

SZKOŁA DOKTORSKA NAUK ŚCISŁYCH I PRZYRODNICZYCH  
UNIwersYTETU ŁÓDZKIEGO

# ROZPRAWA DOKTORSKA

**Łukasz Szymon Biegała**

---

**Wykorzystanie szlaku kinazy ATR/CHK1 w celu  
zwiększenia efektywności terapii olaparibem.**

**Porównanie efektów terapeutycznych  
w modelu *in vitro* oraz *in vivo* raka jajnika  
opornego na leczenie inhibitorem PARP**

---

The use of the ATR/CHK1 pathway to enhance olaparib efficacy.  
A comparison of therapeutic effects in PARP inhibitor-resistant  
ovarian cancer models *in vitro* and *in vivo*

Praca doktorska wykonana w  
Katedrze Biofizyki Medycznej,  
Instytut Biofizyki, Uniwersytet Łódzki

Promotor  
dr hab. Aneta Rogalska, prof. UŁ

Promotor pomocniczy  
dr Arkadiusz Gajek

ŁÓDŹ, 2024

Serdecznie dziękuję moim promotorom **dr hab. Anecie Rogalskiej, prof. UŁ**,  
oraz **dr. Arkadiuszowi Gajkowi** za opiekę naukową, możliwość realizacji badań,  
zaangażowanie i pomoc merytoryczną.

Składam również podziękowania dla wszystkich **współautorów publikacji naukowych**,  
w szczególności dla prof. dr hab. Agnieszki Marczak,  
dr hab. n.med. Agnieszki Śliwińskiej, prof. Uczelni,  
dr n. med. Izabeli Szymczak-Pajor,  
mgr. Damiana Kołata,  
za owocną współpracę i pomoc w realizacji projektów.

Dziękuję **koleżankom i kolegom z mojej Uczelni**, w szczególności dr Patrycji Gralewskiej,  
za wszelką pomoc i wspierającą atmosferę w pracy.

Szczególnie chciałabym podziękować **Rodzicom**,  
za ich wsparcie i wiarę we mnie podczas całej mojej drogi edukacji.

---

# SPIS TREŚCI

---

<b>ŹRÓDŁO FINANSOWANIA</b>	<b>4</b>
<b>WSPÓŁPRACA</b>	<b>5</b>
<b>DOROBEK NAUKOWY</b>	<b>6</b>
<b>STRESZCZENIE</b>	<b>11</b>
<b>ABSTRACT</b>	<b>13</b>
<b>WYKAZ SKRÓTÓW</b>	<b>15</b>
<b>WSTĘP TEORETYCZNY</b>	<b>17</b>
CHARAKTERYSTYKA RAKA JAJNIKA	17
ROLA SZLAKU ODPOWIEDZI NA USZKODZENIA DNA W RAKU JAJNIKA	18
LECZENIE NISKOZRÓŻNICOWANEGO RAKA JAJNIKA – INHIBITORY PARP	19
PRZYCZYNY ROZWOJU OPORNOŚCI NA OLAPARIB	21
PRZEŁAMYWANIE OPORNOŚCI NA OLAPARIB A SZLAK ATR/CHK1	21
ZNACZENIE MIKRORNA W RAKU JAJNIKA	23
<b>CEL PRACY</b>	<b>25</b>
<b>MATERIAŁY I METODY</b>	<b>27</b>
MATERIAŁ BADAWCZY	27
BADANE ZWIĄZKI	28
METODY BADAWCZE	28
<b>WYNIKI I DYSKUSJA</b>	<b>31</b>
ETAP 1	32
ETAP 2	37
ETAP 3	42
ETAP 4	47
<b>PODSUMOWANIE I WNIOSKI</b>	<b>53</b>
<b>BIBLIOGRAFIA</b>	<b>56</b>
<b>KOPIE ARTYKUŁÓW OPUBLIKOWANYCH I MANUSKRYPTU</b>	<b>58</b>
PUBLIKACJA #1	59
PUBLIKACJA #2	76
PUBLIKACJA #3	129
PUBLIKACJA #4	150
MANUSKRYPT ARTYKUŁU #5	211
<b>OŚWIADCZENIA WSPÓŁAUTORÓW</b>	<b>242</b>

## ŹRÓDŁO FINANSOWANIA

---

Badania przeprowadzone w ramach rozprawy doktorskiej zostały sfinansowane z następujących źródeł:

### **PROJEKT SONATA BIS 9**

Projekt badawczy SONATA BIS 9 nr 2019/34/E/NZ7/00056 finansowany przez Narodowe Centrum Nauki pt. „Wykorzystanie olaparibu i inhibitorów kinazy ATR/CHK1 jako celowanej terapii przeciwnowotworowej opartej na syntetycznej letalności”. Kierownik projektu: dr hab. Aneta Rogalska, prof. UŁ.



### **SZKOŁA DOKTORSKA NAUK ŚCISŁYCH I PRZYRODNICZYCH UŁ**

Dofinansowania w ramach działalności naukowej doktorantów Szkoły Doktorskiej Nauk Ścisłych i Przyrodniczych UŁ w latach 2021–2024.





## WSPÓŁPRACA

---

Część badań przedstawionych w zbiorze opublikowanych artykułów i nieopublikowanego manuskryptu, stanowiącym podstawę rozprawy doktorskiej, przeprowadzono we współpracy z poniższymi jednostkami naukowymi:

### **UNIwersYTET MEDYCZNY W ŁODZI**

- ✦ Zakład Biochemii Kwasów Nukleinowych
- ✦ Zakład Genomiki Funkcjonalnej



UNIwersYTET  
MEDYCZNY  
W ŁODZI

### **NARODOWY INSTYTUT ONKOLOGII IM. MARII SKŁODOWSKIEJ-CURIE – PAŃSTWOWY INSTYTUT BADAWCZY**

- ✦ Zakład Genetyki
- ✦ Zakład Immunoterapii Eksperymentalnej



**Narodowy  
Instytut  
Onkologii**

im. Marii Skłodowskiej-Curie  
Państwowy Instytut Badawczy

# DOROBEK NAUKOWY

---

## ARTYKUŁY WCHODZĄCE W SKŁAD ROZPRAWY DOKTORSKIEJ

Na niniejszą rozprawę doktorską składa się cykl czterech opublikowanych i powiązanych tematycznie artykułów naukowych uzupełniony o jeden nieopublikowany manuskrypt artykułu gotowy do wysłania do recenzowanego czasopisma. Wartość współczynnika wpływu Impact Factor (IF) oraz liczbę punktów Ministerstwa Nauki i Szkolnictwa Wyższego (MNiSW) dla danego artykułu naukowego ustalono zgodnie z rokiem opublikowania artykułów.

### Publikacja przeglądowa

- ✦ **Biegała Ł.**, Gajek A., Marczak A., Rogalska A. *PARP inhibitor resistance in ovarian cancer: Underlying mechanisms and therapeutic approaches targeting the ATR/CHK1 pathway*. Biochim Biophys Acta Rev Cancer. 2021. 1876(2):188633. doi: 10.1016/j.bbcan.2021.188633.

Punkty MNiSW = 200 pkt, IF = 11,414 (2-letni)

### Publikacje doświadczalne

- ✦ **Biegała Ł.**, Gajek A., Marczak A., Rogalska A. *Olaparib-resistant BRCA2<sup>MUT</sup> ovarian cancer cells with restored BRCA2 abrogate olaparib-induced DNA damage and G2/M arrest controlled by the ATR/CHK1 pathway for survival*. Cells. 2023. 12(7):1038. doi: 10.3390/cells12071038.

Punkty MNiSW = 140 pkt, IF = 6,0

- ✦ **Biegała Ł.**, Gajek A., Szymczak-Pajor I., Marczak A., Śliwińska A., Rogalska A. *Targeted inhibition of the ATR/CHK1 pathway overcomes resistance to olaparib and dysregulates DNA damage response protein expression in BRCA2<sup>MUT</sup> ovarian cancer cells*. Sci Rep. 2023. 13(1):22659.

doi: 10.1038/s41598-023-50151-y.

Punkty MNiSW = 140 pkt, IF = 4,6

- ✦ **Biegała Ł.**, Kołat D., Gajek A., Płuciennik E., Marczak A., Śliwińska A., Mikula M., Rogalska A. *Uncovering miRNA-mRNA Regulatory Networks Related to Olaparib Resistance and Resensitization of BRCA2<sup>MUT</sup> Ovarian Cancer PEO1-OR Cells with the ATR/CHK1 Pathway Inhibitors*. Cells. 2024. 13(10):857. doi: 10.3390/cells13100867.

Punkty MNiSW = 140 pkt, IF = 6,0

### Nieopublikowany manuskrypt artykułu doświadczalnego

- ✦ **Biegała Ł.**, Statkiewicz M., Gajek A., Szymczak-Pajor I., Rusetska N., Śliwińska A., Marczak A., Mikula M., Rogalska A. *Olaparib rechallenge combined with the ATR/CHK1 pathway inhibitors in olaparib-resistant PDX models of ovarian cancer: Mechanisms behind synergistic tumor growth inhibition*.

Sumaryczna liczba punktów MNiSW cyklu prac wynosi:

620

Sumaryczny IF cyklu publikacji wynosi:

28,014

## POZOSTAŁE ARTYKUŁY STANOWIĄCE DOROBK NAUKOWY

- ✦ Drzazga A., Okulus M., Rychlicka M., **Biegała Ł.**, Gliszczyńska A., Gendaszewska-Darmach E. *Lysophosphatidylcholine Containing Anisic Acid Is Able to Stimulate Insulin Secretion Targeting G Protein Coupled Receptors*. *Nutrients*. 2020. 12(4):1173. doi: 10.3390/nu12041173.

Punkty MNiSW = 140 pkt, IF = 5,717

Sumaryczna liczba punktów MNiSW dorobku naukowego wynosi:	760
Sumaryczny IF dorobku naukowego wynosi:	33,731
Łączna ilość cytowań według bazy Web of Science:	42

## DONIESIENIA KONFERENCYJNE

### Konferencje międzynarodowe

- ✦ **Łukasz Biegała**, Damian Kołat, Arkadiusz Gajek, Elżbieta Płuciennik, Agnieszka Marczak, Agnieszka Śliwińska, Michał Mikula, Aneta Rogalska. „Insights into olaparib resistance in *BRCA2*<sup>MUT</sup> ovarian cancer cells and its reversal with the ATR/CHK1 pathway inhibitors: miRNA-mRNA regulatory network and growth factor signaling”.

**Wystąpienie ustne | 62<sup>nd</sup> Polish and 20<sup>th</sup> International Training & Scientific Medical Congress of Students' Scientific Society – Juvenes Pro Medicina 2024.**  
Łódź, Polska | 9–12.05.2024,

- ✦ **Łukasz Biegała**, Arkadiusz Gajek, Agnieszka Marczak, Aneta Rogalska. „Targeting the ATR/CHK1 pathway resensitizes olaparib-resistant *BRCA2*<sup>MUT</sup> ovarian cancer cells via induction of caspase mediated apoptosis”.

**Wystąpienie ustne | The International Cell Science and Molecular Biology Forum 2023.**  
Walencja, Hiszpania | 13–15.04.2023,

- ✦ **Łukasz Biegała**, Arkadiusz Gajek, Agnieszka Marczak, Aneta Rogalska. „Chromosomal aberrations and homologous recombination DNA repair activity in response to olaparib combined with inhibitors of ATR/CHK1 pathway in ovarian cancer cells sensitive and resistant to PARPi”.

**Poster | The Biochemistry Global Submit – the 25<sup>th</sup> IUBMB, 46<sup>th</sup> FEBS, and 15<sup>th</sup> PABMB Congresses.** Lizbona, Portugalia | 09–14.07.2022,

- ✦ **Łukasz Biegała**, Arkadiusz Gajek, Agnieszka Marczak, Aneta Rogalska. „The combination of olaparib and the inhibitors of ATR/CHK1 pathway exerts synergistic antitumor effects in *BRCA2*-proficient PEO4 ovarian cancer cell line”.

**Poster | 8<sup>th</sup> Central European Congress of Life Sciences EUROBIOTECH.**  
Kraków, Polska | 20–22.06.2022,

- ✦ **Łukasz Biegała**, Karolina Górna, Arkadiusz Gajek, Agnieszka Marczak, Aneta Rogalska. „Preliminary studies assessing the impact of PARP inhibitor and ATR/CHK1 pathway blockade on the expression level of targeted proteins in PEO1 *BRCA2*<sup>MUT</sup> ovarian cancer cells”.

**Poster | 25<sup>th</sup> Gliwice Scientific Meetings.** Gliwice, Polska | 19–20.11.2021,

- ✦ **Łukasz Biegała**, Arkadiusz Gajek, Agnieszka Marczak, Aneta Rogalska. „Olaparib in combination with the inhibitors of ATR/CHK1 pathway leads to increased cell death in ovarian cancer cells sensitive and resistant to PARPi”.

**Poster | 22<sup>nd</sup> European Gynaecological Oncology Congress of the European Society of Gynaecological Oncology.** Praga, Czechy | 23–25.10.2021.

### **Konferencje ogólnopolskie**

- ✦ **Łukasz Biegała**, Arkadiusz Gajek, Agnieszka Marczak, Aneta Rogalska. „Wpływ olaparibu i inhibitorów szlaku ATR/CHK1 na uszkodzenia DNA i ich naprawę z udziałem rekombinazy RAD51 w komórkach raka jajnika”.

**Wystąpienie ustne | VII Ogólnopolska Konferencja Doktorantów Nauk o Życiu BioOpen.** Łódź, Polska | 07–08.04.2022.

### **| NAGRODY, WYRÓŻNIENIA I STYPENDIA**

- ✦ I Nagroda w konkursie „Nagroda Naukowa Rektora Uniwersytetu Łódzkiego” dla doktorantek i doktorantów realizujących czwarty rok kształcenia w Szkołach Doktorskich UŁ w roku akademickim 2023/24 za osiągnięcia w zakresie działań związanych z aktywnością publikacyjną i umiędzynarodowieniem kształcenia oraz pracy naukowej i badawczej. Nagrodę uzyskano w obrębie Szkoły Doktorskiej Nauk Ścisłych i Przyrodniczych UŁ | 19.04.2024,
- ✦ Wyróżnienia za plakat w konkursie „Best Poster Distinction” podczas międzynarodowej konferencji „8<sup>th</sup> Central European Congress of Life Sciences EUROBIOTECH” w Krakowie | 22.06.2022,
- ✦ Stypendium konferencyjne dla młodych naukowców finansowane przez Federation of European Biochemical Societies (FEBS) w ramach konkursu na dofinansowanie uczestnictwa w kongresie międzynarodowym „The Biochemistry Global Submit – the 25<sup>th</sup> IUBMB, 46<sup>th</sup> FEBS and 15<sup>th</sup> PABMB Congresses” w Lizbonie | 07.04.2022.

### **| ORGANIZACJA KONFERENCJI I SZKOLEŃ NAUKOWYCH**

- ✦ Członek komitetu naukowego Ogólnopolskiej Konferencji Doktorantów Nauk o Życiu BioOpen organizowanej przez Wydział Biologii i Ochrony Środowiska Uniwersytetu Łódzkiego:
  - sekcja „Biologia Molekularna i Medyczna”, VIII edycja w 2023 r. | 13–14.04.2023,
  - sekcja „Biologia Molekularna i Medyczna”, VII edycja w 2022 r. | 07–08.04.2022.
- ✦ Wykład i pokaz praktyczny sprzętu laboratoryjnego w trakcie seminariów w tematyce „Optymalizacja technik pracy z białkami” organizowanych przez firmę Merck Sp. z o. o. | Łódź, 08.11.2023 oraz Warszawa, 22.11.2023.

### **| PROJEKT BADAWCZY**

- ✦ Wykonawca projektu badawczego „Wykorzystanie olaparibu i inhibitorów kinazy ATR/CHK1 jako celowanej terapii przeciwnowotworowej opartej na syntetycznej letalności” finansowanego przez NCN w ramach projektu krajowego SONATA BIS 9 numer 2019/34/E/NZ7/00056 | 02.11.2020–30.04.2024.

## **SZKOLENIA NAUKOWE**

- ✦ Szkolenie stacjonarne „Optymalizacja technik pracy z białkami” organizowane przez firmę Merck Sp. z o. o. | Łódź, 08.11.2023 oraz Warszawa, 22.11.2023,
- ✦ Szkolenie on-line pt. „Expert Insights on qPCR and dPCR Validation for Gene Therapy” organizowane przez firmę Thermo Fisher Scientific & BioAgilytix | 15.06.2023,
- ✦ Szkolenie stacjonarne pt. „Jak uzyskać wiarygodne wyniki w technikach real-time PCR oraz digital PCR z Thermo Fisher Scientific” organizowane przez firmę Thermo Fisher Scientific | Łódź, 15.09.2022,
- ✦ Szkolenie on-line pt. „Simple steps to publication-quality western blots” organizowane przez firmę Thermo Fisher Scientific | 12–14.10.2021,
- ✦ Szkolenie on-line pt. „Western blotting – wskazówki i porady dotyczące optymalizacji procesu” organizowane przez firmę Merck Sp. z o. o. | 28.05.2021,
- ✦ Szkolenie on-line pt. „Hodowle komórek w 3D” organizowane przez firmę Merck Sp. z o. o. | 23.04.2021,
- ✦ Szkolenie on-line pt. „Zakażenia hodowli mykoplazmą – zapobieganie oraz detekcja” organizowane przez firmę Merck Sp. z o. o. | 19.03.2021,
- ✦ Kurs dla osób uczestniczących w wykonywaniu procedur i doświadczeń prowadzonych na zwierzętach laboratoryjnych organizowany przez Zwierzętarnie UŁ | 30.11–04.12.2020.

## **POPULARYZOWANIE NAUKI**

- ✦ Prowadzenie warsztatów eksperymentalnych pt. „Jak hodować komórki w warunkach *in vitro*?” w ramach zajęć Instytutu Kreatywnej Biologii organizowanego przez Wydziału Biologii i Ochrony Środowiska Uniwersytetu Łódzkiego:
  - edycja 2023/2024 | 19.01.2024, 23.02.2024, 19.04.2024
  - edycja 2022/2023 | 18.11.2022, 24.02.2023, 21.04.2023, 16.06.2023,
  - edycja 2021/2022 | 10.06.2022,
- ✦ Prowadzenie warsztatów eksperymentalnych pt. „Jak hodować komórki w warunkach *in vitro*?” w ramach XX Festiwalu Nauki, Techniki i Sztuki na Wydziale Biologii i Ochrony Środowiska Uniwersytetu Łódzkiego | Łódź, 19.10.2021.

## **WSPÓŁPRACA Z PRACODAWCAMI I BIZNESEM**

- ✦ Przeprowadzenie testów urządzenia do przygotowywania żeli poliakrylamidowych „mPAGE® Lux Casting System for SDS-PAGE Gels” do techniki SDS-PAGE (część II) dla firmy Merck Sp. z o. o. z obszaru Life Science | Katedra Biofizyki Medycznej, Uniwersytet Łódzki, Łódź, 01–31.01.2023,
- ✦ Przeprowadzenie testów urządzenia do elektroforezy i transferu białek metodą Western Blot dla firmy Merck Sp. z o. o. z obszaru Life Science | Katedra Biofizyki Medycznej, Uniwersytet Łódzki, Łódź, 01–14.08.2022,

- ✦ Przeprowadzenie testów urządzenia do przygotowywania żeli poliakrylamidowych „mPAGE® Lux Casting System for SDS-PAGE Gels” do techniki SDS-PAGE (część I) dla firmy Merck Sp. z o. o. z obszaru Life Science | Katedra Biofizyki Medycznej, Uniwersytet Łódzki, Łódź, 06–19.12.2021.

## **POZOSTAŁY DOROBEK NAUKOWY**

- ✦ Członek Europejskiego Towarzystwa Onkologii Medycznej (ESMO) od 13.03.2024–obecnie,
- ✦ Członek Polskiego Towarzystwa Biochemicznego od 16.09.2021–obecnie,
- ✦ Opieka nad częścią eksperymentalną pracy magisterskiej Pani Karoliny Górnej, studentki kierunku Biologia na Wydziale Biologii i Ochrony Środowiska Uniwersytetu Łódzkiego w roku akademickim 2021/2022. Tytuł pracy magisterskiej: „Uwrażliwienie komórek raka jajnika o wysokim stopniu złośliwości na olaparib z wykorzystaniem inhibitorów szlaku ATR/CHK1”.

# STRESZCZENIE

---

## **„Wykorzystanie szlaku kinazy ATR/CHK1 w celu zwiększenia efektywności terapii olaparibem. Porównanie efektów terapeutycznych w modelu *in vitro* oraz *in vivo* raka jajnika opornego na leczenie inhibitorem PARP”**

Niskozróżnicowany surowiczy rak jajnika (HGSOC, ang. *high-grade serous ovarian cancer*) to najczęstszy i najgorzej rokujący typ histologiczny raka jajnika, który cechuje się wysoką heterogennością i w przypadku nawrotów uważany jest za chorobę przewlekłą. Od pewnego czasu w leczeniu HGSOC coraz większą rolę odgrywają leki ukierunkowane molekularnie. Olaparib, to niskocząsteczkowy inhibitor polimerazy poli(ADP)rybozy (PARPi, ang. *poly(ADP)ribose polymerase inhibitor*) stosowany w raku jajnika zwykle w leczeniu podtrzymującym platynowrażliwego HGSOC, który został po raz pierwszy zarejestrowany w leczeniu raka jajnika w 2014 roku. Przeprowadzane w kolejnych latach badania kliniczne umożliwiły rozszerzenie wskazań do stosowania tego leku w terapii HGSOC, uwzględniając charakterystykę guzów pacjentek, które mogą uzyskać największe korzyści terapeutyczne. Mechanizm przeciwnowotworowego działania olaparibu w komórkach HGSOC opiera się na wykorzystaniu zjawiska syntetycznej letalności. W przypadku komórek nowotworowych z mutacjami w genach *BRCA1/2*, zaburzającymi szlak naprawy DNA przez rekombinację homologiczną (HR, ang. *homologous recombination*), zahamowanie dodatkowo alternatywnych szlaków naprawy regulowanych przez PARP z użyciem olaparibu prowadzi do akumulacji uszkodzeń DNA prowadzących w konsekwencji do śmierci komórki. Jednak istotnym problemem w terapii raka jajnika z użyciem olaparibu jest nabywanie oporności na ten lek, co znacząco ogranicza potencjał PARPi u pacjentek z HGSOC. Jak dotąd, poznano część mechanizmów odpowiedzialnych za rozwój oporności na ten PARPi w raku jajnika. Aktualnie podejmowane są także próby przełamywania oporności na olaparib z zastosowaniem celowanych terapii skojarzonych. Jedną z obecnie badanych strategii ponownego uwrażliwiania komórek HGSOC na olaparib jest inhibicja szlaku ATR/CHK1, który odpowiedzialny jest za regulację odpowiedzi na uszkodzenia DNA oraz przebiegu cyklu komórkowego. Dalsze badania nad nabywaniem i przełamywaniem oporności na olaparib, uwzględniające różnorodność komórek HGSOC, mogą przyczynić się do lepszego zrozumienia tych zjawisk, a w efekcie poprawę skuteczności terapii raka jajnika przedłużającą czas życia pacjentek.

Uwzględniając powyższe przesłanki, celem niniejszej rozprawy doktorskiej była ocena przeciwnowotworowego działania oraz potencjału terapeutycznego połączenia olaparibu z inhibitorem kinazy ATR (ATRi) lub kinazy CHK1 (CHK1i) odpowiednio w modelu *in vitro* oraz *in vivo* HGSOC z mutacjami w genach *BRCA1* i/lub *BRCA2* (*BRCA1/2<sup>MUT</sup>*) oraz nabytą opornością na olaparib. Jednocześnie porównano skuteczność badanych kombinacji olaparibu ze skutecznością każdego z inhibitorów osobno w hamowaniu wzrostu i przeżycia opornych komórek HGSOC. Ponadto, celem pracy było poznanie mechanizmów związanych z nabywaniem oporności na olaparib oraz jej przełamywaniem poprzez inhibicję szlaku ATR/CHK1.

W pierwszej części badań *in vitro* wyprowadzono linię komórkową raka jajnika PEO1-OR oporną na olaparib z macierzystej linii wrażliwej PEO1 oraz zbadano molekularne mechanizmy odpowiedzialne za nabywanie fenotypu opornego. Jednym ze zidentyfikowanych w warunkach

*in vitro* mechanizmów oporności była selekcja klonalna w kierunku komórek posiadających rewersję mutacji w genie *BRCA2* przywracająca prawidłową ramkę odczytu. Następnie wytypowano stężenia inhibitorów wykazujących w kombinacji synergistycznie działanie przeciwnowotworowe w komórkach linii wrażliwych (PEO1 i PEO4) przy jednoczesnym niewielkim wpływie na przeżycie komórek linii niewrażliwej (PEO1-OR) w celu porównania na poziomie molekularnym odpowiedzi komórek HGSOC zależne od wrażliwości na PARPi. W związku z tym zbadano między innymi ekspresję polimerazy PARP1 i glikohydrolazy PARG, kinazy ATR i CHK1 oraz ich fosforylację, a także białek zaangażowanych w szlaki naprawy DNA (BRCA1, BRCA2, RAD51, 53BP1,  $\gamma$ H2AX). Ponadto oceniono rolę glikoproteiny P w odpowiedzi na badane inhibitory oraz zbadano przebieg cyklu komórkowego i poziom uszkodzeń DNA indukowanych przez badane związki.

Kolejny etap badań *in vitro* obejmował porównanie przeciwnowotworowego działania inhibitorów stosowanych osobno, jak i w kombinacji w wyższych stężeniach wykazujących synergistyczne działanie przeciwnowotworowe w komórkach PEO1-OR. Co ważne, potwierdzono, że inhibicja szlaku ATR/CHK1 umożliwia przełamanie oporności na olaparib w warunkach *in vitro*. Dodatkowo, zbadano odpowiedź uwrażliwionych komórek PEO1-OR na badane kombinacje, w tym oceniono udział apoptozy, aktywność kaspaz-3/7 oraz ekspresję panelu 27 białek zaangażowanych w szlak naprawy DNA.

W następnej części badań *in vitro* skupiono się na roli cząsteczek mikroRNA (miRNA) w nabywaniu i przełamywaniu oporności na olaparib. W tym celu przeprowadzono profilowanie ekspresji miRNA we wszystkich trzech liniach komórkowych HGSOC. Następnie wykonano analizy bioinformatyczne umożliwiające zidentyfikowanie genów docelowych dla miRNA o zmienionej ekspresji oraz procesów komórkowych i szlaków sygnałowych związanych z wytypowanymi genami. Na koniec oceniono związek pomiędzy miRNA o zmienionej ekspresji w linii PEO1-OR oraz ich genami docelowymi a przeżyciem pacjentek z surowiczym rakiem jajnika na podstawie danych klinicznych z repozytorium.

Ostatni etap badań obejmował ocenę potencjału terapeutycznego kombinacji olaparibu z inhibitorami szlaku ATR/CHK1 w warunkach *in vivo* w mysim modelu opornego na olaparib heteroprzeszczepu guza pochodzącego od pacjentki z HGSOC. Co ważne, potwierdzono, że dodanie do olaparibu ATRi lub CHK1i prowadzi do synergistycznego zahamowania wzrostu guzów opornych na olaparib. Dodatkowo, scharakteryzowano zmiany zachodzące podczas nabywania oporności na olaparib oraz odpowiedź uwrażliwionych guzów na badane kombinacje, w tym przeprowadzono analizy histopatologiczne oraz badania molekularne.

Podsumowując, zrealizowane w ramach niniejszej rozprawy badania potwierdziły, że dodanie ATRi lub CHK1i do olaparibu przełamuje oporność na PARPi w komórkach raka jajnika z nabytą opornością na olaparib. Synergistyczne przeciwnowotworowe działanie kombinacji olaparibu z inhibitorami szlaku ATR/CHK1 stwierdzono zarówno w modelu *in vitro* opartym o ludzką linię komórkową HGSOC, jak i w mysim modelu *in vivo* opartym o heteroprzeszczep guza pozyskanego od pacjentki z HGSOC. Uzyskane wyniki wskazują na duży potencjał celowanej terapii skojarzonej łączącej olaparib z inhibitorami szlaku ATR/CHK1 u opornych na olaparib pacjentek z rakiem jajnika będących nosicielkami mutacji w genach *BRCA1/2*.



# ABSTRACT

---

**„Targeting the ATR/CHK1 pathway to increase the efficacy of olaparib therapy.  
A comparison of therapeutic effects in ovarian cancer models  
resistant to PARP inhibitors *in vitro* and *in vivo*”**

High-grade serous ovarian cancer (HGSOC) is the most common and lethal histotype of ovarian cancer, characterized by tumor heterogeneity and regarded as a chronic condition upon recurrence. Recently, targeted therapy drugs have gained increasing relevance in HGSOC treatment. Olaparib, a small-molecule poly(ADP)ribose polymerase inhibitor (PARPi), received its initial approval for ovarian cancer therapy in 2014. Currently, olaparib is primarily recommended for use in HGSOC as maintenance therapy for platinum-sensitive patients. Clinical trials assessing olaparib's efficacy in various HGSOC cohorts have allowed for the expansion of its indications based on the characteristics of patients' tumors, which help predict drug efficacy. Olaparib's antitumor mechanism of action relies on the concept of synthetic lethality. In the context of *BRCA1/2*-mutated tumors with homologous recombination deficiency, this concept refers to a phenomenon where simultaneous inhibition of alternative DNA repair pathways controlled by PARP1 with olaparib leads to the accumulation of DNA damage and cell death. Unfortunately, acquired resistance to olaparib poses a significant challenge in the treatment of ovarian cancer, limiting its effectiveness in HGSOC patients. To date, several mechanisms of resistance to PARPi have been elucidated in ovarian cancer. Nowadays, combination targeted therapies constitute a promising approach to overcoming olaparib resistance. Current studies investigate the potential of inhibiting the ATR/CHK1 pathway, regulating DNA damage response and cell cycle, to resensitize HGSOC to olaparib. Future studies linking HGSOC heterogeneity with acquiring and overcoming resistance to olaparib can enhance our understating of these processes, leading to the development of therapies with enhanced efficacy in ovarian cancer.

In view of the above, the presented doctoral dissertation aimed to assess the antitumor activity and therapeutic potential of combining olaparib with the ATR kinase inhibitor (ATRi) and CHK1 kinase inhibitor (CHK1i) in both *in vitro* and *in vivo* models of olaparib-resistant *BRCA1/2*<sup>MUT</sup> HGSOC, respectively. Additionally, the activity of each single-agent inhibitor was compared with their combinations regarding tumor growth inhibition and survival. Furthermore, the conducted studies sought to elucidate the mechanisms associated with both conferring and overcoming resistance to olaparib through the ATR/CHK1 pathway inhibition.

In the first part of *in vitro* studies, the olaparib-resistant ovarian cancer PEO1-OR cell line was developed from the parental olaparib-sensitive PEO1 cell line. Molecular mechanisms underlying the resistant phenotype were established, which included the subclonal enrichment of the *BRCA2* secondary mutation restoring the protein's open reading frame. Subsequent investigations enabled me to identify concentrations of combined inhibitors that exerted synergistic antitumor activity in olaparib-sensitive cell lines (PEO1 and PEO4), while minimally affecting the survival of the olaparib-resistant cell line (PEO1-OR). Using these selected doses, HGSOC cell responses were compared across cell lines with varying sensitivities to olaparib. This comparison encompassed the PARP1 polymerase and PARG glycohydrolase expression, ATR and CHK1 kinases expression and

phosphorylation as well as levels of DNA damage repair-related proteins (BRCA1, BRCA2, RAD51, 53BP1,  $\gamma$ H2AX). Moreover, we investigated the role of glycoprotein P (MDR1), changes in cell cycle progression, and DNA damage in the context of the HGSOC responses to tested inhibitors.

In the subsequent phase of *in vitro* studies, the antitumor activity of each single-agent inhibitor was compared with their combinations at higher concentrations, which demonstrated synergistic activity in PEO1-OR cells. Importantly, overcoming resistance to olaparib through targeted inhibition of the ATR/CHK1 pathway was confirmed. Furthermore, the response of PEO1-OR cells resensitized to olaparib with the ATR/CHK1 pathway inhibitors was characterized. This characterization included the role of apoptosis, caspase-3/7 activity, and the expression of 27 proteins involved in DNA damage response.

The subsequent part of *in vitro* studies was dedicated to investigating the role of microRNA (miRNA) in both acquiring and overcoming resistance to olaparib. To begin, miRNA profiles were established in all three HGSOC cell lines. Subsequently, bioinformatic analyses were conducted to identify genes targeted by differentially-expressed miRNAs and to unveil enriched biological processes and signaling pathways linked to these genes. Lastly, the association between miRNAs that were differentially-expressed in the PEO1-OR cell line, along with their target genes, and survival outcomes of HGSOC patients based on available clinical data.

The final part of the studies was focused on assessing the therapeutic potential of combining olaparib with the ATR/CHK1 pathway inhibitors *in vivo*, utilizing the olaparib-resistant mouse xenograft model of HGSOC derived from a patient's tumor. Notably, the addition of ATRi or CHK1i to olaparib resulted in synergistic growth inhibition of tumors with acquired resistance to olaparib. Moreover, changes associated with acquiring and overcoming resistance to olaparib were characterized through histopathological and molecular analyses of the resensitized tumors.

In summary, conducted studies confirmed that adding ATRi or CHK1 to olaparib effectively overcomes resistance to tested PARPi in HGSOC cells that had acquired resistance to olaparib. Synergistic antitumor activity of olaparib combined with the ATR/CHK1 pathway inhibitors was documented in both *in vitro* the HGSOC cell line model and *in vivo* in the HGSOC patients-derived xenograft model. These findings highlight the potential of a targeted therapy combining olaparib with the ATR/CHK1 pathway inhibitors for ovarian cancer patients harboring *BRCA1/2* mutations.

## WYKAZ SKRÓTÓW

---

<b>A</b>	inhibitor kinazy ATR (ceralasertib)
<b>ATR</b>	kinaza związana z ataksją teleangiektazją i Rad3 (ang. <i>ataxia-telangiectasia and Rad3-related</i> )
<b>ATRi</b>	inhibitor(y) kinazy ATR (ang. <i>ATR inhibitor</i> )
<b>BRCA2<sup>MUT</sup></b>	mutacja w genie BRCA2
<b>C</b>	inhibitor kinazy CHK1 (MK-8776)
<b>CDI</b>	współczynnik oddziaływania leków (ang. <i>coefficient of drug interaction</i> )
<b>CHK1</b>	kinaza punktu kontrolnego 1 (ang. <i>checkpoint kinase 1</i> )
<b>CHK1i</b>	inhibitor(y) kinazy CHK1 (ang. <i>CHK1 inhibitor</i> )
<b>CI</b>	współczynnik kombinacji (ang. <i>combination index</i> )
<b>DDR</b>	odpowiedź na uszkodzenia DNA (ang. <i>DNA damage response</i> )
<b>DSB</b>	podwójne pęknięcie DNA (ang. <i>double-strand break</i> )
<b>ECACC</b>	Europejska Kolekcja Uwierzytelnionych Kultur Komórkowych (ang. <i>European Collection of Authenticated Cell Cultures</i> )
<b>EGFR</b>	receptor nabłonkowego czynnika wzrostu (ang. <i>epidermal growth factor receptor</i> )
<b>EMA</b>	Europejska Agencja Leków (ang. <i>European Medicines Agency</i> )
<b>EMT</b>	przejście epitelialno-mezenchymalne (ang. <i>epithelial-to-mesenchymal transition</i> )
<b>ESMO</b>	Europejskie Towarzystwo Onkologii Klinicznej (ang. <i>European Society for Medical Oncology</i> )
<b>FDA</b>	Agencja ds. Żywności i Leków (ang. <i>Food and Drug Administration</i> )
<b>FGF</b>	czynnik wzrostu fibroblastów (ang. <i>fibroblast growth factor</i> )
<b>FGFR</b>	receptor czynnika wzrostu fibroblastów (ang. <i>fibroblast growth factor receptor</i> )
<b>HB-EGF</b>	czynnik wzrostu EGF-podobny wiążący heparynę (ang. <i>heparin-binding EGF-like growth factor</i> )
<b>HGSOC</b>	niskozróżnicowany surowiczy rak jajnika (ang. <i>high-grade serous ovarian cancer</i> )
<b>HR</b>	współczynnik ryzyka (ang. <i>hazard ratio</i> )
<b>HRD</b>	niedobór homologicznej rekombinacji (ang. <i>homologous recombination deficiency</i> )
<b>HRR</b>	naprawa poprzez rekombinację homologiczną (ang. <i>homologous recombination repair</i> )

<b>IGFBP</b>	białko wiążącego insulinopodobny czynnik wzrostu (ang. <i>insulin-like growth factor-binding protein</i> )
<b>NGF</b>	czynnik wzrostu nerwów (ang. <i>nerve growth factor</i> )
<b>NGS</b>	sekwencjonowanie nowej generacji (ang. <i>next-generation sequencing</i> )
<b>NHEJ</b>	łączenie niehomologicznych końców (ang. <i>non-homologous end joining</i> )
<b>O</b>	olaparib
<b>OC</b>	rak jajnika (ang. <i>ovarian cancer</i> )
<b>OS</b>	całkowity czas przeżycia (ang. <i>overall survival</i> )
<b>PARP</b>	polimeraza poli(ADP-rybozy) (ang. <i>poly(ADP-ribose) polymerase</i> )
<b>PARPi</b>	inhibitor(y) PARP (ang. <i>PARP inhibitors</i> )
<b>PDGF</b>	platekopochozny czynnik wzrostu (ang. <i>platelet-derived growth factor</i> )
<b>PDGFR</b>	receptor platekopochoznego czynnik wzrostu (ang. <i>platelet-derived growth factor receptor</i> )
<b>PDT</b>	czas podwojenia populacji (ang. <i>population doubling time</i> )
<b>PDX</b>	heteroprzeszczep guza pozyskanego od pacjentki (ang. <i>patient-derived xenograft</i> )
<b>PEO1-OR</b>	linia komórkowa raka jajnika oporna na olaparib
<b>PFI</b>	interwały wolne od progresji (ang. <i>progression-free intervals</i> )
<b>PLGF</b>	łożyskowy czynnik wzrostu (ang. <i>placental growth factor</i> )
<b>RTV</b>	względna objętość guza (ang. <i>relative tumor volume</i> )
<b>SCF</b>	czynnik wzrostu komórek macierzystych (ang. <i>stem-cell factor</i> )
<b>T/C ratio</b>	stosunek objętości guza do kontroli (ang. <i>tumor-to-control ratio</i> )
<b>TGFβR</b>	receptor transformującego czynnik wzrostu beta (ang. <i>transforming growth factor beta receptor</i> )
<b>TGI</b>	zahamowanie wzrostu guza (ang. <i>tumor growth inhibition</i> )
<b>VEGF</b>	czynnik wzrostu śródbłónka naczyniowego (ang. <i>vascular endothelial growth factor</i> )
<b>VEGFR</b>	receptor czynnika wzrostu śródbłónka naczyniowego (ang. <i>vascular endothelial growth factor receptor</i> )
<b>WES</b>	sekwencjonowanie całego eksomu (ang. <i>whole-exome sequencing</i> )

# 1

## WSTĘP TEORETYCZNY

---

**R**ak jajnika (OC, ang. *ovarian cancer*) wciąż pozostaje jednym z największych wyzwań pod względem diagnostycznym i terapeutycznym współczesnej onkologii klinicznej, ze względu na wysoką heterogenność nowotworów wywodzących się z jajnika [1]. W 2020 roku, na całym świecie, zdiagnozowano raka jajnika u ponad 310 000 kobiet, a blisko 210 000 pacjentek umarło z jego powodu [2]. Szacuje się, że w 2024 roku rak jajnika będzie przyczyną śmierci 12 700 osób w Stanach Zjednoczonych [3]. Jak dotąd, nie opracowano wiarygodnej metody diagnostycznej pozwalającej wykryć tę chorobę we wczesnych etapach, co przyczynia się do stosunkowo wysokiej śmiertelności pacjentek z rakiem jajnika [4].

### **CHARAKTERYSTYKA RAKA JAJNIKA**

Rak jajnika to zróżnicowana jednostka chorobowa, która klasyfikowana jest ze względu na typ histologiczny. Najpowszechniejszym typem rak jajnika jest nabłonkowy rak jajnika (EOC, ang. *epithelial ovarian cancer*), który stanowi około 90% wszystkich przypadków [5]. Zgodnie z ostatnią klasyfikacją WHO z 2020 roku EOC dzieli się na pięć typów histologicznych, które różnią się patogenezą, morfologią i charakterystyką molekularną, przez co uważane są za oddzielne jednostki chorobowe i poddawane są różnym sposobom leczenia [6]. Najczęściej występującym typem histologicznym EOC jest niskozróżnicowany surowiczy rak jajnika (HGSOC, ang. *high-grade serous ovarian cancer*) charakteryzujący się niestabilnością genetyczną, znaczącym odsetkiem mutacji w genie *TP53* (95% przypadków) oraz wysoką śmiertelnością ze względu na skłonność do nawrotów po leczeniu [7]. Niestety, w większości przypadków rak jajnika wykrywany jest w późnym stadium zaawansowania choroby, tzn. w III i IV stopniu zgodnie z klasyfikacją FIGO, ze względu na bezobjawowy przebieg choroby w początkowych stadiach jej rozwoju, co utrudnia skuteczne leczenie [4, 8].

W raku jajnika zmiany na poziomie genów są ważnym czynnikiem bezpośrednio związanym z ryzykiem rozwoju tej choroby nowotworowej. Jednym z najczęściej wykonywanych badań genetycznych są badania w kierunku mutacji genów supresji nowotworowej *BRCA1/2* (ang. *breast cancer susceptibility 1 and 2*), które zaangażowane są w naprawę DNA. Mutacje w genach *BRCA1/2* są ważnymi czynnikami prognostycznymi i predykcyjnymi w raku jajnika, na podstawie których można częściowo przewidzieć przebieg choroby oraz skuteczność podjętego leczenia [9]. Potencjalnie patogenne mutacje somatyczne i germinalne w genach *BRCA1/2* są identyfikowane u około 17–25% pacjentek z EOC [10, 11]. Geny *BRCA1/2* kodują białka bezpośrednio zaangażowane

w naprawę uszkodzeń DNA poprzez rekombinację homologiczną (HRR, ang. *homologous recombination repair*), przez co mutacje w tych genach mogą doprowadzać do zaburzeń w naprawie DNA [12]. Nosicielki mutacji *BRCA1/2* zwykle lepiej odpowiadają na leczenie związkami indukującymi uszkodzenia DNA [9]. Dane z repozytorium programu genomu raka The Cancer Genome Atlas (TCGA) pokazują, że około 50% pacjentek z HGSOC posiada mutacje w genach związanych ze szlakami HRR [13]. Badania genetyczne na grupie prawie 500 pacjentek z HGSOC potwierdziły, że aż 52% z nich została diagnozowana ze statusem niedoboru rekombinacji homologicznej (HRD, ang. *homologous recombination deficiency*) [14].

### **ROLA SZLAKU ODPOWIEDZI NA USZKODZENIA DNA W RAKU JAJNIKA**

Każdego dnia w komórce indukowane są dziesiątki tysięcy spontanicznych uszkodzeń DNA, które naprawiane są przez systemy wewnątrzkomórkowe związane ze szlakami odpowiedzi na uszkodzenia DNA (DDR, ang. *DNA damage response*) utrzymujące stabilność genomową. Podwójne pęknięcia DNA (DSB, ang. *double-strand break*) należą do jednych z najbardziej genotoksycznych typów uszkodzeń [15]. Powstają one w wyniku działania czynników endogennych m. in. poprzez zatrzymanie widełek replikacyjnych w czasie syntezy DNA i nieefektywną naprawę pęknięć pojedynczej nici DNA przez polimerazy poli(ADP-rybozy (PARP, ang. *poly(ADP-ribose) polymerase*), oraz czynniki egzogenne tj. promieniowanie jonizujące i chemioterapeutyki [15].

Białka z rodziny PARP sygnalizują wykrycie zarówno pojedynczych, jak i podwójnych uszkodzeń DNA oraz biorą udział w ich naprawie. Głównym przedstawicielem tej grupy białek jest polimeraza PARP1. Aktywowany PARP1 katalizuje przyłączanie pojedynczych cząsteczek lub polimerów ADP-rybozy (PAR, ang. *poly(ADP-ribose)*) do własnej cząsteczki polimerazy oraz do innych białek akceptorowych. Proces ten, zwany PARylacją, jest jednym z rodzajów potranslacyjnej modyfikacji białek i ma na celu przekazanie informacji o detekcji uszkodzeń DNA w komórce [16].

Do dwóch głównych szlaków naprawy DSB zaliczyć można HRR oraz naprawę poprzez łączenie niehomologicznych końców (NHEJ, ang. *non-homologous end joining*). Mechanizm naprawy oparty o HRR, który zachodzi głównie w fazie S i G2 cyklu komórkowego, uważany jest za praktycznie bezbłędny w związku z wykorzystywaniem homologicznych sekwencji DNA służących jako matryce do naprawy. W proces ten zaangażowana jest cała grupa białek odpowiedzialnych za rozpoznanie uszkodzeń i ich dalszą naprawę, w tym kompleks MRN (MRE11-RAD50-NBS1), histon H2AX, BRCA1, BRCA2, RAD51 oraz PALB2 [17]. W odróżnieniu od HRR, NHEJ zachodzić może we wszystkich fazach cyklu komórkowego, ale charakteryzuje się mniejszą wiernością naprawy pod względem zachowania prawidłowej informacji genetycznej [18]. Zaburzenia w działaniu jednego z białek szlaków naprawy, w tym BRCA1 czy BRCA2, może wiązać się z ograniczoną wydajnością działania HRR, co od pewnego czasu wykorzystywane jest w terapii HGSOC opartej o inhibicję PARP. Szacuje się, że w około 50% przypadków HGSOC system HRR jest нефunkcjonalny, co stanowi podstawę działania dla ukierunkowanych molekularnie związków przeciwnowotworowych w tym typie raka jajnika [18].

## **LECZENIE NISKOZRÓŻNICOWANEGO RAKA JAJNIKA – INHIBITORY PARP**

Standardowe leczenie nowo zdiagnozowanego HGSOE opiera się na terapii skojarzonej, łączącej operację cytoredukcyjną z pooperacyjną chemioterapią opartą na związkach platyny. Zabieg chirurgiczny poza usunięciem jak największej ilości tkanki nowotworowej pozwala na zdiagnozowanie histologicznego typu raka jajnika oraz stopnia zaawansowania choroby [19]. Długotrwała skuteczność terapeutyczna chemioterapii jest jednak w wielu przypadkach ograniczona ze względu na częsty nawrót choroby (70–80% przypadków) w przeciągu trzech lat oraz narastającą chemiooporność [3, 4]. W przypadku nawrotowego HGSOE, dalsze leczenie podyktowane jest przede wszystkim odpowiedzią na chemioterapię opartą na związkach platyny w poprzednich liniach leczenia oraz obecnością mutacji w genach *BRCA1/2* [4]. W zależności od skuteczności leczenia pochodnymi platyny w pierwszej linii, pacjentki są klasyfikowane jako platynowrażliwe lub platynooporne. Zgodnie z wytycznymi ESMO z 2023 roku, pacjentki z nawrotowym platynowrażliwym rakiem jajnika mogą zostać poddane leczeniu chemioterapeutykami w kolejnych liniach w skojarzeniu z bewacyzumabem lub w połączeniu z terapią podtrzymującą inhibitorami PARP (PARPi) [4]. W przypadku nawrotowego platynoopornego raka jajnika, rekomendowane jest przede wszystkim włączenie leczenia paliatywnego, w tym terapii opartej o inne chemioterapeutyki tj. paklitaksel, topotekan, czy gemcytabina w skojarzeniu z bewacyzumabem lub udział w badaniach klinicznych z użyciem nowych terapii celowanych [4]. Jednak ograniczona skuteczność stosowanej obecnie chemioterapii oraz jej stosunkowo wysoka toksyczność ogólnoustrojowa wskazują, że tradycyjne metody leczenia raka jajnika nie przyczynią się do dalszego zwiększenia korzyści terapeutycznych. Rak jajnika obecnie stał się chorobą przewlekłą, gdzie okresy choroby przeplatają się z okresami wolnymi od progresji, nawet w przypadku stosowania PARPi. Ostatnie dane pokazują, że pięcioletni wskaźnik przeżycia pacjentek z rakiem jajnika w latach 1975–2019 wzrósł umiarkowanie z 36% do 51% [3]. Stąd, kluczowe jest opracowywanie nowych schematów leczenia wykorzystujących cząsteczki ukierunkowane na określone cele molekularne dobierane na podstawie indywidulanej charakterystyki molekularnej i genetycznej pacjentki.

Wprowadzenie w ostatnich latach nowoczesnych terapii celowanych opartych o niskocząsteczkowe inhibitory pozwoliło poprawić wyniki leczenia HGSOE. Jednymi z najistotniejszych leków nowej generacji hamujących szlaki DDR są PARPi, które zwiększyły efektywność terapii i wprowadziły nowe perspektywy dla leczenia tego typu raka jajnika wykorzystując koncepcję syntetycznej letalności [15]. Jest to zjawisko indukowania śmierci komórki nowotworowej w wyniku zahamowania funkcjonalności dwóch genów lub ich produktów białkowych. Jednocześnie, jeden z genów lub kodowanych przez niego białek, musi być kluczowy dla przeżycia komórki, a zaburzenie jego funkcji prowadzić do posługiwania się funkcją drugiego genu lub białka w alternatywnym szlaku [20].

Jak wspomniano wcześniej, w komórkach raka jajnika białka PARP odrywają kluczową rolę w procesach naprawy pojedynczych i podwójnych pęknięć nici DNA [15]. Inhibitory PARP działają na komórki nowotworowe poprzez dwa główne mechanizmy. Zahamowanie PARP po pierwsze ogranicza aktywność enzymatyczną polimerazy i blokuje rekrutację białek naprawczych podlegających PARylacji w szlakach DDR. Po drugie, inhibicja PARP blokuje interakcję cząsteczek tego enzymu z miejscami uszkodzenia DNA, co ogranicza zdolność systemów naprawczych DNA

i prowadzi do akumulacji uszkodzeń [21]. W przypadku stosowania PARPi, utrata funkcji *BRCA1/2* lub innych genów zaangażowanych w naprawę HRR, z jednoczesną inhibicją PARP1, może doprowadzić do śmierci komórek raka jajnika na drodze syntetycznej letalności poprzez zahamowanie alternatywnego szlaku naprawy DNA [16].

Jak dotąd, trzy PARPi uzyskały rejestrację Europejskiej Agencji Leków (EMA, ang. *European Medicines Agency*) i Agencji ds. Żywności i Leków (FDA, ang. *Food and Drug Administration*) do stosowania w leczeniu raka jajnika. Do tej grupy leków należą olaparib, niraparib i rucaparib [16]. Skuteczność olaparibu w terapii raka jajnika zaobserwowano po raz pierwszy u pacjentek z mutacją *BRCA1/2* [22]. Jednak dalsze badania, pokazały, że nie wszystkie pacjentki będące nosicielkami mutacji w *BRCA1/2* odpowiadają na leczenie olaparibem, a z drugiej strony część pacjentek z prawidłowymi wersjami tych genów wykazują wrażliwość na PARPi. Obserwacje te były podstawą do zidentyfikowania dokładniejszego czynnika predykcyjnego wskazującego na potencjalne korzyści terapeutyczne ze stosowania olaparibu. Jak się okazało, identyfikacja statusu HRD poprzez profilowanie molekularne guzów może dokładniej odzwierciedlać skuteczność terapii olaparibem w większej grupie pacjentów [15]. Przykładem testu do oceny potencjalnych korzyści ze stosowania olaparibu jest zatwierdzony przez FDA test MyChoice® CDx oceniający status HDR [14].

Randomizowane badanie kliniczne III fazy SOLO2, oceniające leczenie podtrzymujące olaparibem pacjentek z nawrotowym rakiem jajnika z mutacją *BRCA1/2* wrażliwym na chemioterapię, wykazało, że całkowity czas przeżycia pacjentek wydłużył się o ponad rok (12,9 miesiąca) w porównaniu z grupą placebo [23]. Ostatnie wyniki kolejnego badania klinicznego III fazy SOLO3 z 2022 roku, pokazały, że monoterapia olaparibem istotnie wydłuża czas przeżycia wolnego od progresji choroby u platynowrażliwych pacjentek z mutacjami *BRCA1/2* w porównaniu z chemioterapią. Kolejne badania kliniczne umożliwiły w następnych latach poszerzenie wskazań do stosowania PARPi, również jako monoterapii pierwszej linii, u pacjentek z HGSOV [21].

Od kilku lat w Polsce PARPi są refundowane do stosowania w praktyce klinicznej. Pierwszym z nich był olaparib, który znalazł się na liście refundacyjnej w 2016 roku w ramach leczenia podtrzymującego, jednak dla ograniczonej grupy pacjentek z zaawansowanym rakiem jajnika. Dodatkowym przełomem w terapii raka jajnika w Polsce było zapewnienie szerokiego dostępu do zastosowania niraparibu w leczeniu podtrzymującym HGSOV od 1 stycznia 2022 r., bez względu na obecność mutacji w genach *BRCA1/2* oraz status HRD. Zgodnie z ostatnim obwieszczeniem Ministra Zdrowia z 1 kwietnia 2024 roku, refundowany przez NFZ program lekowy B.50 pozwala obecnie na leczenie podtrzymujące w pierwszej linii nowo zdiagnozowanego HGSOV z zastosowaniem:

- olaparibu w przypadku obecności mutacji w genach *BRCA1/2*,
- niraparibu niezależnie od obecności mutacji w genach *BRCA1/2* oraz statusu HRD,
- olaparibu w skojarzeniu z bewacyzumabem w przypadku obecności mutacji w genach *BRCA1/2* lub potwierdzonym HRD.

Ponadto, terapia podtrzymująca nawrotowego HGSOV w drugiej linii obejmuje wykorzystanie olaparibu u pacjentek ze zdiagnozowaną mutacją w *BRCA1/2* lub bez mutacji *BRCA1/2*, gdy zakończono co najmniej dwie linie chemioterapii i nie stwierdzono nawrotu choroby w przeciągu co najmniej 6 miesięcy. Jednak w każdym z wyżej wymienionych wskazań, czas leczenia podtrzymującego trwa do 36 miesięcy u pacjentek z nowo zdiagnozowanym rakiem jajnika lub do czasu wystąpienia progresji choroby czy znaczącej toksyczności.



## PRZYCZYNY ROZWOJU OPORNOŚCI NA OLAPARIB

Pomimo ogromnego sukcesu klinicznego PARPi, oporność na olaparib pozostaje główną przyczyną ograniczającą skuteczność leczenia HGSOE. Część pacjentek nie odpowiada zupełnie na leczenie PARPi, co związane jest z opornością wrodzoną na te niskocząsteczkowe leki. Do drugiej grupy ograniczeń należy oporność nabyta, czyli stopniowe zmniejszanie się wrażliwości komórek raka jajnika w trakcie leczenia. Obecna wiedza wskazuje, że nabyta oporność na olaparib jest związana z wieloma różnymi czynnikami molekularnymi i komórkowymi [5]. Badania nad mechanizmami oporności na olaparib pozwalają zrozumieć przyczyny niepowodzenia tego typu leczenia oraz wskazać potencjalne sposoby na jej przełamanie. Kluczową rolę w poznawaniu przyczyn nabywania oporności na olaparib są zarówno modele *in vitro* oparte o linie komórkowe, jak i modele *in vivo* bazujące na materiale pochodzącym od pacjentek. Procesy związane z nabywaniem oporności w raku jajnika poznane w ostatnich latach zostały szczegółowo opisane w publikacji przeglądowej będącej podstawą teoretyczną powyższej rozprawy doktorskiej [24].

Jedną z najlepiej poznanych przyczyn nabywania oporności na olaparib jest przywracanie funkcjonalności szlaku HRR, głównie poprzez rewersję mutacji w genach *BRCA1/2*, która uniemożliwia wykorzystanie koncepcji syntetycznej letalności będącej podstawą działania PARPi. Inne mechanizmy mogą również wiązać się z przywróceniem działania ścieżki HRR i zmniejszeniem wrażliwości na olaparib, w tym: demetylacja promotora *BRCA1*, mutacje hipomorficzne *BRCA1*, promowanie formowania się skupisk RAD51 w miejscu uszkodzenia DNA, nadekspresja genów zaangażowanych w HRR, czy reaktywacja szlaku HRR poprzez inaktywację białek 53BP1 przy braku *BRCA1* [24]. Ponadto, nabywanie oporności na olaparib w komórkach raka jajnika [24] powiązano między innymi z procesami tj.:

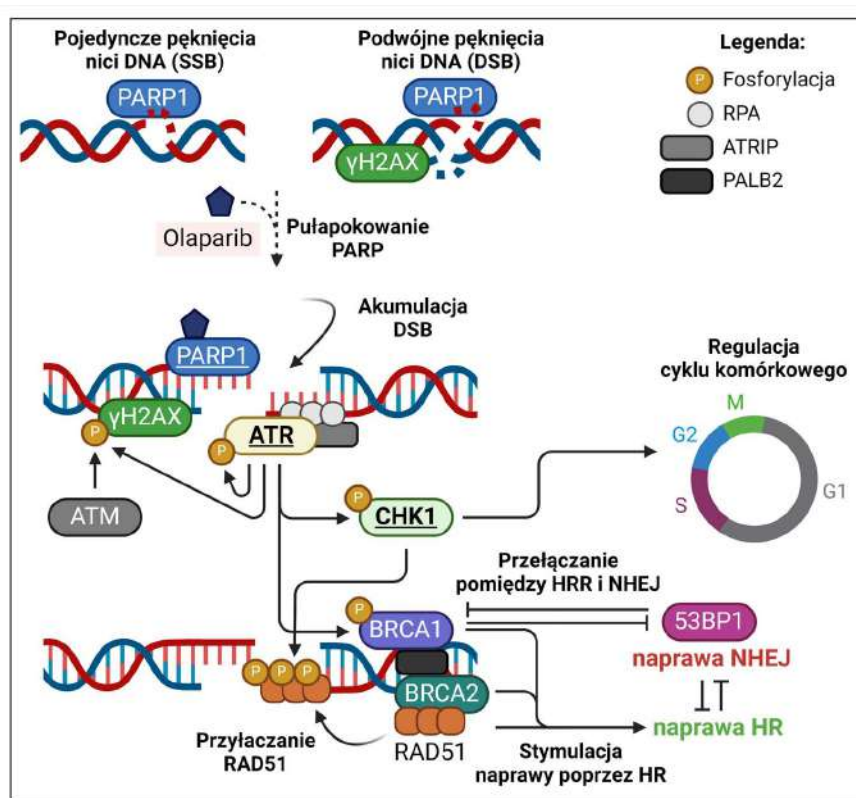
- przywrócenia stabilności widełek replikacyjnych poprzez inhibicję MRE11,
- ograniczenie zatrzymywania widełek replikacyjnych przez PARP1 w wyniku utraty lub mutacji *PARP1*,
- przywrócenie procesu PARylacji poprzez utratę glikohydrolazy PARG,
- zwiększenie czynnego usuwania leków z komórki poprzez nadekspresję glikoproteiny P, zwanej również MDR1 (ang. *multi drug resistance 1*)

Warto zauważyć, że w HGSOE oporność na olaparib często koreluje ze zmniejszoną wrażliwością na cisplatynę, gdyż część z mechanizmów nabywania oporności na te dwie grupy leków jest wspólna [25]. Wyniki badań klinicznych pokazały, że znaczny odsetek pacjentek z HGSOE nie odpowiada na leczenie olaparibem w przypadku braku ich wrażliwości na pochodne platyny [16, 23]. U pacjentek z tym typem raka jajnika, wrażliwość na cisplatynę jest jednym z czynników predykcyjnych, który wykorzystywany jest do przewidywania odpowiedzi na PARPi.

## PRZEŁAMYWANIE OPORNOŚCI NA OLAPARIB A SZLAK ATR/CHK1

Dotychczasowe badania dotyczące zastosowania PARPi w raku jajnika skupiają się głównie na monoterapii. Od czasu zaobserwowania zwiększającej się ilości przypadków nabywania oporności, naukowcy zainteresowali się podjęciem prób zwiększania przeciwnowotworowego działania olaparibu poprzez jego łączenie z inhibitorami ukierunkowanymi na odmienne cele molekularne, które mogą działać synergistycznie [24].

Szlaki DDR ze względu na swoją kluczową rolę i częste zaburzenia działania w raku jajnika stały się obiektem wielu badań nad opracowywaniem nowych metod leczenia tego typu nowotworu, także w kontekście przełamania oporności na olaparib [17]. Od kilku lat szczególne zainteresowanie wzbudza między innymi inhibicja szlaku ATR/CHK1 w terapii raka jajnika. Kinaza ATR (ang. *ataxia telangiectasia and Rad3 related*) jest jednym z przekazników sygnału informującym o rozpoznaniu uszkodzeń DNA. Zostaje ona aktywowana w przypadku powstania między innymi pojedynczych i podwójnych pęknięć nici DNA. Aktywowana kinaza ATR fosforyluje wiele białek mediatorowych, w tym CHK1 (ang. *checkpoint kinase 1*), BRCA1, NBS1 oraz p53 [26]. Dalsza aktywacja kinazy CHK1 prowadzi do fosforylacji białek regulujących punkty kontrolne cyklu komórkowego [5]. Istotnie, ścieżka sygnałowa ATR/CHK1 jest odpowiedzialna zarówno za regulację procesów naprawy uszkodzeń DNA, stabilność oraz dynamikę widełek replikacyjnych, jak i kontrolowanie cyklu komórkowego i decyduje o przeżyciu lub śmierci komórek raka jajnika (Rys. 1) [27].



**Rysunek 1. Rola szlaku ATR/CHK1 w kontrolowaniu odpowiedzi na uszkodzenia DNA oraz cyklu komórkowego w obecności olaparibu.** Na schemacie przedstawiono potencjał wykorzystania inhibicji kinazy ATR i CHK1 w celu zwiększania cytotoksycznego działania olaparibu w komórkach raka jajnika. W obecności olaparibu, indukującego akumulację podwójnych uszkodzeń nici DNA (DSB), kinaza ATR fosforyluje m. in. histon H2AX i BRCA1 (promując naprawę poprzez HRR), oraz kinazę CHK1. Ta ostatnia w wyniku aktywacji fosforyluje m. in. RAD51 (umożliwiając rekrutację kompleksów RAD51-BRCA2 w miejsca uszkodzenia DNA) oraz białka bezpośrednio regulujące cykl komórkowy. Farmakologiczne zahamowanie procesów regulowanych przez szlak ATR/CHK1 może ponownie zaindukować cytotoksyczność olaparibu na drodze syntetycznej letalności.

Stąd, szlak ATR/CHK1 stał się obiecującym celem molekularnym w terapii raka jajnika, gdyż jego inhibicja może zwiększyć efektywność olaparibu lub przywrócić jego przeciwnowotworowe

działanie w komórkach nowotworowych, które wykształciły oporność na ten lek [28]. Badania przeprowadzone na liniach komórkowych oraz pierwotnych komórkach raka jajnika pokazały, że inhibitor ATR, zwany VE-821, uwrażliwia komórki z mutacją *BRCA1* na olaparib [29]. Zahamowanie kinazy ATR zwiększyło również przeciwnowotworowe działanie olaparibu w komórkach opornych raka jajnika z mutacją *BRCA2* w warunkach *in vitro*, jak i *in vivo* [30]. Badania nad inhibitorami kinazy CHK1 potwierdziły, że prexasertib, inhibitor CHK1, zwiększa aktywność przeciwnowotworową olaparibu w komórkach raka jajnika bez mutacji *BRCA1/2* w warunkach *in vitro* [31]. Wyniki innych eksperymentów zademonstrowały, że zastosowanie innego inhibitora kinazy CHK1, zwanego MK-8776, przywraca komórkom raka jajnika z mutacją *BRCA1* wrażliwość na olaparib [32].

Jak dotąd, niektóre badania kliniczne dotyczące zastosowania inhibitorów szlaku ATR/CHK1 w zwiększaniu efektywności przeciwnowotworowego działania olaparibu okazały się obiecujące. Pierwsze wyniki badania klinicznego II fazy CAPRI, przeprowadzone na pacjentkach z nawrotowym platynoopornym HGSOC, pokazały, że kombinacja olaparibu z inhibitorem ATRi (ceralasertib) nie przyniosła obiektywnej odpowiedzi w całej grupie pacjentek, ale część z nich uzyskała korzyści terapeutyczne w postaci zahamowania progresji choroby [33]. Dalsze analizy pokazały, że ceraslasertib uwrażliwia na olaparib pacjentki z nawrotowym platynowrażliwym HGSOC i statusem HRD (głównie związanym z mutacjami *BRCA1/2*) [34]. Zastosowanie inhibitora kinazy CHK1 w warunkach klinicznych również może przyczynić się do zwiększenia efektywności olaparibu. Badanie kliniczne II fazy, w którym udział wzięły pacjentki z nawrotowym HGSOC, pokazało, że w grupie leczonej jednocześnie prexasertibem i olaparibem osiągnięto częściową odpowiedź na terapię [35]. Częściową aktywność kliniczną tej terapii łączonej stwierdzono także u pacjentek z mutacjami *BRCA1/2* uprzednio leczonymi PARPi [36]. Pomimo korzystnych doniesień dotyczących przełamывania oporności na olaparib, jak dotąd nie opracowano schematu terapeutycznego opartego na terapii skojarzonej, która byłaby wprowadzona do praktyki klinicznej. Zarówno w przypadku inhibitorów kinazy ATR, jak i CHK1, niezbędne są dalsze badania, w tym badania kliniczne III fazy na większych, stratyfikowanych grupach pacjentek w oparciu o status HRD, aby ocenić długoterminowe efekty ich stosowania w połączeniu z olaparibem.

Niemniej, każde kolejne badanie przyczynia się do lepszego poznania mechanizmów odpowiedzialnych za nabywanie oporności na olaparib i jej przełamывanie. Ze względu na wysoką heterogenność raka jajnika, dalsze analizy są kluczowe w celu zwiększenia oraz identyfikacji grupy pacjentek mogących uzyskać korzyści terapeutyczne ze stosowania leczenia PARPi, zarówno w przypadku monoterapii, jak i terapii skojarzonych.

## **ZNACZENIE MIKRORNA W RAKU JAJNIKA**

W ostatnich latach co raz więcej uwagi skupia się na roli mikroRNA (miRNA) w patogenezie raka jajnika. MiRNA to krótkie, niekodujące cząsteczki RNA odpowiedzialne za potranskrypcyjną regulację ekspresji genów. Zaangażowanie ogromnej liczby miRNA w różne procesy w komórkach nowotworowych stanowiły podstawę do poszerzenia obszaru towarzyszących im badań [37]. Liczne eksperymenty potwierdziły istotną rolę miRNA w diagnostyce oraz leczeniu raka jajnika. Profilowanie ekspresji miRNA pozwoliło opracować grupę biomarkerów o potencjalnej wartości diagnostycznej w raku jajnika [37, 38]. W zależności od poziomu ekspresji miRNA, mogą one działać zarówno jako onkogeny, jak i geny supresji nowotworowej. Zmiana ekspresji miRNA, a zatem białek kodowanych przez docelowe geny, może istotnie wpływać na przebieg wielu procesów

biologicznych, w tym na proliferację, angiogenezę, przerzutowanie, czy oporność na leczenie. Przykładowo, nadekspresję miR-126-3p powiązano z zatrzymaniem cyklu komórkowego w komórkach raka jajnika *in vitro* [39]. Inne badania pokazały, że miR-424-3p może zwiększać wrażliwość komórek raka jajnika na cisplatynę poprzez obniżanie ekspresji antyapoptotycznych białek [40].

Obecnie, obszar badań nad rolą miRNA w raku jajnika dynamicznie się rozwija, głównie dzięki upowszechnieniu technik wysokoprzepustowych do identyfikacji miRNA oraz narzędzi nieinformatycznych do ich analiz. Stanowi to ciekawą tematykę, która może pomóc w przewidywaniu odpowiedzi na stosowane obecne leczenie, monitorowaniu odpowiedzi na terapię, jak i opracowywaniu nowych schematów terapeutycznych.

# 2

## CEL PRACY

---

W ostatnich latach opracowano nowe schematy leczenia pacjentek z HGSOE, które dzięki zastosowaniu PARPi przyniosły zauważalne korzyści terapeutyczne dla tej grupy pacjentek. Jednak wydają się one niewystarczająco przełomowe, zwłaszcza w przypadku nowotworów nawrotowych. Stąd głównym celem rozprawy doktorskiej było określenie czy **zastosowanie kombinacji olaparibu z inhibitorami szlaku ATR/CHK1 prowadzi do zwiększenia śmierci komórek raka jajnika opornych na olaparib w warunkach *in vitro* oraz *in vivo*.**

Badania zrealizowane w ramach weryfikacji powyższej hipotezy badawczej zostały podzielone na cztery etapy, obejmujące poszczególne cele szczegółowe:

- ✦ **Etap 1:** Określenie mechanizmów związanych z rozwojem oporności na olaparib w komórkach raka jajnika *in vitro* oraz porównanie odpowiedzi komórek wrażliwych i opornych na połączenie olaparibu z inhibitorami szlaku ATR/CHK1 w stężeniach wykazujących synergistyczną cytotoksyczność w komórkach wrażliwych:
  - Wyprowadzenie stabilnej linii komórkowej raka jajnika o fenotypie opornym na olaparib z wrażliwej linii komórkowej z mutacją *BRCA2* i wyjaśnienie molekularnych mechanizmów związanych z nabywaniem oporności w warunkach *in vitro*,
  - Wytypowanie stężeń badanych związków wykazujących w kombinacjach synergistyczną aktywność cytotoksyczną w komórkach wrażliwych na olaparib,
  - Porównanie odpowiedzi komórek raka jajnika o różnej wrażliwości na olaparib na połączenie olaparibu z inhibitorami szlaku ATR/CHK1 przy zastosowaniu kombinacji inhibitorów w stężeniach subletalnych dla komórek wrażliwych.
- ✦ **Etap 2:** Analiza potencjału przeciwnowotworowego połączenia olaparibu z inhibitorami szlaku ATR/CHK1 jako kombinacji przełamującej oporność na PARPi w komórkach raka jajnika niewrażliwych na olaparib w warunkach *in vitro*:
  - Wytypowanie stężeń badanych związków wykazujących synergistyczną aktywność cytotoksyczną w komórkach opornych na olaparib,
  - Określenie udziału apoptozy w śmierci komórek indukowanej przez badane związki stosowane w kombinacjach,

- Analiza zmian poziomu ekspresji białek zaangażowanych w szlak odpowiedzi na uszkodzenia DNA przy przełamywaniu oporności na PARPi w komórkach opornych oraz wrażliwych na olaparib.
- ✦ **Etap 3:** Ocena roli cząsteczek miRNA w nabywaniu oporności na olaparib oraz jej przełamywaniu w komórkach raka jajnika z zastosowaniem inhibitorów szlaku ATR/CHK1 *in vitro*:
  - Profilowanie ekspresji miRNA i identyfikacja dojrzałych transkryptów miRNA o zmienionej ekspresji specyficznej dla komórek opornych i uwrażliwionych – analiza różnicowej ekspresji,
  - Określenie potencjalnie ważnych szlaków i procesów biologicznych poprzez analizę funkcjonalnego wzbogacenia genów docelowych dla deregulowanych miRNA,
  - Analiza zmian poziomu ekspresji białek zaangażowanych w szlaki sygnałowe czynników wzrostu i ich receptorów,
  - Skonstruowanie sieci regulatorowych kluczowych oddziaływań miRNA-mRNA w komórkach opornych oraz uwrażliwionych na olaparib,
  - Powiązanie ekspresji wybranych miRNA oraz genów z przeżyciem pacjentek, jako potencjalnych czynników predykcyjnych odpowiedzi na olaparib oraz skuteczności terapii przełamującej oporność.
- ✦ **Etap 4:** Ocena potencjału terapeutycznego połączenia olaparibu z inhibitorami szlaku ATR/CHK1 w kontekście uwrażliwiania komórek raka jajnika na olaparib w warunkach *in vivo*:
  - Opracowanie oraz charakterystyka molekularna opornego na olaparib mysiego modelu heteroprzeszczepu tkanek nowotworowych pochodzących od pacjentki (PDX, ang. *patient-derived xenograft*) z rakiem jajnika (HGSOC),
  - Porównanie skuteczności monoterapii i terapii skojarzonej łączącej olaparib z inhibitorami kinazy ATR lub CHK1 w modelu PDX raka jajnika niewrażliwym na olaparib,
  - Zbadanie wpływu połączenia olaparibu z inhibitorami szlaku ATR/CHK1 na zmiany histologiczne i molekularne zachodzące w heteroprzeszczepach uwrażliwionych na olaparib poprzez inhibicję szlaku ATR/CHK1.

# 3

## MATERIAŁY I METODY

---

Szczegółowy opis materiałów badawczych oraz procedur wykorzystanych w niniejszych badaniach został przedstawiony w artykułach doświadczalnych oraz nieopublikowanym manuskrypcie pracy eksperymentalnej, stanowiących podstawę rozprawy doktorskiej.

### MATERIAŁ BADAWCZY

---

Eksperymenty w ramach niniejszej pracy przeprowadzono z wykorzystywaniem dwóch typów modeli badawczych:

#### ✦ Model *in vitro*

W badaniach podstawowych wykorzystano trzy linie komórkowe ludzkiego niskozróżnicowanego surowiczego raka jajnika z mutacją *TP53* (c.G731A; p.G244D) wykazujące zróżnicowaną wrażliwość na olaparib:

- **PEO1** – linia komórkowa wrażliwa na olaparib z mutacją nonsensowną *BRCA2* (c.4965C>G; p.Y1655\*), zakupiona z kolekcji ECACC (nr kat. 10032308),
- **PEO4** – linia komórkowa wrażliwa na olaparib z mutacją rewersyjną *BRCA2* (c.4965C>T; p.Y1655Y), zakupiona z kolekcji ECACC (nr kat. 10032309),
- **PEO1-OR** – linia komórkowa z wyindukowaną opornością na olaparib i mutacją rewersyjną *BRCA2* (c.[4964A>T; 4965C>G], p.Y1655L), wyprowadzona z komórek linii PEO1 w warunkach laboratoryjnych.

#### ✦ Model *in vivo*

W badaniach *in vivo* wykorzystano trzy mysie heterotropowe modele heteroprzeszczepów raka jajnika z mutacjami w genach *BRCA1/2* wyprowadzone z tkanek nowotworowych pozyskanych po chirurgicznym usunięciu guza u trzech pacjentek z HGSOE niepoddanych przedoperacyjnemu leczeniu przeciwnowotworowemu: **PDX-X127**, **PDX-X160** i **PDX-X179**.

Modele te zostały użyte w próbach wyprowadzania docelowych heterotropowych modeli PDX raka jajnika z nabytą opornością na olaparib. Uniewrażliwienie na olaparib skutecznie zaindukowano w heteroprzeszczepach z modelu PDX-X179, zastosowanych dalej do oceny skuteczności terapeutycznej połączenia olaparibu z inhibitorami szlaku ATR/CHK1 w kontekście przełamывania oporności na badany PARPi.

## BADANE ZWIĄZKI

---

Przedmiotem badań były trzy niskocząsteczkowe inhibitory ukierunkowane molekularnie:

- **olaparib** – inhibitor polimerazy PARP1 (O),
- **ceralasertib** – inhibitor kinazy ATR (ATRi, A),
- **MK-8776** – inhibitor kinazy CHK1 (CHK1i, C).

## METODY BADAWCZE

---

### **BADANIA *in vitro***

- ✦ Wyprowadzenie linii komórkowej raka jajnika z wyindukowaną opornością na olaparib z linii macierzystej PEO1.
- ✦ Wyznaczenie tempa proliferacji komórek i określenie czasu podwojenia populacji na podstawie krzywych wzrostu.
- ✦ Mikroskopowa ocena zmian morfologicznych komórek.
- ✦ Ocena aktywności cytotoksycznej oraz określenie współczynników interakcji dla olaparibu, ATRi, CHK1i oraz ich kombinacji:
  - ocena przeżywalności komórek i wyznaczenie wartości IC<sub>50</sub> dla inhibitorów – test MTT,
  - ocena zdolności komórek do tworzenia kolonii – test wzrostu klonalnego.
- ✦ Ocena cytotoksyczności badanych związków i ich kombinacji w obecności inhibitorów glikoproteiny P (MDR1) – test MTT.
- ✦ Izolacja genomowego DNA z hodowli komórkowych.
- ✦ Ocena jakości, czystości i integralności wyizolowanego DNA za pomocą elektroforezy w żelu agarozowym oraz metodami spektrofotometrycznymi.
- ✦ Sekwencjonowanie całego eksomu (WES, ang. *whole-exome sequencing*) metodą NGS i analiza surowych wyników sekwencjonowania (zlecone firmie zewnętrznej).
- ✦ Annotacja i interpretacja wariantów sekwencyjnych za pomocą programu Qiagen Clinical Insight Interpret Translational, w tym przewidywanie ich wpływu na funkcję genów.
- ✦ Przygotowanie lizatów białkowych z linii komórkowych oraz oznaczenie całkowitego stężenia białek metodą Bradforda oraz BCA.
- ✦ Określenie poziomu ekspresji i/lub fosforylacji białek metodą Western Blot, w tym białek:
  - będących celami molekularnymi badanych inhibitorów (PARP1, ATR, fosfo-ATR (Thr1989), CHK1 oraz fosfo-CHK1 (Ser345)),
  - zaangażowanych w naprawę uszkodzeń DNA poprzez szlak HRR (BRCA1, BRCA2, fosfo-H2AX (Ser139) dalej określony jako γH2AX, RAD51) oraz szlak NHEJ (53BP1),
  - odpowiedzialnych za transport leków (MDR1),
  - będących markerami programowanej śmierci komórki (kaspaza-3, cięta kaspaza-3, cięty PARP1),
  - zaangażowanych w dePARylację (PARG),



- ✦ Określenie dystrybucji komórek w fazach cyklu komórkowego z jednoczesną oceną poziomu  $\gamma$ H2AX w komórkach – analiza cytometryczna z zastosowaniem barwienia wielokolorowego (połączenie testu na inkorporację BrdU z immunofluorescencyjnym barwieniem białek).
- ✦ Ocena poziomu indukowania podwójnych pęknięć nici DNA i ich naprawy – immunofluorescencyjna analiza tworzenia skupisk  $\gamma$ H2AX i RAD51.
- ✦ Analiza poziomu uszkodzeń DNA:
  - Preparatyka chromosomów metafazowych (strukturalne uszkodzenia chromosomów),
  - Test kometowy w warunkach neutralnych (dwuniciowe pęknięcia DNA).
- ✦ Izolacja całkowitego RNA z hodowli komórkowych.
- ✦ Synteza cDNA na matrycy mRNA oraz badanie ekspresji genów metodą RT-qPCR z uwzględnieniem walidacji stabilnej ekspresji genów referencyjnych.
- ✦ Analiza cytometryczna aktywności kaspazy-3/7.
- ✦ Analiza cytometryczna zmian apoptotycznych z równoczesnym pomiarem zmian integralności błony komórkowej (wyznakowanie komórek aneksyną V i jodkiem propidyny).
- ✦ Określenie poziomu ekspresji białek z użyciem macierzy przeciwciał dla 27 białek zaangażowanych w odpowiedź na uszkodzenia DNA oraz 41 białek związanych ze szlakami sygnałowymi czynników wzrostu i ich receptorów.
- ✦ Synteza cDNA na matrycy mikroRNA (miRNA) oraz badanie różnicowej ekspresji miRNA metodą RT-qPCR (profilowanie miRNA) z uwzględnieniem walidacji stabilnej ekspresji trzech genów referencyjnych.
- ✦ Bioinformatyczna analiza danych z różnicowej ekspresji miRNA w liniach komórkowych:
  - Klastrowanie wartości ekspresji miRNA za pomocą programu ClustVis,
  - Identyfikacja eksperymentalnie potwierdzonych genów docelowych dla miRNA z bazy danych miRTarBase v8.0 i TarBase v8.0, zbudowanie sieci regulatorowej miRNA-mRNA z uwzględnieniem oddziaływań białko-białko za pomocą programu miRNet 2.0,
  - Analiza funkcjonalnego wzbogacenia grupy z użyciem testu hipergeometrycznego na podstawie bazy danych Reactome oraz GO:BP za pomocą programu miRNet 2.0,
  - Dostosowanie, edycja sieci regulatorowych i identyfikacja centralnych miRNA i genów za pomocą oprogramowania Cytoscape,
- ✦ Bioinformatyczna analiza danych klinicznych pochodzących od pacjentek z rakiem jajnika:
  - Analiza różnicowej ekspresji miRNA i genów na podstawie danych RNAseq pobranych z bazy TCGA (The Cancer Genome Atlas) dla pacjentek z rakiem jajnika za pomocą pakietu Limma,
  - Analiza różnicowej ekspresji genów na podstawie danych RNAseq z baz TCGA i GTEx dla odpowiednio pacjentek z rakiem jajnika oraz normalnych jajników za pomocą programu TNMplot,
  - Analiza przeżycia Kaplana-Meiera dla pacjentek z HGSOE na podstawie danych RNAseq z bazy TCGA za pomocą programu ToPP,
  - Analiza poziomu ekspresji genów na poziomie białka na podstawie danych immunohistochemicznych z bazy HPA (Human Protein Atlas).
- ✦ Analiza statystyczna wyników za pomocą oprogramowania GraphPad Prism.

**BADANIA *in vivo***

- ✦ Izolacja DNA oraz celowe sekwencjonowanie genów *BRCA1/2* metodą NGS w mysich modelach heteroprzeszczepu raka jajnika pochodzących od pacjentek (PDX, ang. *patient-derived xenograft*).
- ✦ Pomiar objętości guzów i sporządzenie krzywych wzrostu heteroprzeszczepów w modelach PDX oraz pomiar masy myszy.
- ✦ Wyprowadzenie opornego na olaparib mysiego modelu PDX raka jajnika.
- ✦ Ocena skuteczności terapeutycznej stosowanych osobno inhibitorów i ich kombinacji w modelu PDX opornym na olaparib po zastosowaniu badanych terapii za pomocą poniższych parametrów:
  - Względna objętość guza (RTV, ang. *relative tumor volume*),
  - Stosunek wzrostu guz względem kontroli (T/C ratio, ang. *tumor-to-control ratio*),
  - Inhibicja zahamowania guza (TGI, ang. *tumor growth inhibition*),
  - Współczynnik kombinacji (CI, ang. *combination index*).
- ✦ Przygotowanie próbek tkanek utrwalonych w formalinie i zatopionych w parafinie (FFPE, ang. *formalin-fixed paraffin-embedded*)
- ✦ Barwienie hematoksykliną i eozyną wraz z oceną indeksu mitotycznego oraz cech histopatologicznych (nekroza, pleomorfizm jądrowy, wakuolizacja komórek) w tkankach guzów pobranych z modelu PDX,
- ✦ Ocena stopnia i częstości uszkodzenia mięśnia sercowego w materiale pobranym z modelu PDX,
- ✦ Analiza poziomu ekspresji Ki-67 oraz fosfo-CHK1 (Ser345) za pomocą barwienia immunohistochemicznego w tkankach guzów pobranych z modelu PDX.
- ✦ Przygotowanie lizatów białkowych z tkanek guzów oraz oznaczenie całkowitego stężenia białek metodą Bradforda oraz BCA.
- ✦ Określenie poziomu ekspresji i/lub fosforylacji białek metodą Western Blot, w tym wyżej wymienionych białek badanych w eksperymentach *in vitro* oraz białek zaangażowanych w przejście epithelialno-mezenchymalne (E-kadheryna, TIMP2, MMP2, wimentyna).
- ✦ Izolacja całkowitego RNA z tkanek guzów pobranych z modelu PDX.
- ✦ Synteza cDNA na matrycy mRNA oraz badanie ekspresji genów metodą RT-qPCR z uwzględnieniem walidacji stabilnej ekspresji genów referencyjnych.
- ✦ Analiza statystyczna wyników za pomocą oprogramowania GraphPad Prism.

# 4

## WYNIKI I DYSKUSJA

---

Wyniki badań realizowanych w ramach niniejszej rozprawy doktorskiej i opisanych w zbiorze publikacji naukowych podzielono na część teoretyczną oraz część eksperymentalną. Zbiór powiązanych tematycznie artykułów, będących przedmiotem niniejszej rozprawy doktorskiej, otwiera publikacja przeglądowa pt.: „**PARP inhibitor resistance in ovarian cancer: Underlying mechanisms and therapeutic approaches targeting the ATR/CHK1 pathway**” [24]. Praca ta stanowi przegląd aktualnych doniesień na temat mechanizmów nabywania oporności na PARPi, w szczególności olaparib oraz jej przełamania w komórkach raka jajnika za pomocą kombinacji PARPi z cząsteczkami ukierunkowanymi na inne cele molekularne.

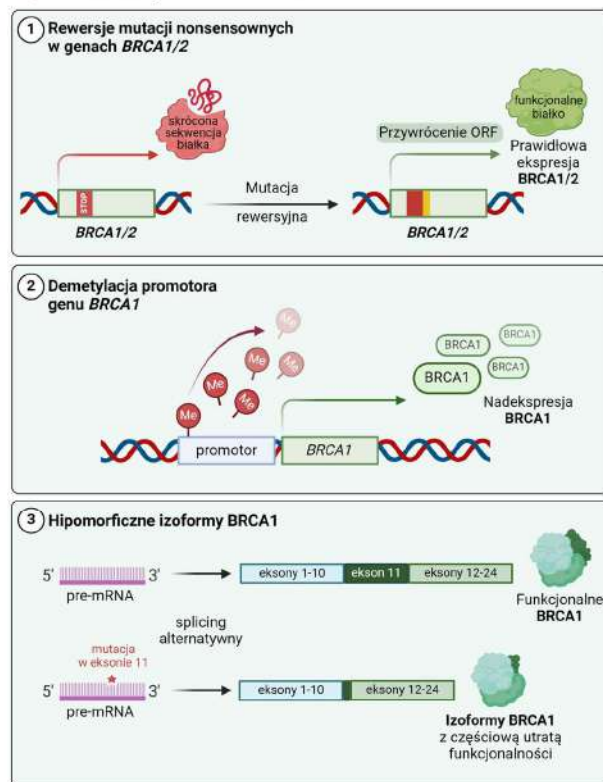
W publikacji przeglądowej zaznaczono jak istotnym problemem w obecnej praktyce klinicznej jest wrodzona oporność na olaparib oraz jej nabywanie w trakcie terapii u pacjentek z najczęstszym typem rakiem jajnika – HGSOC. Następnie szczegółowo omówiono zidentyfikowane wcześniej mechanizmy pełniące istotną rolę w rozwijaniu się oporności na olaparib z uwzględnieniem wpływu szlaku ATR/CHK1 na to zjawisko w kontekście regulacji ścieżek DDR i zjawiska syntetycznej letalności. Jedną z głównych grup mechanizmów nabywania oporności na PARPi jest przywracanie funkcjonalności szlaku naprawy DNA poprzez HRR, gdzie wyróżnić można kilka procesów odpowiedzialnych za to zjawisko (Rys. 2). Co więcej, znajomość tych mechanizmów może przyczynić się do opracowania strategii uwrażliwiania komórek raka jajnika na PARPi.

W dalszej części pracy opisano potencjalnie możliwości przełamania oporności na olaparib z wykorzystaniem niskocząsteczkowych inhibitorów oraz przeciwciał monoklonalnych, w tym inhibitorów kinazy AKT, ATR, PI3K. Usystematyzowano doniesienia na ten temat pochodzące zarówno z badań *in vitro*, przedklinicznych, jak i klinicznych. Co ciekawe, większość badań klinicznych skupia się na terapiach łączących PARPi z jednoczesną inhibicją kinaz (AKT, ATR, CHK1, MEK1/2, PI3K czy WEE1) lub punktów kontrolnych układu odpornościowego (CTLA-4, PD-1, PD-L1).

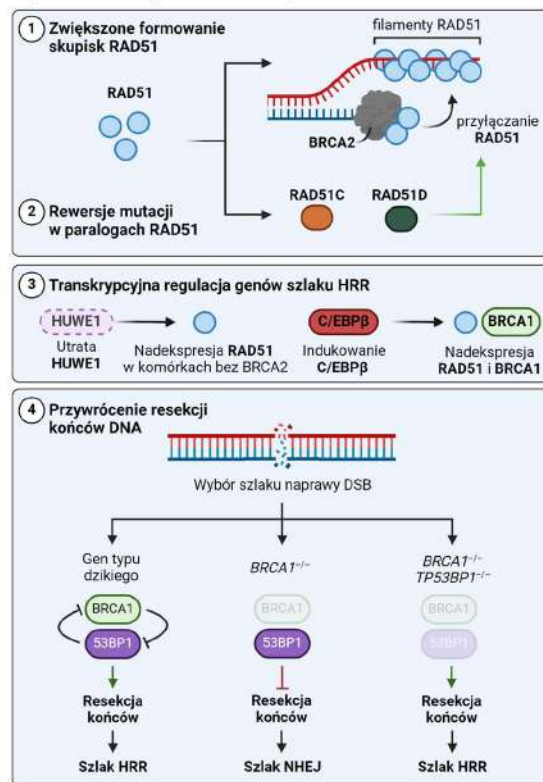
W pracy szczegółowo przedstawiono potencjał łączenia PARPi z inhibitorami szlaku ATR/CHK1 jako obiecującej metody uwrażliwiania komórek raka jajnika na olaparib. Uważa się, że komórki raka jajnika podczas nabywania oporności mogą korzystać z funkcji alternatywnych białek i procesów umożliwiających im przeżycie. Biorąc pod uwagę, że ścieżka ATR/CHK1 pełni istotną rolę w kontrolowaniu DDR, stresu replikacyjnego oraz cyklu komórkowego, jej zahamowanie może przyczynić się do akumulacji uszkodzeń DNA i uniemożliwienia ich naprawy w obecności olaparibu, a w konsekwencji śmierci komórek raka jajnika.

## Przywrócenie naprawy poprzez rekombinację homologiczną (HRR)

## A | Mechanizmy zależne od BRCA



## B | Mechanizmy niezależne bezpośrednio od BRCA



**Rysunek 2. Wewnątrzkomórkowe procesy odpowiedzialne za nabywanie oporności na inhibitory PARP w komórkach raka jajnika, które przywracają funkcjonalność szlaku naprawy uszkodzeń DNA poprzez rekombinację homologiczną (HRR).** Poszczególne mechanizmy sklasyfikowano jako zależne oraz niezależne od genów *BRCA1/2*.

W dalszej części przedstawiono i omówiono osiągnięcia uzyskane dzięki realizacji poszczególnych etapów pracy eksperymentalnej:

## ETAP 1

**Określenie mechanizmów związanych z rozwojem oporności na olaparib w komórkach raka jajnika *in vitro* oraz porównanie odpowiedzi komórek wrażliwych i opornych na olaparib na połączenie olaparibu z inhibitorami szlaku ATR/CHK1 w stężeniach wykazujących synergistyczną cytotoksyczność w komórkach wrażliwych.**

Pierwszy etap badań podsumowuje praca doświadczalna pt.: „**Olaparib-resistant *BRCA2*<sup>MUT</sup> ovarian cancer cells with restored *BRCA2* abrogate olaparib-induced DNA damage and G2/M arrest controlled by the ATR/CHK1 pathway for survival**” [41].

Do badań nad molekularnym podłożem nabywania oporności na olaparib oraz do badań odpowiedzi komórek na kombinacje PARPi z inhibitorami szlaku ATR/CHK1 wykorzystano linie komórkowe HGSOc wrażliwe (PEO1, PEO4) i oporne na olaparib (PEO1-OR). Linie komórkowe PEO1 oraz PEO4 to komercyjnie dostępne modele wyprowadzone w latach 80-tych ubiegłego wieku od tej samej pacjentki z HGSOc [42], która jak się później okazało była nosicielką nonsensownej mutacji *BRCA2*

[43]. Komórki PEO1 i PEO4 wyizolowano z nawrotowych tkanek nowotworowych pobranych po pierwszym etapie leczenia chemioterapią (PEO1) oraz po drugim etapie leczenia z nabytą kliniczną opornością na cytostatyki (PEO4) [42, 44]. Ze względu na wysoką heterogenność oraz komercyjną dostępność wielu linii komórkowych raka jajnika, w badaniach nad tym typem nowotworu niezmiernie istotne jest wykorzystanie odpowiedniego modelu. Ostatnie badania klasyfikujące linie komórkowe raka jajnika potwierdziły, że zarówno komórki PEO1, jak i PEO4 wykazują typ histologiczny HGSOE i stanowią wiarygodny model do badań *in vitro* nad tą jednostką chorobową [45].

W pierwszej części pracy opisano wyprowadzenie stabilnej linii komórkowej PEO1-OR z wyindukowaną opornością na olaparib z linii macierzystej PEO1 z mutacją *BRCA2*. W tym celu przeprowadzono selekcję komórek podczas ciągłej inkubacji z wzrastającymi stężeniami olaparibu (0–80  $\mu\text{M}$ ). Następnie prowadzono hodowlę stabilizującą wyselekcjonowane klony w nieobecności leku oraz namnożono komórki ustabilizowanej linii do przygotowania banków komórkowych do dalszych badań (Rys. 3). Ostatecznie uzyskano stabilną linię PEO1-OR z nabytą opornością na PARPi, dla której wartość  $\text{IC}_{50}$  dla olaparibu przy 5-cio dniowej inkubacji wzrosła aż 3,3-krotnie do wartości 82,1  $\mu\text{M}$  względem komórek PEO1. Dodatkowo na podstawie wyznaczonych krzywych wzrostu i czasu podwojenia populacji (PDT, ang. *population doubling time*) pokazano, że tempo proliferacji komórek PEO1-OR jest znacznie wyższe niż komórek PEO1 oraz PEO4 (PDT = 31,9 godz. vs. 37,1 godz. oraz 46,3 godz.).



**Rysunek 3. Schematyczne przedstawienie poszczególnych etapów wyprowadzania linii PEO1-OR z wyindukowaną opornością na olaparib.** W pierwszym etapie komórki macierzyste PEO1 hodowano w obecności wzrastających stężeń olaparibu (10, 20, 40 i 80  $\mu\text{M}$ ). Po 20-stu dniach selekcji klonów tolerujących coraz wyższe stężenia leku, komórki hodowano w nieobecności leku oraz okresowo badano wartość  $\text{IC}_{50}$  dla olaparibu. Dodatkowo przeprowadzono cykl zamrażania i rozmrażania w celu ustabilizowania zmian fenotypu o zwiększonej oporności na olaparib. Na końcu wyselekcjonowane komórki PEO1-OR namnożono i poddano bankowaniu. Ostateczną wartość  $\text{IC}_{50}$  dla olaparibu oceniono po całym procesie wyprowadzania linii odpornej.

Następnie oceniono aktywność cytotoksyczną olaparibu i inhibitorów szlaku ATR/CHK1 oraz ich kombinacji w komórkach PEO1, PEO4 oraz PEO1-OR. Badania te miały na celu wyznaczenie stężeń związków wykazujących w połączeniu synergizm wobec komórek wrażliwych na olaparib, aby w dalszych eksperymentach zbadać odpowiedź badanych linii na poziomie komórkowym i molekularnym. Na podstawie wyznaczonych testem MTT wartości  $\text{IC}_{50}$  dla pozostałych inhibitorów po 5 dniach inkubacji pokazano, że komórki PEO1-OR odporne na olaparib wykazują również istotnie zmniejszoną wrażliwość na ATRi (3,3  $\mu\text{M}$ ) względem odpowiednio komórek PEO1 (0,89  $\mu\text{M}$ ) oraz PEO4 (1,7  $\mu\text{M}$ ) i zmniejszoną wrażliwość na CHK1i (17,8  $\mu\text{M}$ ) względem komórek PEO1 (3,9  $\mu\text{M}$ ). Wyznaczone wartości  $\text{IC}_{50}$  pozwoliły wytypować szereg stężeń olaparibu (0,5  $\mu\text{M}$ ; 2,5  $\mu\text{M}$ ; 5  $\mu\text{M}$ ;

10  $\mu$ M) i inhibitorów kinazy ATR (0,5  $\mu$ M) i CHK1 (2,5  $\mu$ M) do określenia efektywnych stężeń wykazujących silnie synergistyczne działanie przeciwnowotworowe w kombinacjach względem komórek wrażliwych na olaparib. Słuszność koncepcji podania skojarzonego inhibitorów szlaku ATR/CHK1 oraz olaparibu potwierdzono na podstawie wartości współczynnika interakcji leków (CDI, ang. *coefficient of drug interaction*) dla każdej kombinacji związków. Na podstawie testu MTT oraz testu wzrostu klonalnego do dalszych badań wybrano 5  $\mu$ M olaparib, 0,5  $\mu$ M ATRi, oraz 2,5  $\mu$ M CHK1i. Dodanie ATRi do olaparibu synergistycznie zmniejszyło przeżywalność komórek PEO1 oraz PEO4 do odpowiednio 49% (CDI = 0,98) i 23% (CDI = 0,40). Podobny efekt zaobserwowano przy połączeniu CHK1i z olaparibem, gdzie przeżywalność komórek PEO1 oraz PEO4 została obniżona do odpowiednio 26% (CDI = 0,80) i 41% (CDI = 0,71). Jednocześnie, kombinacje inhibitorów w powyższych stężeniach nie wpłynęły istotnie na przeżywalność komórek PEO1-OR.

Wyniki testu klonalnego potwierdziły, że inkubacja komórek PEO1 oraz PEO4 równocześnie z olaparibem i inhibitorami szlaku ATR/CHK1 po 5 dniach traktowania związkami wykazuje synergistyczne działania przeciwnowotworowe (CDI w zakresie 0,44–0,49 dla komórek PEO1 oraz 0,20–0,25 dla komórek PEO4). Co ważne, połączenie olaparibu z ATRi lub CHK1i obniżyło zdolność komórek wrażliwych na olaparib do tworzenia kolonii do około 6–12% w linii PEO1 i około 1–2% w linii PEO4, wskazując na niewątpliwe działanie przeciwnowotworowe kombinacji w kontekście zdolności komórek do przeżycia i proliferacji. Na szczególną uwagę zasługuje fakt, iż komórki linii PEO1-OR wykazywały ograniczoną zdolność do tworzenia kolonii (35–49%) w obecności kombinacji związków, pomimo braku istotnego wpływu zastosowanych stężeń inhibitorów na aktywność metaboliczną komórek, wskazując, że koncepcja podania skojarzonego inhibitorów może być efektywna w przełamywaniu nabytej oporności na olaparib po zoptymalizowaniu stężeń inhibitorów.

W dalszej części pracy skupiono się na identyfikacji mechanizmów nabywania oporności na olaparib przez komórki PEO1-OR. W pierwszej kolejności skupiono się na ocenie zmian genetycznych odpowiedzialnych za fenotyp o obniżonej wrażliwości na PARPi, w szczególności mutacji w rejonach kodujących genów zaangażowanych w szlak DDR, cykl komórkowy i aktywny transport leków. Wyniki sekwencjonowania całego eksomu metodą NGS potwierdziły obecność charakterystycznej dla HGSOC mutacji zmiany sensu w *TP53* (c.731G>A; p.G244D) w komórkach PEO1 oraz PEO1-OR, a także mutacji nonsensownej w *BRCA2* (c.4965C>G; p.Y1655\*) w komórkach PEO1. Ponadto w linii PEO1 oraz PEO1-OR zidentyfikowano wiele wspólnych mutacji w wariantach genów, w tym *BRCA1*, *PARP1*, *ATR*, *CHKE1* i innych opisanych szczegółowo w artykule. Co najważniejsze, badania ujawniły, że podczas wyprowadzania linii PEO1-OR nastąpiła selekcja komórek w kierunku klonów z wtórną mutacją w genie *BRCA2* (c.[4964A>T; 4965C>G], p.Y1655L) przywracającą otwartą ramkę odczytu. Obecność zidentyfikowanego wariantu *BRCA2* i zdolność komórek do ekspresji pełnołańcuchowego białka potwierdzono biochemicznie techniką Western Blot.

Następnie wykluczono rolę glikoproteiny P (MDR1) w nabywaniu oporności na olaparib. Oceniając poziom ekspresji tego białka oraz aktywność cytotoksyczną związków w obecności specyficznego inhibitora MDR1 – tariquidaru, stwierdzono, że powyższy transporter nie uczestniczy w odpowiedzi komórek raka jajnika na badane inhibitory i ich kombinacje. Dodatkowo stwierdzono, że poziom

ekspresji celu molekularnego olaparibu, polimerazy PARP1, również nie odgrywa znaczącej roli we wrażliwości komórek HGSOc na inhibitory PARP, ATR, CHK1 i ich kombinacje.

W dalszej kolejności wykazano, że połączenie olaparibu z inhibitorami szlaku ATR/CHK1 synergistycznie zwiększa poziom ciętego PARP1, będącego markerem programowanej śmierci komórki kontrolowanej przez kaspazy, w liniach komórkowych wrażliwych na PARPi. Obserwacje te stały się podstawą do weryfikacji udziału apoptozy w przeciwnowotworowym działaniu związków w dalszej części pracy (publikacja nr 2).

W komórkach raka jajnika z mutacją *TP53* regulacja punktu kontrolnego G2/M cyklu komórkowego jest silnie zależna od aktywacji ścieżki sygnałowej ATR/CHK1 w odpowiedzi na uszkodzenia DNA. Stąd, sprawdzono poziom fosforylowanej, aktywnej kinazy ATR (Thr1989) oraz CHK1 (Ser345) w odpowiedzi na stosowane inhibitory. Badania pokazały, że komórki PEO1-OR unikają aktywacji szlaku ATR/CHK1, obserwowanej w komórkach wrażliwych na PARPi jako odpowiedź na cytotoksyczne stężenia olaparibu.

Cytotoksyczne działanie PARPi opiera się na zwiększaniu akumulacji DSB w komórkach nowotworowych, doprowadzając do ich śmierci. W celu określenia stopnia indukowania DSB, zbadano poziom fosforylacji histonu H2AX ( $\gamma$ H2AX). Po pierwsze, wyniki wykazały, że komórki PEO1-OR mają znacznie niższy podstawowy poziom DSB niż komórki PEO1. Podwyższony poziom  $\gamma$ H2AX w komórkach wrażliwych na PARPi w odpowiedzi na kombinacje olaparibu z ATRi względem związków stosowanych osobno, wskazuje na akumulację DSB, zgodnie z zaobserwowaną aktywnością cytotoksyczną związków. Ponadto, w komórkach PEO1-OR nie stwierdzono znacznych zmian w poziomie  $\gamma$ H2AX, co wskazuje na relatywnie nieistotny wpływ kombinacji na indukowanie DSB w komórkach o zwiększonej oporności. W celu pogłębienia wiedzy na temat indukowania DSB przez analizowane inhibitory oraz potencjalnej zdolności komórek do ich naprawy zbadano kolokalizację  $\gamma$ H2AX oraz rekombinazy RAD51 (marker sprawności naprawy przez HRR). Było to szczególnie ważne ze względu na fakt, iż RAD51 rekrutowana jest do miejsc uszkodzeń DNA za pośrednictwem BRCA2, w którym stwierdzono obecność mutacji niesynonimicznych w badanych liniach komórkowych. Analiza immunofluorescencyjna pokazała, że we wszystkich liniach komórkowych tworzone są sąsiadujące skupiska  $\gamma$ H2AX i RAD51, co wskazuje na funkcjonalność szlaku HRR. Dodatkowo potwierdzono wcześniej opisane wyniki poziomu ekspresji  $\gamma$ H2AX, gdyż w komórkach PEO1-OR zaobserwowano najmniej widocznych skupisk ufosforylowanego histonu.

DSB są typem uszkodzeń DNA, które mogą doprowadzać do poważnych aberracji strukturalnych chromosomów. W celu weryfikacji zaobserwowanej zdolności badanych inhibitorów do indukowania DSB, zbadano bezpośrednio stopień uszkodzeń DNA przy pomocy testu kometowego oraz mikroskopowej oceny morfologicznych zmian metafazowych postaci chromosomów. Uzyskane wyniki pokazały, że dodanie inhibitorów szlaku ATR/CHK1 do olaparibu potęgowało genotoksyczne działanie inhibitorów stosowanych osobno w komórkach wrażliwych na PARPi. Ponadto zaobserwowano, że linia PEO1-OR cechuje się znacznie mniejszym poziomem akumulacji DSB oraz strukturalnych uszkodzeń chromosomów w obecności badanych inhibitorów w porównaniu z komórkami wrażliwymi. Co ważne, w komórkach PEO1-OR jedynie połączenie olaparibu z jednoczesną inhibicją ścieżki ATR/CHK1 przyczyniło się do akumulacji uszkodzeń DNA, jednak w znacznie mniejszym stopniu niż w komórkach PEO1 i PEO4, co odzwierciedla poziom  $\gamma$ H2AX.

Istotnie, obserwacje te po raz kolejny potwierdziły wyniki testów cytotoksyczności i ujawniły zdolność inhibitorów do wywoływania genotoksycznych efektów.

Biorąc pod uwagę, że szlak ATR/CHK1 kontroluje cykl komórkowy, a inhibicja PARP z jednoczesnym blokowaniem kinaz ATR i CHK1 może prowadzić do śmierci komórek raka jajnika, w dalszej części badań skupiono się na ocenie dystrybucji komórek w fazach cyklu komórkowego. Jednocześnie określono poziom DSB w czasie progresji komórek przez fazy cyklu komórkowego. Olaparib indukował blokowanie komórek PEO1 i PEO4 w fazie G2/M, jednak dodanie inhibitorów szlaku ATR/CHK1 nie spotęgowało tego efektu.

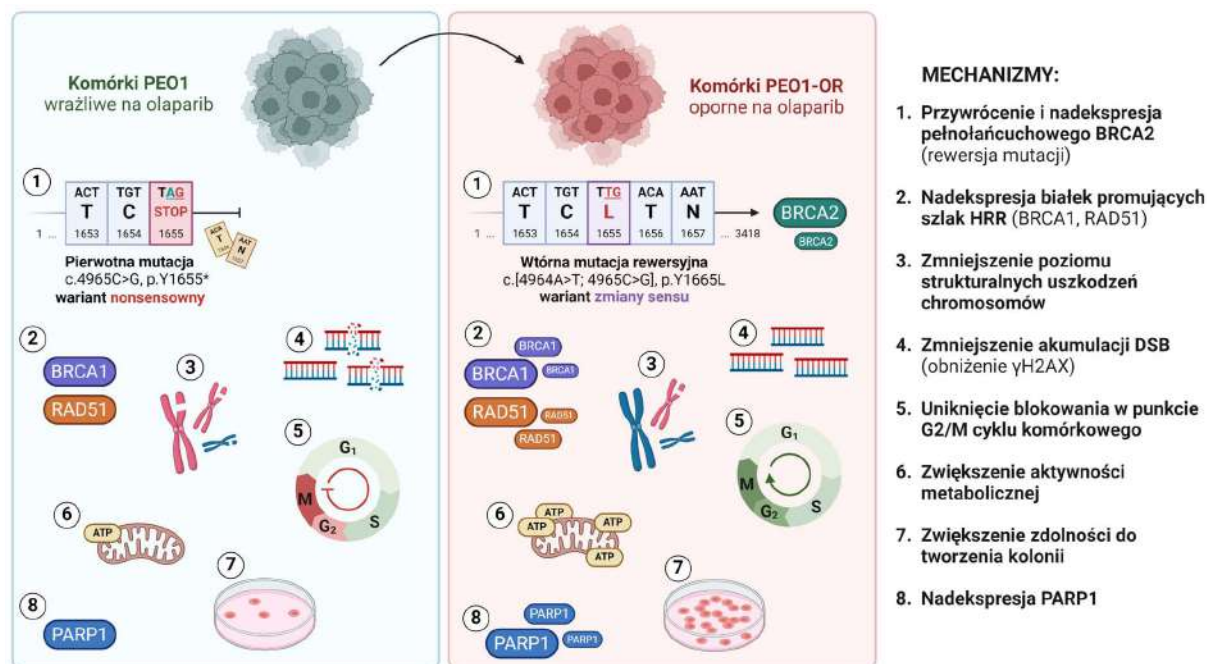
Co ważne, zarówno związki stosowane osobno, jak i ich kombinacje nie miały wpływu na progresję komórek PEO1-OR przez kolejne fazy cyklu komórkowego. Jednocześnie w komórkach opornych potwierdzono brak zmian w poziomie fosforylacji H2AX, w przeciwieństwie do linii PEO1. Wyniki te pokazały, że komórki PEO1-OR unikają zahamowania cyklu komórkowego w obecności badanych związków przez co prawdopodobnie nie są kierowane na drogę programowanej śmierci komórki.

Dane literaturowe wskazują, że utrata białka 53BP1 w komórkach raka jajnika pozbawionych BRCA1 może przyczynić się do reaktywacji szlaku naprawy DNA poprzez HRR i zmniejszać wrażliwość na olaparib. W związku z tym zbadano poziom ekspresji białek BRCA1 oraz 53BP1 wzajemnie regulujących odmienne szlaki naprawy DNA aktywowane w obecności uszkodzeń materiału genetycznego tzn. HRR i NHEJ. Nie stwierdzono różnic w ekspresji podstawowej 53BP1 pomiędzy badanymi liniami komórkowymi. Niemniej, komórki PEO1-OR cechowały się zwiększonym poziomem podstawowej ekspresji BRCA1, spotęgowanym przez inkubację z nietoksycznym stężeniem olaparibu, co wskazuje na potencjalną rolę tego białka regulującego HRR w zmniejszonej wrażliwości na PARPi. Z drugiej strony, dodanie ATRi lub CHK1i do olaparibu obniżyło poziom BRCA1 w linii PEO1-OR względem komórek nietraktowanych, przy jednoczesnym braku wpływu kombinacji na ekspresję 53BP1. Biorąc pod uwagę, że jednoczesne stosowanie badanych związków ograniczyło zdolność komórek PEO1-OR do tworzenia kolonii, przypuszczać można, że obniżenie poziomu BRCA1 promującego HRR może być wskaźnikiem potencjału przeciwnowotworowego badanych kombinacji.

Ostatnim czynnikiem zbadanym pod kątem potencjalnego wpływu na odmienne wrażliwości komórek na olaparib była glikohydrolaza PARG, która usuwa potranslacyjną PARylację białek przez PARP1, a jej utrata może być prawdopodobnie związana z opornością na PARPi. Brak różnic w podstawowej ekspresji PARG pomiędzy komórkami PEO1 i PEO1-OR wskazuje na brak roli tego białka w nabywaniu oporności na olaparib. Stwierdzono jednak, że linia PEO1-OR nie wykazuje obniżonej ekspresji PARG w obecności kombinacji badanych inhibitorów, która została z kolei wykryta w linii PEO1. Jak wcześniej opisano, dodanie ATRi lub CHK1i do olaparibu zwiększało ekspresję PARR1 względem linii wrażliwej. Wydaje się zatem, że regulacja poziomu PARylacji białek przez PARP1 i PARG może mieć wpływ na odmienną odpowiedzi komórek wrażliwych i opornych na połączenie olaparibu z inhibitorami szlaku ATR/CHK1. Obserwacje te stały się podstawą do analizy tej modyfikacji potranslacyjnej w warunkach *in vivo* w dalszej części pracy.



Podsumowując, pierwsza część badań ujawniła jak komórki wyprowadzonej linii PEO1-OR nabywają oporność na olaparib w warunkach *in vitro*, wskazując jednocześnie na rolę wielu różnych mechanizmów odpowiedzialnych za rozwój tego fenotypu (Rys. 4).



**Rysunek 4. Podsumowanie mechanizmów prowadzących do obniżonej wrażliwości na olaparib w linii komórkowej PEO1-OR.**

Selekcja klonalna w kierunku mutacji rewersyjnej *BRCA2* oraz krotność zmian cytotoksyczności olaparibu w komórkach PEO1-OR względem PEO1 potwierdziła, że uzyskany model badawczy do badań *in vitro* w zadowalający sposób odzwierciedla zmiany w warunkach klinicznych opisywane w literaturze. Ponadto potwierdzono synergistyczne potęgowanie cytotoksyczności i genotoksyczności olaparibu podczas blokowania szlaku ATR/CHK1 w komórkach wrażliwych. Wskazano również na potencjał przeciwnowotworowy połączenia badanych związków w komórkach opornych na PARPi przy stężeniach subletalnych dla komórek wrażliwych, jednak linia PEO1-OR cechowała się znacznie niższą wrażliwością na testowane kombinacje. Jednocześnie opisano różne formy odpowiedzi komórek na jednoczesne stosowanie olaparibu z ATRi lub CHK1i w liniach raka jajnika wrażliwych i opornych na olaparib.

## ETAP 2

**Szczegółowa analiza potencjału przeciwnowotworowego połączenia olaparibu z inhibitorami szlaku ATR/CHK1 jako kombinacji przełamującej oporność na inhibitor PARP w komórkach raka jajnika niewrażliwych na olaparib w warunkach *in vitro*.**

Drugi etap badań podsumowuje praca doświadczalna pt.: „**Targeted inhibition of the ATR/CHK1 pathway overcomes resistance to olaparib and dysregulates DNA damage response protein expression in *BRCA2*<sup>MUT</sup> ovarian cancer cells**” [46].

Jak wykazano w poprzedniej części badań, połączenie olaparibu z inhibitorami szlaku ATR/CHK1 wykazuje potencjał przeciwnowotworowy w komórkach PEO1-OR opornych na olaparib przy zastosowaniu subletalnych stężeń związków dla komórek wrażliwych (5  $\mu$ M olaparib; 0,5  $\mu$ M ATRi oraz 2,5  $\mu$ M CHK1i), jednak komórki odporne są znacznie mniej podatne na działanie kombinacji.

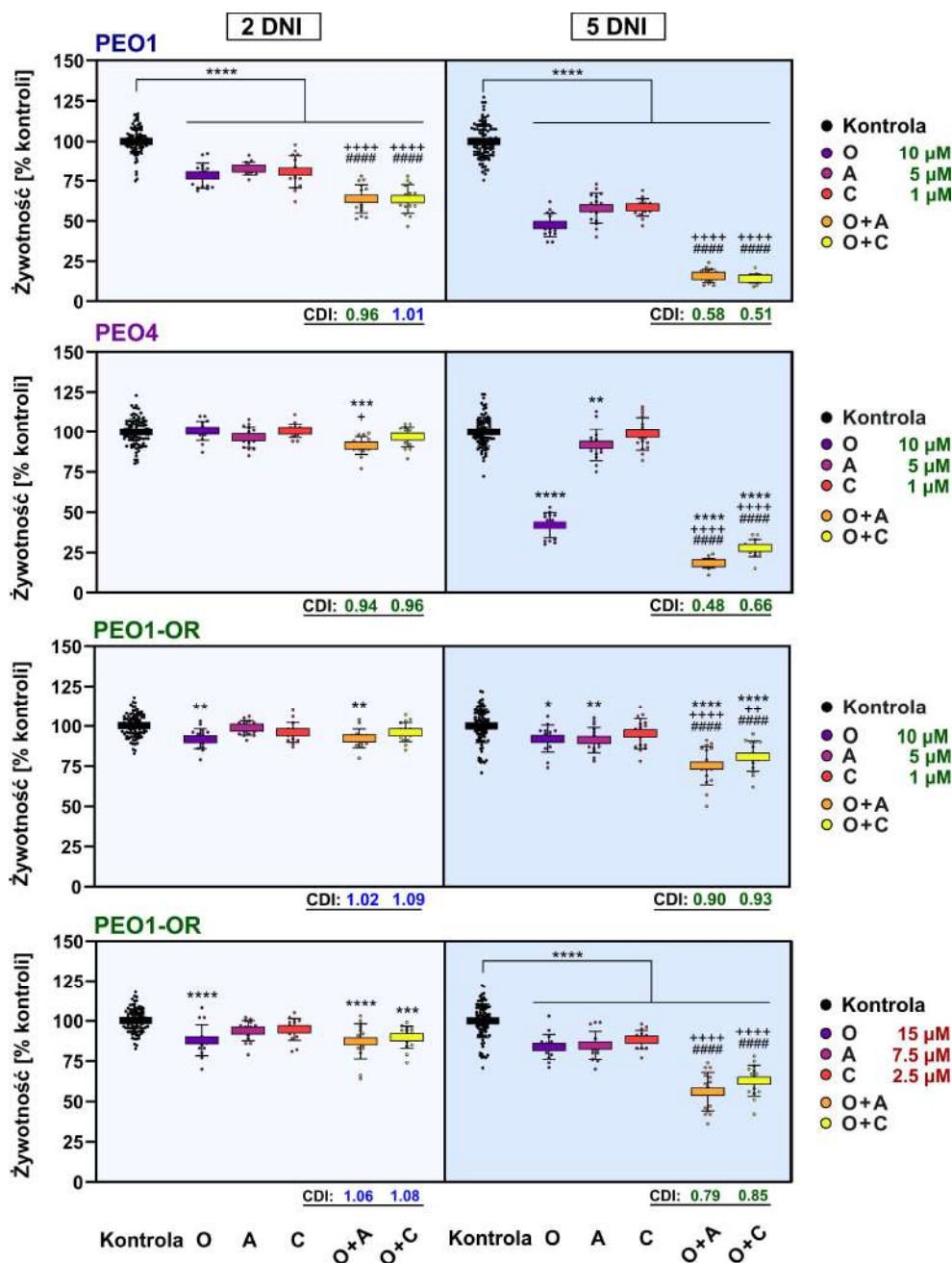
Głównym celem tego etapu badań było wykazanie, że kombinacja olaparibu z ATRi lub CHK1i w odpowiednich stężeniach synergistycznie indukuje śmierć komórek opornych na olaparib PEO1-OR z rewersją mutacji *BRCA2*. Określenie aktywności cytotoksycznej inhibitorów po 2 i 5 dniach ich działania za pomocą testu MTT (Rys. 5) pozwoliło wykazać, że wybrane stężenia związków działają synergistycznie w silnym stopniu w komórkach:

- wrażliwych (PEO1 i PEO4): 10  $\mu$ M olaparib; 5  $\mu$ M ATRi oraz 1  $\mu$ M CHK1i,
- opornych (PEO1-OR): 15  $\mu$ M olaparib; 7,5  $\mu$ M ATRi oraz 2,5  $\mu$ M CHK1i.

Przy niższych stężeniach związków, silnie synergistycznie zmniejszenie żywotności komórek było widoczne po 5 dniach inkubacji w linii PEO1 oraz PEO4 (Rys. 5). Dodanie ATRi (5  $\mu$ M) lub CHK1i (1  $\mu$ M) znacząco zwiększyło cytotoksyczność olaparibu (10  $\mu$ M) z 45% do odpowiednio 16% (CDI = 0,58) i 14% (CDI = 0,51) w komórkach PEO1 oraz z 42% do odpowiednio 18% (CDI = 0,48) i 28% (CDI = 0,66) w komórkach PEO4. W komórkach PEO1-OR wykazano synergizm [47], jednak stosunkowo słaby, pomiędzy badanymi związkami w tych stężeniach inhibitorów (CDI = 0,90 dla olaparibu + ATRi, CDI = 0,93 dla olaparibu + CHK1i). Potwierdza to wcześniejsze obserwacje o mniejszej wrażliwości komórek PEO1-OR na połączenia badanych inhibitorów. Co ważne, w linii PEO1-OR zastosowanie wyższych stężeń inhibitorów (15  $\mu$ M olaparib, 7,5  $\mu$ M ATRi, oraz 2,5  $\mu$ M CHK1i) spowodowało bardziej zauważalny synergistyczny efekt cytotoksyczny (CDI < 0,9). Jak wykazano, połączenie olaparibu (15  $\mu$ M) z ATRi (7,5  $\mu$ M) lub CHK1i (2,5  $\mu$ M) zmniejszyło znacząco przeżywalność komórek z 84% do odpowiednio 56% (CDI = 0,79) i 63% (CDI = 0,85) (Rys. 4). Jednocześnie, zwiększenie stężeń inhibitorów w komórkach PEO1-OR nie wpłynęło istotnie na cytotoksyczność związków stosowanych osobno po 5 dniach inkubacji (olaparib: 88% vs. 84%, ATRi: 91% vs. 85%, CHK1i 95% vs. 88%). Pokazuje to, że komórki PEO1-OR są wyjątkowo mało wrażliwe na badane inhibitory, ale zastosowanie ich w kombinacji przyczynia się do istotnego zwiększenia cytotoksyczności.

W celu potwierdzenia synergistycznej aktywności przeciwnowotworowej w komórkach opornych na olaparib, przeprowadzono test wzrostu klonalnego. Uzyskane wyniki potwierdziły, że wytypowane dla komórek PEO1-OR stężenia inhibitorów przełamują oporność na olaparib. Dodanie do olaparibu ATRi lub CHK1i zmniejszyło zdolność komórek do tworzenia kolonii z 68% do odpowiednio jedynie 1% (CDI = 0,04) i 19% (CDI = 0,34) po 5 dniach inkubacji. Co ważne, zdolność do przeżycia i proliferacji komórek była wyraźnie obniżona zarówno w komórkach wrażliwych, jak i opornych na olaparib.

Powyższe wyniki wskazują, na większy potencjał przełamывania oporności na olaparib przy użyciu ATRi, jednak obie badane kombinacje wykazały zadowalający efekt przeciwnowotworowy. Stąd, w dalszych badaniach *in vitro* stosowano powyżej opisane stężenia leków odpowiednio dla komórek wrażliwych i opornych na olaparib, aby porównać dalsze efekty wywoływane przez związki na poziomie molekularnym i komórkowym.



**Rysunek 5. Połączenie olaparibu z inhibitorami szlaku ATR/CHK1 synergistycznie zwiększa cytotoksyczność badanych leków zarówno w komórkach wrażliwych (PEO1 i PEO4), jak i opornych na olaparib (PEO1-OR) przy zastosowaniu odpowiednich stężeń związków.** Wykresy przedstawiają żywotność komórek po 2 i 5 dniach inkubacji oznaczoną za pomocą testu MTT. Istotność statystyczną określono za pomocą dwuczynnikowej analizy ANOVA oraz testu wielokrotnych porównań Tukey'a: \* $p < 0,01$ , \*\* $p < 0,01$ , \*\*\* $p < 0,001$ , \*\*\*\* $p < 0,0001$  (inhibitor(y) vs. kontrola); + $p < 0,05$ , ++ $p < 0,01$ , +++ $p < 0,0001$  (olaparib vs. kombinacja z ATRi lub CHK1i); #### $p < 0,0001$  (ATRi lub CHK1i vs. odpowiednia kombinacja z olaparibem).

W dalszej części badań oceniono czy dodanie do olaparibu inhibitorów szlaku ATR/CHK1 potęguje śmierć komórek opornych na olaparib na drodze apoptozy. Wyniki oznaczenia poziomu eksternalizacji fosfatydylseryny w linii PEO1-OR po 2 dniach inkubacji pokazały, że użycie samego olaparibu czy ATRi nie ma statystycznie istotnego wpływu na zmianę odsetka komórek wyznakowanych aneksyną V względem komórek kontrolnych (wzrost z 3,8% do odpowiednio 6,5%

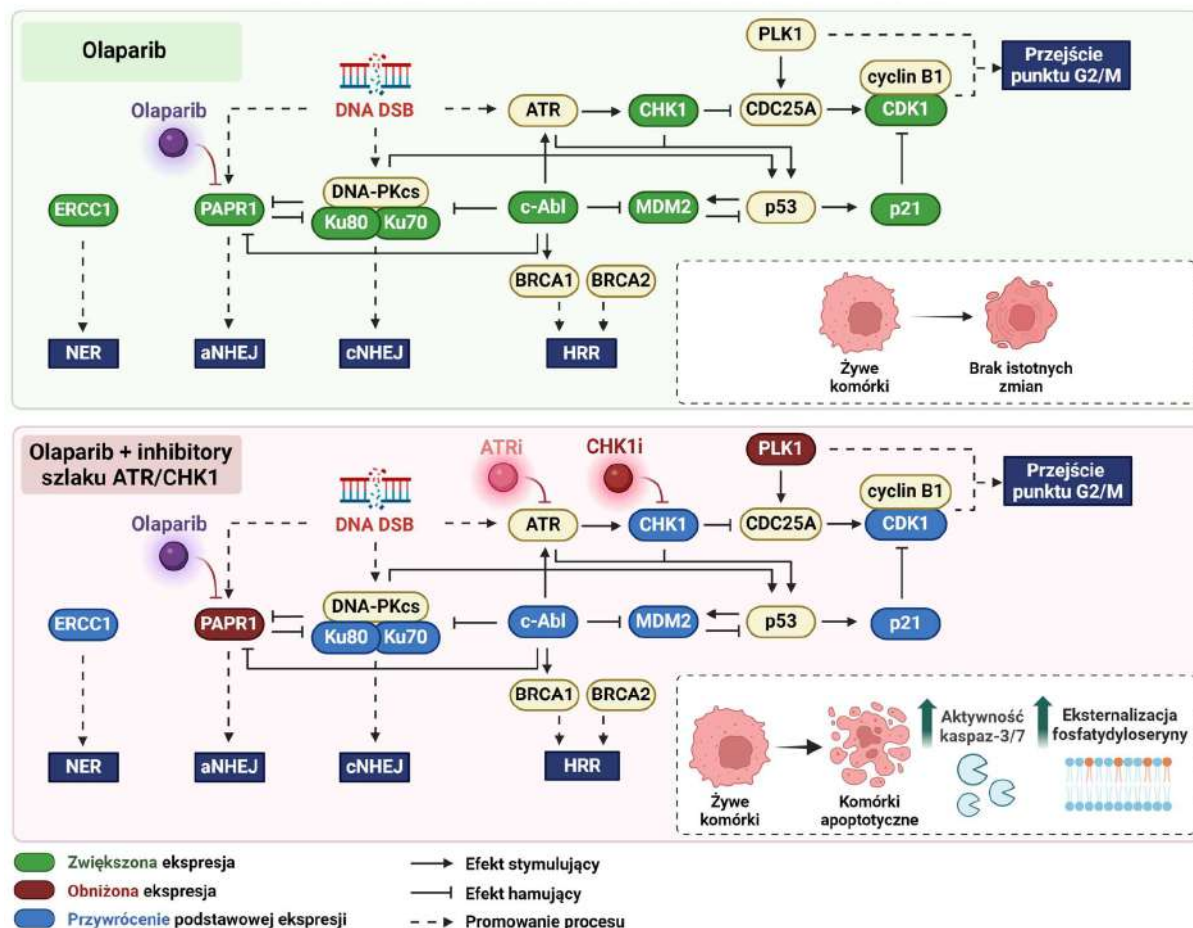
oraz 5,7%). Jednak zastosowanie połączenia obu inhibitorów przyczyniło się do istotnego 2,2-krotnego zwiększenia udziału komórek apoptotycznych w całej populacji. Inkubacja zarówno z samym CHK1i, jak i w połączeniu z olaparibem spowodowała wzrost odsetka komórek z wyeksponowaną fosfatydyloseryną do odpowiednio 8,6% oraz 9,6% względem komórek nietraktowanych. Następnie oceniono, czy kaspazy biorą udział w indukowaniu apoptozy we wczesnych etapach działania związków w komórkach raka jajnika poprzez pomiar aktywności kaspaz wykonawczych-3/7 po 2 dniach inkubacji. Traktowanie komórek PEO1-OR samym olaparibem nie przyczyniło się do istotnego zwiększenia aktywności kaspaz-3/7 względem komórek kontrolnych, zgodnie z opornym fenotypem komórek. Co ważne, w linii PEO1-OR stwierdzono synergistyczną aktywację kaspaz-3/7 w wyniku połączenia olaparibu z ATRi lub CHK1i, których dodanie przyczyniło się do odpowiednio 1,5-krotnego i 2,3-krotnego zwiększenia odsetku komórek kaspazododatnich względem samego inhibitora PARP. Ocena poziomu ekspresji mRNA dla kaspazy 3 nie wykazała nadekspresji genu w komórkach PEO1-OR w odpowiedzi na stosowane osobno związki ani ich kombinacje, w przeciwieństwie do komórek PEO1, gdzie stwierdzono synergistycznie zwiększony poziom *CASP3* w odpowiedzi na łączne działanie olaparibu z ATRi lub CHK1i. Podsumowując, inhibitory szlaku ATR/CHK1 w połączeniu z olaparibem wykazują spotęgowane działanie proapoptotyczne w komórkach PEO1-OR już po 2 dniach, co uwidacznia się w przeciwnowotworowej aktywności kombinacji związków po 5 dniach.

Wyniki badań z pierwszego etapu pracy, wskazujące na genotoksyczne działania badanych inhibitorów, skłoniły mnie do dalszej oceny znaczenia szlaków DDR w komórkach PEO1-OR oraz ich linii macierzystej. W tym celu oznaczono poziom ekspresji 27 białek zaangażowanych w DDR, aby ocenić, czy przyczyniają się one do uwrażliwiania komórek PEO1-OR na olaparib podczas inhibicji szlaku ATR/CHK1.

W pierwszej kolejności skupiono się na porównaniu odpowiedzi komórek wrażliwych i opornych podczas inkubacji z samym olaparibem, który jak pokazano wcześniej, wykazuje aktywność cytotoksyczną jedynie w linii PEO1. PARPi spowodował istotne zwiększenie ekspresji 10 białek w linii PEO1-OR względem komórek wrażliwych, w tym zaangażowanych w naprawę HRR (BRCA1, BRCA2, c-Abl), NHEJ (Ku80), bezpośrednią naprawę uszkodzeń (MGMT), regulację cyklu komórkowego (CHK1, CHK2, cyklina B1), apoptozę (MDM2) oraz białka PARP1. Wzrost poziomu większości z tych białek w komórkach PEO1-OR w porównaniu z komórkami PEO1 przyczynił się do przywrócenia podstawowego poziomu ekspresji obserwowanego w komórkach nietraktowanych. Poza tym, zwiększenie ekspresji c-Abl, CHK1, Ku80, MDM2 i PARP1 w komórkach PEO1-OR w porównaniu z komórkami PEO1 sugeruje rolę tych białek w zmniejszaniu wrażliwości na olaparib.

W dalszym etapie analiz porównano odpowiedzi komórek PEO1-OR na traktowanie ich jedynie olaparibem oraz jego połączeniami z inhibitorami szlaku ATR/CHK1, które przełamują oporność (Rys. 6). Traktowanie linii PEO1-OR olaparibem zwiększyło poziom 9 białek zaangażowanych w DDR. W porównaniu z inhibitorem PARP, dodanie ATRi lub CHK1i spowodowało przywrócenie ich podstawowej ekspresji (ERCC1, Ku70, Ku80, c-Abl, MDM2, CHK1, CDK1 i p21) lub jej zmniejszenie (PARP1) względem komórek nietraktowanych. Ponadto, połączenie olaparibu z ATRi lub CHK1i zaindukowano obniżenie poziomu PLK1. Rolę każdego z tych białek w szlaku DDR przedstawiono na Rysunku 6.

## ODPOWIEŹ NA USZKODZENIA DNA W KOMÓRKACH PEO1-OR



**Rysunek 6.** Olaparib w połączeniu z inhibitorami ścieżki sygnałowej ATR/CHK1 powoduje w komórkach PEO1-OR zmiany w ekspresji białek zaangażowanych w różne procesy będące elementami szlaku DDR. aNHEJ – alternatywne łączenie niehomologicznych końców, cNHEJ – kanoniczne łączenie niehomologicznych końców, DSB – podwójne pęknięcia nici DNA, HRR – naprawa poprzez rekombinację homologiczną, NER – naprawa przez wycinanie nukleotydów.

Warto zaznaczyć, że kombinacje badanych inhibitorów nie miały wpływu na poziom głównych mediatorów naprawy przez HRR tzn. BRCA1 i BRCA2, ale obniżyły poziom kinazy c-Abl (pośredni regulator HRR) do obserwowanego w komórkach nietraktowanych badanymi związkami. Analiza poziomu białek zaangażowanych w mechanizm naprawy za pośrednictwem NHEJ pokazała, że dodanie ATRi lub CHK1i zniósło nadekspresję Ku70 i Ku80 indukowaną przez olaparib. Jednocześnie nie stwierdzono wpływu działania związków na główną kinazę regulującą ten szlak – DNA-PKcs.

Reasumując, zahamowanie szlaku ATR/CHK1 skutecznie uwrażliwia komórki PEO1-OR na olaparib. Zwiększenie apoptozy poprzez synergistyczny wzrost aktywności kaspaz-3/7 odgrywa ważną rolę w przełamywaniu oporności na PARPi. Przywrócenie cytotoksycznej aktywności olaparibu podczas inhibicji szlaku ATR/CHK1 wiąże się z deregulacją ekspresji białek szlaku DDR. Badania te w istotny sposób poszerzają wiedzę na poziomie molekularnym dotyczącą nabywania i przełamywania oporności na olaparib w komórkach z rewersją mutacji *BRCA2* w warunkach *in vitro*.

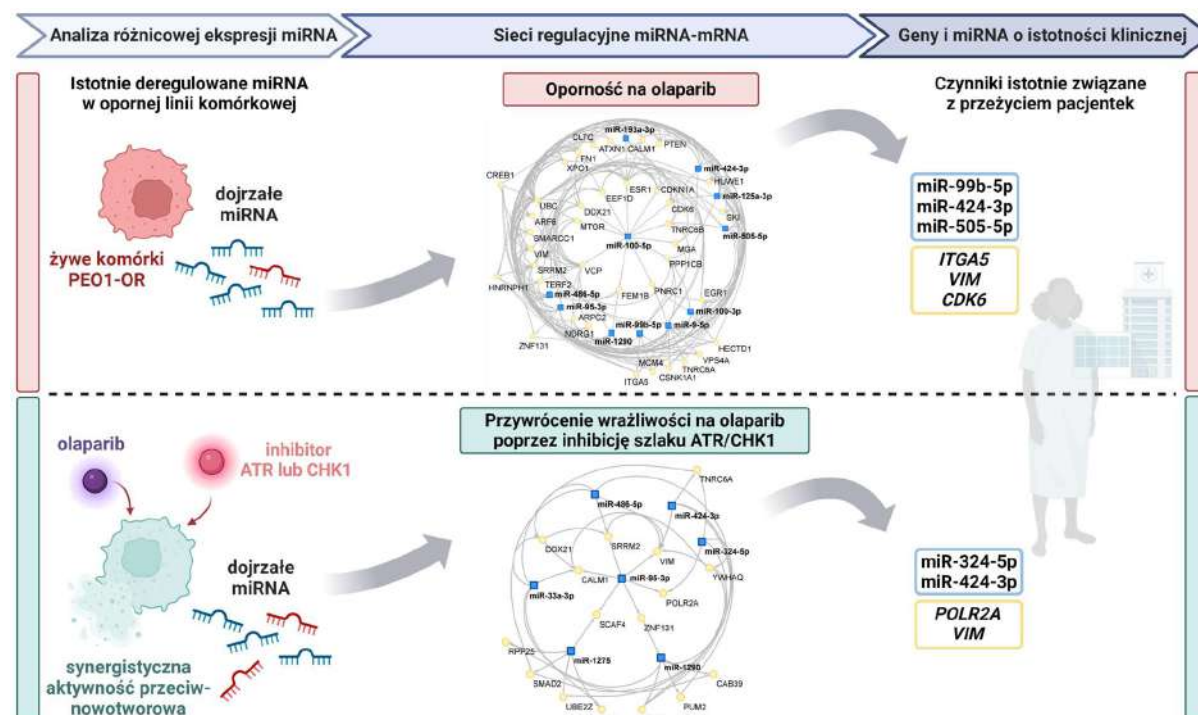


## ETAP 3

**Ocena roli cząsteczek miRNA w nabywaniu oporności na olaparib w komórkach raka jajnika oraz jej przełamywaniu z zastosowaniem inhibitorów szlaku ATR/CHK1.**

Trzeci etap badań podsumowuje praca doświadczalna pt.: „**Uncovering miRNA-mRNA regulatory networks related to olaparib resistance and resensitization of *BRCA2*<sup>MUT</sup> ovarian cancer PEO1-OR cells with the ATR/CHK1 pathway inhibitors**” [48].

W tej części badań *in vitro* przeprowadzono analizę różnicowej ekspresji cząsteczek miRNA (identyfikacja miRNA różniących się poziomem ekspresji dojrzałych transkryptów pomiędzy badanymi warunkami) w celu zidentyfikowania miRNA, ich genów docelowych i potencjalnych procesów biologicznych powiązanych z nabywaniem i przełamywaniem oporności na olaparib w komórkach PEO1-OR. Następnie określono, które z wytypowanych w badaniach *in vitro* miRNA i ich genów docelowych są związane istotnie z przeżyciem pacjentek na podstawie analiz *in silico* danych klinicznych (Rys. 7).



**Rysunek 7. Uogólniony schemat postępowania przy określaniu roli miRNA w nabywaniu i przełamywaniu oporności na olaparib w komórkach raka jajnika.** Na podstawie wyników analizy różnicowej ekspresji miRNA w komórkach raka jajnika *in vitro* określono, które cząsteczki wykazują zmienioną ekspresję. Następnie za pomocą narzędzi bioinformatycznych przewidziano geny docelowe dla wytypowanych miRNA, opracowano sieci regulatorowe miRNA-mRNA z uwzględnieniem oddziaływań białko-białko oraz przeprowadzono analizę funkcjonalnego wzbogacenia. Na koniec oceniono wartość prognostyczną wybranych miRNA i ich genów docelowych w próbkach klinicznych na podstawie danych z bazy TCGA i wybrano cząsteczki, których zmieniona ekspresja była skorelowana z przeżyciem pacjentek.

Na początku przeprowadzono badania przesiewowe za pomocą komercyjnie dostępnych macierzy miRNA w celu określenia profilów ekspresji 754 miRNA w komórkach PEO1 i PEO1-OR

nietraktowanych oraz traktowanych badanymi inhibitorami przez 2 dni. Etap ten pozwolił wytypować obiecujące cząsteczki o znacząco zmienionej ekspresji (bezwzględna krotność zmian  $\pm 1,5$ ), spośród których wybrano 44 miRNA do oceny różnic w ich poziomie ekspresji we wszystkich liniach raka jajnika za pomocą zaprojektowanych macierzy miRNA z odpowiednio dobranymi genami referencyjnymi o potwierdzonej stabilnej ekspresji pomiędzy warunkami eksperymentalnymi.

Na podstawie wyników walidacyjnych, najpierw porównano profile ekspresji wyselekcjonowanych miRNA pomiędzy nietraktowanymi komórkami PEO1 oraz PEO4 i PEO1-OR w celu określenia, które z cząsteczek ulegały istotnie zmienionej ekspresji, dalej określanych jako deregulowane, związanej z wrażliwością komórek na olaparib. Szczególną uwagę poświęcono linii odpornej PEO1-OR oraz jej linii macierzystej. Za istotnie deregulowane miRNA uważano te cząsteczki, dla których bezwzględna krotność zmian wynosiła co najmniej 1,5 przy wartości  $p < 0,05$ . Jak pokazały wyniki, w komórkach PEO1-OR oraz PEO4 doszło do istotnej zmiany ekspresji odpowiednio 11 i 16 miRNA względem komórek PEO1, przy czym ponad 90% z nich uległa obniżonej ekspresji. Jednym z najbardziej deregulowanych miRNA w komórkach PEO1-OR był miR-486-5p, którego ekspresja obniżyła się ponad 10-krotnie względem komórek macierzystych. Fakt, że aż 25% miRNA spośród docelowo badanych uległo istotnej zmianie ekspresji w komórkach PEO1-OR wskazuje na to, że komórki odporne mogą znacznie różnić się potranslacyjną regulacją ekspresji docelowych genów.

Następnie określono profil ekspresji miRNA w komórkach raka jajnika w odpowiedzi na badane inhibitory lub ich kombinacje w celu określenia, które z miRNA mogą być potencjalnie związane z przełamywaniem oporności na olaparib. Wyniki analizy pokazały, że profile miRNA w komórkach PEO1-OR traktowanych każdym inhibitorem osobno różnią się od tych w komórkach inkubowanych z kombinacjami związków. W linii PEO1-OR sam olaparib spowodował zmianę ekspresji jedynie 3 miRNA (miR-96-5p, miR-486-5p i miR-766-3p). Kombinacja olaparibu z inhibitorami szlaku ATR/CHK1 przyczyniła się do istotnej zmiany ekspresji w sumie 7 miRNA w komórkach PEO1-OR, przy czym ekspresja 4 z nich uległa zmianie jedynie w tej linii (miR-33a-3p, miR-95-3p, miR-424-3p i miR-1275) w porównaniu z liniami wrażliwymi PEO1 i PEO4. Co ciekawe, połączenie olaparibu z ATRi lub CHK1i przywracało w komórkach PEO1-OR ekspresję miR-95-3p i miR-1290 do poziomu obserwowanego w linii wrażliwej PEO1. Ponadto, kombinacje inhibitorów wywoływały podobny efekt zmiany ekspresji w komórkach PEO1 oraz PEO1-OR. Powyższe obserwacje wskazują, że zmiany ekspresji pewnych miRNA mogą być związane z uwrażliwianiem komórek opornych na olaparib poprzez inhibicję szlaku ATR/CHK1.

Kolejno na podstawie wyników analizy różnicowej ekspresji miRNA przeprowadzono analizy bioinformatyczne w celu zrozumienia roli wybranych miRNA. Na początku zidentyfikowano docelowe geny dla miRNA z istotnie zmienioną ekspresją i zbudowano odrębne sieci regulatorowe miRNA-mRNA dla cząsteczek miRNA związanych z opornością na olaparib bądź przełamywaniem oporności za pomocą kombinacji badanych inhibitorów (Rys. 7).

Zaburzona ekspresja miRNA może mieć istotny wpływ na regulację szlaków sygnałowych i procesów komórkowych w nowotworach. Wobec tego, w dalszej części zidentyfikowano eksperymentalnie potwierdzone docelowe geny dla miRNA, skonstruowano sieci regulatorowe miRNA-mRNA oraz

przeprowadzono analizy funkcjonalnego wzbogacenia dla grupy docelowych genów za pomocą narzędzia bioinformatycznego miRNet 2.0 [49].

Każda pierwotna sieć regulatorowa o wysokim stopniu złożoności, zawierająca nawet kilkadziesiąt tysięcy bezpośrednich interakcji pomiędzy elementami sieci, została zredukowana do sieci przedstawiających kluczowe oddziaływania współorganizujące sieć za pomocą algorytmu „minimum connected network” dostępnego w miRNet 2.0. Czynność ta pozwoliła skupić się na zbadaniu roli kluczowych interakcji.

Zredukowana sieć regulatorowa miRNA-mRNA dla nietraktowanych komórek PEO1-OR składała się z 11 deregulowanych miRNA oraz 38 genów docelowych, gdzie każdy z miRNA okazał się regulować od 7 do 21 genów. Wyniki analizy wzbogacenia funkcjonalnego grupy genów z użyciem baz danych dla ścieżek sygnałowych (Reactome) oraz procesów biologicznych (GO:BP) pokazały, że w proces nabywania oporności mogą być zaangażowane szlaki sygnałowe wielu czynników wzrostu i ich receptorów, w tym FGFR, EGFR, PDGF, SCF-KIT, TGF $\beta$ R, oraz ścieżki związane z kancerogenezą, proliferacją, migracją i cyklem komórkowym. Ponadto przewidziano, że za oporny fenotyp mogą również odpowiadać procesy komórkowe związane z DDR, co wiąże się z danymi eksperymentalnymi uzyskanymi we wcześniejszych etapach badań.

W przypadku komórek PEO1-OR uwrażliwionych na olaparib poprzez inhibicję szlaku ATR/CHK1, w skład zredukowanej sieci regulatorowej wchodziło 7 miRNA, każdy istotnie regulujący 4–6 geny spośród wszystkich 23 zidentyfikowanych jako geny docelowe. Na podstawie rezultatów analizy wzbogacenia funkcjonalnego wykazano, że w proces przełamania oporności na olaparib może być zaangażowany szlak sygnałowy Wnt niezależny od  $\beta$ -kateniny, szlaki związane z apoptozą regulowaną przez kaspazy oraz regulacja cyklu komórkowego w punkcie kontrolnym G2/M. Istotnie, we wcześniejszym etapie badań udowodniono, że część tych procesów jest związana z odpowiedzią komórek PEO1-OR na kombinacje badanych inhibitorów, co zwiększa wiarygodność przewidywań za pomocą analiz *in silico*. Ponadto, badania te pokazały, że uwrażliwianie komórek PEO1-OR na olaparib może mieć związek również ze ścieżkami sygnałowymi czynników wzrostu i ich receptorów (TGF $\beta$ , EGFR, FGFR1, NGF, VEGFR2 oraz PDGF).

Wyniki analizy funkcjonalnej wzbogacenia grupy genów dla deregulowanych miRNA, wskazujące na rolę wielu różnych czynników wzrostu i ich receptorów, wymagały weryfikacji poprzez określenie poziomu ekspresji panelu czynników wzrostu i ich receptorów na poziomie białka. Badania poziomu ekspresji 41 wybranych białek przeprowadzono za pomocą macierzy przeciwciał w komórkach PEO1 oraz PEO1-OR po zastosowaniu inhibitorów lub ich kombinacji przez 2 dni. W obu liniach komórkowych udało się wykryć i ilościowo określić poziom 38 czynników wzrostu i ich receptorów. Za białka, których ekspresja uległa istotnej zmianie uważano te, których poziom ekspresji zmienił się co najmniej  $\pm 1,5$ -krotnie przy  $p < 0,05$ . W komórkach PEO1-OR inkubacja z samym olaparibem zmieniła poziom jedynie czynnika FGF6 (1,6-krotny spadek względem komórek kontrolnych). Inhibicja PARP w połączeniu z ATRi lub CHK1i zaburzył ekspresję 7 białek w komórkach PEO1-OR oraz aż 15 białek w komórkach PEO1. Spośród wszystkich białek o istotnie zmienionej ekspresji, kombinacja olaparibu z inhibitorami szlaku ATR/CHK1 spowodowała obniżenie ekspresji 5 białek jedynie w linii odpornej (FGF4, FGF7, NT-4, PLGF, and TGF $\beta$ 1). Ponadto, w komórkach PEO1-OR nie odnotowano nadekspresji 12 białek indukowanej przez kombinację inhibitorów w linii PEO1

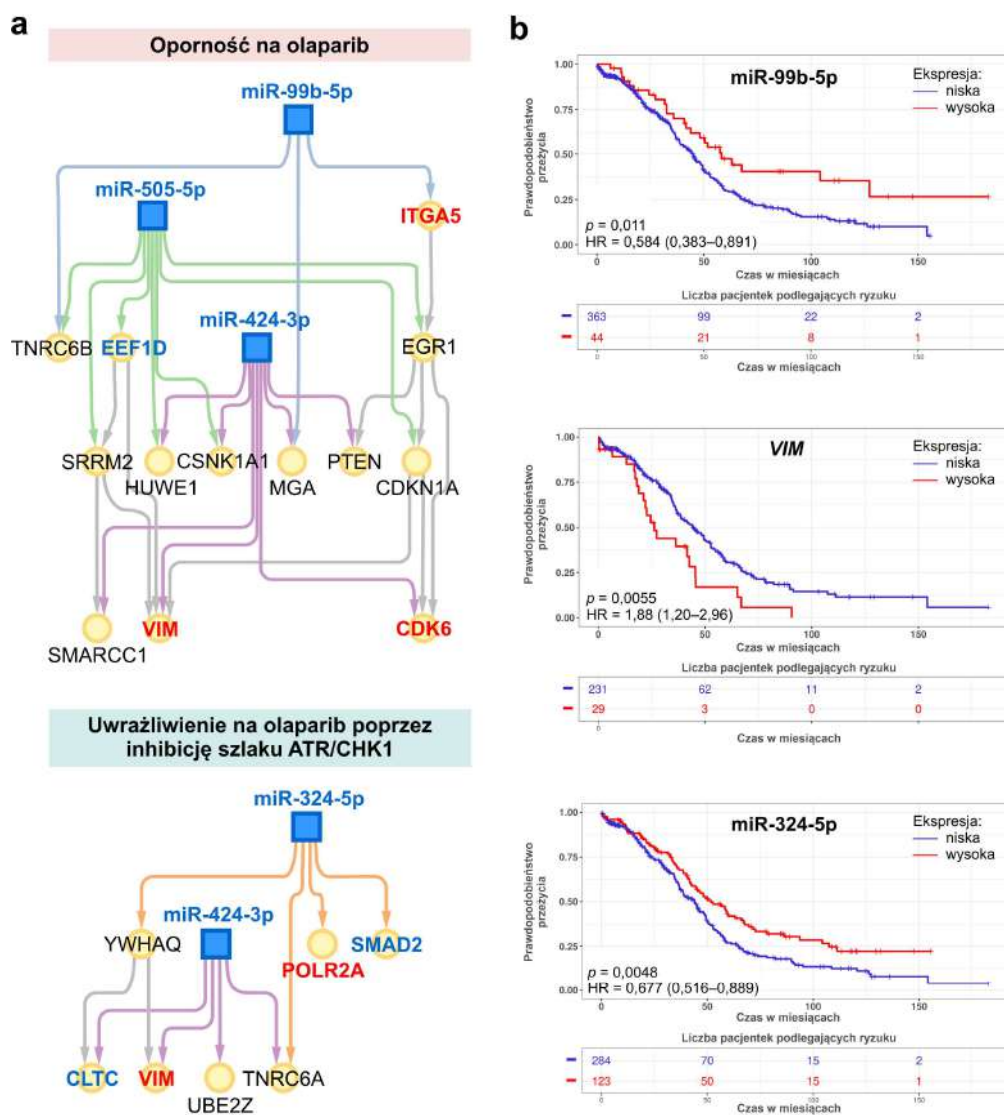


(amfiredulina, HB-EGF, HGF, IGFBP-1, IGFBP-3, IGFBP-4, IGFBP-6, PDGFR $\alpha$ , PDGFR $\beta$ , PDGF-AA, VEGF-A i VEGFR2). Co ważne, wyniki eksperymentalne potwierdziły przewidywane zaburzenia w ekspresji czynników wzrostu i ich receptorów. Naświetla to istotną rolę białek zaangażowanych w regulowanie wzrostu i proliferacji w przełamywaniu oporności na olaparib.

Dalsza część badań była poświęcona analizom *in silico* danych klinicznych z bazy danych TCGA dla pacjentek z surowiczym rakiem jajnika w zaawansowanym stadium po farmakoterapii dla istotnie deregulowanych miRNA i ich genów docelowych zidentyfikowanych *in vitro*. Celem tych analiz było przede wszystkim określenie, czy wytypowane miRNA oraz geny, w kontekście nabywania i przełamywania oporności na olaparib, mają związek z przeżyciem pacjentek. Spośród wyznaczonych wcześniej miRNA deregulowanych w komórkach PEO1-OR do analiz wybrano te, których poziom ekspresji na podstawie danych klinicznych może mieć znaczenie biologiczne *in vivo*. Jako kryterium przyjęto wartość progową ekspresji określoną jako zaliczenia na milion (CPM, ang. *count per milion*) powyżej 10 w co najmniej 50% próbek. Spośród wszystkich miRNA związanych z nabywaniem i przełamywaniem oporności kryterium progu poziomu ekspresji u pacjentek spełniło 8 miRNA (miR-9-5p, miR-99b-5p, miR-100-5p, miR-125a-3p, miR-324-5p, miR-424-3p, miR-486-5p i miR-505-5p).

Najpierw skupiono się na powiązaniu roli wybranych miRNA ze zmniejszoną wrażliwością na olaparib. Wśród 8 zakwalifikowanych do analiz miRNA, 7 z nich określono wcześniej jako powiązane z nabywaniem oporności w komórkach PEO1-OR. Analiza przeżycia metodą Kaplana-Meiera dla pacjentek z HGSOE z użyciem programu ToPP pokazała, że w grupach z obniżonym poziomem ekspresji dla 3 miRNA stwierdzono krótszy czas przeżycia całkowitego (OS, ang. *overall survival*) oraz krótsze interwały wolne od progresji (PFI, ang. *progression-free intervals*). Skrócony czas OS powiązano z obniżonym poziomem miR-99b-5p (HR = 0,84;  $p = 0,011$ ), miR-424-3p (HR = 0,738;  $p = 0,021$ ) i miR-505-5p (HR = 0,605;  $p = 0,0009$ ) (Rys. 8).

Podstawowy poziom ekspresji tych miRNA był również obniżony w komórkach PEO1-OR. Ekspresja wspomnianych miRNA nie różniła się istotnie pomiędzy pacjentkami w II, III i IV stadium zaawansowania, a ich stabilny poziom ekspresji może wskazywać na rolę tych cząsteczek w progresji choroby. Przeprowadzona dalej redukcja wielkości sieci regulatorowej miRNA-mRNA dla komórek PEO1-OR do trzech miRNA o wartości prognostycznej (miR-99b-5p, miR-424-3p i miR-505-5p) wyselekcjonowała 13 potencjalnie ważnych genów docelowych (Rys. 8). Pośród nich poszukiwano takich, których podwyższony poziom ekspresji korelowałby negatywnie z przeżyciem pacjentek. Wyniki pokazały, że pacjentki ze zwiększonym poziomem genu dla eukariotycznego czynnika elongacyjnego 1 delta (*EEF1D*), integryny 5 (*ITGA5*), wimentyny (*VIM*) oraz zależnej od cyklin kinazy 6 (*CDK6*) charakteryzowały się istotnie gorszym przeżyciem (krótszy czas OS oraz PFI). Porównanie poziomu ekspresji tych genów u pacjentek w różnych stadiach zaawansowania wykazało nadekspresję *VIM* w stadium III w porównaniu do II oraz nadekspresję *CDK6* w stadium IV w porównaniu do III, co może świadczyć o roli tych genów w progresji nowotworu. Ponadto stwierdzono, że zarówno *ITGA5*, jak i *VIM* wykazują obniżoną ekspresję na poziomie mRNA w tkankach pochodzących z guzów nowotworowych w porównaniu z prawidłowymi tkankami jajnika. Obniżenie poziomu ekspresji wimentyny u pacjentek z surowiczym rakiem jajnika potwierdzono na poziomie białka na podstawie danych z bazy Human Protein Atlas (ang. HPA).



**Rysunek 8. Powiązanie miRNA deregulowanych w komórkach PEO1-OR oraz ich genów docelowych z przeżyciem pacjentek z HGSOC podzielonych na grupy zależnie od poziomu ekspresji. (a)** Sieci regulatorowe miRNA-mRNA ograniczone do miRNA o potencjalnej wartości predykcyjnej związanej z nabywaniem i przełamywaniem oporności na olaparib. Na niebiesko i czerwono zaznaczono miRNA oraz geny, których odpowiednio niska i wysoka ekspresja istotnie wpływa na przeżycie **(b)** Krzywe Kaplana-Meiera przedstawiające czas całkowitego przeżycia u pacjentek zależnie od poziomu miRNA i genów najbardziej wpływających na różnicę w przeżyciu pomiędzy grupami o niskim (niebieski) i wysokim (czerwony) poziomie ekspresji. HR–współczynnik ryzyka (ang. *hazard ratio*) z 95% przedziałami ufności.

Następnie skoncentrowano się na określeniu prognostycznej wartości miRNA dla cząsteczek związanych z przełamywaniem oporności na olaparib w komórkach PEO1-OR (miR-324-5p, miR-424-3p i miR-486-5p). Analiza przeżycia Kaplana-Meiera dla pacjentek z HGSOC wykazała, że niski poziom miR-324-5p i miR-424-3p związany był ze skróconym czasem OS oraz PFI. Istotnie, obniżenie ekspresji tych miRNA również zidentyfikowano w komórkach PEO1-OR uwrażliwionych na olaparib z użyciem inhibitorów szlaku ATR/CHK1. Oba miRNA wykazywały stabilną ekspresję u pacjentek w stadiach II-IV, co może wskazywać na ich rolę w progresji choroby. Zredukowana dalej sieć regulatorowa miRNA-mRNA dla uwrażliwiania komórek raka jajnika na olaparib wykazała,

że miR-324-5p i miR-424-3p regulują 7 genów docelowych (Rys. 8), przy czym istotną wartość prognostyczną stwierdzono dla genu kodującego podjednostkę RPB1 polimerazy RNA II zależnej od DNA (*POLR2A*), wimentynę (*VIM*), klatrynę (*CLTC*), i białko SMAD2 (*SMAD2*). W grupach pacjentek z podwyższonym poziomem ekspresji dwóch z tych genów (*POLR2A* i *VIM*) stwierdzono istotnie skrócony czas OS i PFI (Rys. 8). Ponadto ekspresja *POLR2A* była obniżona u pacjentek w stadium zaawansowania III i IV w porównaniu ze stadium II oraz u pacjentek z rakiem jajnika w porównaniu z prawidłową tkanką.

Podsumowując, zaburzona ekspresja miRNA w komórkach PEO1-OR wskazuje na znaczne zmiany zachodzące w komórkach raka jajnika w trakcie nabywania oporności na olaparib. Deregulowane miRNA mogą odgrywać szczególną rolę w tych procesach poprzez pośredni wpływ na deregulację ekspresji czynników wzrostu i ich receptorów. Scharakteryzowane profile ekspresji miRNA w linii PEO1-OR wykazującej oporność na olaparib oraz w tych komórkach po przełamaniu oporności, mogą w przyszłości być wartościowym punktem wyjściowym do opracowania markerów związanych z odpowiedzią raka jajnika na olaparib oraz jego kombinacji z inhibitorami szlaku ATR/CHK1. Określone zależności pomiędzy poziomem ekspresji wybranych miRNA i ich docelowymi genami, a przeżyciem pacjentek wskazują na wysoki potencjał dalszych badań prowadzonych w tym kierunku.

## ETAP 4

### Ocena potencjału terapeutycznego połączenia olaparibu z inhibitorami szlaku ATR/CHK1 w kontekście uwrażliwiania komórek raka jajnika na olaparib w warunkach *in vivo*.

Ostatni etap badań podsumowuje manuskrypt pracy doświadczalna pt.: „**Olaparib rechallenge combined with the ATR/CHK1 pathway inhibitors in olaparib-resistant PDX models of ovarian cancer: Mechanisms behind synergistic tumor growth inhibition**”

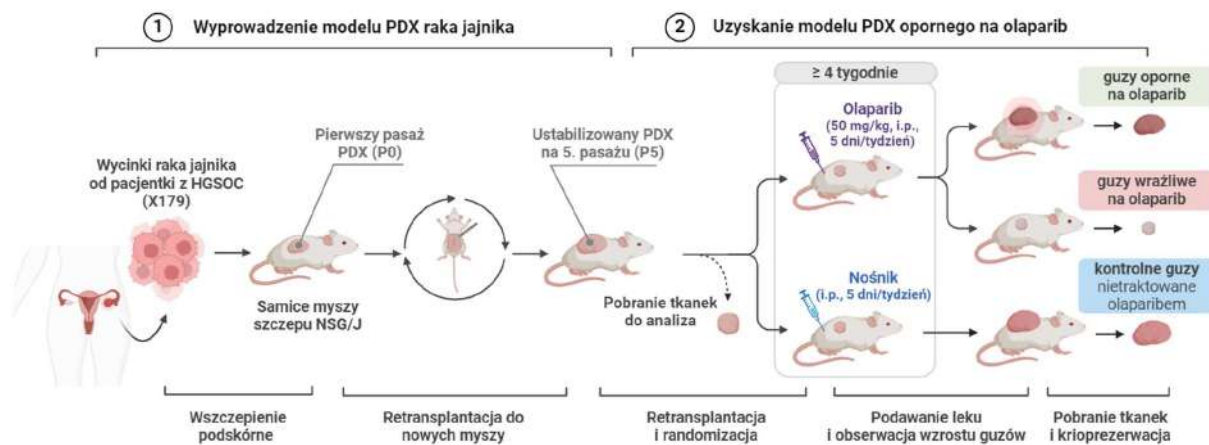
W badaniach przedklinicznych często wykorzystywanymi zwierzęcymi modelami nowotworów są mysie modele oparte o heteroprzeszczepy guzów pobranych bezpośrednio od pacjentów (PDX, ang. *patient-derived xenograft*). Umożliwiają one m. in. ocenę skuteczności terapii przeciwnowotworowych oraz badanie mechanizmów leżących u podstaw działania potencjalnych leków, jak i oporności na stosowane terapie. Modele PDX raka jajnika, tak jak i wielu innych nowotworów, są cennym narzędziem do badań przedklinicznych, gdyż stosunkowo wiarygodnie odzwierciedlają wzrost, charakterystykę genetyczną i molekularną oraz odpowiedź terapeutyczną guza pacjentki [50-52].

Głównym celem tego etapu badań było określenie wpływu połączenia olaparibu z inhibitorami szlaku ATR/CHK1 na zahamowanie wzrostu HGSOc w modelu PDX z wyindukowaną opornością na olaparib w warunkach *in vivo*. Dodatkowo zbadano zmiany związane z rozwojem oporności na olaparib i jej przełamywanie zachodzące w uzyskanych modelach heteroprzeszczepów.

Aby zrealizować założone cele, najpierw rozmrożono i rozpropagowano w myszach z immunodefektem szczepu NSG/J opracowane wcześniej heterotropowe heteroprzeszczepy raka jajnika z mutacjami w genach *BRCA1/2* pochodzące od trzech pacjentek z HGSOc (etap I). Następnie po przeszczepieniu do nowych myszy rozpropagowanych guzów wyprowadzono heterotropowy model

PDX raka jajnika z nabytą opornością na olaparib (etap II) (Rys. 9). Na koniec zbadano jak odporne na olaparib heteroprzeszczepu reagują na terapię skojarzoną łączącą olaparib z inhibitorem kinazy ATR lub CHK1 (etap III). Eksperymenty na zwierzętach zostały przeprowadzone we współpracy z Narodowym Instytutem Onkologii im. Marii Skłodowskiej-Curie – Państwowym Instytutem Badawczym w Warszawie w oparciu o zgodę Lokalnej Komisji Etycznej ds. Doświadczeń na Zwierzętach oraz zgodę Komisji Bioetycznej przy Centrum Onkologii w Warszawie.

Próbie uzyskania oporności na olaparib *in vivo* podjęto w trzech modelach PDX (X127, X160 oraz X179) z mutacjami *BRCA1/2* uprzednio nietraktowanych inhibitorami PARP. Po rozpropagowaniu u myszy heteroprzeszczepów, zwierzęta zostały poddane randomizacji do grupy kontrolnej otrzymującej nośnik składający się z roztworu 10% (v/v) DMSO, 40% (v/v) PEG300 i 5% (v/v) Tween 80 w wodzie podwójnie destylowanej (5 dni w tygodniu, dootrzewnowo) oraz grupy otrzymującej olaparib (50 mg/kg, 5 dni w tygodniu, dootrzewnowo). Za guzy z nabytą opornością na olaparib uznano takie, których objętość uległa co najmniej 2-krotnemu zwiększeniu po otrzymywaniu leku przez co najmniej 4 tygodnie względem pierwszego dnia podawania leku ( $RTV \geq 2$ ). W modelach PDX-X127 oraz PDX-X160 stwierdzono nietypowo wysokie tempo wzrostu guzów uniemożliwiające podawanie myszom olaparibu przez założony okres co najmniej 4 tygodni. W celu uniknięcia pogorszenia dobrostanu zwierząt, eksperymenty z zastosowaniem tych dwóch modeli heteroprzeszczepów zostały przerwane. Istotnie, oporność na olaparib uzyskano po 6 tygodniach w dwóch (#11 oraz #14) z ośmiu wszczepionych do myszy guzów z modelu PDX-X179 (Rys. 9).



**Rysunek 9. Schematyczne przedstawienie poszczególnych etapów wyprowadzania mysiego modelu PDX raka jajnika z wyindukowaną opornością na olaparib.** Myszy z rozpropagowanymi heteroprzeszczepami z modelu PDX-X179 z pasażu piątego (etap I) podzielono na grupę kontrolną otrzymującą nośnik poprzez iniekcje dootrzewnowe (i.p.) 5 dni w tygodniu oraz docelową grupę eksperymentalną traktowaną olaparibem (50 mg/kg, 5 dni w tygodniu, i.p.) (etap II). Po 6 tygodniach leczenia olaparibem u myszy zaobserwowano zahamowanie wzrostu guza lub jego regresję (wrażliwe na olaparib) lub wzrost guza prowadzący do ostatecznie podwojenia jego rozmiarów (oporne na olaparib). Model PDX z nabytą opornością na olaparib wykorzystano do oceny skuteczności badanych terapii skojarzonych (etap III).

Co ważne, model oporny został wyprowadzony z PDX-X179 posiadającego patogenne mutacje w genie *BRCA1* (c.181T>G; p.Cys61Gly) oraz *BRCA2* (c.4677delT; p.Phe1559\*), które odzwierciedlają kliniczny status HDR tzn. zaburzenia w procesie HR [53, 54]. Analiza kinetyki zmian wielkości uniewrażliwionych na olaparib guzów w trakcie indukowania oporności pokazała, że po

początkowym wzroście heteroprzeszczepów w pierwszym okresie podawania inhibitora doszło do chwilowej redukcji objętości guzów. Następnie w 28 dniu od pierwszego dnia podania olaparibu zaobserwowano nawrotowy wzrost guzów uzyskujących ostatecznie 2,7-krotnie (#11) oraz 2,0-krotnie (#14) zwiększoną objętość względem pierwszego dnia iniekcji leku. Jednocześnie, nie zaobserwowano istotnych zmian masy zwierząt w trakcie podawania leku. Ponadto, u trzech z ośmiu wszczepionych do myszy heteroprzeszczepów poddanych indukowaniu oporności stwierdzono częściową wrażliwość na olaparib bez zmian objętości guza (#12: RTV = 1,0) lub zwiększoną wrażliwość na olaparib prowadzącą do redukcji objętości guzów (#5: RTV = 0,16 oraz #9: RTV = 0,59). Heteroprzeszczepy pochodzące od trzech pozostałych myszy wykluczono z analizy ze względu na cystowatość guza, nietypowe zachowanie zwierzęcia lub zbyt krótki okres podawania olaparibu.

Porównanie ekspresji panelu białek pomiędzy guzami z nabytą opornością tuż po zakończeniu podawania olaparibu, a kontrolnymi guzami traktowanymi nośnikiem pozwoliło ujawnić zmiany molekularne związane z uniewrażliwieniem HGSOc na PARPi *in vivo*. W ramach scharakteryzowania fenotypu opornego zbadano ekspresję białek zaangażowanych w sygnalizację PARP, szlak ATR/CHK1, naprawę DNA oraz przejście epitelialno-mezenchymalne (EMT, ang. *epithelial-to-mesenchymal transition*). Na podstawie uzyskanych wyników stwierdzono, że heteroprzeszczepy raka jajnika z nabytą opornością na olaparib charakteryzowały się istotnie obniżonym poziomem ekspresji PARP1, PARG, a także zmniejszoną post-translacyjną PARylacją białek, wskazującą na indukowaną przez olaparib inhibicję PARP1 bez wywoływania jednocześnie istotnej inhibicji wzrostu guza. Wyniki te wskazują na zaburzenie sygnalizacji komórkowej regulowanej przez polimerazy PARP, które kontrolują naprawę DNA, utrzymanie stabilności genomu i wiele innych procesów komórkowych. Jednocześnie stwierdzić można, że w obecności olaparibu faworyzowane było przeżycie komórek opornych, które obniżyły ekspresję celu molekularnego leku – PARP1. Dodatkowo, zaobserwowano istotne obniżenie ekspresji zarówno kinazy ATR, jak i CHK1 oraz ich aktywnych, fosforylowanych form, co ujawniło zmiany w aktywności szlaku ATR/CHK1 regulującego odpowiedź na uszkodzenia DNA oraz przebieg cyklu komórkowego. Ponadto, guzy odporne na olaparib charakteryzowały się istotnie obniżoną ekspresją  $\gamma$ H2AX, BRCA2 i RAD51, sugerującą obniżoną akumulację DSB oraz zmniejszenie zależności od szlaku naprawy DNA poprzez HR. Z drugiej strony, w guzach tych zaobserwowano także obniżenie poziomu ekspresji białka 53BP1 promującego NHEJ, co w przypadku komórek HGSOc z mutacją w genie *BRCA1* może świadczyć o reaktywacji szlaku HR [55]. Znaczące różnice na poziomie białka stwierdzono także w przypadku ekspresji E-kadheryny i metaloproteinazy MMP2 pomiędzy guzami opornymi a kontrolnymi, jednak ze względu na przeciwne kierunki zmian ekspresji tych białek nie udało się stwierdzić czy nabywanie oporności związane jest ze zjawiskiem EMT. Jednocześnie, w guzach z nabytą opornością nie stwierdzono zmian w ekspresji MDR1, co wskazuje na brak roli tej glikoproteiny, odpowiedzialnej za usuwanie leków z komórki, w obniżeniu wrażliwości na olaparib.

W następnej części badań *in vivo* porównano skuteczność terapeutyczną inhibitorów stosowanych osobno i ich kombinacji w heteroprzeszczepach z nabytą opornością na olaparib. W tym celu, po przeszczepieniu i rozpropagowaniu opornych guzów (#11 i #14) w nowych myszach, zwierzęta poddano randomizacji do grupy kontrolnej otrzymującej wcześniej opisany nośnik (5 dni w tygodniu, dootrzewnowo) oraz do grup badanych traktowanych olaparibem (50 mg/kg, 5 dni

w tygodniu, dootrzewnowo), ATRi (25 mg/kg, 5 dni w tygodniu, doustnie), CHK1i (50 mg/kg, 2 dni w tygodniu, dootrzewnowo) lub kombinacjami olaparibu z ATRi lub CHK1i stosując ten sam schemat dawkowania co przy użyciu każdego ze związków osobno. Myszy otrzymywały badane inhibitory i ich kombinacje przez maksymalnie 37 dni (mediana 5 tygodni), po czym oceniono skuteczność terapeutyczną inhibitorów. Jednocześnie, nie stwierdzono znaczącego spadku masy myszy w trakcie podawania badanych inhibitorów i ich kombinacji.

W pierwszej części badań poświęconych ocenie skuteczności terapeutycznej inhibitorów w guzach opornych skupiono się na odpowiedzi komórek HGSOC uniewrażliwionych na olaparib po ponownym leczeniu PARPi. Co ważne, ponowne traktowanie olaparibem heteroprzeszczepów wszczepionych do nowych myszy potwierdziło oporny fenotyp guzów, które od momentu otrzymania pierwszej dawki leku przez myszy zwiększyły swoją objętość aż 4,2-krotnie. Guzy kontrolne w większym stopniu zwiększyły swoje rozmiary (RTV = 7,0), jednak nie zaobserwowano istotnych różnic we wzroście heteroprzeszczepów w punktach końcowych eksperymentu pomiędzy grupą otrzymującą olaparib a nośnik ( $p = 0,358$ ). Na poziomie molekularnym, odporne guzy poddane ponownemu działaniu olaparibu wykazywały obniżoną PARylację białek względem grupy kontrolnej, świadczącą o indukowanym przez olaparib częściowym zahamowaniu aktywności PARP1 bez wystąpienia istotnego efektu cytotoksycznego. Dodatkowo w tych guzach stwierdzono obniżenie poziomu  $\gamma$ H2AX oraz fosforylacji kinaz ATR i CHK1, sugerujące brak akumulacji DSB oraz aktywacji szlaku ATR/CHK1 w odpowiedzi na olaparib. Analiza ekspresji białek zaangażowanych w naprawę DNA wykazała obniżenie poziomu BRCA1, przy jednoczesnym podwyższeniu poziomu BRCA2 oraz 53BP1, wskazując na rolę tych dwóch ostatnich białek w odpowiedzi komórek opornych przy ponownym traktowaniu olaparibem. Biorąc pod uwagę zmiany poziomu badanych markerów EMT, olaparib nieoczekiwanie zwiększył ekspresję wimentyny, sugerując nabywanie przez komórki odporne cech komórek mezenchymalnych potencjalnie umożliwiających ich migrację oraz inwazję podczas ponownej terapii PARPi.

W drugiej części badań przeprowadzonych na rzecz oceny skuteczności terapeutycznej inhibitorów w guzach opornych skupiono się na odpowiedzi opornych guzów po uwrażliwieniu na olaparib poprzez inhibicję szlaku ATR/CHK1. Uzyskane efekty terapeutyczne związane z równoczesnym podawaniem dwóch inhibitorów oceniono na podstawie wartości współczynnika kombinacji (CI, ang. *combination index*), którego wartość poniżej 1 wskazuje na synergizm [56]. Co najważniejsze, wykazano synergistyczne zwiększenie zahamowania wzrostu guzów (TGI, ang. *tumor growth inhibition*) opornych na PARPi w grupie myszy otrzymujących jednocześnie olaparib oraz ATRi (TGI = 96%, CI = 0,84) lub CHK1i (TGI = 85%, CI = 0,75). Analiza zmian objętości guzów od pierwszego do ostatniego dnia podawania inhibitorów pokazała, że wielkość heteroprzeszczepów zwiększyła się w czasie terapii średnio 1,4-krotnie w grupie otrzymującej jednocześnie olaparib i ATRi oraz 2,6-krotnie w grupie otrzymującej równocześnie olaparib i CHK1i. Jak wspomniano wcześniej, heteroprzeszczepy w grupie kontrolnej oraz traktowanej olaparibem zwiększyły swoją objętość średnio 7,0-krotnie oraz 4,2-krotnie. Uzyskane wyniki wskazują zatem na synergistyczne działanie przeciwnowotworowe kombinacji inhibitorów w komórkach HGSOC opornych na olaparib.

Ocena efektów terapeutycznych kombinacji z użyciem wskaźnika T/C po zakończeniu leczenia, czyli stosunku wzrostu guzów traktowanych inhibitorami względem guzów kontrolnych [57], pokazała,

że grupy otrzymującą olaparib w połączeniu z ATRi (T/C = 0,21) lub CHK1i (T/C = 0,38) uzyskały korzystną odpowiedź przeciwnowotworową (uwzględniając przyjęte kryterium  $T/C \leq 0,42$  mówiące o korzystnym efekcie terapeutycznym). Porównując przeciwnowotworowe działanie dwóch badanych kombinacji inhibitorów, dodanie ATRi do olaparibu przyczyniło się do uzyskania lepszych efektów terapeutycznych niż zastosowanie połączenia olaparibu z CHK1i, co stwierdzono na podstawie analizy przebiegu krzywych wzrostu guzów oraz wartości wskaźników RTV, TGI i T/C. Szczegółowa ocena odpowiedzi na kombinacje olaparibu i ATRi u każdej myszy z osobna pokazała, że u dwóch z pięciu myszy (#22 oraz #47) uzyskano odpowiedź zaklasyfikowaną jako stabilną chorobę ( $0,70 \leq RTV \leq 1,20$ ) w postaci prawie całkowitego zahamowania wzrostu guza i stabilizacji choroby aż do końca skojarzonego podawania związków. Dodatkowo, u trzeciej z pięciu myszy otrzymującej olaparib i ATRi stwierdzono odpowiedź bliską stabilnej chorobie ( $RTV = 1,25$ ). W grupie otrzymującej olaparib w połączeniu z CHK1 najsilniejszą aktywność przeciwnowotworową zaobserwowano u myszy #25, u której inhibicja wzrostu heteroprzeszczepu względem kontroli wyniosła 96%, prowadząc do 1,4-krotnego zwiększenia rozmiaru guza od początku do końca leczenia. Przyczyny silniejszej aktywności przeciwnowotworowej kombinacji olaparibu z ATRi niż z CHK1i przypuszczalnie związane były z różnym schematem podawania oraz dawkami obu inhibitorów kinaz i ich farmakokinetyką. Przypuszczać również można, że zahamowanie szlaku ATR/CHK1 na poziomie kinazy ATR, a zatem i zmian w aktywności białek kontrolowanych przez nią, może wywoływać bardziej korzystny efekt terapeutyczny w postaci uwrażliwiania HGSOE na olaparib niż inhibicja kinazy CHK1. Niewątpliwie stanowi to ciekawy obszar dalszych badań. Związana z oceną efektów terapeutycznych analiza zmian mas myszy w trakcie leczenia pokazała, że olaparib, ATRi i CHK1i oraz ich kombinacje nie wpływają znacząco na wzrost zwierząt przy zastosowanym schemacie i dawkach leczenia. Istotnie, analiza uszkodzeń mięśnia sercowego ujawniła, że CHK1i oraz jego kombinacja z olaparibem powodowała u niektórych myszy zwłóknienie szkliste mięśnia sercowego oraz zmiany zwyrodnieniowe w kardiomiocytach, jednak stopień nasilenia obu zmian patologicznych był minimalny ( $< 10\%$ ). Niemniej, prawdopodobnie wyklucza to możliwość stosowania większych dawek lub częstotści podawania CHK1i osobno i w kombinacji, przy użyciu których można byłoby potencjalnie uzyskać większy efekt terapeutyczny.

Dalsze badania były poświęcone scharakteryzowaniu odpowiedzi opornych guzów po ich uwrażliwieniu na olaparib za pomocą inhibitorów szlaku ATR/CHK1, skupiając się szczególnie na kombinacji z ATRi. Badania histologiczne pokazały, obniżony indeks mitotyczny oraz poziom markera Ki-67 w tkankach guzów traktowanych olaparibem w połączeniu z ATRi, co świadczyło o obniżonej proliferacji uwrażliwionych komórek. Jednocześnie zaobserwowano umiarkowane oznaki nekrozy oraz zwiększony pleomorfizm jądrowy i wakuolizację komórek, co powiązano z przeciwnowotworowym mechanizmem działania badanych kombinacji olaparibu. Wyniki badań poziomu aktywnej postaci kaspazy-3 wskazują na brak udziału apoptozy zależnej od kaspazy-3 w zahamowaniu wzrostu uwrażliwionych guzów. Ponadto kombinacja olaparibu z ATRi przyczyniła się do synergistycznego obniżenia PARylacji białek oraz ekspresji PARP1 i PARC. Efekt ten był silniejszy niż przy użyciu każdego z inhibitorów osobno, co uwidacznia rolę zahamowywania aktywności PARP1 i PARylacji białek w uwrażliwianiu HGSOE na olaparib, przypuszczalnie powodując zaburzenia w rekrutacji białek zaangażowanych w naprawę DNA. Jednocześnie stwierdzono obniżenie poziomu  $\gamma$ H2AX w odpowiedzi na olaparib w połączeniu z inhibitorami



szlaku ATR/CHK1, co dodatkowo sugeruje wystąpienie nieprawidłowości w szlakach naprawy DNA. Z racji tego, że histon H2AX fosforylowany jest przez kinazę ATR, przypuszczać można, że spadek poziomu  $\gamma$ H2AX mógł być związany z obniżonym poziomem ekspresji ATR oraz inhibicją aktywności tej kinazy przez ATRi. Ocena poziomu ekspresji białek zaangażowanych w HR i NHEJ pokazała, że kombinacja olaparibu z ATRi doprowadziła do zmniejszenia poziomu ekspresji BRCA1, BRCA2 i 53BP1, wskazując na zaburzenia w szlakach naprawy DNA, które mogły przyczynić się do zahamowania wzrostu guzów. Dodatkowo, nie stwierdzono różnic w ekspresji analizowanych białek związanych z EMT (E-kadheryna, wimentyna, MMP2 oraz TIMP2), zatem uwrażliwienie komórek prawdopodobnie nie było związane ze zmianą ich zdolności do migracji i inwazji, w przeciwieństwie do terapii samym olaparibem.

Podsumowując, inhibicja szlaku ATR/CHK1 uwrażliwia komórki *BRCA1/2*<sup>MUT</sup> HGSOC odporne na olaparib, prowadząc do synergistycznego zahamowania ich wzrostu w mysim modelu PDX *in vivo*. Udokumentowanie potencjału przeciwnowotworowego badanych kombinacji w kontekście komórek HGSOC posiadających mutacje w genach *BRCA1/2* przyczyniło się do poszerzenia wiedzy dotyczącej przełamywania oporności na olaparib dla określonej grupy pacjentek. Szczegółowa charakterystyka histologiczna i molekularna pozwoliła opisać zmiany zachodzące w komórkach HGSOC podczas nabywania oporności na olaparib, jak i jej przełamywania z użyciem inhibitorów kinazy ATR oraz CHK1.



# 5

## PODSUMOWANIE I WNIOSKI

---

**C**harakterystyka genetyczna i molekularna raka jajnika jest jednym z głównych czynników wpływających na skuteczność leczenia przeciwnowotworowego, co wydaje się mieć kluczowe znaczenie przy stosowaniu leków ukierunkowanych molekularnie. Badania przeprowadzone w ramach rozprawy doktorskiej pozwoliły wykazać potencjał stosowania inhibitorów szlaku ATR/CHK1 w przełamywaniu oporności na olaparib w niskozróżnicowanym surowiczym raku jajnika. Dodatkowo, wykorzystanie wielu metod badawczych przyczyniło się do poszerzenia wiedzy na temat złożoności odpowiedzi na badane inhibitory w komórkach raka jajnika o różnej wrażliwości na olaparib. W przyszłości uzyskane wyniki mogą pomóc w opracowaniu biomarkerów służących do przewidywania ryzyka nabywania oporności na olaparib oraz skuteczności terapii łączących olaparib z inhibitorami szlaku ATR/CHK1 u pacjentek z rakiem jajnika.

**Podsumowując, wyniki uzyskane w ramach pracy doktorskiej pozwalają stwierdzić, że:**

- ✦ Komórki raka jajnika linii PEO1-OR z wyindukowaną opornością na olaparib *in vitro* wykazują wiele współistniejących mechanizmów związanych z obniżoną wrażliwością na inhibitor PARP, w tym rewersję mutacji w genie *BRCA2* czy nadekspresję białek odpowiedzialnych za sprawność naprawy uszkodzeń DNA poprzez rekombinację homologiczną.
- ✦ Komórki odporne na olaparib linii PEO1-OR wykazują mniejszą niż komórki wrażliwe podatność na indukowane przez olaparib uszkodzenia DNA i nie są zatrzymywane w punkcie kontrolnym G2/M cyklu komórkowego kontrolowanym przez szlak kinaz ATR/CHK1.
- ✦ W warunkach *in vitro* olaparib w połączeniu z inhibitorami szlaku ATR/CHK1 wykazuje synergistyczne działanie cytotoksyczne w komórkach raka jajnika zarówno wrażliwych, jak i opornych na inhibitor PARP. Stosowanie olaparibu z jednoczesną inhibicją kinaz ATR i CHK1 przełamuje oporność na olaparib w komórkach z rewersją mutacji *BRCA2*.
- ✦ Synergistyczne zwiększenie cytotoksyczności olaparibu przez inhibitory szlaku ATR/CHK1 w komórkach opornych PEO1-OR jest indukowane na drodze apoptozy zależnej od kaspaz-3/7.
- ✦ Zmiany ekspresji białek zaangażowanych w szlak odpowiedzi na uszkodzenia DNA mogą mieć istotną rolę w procesie nabywania i przełamywania oporności na olaparib poprzez ukierunkowaną inhibicję szlaku ATR/CHK1 w komórkach PEO1-OR.

- ✦ Zmieniony profil ekspresji miRNA w linii PEO1-OR odpornej na olaparib oraz komórkach PEO1-OR uwrażliwionych z użyciem inhibitorów szlaku ATR/CHK1 wskazuje na istotne zmiany zachodzące podczas nabywania i przełamywania oporności na inhibitor PARP na poziomie molekularnym. Nieprawidłową ekspresję miRNA, charakterystyczną dla komórek opornych oraz uwrażliwionych, powiązano istotnie z przeżyciem pacjentek z rakiem jajnika. W przyszłości odpowiednio dobrany panel miRNA może stać się ważnym wskaźnikiem prognostycznymi i/lub predykcyjnym do przewidywania odpowiedzi na olaparib oraz skuteczności terapii skojarzonej z inhibitorami szlaku ATR/CHK1.
- ✦ Zaburzoną ekspresję miRNA w komórkach PEO1-OR opornych oraz uwrażliwionych na olaparib powiązano ze szlakami czynników wzrostu na podstawie analiz bioinformatycznych. Zmiany w ekspresji panelu czynników wzrostu i ich receptorów potwierdzono eksperymentalnie na poziomie białka, co świadczy o u nich potencjalnym udziale w tych procesach.
- ✦ Komórki HGSOC z mutacjami w genach BRCA1/2 pozyskane z guza pacjentki mogą nabywać oporność na olaparib w mysim modelu *in vivo*. Uniewrażliwienie komórek raka jajnika na olaparib powiązano ze zmianami w ekspresji panelu białek, świadczącymi o zaburzeniach w sygnalizacji PARP, zmianach w aktywności szlaku ATR/CHK1 oraz szlakach naprawy DNA i procesie EMT.
- ✦ Połączenie olaparibu z inhibitorami szlaku ATR/CHK1 skutecznie hamuje wzrost heteroprzeszczepów HGSOC opornych na olaparib w mysim modelu *in vivo*, przy czym dodanie do olaparibu inhibitora ATR wywołuje lepszy efekt terapeutyczny niż dodanie inhibitora CHK1.
- ✦ Indukowane przez badane kombinacje synergistyczne hamowanie wzrostu heteroprzeszczepów raka jajnika opornych na olaparib związane jest obniżeniem proliferacji komórek, niewielkim poziomem nekrozy, zwiększonym pleomorfizmem jądrowym i wakuolizacją komórek. Przeprowadzone badania nie potwierdziły udziału apoptozy zależnej od kaspasy-3 w śmierci komórek nowotworowych.
- ✦ Oporne komórki HGSOC po uwrażliwieniu na olaparib poprzez inhibicję szlaku ATR/CHK1 w warunkach *in vivo* wykazywały obniżony poziom PARylacji białek, ekspresji PARP1, PARG, ATR, BRCA1, BRCA2 i 53BP1 oraz fosforylacji H2AX i ATR. Zmiany te wskazują na nieprawidłowości w sygnalizacji PARP, aktywności szlaku ATR/CHK1 oraz dysfunkcję szlaków naprawy DNA w trakcie przełamywania oporności na olaparib.

**Kluczowe wnioski** płynące z przeprowadzonych badań prezentują się następująco:

- 1. Oporność** komórek raka jajnika linii PEO1-OR na olaparib związana jest z wieloma współistniejącymi mechanizmami zachodzącymi na poziomie molekularnym, w tym rewersją mutacji w genie *BRCA2*, nadekspresją PARP1 i białek promujących rekombinację homologiczną, oraz zmianami w przebiegu cyklu komórkowego.
- 2. Kombinacja** olaparibu z inhibitorami szlaku ATR/CHK1 wykazuje synergistyczne działanie przeciwnowotworowe w komórkach linii PEO1-OR z nabytą opornością na olaparib, świadczące o przełamaniu oporności na PARPi w komórkach HGSOC w warunkach *in vitro*.
- 3. Nabywanie** oporności na olaparib przez komórki raka jajnika linii PEO1-OR oraz ich uwrażliwianie poprzez inhibicje szlaku ATR/CHK1 wiąże się ze zmianami w regulacji ekspresji miRNA.
- 4. Połączenie** olaparibu z inhibitorami szlaku ATR/CHK1 prowadzi do synergistycznego zahamowania wzrostu opornego na olaparib raka jajnika w mysim modelu PDX z mutacjami w genach *BRCA1/2*, potwierdzając korzyści terapeutyczne wynikające ze stosowania kombinacji wobec komórek HGSOC w warunkach *in vivo*.
- 5. Nabywanie** oporności na olaparib oraz jej przełamywanie poprzez inhibicje szlaku ATR/CHK1 w komórkach raka jajnika w modelu *in vivo* wiąże się ze zmianami ekspresji białek zaangażowanych w sygnalizację PARP, szlak ATR/CHK1, naprawę uszkodzeń DNA oraz proces EMT.
- 6. Zidentyfikowane** zmiany w ekspresji białek, wskazujące na potencjalne mechanizmy nabywania i przełamywania oporności na olaparib w komórkach HGSOC, mogą w przyszłości pomóc w określeniu, które pacjentki z rakiem jajnika mają szanse na uzyskanie korzyści terapeutycznych podczas leczenia olaparibem w połączeniu z inhibitorami szlaku ATR/CHK1.

## BIBLIOGRAFIA

---

1. Veneziani, A.C., et al., *Heterogeneity and treatment landscape of ovarian carcinoma*. Nat Rev Clin Oncol, **2023**. 20(12): p. 820-842.
2. Huang, J., et al., *Worldwide Burden, Risk Factors, and Temporal Trends of Ovarian Cancer: A Global Study*. Cancers (Basel), **2022**. 14(9).
3. Siegel, R.L., A.N. Giaquinto, and A. Jemal, *Cancer statistics, 2024*. CA Cancer J Clin, **2024**. 74(1): p. 12-49.
4. Gonzalez-Martin, A., et al., *Newly diagnosed and relapsed epithelial ovarian cancer: ESMO Clinical Practice Guideline for diagnosis, treatment and follow-up*. Ann Oncol, **2023**. 34(10): p. 833-848.
5. Akter, S., et al., *Recent Advances in Ovarian Cancer: Therapeutic Strategies, Potential Biomarkers, and Technological Improvements*. Cells, **2022**. 11(4).
6. Kobel, M. and E.Y. Kang, *The Evolution of Ovarian Carcinoma Subclassification*. Cancers (Basel), **2022**. 14(2).
7. Talbot, T., H. Lu, and E.O. Aboagye, *Amplified therapeutic targets in high-grade serous ovarian carcinoma - a review of the literature with quantitative appraisal*. Cancer Gene Ther, **2023**. 30(7): p. 955-963.
8. Pavlik, E.J., et al., *Disease-Specific Survival of Type I and Type II Epithelial Ovarian Cancers-Stage Challenges Categorical Assignments of Indolence & Aggressiveness*. Diagnostics (Basel), **2020**. 10(2).
9. Shah, S., et al., *Epithelial Ovarian Cancer: Providing Evidence of Predisposition Genes*. Int J Environ Res Public Health, **2022**. 19(13).
10. Eoh, K.J., et al., *Mutation landscape of germline and somatic BRCA1/2 in patients with high-grade serous ovarian cancer*. BMC Cancer, **2020**. 20(1): p. 204.
11. Fumagalli, C., et al., *Tumor BRCA Testing in Epithelial Ovarian Cancers: Past and Future-Five-Years' Single-Institution Experience of 762 Consecutive Patients*. Cancers (Basel), **2022**. 14(7).
12. Farmer, H., et al., *Targeting the DNA repair defect in BRCA mutant cells as a therapeutic strategy*. Nature, **2005**. 434(7035): p. 917-21.
13. Iijima, M., et al., *Genome-wide analysis of gynecologic cancer: The Cancer Genome Atlas in ovarian and endometrial cancer*. Oncol Lett, **2017**. 13(3): p. 1063-1070.
14. Loverix, L., et al., *PARP inhibitor predictive value of the Leuven HRD test compared with Myriad MyChoice CDx PLUS HRD on 468 ovarian cancer patients from the PAOLA-1/ENGOT-ov25 trial*. Eur J Cancer, **2023**. 188: p. 131-139.
15. Rabenau, K. and E. Hofstätter, *DNA Damage Repair and the Emerging Role of Poly(ADP-ribose) Polymerase Inhibition in Cancer Therapeutics*. Clin Ther, **2016**. 38(7): p. 1577-88.
16. Wu, Y., et al., *Clinical application of PARP inhibitors in ovarian cancer: from molecular mechanisms to the current status*. J Ovarian Res, **2023**. 16(1): p. 6.
17. Mirza-Aghazadeh-Attari, M., et al., *DNA damage response and repair in ovarian cancer: Potential targets for therapeutic strategies*. DNA Repair (Amst), **2019**. 80: p. 59-84.
18. Gee, M.E., et al., *DNA damage repair in ovarian cancer: unlocking the heterogeneity*. J Ovarian Res, **2018**. 11(1): p. 50.
19. Moschetta, M., et al., *Neoadjuvant treatment for newly diagnosed advanced ovarian cancer: where do we stand and where are we going?* Ann Transl Med, **2020**. 8(24): p. 1710.
20. Toma, M., T. Skorski, and T. Sliwinski, *Syntetyczna letalność jako funkcjonalne narzędzie w badaniach podstawowych oraz w terapii przeciwnowotworowej*. Postepy Hig Med Dosw, **2014**. 68: p. 1091-103.
21. Zheng, F., et al., *Mechanism and current progress of Poly ADP-ribose polymerase (PARP) inhibitors in the treatment of ovarian cancer*. Biomed Pharmacother, **2020**. 123: p. 109661.
22. Audeh, M.W., et al., *Oral poly(ADP-ribose) polymerase inhibitor olaparib in patients with BRCA1 or BRCA2 mutations and recurrent ovarian cancer: a proof-of-concept trial*. Lancet, **2010**. 376(9737): p. 245-51.
23. Poveda, A., et al., *Olaparib tablets as maintenance therapy in patients with platinum-sensitive relapsed ovarian cancer and a BRCA1/2 mutation (SOLO2/ENGOT-Ov21): a final analysis of a double-blind, randomised, placebo-controlled, phase 3 trial*. Lancet Oncol, **2021**. 22(5): p. 620-631.
24. Biegała, Ł., et al., *PARP inhibitor resistance in ovarian cancer: Underlying mechanisms and therapeutic approaches targeting the ATR/CHK1 pathway*. Biochim Biophys Acta Rev Cancer, **2021**. 1876(2): p. 188633.
25. Konstantinopoulos, P.A., et al., *Homologous Recombination Deficiency: Exploiting the Fundamental Vulnerability of Ovarian Cancer*. Cancer Discov, **2015**. 5(11): p. 1137-54.
26. Blackford, A.N. and S.P. Jackson, *ATM, ATR, and DNA-PK: The Trinity at the Heart of the DNA Damage Response*. Mol Cell, **2017**. 66(6): p. 801-817.
27. Gralewski, P., et al., *PARP Inhibition Increases the Reliance on ATR/CHK1 Checkpoint Signaling Leading to Synthetic Lethality-An Alternative Treatment Strategy for Epithelial Ovarian Cancer Cells Independent from HR Effectiveness*. Int J Mol Sci, **2020**. 21(24).
28. Huntton, C.J., et al., *ATR inhibition broadly sensitizes ovarian cancer cells to chemotherapy independent of BRCA status*. Cancer Res, **2013**. 73(12): p. 3683-91.
29. Yazinski, S.A., et al., *ATR inhibition disrupts rewired homologous recombination and fork protection pathways in PARP inhibitor-resistant BRCA-deficient cancer cells*. Genes Dev, **2017**. 31(3): p. 318-332.
30. Kim, H., et al., *Combining PARP with ATR inhibition overcomes PARP inhibitor and platinum resistance in*

- ovarian cancer models. *Nat Commun*, **2020**. 11(1): p. 3726.
31. Brill, E., et al., *Prexasertib, a cell cycle checkpoint kinases 1 and 2 inhibitor, increases in vitro toxicity of PARP inhibition by preventing Rad51 foci formation in BRCA wild type high-grade serous ovarian cancer*. *Oncotarget*, **2017**. 8(67): p. 111026-111040.
  32. Burgess, B.T., et al., *Olaparib Combined with an ATR or Chk1 Inhibitor as a Treatment Strategy for Acquired Olaparib-Resistant BRCA1 Mutant Ovarian Cells*. *Diagnostics (Basel)*, **2020**. 10(2).
  33. Shah, P.D., et al., *Combination ATR and PARP Inhibitor (CAPRI): A phase 2 study of ceralasertib plus olaparib in patients with recurrent, platinum-resistant epithelial ovarian cancer*. *Gynecol Oncol*, **2021**. 163(2): p. 246-253.
  34. Wethington, S.L., et al., *Combination ATR (cerlasertib) and PARP (olaparib) Inhibitor (CAPRI) Trial in Acquired PARP Inhibitor-Resistant Homologous Recombination-Deficient Ovarian Cancer*. *Clin Cancer Res*, **2023**. 29(15): p. 2800-2807.
  35. Lee, J.M., et al., *Prexasertib, a cell cycle checkpoint kinase 1 and 2 inhibitor, in BRCA wild-type recurrent high-grade serous ovarian cancer: a first-in-class proof-of-concept phase 2 study*. *Lancet Oncol*, **2018**. 19(2): p. 207-215.
  36. Do, K.T., et al., *Phase 1 Combination Study of the CHK1 Inhibitor Prexasertib and the PARP Inhibitor Olaparib in High-grade Serous Ovarian Cancer and Other Solid Tumors*. *Clin Cancer Res*, **2021**. 27(17): p. 4710-4716.
  37. Zhao, L., et al., *The Role of miRNA in Ovarian Cancer: an Overview*. *Reprod Sci*, **2022**. 29(10): p. 2760-2767.
  38. Frisk, N.L.S., et al., *Circulating microRNAs for Early Diagnosis of Ovarian Cancer: A Systematic Review and Meta-Analysis*. *Biomolecules*, **2023**. 13(5).
  39. Xiang, G. and Y. Cheng, *MiR-126-3p inhibits ovarian cancer proliferation and invasion via targeting PLXNB2*. *Reprod Biol*, **2018**. 18(3): p. 218-224.
  40. Bieg, D., et al., *MiR-424-3p suppresses galectin-3 expression and sensitizes ovarian cancer cells to cisplatin*. *Arch Gynecol Obstet*, **2019**. 299(4): p. 1077-1087.
  41. Biegała, Ł., et al., *Olaparib-Resistant BRCA2(MUT) Ovarian Cancer Cells with Restored BRCA2 Abrogate Olaparib-Induced DNA Damage and G2/M Arrest Controlled by the ATR/CHK1 Pathway for Survival*. *Cells*, **2023**. 12(7).
  42. Langdon, S.P., et al., *Characterization and properties of nine human ovarian adenocarcinoma cell lines*. *Cancer Res*, **1988**. 48(21): p. 6166-72.
  43. Sakai, W., et al., *Functional restoration of BRCA2 protein by secondary BRCA2 mutations in BRCA2-mutated ovarian carcinoma*. *Cancer Res*, **2009**. 69(16): p. 6381-6.
  44. Langdon, S.P., et al., *Oestrogen receptor expression and the effects of oestrogen and tamoxifen on the growth of human ovarian carcinoma cell lines*. *Br J Cancer*, **1990**. 62(2): p. 213-6.
  45. Beaufort, C.M., et al., *Ovarian cancer cell line panel (OCCP): clinical importance of in vitro morphological subtypes*. *PLoS One*, **2014**. 9(9): p. e103988.
  46. Biegała, Ł., et al., *Targeted inhibition of the ATR/CHK1 pathway overcomes resistance to olaparib and dysregulates DNA damage response protein expression in BRCA2(MUT) ovarian cancer cells*. *Sci Rep*, **2023**. 13(1): p. 22659.
  47. Ali, K.A., et al., *Ex vivo discovery of synergistic drug combinations for hematologic malignancies*. *SLAS Discov*, **2024**. 29(2): p. 100129.
  48. Biegała, Ł., et al., *Uncovering miRNA-mRNA Regulatory Networks Related to Olaparib Resistance and Resensitization of BRCA2MUT Ovarian Cancer PEO1-OR Cells with the ATR/CHK1 Pathway Inhibitors*. *Cells*, **2024**. 13(10): p. 867.
  49. Chang, L., et al., *miRNet 2.0: network-based visual analytics for miRNA functional analysis and systems biology*. *Nucleic Acids Res*, **2020**. 48(W1): p. W244-W251.
  50. Cybula, M., et al., *Patient-Derived Xenografts of High-Grade Serous Ovarian Cancer Subtype as a Powerful Tool in Pre-Clinical Research*. *Cancers (Basel)*, **2021**. 13(24).
  51. Liu, J.F., et al., *Establishment of Patient-Derived Tumor Xenograft Models of Epithelial Ovarian Cancer for Preclinical Evaluation of Novel Therapeutics*. *Clin Cancer Res*, **2017**. 23(5): p. 1263-1273.
  52. Chen, J., et al., *Using Patient-Derived Xenograft (PDX) Models as a 'Black Box' to Identify More Applicable Patients for ADP-Ribose Polymerase Inhibitor (PARPi) Treatment in Ovarian Cancer: Searching for Novel Molecular and Clinical Biomarkers and Performing a Prospective Preclinical Trial*. *Cancers (Basel)*, **2022**. 14(19).
  53. Kowalik, A., et al., *BRCA1 founder mutations and beyond in the Polish population: A single-institution BRCA1/2 next-generation sequencing study*. *PLoS One*, **2018**. 13(7): p. e0201086.
  54. Ratajska, M., et al., *Detection of BRCA1/2 mutations in circulating tumor DNA from patients with ovarian cancer*. *Oncotarget*, **2017**. 8(60): p. 101325-101332.
  55. Hurley, R.M., et al., *53BP1 as a potential predictor of response in PARP inhibitor-treated homologous recombination-deficient ovarian cancer*. *Gynecol Oncol*, **2019**. 153(1): p. 127-134.
  56. Duarte, D. and N. Vale, *Evaluation of synergism in drug combinations and reference models for future orientations in oncology*. *Curr Res Pharmacol Drug Discov*, **2022**. 3: p. 100110.
  57. Malcolm, J.E., et al., *Factors that influence response classifications in chemotherapy treated patient-derived xenografts (PDX)*. *PeerJ*, **2019**. 7: p. e6586.

**KOPIE ARTYKUŁÓW OPUBLIKOWANYCH  
I MANUSKRYPTU**

---

WCHODZĄCYCH W SKŁAD ROZPRAWY DOKTORSKIEJ

## **PUBLIKACJA #1**



## Review

# PARP inhibitor resistance in ovarian cancer: Underlying mechanisms and therapeutic approaches targeting the ATR/CHK1 pathway

Łukasz Biegała, Arkadiusz Gajek, Agnieszka Marczak, Aneta Rogalska<sup>\*</sup>

Department of Medical Biophysics, Institute of Biophysics, Faculty of Biology and Environmental Protection, University of Lodz, Pomorska 141/143, 90-236 Lodz, Poland



## ARTICLE INFO

## Keywords:

Ovarian cancer  
PARP inhibitor  
Resistance  
Targeted therapy  
ATR  
CHK1

## ABSTRACT

Ovarian cancer (OC) constitutes the most common cause of gynecologic cancer-related death in women worldwide. Despite consistent developments in treatment strategies for OC, the management of advanced-stage disease remains a significant challenge. Recent improvements in targeted treatments based on poly(ADP-ribose) polymerase (PARP) inhibitors (PARPi) have provided invaluable benefits to patients with OC. Unfortunately, numerous patients do not respond to PARPi due to intrinsic resistance or acquisition of resistance. Here, we discuss mechanisms of resistance to PARPi that have specifically emerged in OC including increased drug efflux, restoration of HR repair, re-establishment of replication fork stability, reduced PARP1 trapping, abnormalities in PARP signaling, and less common pathways associated with alternative DNA sensing and repair pathways. Elucidation of the precise mechanisms is essential for the development of novel strategies to re-sensitize OC cells to PARPi agents. Additionally, novel potential concepts for preventing and combating resistance to PARPi under development and relevant clinical reports on treatment strategies have been reviewed, with emphasis on the exploitation of the ATR/CHK1 kinase pathway in sensitization to PARPi to overcome resistance-induced vulnerability in ovarian cancer.

## 1. Introduction

In view of the progressive increase in the incidence of neoplastic diseases, especially in industrialized countries, the scientific and medical community has prioritized the development of more effective and

“patient-friendly” therapeutic options. Despite considerable research and financial outlays, modern medicine is yet to achieve fully effective management strategies. Relatively satisfactory results have been obtained for only a few neoplasm types with currently available drugs. Common cancers responsible for millions of deaths each year are

**Abbreviations:** 17-AAG, 17-allylamino-17-demethoxygeldanamycin; 53BP1, p53 binding protein 1; ABC, ATP-binding cassette; ABCB1, ATP binding cassette subfamily B member 1; ALDH1L1, aldehyde dehydrogenase 1 family member L1; ATR, ataxia telangiectasia and RAD3-related protein; ATRIP, ATR-interacting protein; BARD1, BRCA1 associated RING domain 1; BRCA1, breast cancer type 1 susceptibility protein; BRCA2, breast cancer type 2 susceptibility protein; BRD4, bromodomain-containing protein 4; C/EBP $\beta$ , CCAAT-enhancer-binding protein  $\beta$ ; CARM1, coactivator associated arginine methyltransferase 1; cGAMP, cyclic GMP-AMP; cGAS, cyclic GMP-AMP synthetase; CHK1, checkpoint kinase 1; ctDNA, circulating tumor DNA; CTLA-4, cytotoxic T lymphocyte-associated protein 4; dsDNA, double-stranded DNA; DYNLL1, dynein light chain LC8-type 1; DCR, disease control rate; EMA, European Medicines Agency; ESC, embryonic stem cell; EZH2, enhancer of zeste homolog 2; FDA, Food and Drug Administration; HDR, homology-directed repair; HGSO, high-grade serous ovarian cancer; HLTF, helicase-like transcription factor; HR, homologous recombination; HSP, heat shock protein; ICI, immune checkpoint inhibitor; INF, interferons; IRF3, interferon regulatory factor 3; MAPK, mitogen-activated protein kinase; MDR, multidrug resistance; MDR1, multidrug resistance protein 1; MEK, mitogen-activated protein kinase kinase; MMEJ, microhomology-mediated end joining; NAD, nicotinamide adenine dinucleotide; NAD<sup>+</sup>, oxidized form of nicotinamide adenine dinucleotide; NAMPT, nicotinamide phosphoribosyltransferase; NF- $\kappa$ B, nuclear factor kappa B; OC, ovarian cancer; ORF, open reading frame; ORR, overall response rate; OS, overall survival; PALB2, partner and localizer of BRCA2; PAR, poly(ADP-ribose); PARG, poly(ADP-ribose) glycohydrolase; PARP, poly(ADP-ribose) polymerase; PARPi, poly(ADP-ribose) polymerase inhibitor; PDX, patient-derived xenograft; PD-1, programmed cell death 1; PD-L1, programmed death-ligand 1; PFS, progression-free survival; P-gp, P-glycoprotein; PI3K, phosphoinositide 3-kinase; PID, PALB2-interacting domain; PTIP, pax transactivation domain-interacting protein; RIF1, Rap1-interacting factor 1; RPA, replication protein A; SMARCA1, SWI/SNF-related matrix-associated actin-dependent regulator of chromatin subfamily A-like protein 1; ssDNA, single-stranded DNA; STING, stimulator of interferon genes; TP53BP1, tumor protein p53 binding protein 1; ZRANB3, zinc finger RANBP2-type containing 3.

<sup>\*</sup> Corresponding author.

E-mail addresses: [lukasz.biegala@edu.uni.lodz.pl](mailto:lukasz.biegala@edu.uni.lodz.pl) (Ł. Biegała), [arkadiusz.gajek@biol.uni.lodz.pl](mailto:arkadiusz.gajek@biol.uni.lodz.pl) (A. Gajek), [agnieszka.marczak@biol.uni.lodz.pl](mailto:agnieszka.marczak@biol.uni.lodz.pl) (A. Marczak), [aneta.rogalska@biol.uni.lodz.pl](mailto:aneta.rogalska@biol.uni.lodz.pl) (A. Rogalska).

<https://doi.org/10.1016/j.bbcan.2021.188633>

Received 23 July 2021; Received in revised form 14 September 2021; Accepted 1 October 2021

Available online 4 October 2021

0304-419X/© 2021 The Authors. Published by Elsevier B.V. This is an open access article under the CC BY license (<http://creativecommons.org/licenses/by/4.0/>).



relatively resistant to treatment and only a modest proportion of patients respond reasonably well to conventional therapy [1].

Ovarian cancer (OC) is one of the greatest diagnostic and therapeutic challenges in modern oncological gynecology. According to the American Cancer Society, over 21,000 new cases of OC are estimated in 2021 in the United States alone [1]. About 75% of all ovarian tumors and 95% ovarian malignancies constitute epithelial ovarian cancer (EOC), presenting mainly as the high-grade serous ovarian cancer (HGSOC) histologic subtype [2]. EOC contributes to female mortality to a greater extent than any other gynecological malignancies combined and it is reported as the fifth most common cause of cancer-associated death among women. This considerably high fatality rate is linked to the complexity of making an accurate diagnosis, with most cases being identified at the third or fourth stage of disease [3]. For new diagnoses with advanced-stage EOC, cytoreductive surgery followed by chemotherapy with paclitaxel or platinum derivatives combined with the anti-angiogenic drug, bevacizumab, remains the standard first-line treatment in patients with high risk of progression [4–6]. Although systemic treatment can significantly prolong patient survival, overall prognosis remains unfavorable. About 70–80% patients show relapse after first-line therapy [6]. The greatest obstacles in the efficacy of widely available chemotherapeutic agents are multidrug resistance (MDR) development, low selectivity and high systemic toxicity, leading to the general consensus that traditional methods of OC treatment have reached a therapeutic limit. Further progress in oncological outcome, evaluated mainly as extended overall survival time of patients, requires other solutions [7,8].

Currently, high hopes are associated with novel rational-based therapies targeting DNA repair mechanisms. One of the most extensively studied strategies in recent years is blockage of the activity of poly (ADP-ribose) polymerases (PARP) by specific small-molecule inhibitors. PARP inhibitors (PARPi) present a long-awaited step forward in the treatment of OC [9–11]. So far, three PARPi agents, olaparib, rucaparib, and niraparib, have been approved by the European Medicines Agency (EMA) and Food and Drug Administration (FDA) to treat OC. Throughout recent years, indications of these PARPi have been expanding. At present, PARPi are used as first-line, second-line, or maintenance therapy following response to platinum-based therapy [12,13].

The mechanism of action of PARPi relies on the accumulation of unrepaired single-strand breaks (SSB) in DNA, which, in turn, causes errors during DNA replication and, as a consequence, double-stranded breaks (DSB). In normal cells, DSBs are mainly repaired by the homologous recombination (HR) repair pathway. Proteins encoded by *BRCA1* and *BRCA2* genes are involved in this mechanism, contributing to preservation of genetic stability. Loss of *BRCA1/2* function triggers alternative repair mechanisms, including non-homologous end joining (NHEJ), that potentially result in emergence of chromosomal aberrations and consequently, cell death. *BRCA1* and *BRCA2* mutations underlie ~50% of HGSOC cases. The use of PARPi in patients with loss of *BRCA1/2* activity promotes the occurrence of so-called synthetic lethality, a concept that concurrent defects in two or more genes or related cellular components result in cell death whereas individual perturbations have minor or no effects [14–16]. The selectivity of PARPi action against cells with a defective HR system, in particular, homozygous mutations in *BRCA1/2*, supports their utility as effective anti-cancer agents. Interestingly, recent trials focusing on niraparib have revealed that the clinical efficacy of PARPi is not limited to patients with mutations in *BRCA1/2* or HR deficiencies, arguably broadening the utility of some of these inhibitors in treatment of all HGSOC as recommended in the latest guidelines [12,17].

Elucidation of the molecular mechanisms underlying acquired and intrinsic resistance to PARPi should facilitate improvement of PARPi efficacy. The current review has focused on these mechanisms in OC as well as strategies to overcome PARPi resistance.

## 2. Mechanisms of resistance to PARP inhibitors in ovarian cancer

PARPi resistance is mediated through diverse pathways. Accumulating reports and clinical examinations have addressed the issue of PARPi resistance in OC, leading to better understanding of the molecular basis of this unfavorable phenomenon (Table 1).

### 2.1. Enhanced drug efflux

Several ATP-dependent efflux pumps belong to the superfamily of proteins conferring multi-drug resistance (MDR) to numerous chemotherapeutics [18] as well as PARPi (Fig. 1) [19–21]. General upregulation of ATP-binding cassette (ABC) transporters in cancer cells is one of the mechanisms of MDR and leads to reduced intracellular drug concentrations [22,23]. P-glycoprotein (P-gp, also known as ABCB1 or MDR1) is one of the most extensively studied ABC multidrug transporters. P-gp has very broad substrate specificity, facilitating interactions with multiple chemical agents, and is highly expressed in many solid tumors, including OC [18]. Initial suggestions on the association between olaparib resistance and drug efflux were presented by Rottenberg et al. (2008). The group reported that resistance to olaparib was correlated with overexpression of P-gp, which was reversed in the presence of the MDR1 inhibitor, tariquidar [19]. More recently, the involvement of ABC transporters in PARPi resistance was investigated in OC cell lines. For instance, IGROV-1 cells were shown to be significantly more sensitive to olaparib than IGROVDDP P-gp-overexpressing cells. In the presence of P-gp inhibitors, such as elacridar, zosuquidar, and valspodar, resistance to olaparib was partially reversed. However, no differences in P-gp protein expression were detected between IGROVDDP cells treated with olaparib for three days and those left untreated. The authors proposed that an increase in P-gp levels is usually only induced following long-term exposure to the drug [20].

Subsequent studies showed decreased sensitivity of A2780-derived OC cells to olaparib compared to parental cells, which was associated with elevated *ABCB1* expression. Interestingly, cells were cross-resistant to rucaparib but not veliparib. Additionally, no changes in mRNA level of *MRP1*, another member of the ABC transporter family encoded by *ABCC1*, were observed. A2780 cells resistant to olaparib exhibited decreased levels of a number of MDR efflux pumps (*ABCB6*, *ABCB9*, *ABCC4*, *ABCD3*, *ABCE1*, *ABCF2*, and *ABCG4*), as confirmed via microarray analysis [21]. Data from this report highlight that development of P-gp-mediated drug resistance to specific PARPi in OC does not exclude sensitivity to alternative ones owing to multiple mechanisms of acquired resistance [21]. Accordingly, it was suggested that clinical application of PARPi as second-line or maintenance therapy after exposure to

**Table 1**  
Mechanisms of resistance to PARP inhibitors in ovarian cancer.

Mode of resistance	Mechanism of resistance
Increased PARPi efflux	Overexpression of P-gp efflux pumps
Restoration of homologous recombination	Reactivation of <i>BRCA1</i> and <i>BRCA2</i> by secondary mutations Reactivation of <i>BRCA1</i> by promoter demethylation <i>BRCA1</i> hypomorphic isoforms activity Increased RAD51 foci formation Restoration of RAD51 paralogs Transcriptional upregulation of HR genes Reacquisition of DNA end resection through loss of 53BP1 or MRE11 facilitators
Reestablishment of replication fork stability	Inhibition of MRE11-mediated replication fork degradation
Decreased PARP1 trapping	Loss or mutations of PARP1
Restoration of PARP signaling	Loss of PARG
Mechanisms beyond mainstream	Downregulation of essential factors for NHEJ Enhanced MMEJ activity Upregulation of the Wnt/ $\beta$ -catenin pathway

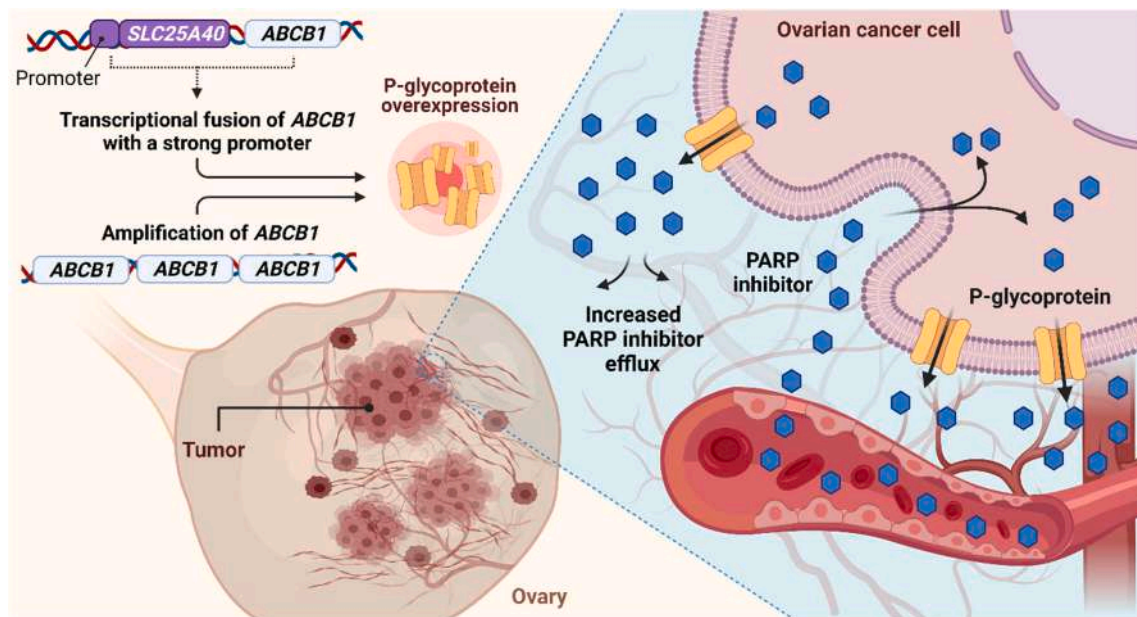


Fig. 1. Increased drug efflux mediated by overexpression of P-glycoprotein confers resistance to PARPi in ovarian cancer.

doxorubicin or paclitaxel may not be beneficial for patients showing relapse after first-line therapy due to shared drug transporter-related resistance mechanisms for standard chemotherapy drugs [21]. Significant P-gp overexpression was also detected by Kim and co-workers in olaparib-resistant PEO1 cells. In contrast, no increase in the efflux pump level was observed in JHOS4 cells, which are also resistant to olaparib [24]. Recent studies on clinical breast cancer and HGSOC suggest that upregulation of P-gp is attributable to transcriptional fusion involving *ABCB1*. The emergence of these genetic alterations is a consequence of placing the undisturbed open reading frame (ORF) of *ABCB1* under control of the strong promoter of *SLC25A40* encoding a membrane transporter, identified as the most common gene fusion partner [25]. Several studies have addressed the contribution of ABC transporters to PARPi resistance, little is currently known on the role of the efflux pumps in resistance to rucaparib. One of the first studies reporting that rucaparib is a substrate for both *ABCB1* and *ABCG2* in vitro showed that the drug is transported efficiently by mouse *Abcg2* and moderately by both human *ABCB1* and *ABCG2* [26].

From the clinical viewpoint, important findings associated *ABCB1* overexpression with gene amplification in every seventh biopsy sample in a study conducted in patients with HGSOC that have progressed on PARPi therapy. Moreover, upregulation of *ABCB1* is correlated with poorer progression-free survival (PFS) and overall survival [27]. Clinical resistance is significantly associated with increased drug efflux, which results in decreased effective intracellular drug concentration. Hence, comprehensive analysis of *ABCB1* expression and effects is strongly recommended in ongoing and future clinical trials.

As specified above, P-gp-mediated enhanced drug efflux is mainly driven by protein overexpression. However, an extensive literature review highlighted that resistance to PARPi may occur without a concurrent increase in levels of P-gp. A number of research groups have demonstrated no differences in expression of P-gp in olaparib-resistant HGSOC cell lines compared with parental sensitive cells, with further evidence obtained for both HR-deficient and HR-proficient cells [28].

## 2.2. Restoration of homologous recombination repair

HR repair restoration in HR-deficient tumors is one of the pivotal mechanisms of PARPi resistance (Fig. 2) [29,30]. HR repair can be reintroduced by both BRCA-dependent and BRCA-independent

mechanisms [31–33] and mainly promoted by re-establishment of expression of functional proteins involved in HR via secondary mutations (Table 2) or epigenetic modifications as well as loss of proteins regulating non-homologous end-joining (NHEJ) in OC tumors. In EOC, HR deficiency (HRD) underlies the concept of synthetic lethality exploited by PARPi. HR response is the main mechanism for DSB repair during S and G2 phases. However, in HR-deficient cells, these lesions are repaired by error-prone NHEJ, eventually leading to genomic instability. The occurrence of aberrations in the HR pathway is generally exploited by PARPi, which induces accumulation of unrepaired SSB leading to conversion to DSB. Consequently, PARPi induces death of tumor cells defective in HR [34,35]. Reacquisition of HR capacity has been linked to increased PARPi tolerance [29,30].

### 2.2.1. Restoration of BRCA1 and BRCA2 functionality

BRCA1 and BRCA2 play key roles in HR-dependent DSB repair and loss of their functions results in a defective HR repair pathway [36]. BRCA1 promotes BRCA2 and RAD51 recombinase loading onto single-stranded DNA (ssDNA) via interactions with partner and localizer of BRCA2 (PALB2), resulting in RAD51 nucleoprotein filament formation during HR [37]. The protective role of BRCA1/2 in the field of HR and fork stabilization may account for sensitivity to PARPi of cells lacking functional BRCA1/2 [38]. Molecular aberrations documented in HR repair mechanisms in HGSOC are mainly associated with germline or somatic mutations in *BRCA1* and *BRCA2*, which account for up to 25% of all cases [39]. Genetic testing of *BRCA1/2* in advanced-stage OC revealed that numerous abnormalities in tumor samples, predominantly point mutations, indels and copy-number variations, can lead to loss of *BRCA1/2* function [40].

One of the most well-characterized mechanisms underlying PARPi resistance is somatic reversion mutations in either *BRCA1* or *BRCA2* (Fig. 2A-1) that restore ORFs of genes [33,41]. Preliminary studies concerning reversion mutations in OC with acquired resistance to PARPi focused on *BRCA2*. While treatment of OC with PARPi may be effective for *BRCA1/2*<sup>mut</sup> tumors, development of resistance is also common [30,35].

Several reversion events have been identified as molecular characteristics of acquired resistance using whole-genome sequencing in samples of OC [43]. Acquisition of secondary *BRCA1* and *BRCA2* mutations has also been detected in circulating tumor DNA (ctDNA) from

RESTORATION OF HOMOLOGOUS RECOMBINATION REPAIR

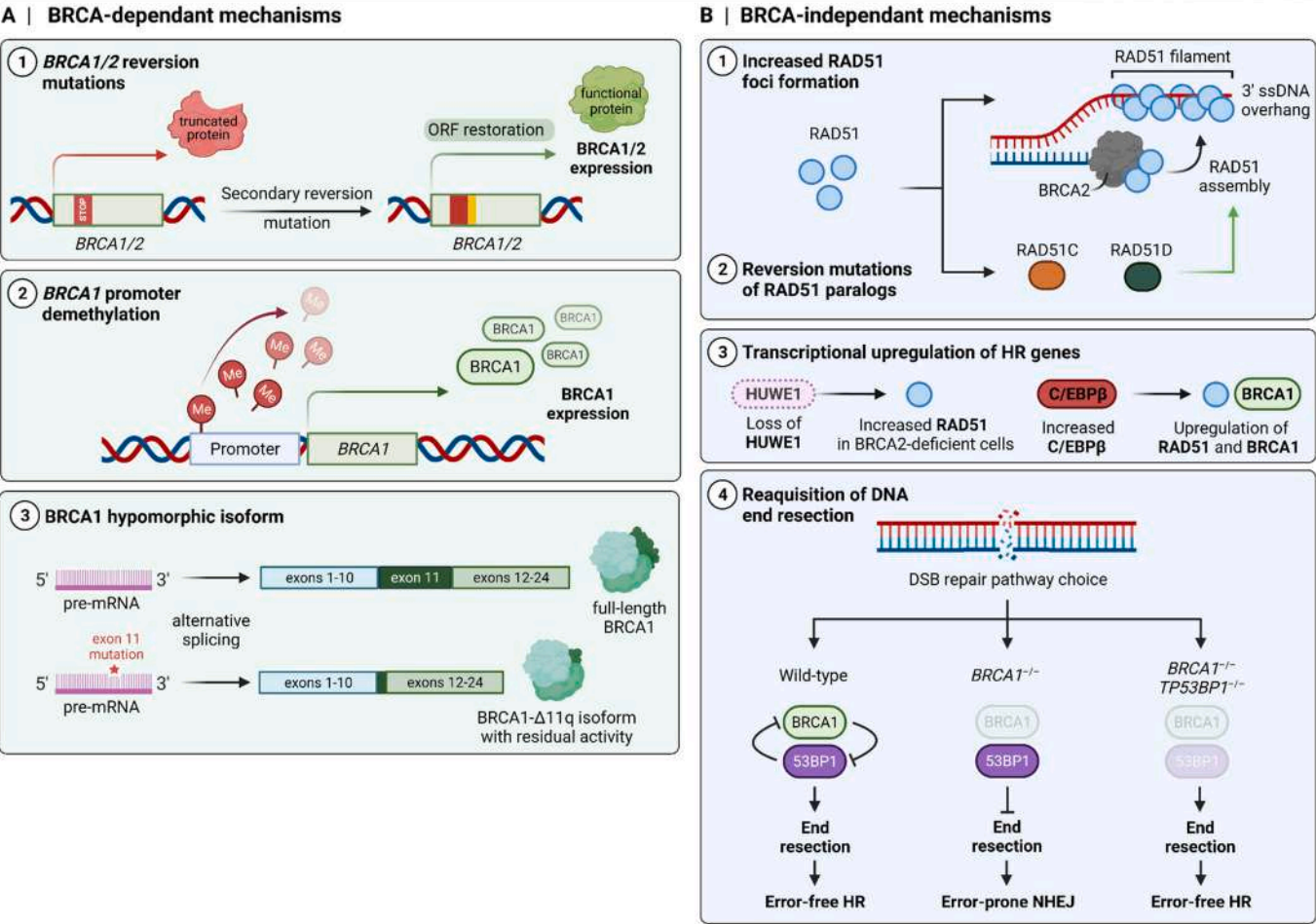


**Fig. 2.** Restoration of homologous recombination (HR) as a molecular mechanism conferring resistance to PARPi in ovarian cancer. HR restoration can be induced by both BRCA-dependent and -independent mechanisms. A | BRCA-dependent resistance is directly correlated with BRCA1/2 and associated with (1) reversion secondary mutations in *BRCA1/2* genes, (2) *BRCA1* promoter demethylation, and (3) expression of *BRCA1* hypomorphic isoforms with residual activity. B | BRCA-independent resistance does not directly depend on *BRCA1/2* and is associated with (1) increased RAD51 foci formation, (2) reversion mutations in *RAD51C* and *RAD51D* paralogs, (3) transcriptional upregulation of HR genes through loss of HUWE1 ubiquitin ligase and increased transcriptional factor, C/EBPβ, and (4) reacquisition of DNA end resection via loss of 53BP1 in *BRCA1*-depleted cells.

**Table 2**  
Secondary mutations in key genes resulting in restoration of transcript ORFs in PARPi-resistant ovarian cancer. Sequence variants are described according to HGVS nomenclature.

Gene	Primary mutation	Origin	Secondary mutations	Sample source
<i>BRCA1</i>	p.L392Qfs*5, c.1175_1214del	Germline	p.S377_N417del, c.1129_1251del	Solid tumor biopsy [31]
	p.L631Qfs*4, c.1892_1893del	Somatic	p.E427_S713del, c.1279_2139del	Solid tumor biopsy [31]
	p.N682*, c.2043dup	Germline	p.R612_S681delins27 c.[1835_1964del;2043dup] c.4096 + 1G > A	Solid tumor biopsy [31]
	p.Q855*, c.2563C > T	Somatic	p.E846_N859, c.2535_2576del p.E849_K862, c.2546_2587del	ctDNA from plasma [36]
<i>BRCA2</i>	p.E1493Vfs*9, c.4705_4708del	Germline	p.I1490_E1493del, c.4698_4709del	Solid tumor sample [42]
<i>RAD51C</i>	p.R193* c.577C > T	Germline	p.R193W, c.577_579delinsTGG p.(=), c.577C > A, p.H192_R193delinsGG, c.574_577delinsGGCG p.R193L, c.577_578delinsTT	Solid tumor biopsy [31]
<i>RAD51D</i>	p.G258Sfs*50 c.770_776del	Germline	p.S257_R259delinsK, c.770_776delinsA	Solid tumor biopsy

blood plasma samples of HGSOc patients and associated with disease progression in patients on rucaparib [44]. Reversion mutations in *BRCA1* were documented in ctDNA from another patient resistant to PARPi in a separate study [36]. Interestingly, different types of *BRCA1* reversion mutations were identified with various therapies, including olaparib and rucaparib [36]. Comprehensive analysis of secondary

reversion mutations of *BRCA1/2* genes in an OC patient cohort during progression on PARPi treatment led to the identification of several types of genetic abnormalities, predominantly including multiple base deletions and, to a lesser extent, one base-pair deletion, insertion, indel mutation, and single-nucleotide variations, in both *BRCA1* and *BRCA2*. The majority of *BRCA* mutations could correct the primary mutation and



restore functional activity of proteins [41]. A recently published report analyzing data from the ARIEL2 clinical trial demonstrated association of *BRCA1/2* reversion mutations in HGSOC patients with lack of responsiveness to rucaparib [45].

In addition to the well-studied common secondary *BRCA1/2* mutations resulting in restoration of in-frame gene transcripts, other mechanisms underlying restoration of *BRCA1* function have gained significant attention. Changes in methylation of *BRCA1* promoter constitute the second most commonly encountered defect associated with abrogation of HR underlying *BRCA1* mutations (Fig. 2A-2). Defects in promoter methylation of *BRCA1* have been detected in 7–12% samples of OC [39,46]. One of the first reports concerning methylation of *BRCA1* promoter in OC was documented over 20 years ago. Since then hypermethylation of promoter CpG islands has been associated with *BRCA1* silencing in ovarian and breast cancer [47,48]. *BRCA1* promoter methylation status is therefore considered a useful predictor of responsiveness to PARPi. However, the association between *BRCA1* methylation and response to treatment has not been fully elucidated [49,50]. Genomic characterization of *BRCA1* methylation status revealed that treatment with olaparib results in a long-term complete response in OC patients with highly methylated promoters. On the other hand, attenuated response to olaparib was associated with hypomethylation or complete lack of methylation of *BRCA1* promoter in most but not all cases [50]. Considering PARPi resistance, lack of responsiveness to rucaparib was associated with *BRCA1* restoration via demethylation of the *BRCA1* promoter. Additionally, the authors addressed the unresolved correlation between zygosity status of *BRCA1* methylation and responsiveness to rucaparib. Research conducted using OC cells and HGSOC patient-derived xenografts (PDX) provides evidence that heterozygous methylation is related to partial loss of promoter methylation and impaired responsiveness to PARPi, contributing to resistance to rucaparib [49].

Variations in *BRCA1* mutations are further correlated with distinct responsiveness to PARPi. The *BRCA1*- $\Delta$ 11q isoform harboring a mutation in exon 11 partially retained its function, but to a lower extent than wild-type protein (Fig. 2A-3). UWB1.289 OC cells containing *BRCA1* mutations within exon 11 demonstrated partial resistance to rucaparib and olaparib compared with *BRCA1* cells harboring mutations outside exon 11, which were highly sensitive to PARPi. Specific mutations in exon 11 could lead to a shift of ORF in *BRCA1*, resulting in generation of a hypomorphic isoform lacking the end of exon 11, specifically, a *BRCA1* protein with partial loss of function or reduced expression. Truncated, hypomorphic *BRCA1* is associated with residual function in response to HR and development of incomplete resistance [51]. Further analysis of 5-year overall survival of OC patients showed that exon 11 mutation carriers respond partially to platinum-based chemotherapy. However, the potential correlation of the mutation status of *BRCA1* exon 11 with the therapeutic efficacy of PARPi requires investigation [51].

### 2.2.2. Increased formation of RAD51 foci and restoration of RAD51 paralogs

Recent findings suggest that changes in RAD51 are involved in restoration of HR (Fig. 2B). RAD51 recombinase protein plays a key role in the first phases of DSB repair by HR. RAD51 promotes HR repair, replication fork reversal, and protection of stalled fork [52]. One of the initial steps of HR, homology search and strand exchange, involves encounter of two homologous sequences and is based on bringing together to the physical vicinity a single strand of a damaged sequence with complementary DNA of an undamaged template. RAD51 possesses two DNA-binding sites that allow this pairing, the first for the resected end of ssDNA at the break site of a damaged strand and the second interacting with the target strand of double-stranded DNA (dsDNA). Recognition and binding of homologous DNA sequences are mediated by RAD51, initially leading to formation of nucleoprotein filaments on the 3' ssDNA overhang, known as RAD51 assembly, followed by complementary pairing with a dsDNA strand [53]. Formation of RAD51

filaments in human cells is mediated by *BRCA2* function as a RAD51 loader with the assistance of RAD51C and RAD51D [52].

In the literature, several examples of association of RAD51 with PARPi resistance in OC (Fig. 2B) are documented, including reports from OC patient-derived organoids [29]. Recent studies have demonstrated restoration of HR during S and G2 phases in PARPi-resistant HGSOC cells harboring original *BRCA2* mutations following treatment with olaparib compared with sensitive cells with no RAD51 accumulation. Notably, both PEO1 cells resistant to olaparib (PEO1-PR) and parental sensitive cells did not express functional *BRCA2* protein, which was confirmed by whole-genome sequencing (*BRCA2*: c.6620C > G, p. T1655X). HR restoration in PARPi-resistant *BRCA2*<sup>mut</sup> cells was correlated with formation of RAD51 foci. Resistance to PARPi may therefore be conferred by HR restoration through increased RAD51 formation irrespective of reversion mutation in *BRCA2*. At the same time, no RAD51 foci were detected in *BRCA1*<sup>mut</sup> cells resistant to PARPi (JHOS4-PR) in the presence of olaparib. The results obtained by Kim et al. [24] suggest that PARPi resistance is based on another mechanism in this cell line and not restricted to HR restoration via formation of RAD51 nucleoprotein filaments in OC cells.

Abnormalities in HR genes other than *BRCA1/2* favor effective response to PARPi. Consequently, somatic reversion mutations restoring the HR repair pathway and decreasing sensitivity to PARPi are not restricted to *BRCA1* and *BRCA2*. The recovery of functions of other key proteins involved in HR by secondary mutations has also been documented. Germline mutations in *RAD51* genes were widely investigated in a study involving almost 3500 patients with invasive epithelial OC. The results showed that mutations in *RAD51C* and *RAD51D* encoding RAD51 paralogs contributed to susceptibility to OC [54]. Thus, the occurrence of mutations in core HR genes other than *BRCA1/2* in OC cells, such as *RAD51*, may confer responsiveness to PARPi [31]. Clinical effectiveness of rucaparib in HR-defective OC (either in *BRCA1*<sup>mut</sup> or *RAD51*<sup>mut</sup> cells) has been demonstrated [31]. Recent findings support a role of secondary reversion mutations in *RAD51* genes in acquired resistance to PARPi including rucaparib in clinical settings (Fig. 2B). Preliminary NGS studies conducted by Kondrashova et al. [31] on samples from HGSOC patients showing relapse following rucaparib treatment focused on core HR genes. A number of deleterious mutations resulting in C-terminal truncated RAD51C and RAD51D paralogs were found in pretreatment tumor samples, which could have conferred sensitivity to PARPi treatment. However, secondary mutations were detected in the majority of paired biopsy samples obtained from patients with initial deleterious mutations after relapse on rucaparib. The ORFs of *RAD51* genes may be restored via secondary genetic alterations leading to restoration of the HR pathway and eventually rucaparib resistance. Further assays confirmed the restoration of repair by HR. Overall, reversion mutations in *RAD51C* and *RAD51D* genes have been identified as one of the mechanisms of acquired PARPi resistance irrespective of *BRCA1/2* status under PARPi selection pressure [31]. However, recent observations indicate that not all germline mutations in *RAD51C* are associated with restoration of HR repair. Based on results obtained from HGSOC-derived 3D organoid cultures, Hill et al. [29] proposed that the model was sensitive to olaparib, possibly due to defects in HR.

Additionally, genome-wide CRISPR-based screening by Clements et al. [55] revealed that increased RAD51 expression induced by ubiquitin-ligase HUWE1 depletion promotes olaparib resistance due to partial restoration of HR repair in *BRCA2*-deficient cells (Fig. 2B). Interestingly, their results support an association between HUWE1 and RAD51 transcriptional regulators. However, screening was performed in HeLa cells representing a model of gynecological cancer without considering OC cells [55]. Moreover, HR restoration was induced by transcriptional upregulation of RAD51 and *BRCA1* mediated by a transcription factor, CCAAT-enhancer-binding protein  $\beta$  (C/EBP $\beta$ ), directly regulating genes encoding key HR machinery. Recent findings have demonstrated that increased levels of C/EBP $\beta$  are common in HGSOC.

Moreover, C/EBP $\beta$  expression is inducible by olaparib in OC and promotes PARPi resistance through HR gene targeting [56].

### 2.2.3. Reacquisition of DNA end resection

Abrogation of protein components of the NHEJ pathway can re-establish HR. For instance, reactivation of HR induced by reacquisition of DNA end resection through loss of p53 binding protein 1 (53BP1) as well as end resection-associated proteins represents another novel mechanism of PARPi resistance (Fig. 2B). NHEJ functions as an alternative prevalent pathway to HR for repair of DSB in mammalian cells. DSB repair by NHEJ is mediated predominantly in a 53BP1-dependent manner and can be exploited as an alternative mechanism of DNA damage repair. Importantly, antagonistic actions of 53BP1 and BRCA1 determine the pathway choices between erroneous HNEJ and high-fidelity HR, respectively [57]. 53BP1 is an NHEJ-promoting protein that protects DNA ends from resection at the break site, resulting in inhibition of HR repair [57].

HR reactivation by concurrent loss of 53BP1 and BRCA1, and in some cases, correlation of this phenomenon with PARPi resistance, have been widely documented in breast tumor models [58–60]. Importantly, abrogation of 53BP1 recruitment to DSB could lead to loss of end resection inhibition and restore attenuated HR in cells deficient in BRCA1 [58]. Recent efforts have considerably focused on the role of TP53BP1 status in OC cells in relation to HR reactivation and PARPi resistance. In vitro results showed that HR- and BRCA1-deficient COV362 HGSOC cells display acquisition of HR proficiency as a result of 53BP1 deletion, with concurrent enhanced resistance to PARPi. Interestingly, no impact on PARPi sensitivity was evident in 53BP1 knockout COV362 cells harboring BRCA1<sup>mut</sup> with increased HR [32]. Separate preclinical studies demonstrated upregulation of BRCA1 protein levels in OVCAR8 olaparib-resistant clones compared with the HR-deficient parental cell line (BRCA1-depleted) as a result of gene promoter hypermethylation. Interestingly, two out of four resistant clones exhibited simultaneously reduced levels of 53BP1, indicating promotion of HR over NHEJ [28]. PARPi resistance was also attributed to loss of 53BP1 in HR-deficient OC in an earlier clinical examination [32]. Analysis of tumor cells via whole-exome sequencing from a BRCA1-mutant HGSOC PDX model resistant to olaparib revealed decreased expression of 53BP1, which was further associated with mutation of TP53BP1 leading to HR restoration [61]. Reactivation of HR in BRCA1-

deficient and TP53BP1-deficient cells is dependent on the ubiquitin E3 ligase, RNF168, which mediates RAD51 loading (Fig. 3A). PALB2 joins damaged chromatin via the WD40 domain and the PALB2-interacting domain (PID) of RNF168. Data from this study suggest that HR reactivation in BRCA1- and TP53BP1-deficient cells is promoted by combination of the BRCA1-independent recruitment mode of PALB2 and increased resection due to loss of the 53BP1–RIF1–shieldin axis. Moreover, the downstream role of BRCA1 in RAD51 loading is suggested to be unnecessary in the absence of 53BP1 [62,63].

Moreover, 53BP1 constitutes the scaffold for numerous signaling and repair proteins at the DSB site during HR repair (Fig. 3B) [64]. Rap1-interacting factor 1 (RIF1) and shieldin consisting of REV7, SHLD1, SHLD2, and SHLD3 are recruited to DSB and block HR by limiting DNA end resection. Therefore, nuclease activity is blocked at the DSB site inhibiting end resection in a BRCA-independent manner. Association of SHLD3 with REV7 is a signal for attachment of other proteins, such as SHLD1 and SHLD2 [65,66]. The trimeric CST complex (composed of Ctc1, Stn1, and Ten1 subunits) and DNA polymerase alpha (Pol $\alpha$ ) may participate in refill of resected DSB ends, which allows shieldin to prevent resection in BRCA1-deficient cells [67,68]. Binding of ssDNA to SHLD2 is crucial for shieldin protection of DNA ends to mediate 53BP1-dependent DNA repair. The first step is recruitment of ubiquitin E3 ligase followed by another E3 ligase, RNF168 [69]. RNF168 directly ubiquitylates duplex-resolving helicase DHX9 to facilitate its recruitment to R-loop loci in PEO-1 BRCA<sup>mut</sup> OC cells. Thus, loss of RNF168 in BRCA1/2-deficient cells impairs recruitment of the R-loops to duplex-resolving DHX9, leading to accumulation and genomic instability [70]. Upon localization to the DSB region, RNF168 ubiquitylates histone H2AX, facilitating attachment of other DNA repair factors, such as 53BP1, and downstream effectors, including RIF1, pax transactivation domain-interacting protein (PTIP), and the shieldin complex. Phosphorylated  $\gamma$ H2AX recruits the chromatin associated adaptor protein, MDC1, which interacts with multiple partners, such as MRN (MRE11-RAD50-NBS1) and RNF168. Upon loss of resection, HR can be reactivated in a BRCA-independent manner via recruitment of PALB2 [69].

Recent CRISPR knockout screening has led to the identification of DYNLL1 as an organizer of multimeric 53BP1 complexes and critical regulator of PARPi resistance in BRCA1<sup>mut</sup> HGSOC cell lines. In general, DYNLL1 stimulates NHEJ through interactions with MRE11 and

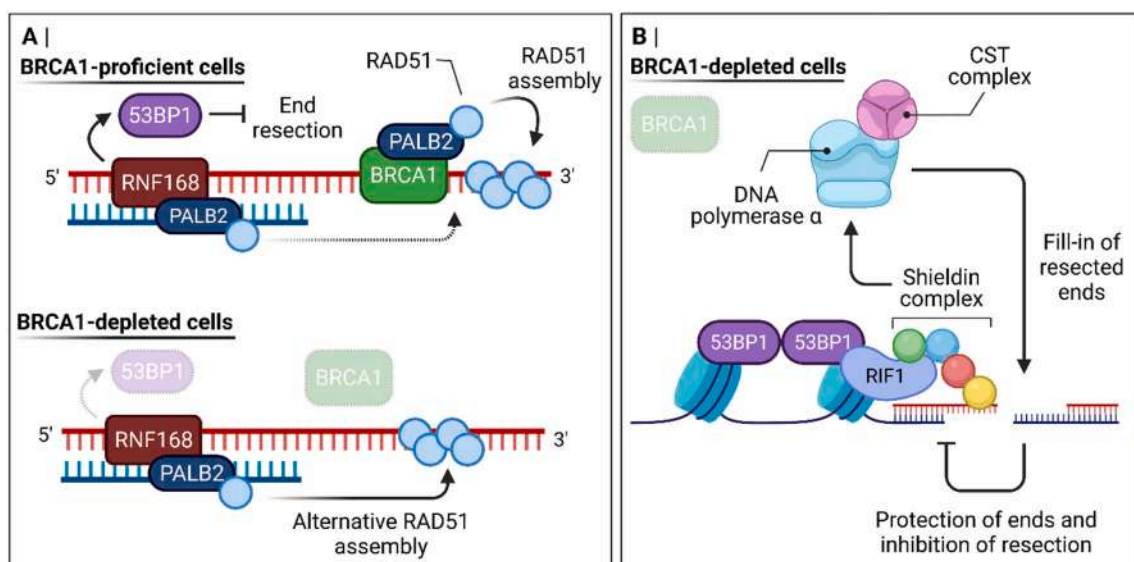


**Fig. 3.** Regulation of DNA end protection and resection. A | An alternative mechanism of RAD51 loading onto ssDNA mediated via RNF168 interactions with PALB2 in the presence or absence of BRCA1. B | Role of 53BP1 and shieldin complex in end resection inhibition in BRCA1-deficient cells. Shieldin inhibits resection through interactions with the CST complex, in turn, mediating Pol $\alpha$  recruitment at the DSB site. DNA polymerase catalyzes the fill-in reaction of resected ends. Loss of this mechanism restores homologous recombination.

53BP11, resulting in downregulation of DNA end resection. Loss of DYNLL1 is correlated with cross-resistance to olaparib and niraparib in BRCA1-deficient but not BRCA2-deficient cells. Further studies considering the PARPi resistance phenotype have demonstrated that DYNLL1-deficient cells exhibit increased DNA end resection after olaparib treatment. In a previous clinical study, cohorts of patients with HGSOC and low DYNLL1 expression were associated with poor PFS, reduced genomic alterations, and increased homology at lesions [71].

Recent studies have additionally revealed a role of enhancer of zeste homolog 2 (EZH2), a histone *N*-methyltransferase, in regulating NHEJ activity in coactivator associated arginine methyltransferase 1 (CARM1)-high OC cells. CARM1 is a protein methyltransferase that recruits chromatin remodeler, EZH2, responsible for silencing *MAD2L2* that encodes a component of the shieldin complex that preserves DNA end resection. The group demonstrated that EZH2-mediated downregulation of *MAD2L2* contributes to increased resistance to PARPi in CARM1-high HR-proficient OC and loss of end resection inhibition compared with EZH2-inhibited cells. These findings were associated with reduced activity of NHEJ without effects on HR. Further experiments confirmed that the CARM1-high EOC mouse model is not sensitive to olaparib treatment, as evident from the lack of effect on tumor growth [72,73].

### 2.3. Restoration of replication fork stabilization

Restoration of HR is one of the most extensively characterized mechanisms underlying lack of responsiveness to PARPi. However, elucidation of other contributory mechanisms to resistance to therapeutic agents is pivotal for improving overall therapeutic outcomes of OC. Another PARPi resistance mechanism independent of HR restoration is the restoration of stalled fork stabilization (Fig. 4A). Replication stress involves slowing or stalling of the replication fork during DNA synthesis resulting in genome instability [65]. Numerous obstacles encountered during DNA replication, including DNA lesions or collision with transcription machinery, contribute to replication fork stalling.

Stalled replication forks can be rescued by subsequent stabilization and restarting [66]. Replication fork dynamics has gained significant attention in research focused on deciphering PARPi resistance, since PARPi influences replication for stability. With respect to synthetic lethality, the mechanism of action of PARPi considerably relies on PARPi-induced suppression of fork protection and perturbation of replication fork reversal [74]. During DNA synthesis, inactivation of replication caused by the inability of the fork to resume replication is generally defined as 'fork collapse'. Collapse of stalled replication forks is associated with uncoupling of DNA replication machinery and failure to stabilize the stalled fork, eventually leading to formation of DSBs. In addition to the significant roles of PARP1, BRCA1, BRCA2, and RAD51 in promotion of DNA DSB repair, these proteins function in replication fork maintenance [75–77]. BRCA1, accompanied by a BRCA1 binding partner (designated BRCA1-associated RING domain 1 (BARD1)) as well as BRCA2, play key roles in replication fork protection although the functions are variable [76]. For instance, BRCA2 protects against replication fork stalling by recruiting and stabilizing RAD51 into ssDNA, which prevents exposed DNA strands from degradation by MRE11 nuclease [76]. However, only RAD51 is reported to drive reversion of stalled replication fork independently prior to fork protection [76].

In the absence of BRCA1/2, nuclease MRE11 and crossover junction endonuclease MUS81 attack stalled replication forks, leading to fork collapse and chromosomal instability (Fig. 4A). The methyltransferase, EZH2, which participates in histone methylation and transcriptional repression, and PTIP are responsible for recruiting MUS81 and MRE11 to the stalled replication fork, respectively [78]. However, in *BRCA1/2*<sup>mut</sup> cells, EZH2 and PTIP activities are downregulated at the fork, reducing recruitment of nucleases and resulting in fork protection. Low EZH2 expression is proposed to lead to reduced H3K27 methylation, prevent MUS81 recruitment at stalled forks, and trigger fork stabilization. Moreover, in a panel of BRCA2-deficient but not BRCA1-deficient ovarian and breast cancer cell lines, the EZH2/MUS81 axis has been shown to act independently of the recently characterized MLL3–4/PTIP/MRE11 pathway of chemoresistance [79]. PTIP deficiency inhibited the

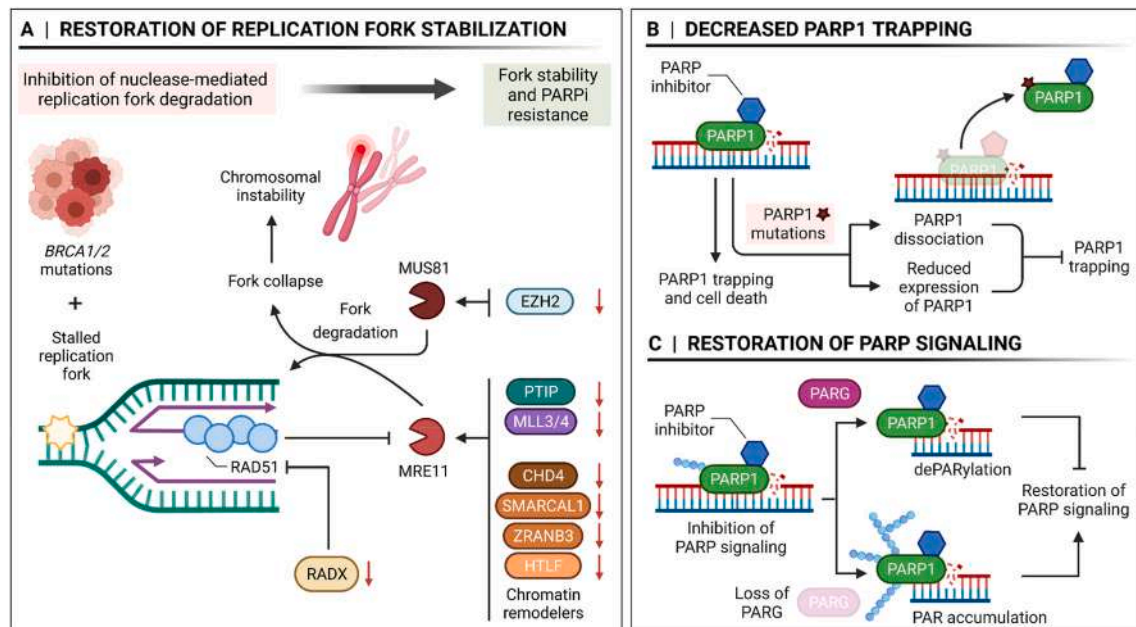


**Fig. 4.** Different modes of PARPi resistance in ovarian cancer. **A** | Restoration of stalled fork stabilization underlying PARPi resistance in *BRCA1/2*-mutated cancers. In OC cells, MRE11 and MUS81 nuclease-mediated fork degradation leads to destabilization of stalled replication forks. Nuclease recruitment and activity are facilitated by numerous proteins. Chromatin remodelers CHD4, SMARCA1, ZRANB3, H1TF, and MLL3–4/PTIP recruit MRE11 whereas EZH2 recruits MUS81. RAD51 antagonizes the protective role of RAD51-regulated nuclease inhibition. Loss of facilitators (↓) impairs nuclease-dependent fork degradation, leading to increased fork stabilization, and PARPi resistance. **B** | Decreased PARP1 trapping contributes to resistance to PARPi. Mutations in *PARP1* can result in reduced expression of PARP1 or increased dissociation of PARPi from the DNA damage site, limiting PARPi cytotoxicity. **C** | PARPi resistance induction through loss of PARG glycohydrolase.



recruitment of MRE11 nuclease to stalled replication forks, in turn, protecting nascent DNA strands from extensive degradation. Experiments were conducted on BRCA2-null embryonic stem cells (ESC), patients with BRCA1/2<sup>mut</sup> ovarian serous adenocarcinoma treated with platinum chemotherapy, ESC, and OC cell lines. Moreover, loss of PTIP conferred resistance to multiple DNA-damaging agents in BRCA-deficient cells [38].

Fork reversal by the chromatin remodelers SWI/SNF-related matrix-associated actin-dependent regulator of chromatin subfamily A-like protein 1 (SMARCA1), DNA annealing helicase, endonuclease ZRANB3, and helicase-like transcription factor (HLTF) is required for MRE11-dependent degradation of replication forks (Fig. 4A) [80]. Ataxia-telangiectasia and RAD3-related protein (ATR)-mediated phosphorylation of SMARCA1 serine at S652 regulates SMARCA1 and constitutes one pathway by which ATR maintains genome integrity during DNA replication [81]. Loss of the factors mediating nuclease-dependent fork degradation in BRCA1/2-deficient cells is pivotal in fork protection and PARPi resistance [38,66].

The activity of replication protein A (RPA)-like ssDNA binding protein, RADX, is another contributory factor to fork protection (Fig. 4A). A newly discovered protein, RADX has been shown to antagonize RAD51 activity. In cancer cells lacking BRCA2, RADX deletion led to re-establishment of fork protection without restoring homology-directed repair (HDR). Upon inactivation of RADX, excessive RAD51 activity slows replication elongation and causes DSBs. Thus, RADX acts as a regulator of RAD51 that functions at replication forks to maintain genome stability and is potentially an important determinant of chemosensitivity in cancer [82].

Interestingly, a recent study showed that restoration of replication fork protection in BRCA2-deficient HGSOc cells without recovery of HR conveys PARPi resistance. The researchers suggested that restoration of replication fork stability is associated with depletion of nucleosome remodeling factor, CHD4, in PEO1 cells (Fig. 4A) that results in inhibition of MRE11-mediated replication fork degradation [38]. Considerable efforts have been devoted to establishing the role of fork protection in OC cells. However, functional assays of DNA repair activity in organoids developed from HGSOc revealed no association of PARPi resistance with impaired replication fork protection. Results regarding the functionality of fork protection may be useful in predicting clinical response of cancer patients to PARPi, however studies were performed on organoids from only 20 patients displaying PARPi resistance [29]. Subsequently, Sanij and co-workers demonstrated that resistance to PARPi in HGSOc PDX models is a result of replication fork stabilization. In their study, CX-5461 exhibited significant therapeutic efficacy by overcoming fork protection via induction of MRE11 nuclease activity in OC cells with reduced responsiveness to olaparib [83].

#### 2.4. Reduced PARP1 trapping

The presence of functional PARP1 is essential for the PARPi mode of action that relies on PARP1 trapping at damaged DNA for induction of inhibitor cytotoxicity. A positive correlation between PARP1 expression and efficiency of a set of PARPi agents was confirmed in OC cell lines [84]. Consequently, acquired resistance to PARPi was correlated with decreased poly(ADP-ribose) (PAR) formation and PARP1 expression in OC cell lines (Fig. 4B) [85]. Moreover, knockdown of PARP1 with siRNA induced significant reduction of PARPi cytotoxicity in OVCAR8 cells [85]. CRISPR-Cas9-mediated induction of mutations in genes encoding PARP1 in BRCA1<sup>mut</sup> OC cells has been linked to emergence of a resistant phenotype, indicating that PARP1 activity is critical for sensitivity to talazoparib [86]. PARPi resistance has been established in clones of BRCA1<sup>mut</sup> COV362 OC cells with residual BRCA1 activity after induction of PARP1 mutations, including deletions involving residues neighboring K119 and Y848. A mutation of PARP1 resulting in nonsynonymous substitution (p.R591C) has been also detected in clinical settings in OC patients exhibiting intrinsic resistance to olaparib. Further investigation

revealed that the R591C mutation enhanced PARP1 dissociation from DNA and potentially decreased trapping in the presence of talazoparib relative to wild-type protein [86]. Resistance to numerous PARPi agents has been also identified in BRCA1<sup>mut</sup> and BRCA1 promoter-methylated OC cell lines with reduced expression of PARP1 as a result of directed gene deletion [87]. Our collective findings suggest that PARPi resistance is induced by inhibition of PARP1 trapping as a consequence of loss of drug-target expression.

#### 2.5. Restoration of PARP signaling and loss of PARG

PARP signaling is a component of the PARYlation system regulated by synthesizers and erasers of PAR. PARYlation is a post-translational protein modification that controls key cellular mechanisms, such as DNA damage response, as PAR chains loosen chromatin and facilitate recruitment of repair proteins. Covalent formation of PAR on target proteins is regulated by PARP and simultaneously, removal of PAR from PARYlated proteins is catalyzed by hydrolases, such as PARG [88]. Recent findings suggest that successful PARPi therapy at least partially depends on cellular PARG activity, and its loss reestablishes PARP1 signaling upon PARPi treatment (Fig. 4C). In general, PARP1 catalyzes self-PARYlation as well as that of other target proteins, which is a transient modification attributable to PARG glycohydrolase activity, resulting in PAR removal from target proteins [89]. PARPi agents induce a significant reduction in PARP1 enzymatic activity. However, the residual PARYlation ability of PARP1 remains intact. PARP signaling is further decreased by the action of PARG, which hydrolyzes PAR chains. Indeed, loss of PARG activity underlies partial maintenance of PARP1 signaling via inhibition of PAR degradation and PARPi resistance mechanisms. Lack of PARG has been shown to suppress PARP1 trapping on DNA through partial restoration of PARYlation. While the majority of earlier studies have been conducted in mammary tumor models, a correlation between decreased PARG expression and PARPi resistance is also reported in serous OC [90]. Reduced levels of PARG have been documented in HR-deficient HGSOc clones after selection with olaparib compared with sensitive parental cell lines [28]. Overall, PARG depletion serves as one of the HR-independent mechanisms of resistance to PARPi via re-introduction of PARP signaling [90]. On the other hand, in a recent study, loss of PARG activity induced by treatment with PARG inhibitor restored the formation of PAR chains and re-sensitized olaparib-resistant UWB1.289 (SYr12) OC cells [91].

#### 2.6. Role of the ATR/CHK1 pathway in PARP inhibitor resistance

In eukaryotic cells, errors and damage emerging during DNA replication contribute to replication stress, characterized by increased risk of DNA stress resulting in slowing or stalling of replication origins (known as replication forks). Therefore, the replicative stress response is activated by cells to maintain genome integrity. The emergence of physical structures typical of replication stress, such as ssDNA and stalled forks, initiates activation of DNA damage sensors including ATR protein kinases and effector proteins (Fig. 5) [65]. Generally, during replication stress in cancer cells, the presence of ssDNA initiates a response system based on ATR/CHK1 (checkpoint kinase 1) signaling [92]. The extensive role of ATR/CHK1 in DNA damage sensing and response is relatively well established. The ATR-mediated replication stress response involves initial recruitment of ATR and its partner co-factor ATR-interacting protein (ATRIP) to the damage site characterized by stretches of ssDNA, and subsequent activation of ATR major downstream effector kinase CHK1 via phosphorylation (Ser345) [93]. Activation of the ATR/CHK1 signaling pathway leads to global inhibition of cell cycle progression and local restoration of stalled replication forks, one of the previously described mechanisms responsible for PARPi resistance in OC [83,94]. Clarification of the role of the ATR/CHK1 axis in cancer response to replicative stress has led to the development of novel compounds targeting this pathway. Thus, one of the goals of effective therapeutic

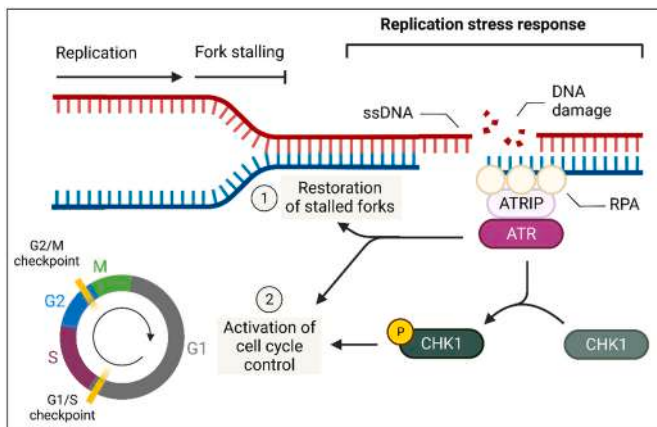


**Fig. 5.** Role of the ATR/CHK1 pathway in PARPi resistance. Replicative stress response mediated by ATR and CHK1 is induced by cell sensing machinery in the presence of ssDNA or stalled replication fork in response to DNA damage. Activation of the ATR/CHK1 axis leads to induction of cell cycle checkpoints and stabilization of the stalled fork.

strategies is to further enhance replication stress, fork stalling and collapse, and ultimately cell death [92].

## 2.7. Mechanisms under further exploration

In addition to the primary role of 53BP1 and BRCA1 in pathway choice between HR- and NHEJ-mediated DSB repair, recent reports have associated PARPi resistance with other factors contributing to regulation of this balance. The Ku complex (comprising Ku70 and Ku80 proteins), the main component of the NHEJ pathway, has been shown to play an important role in this phenomenon. Interestingly, in *BRCA1*-deficient OC cells, the Ku complex is downregulated by miRNA-622 during the S

phase, resulting in promotion of DSB repair by HR and olaparib resistance [95]. Defects in NHEJ have been linked to resistance to rucaparib in primary OC cultures of HR-deficient cells. Non-functional NHEJ is associated with reduced protein expression of Ku70, Ku80, and the catalytic subunit of DNA protein kinase, which are key factors recruited during NHEJ-mediated DSB repair [96]. More recent evidence suggests that upregulation of Wnt/ $\beta$ -catenin signaling confers PARPi resistance in HGSOC cell lines as well as the intraperitoneal PDX model. Furthermore, OC cells were re-sensitized to olaparib by co-administration of olaparib with pyruvium pamoate which downregulated  $\beta$ -catenin [97]. Intensified microhomology-mediated end joining (MMEJ) has also been shown to mediate PARPi resistance in *BRCA2*-deficient EOC. More specifically, it is suggested that upregulation of ALDH1A1, a member of the aldehyde dehydrogenase family, is driven by olaparib-induced overexpression of bromodomain-containing protein 4 (BRD4) and mediates resistance to PARPi through enhanced MMEJ activity. Interestingly, blockage of ALDH1A1 via specific inhibitors in the presence of olaparib is reported as an effective therapeutic approach in resistant cells in vitro as well as the olaparib-resistant PEO1 xenograft model. However, enhanced efficacy of olaparib in ALDH1A1-inhibited PARPi-resistant cells has been demonstrated only in cells possessing *BRCA2* mutations, a hallmark of HR deficiency, indicating dependence on MMEJ [98].

## 3. Overcoming resistance to PARP inhibitors

Regardless of intrinsic or acquired resistance, all patients considered PARPi resistant require appropriate treatment (Fig. 6). Knowledge of the mechanisms underlying PARPi resistance provide a starting point to overcome this phenomenon in OC. Various combinations of PARPi and other inhibitors are under investigation in clinical trials at present (Tables 3 and 4). The collective results should provide essential guidance for treatment of OC, including PARPi-resistant cases. In general, combination of PARPi with inhibitors targeting proteins involved in the DNA damage response is considered a promising approach to induce

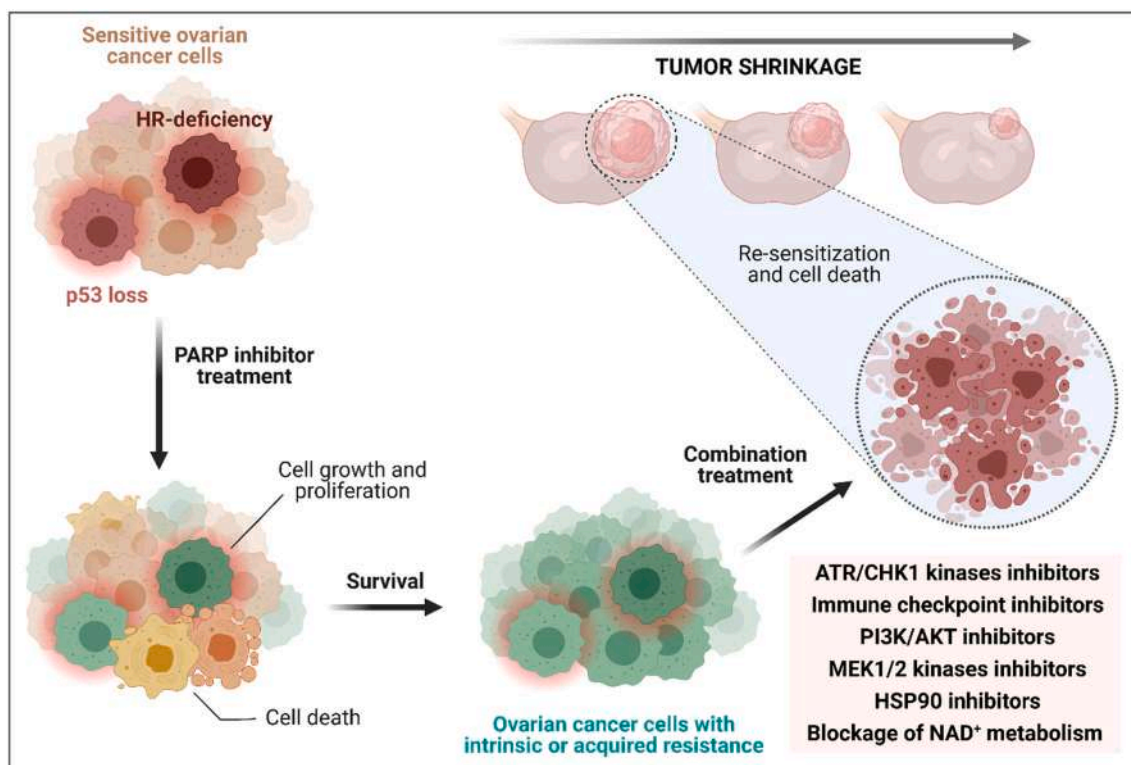


**Fig. 6.** Combination treatment options for ovarian cancer resistant to PARPi. Available targeted treatments to re-sensitize ovarian cancer cells to PARPi involve inhibition of ATR/CHK1 kinases.



**Table 3**

Overview of clinical trials assessing treatments for ovarian cancer patients resistant to PARP inhibitors.

Study name or identifier	Phase	Treatment	Participant's disease relevant to PARP inhibitor therapy	Key outcome measures	Study status
ComPAKT NCT02338622 [109]	I	Olaparib + Capivasertib (AZD5363, AKT inhibitor)	Specific malignant advanced solid tumors including <i>BRCA1/2</i> mutation HGSOc which progressed on PARP inhibitor monotherapy or HGSOc which may harbor HR defects	<ul style="list-style-type: none"> <li>– Safety and tolerability of the combination</li> <li>– MTD and recommended phase II dose of the combination</li> <li>– ORR</li> <li>– Pharmacokinetics</li> <li>– Exploratory biomarkers, including <i>BRCA</i> and PARP expression</li> </ul>	Completed (2017)
NCT04149145	I	Niraparib + M4344 (ATR inhibitor)	PARP inhibitor resistant recurrent OC	<ul style="list-style-type: none"> <li>– Emergence of adverse events</li> <li>– MTD of M4344 and niraparib</li> <li>– ORR</li> <li>– PFS (6 months)</li> </ul>	Not yet recruiting
NCT04586335	Ib	Olaparib + CYH33 (PI3K $\alpha$ inhibitor)	Advanced OC with acquired PARP inhibitor, or recurrent HGSOc, fallopian tube, and primary peritoneal cancer that are platinum-resistant or refractory	<ul style="list-style-type: none"> <li>– Dose limiting toxicities</li> <li>– ORR</li> <li>– Emergence of adverse events</li> <li>– DCR</li> <li>– Pharmacokinetics of CHY33 and olaparib</li> </ul>	Recruiting
NCT04267939	Ib	Niraparib + BAY1895344 (ATR inhibitor)	Advanced solid tumors, including OC after progression on PARP inhibitor	<ul style="list-style-type: none"> <li>– Emergence of adverse events</li> <li>– MTD of BAY1895344</li> <li>– ORR</li> <li>– DCR</li> <li>– Pharmacokinetics of BAY1895344</li> </ul>	Recruiting
NCT03586661	Ib	Niraparib and Copanlisib (PI3K inhibitor)	Endometrial, primary peritoneal, or fallopian tube cancer, or OC with a <i>BRCA</i> mutation that may have progressed on prior PARP inhibitor	<ul style="list-style-type: none"> <li>– MTD and recommended phase II dose of the combination</li> <li>– ORR</li> <li>– PFS (6 months)</li> <li>– Pharmacokinetics of the combination</li> </ul>	Recruiting
NCT03057145 [108]	I	Olaparib + Prexasertib (CHK1i)	Advanced solid tumors, including HGSOc with <i>BRCA1/2</i> mutation in the expansion cohort	<ul style="list-style-type: none"> <li>– MTD</li> <li>– Dose limiting toxicities</li> <li>– Pharmacokinetics</li> <li>– Anti-tumor activity</li> </ul>	Completed (2021)
NCT03162627	I/II	Olaparib + Selumetinib (MEK1/2 inhibitor)	Solid tumors that are advanced or recurrent, including ovarian tumors with PARPi resistance	<ul style="list-style-type: none"> <li>– MTD for combination</li> <li>– Dose expansion</li> <li>– Drug levels</li> <li>– Anti-tumor activity</li> </ul>	Recruiting
CAPRI NCT03462342	II	Olaparib + AZD6738 (ATRI)	Recurrent OC (platinum-sensitive or platinum-resistant, prior treatment with PARPi allowed if followed by disease progression)	<ul style="list-style-type: none"> <li>– Emergence of adverse events</li> <li>– PFS (2 years)</li> </ul>	Recruiting
NCT03579316	II	Olaparib + Adavosertib (WEE1 inhibitor) or Adavosertib alone	PARP inhibitor resistance (disease progression on PARP inhibitor therapy) or recurrent OC after completion of PARP inhibitor therapy	<ul style="list-style-type: none"> <li>– ORR</li> <li>– Disease control rate</li> </ul>	Recruiting

CR – complete response, DCR – disease control rate, MTD – maximally tolerated dose, ORR – overall response rate, PD – progressive disease, PFS – progression-free survival, PR – partial response, SD – stable disease.

synthetic lethality. One of the strategies to avoid diminished responsiveness to PARPi relies on preventing resistance before its occurrence via development of therapies that maintain PARPi effectiveness [99]. Alternative therapies may be developed as management options following PARPi progression. Currently, several clinical trials are underway to improve PARPi efficiency in combination with other small-molecule inhibitors that mainly target checkpoint kinases (Table 3).

Notably, basic strategies can also be applied to combat PARPi resistance. Resistance induced by risk of increased drug efflux can be counteracted using inhibitors with low affinity to PARP. A number of reports have shown that not all PARPi are P-gp substrates and neither does P-gp contribute to resistance to all known agents inhibiting PARP. Lawlor and co-workers proposed that veliparib is not a potential P-gp substrate [20]. One of the next-generation PARPi molecules, AZD2461, was developed as a poor substrate for the P-gp transporter to generate an efficacious inhibitor. The agent was shown to be potent against a *BRCA2*-deficient mouse breast cancer cell line with olaparib resistance overexpressing P-gp [100]. Interestingly, olaparib-resistant OC A2780 cells overexpressing P-gp were also sensitive to AZD2461 [21]. Further in vivo studies demonstrated efficacy of AZD2461 against tumors with ABCB1-induced resistance to olaparib [100]. However, the majority of

strategies developed to overcome PARPi resistance in the literature focused on reintroduction of HR dysfunction or dysregulation of cell cycle control.

### 3.1. Combination therapy targeting PARP1 and ATR/CHK1 pathways

Epithelial OC is characterized by loss of wild-type p53 activity, manifested by the occurrence of *TP53* mutations in 94–96% cases of HGSOc [101]. Around 50% HGSOc cases are considered HR-deficient due to numerous genetic abnormalities in the HR pathway [102]. The PARPi damaging mode of action in combination with targeting intrinsic perturbations in DNA repair or cell cycle regulation in OC cells is of significant research interest for development of combination therapies in view of their potential synergistic activity. These novel strategies target not only acquired resistance to PARPi but also aim to elicit responsiveness to PARPi in HR-proficient OC cells. Induction of DNA damage accumulation in cells with unbalanced repair mechanisms could potentially improve efficiency of PARPi and induce cell death.

Another approach to abolish PARPi resistance relies on exploiting OC vulnerabilities that develop concurrently with resistance. In cancer cells with restored HR and fork protection, acquired vulnerabilities comprise

**Table 4**

Clinical trials testing selected combinations of immune checkpoint inhibitor-based immunotherapies with PARP inhibitors for ovarian cancer patients.

Study name or identifier	Phase	Treatment	Features of participant's disease concerning ovarian cancer	Key outcome measures	Study status
NCT02571725	I/II	Olaparib + Tremelimumab (anti-CTLA-4 antibody)	Recurrent EOC with germline <i>BRCA1/2</i> mutation	<ul style="list-style-type: none"> <li>– Safety and efficacy of the combination</li> <li>– Recommended phase II dose of the combination</li> <li>– ORR, PFS</li> </ul>	Active, not recruiting
TOPACIO/ Keynote-162 NCT02657889	I/II	Niraparib + Pembrolizumab (anti-PD-1 antibody)	Any type of platinum-resistant, recurrent EOC (phase I) and platinum-resistant, recurrent HGSOC or endometrioid OC (phase II)	<ul style="list-style-type: none"> <li>– Safety and efficacy of the combination</li> <li>– Dose limiting toxicities</li> <li>– ORR, DCR, PFS, OS</li> <li>– Duration of response</li> <li>– Pharmacokinetics of niraparib during combination</li> </ul>	Active, not recruiting
NCT02953457	I/II	Olaparib + Durvalumab (anti-PD-L1 antibody) or Olaparib + Tremelimumab	Recurrent platinum-sensitive, resistant or refractory EOC with <i>BRCA1/2</i> mutation	<ul style="list-style-type: none"> <li>– Safety and efficacy of the combination</li> <li>– Dose limiting toxicities</li> <li>– PFS, OS</li> <li>– Changes in expression level of PD-L1 and tumor-infiltrating lymphocytes in tumor biopsies</li> </ul>	Active, not recruiting
NCT02484404	I/II	Durvalumab + Olaparib and/or Cediranib	Advanced or recurrent OC	<ul style="list-style-type: none"> <li>– Safety and efficacy of the combination</li> <li>– Recommended phase II dose of the combination</li> <li>– ORR, PFS</li> <li>– Pharmacokinetics of combinations</li> </ul>	Recruiting
MEDIOLA NCT02734004	I/II	Durvalumab + Olaparib or Olaparib and Bevacizumab	Advanced OC	<ul style="list-style-type: none"> <li>– Safety and efficacy of the combination</li> <li>– ORR, DCR, PFS, OS</li> <li>– Duration of response</li> <li>– Time treatment discontinuation, or death</li> <li>– Pharmacokinetics of combinations</li> </ul>	Active, not recruiting
NCT03740165	III	Chemotherapy + Pembrolizumab and maintenance Olaparib	Advanced EOC with non-mutated <i>BRCA1/2</i> (stage III or IV)	<ul style="list-style-type: none"> <li>– Safety and efficacy of the combination</li> <li>– PFS, OS</li> <li>– Emergence of adverse events</li> <li>– Time to first or second subsequent treatment, discontinuation of the study, or death</li> </ul>	Active, not recruiting
ANITA NCT03598270	III	Chemotherapy + Atezolizumab (anti-PD-L1 antibody) and maintenance Niraparib with or without Atezolizumab	Platinum-sensitive, relapsed EOC (stage III or IV)	<ul style="list-style-type: none"> <li>– ORR, PFS, OS</li> <li>– Duration of response</li> <li>– Emergence of adverse events</li> <li>– Time to first or second subsequent treatment, or death</li> <li>– PD-L1 and BRCA status</li> </ul>	Recruiting
NCT03522246	III	Rucaparib + Nivolumab (anti-PD-1 antibody) as maintenance	Newly diagnosed advanced EOC (stage III or IV)	<ul style="list-style-type: none"> <li>– Safety and efficacy of the combination</li> <li>– ORR, PFS, OS</li> <li>– Duration of response</li> <li>– Emergence of adverse events</li> </ul>	Active, not recruiting

DCR – disease control rate, ORR – overall response rate, OS – overall survival, PFS – progression-free survival.

reliance on RAD51 foci formation at the fork and BRCA2 recruitment at DNA damage sites [103]. Taking into consideration the ATR/CHK1 pathway that regulates HR, cell cycle control, and replication fork dynamics, inhibition of the axis in combination with PARPi presents an interesting approach to combat PARPi resistance. In general, inhibition of the ATR/CHK1 axis should bypass intra-S phase and G2/M cell cycle checkpoints. Eventually, in the presence of DNA strand breaks or stalled replication forks, cells enter mitosis under stress conditions with unrepaired damage, potentially leading to death [104,105]. Currently, numerous inhibitors of ATR and CHK1 are under investigation as potentially effective therapeutic agents in various cancer types. However, combinatorial therapies appear necessary in some regimens due to moderate efficiency of monotherapies and, in some cases, resistance to inhibition of CHK1 alone [105].

Studies attempting to overcome PARPi resistance in *BRCA1*<sup>mut</sup> cells showed that ATR plays a critical role in RAD51 foci formation in DSB sites, leading to cell survival. Inhibition of ATR with VE-821 has been shown to be effective in re-sensitizing *BRCA1*-deficient olaparib-

resistant OC cell lines and primary tumor cells from OC patients. Interestingly, VE-821 circumvented de novo resistance and acquired resistance to PARPi in vitro [103]. Additional experiments have confirmed that ATRi agents suppress PARPi resistance in OC [24,99]. Olaparib increased reliance of OC cells on the ATR/CHK1 pathway, as confirmed by increased phosphorylation of ATR and CHK1 in resistant cell lines [24]. Burgess et al. [106] showed that combination of olaparib with ATRi (VE-821) exerts synergistic effects in *BRCA1*<sup>mut</sup> OC cell lines both sensitive and resistant to olaparib. The preclinical efficacy of simultaneous administration of the ATRi ceralasertib (AZD6738) and olaparib has been demonstrated in the orthotopic HGSOC PDX model. Kim and co-workers reported that addition of ceralasertib to olaparib enhanced cytotoxicity and apoptosis relative to monotherapy in *BRCA*<sup>mut</sup> and *BRCA*<sup>wt</sup> OC cells. ATRi and olaparib exhibited a synergistic effect on tumor growth suppression in the *BRCA2*<sup>mut</sup> HGSOC PDX model [99]. Subsequently, combination of ATRi with olaparib showed efficacy in inducing complete regression of tumors in *BRCA2*<sup>mut</sup> PDX models of acquired resistance to PARPi relative to individual monotherapy

regimens [24].

CHK1, an ATR-dependent downstream effector protein, has been highlighted as a potential therapeutic target, since OC cells strongly rely on G2/M cell-cycle arrest regulated by CHK1 in *TP53*<sup>mut</sup> cells with disabled G1/S checkpoints. Earlier research efforts have focused on evaluating a combination of prexasertib, a CHK1 inhibitor, and olaparib in OC models. Co-treatment with prexasertib and olaparib induced synergistic cytotoxicity in the HGSOC cell line with *BRCA2* reversion mutation, a hallmark of PARPi resistance [107]. Combination of a CHK1 inhibitor with olaparib in further preclinical studies led to re-sensitization to PARPi in a *BRCA1*<sup>mut</sup> HGSOC PDX model [61]. In compliance with previous reports, combination of olaparib with another CHK1 inhibitor, MK-8776, increased sensitivity to olaparib in the PARPi-resistant *BRCA1*<sup>mut</sup> UWB1 OC cell line [106]. Results of phase 1 clinical trials evaluating simultaneous treatment with olaparib and prexasertib showed that *BRCA1*<sup>mut</sup> HGSOC patients with progression on prior PARPi treatment benefited from the combination regimen [108].

The collective findings suggest that PARPi-resistant cells depend more strongly on the ATR/CHK1 axis than sensitive cells and support the efficacy of combination strategies to overcome resistance [24,106]. DNA damage sensors, such as ATR and its downstream protein, CHK1, provide novel therapeutic targets for resistant OC.

### 3.2. Combined PARP inhibition and immune checkpoint therapy

Immunotherapy targeting immune checkpoint pathways has significantly contributed to the progress in treatment of several types of tumors. Immune checkpoint therapy is based on novel agents enhancing antitumor immunity, and attenuating the immunosuppressive micro-environment through checkpoint molecules, which are immune-cell surface receptors regulating the immune response. Currently, immunotherapy approaches employing single-agent blockage of immune checkpoints have shown modest efficacy in clinical trials for patients with OC, and are not yet approved for human use. However, this strategy is being under intensive development for OC, and has provided encouraging results as combination therapy with chemotherapy, radiation therapy, and PARP inhibitors [110,111]. One of the most promising immune checkpoint inhibitors (ICI) in OC target negative modulators of T cell activation involved in the attenuation of immune response against host's tumor, including cytotoxic T lymphocyte-associated protein 4 (CTLA-4) and programmed cell death 1 (PD-1) [112,113]. Immune checkpoint therapy has been extensively explored in OC since the discovery and development of monoclonal antibody-based ICI directed against inhibitory checkpoint molecules [114].

The rationale behind combining ICI with PARPi for treatment of OC arises from the findings that have demonstrated association between mutations in *BRCA1/2* and *TP53* with elevated expression of PD-1 and

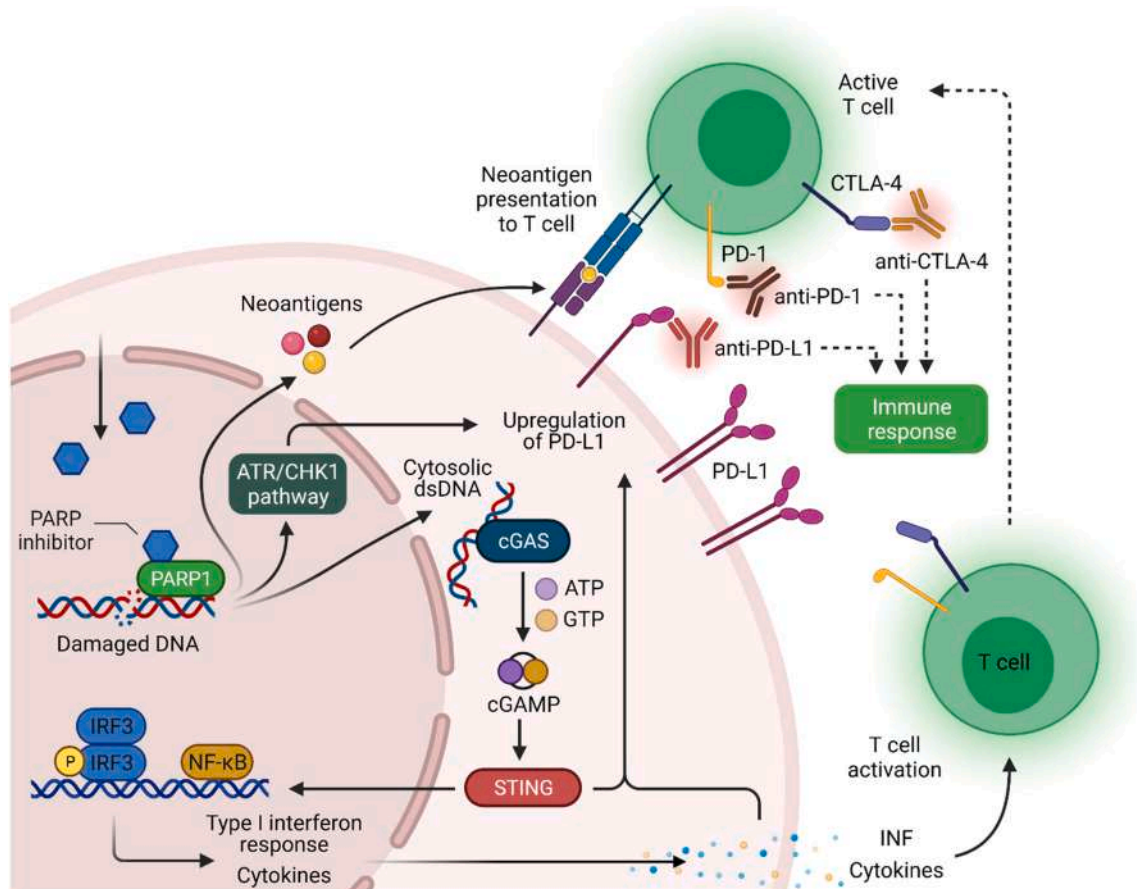


**Fig. 7.** Rationale for combining PARPi with immune checkpoint inhibitors highlighting association between DNA damage and the response of immune system in ovarian cancer. PARPi-mediated antitumor activity leads to release of tumor-derived dsDNA to cytoplasm, which can be detected by cytosolic cyclic GMP-AMP (cGAMP) synthase (cGAS). Once activated, cGAS synthesizes cGAMP triggering activation of stimulator of interferon (INF) genes (STING) pathway. Subsequently, genes encoding type I INF and inflammatory cytokines are induced by transcription factors – interferon regulatory factor 3 (IRF3) and nuclear factor kappa B (NF-κB). In turn, antitumor immune response may be initiated. Moreover, inhibition of PARP can stimulate immune response by increasing release of tumor neo-antigens, subsequently presented to T cells. PARPi also induce upregulation of PD-L1, either by promoting STING signaling or ATR/CHK1 pathway. Importantly, antibody-mediated immune checkpoint blockage targeting negative modulators of T cell activation, PD-1/PD-L1 axis and CTLA-4 negative co-stimulatory molecule, may be utilized to prolong PARPi activity [116–118,120].

programmed death-ligand 1 (PD-L1) in the cohort of patients with HGSOC [115]. Interestingly, recent studies have revealed that treatment with PARPi upregulate PD-L1 expression by activation of CHK1 in OC cells, leading to increased tumor susceptibility to co-administered agents targeting checkpoint molecules [116]. Moreover, PARPi-induced DNA damage promote tumor cell death and release of tumor-specific neoantigens, which may synergize in antitumor activity with ICI [117]. Promising synergism between PARPi and anti-PD-1 antibody has been reported in preclinical trials in *Brca1*-deficient murine OC model. It has also been presented that blockage of PD-1 may potentially prevent emergence of acquired resistance to PARPi after prolonged treatment [118]. In addition, synergistic antitumor effect was observed when niraparib was combined with anti-PD-1 therapy in various cancer cell models, including OC regardless of *BRCA* status [119]. Mechanism underlying correlation between DNA damage induced by PARPi and antitumor immune response in OC, which lays the foundation for combination of PARPi with ICI, was associated with activation of stimulator of interferon genes (STING) pathway (Fig. 7) [118,120]. Release of tumor dsDNA in response to treatment with PARPi is sensed by cyclic GMP-AMP (cGAMP) cGAMP synthetase (cGAS), which catalyzes production of second messenger cGAMP. In turn, expression of STING-regulated genes encoding type I interferons and proinflammatory cytokine can be induced, mediating antitumor immune response following treatment with PARPi [118]. Moreover, inhibition of PARP can upregulate expression of PD-L1 in OC cells potentially limiting PARPi efficacy, however, blockage of PD-1 was shown to prolong PARPi activity [118].

Currently, many ongoing trials are assessing usage of ICI in combination with various therapies in treatment of OC, including PARPi (Table 4). As an example, in a phase I/II TOPACIO/Keynote-162 trial safety and efficacy of combination therapy with niraparib and pembrolizumab, an anti-PD-1 antibody, has been evaluated in women with recurrent OC. Integrated response assessment has revealed promising results with ORR of about 18% in all platinum-resistance patients and subgroups regardless of *BRCA1/2* mutation or HRD status [121]. Data from a phase I/II MEDIOLA trial (NCT02734004), recruiting germline *BRCA1/2*<sup>mut</sup> participants with recurrent OC, showed that patients receiving combination of olaparib with durvalumab, anti-PD-L1 antibody, exhibited ORR of 72% and median PFS duration of 11.1 months [122]. Interestingly, the OC cohort from another study (NCT02484404) of mainly *BRCA*<sup>wt</sup> patients, accounting for 77% of enrolled women, showed to be less responsive to treatment with olaparib and durvalumab. In this single-center phase I/II trial co-administration of the drugs resulted in clinical benefit lasting over half a year for 30% of patients with recurrent OC. Moreover, participants had ORR of only 14% and a median PFS duration of 3.9 months [111]. Still, concurrent inhibition of PARP and blockage of immune-checkpoints is a promising approach for treatment of OC due to the suggestions that PARPi may improve response to ICI and upregulate antitumor immune activity [112,123]. Further results of ICI efficacy in OC are awaited with interest. Little is known about efficacy of various combination therapies with ICI in PARPi-resistant OC patients. However, few reports described above shed light on potential of combination of PARPi with ICI for avoiding resistance to PARPi [118,119].

### 3.3. Alternative combination strategies for overcoming resistance to PARP inhibitors

The phosphoinositide 3-kinase/AKT (PI3K/AKT) signaling pathway regulates key cellular processes in OC and contributes to cell survival. Inhibition of this pathway is correlated with reduced expression of *BRCA1/2* and HDR [124,125]. Suppression of PI3K/AKT signaling in combination with PARPi is a current focus of investigation as a strategy for control of PARPi resistance in a clinical setting. For instance, a completed phase I trial assessed disease response to a combination of olaparib and the AKT inhibitor, capivasertib, in a diverse cohort

including HGSOC patients. Their results showed that among eleven patients with advanced OC who achieved clinical benefits from the combination, four were PARPi-resistant. All patients with PARPi resistance that benefited from the treatment possessed *BRCA1* or *BRCA2* somatic mutations [109]. Several ongoing trials using PARPi in combination with inhibitors of PI3K (CYH33, copanlisib) are underway (NCT04586335, NCT03586661; Table 3).

Other groups have reported upregulation of the RAS/MAPK (mitogen-activated protein kinase) pathway in PARPi-resistant cell lines, as confirmed by the observation that PARPi and mitogen-activated protein kinase kinase (MEK) inhibitor (AZD6624) act synergistically to reverse acquired PARPi resistance. In view of this finding, combination of PARPi with MEK inhibitors has been highlighted as a potentially effective strategy for re-sensitization of PARPi-resistant cells [85]. Active phase I/II clinical trials (NCT03162627) on a combination of MEK1/2 inhibitor (selumetinib) and olaparib are currently underway in patients diagnosed with various solid tumors, including OC resistant to PARPi.

High expression of heat shock proteins (HSP), stress responsive molecules, has been observed in numerous types of cancers, including OC [126]. Overexpression of HSP27, HSP60, HSP70 and especially HSP90, has been linked to tumor aggressiveness metastasis, resistance to chemotherapeutics, and was correlated with poor prognosis in OC. For that reason, many studies consider HSP as ideal therapeutic targets for effective cancer therapy [127]. In the context of combined therapy with PARPi and HSP inhibitors, particular attention is paid to inhibitors of HSP90. Potential use of HSP90 inhibition has been based on the discovery of HSP90 role in stabilization of proteins involved in DNA damage repair and cell cycle checkpoint, including CHK1, *BRCA1*, *BRCA2*, *RAD51*, and *MRE11*. Therefore, blockage of HSP90 was suggested to abrogate HR-mediated resistance to PARPi. For instance, researchers have demonstrated that 17-AAG (17-allylamino-17-demethoxygeldanamycin) sensitized HR-proficient OC cell lines to olaparib via suppression of HR. Importantly, 17-AAG downregulated *BRCA1* and *RAD51* protein levels and reduced *RAD51* foci formation in OC cells with functional HR [128]. Moreover, treatment with HSP90 inhibitor ganetespib and PARPi talazoparib exerted synergistic antitumor activity in HR-proficient HGSOC cell lines [129]. Preclinical data demonstrated that inhibition of HSP90 with onalespib (AT13387) restrained tumor growth in 57% of PDX models of HGSOC. Interestingly, the efficacy of combination has been also confirmed in one PARPi-resistant model with mutation in *BRCA1* [130]. HSP90 has been also targetable by onalespib in combination with olaparib in an ongoing phase I trial (NCT02898207) designed to evaluate side effects and best dose in various solid tumors, including recurrent EOC.

Targeting nicotinamide adenine dinucleotide (NAD) metabolism has been proposed as another promising combination approach for treatment of OC with PARPi, since PARP signaling affects cellular energy homeostasis by consumption of oxidized form of NAD (NAD<sup>+</sup>) for PARylation of target proteins, and other intracellular events. Notably, DNA damage-induced hyperactivation of PARP1 was suggested to drive deprivation of NAD<sup>+</sup> and ATP, requiring replenishment through metabolic shift to oxidative phosphorylation over glycolysis sustaining cell survival [131]. On the other hand, the study by Lahiguera et al. indicated that shift to a more glycolytic metabolism was associated with olaparib resistance in OC cells. Furthermore, blockage of pyruvate dehydrogenase (PDH) kinase with dichloroacetate resulted in restoration of PDH activity, increased oxidative phosphorylation and enhanced sensitivity to olaparib. Thus, metabolic profile of tumor cells can be associated with sensitivity to olaparib [132]. The co-administration of PARPi with agents limiting production of NAD<sup>+</sup> may have implications in cancer treatment. For instance, inhibition of nicotinamide phosphoribosyltransferase (NAMPT), an enzyme catalyzing the rate-determining step for biosynthesis of NAD<sup>+</sup>, with concurrent olaparib treatment additively suppressed the growth of breast tumor [133]. To date, modulation of NAD<sup>+</sup> metabolism in combination with PARP



inhibition has been poorly assessed in OC. However, recent studies have indicated that blockage of NAD<sup>+</sup> metabolism with NAMPT inhibitor FK866 can inhibit growth of OC cells both in vitro and in vivo [134,135].

# 4. Conclusions

The emerging success of PARPi has led to significant alterations in treatment settings for EOC patients, with rapid expansion of the use of these agents in the clinic. Despite the effectiveness of PARPi, resistance to applied treatments is relatively common and remains a considerable clinical challenge. Resistance may develop rapidly, even from the starting point of the initial regimen, since PARPi agents have been recommended earlier in recent years during the treatment course as front-line maintenance therapy [136]. With the increasing usage of these novel drugs, the number of PARPi-resistant cases is also expected to increase, highlighting the importance of developing efficient strategies to overcome resistance. Successful treatment of resistant OC may be effectively based on characterization of molecular biomarkers assessed via non-invasive tumor liquid biopsy using ctDNA. This method of detection of mutations and promoter methylation in HR repair genes driving resistance should benefit patients in clinical practice as it allows deployment of evidence-based monitoring of disease progression and implementation of putative treatment options [27].

In conclusion, combination treatment of PARPi with novel inhibitors presents a promising approach to improve the efficacy of single-agent therapy, especially in patients with OC showing therapeutic resistance, and warrants more comprehensive investigation.

# Author contributions

Lukasz Biegała: Conceptualization, Writing - Original Draft, Visualization. Arkadiusz Gajek: Conceptualization, Writing - Original Draft, Visualization. Agnieszka Marczak: Writing - Original Draft, Supervision. Aneta Rogalska: Conceptualization, Writing - Original Draft, Funding acquisition, Supervision.

# Funding

This work was funded by the National Science Centre, Poland (Project grant number: Sonata Bis 2019/34/E/NZ7/00056).

# Declaration of Competing Interest

The authors declare no conflicts of interest.

# Acknowledgment

Figures have been created with [BioRender.com](#).

# References

- [1] R.L. Siegel, et al., Cancer statistics, 2021, *CA Cancer J. Clin.* 71 (1) (2021) 7–33, <https://doi.org/10.3322/caac.21654>.
- [2] N. Terraneo, et al., Novel therapeutic strategies for ovarian cancer stem cells, *Front. Oncol.* 10 (2020) 319, <https://doi.org/10.3389/fonc.2020.00319>.
- [3] E.J. Pavlik, et al., Disease-specific survival of type I and type II epithelial ovarian cancers-stage challenges categorical assignments of indolence & aggressiveness, *Diagnostics (Basel)* 10 (2) (2020), <https://doi.org/10.3390/diagnostics10020056>.
- [4] A.M. Oza, et al., Standard chemotherapy with or without bevacizumab for women with newly diagnosed ovarian cancer (ICON7): overall survival results of a phase 3 randomised trial, *Lancet Oncol.* 16 (8) (2015) 928–936, [https://doi.org/10.1016/s1470-2045\(15\)00086-8](https://doi.org/10.1016/s1470-2045(15)00086-8).
- [5] I. Tsioulak, A.G. Zeimet, C. Marth, Hopes and failures in front-line ovarian cancer therapy, *Crit. Rev. Oncol. Hematol.* 143 (2019) 14–19, <https://doi.org/10.1016/j.critrevonc.2019.08.002>.
- [6] D. Lorusso, et al., Newly diagnosed ovarian cancer: which first-line treatment? *Cancer Treat. Rev.* 91 (2020), 102111 <https://doi.org/10.1016/j.ctrv.2020.102111>.
- [7] R. Pokhriyal, et al., Chemotherapy resistance in advanced ovarian cancer patients. *Biomark. Cancer* 11 (2019) <https://doi.org/10.1177/1179299X19860815>, p. 1179299X19860815.
- [8] A. Chandra, et al., Ovarian cancer: current status and strategies for improving therapeutic outcomes, *Cancer Med.* 8 (16) (2019) 7018–7031, <https://doi.org/10.1002/cam4.2560>.
- [9] U.A. Matulonis, et al., Olaparib maintenance therapy in patients with platinum-sensitive, relapsed serous ovarian cancer and a BRCA1/2 mutation: overall survival adjusted for postprogression poly(adenosine diphosphate ribose) polymerase inhibitor therapy, *Cancer* 122 (12) (2016) 1844–1852, <https://doi.org/10.1002/cncr.29995>.
- [10] E. Pujade-Lauraine, et al., Olaparib tablets as maintenance therapy in patients with platinum-sensitive, relapsed ovarian cancer and a BRCA1/2 mutation (SOLO2/ENGOT-Ov21): a double-blind, randomised, placebo-controlled, phase 3 trial, *Lancet Oncol.* 18 (9) (2017) 1274–1284, [https://doi.org/10.1016/S1470-2045\(17\)30469-2](https://doi.org/10.1016/S1470-2045(17)30469-2).
- [11] A.J. Cortez, et al., Advances in ovarian cancer therapy, *Cancer Chemother. Pharmacol.* 81 (1) (2018) 17–38, <https://doi.org/10.1007/s00280-017-3501-8>.
- [12] W.P. Tew, et al., PARP Inhibitors in the management of ovarian cancer: ASCO guideline, *J. Clin. Oncol.* 38 (30) (2020) 3468–3493, <https://doi.org/10.1200/JCO.20.01924>.
- [13] M.R. Mirza, et al., The forefront of ovarian cancer therapy: update on PARP inhibitors, *Ann. Oncol.* 31 (9) (2020) 1148–1159, <https://doi.org/10.1016/j.annonc.2020.06.004>.
- [14] J. Mateo, et al., A decade of clinical development of PARP inhibitors in perspective, *Ann. Oncol.* 30 (9) (2019) 1437–1447, <https://doi.org/10.1093/annonc/mdz192>.
- [15] E. Franzese, et al., PARP inhibitors in ovarian cancer, *Cancer Treat. Rev.* 73 (2019) 1–9, <https://doi.org/10.1016/j.ctrv.2018.12.002>.
- [16] H. Li, et al., PARP inhibitor resistance: the underlying mechanisms and clinical implications, *Mol. Cancer* 19 (1) (2020) 107, <https://doi.org/10.1186/s12943-020-01227-0>.
- [17] A. Gonzalez-Martin, et al., Niraparib in patients with newly diagnosed advanced ovarian cancer, *N. Engl. J. Med.* 381 (25) (2019) 2391–2402, <https://doi.org/10.1056/NEJMoa1910962>.
- [18] A.C. Jaramillo, et al., How to overcome ATP-binding cassette drug efflux transporter-mediated drug resistance? *Cancer Drug Resist.* 1 (1) (2018) 6–29, <https://doi.org/10.20517/cdr.2018.02>.
- [19] S. Rottenberg, et al., High sensitivity of BRCA1-deficient mammary tumors to the PARP inhibitor AZD2281 alone and in combination with platinum drugs, *Proc. Natl. Acad. Sci. U. S. A.* 105 (44) (2008) 17079–17084, <https://doi.org/10.1073/pnas.0806092105>.
- [20] D. Lawlor, et al., PARP inhibitors as P-glycoprotein substrates, *J. Pharm. Sci.* 103 (6) (2014) 1913–1920, <https://doi.org/10.1002/jps.23952>.
- [21] A. Vaidyanathan, et al., ABCB1 (MDR1) induction defines a common resistance mechanism in paclitaxel- and olaparib-resistant ovarian cancer cells, *Br. J. Cancer* 115 (4) (2016) 431–441, <https://doi.org/10.1038/bjc.2016.203>.
- [22] K. Bukowski, M. Kciuk, R. Kontek, Mechanisms of multidrug resistance in cancer chemotherapy, *Int. J. Mol. Sci.* 21 (9) (2020), <https://doi.org/10.3390/ijms21093233>.
- [23] L. Andrei, et al., Advanced technological tools to study multidrug resistance in cancer, *Drug Resist. Updat.* 48 (2020), 100658, <https://doi.org/10.1016/j.drug.2019.100658>.
- [24] H. Kim, et al., Combining PARP with ATR inhibition overcomes PARP inhibitor and platinum resistance in ovarian cancer models, *Nat. Commun.* 11 (1) (2020) 3726, <https://doi.org/10.1038/s41467-020-17127-2>.
- [25] E.L. Christie, et al., Multiple ABCB1 transcriptional fusions in drug resistant high-grade serous ovarian and breast cancer, *Nat. Commun.* 10 (1) (2019), <https://doi.org/10.1038/s41467-019-09312-9>.
- [26] S. Durmus, et al., Breast cancer resistance protein (BCRP/ABCG2) and P-glycoprotein (P-GP/ABCB1) restrict oral availability and brain accumulation of the PARP inhibitor rucaparib (AG-014699), *Pharm. Res.* 32 (1) (2015) 37–46, <https://doi.org/10.1007/s11095-014-1442-z>.
- [27] S. Lheureux, et al., EVOLVE: a multicenter open-label single-arm clinical and translational phase II trial of cediranib plus olaparib for ovarian cancer after PARP inhibition progression, *Clin. Cancer Res.* 26 (16) (2020) 4206–4215, <https://doi.org/10.1158/1078-0432.CCR-19-4121>.
- [28] M.K. Gomez, et al., Identifying and overcoming mechanisms of PARP inhibitor resistance in homologous recombination repair-deficient and repair-proficient high grade serous ovarian cancer cells, *Cancers* 12 (6) (2020) 1503, <https://doi.org/10.3390/cancers12061503>.
- [29] S.J. Hill, et al., Prediction of DNA repair inhibitor response in short-term patient-derived ovarian cancer organoids, *Cancer Discov.* 8 (11) (2018) 1404–1421, <https://doi.org/10.1158/2159-8290.CD-18-0474>.
- [30] M.J. Wakefield, et al., Diverse mechanisms of PARP inhibitor resistance in ovarian cancer, *Biochim. Biophys. Acta* 1872 (2) (2019), 188307, <https://doi.org/10.1016/j.bbcan.2019.08.002>.
- [31] O. Kondrashova, et al., Secondary somatic mutations restoring RAD51C and RAD51D associated with acquired resistance to the PARP inhibitor rucaparib in high-grade ovarian carcinoma, *Cancer Discov.* 7 (9) (2017) 984–998, <https://doi.org/10.1158/2159-8290.CD-17-0419>.
- [32] R.M. Hurley, et al., 53BP1 as a potential predictor of response in PARP inhibitor-treated homologous recombination-deficient ovarian cancer, *Gynecol. Oncol.* 153 (1) (2019) 127–134, <https://doi.org/10.1016/j.ygyno.2019.01.015>.

- [33] M. Chiappa, et al., Overcoming PARPi resistance: preclinical and clinical evidence in ovarian cancer, *Drug Resist. Updat.* 55 (2021), 100744, <https://doi.org/10.1016/j.drug.2021.100744>.
- [34] J.A. Ledermann, Y. Drew, R.S. Kristeleit, Homologous recombination deficiency and ovarian cancer, *Eur. J. Cancer* 60 (2016) 49–58, <https://doi.org/10.1016/j.ejca.2016.03.005>.
- [35] K. Matsumoto, et al., PARP inhibitors for BRCA wild type ovarian cancer; gene alterations, homologous recombination deficiency and combination therapy, *Jpn. J. Clin. Oncol.* 49 (8) (2019) 703–707, <https://doi.org/10.1093/jco/hyz090>.
- [36] S.L. Jacob, L.A. Kiedrowski, Y.K. Chae, The dynamic landscape of BRCA1 reversion mutations from indel to SNV in a patient with ovarian cancer treated with PARP-inhibitors and immunotherapy, *Heliyon* 6 (5) (2020), e03841, <https://doi.org/10.1016/j.heliyon.2020.e03841>.
- [37] T.C. Nepomuceno, et al., The Role of PALB2 in the DNA damage response and cancer predisposition, *Int. J. Mol. Sci.* 18 (9) (2017), <https://doi.org/10.3390/ijms18091886>.
- [38] A. Ray Chaudhuri, et al., Replication fork stability confers chemoresistance in BRCA-deficient cells, *Nature* 535 (7612) (2016) 382–387, <https://doi.org/10.1038/nature18325>.
- [39] Cancer Genome Atlas Research, Integrated genomic analyses of ovarian carcinoma, *Nature* 474 (7353) (2011) 609–615, <https://doi.org/10.1038/nature10166>.
- [40] E. Aref-Eshghi, et al., Genetic and epigenetic profiling of BRCA1/2 in ovarian tumors reveals additive diagnostic yield and evidence of a genomic BRCA1/2 DNA methylation signature, *J. Hum. Genet.* 65 (10) (2020) 865–873, <https://doi.org/10.1038/s10038-020-0780-4>.
- [41] L. Tobalina, et al., A meta-analysis of reversion mutations in BRCA genes identifies signatures of DNA end-joining repair mechanisms driving therapy resistance, *Ann. Oncol.* 32 (1) (2021) 103–112, <https://doi.org/10.1016/j.annonc.2020.10.470>.
- [42] L.J. Barber, et al., Secondary mutations in BRCA2 associated with clinical resistance to a PARP inhibitor, *J. Pathol.* 229 (3) (2013) 422–429, <https://doi.org/10.1002/path.4140>.
- [43] A.M. Patch, et al., Whole-genome characterization of chemoresistant ovarian cancer, *Nature* 521 (7553) (2015) 489–494, <https://doi.org/10.1038/nature14410>.
- [44] K.K. Lin, et al., BRCA reversion mutations in circulating tumor DNA predict primary and acquired resistance to the PARP inhibitor rucaparib in high-grade ovarian carcinoma, *Cancer Discov.* 9 (2) (2019) 210–219, <https://doi.org/10.1158/2159-8290.CD-18-0715>.
- [45] E.M. Swisher, et al., Molecular and clinical determinants of response and resistance to rucaparib for recurrent ovarian cancer treatment in ARIEL2 (Parts 1 and 2), *Nat. Commun.* 12 (1) (2021) 2487, <https://doi.org/10.1038/s41467-021-22582-6>.
- [46] S.S. Bernards, et al., Clinical characteristics and outcomes of patients with BRCA1 or RAD51C methylated versus mutated ovarian carcinoma, *Gynecol. Oncol.* 148 (2) (2018) 281–285, <https://doi.org/10.1016/j.ygyno.2017.12.004>.
- [47] A. Catteau, et al., Methylation of the BRCA1 promoter region in sporadic breast and ovarian cancer: correlation with disease characteristics, *Oncogene* 18 (11) (1999) 1957–1965, <https://doi.org/10.1038/sj.onc.1202509>.
- [48] T. Bianco, et al., Tumour-specific distribution of BRCA1 promoter region methylation supports a pathogenetic role in breast and ovarian cancer, *Carcinogenesis* 21 (2) (2000) 147–151, <https://doi.org/10.1093/carcin/21.2.147>.
- [49] O. Kondrashova, et al., Methylation of all BRCA1 copies predicts response to the PARP inhibitor rucaparib in ovarian carcinoma, *Nat. Commun.* 9 (1) (2018) 3970, <https://doi.org/10.1038/s41467-018-0564-z>.
- [50] E. Franzese, et al., Genomic profile and BRCA-1 promoter methylation status in BRCA mutated ovarian cancer: new insights in predictive biomarkers of olaparib response, *Front. Oncol.* 9 (2019) 1289, <https://doi.org/10.3389/fonc.2019.01289>.
- [51] Y. Wang, et al., The BRCA1-Δ11q alternative psplice isoform bypasses germline mutations and promotes therapeutic resistance to PARP inhibition and cisplatin, *Cancer Res.* 76 (9) (2016) 2778–2790, <https://doi.org/10.1158/0008-5472.can-16-0186>.
- [52] K.P. Bhat, D. Cortez, RPA and RAD51: fork reversal, fork protection, and genome stability, *Nat. Struct. Mol. Biol.* 25 (6) (2018) 446–453, <https://doi.org/10.1038/s41594-018-0075-z>.
- [53] J. Renkawitz, C.A. Lademann, S. Jentsch, Mechanisms and principles of homology search during recombination, *Nat. Rev. Mol. Cell Biol.* 15 (6) (2014) 369–383, <https://doi.org/10.1038/nrm3805>.
- [54] H. Song, et al., Contribution of germline mutations in the RAD51B, RAD51C, and RAD51D genes to ovarian cancer in the population, *J. Clin. Oncol.* 33 (26) (2015) 2901–2907, <https://doi.org/10.1200/JCO.2015.61.2408>.
- [55] K.E. Clements, et al., Identification of regulators of poly-ADP-ribose polymerase inhibitor response through complementary CRISPR knockout and activation screens, *Nat. Commun.* 11 (1) (2020) 6118, <https://doi.org/10.1038/s41467-020-19961-w>.
- [56] J. Tan, et al., C/EBPβ promotes poly(ADP-ribose) polymerase inhibitor resistance by enhancing homologous recombination repair in high-grade serous ovarian cancer, *Oncogene* (2021), <https://doi.org/10.1038/s41388-021-01788-4>.
- [57] M.R. Sullivan, K.A. Bernstein, RAD-ical new insights into RAD51 regulation, *Genes (Basel)* 9 (12) (2018), <https://doi.org/10.3390/genes9120629>.
- [58] J.E. Jaspers, et al., Loss of 53BP1 causes PARP inhibitor resistance in Brca1-mutated mouse mammary tumors, *Cancer Discov.* 3 (1) (2013) 68–81, <https://doi.org/10.1158/2159-8290.CD-12-0049>.
- [59] Z.M. Yang, et al., Combining 53BP1 with BRCA1 as a biomarker to predict the sensitivity of poly(ADP-ribose) polymerase (PARP) inhibitors, *Acta Pharmacol. Sin.* 38 (7) (2017) 1038–1047, <https://doi.org/10.1038/aps.2017.8>.
- [60] H. Dev, et al., Shieldin complex promotes DNA end-joining and counters homologous recombination in BRCA1-null cells, *Nat. Cell Biol.* 20 (8) (2018) 954–965, <https://doi.org/10.1038/s41556-018-0140-1>.
- [61] K. Parmar, et al., The CHK1 inhibitor prexasertib exhibits monotherapy activity in high-grade serous ovarian cancer models and sensitizes to PARP inhibition, *Clin. Cancer Res.* 25 (20) (2019) 6127–6140, <https://doi.org/10.1158/1078-0432.CCR-19-0448>.
- [62] M.S. Luijsterburg, et al., A PALB2-interacting domain in RNF168 couples homologous recombination to DNA break-induced chromatin ubiquitylation, *Elife* 6 (2017), <https://doi.org/10.7554/eLife.20922>.
- [63] D. Zong, et al., BRCA1 haploinsufficiency is masked by RNF168-mediated chromatin ubiquitylation, *Mol. Cell* 73 (6) (2019) 1267–1281, <https://doi.org/10.1016/j.molcel.2018.12.010>, e7.
- [64] S. Panier, S.J. Boulton, Double-strand break repair: 53BP1 comes into focus, *Nat. Rev. Mol. Cell Biol.* 15 (1) (2014) 7–18, <https://doi.org/10.1038/nrm3719>.
- [65] M.K. Zeman, K.A. Cimprich, Causes and consequences of replication stress, *Nat. Cell Biol.* 16 (1) (2014) 2–9, <https://doi.org/10.1038/ncb2897>.
- [66] H. Liao, et al., Mechanisms for stalled replication fork stabilization: new targets for synthetic lethality strategies in cancer treatments, *EMBO Rep.* 19 (9) (2018), <https://doi.org/10.15252/embr.201846263>.
- [67] C. Rice, E. Skordalakis, Structure and function of the telomeric CST complex, *Comput. Struct. Biotechnol. J.* 14 (2016) 161–167, <https://doi.org/10.1016/j.csbj.2016.04.002>.
- [68] Z. Mirman, et al., 53BP1-RIF1-shieldin counteracts DSB resection through CST- and Polapha-dependent fill-in, *Nature* 560 (7716) (2018) 112–116, <https://doi.org/10.1038/s41586-018-0324-7>.
- [69] M. McMullen, et al., Overcoming platinum and PARP-inhibitor resistance in ovarian cancer, *Cancers (Basel)* 12 (6) (2020), <https://doi.org/10.3390/cancers12061607>.
- [70] P.S. Patel, et al., RNF168 regulates R-loop resolution and genomic stability in BRCA1/2-deficient tumors, *J. Clin. Invest.* 131 (3) (2021), <https://doi.org/10.1172/JCI140105>.
- [71] Y.J. He, et al., DYNLL1 binds to MRE11 to limit DNA end resection in BRCA1-deficient cells, *Nature* 563 (7732) (2018) 522–526, <https://doi.org/10.1038/s41586-018-0670-5>.
- [72] S. Karakashev, et al., CARM1-expressing ovarian cancer depends on the histone methyltransferase EZH2 activity, *Nat. Commun.* 9 (1) (2018) 631, <https://doi.org/10.1038/s41467-018-03031-3>.
- [73] S. Karakashev, EZH2 inhibition sensitizes CARM1-high, homologous recombination proficient ovarian cancers to PARP inhibition, *Cancer Cell* 37 (2) (2020) 157–167, <https://doi.org/10.1016/j.ccell.2019.12.015>, e6.
- [74] Y. Chen, H. Du, The promising PARP inhibitors in ovarian cancer therapy: from Olaparib to others, *Biomed. Pharmacother.* 99 (2018) 552–560, <https://doi.org/10.1016/j.biopha.2018.01.094>.
- [75] W. Feng, M. Jasin, Homologous recombination and replication fork protection: BRCA2 and more!, *Cold Spring Harb. Symp. Quant. Biol.* 82 (2017) 329–338, <https://doi.org/10.1101/sqb.2017.82.035006>.
- [76] K. Rickman, A. Smogorzewska, Advances in understanding DNA processing and protection at stalled replication forks, *J. Cell Biol.* 218 (4) (2019) 1096–1107, <https://doi.org/10.1083/jcb.201809012>.
- [77] G.E. Ronson, et al., PARP1 and PARP2 stabilise replication forks at base excision repair intermediates through Fbh1-dependent Rad51 regulation, *Nat. Commun.* 9 (1) (2018) 746, <https://doi.org/10.1038/s41467-018-03159-2>.
- [78] X. Lyu, et al., Human CST complex protects stalled replication forks by directly blocking MRE11 degradation of nascent-strand DNA, *EMBO J.* 40 (2) (2021), e103654, <https://doi.org/10.15252/emboj.2019103654>.
- [79] B. Rondinelli, et al., EZH2 promotes degradation of stalled replication forks by recruiting MUS81 through histone H3 trimethylation, *Nat. Cell Biol.* 19 (11) (2017) 1371–1378, <https://doi.org/10.1038/ncb3626>.
- [80] A. Tagliatela, et al., Restoration of replication fork stability in BRCA1- and BRCA2-deficient cells by inactivation of SNF2-family fork remodelers, *Mol. Cell* 68 (2) (2017) 414–430 e8, <https://doi.org/10.1016/j.molcel.2017.09.036>.
- [81] F.B. Couch, et al., ATR phosphorylates SMARCA1 to prevent replication fork collapse, *Genes Dev.* 27 (14) (2013) 1610–1623, <https://doi.org/10.1101/gad.214080.113>.
- [82] H. Dugrawala, et al., RADX promotes genome stability and modulates chemosensitivity by regulating RAD51 at replication forks, *Mol. Cell* 67 (3) (2017) 374–386, <https://doi.org/10.1016/j.molcel.2017.06.023>, e5.
- [83] E. Sanji, et al., CX-5461 activates the DNA damage response and demonstrates therapeutic efficacy in high-grade serous ovarian cancer, *Nat. Commun.* 11 (1) (2020), <https://doi.org/10.1038/s41467-020-16393-4>.
- [84] M. Makvandi, et al., A radiotracer strategy to quantify PARP-1 expression in vivo provides a biomarker that can enable patient selection for PARP inhibitor therapy, *Cancer Res.* 76 (15) (2016) 4516–4524, <https://doi.org/10.1158/0008-5472.CAN-16-0416>.
- [85] C. Sun, et al., Rational combination therapy with PARP and MEK inhibitors capitalizes on therapeutic liabilities in RAS mutant cancers, *Sci. Transl. Med.* 9 (392) (2017), <https://doi.org/10.1126/scitranslmed.aal5148>.
- [86] S.J. Pettitt, et al., Genome-wide and high-density CRISPR-Cas9 screens identify point mutations in PARP1 causing PARP inhibitor resistance, *Nat. Commun.* 9 (1) (2018), <https://doi.org/10.1038/s41467-018-03917-2>.

- [87] M. Makvandi, et al., A PET imaging agent for evaluating PARP-1 expression in ovarian cancer, *J. Clin. Invest.* 128 (5) (2018) 2116–2126, <https://doi.org/10.1172/JCI97992>.
- [88] T. Kamaletdinova, Z. Fanaei-Kahrani, Z.-Q. Wang, The enigmatic function of PARP1: from PARYlation activity to PAR readers, *Cells* 8 (12) (2019) 1625, <https://doi.org/10.3390/cells8121625>.
- [89] P. Francia, S. Rottenberg, Mechanisms of PARP inhibitor resistance in cancer and insights into the DNA damage response, *Genome Med.* 10 (1) (2018) 101, <https://doi.org/10.1186/s13073-018-0612-8>.
- [90] E. Gogola, et al., Selective loss of PARG restores PARYlation and counteracts PARP inhibitor-mediated synthetic lethality, *Cancer Cell* 35 (6) (2019) 950–952, <https://doi.org/10.1016/j.ccell.2019.05.012>.
- [91] S.H. Chen, X. Yu, Targeting dePARYlation selectively suppresses DNA repair-defective and PARP inhibitor-resistant malignancies, *Sci. Adv.* 5 (4) (2019), <https://doi.org/10.1126/sciadv.aav4340> p. eaav4340.
- [92] J. Zhang, et al., Targeting DNA replication stress for cancer therapy, *Genes* 7 (8) (2016) 51, <https://doi.org/10.3390/genes7080051>.
- [93] A.N. Blackford, S.P. Jackson, ATM, ATR, and DNA-PK: the trinity at the heart of the DNA damage response, *Mol. Cell* 66 (6) (2017) 801–817, <https://doi.org/10.1016/j.molcel.2017.05.015>.
- [94] A. Ray Chaudhuri, et al., Replication fork stability confers chemoresistance in BRCA-deficient cells, *Nature* 535 (7612) (2016) 382–387, <https://doi.org/10.1038/nature18325>.
- [95] Y.E. Choi, et al., Platinum and PARP inhibitor resistance due to overexpression of MicroRNA-622 in BRCA1-mutant ovarian cancer, *Cell Rep.* 14 (3) (2016) 429–439, <https://doi.org/10.1016/j.celrep.2015.12.046>.
- [96] A. McCormick, et al., Ovarian cancers harbor defects in nonhomologous end joining resulting in resistance to rucaparib, *Clin. Cancer Res.* 23 (8) (2017) 2050–2060, <https://doi.org/10.1158/1078-0432.CCR-16-0564>.
- [97] T.M. Yamamoto, et al., Activation of Wnt signaling promotes olaparib resistant ovarian cancer, *Mol. Carcinog.* 58 (10) (2019) 1770–1782, <https://doi.org/10.1002/mc.23064>.
- [98] L. Liu, et al., ALDH1A1 contributes to PARP inhibitor resistance via enhancing DNA repair in BRCA2(-/-) ovarian cancer cells, *Mol. Cancer Ther.* 19 (1) (2020) 199–210, <https://doi.org/10.1158/1535-7163.MCT-19-0242>.
- [99] H. Kim, et al., Targeting the ATR/CHK1 axis with PARP inhibition results in tumor regression in BRCA-mutant ovarian cancer models, *Clin. Cancer Res.* 23 (12) (2017) 3097–3108, <https://doi.org/10.1158/1078-0432.CCR-16-2273>.
- [100] L. Oplustil O'Connor, et al., The PARP inhibitor AZD2461 provides insights into the role of PARP3 inhibition for both synthetic lethality and tolerability with chemotherapy in preclinical models, *Cancer Res.* 76 (20) (2016) 6084–6094, <https://doi.org/10.1158/0008-5472.CAN-15-3240>.
- [101] A.J. Cole, et al., Assessing mutant p53 in primary high-grade serous ovarian cancer using immunohistochemistry and massively parallel sequencing, *Sci. Rep.* 6 (1) (2016) 26191, <https://doi.org/10.1038/srep26191>.
- [102] H. Takaya, et al., Homologous recombination deficiency status-based classification of high-grade serous ovarian carcinoma, *Sci. Rep.* 10 (1) (2020), <https://doi.org/10.1038/s41598-020-59671-3>.
- [103] S.A. Yazinski, et al., ATR inhibition disrupts rewired homologous recombination and fork protection pathways in PARP inhibitor-resistant BRCA-deficient cancer cells, *Gene Dev.* 31 (3) (2017) 318–332, <https://doi.org/10.1101/gad.290957.116>.
- [104] L. Mei, et al., Ataxia telangiectasia and Rad3-related inhibitors and cancer therapy: where we stand, *J. Hematol. Oncol.* 12 (1) (2019) 43, <https://doi.org/10.1186/s13045-019-0733-6>.
- [105] L. Gorecki, M. Andrs, J. Korabecny, Clinical candidates targeting the ATR-CHK1-WEE1 axis in cancer, *Cancers (Basel)* 13 (4) (2021), <https://doi.org/10.3390/cancers13040795>.
- [106] B.T. Burgess, et al., Olaparib combined with an ATR or Chk1 inhibitor as a treatment strategy for acquired olaparib-resistant BRCA1 mutant ovarian cells, *Diagnostics (Basel)* 10 (2) (2020), <https://doi.org/10.3390/diagnostics10020121>.
- [107] E. Brill, et al., Prexasertib, a cell cycle checkpoint kinases 1 and 2 inhibitor, increases in vitro toxicity of PARP inhibition by preventing Rad51 foci formation in BRCA wild type high-grade serous ovarian cancer, *Oncotarget* 8 (67) (2017) 111026–111040, <https://doi.org/10.18632/oncotarget.22195>.
- [108] K.T. Do, et al., Abstract CT232: Phase I combination study of the CHK1 inhibitor prexasertib (LY2606368) and olaparib in patients with high-grade serous ovarian cancer and other advanced solid tumors, *Cancer Res.* 79 (13 Supplement) (2019), <https://doi.org/10.1158/1538-7445.Am2019-ct232> p. CT232-CT232.
- [109] T.A. Yap, et al., Phase I trial of the PARP inhibitor olaparib and AKT inhibitor capivasertib in patients with BRCA1/2- and non-BRCA1/2-mutant cancers, *Cancer Discov.* 10 (10) (2020) 1528–1543, <https://doi.org/10.1158/2159-8290.cd-20-0163>.
- [110] E. Hinchcliff, et al., Characteristics and outcomes of patients with recurrent ovarian cancer undergoing early phase immune checkpoint inhibitor clinical trials, *Gynecol. Oncol.* 151 (3) (2018) 407–413, <https://doi.org/10.1016/j.ygyno.2018.10.008>.
- [111] E.J. Lampert, et al., Combination of PARP inhibitor olaparib, and PD-L1 inhibitor durvalumab, in recurrent ovarian cancer: a proof-of-concept phase II study, *Clin. Cancer Res.* 26 (16) (2020) 4268–4279, <https://doi.org/10.1158/1078-0432.CCR-20-0056>.
- [112] E. Ghisoni, et al., Ovarian cancer immunotherapy: turning up the heat, *Int. J. Mol. Sci.* 20 (12) (2019), <https://doi.org/10.3390/ijms20122927>.
- [113] C. Yang, et al., Immunotherapy for ovarian cancer: adjuvant, combination, and neoadjuvant, *Front. Immunol.* 11 (2020), 577869, <https://doi.org/10.3389/fimmu.2020.577869>.
- [114] I. Palaia, et al., Immunotherapy for ovarian cancer: recent advances and combination therapeutic approaches, *Onco Targets Ther.* 13 (2020) 6109–6129, <https://doi.org/10.2147/OTT.S205950>.
- [115] V. Wieser, et al., BRCA1/2 and TP53 mutation status associates with PD-1 and PD-L1 expression in ovarian cancer, *Oncotarget* 9 (25) (2018) 17501–17511, <https://doi.org/10.18632/oncotarget.24770>.
- [116] C. Xue, et al., Expression of PD-L1 in ovarian cancer and its synergistic antitumor effect with PARP inhibitor, *Gynecol. Oncol.* 157 (1) (2020) 222–233, <https://doi.org/10.1016/j.ygyno.2019.12.012>.
- [117] E.G. Hartnett, et al., Immunotherapy advances for epithelial ovarian cancer, *Cancers (Basel)* 12 (12) (2020), <https://doi.org/10.3390/cancers12123733>.
- [118] L. Ding, et al., PARP inhibition elicits STING-dependent antitumor immunity in Brca1-deficient ovarian cancer, *Cell Rep.* 25 (11) (2018) 2972–2980, <https://doi.org/10.1016/j.celrep.2018.11.054>, e5.
- [119] Z. Wang, et al., Niraparib activates interferon signaling and potentiates anti-PD-1 antibody efficacy in tumor models, *Sci. Rep.* 9 (1) (2019) 1853, <https://doi.org/10.1038/s41598-019-38534-6>.
- [120] F. Peyraud, A. Italiano, Combined PARP inhibition and immune checkpoint therapy in solid tumors, *Cancers (Basel)* 12 (6) (2020), <https://doi.org/10.3390/cancers12061502>.
- [121] P.A. Konstantinopoulos, et al., Single-arm phases 1 and 2 trial of niraparib in combination with pembrolizumab in patients with recurrent platinum-resistant ovarian carcinoma, *JAMA Oncol.* 5 (8) (2019) 1141–1149, <https://doi.org/10.1001/jamaoncol.2019.1048>.
- [122] Y. Drew, et al., Phase II study of olaparib + durvalumab (MEDIOLA): ppdated results in germline BRCA-mutated platinum-sensitive relapsed (PSR) ovarian cancer (OC), *Ann. Oncol.* 30 (2019) 485–486, <https://doi.org/10.1093/annonc/mdz253.016>.
- [123] Z. Wu, et al., The synergistic effect of PARP inhibitors and immune checkpoint inhibitors, *Clin. Med. Insights Oncol.* 15 (2021), <https://doi.org/10.1177/1179554921996288>, 1179554921996288.
- [124] R. Condorelli, F. Andre, Combining PI3K and PARP inhibitors for breast and ovarian cancer treatment, *Ann. Oncol.* 28 (6) (2017) 1167–1168, <https://doi.org/10.1093/annonc/mdx218>.
- [125] T.T. Huang, et al., Targeting the PI3K pathway and DNA damage response as a therapeutic strategy in ovarian cancer, *Cancer Treat. Rev.* 86 (2020), 102021, <https://doi.org/10.1016/j.ctrv.2020.102021>.
- [126] S. Chatterjee, T.F. Burns, Targeting heat shock proteins in cancer: a promising therapeutic approach, *Int. J. Mol. Sci.* 18 (9) (2017), <https://doi.org/10.3390/ijms18091978>.
- [127] A. Hoter, H.Y. Naim, Heat shock proteins and ovarian cancer: important roles and therapeutic opportunities, *Cancers (Basel)* 11 (9) (2019) <https://doi.org/10.3390/cancers11091389>.
- [128] Y.E. Choi, et al., Sublethal concentrations of 17-AAG suppress homologous recombination DNA repair and enhance sensitivity to carboplatin and olaparib in HR proficient ovarian cancer cells, *Oncotarget* 5 (9) (2014) 2678–2687, <https://doi.org/10.18632/oncotarget.1929>.
- [129] R. Gabbasov, et al., Targeted blockade of HSP90 impairs DNA-damage response proteins and increases the sensitivity of ovarian carcinoma cells to PARP inhibition, *Cancer Biol. Ther.* 20 (7) (2019) 1035–1045, <https://doi.org/10.1080/15384047.2019.1595279>.
- [130] P. Konstantinopoulos, et al., In vivo synergism between PARP-inhibitor olaparib and HSP90-inhibitor AT13387 in high grade serous ovarian cancer patient derived xenografts, *J. Clin. Oncol.* 34 (15 suppl) (2016) e17045, [https://doi.org/10.1200/JCO.2016.34.15\\_suppl.e17045](https://doi.org/10.1200/JCO.2016.34.15_suppl.e17045).
- [131] M.M. Murata, et al., NAD+ consumption by PARP1 in response to DNA damage triggers metabolic shift critical for damaged cell survival, *Mol. Biol. Cell* 30 (20) (2019) 2584–2597, <https://doi.org/10.1091/mbc.E18-10-0650>.
- [132] A. Lahiguera, et al., Tumors defective in homologous recombination rely on oxidative metabolism: relevance to treatments with PARP inhibitors, *EMBO Mol. Med.* 12 (6) (2020), e12127, <https://doi.org/10.15252/emmm.201911217>.
- [133] S. Bajrami, et al., Synthetic lethality of PARP and NAMPT inhibition in triple-negative breast cancer cells, *EMBO Mol. Med.* 4 (10) (2012) 1087–1096, <https://doi.org/10.1002/emmm.201201250>.
- [134] K. Kudo, et al., Divergent metabolic responses dictate vulnerability to NAMPT inhibition in ovarian cancer, *FEBS Lett.* 594 (9) (2020) 1379–1388, <https://doi.org/10.1002/1873-3468.13736>.
- [135] T. Nacarelli, et al., NAMPT inhibition suppresses cancer stem-like cells associated with therapy-induced senescence in ovarian cancer, *Cancer Res.* 80 (4) (2020) 890–900, <https://doi.org/10.1158/0008-5472.can-19-2830>.
- [136] S. Arora, et al., FDA approval summary: olaparib monotherapy or in combination with bevacizumab for the maintenance treatment of patients with advanced ovarian cancer, *Oncologist* 26 (1) (2021) e164–e172, <https://doi.org/10.1002/onco.13551>.

## **PUBLIKACJA #2**



## Article

# Olaparib-Resistant *BRCA2*<sup>MUT</sup> Ovarian Cancer Cells with Restored *BRCA2* Abrogate Olaparib-Induced DNA Damage and G2/M Arrest Controlled by the ATR/CHK1 Pathway for Survival

Łukasz Biegała, Arkadiusz Gajek , Agnieszka Marczak  and Aneta Rogalska \* 

Department of Medical Biophysics, Institute of Biophysics, Faculty of Biology and Environmental Protection, University of Lodz, 90-236 Lodz, Poland

\* Correspondence: aneta.rogalska@biol.uni.lodz.pl

**Abstract:** The PARP inhibitor (PARPi) olaparib is currently the drug of choice for serous ovarian cancer (OC), especially in patients with homologous recombination (HR) repair deficiency associated with deleterious *BRCA1/2* mutations. Unfortunately, OC patients who fail to respond to PARPi or relapse after treatment have limited therapeutic options. To elucidate olaparib resistance and enhance the efficacy of olaparib, intracellular factors exploited by OC cells to achieve decreased sensitivity to PARPi were examined. An olaparib-resistant OC cell line, PEO1-OR, was established from *BRCA2*<sup>MUT</sup> PEO1 cells. The anticancer activity and action of olaparib combined with inhibitors of the ATR/CHK1 pathway (ceralasertib as ATRi, MK-8776 as CHK1i) in olaparib-sensitive and -resistant OC cell lines were evaluated. Whole-exome sequencing revealed that PEO1-OR cells acquire resistance through subclonal enrichment of *BRCA2* secondary mutations that restore functional full-length protein. Moreover, PEO1-OR cells upregulate HR repair-promoting factors (*BRCA1*, *BRCA2*, *RAD51*) and *PARP1*. Olaparib-inducible activation of the ATR/CHK1 pathway and G2/M arrest is abrogated in olaparib-resistant cells. Drug sensitivity assays revealed that PEO1-OR cells are less sensitive to ATRi and CHK1i agents. Combined treatment is less effective in olaparib-resistant cells considering inhibition of metabolic activity, colony formation, survival, accumulation of DNA double-strand breaks, and chromosomal aberrations. However, synergistic antitumor activity between compounds is achievable in PEO1-OR cells. Collectively, olaparib-resistant cells display co-existing HR repair-related mechanisms that confer resistance to olaparib, which may be effectively utilized to resensitize them to PARPi via combination therapy. Importantly, the addition of ATR/CHK1 pathway inhibitors to olaparib has the potential to overcome acquired resistance to PARPi.

**Keywords:** ovarian cancer; targeted therapy; olaparib; PARP1; ATR/CHK1 pathway



**Citation:** Biegała, Ł.; Gajek, A.; Marczak, A.; Rogalska, A. Olaparib-Resistant *BRCA2*<sup>MUT</sup> Ovarian Cancer Cells with Restored *BRCA2* Abrogate Olaparib-Induced DNA Damage and G2/M Arrest Controlled by the ATR/CHK1 Pathway for Survival. *Cells* **2023**, *12*, 1038. <https://doi.org/10.3390/cells12071038>

Academic Editors: Punit Saraon and Bolin Liu

Received: 20 January 2023

Revised: 7 March 2023

Accepted: 27 March 2023

Published: 29 March 2023



**Copyright:** © 2023 by the authors. Licensee MDPI, Basel, Switzerland. This article is an open access article distributed under the terms and conditions of the Creative Commons Attribution (CC BY) license (<https://creativecommons.org/licenses/by/4.0/>).

## 1. Introduction

Olaparib is the first-in-class approved poly(ADP-ribose) polymerase (PARP) inhibitor (PARPi) which is currently indicated as a monotherapy for the maintenance treatment of recurrent platinum-sensitive ovarian cancer (OC), regardless of *BRCA1/2* status [1]. However, treatment for relapsed epithelial OC (EOC) after PARPi is mainly limited to platinum-based chemotherapy, which achieves modest clinical efficacy [2]. Preliminary data from the OReO trial (NCT03106987) evaluating the clinical benefits of olaparib maintenance retreatment for EOC patients who relapse after initial PARPi indicate that secondary therapy with olaparib could improve progression-free survival irrespective of *BRCA1/2* status. However, overall survival has not been significantly improved in olaparib groups compared to placebo groups. The modest efficacy of re-challenge olaparib therapy has also been documented in a single-institution study [3].

About ~50% of high-grade serous OC (HGSOC) cases have defective homologous recombination (HR) repair, mainly due to *BRCA1* or *BRCA2* deleterious mutations. The

remaining HR deficiency (HRD)-positive patients are defined as non-*BRCA1/2*<sup>MUT</sup> due to harboring other biomarkers of HRD [4,5]. A recent ARIEL4 study demonstrated that intrinsic resistance to PARPi is associated with *BRCA1/2* reversion mutations in PARPi-naïve relapsed HGSOc patients previously treated with chemotherapy [6]. Indeed, an effective response to PARPi is typically dependent on defects emerging in the HR repair pathway due to the phenomenon of PARPi-induced synthetic lethality in tumors [7]. Interestingly, a proportion of HR-deficient OC patients are not responsive to olaparib therapy, indicating that current HRD assays are inadequate for the effective prediction of response to olaparib [8,9].

In addition to the suppression of PARP signaling, olaparib exerts so-called “PARP poisoning” cytotoxicity by trapping the PARP1 enzyme at DNA single-strand breaks, which eventually leads to the accumulation of double-strand breaks (DSBs) and contributes to its anticancer activity [10]. However, the therapeutic efficacy of olaparib is abolished in some cases because of intrinsic or acquired resistance of OC cells resulting from the restoration of HR proficiency (*BRCA1/2* reversion mutation, *BRCA1* promoter demethylation), increased RAD51 foci formation, reduced PARP1 trapping, restoration of replication fork stabilization, and PARP signaling [11,12].

Numerous novel combination strategies with PARPi have been proposed to overcome resistance to olaparib [11,13,14], including small-molecule agents targeting the ATR (ataxia telangiectasia-mutated and Rad3-related) and CHK1 (checkpoint kinase 1) kinases implicated in the DNA damage response (DDR) and cell cycle regulation [15–19]. Concurrent treatments with PARPi and ATR or CHK1 kinase inhibitors have achieved promising results in patients who progress following initial therapy with PARPi, and these strategies are under further investigation [20–22]. However, approved combined therapy for the treatment of OC resistant to olaparib is lacking at present. The main rationale for combining PARPi with inhibitors of the ATR/CHK1 kinase axis is based on the observation that olaparib increases the reliance of olaparib-sensitive OC cells on the ATR/CHK1 pathway for survival [17,23]. DDR, which is regulated by the ATR/CHK1 axis, is a complex network of pathways integrating DNA replication and repair, cell cycle progression, and apoptosis to maintain genomic stability following replication stress and DNA damage [24,25]. However, the majority of HGSOc patients display loss of p53 and *TP53*<sup>MUT</sup> tumor cells predominantly relying on S and G2/M cell cycle checkpoints strictly regulated by the ATR/CHK1 pathway. ATR, one of the most upstream DDR kinases that induce the signal transduction cascade following exposure to various DNA damage stimuli, is auto-phosphorylated at Thr1989. Following activation, ATR phosphorylates downstream effector proteins, including CHK1 kinase at Ser345 and histone H2AX at Ser139, eventually triggering DSB-induced checkpoint arrest and DNA repair mainly via error-free HR [26–28]. Indeed, the HR pathway is activated during the late S and G2 phases of the cell cycle and coordinated via ATR/CHK1-dependent control of S and G2/M checkpoints. In response, RAD51-dependent repair is promoted by *BRCA1* and *BRCA2* [28,29], the latter serving as the main mediator of RAD51 loading onto resected DSBs [28]. Alternatively, error-prone non-homologous end joining (NHEJ) regulated by 53BP1 may be utilized for DNA damage repair. However, this pathway is less accurate and potentially leads to chromosomal instability [4].

Resensitization of OC cells to PARPi is a key measure in expanding the therapeutic utility of olaparib. In the current study, we successfully generated an olaparib-resistant cell line (PEO1-OR) from the parent HGSOc cell line, PEO1, and investigated the complex mechanisms mediating the phenotype of resistance to olaparib in OC in vitro. Subsequently, the differences in the involvement of the ATR/CHK1 pathway in response to PARPi in olaparib-sensitive and -resistant HGSOc cell lines were determined, and the effects of concurrent treatment with olaparib and ATR/CHK1 blockage on DDR and cell cycle progression were examined.

## 2. Materials and Methods

### 2.1. Chemicals

PARPi (O, olaparib, AZD2281), ATRi (A, ceralasertib, AZD6738), and CHK1i (C, MK-8776) were purchased from Selleck Chemicals (Houston, TX, USA). The stock solutions of studied inhibitors were separately prepared from powders dissolved in 100% dimethyl sulfoxide (DMSO), aliquoted, and stored at  $-80^{\circ}\text{C}$  for up to a maximum of six months. RPMI 1640 and DMEM culture media, heat-inactivated fetal bovine serum (HI-FBS), and trypsin-EDTA were obtained from Gibco (Thermo Fisher Scientific, Waltham, MA, USA). Details concerning other key reagents used in the studies are included in Section 2 and Supplementary Tables (Tables S1–S3). Chemicals and solvents were obtained from Sigma-Aldrich (Saint Louis, MO, USA) or Avantor Performance Materials Poland S.A. (Gliwice, Poland).

### 2.2. Cell Lines

Human HGSOC PEO1 and PEO4 cell lines were purchased from ECACC and upon receipt prepared for cryopreservation following recovery of frozen stocks and culture expansion. HGSOC cell lines were cultured as monolayers in RPMI 1640 culture medium containing GlutaMAX supplement and HEPES and supplemented with 10% HI-FBS. Human hepatocellular carcinoma HepG2 cell line was purchased from ATCC and cultured as monolayers in high-glucose DMEM culture medium containing GlutaMAX supplement and HEPES without sodium pyruvate and supplemented with 10% HI-FBS. All cell lines were cultured at  $37^{\circ}\text{C}$  in a humidified atmosphere containing 5%  $\text{CO}_2$ .

### 2.3. Development of Olaparib Resistance in HGSOC Cell Line In Vitro

The human HGSOC cell line resistant to olaparib (PEO1-OR) was derived from a parental PEO1 cell line in our laboratory by constant exposure to gradually increasing concentrations of olaparib by 2-fold ( $10\text{--}80\text{ }\mu\text{M}$ ) during culture of cells growing in log phase in RPMI 1640 culture medium containing 10% HI-FBS over the period of 20 days. Primarily used doses of olaparib were based on an  $\text{IC}_{50}$  value of olaparib determined from a dose–response curve over 5 days in the parental cell line. The preliminarily acquired cell line was cultured in the medium deprived of olaparib for additional 72 days to adapt cells to PARPi-free conditions and maintain and ensure its increased stable resistance to the drug. The sensitivity of PEO1-OR cells to olaparib was re-assessed periodically by MTT cell viability assay throughout the entire process of development to estimate a fold-change of resistance with respect to the PEO1 cell line. Briefly, the cells were exposed to a range of doses of olaparib ( $0\text{--}120\text{ }\mu\text{M}$  or  $0\text{--}240\text{ }\mu\text{M}$ ), and calculated  $\text{IC}_{50}$  values were compared between the established and the parental cell line to define the increase in drug resistance. Immediately after the establishment of the cell line, PEO1-OR cells were expanded from the homogeneous cell suspension for 10 days, banked in RPMI 1640 medium (supplemented with 10% DMSO and 20% HI-FBS), and stored in the vapor phase of liquid nitrogen for future use to ensure genetic stability. Fresh cultures were initiated every 2–3 months and cultivated in RPMI 1640 culture medium containing 10% HI-FBS in the absence of olaparib to conduct biological assays.

### 2.4. Cell Proliferation Rate and Population Doubling Time

Population doubling times (PDTs) of in vitro cultured PEO1, PEO1-OR, and PEO4 cells were determined based on the cell growth curves. Briefly, cells were seeded in 6-well plates ( $4 \times 10^5$  PEO1 and PEO1-OR cells or  $3 \times 10^5$  PEO4 cells) containing 2 mL of RPMI 1640 culture medium with 10% HI-FBS and cultured over a period of 9 days ( $37^{\circ}\text{C}$ , 5%  $\text{CO}_2$ ) until they reached confluency and started to overgrow which finally resulted in growth inhibition. The medium was changed on the fourth and seventh days to ensure suitable nutritional conditions for growth. The number of viable and non-viable cells was examined using the trypan blue exclusion method and a Thoma chamber under a light microscope. Each cell line was seeded in three technical replicates on each plate, and the number of

cells was counted twice for each sample. The experiment was repeated three times ( $n = 3$ ). Cellular growth curves were generated by plotting viable cell counts against the time of culture and using a four-parameter logistic nonlinear regression model that best fitted a set of experimental data. The following formula was used to calculate PDT for the cells exhibiting a logarithmic phase of growth based on the growth curves:

$$\text{PDT} = (t_2 - t_1) / \log_2(N_2/N_1)$$

where  $N_1$  and  $N_2$ —number of viable cells at earlier and later timepoints of the logarithmic phase of growth,  $t_1$  and  $t_2$ —timepoints for  $N_1$  and  $N_2$ , respectively.

### 2.5. MTT Cell Viability Assay

Drug cytotoxic activity and its impact on cell viability, linked with cellular metabolic activity, was measured by MTT assay. Cells were seeded in 96-well plates ( $0.8 \times 10^4$  PEO1 or PEO1-OR cells and  $1.6 \times 10^4$  PEO4 cells per well) in 100  $\mu\text{L}$  of culture medium and incubated for 24 h (37 °C, 5%  $\text{CO}_2$ ). On the following day, 50  $\mu\text{L}$  of fresh culture medium and 50  $\mu\text{L}$  of  $4 \times$  concentrated working dilutions of drugs prepared in culture medium were added to each well. Then the cells were further incubated for two or five days (37 °C, 5%  $\text{CO}_2$ ). Following the treatment, the medium was aspirated, 50  $\mu\text{L}$  of MTT solution (0.5 mg/mL in DPBS) was added to each well, and the plates were incubated for 4 h (37 °C, 5%  $\text{CO}_2$ ). Afterward, 100  $\mu\text{L}$  of DMSO was added to each well, plates were incubated at room temperature (RT) or at 37 °C protected from light until complete solubilization of the formazan crystals, and the samples were mixed for about 30 s using a plate shaker. The absorbance was determined spectrophotometrically on a microplate reader (Synergy HTX, BioTek, Shoreline, WA, USA) at an experimental wavelength of 580 nm, using 720 nm as a reference wavelength. To determine cell survival, the absorbance at 720 nm was subtracted from the absorbance at 580 nm ( $A_{580} - A_{720}$ ) for individual wells. Relative cell viability was calculated as the percentage of untreated control cells using corrected absorbance values. A minimum of three independent experiments ( $n \geq 3$ ) with a minimum of three intraplate technical replicates were performed and the results were presented as mean  $\pm$  standard deviation (SD). MTT assay was preliminarily used to plot dose–response curves for 5 days of olaparib (0.1–240  $\mu\text{M}$ ), ATRi, and CHK1i (0.1–120  $\mu\text{M}$ ) based on a four-parameter logistic model (generated by GraphPad Prism software) from which half-maximal (cytotoxic) inhibitory values ( $\text{IC}_{50}$ ) were calculated.

The total cytotoxic effect exhibited by concurrent administration of two inhibitors for five days was determined by the assessment of the coefficient of drug interaction (CDI) to select the lowest and most effective in olaparib-sensitive cell lines doses of olaparib (0.5, 2.5, 5, 10  $\mu\text{M}$ ) with either ATRi (0.5  $\mu\text{M}$ ) or CHK1i (2.5  $\mu\text{M}$ ) used in further experiments. The CDI was calculated according to the formula  $\text{CDI} = \text{AB}/(\text{A} \times \text{B})$  [30]. Based on the absorbance of each group, AB is the ratio of the two-agent combination group to the untreated control group, and A or B is the ratio of the single-agent group to the control group. CDI values allowed the characterization of whether the interaction effects were significantly synergistic ( $\text{CDI} < 0.7$ ), synergistic ( $\text{CDI} < 1.0$ ), additive ( $\text{CDI} = 1.0$ ), or antagonistic ( $\text{CDI} > 1.0$ ).

To examine the role of multidrug resistance (MDR) transporters in drug cytotoxicity and their influence on drug distribution, PEO1, PEO1-OR, and PEO4 cells were preincubated for 1 h in a culture medium containing the potent, non-competitive P-glycoprotein inhibitor tariquidar (0.1  $\mu\text{M}$ ; Sigma-Aldrich) followed by a co-incubation with pre-selected doses of tested compounds (5  $\mu\text{M}$  olaparib, 0.5  $\mu\text{M}$  ATRi, 2.5  $\mu\text{M}$  CHK1i, or their combinations) for two days in the presence of tariquidar (0.1  $\mu\text{M}$ ). P-glycoprotein inhibitor verapamil was used as a positive control of inhibition of MDR1 in HepG2 cells. Briefly, HepG2 cells were preincubated for 1 h in culture medium containing verapamil (50  $\mu\text{M}$ ; Sigma-Aldrich) and subsequently co-incubated for 2 days with the MDR1 substrate doxorubicin (0.10, 0.25 and 0.50  $\mu\text{M}$ ; Sequoia Research Products Limited, Compton, UK) or tested compounds in the presence of verapamil (50  $\mu\text{M}$ ). Cell viability in the presence of MDR inhibitors (MDRi) was determined using MTT assay as described above.

## 2.6. Clonogenic Assay

The cytotoxic activity of drugs and its influence on cell survival, proliferation, and ability to form colonies were examined using the colony formation assay. Cells were seeded in 6-well plates in 1.5 mL of culture medium ( $2 \times 10^3$  cells per well) and incubated for 24 h (37 °C, 5% CO<sub>2</sub>). The following day, cells were treated with pre-selected doses of tested compounds (5 µM olaparib, 0.5 µM ATRi, 2.5 µM CHK1i, or their combinations) by adding 100 µL of  $16 \times$  concentrated drugs prepared in culture medium and allowed to grow for five days in the presence of drugs. After five days, the medium was changed, and cells were allowed to grow and proliferate in drug-free medium for 10–14 days until single clones in control wells formed non-overlapping colonies. Then colonies were fixed with the mixture of methanol and glacial acetic acid (7:1 (v/v)) for 10 min, stained with 0.5% (w/v) crystal violet in 20% (v/v) ethanol for 20 min, thoroughly rinsed with deionized water to remove residual dye, and air-dried at RT. Each well was photographed, and fixed colonies consisting of at least 50 cells were counted manually. Surviving fractions (SFs) were calculated according to the following formula:

$$\text{SFs} = (\text{number of colonies formed after treatment}) / (\text{number of colonies formed in a control well}) \times 100\%$$

## 2.7. Cellular Morphology Changes

The morphology changes induced by tested compounds in PEO1, PEO1-OR, and PEO4 cells were evaluated by brightfield microscopy technique. Cells were seeded in 12-well plates ( $5 \times 10^4$  cells) containing 1 mL of culture medium and incubated for 24 h (37 °C, 5% CO<sub>2</sub>). The following day 0.5 mL of fresh culture medium was added to each well and cells were treated for five days (37 °C, 5% CO<sub>2</sub>) with olaparib (5 µM), ATRi (0.5 µM), CHK1i (2.5 µM), or their combinations by adding 0.5 mL of  $4 \times$  concentrated working dilutions of drugs prepared in culture medium. Afterward, cellular morphology changes were imaged at  $10\times$  magnification using an inverted optical microscope (Olympus IX70, Tokyo, Japan).

## 2.8. Whole-Exome Sequencing and Variant Calling

Whole-exome sequencing (WES) was performed with the Agilent SureSelect Human All Exon V8 Kit (Agilent Technologies, Santa Clara, CA, USA) on PEO1 and PEO1-OR cell line tumor samples. Paired-end ( $2 \times 150$  bp) next-generation sequencing was performed on a NovaSeq 6000 Sequencing System (Illumina, San Diego, CA, USA) to obtain a mean coverage of more than  $100\times$ . Briefly, freshly thawed and recovered cells from passage 1 were seeded in 100 mm dishes ( $5 \times 10^5$  cells in 8 mL of culture medium) and cultured for four days (37 °C, 5% CO<sub>2</sub>) until reaching 80% confluency. Afterward, cells were harvested by trypsinization, and genomic DNA was isolated and purified using GenElute Mammalian Genomic DNA Miniprep Kits (Sigma-Aldrich) according to the manufacturer's instructions. The quality, integrity, and purity of isolated DNA were evaluated using agarose gel electrophoresis and a spectrophotometer. Genomic DNA was stored in an ultrapure, molecular biology grade Tris-HCl solution (10 mM, pH 8.0) at  $-80$  °C for a week until downstream analysis.

Raw sequence data were aligned and annotated for individual samples to a reference sequence of the human genome (GRCh38). Duplicate reads were excluded from downstream analysis. Next, variants were called utilizing GATK's Haplotype Caller and interpreted using Qiagen Clinical Insight Interpret Translational (QCI-IT) software. Briefly, SnpEff 4.3 prediction toolbox was used to annotate called variants and predict their effects on protein structure and function (gain of function, loss of function, normal function, or change of function). False-positive variants were filtered out using GATK's Variant Filtration module.

Thereafter, we restricted our analysis to the interpretation of single-nucleotide variants (SNVs) and short insertions and deletions (indels) in genes encoding studied proteins, i.e., p53 (TP53, NM\_000546.6), ATR (ATR, NM\_001184.4), CHK1 (CHEK1, NM\_001141212.2), PARP1



(PARP1, NM\_001618.4), PARG (PARG, NM\_003631.5), BRCA1 (BRCA1, NM\_007294.4), BRCA2 (BRCA2, NM\_000059.4), MDR1 (ABCB1, NM\_001348945.2), 53BP1 (TP53BP1, NM\_005657.4), H2AX (H2AX, NM\_002105.3), and RAD51 (RAD51, NM\_002875.5), using the somatic workflow of QCI-IT software. To improve the high confidence of detected variants, we kept high-quality calls that passed upstream pipeline filtering and all of the confidence filters (call quality  $\geq 30$ , genotype quality  $\geq 30$ , and read depth  $\geq 10$ ). To keep only rare variants, any variant with a maximum population frequency  $> 5\%$  in the gnomAD database was classified as benign and excluded from further interpretation (unless previously established as a pathogenic common variant), according to recommendations [31].

High-quality variants were classified based on an automatically computed evidence-based categorization considering their pathogenicity (pathogenic, likely pathogenic, uncertain significance, likely benign, benign) and actionability in terms of therapeutic, diagnostic, and prognostic clinical significance (tier I—strong, tier II—potential, tier III—unknown, tier IV—benign or likely benign) according to the guidelines [32,33].

## 2.9. Western Blotting

For analyses of protein expression levels, cells were seeded in 60 mm dishes ( $0.8 \times 10^6$  cells) or 100 mm dishes ( $2.0 \times 10^6$  cells) and incubated for 24 h ( $37^\circ\text{C}$ ,  $5\% \text{CO}_2$ ) followed by treatment with pre-selected doses of tested compounds or their combinations for two days ( $5 \mu\text{M}$  olaparib,  $0.5 \mu\text{M}$  ATRi,  $2.5 \mu\text{M}$  CHK1i). Whole-cell lysates were prepared on ice by washing with ice-cold DPBS and scraping the cells in ice-cold RIPA buffer (25 mM Tris-HCl, 150 mM NaCl,  $1\% \text{NP-40}$ ,  $1\% \text{sodium deoxycholate}$ ,  $0.1\% \text{SDS}$ ) supplemented with phenylmethylsulfonyl fluoride (1 mM PMSF), Halt Protease Inhibitor Cocktail (1 mM AEBSF, 800 nM aprotinin,  $50 \mu\text{M}$  bestatin,  $15 \mu\text{M}$  E64,  $20 \mu\text{M}$  leupeptin,  $10 \mu\text{M}$  pepstatin A, 5 mM EDTA), and Halt Phosphatase Inhibitor Cocktail ( $\text{NaF}$ ,  $\text{Na}_3\text{VO}_4$ ,  $\text{Na}_4\text{P}_2\text{O}_7$ , and  $\beta$ -glycerophosphate). Lysates were gathered in microcentrifuge tubes, sonicated with a probe sonicator (1 pulse, 10 s,  $15\%$  amplitude), centrifuged ( $14,000 \times g$ , 10 min,  $4^\circ\text{C}$ ), and transferred to new tubes. Samples were prepared in mPAGE 4X LDS Sample Buffer supplemented with 50 mM  $\beta$ -mercaptoethanol and heated for 10 min at  $70^\circ\text{C}$ , and equal amounts of proteins ( $30 \mu\text{g}$ ) were loaded into each lane. Then, proteins were separated by SDS-PAGE at 180–200 V for 30–45 min in mPAGE Bis-Tris gels in an electrophoresis tank (Mini-PROTEAN Tetra Cell, Bio-Rad, Hercules, CA, USA) using MOPS SDS running buffer and transferred using a semi-dry transfer system (Trans-Blot Turbo Blotting System, Bio-Rad) in mPAGE Transfer Buffer onto  $0.45 \mu\text{M}$  PVDF membranes according to the manufacturer's optimized instruction for mPAGE Bis-Tris gels. Membranes were blocked either with  $5\%$  non-fat milk in TBST for 1 h or with SuperBlock (TBS) Blocking Buffer for 15 min and washed with TBST ( $3 \times 5 \text{ min}$ ). Analyzed proteins were immunoblotted with primary antibodies overnight at  $4^\circ\text{C}$  followed by incubation with suitable secondary antibodies conjugated with horseradish peroxidase (HRP) for 1 h at RT. The chemiluminescence signal of immunoreactive proteins was obtained using enhanced chemiluminescent (ECL) substrates (SuperSignal West Pico PLUS or SuperSignal West Atto Ultimate for low-abundance proteins). Images were visualized and captured with Azure 300 Imaging System (Azure Biosystems, Dublin, CA, USA). Densitometric quantification of the bands was performed with ImageJ software (NIH, Bethesda, MD, USA). Each experiment for a quantitative analysis of protein expression was independently repeated at least three times ( $n \geq 3$ ).

The following antibodies were used for immunoblotting: anti-53BP1 (Merck, #MAB3802), anti-ATR (Thermo Fisher Scientific, #MA1-23158), anti-phospho-ATR (Thr1989) (CST, #30632), anti-BRCA1 (Cell Signaling Technology, #9010), anti-BRCA2 C-terminal (Thermo Fisher Scientific, #A300-005A), anti-BRCA2 N-terminal #1 (Thermo Fisher Scientific, #A303-434A), anti-BRCA2 N-terminal #2 (Thermo Fisher Scientific, #MA5-23942), anti-CHK1 (Thermo Fisher Scientific, #MA5-32180), anti-phospho-CHK1 (Ser345) (CST, #2348), anti-MDR1 (Thermo Fisher Scientific, #MA5-32282), anti-PARG (Thermo Fisher Scientific, #MA5-27034), anti-PARP1 (CST, #9532), anti-RAD51 (Merck, #ABE257), anti- $\beta$ -actin (Merck, #A1978), anti- $\gamma$ -H2AX

(Merck, #05-636). Antibody dilution factors and utilized dilution buffers are indicated in the Supplementary Information (Tables S2 and S3).

#### 2.10. Immunofluorescence Analysis of $\gamma$ H2AX and RAD51 Foci Formation

Immunofluorescence microscopy was used to assess the co-localization of the surrogate DNA DSB biomarker  $\gamma$ H2AX (a form of H2AX histone phosphorylated at Ser139) and DNA repair factor RAD51 in response to exposure to tested compounds or their combinations (5  $\mu$ M olaparib, 0.5  $\mu$ M ATRi, 2.5  $\mu$ M CHK1i).

Cells were seeded in CELLview glass-bottom slides ( $1.2 \times 10^4$  in 200  $\mu$ L of culture medium per well) and incubated for 24 h (37  $^{\circ}$ C, 5% CO<sub>2</sub>). The following day, the medium was changed, and cells were exposed to pre-selected doses of tested compounds or their combinations for two days (5  $\mu$ M olaparib, 0.5  $\mu$ M ATRi, 2.5  $\mu$ M CHK1i). Then cells were fixed with formaldehyde (4% (*w/v*) in DPBS 1X) for 15 min at RT, rinsed with DPBS 1X (3  $\times$  5 min), blocked and permeabilized with 5% normal goat serum and 0.3% Triton X-100 in DPBS 1X for 1 h at RT, and co-stained for 2 h at RT with mouse anti- $\gamma$ H2AX (Sigma-Aldrich, #05-636) and rabbit anti-RAD51 (Sigma-Aldrich, #ABE257) monoclonal antibodies diluted with 1% BSA and 0.3% Triton X-100 in DPBS 1X. Next, the specimens were rinsed with DPBS 1X (3  $\times$  5 min) and incubated for 1 h at RT with a mixture of two fluorochrome-conjugated secondary antibodies raised against primary antibodies from mouse (Goat Anti-mouse IgG (H + L) Highly Cross-Adsorbed Secondary Antibody, Alexa Fluor Plus 488, Thermo Fisher Scientific, #A32723) and rabbit (Goat Anti-rabbit IgG (H + L), F(ab')<sub>2</sub> Fragment, Alexa Fluor 555 Conjugate, CST, #4413) prepared in 1% BSA and 0.3% Triton X-100 in DPBS 1X. After rinsing with DPBS 1X, nuclei were stained by incubation with 300 nm DAPI for 3 min at RT, rinsed once with DPBS 1X, and mounted with DPBS 1X for imaging. Immunofluorescence images were acquired using an inverted confocal scanning microscope (SP-8, Leica Microsystems, Wetzlar, Germany) under 63 $\times$  oil magnification.

#### 2.11. Preparation of Metaphase Chromosomes for Structural Aberration Analysis

For analysis of chromosome instability identified as structural chromosomal aberrations induced by examined drugs, cells were seeded in 60 mm dishes ( $0.8 \times 10^6$  cells), incubated for 24 h (37  $^{\circ}$ C, 5% CO<sub>2</sub>), and treated with tested compounds or their combinations for two days (5  $\mu$ M olaparib, 0.5  $\mu$ M ATRi, 2.5  $\mu$ M CHK1i). Then the cells were incubated with colcemid (0.1  $\mu$ g/mL) for 1 h (37  $^{\circ}$ C, 5% CO<sub>2</sub>) to arrest the cells at metaphase for chromosome analysis. Metaphase chromosomes were prepared for visualization based on the in-house modification of the procedure from Howe et al. [34]. Briefly, cells were washed with DPBS 1X, detached from the dishes by trypsinization, collected in tubes, and centrifuged (200 $\times$  g, 10 min). The pellets were resuspended, and cells were incubated in a prewarmed to 37  $^{\circ}$ C hypotonic solution of 0.075 M KCl for 10 min at 37  $^{\circ}$ C in a water bath. Following centrifugation (200 $\times$  g, 5 min), cells were fixed with a fixative solution (3:1 (*v/v*)), methanol and glacial acetic acid). After three cycles of subsequent centrifugation (200 $\times$  g, 5 min), removal of supernatant, and addition of fresh fixative, fixed cells were resuspended in a fixative solution and added drop by drop onto microscope slides tilted at a 45 $^{\circ}$  angle. Then the slides were dried out at RT for about 10 min and placed for 10 min in a Giemsa staining solution. Excessive amounts of dyes were rinsed off with distilled water. Metaphase chromosome spreads were visualized with a light microscope (Nikon Eclipse 50i) equipped with a DS-Fi3 camera (Nikon). Images were acquired at 100 $\times$  magnification. From each biological replicate ( $n = 3$ ), thirty-five metaphases were analyzed in terms of the presence of any structural chromosomal aberrations (chromosome and chromatid breaks, gaps, exchanges, ring chromosomes, pulverized chromosomes, dicentric chromosomes, or centromeric disruption) for a total of 105 metaphases scored for every sample.

### 2.12. Neutral Comet Assay

DNA damage in the form of DSBs was detected and measured at the level of individual cells using the neutral comet assay in response to exposure to studied inhibitors. Cells were seeded in 6-well plates ( $4 \times 10^5$  cells) in 1.5 mL of culture medium, incubated for 24 h (37 °C, 5% CO<sub>2</sub>), and exposed to pre-selected doses of tested compounds or their combinations (5 µM olaparib, 0.5 µM ATRi, 2.5 µM CHK1i) for two days in fresh culture medium. Then cells were harvested by trypsinization, washed, resuspended in DPBS 1X to obtain single-cell suspensions, and counted. Duplicate samples containing 4000 cells in 0.75% low-melting-point agarose dissolved in DPBS 1X (pH 7.4) were spread on glass slides precoated with 0.5% normal-melting-point agarose and immersed in cooled lysis buffer (2.5 M NaCl, 100 mM EDTA, 10 mM Tris, 1% Triton X-100, pH 9.0) for 18–24 h at 4 °C. Subsequently, slides were equilibrated for 20 min in a running buffer (100 mM Tris, 300 mM sodium acetate, pH 9.0 adjusted with glacial acetic acid) and electrophoresed in a fresh running buffer for 60 min (0.41 V/cm, 50 mA). After DNA unwinding and separation, samples were rinsed in distilled water, stained with DAPI (2 µg/mL), and stored in a humidified chamber at 4 °C in darkness before further analysis. For each sample, at least fifty randomly selected comets were visualized at 200× magnification with an Eclipse fluorescence microscope (Nikon, Tokyo, Japan) attached to a COHU 4910 video camera (Cohu Inc., San Diego, CA, USA) equipped with a UV-1 filter block (359 nm excitation filter, and 461 nm barrier filter). Comet tails containing fragments of DSB-induced damaged DNA (% DNA in a tail relative to total DNA in a comet) were quantitatively measured using the Lucia-Comet v. 4.51 image analysis system (Laboratory Imaging, Prague, Czech Republic). Each comet assay was independently repeated three times ( $n = 3$ ) with each sample repeated in two technical replicates during experiments to calculate the mean percentage of tail DNA positively correlating with DNA DSBs.

### 2.13. Cell Cycle Analysis with Quantification of $\gamma$ H2AX by Flow Cytometry

Cells were characterized in terms of their cell cycle position (G0/G1, S, and G2 + M phases) using the bromodeoxyuridine (BrdU) incorporation assay with BD Pharmingen FITC BrdU Flow Kit (BD Biosciences, San Jose, CA, USA) according to the manufacturer's protocol. Simultaneously, phosphorylation of H2AX at Ser139 ( $\gamma$ H2AX) was measured to detect signs of DNA DSB damage within specific cell cycle phases by multicolor flow cytometric analysis.

Briefly, cells were seeded in 60 mm dishes ( $0.8 \times 10^6$  cells) in 3 mL of culture medium per well and allowed to attach for 24 h (37 °C, 5% CO<sub>2</sub>). The following day, the medium was changed, and cells were exposed to pre-selected doses of tested compounds or their combinations for two days (5 µM olaparib, 0.5 µM ATRi, 2.5 µM CHK1i). During the final 3 h of treatment, cells were pulsed with 10 µM BrdU. Cells were harvested by trypsinization, fixed, permeabilized, and co-stained for 30 min at RT with FITC-conjugated anti-BrdU antibody and PE-conjugated anti- $\gamma$ -H2AX antibody (Thermo Fisher Scientific, #12-9865-42) following staining with 7-amino-actinomycin D (7-AAD) for total DNA content. Stained cells were immediately acquired by collecting 10,000 events using flow cytometry (LSR II, Becton Dickinson, San Jose, CA, USA).

Flow cytometric data were analyzed using FlowJo v.7.6.1 analyzing software (Ashland, OR, USA). Briefly, cell populations of interest were gated based on forward scatter (FSC) and side scatter (SSC) to exclude cellular debris. Then doublets were excluded from the analysis of single cells using FSC height vs. FSC area and SSC height vs. SSC area density plots. Finally, cellular events corresponding to suitable cell cycle phases were gated based on two-parameter density plots presenting the cellular content of BrdU (y axis) and 7-AAD (x axis). Gated cells were used for the quantitative analysis of the phosphorylation level of  $\gamma$ H2AX using geometric mean fluorescence intensity (MFI) in arbitrary units in the entire gated population of interest (total  $\gamma$ H2AX) and in populations from respective cell cycle phases (G0/G1, S, and G2/M).



### 2.14. Statistical Analysis

Statistical analysis was performed with GraphPad Prism version 9.4.0 for Windows (GraphPad Software, San Diego, CA, USA) using the tests specified in the description of the figures. One-way ANOVA followed by Tukey's multiple comparison test was used to assess the statistical significance of differences in experiments where three independent groups defined by one factor (cell line) passed the assumption of normal distribution (Shapiro–Wilk or D'Agostino–Pearson test), and homogeneity of variance (Brown–Forsythe test). Welch's ANOVA followed by Dunnett T3 multiple comparison test was applied to compare measurements from three independent groups defined by one factor (cell line) where applicable (data sampled from a Gaussian distribution, but with unequal variances across groups). Two-way ANOVA followed by Tukey's multiple comparison test was used to assess the statistical significance of differences in experiments where three or more independent groups defined by two factors (cell line and drug treatment) passed the assumption of normal distribution (Shapiro–Wilk or D'Agostino–Pearson test).

## 3. Results

### 3.1. The PEO1-OR Cell Line with an Acquired Resistant Phenotype Displays Reduced Sensitivity to Olaparib and Increased Proliferation

PEO1-OR cells with acquired resistance to olaparib were established from the parental BRCA2<sup>MUT</sup> PEO1 cell line to uncover the mechanisms underlying PARPi cytotoxicity and resistance in OC cells in vitro. A multiple-dose selection strategy was employed to gradually increase resistance in the presence of the drug (Figure 1). To ensure consistency in rationale-based repeated oral dosing of olaparib in clinical practice, OC cells were constantly exposed to olaparib for 20 days.

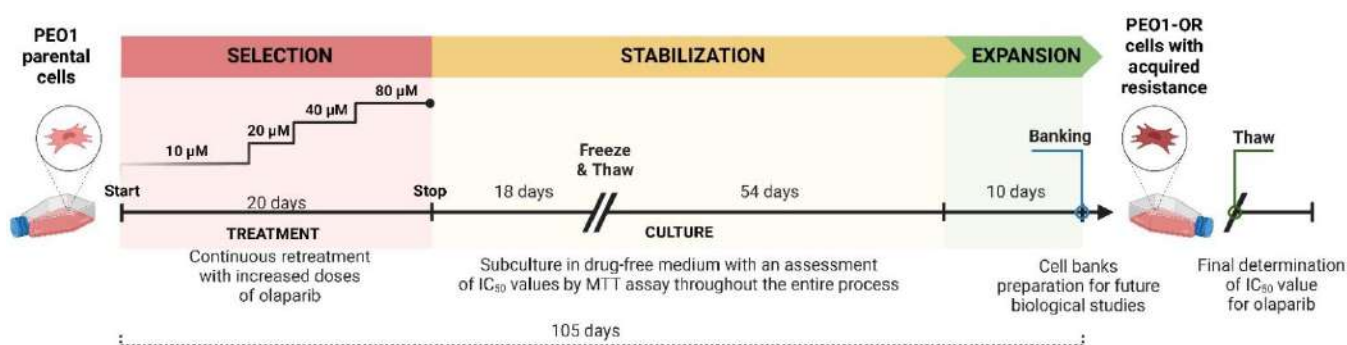


**Figure 1.** Timeline of a continuous selection strategy and stabilization for generating PEO1-OR cells with a phenotype of acquired resistance to olaparib. In the first round of selection, PEO1 parental cells were seeded at moderate confluence and exposed to 10 µM olaparib, and additional doses of drug were administered every 2–5 days during medium change or cell passage. Next, cells were sequentially cultured in the presence of stepwise increasing doses of olaparib (20, 40, and 80 µM) at each round of selection. After 20 days of treatment, cells were cultured in the absence of drug for a total of 72 days to stabilize changes in sensitivity to the drug and subjected to a single cycle of freeze–thaw to ensure the presence of the resistant phenotype. Eventually, the culture of selected cells was expanded and cryopreserved for future use. Untreated parental cells were cultured alongside those used for olaparib selection throughout the procedure.

Firstly, based on a dose–response curve of olaparib (0.1–240 µM) assessed over a 5-day treatment period in the parental PEO1 cell line, we determined the maximum suitable dose at the first stage of induction of resistance (10 µM) that led to significant inhibition of cell viability as assessed with the MTT assay (Figure 2A). Surviving cells were allowed to recover and re-populate during the passage, followed by retreatment with the selected dose, and further incrementally exposed to 2-fold higher doses of olaparib, up to a concentration of 80 µM. The entire population of remaining cells was subsequently cultured in the absence of the drug for a total of 72 days. Continuous treatment with increasing doses

of olaparib resulted in a significant (3.3-fold) increase in drug resistance in PEO1-OR cells ( $IC_{50} = 82.1 \mu M$ ) relative to sensitive PEO1 cells ( $IC_{50} = 25.0 \mu M$ ) (Figure 2B), which may be considered clinically relevant [35]. Although we found a much higher  $IC_{50}$  value for olaparib in PEO1 cells with respect to those reported previously by our team [17], earlier findings collectively show various  $IC_{50}$  values ranging from at least  $0.4 \mu M$  to  $25 \mu M$  [19,36,37]. This apparent discrepancy can be attributed mainly to the reported subclonal evolution of PEO1 cells during passages resulting in the existence of two different subclones [38], the experimental design for the assay, the manufacturer of the drug, and the drug's chemical purity.

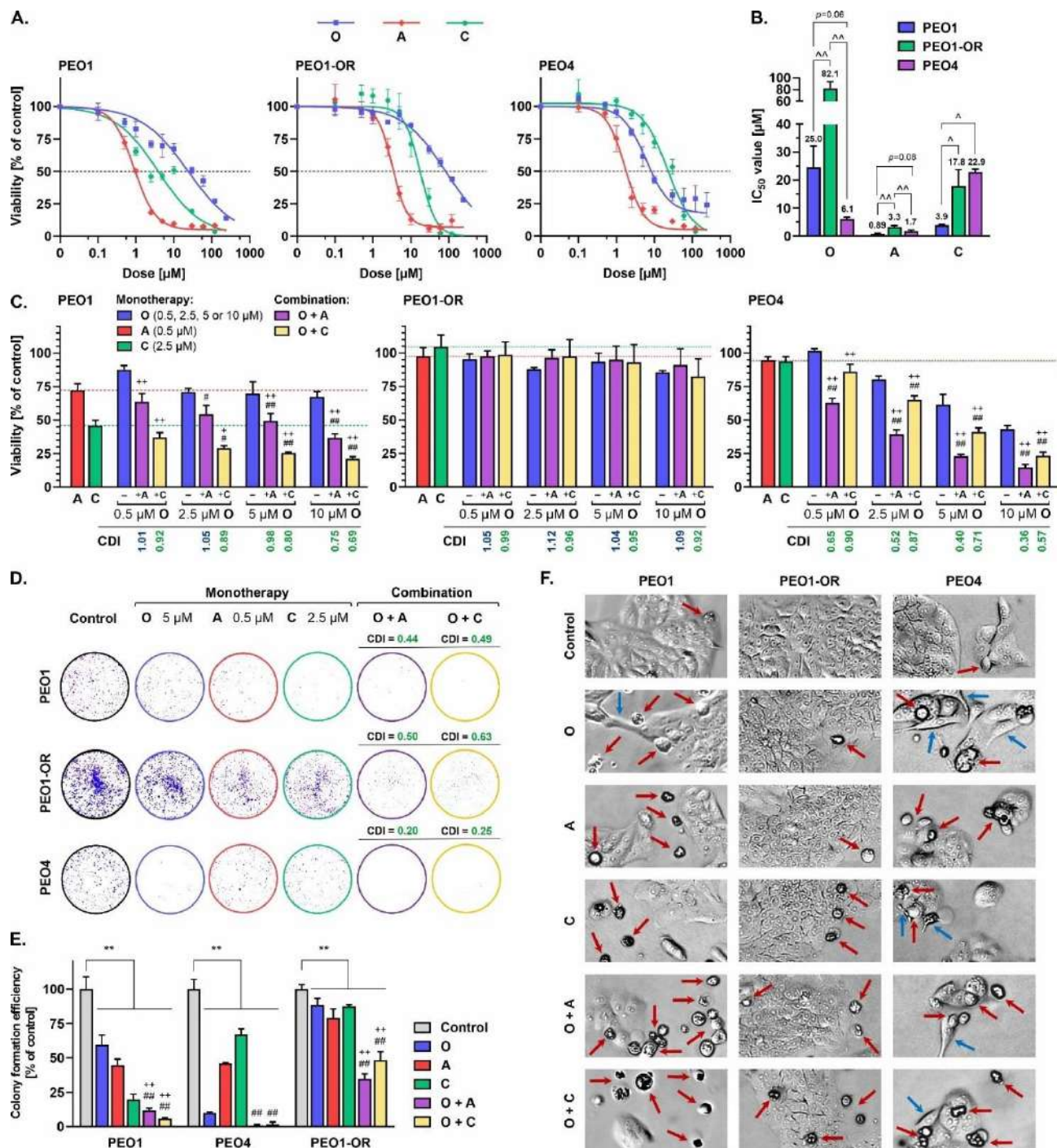


**Figure 2.** Olaparib combined with ATRi and CHK1i induces lower cytotoxicity in PEO1-OR cells compared to olaparib-sensitive cell lines. Cell viability in response to treatment for 5 days with olaparib

(O, 0.1–240  $\mu$ M), ATRi (A, 0.1–120  $\mu$ M), and CHK1i (C, 0.1–120  $\mu$ M) was determined using the MTT assay. (A) A four-parameter logistic regression model was fitted to dose–response data to estimate (B) absolute  $IC_{50}$  values. Data are expressed as mean  $\pm$  SD ( $n \geq 3$ ). (C) Synergistic cytotoxic effects of drugs determined with the MTT assay in response to 5-day treatment with olaparib (0.5, 2.5, 5, or 10  $\mu$ M) combined with ATRi (0.5  $\mu$ M) or CHK1i (2.5  $\mu$ M). Data are expressed as mean  $\pm$  SD ( $n = 3$ –6). (D) The clonogenic assay was performed after incubation with olaparib (5  $\mu$ M), ATRi (0.5  $\mu$ M), CHK1i (2.5  $\mu$ M), or their combinations for 5 days. After treatment, cells were allowed to grow and proliferate in the absence of drugs for 10–14 days. Representative images of colonies and (E) quantification of colony formation ability compared with control cells. Data are expressed as mean  $\pm$  SD ( $n = 4$ ). (F) Morphological changes of OC cell lines in response to olaparib (5  $\mu$ M), ATRi (0.5  $\mu$ M), CHK1i (2.5  $\mu$ M), or their combinations for 5 days. Images were captured at 10 $\times$  magnification. Coefficient of drug interaction (CDI) values indicating whether interaction effects are significantly synergistic ( $CDI < 0.7$ ), synergistic ( $CDI < 1.0$ ), additive ( $CDI = 1.0$ ), or antagonistic ( $CDI > 1.0$ ). Statistical significance was assessed using two-way ANOVA followed by Tukey’s test ( $IC_{50}$  values, viability, and colony formation efficiency).  $^{\wedge} p < 0.05$ ,  $^{\wedge\wedge} p < 0.01$ : significant differences between cell lines;  $^{**} p < 0.01$ : treatment vs. control;  $^{+} p < 0.05$ ,  $^{++} p < 0.01$ : olaparib vs. combination with ATRi or CHK1i;  $^{\#} p < 0.05$ ,  $^{##} p < 0.01$ : ATRi or CHK1i vs. respective combinations with olaparib.

In further biological studies, we used PEO1 and PEO4 cell lines as olaparib-sensitive cells and the PEO1-OR cell line as olaparib-resistant cells. PEO1 and PEO4 cell lines were originally derived at subsequent stages of treatment from ascites of serous OC patients [36] who carried the germline truncating *BRCA2* mutation. PEO4 was developed after disease progression following platinum-based chemotherapy [39] and displays a platinum-resistant phenotype [40]. Although sensitivity to platinum-based chemotherapy is predictive of the efficacy of response to olaparib in vitro and in vivo, suggesting similar mechanisms of resistance [41], the sensitivity of PEO4 cells to olaparib in comparison with OC cell lines with PARPi-induced resistance is ambiguous [19,36,42].

Further preliminary studies were conducted to estimate the proliferation rate and population doubling time (PDT) of PEO1, PEO1-OR, and PEO4 cell lines (Figure S1). All cells demonstrated a sigmoidal-like growth curve pattern typical for immortalized cell lines with a lag phase of about one day, followed by logarithmic growth and a stationary phase (Figure S1A). Notably, PEO1-OR cells began to recover and entered exponential growth as early as one day after plating. PDT estimates revealed the highest rate of proliferation in PEO1-OR cells (PDT = 31.9 h) and slower rates of division of PEO1 (PDT = 37.1 h) and PEO4 cells (PDT = 46.3 h) (Figure S1B) which were in line with original findings for olaparib-sensitive cells [39].

### 3.2. The PEO1-OR Cell Line Displays Increased Resistance to Olaparib and Inhibitors of the ATR/CHK1 Pathway

To evaluate the potential antitumor activities of olaparib, ATRi, CHK1i, and their combinations, the cytotoxic effects of the inhibitors in all OC cell lines were investigated using the MTT assay. Dose–response curves were generated to estimate the absolute  $IC_{50}$  values using a four-parameter logistic regression model following 5-day treatment of cells with increasing concentrations of olaparib (0.1–240  $\mu$ M) and ATRi or CHK1i (0.1–120  $\mu$ M) (Figure 2A). While a notable decrease in the survival of PEO1 cells was observed in response to olaparib at a broad range of drug concentrations (0.5–240  $\mu$ M), the inhibitory influence of olaparib in PEO1-OR cells was markedly lower. Based on  $IC_{50}$  values for olaparib, PEO4 cells were more sensitive to PARPi than PEO1 and PEO1-OR cells (Figure 2B). However, at lower concentrations (0.1–2.5  $\mu$ M), olaparib suppressed cell viability to a greater extent in PEO1 cells. PEO1-OR cells also displayed significantly reduced sensitivity to ATRi and CHK1i ( $IC_{50} = 3.3$   $\mu$ M and 17.8  $\mu$ M, respectively) compared to the parental PEO1 cell line ( $IC_{50} = 0.89$   $\mu$ M and 3.9  $\mu$ M, respectively) (Figure 2B).

We further examined the hypothesis that olaparib cytotoxicity could be potentiated in both sensitive and resistant OC cell lines by the concurrent addition of either ATRi or CHK1i promoting blockage of the ATR/CHK1 pathway [17,20,43]. Specific concentrations



of olaparib (0.5, 2.5, 5, and 10  $\mu\text{M}$ ), ATRi (0.5  $\mu\text{M}$ ), and CHK1i (2.5  $\mu\text{M}$ ) were selected to determine the lowest doses conferring synergistic cytotoxicity across the olaparib-sensitive cell lines without significant reduction in viability of PEO1-OR cells (Figure 2C). The lowest dose of olaparib that exerted synergistic effects with ATRi or CHK1i in PEO1 and PEO4 was 5  $\mu\text{M}$ . The addition of 0.5  $\mu\text{M}$  ATRi markedly augmented the decrease in cell viability induced by 5  $\mu\text{M}$  olaparib in PEO1 (CDI = 0.98) and PEO4 cells (CDI = 0.40), compared to PARPi alone. Synergistic effects were additionally observed upon co-administration of CHK1i with PARPi (0.5–10  $\mu\text{M}$ ) in olaparib-sensitive cell lines, where 2.5  $\mu\text{M}$  CHK1i and 5  $\mu\text{M}$  olaparib resulted in a marked decrease in cell viability (CDI = 0.80 for PEO1 and CDI = 0.71 for PEO4).

Simultaneously, monotherapy and other drug combinations had no significant effects on PEO1-OR metabolic activity, indicating that resistance to olaparib may also be correlated with decreased sensitivity to the inhibition of either ATR or CHK1 kinase. Based on data from the MTT assay, we selected 5  $\mu\text{M}$  olaparib, 0.5  $\mu\text{M}$  ATRi, and 2.5  $\mu\text{M}$  CHK1i as the lowest doses that induced a synergistic decrease in viability of olaparib-sensitive cells for further experiments to compare OC cell responses to combined treatments regarding their distinct sensitivities to PARPi alone.

Next, we performed the clonogenic assay, a commonly used test to establish the long-term effects of cytotoxic agents on cell survival and proliferation [44]. Increased resistance of PEO1-OR cells to olaparib, ATRi, and CHK1i was observed relative to the olaparib-sensitive cell lines after 5 days of treatment (Figure 2D,E). Inhibition of PARP1 with concurrent blockage of ATR or CHK1 significantly decreased the ability of PEO1-OR cells to form colonies compared to untreated cells. Consistent with the results of the MTT assay (Figure 2C), olaparib-sensitive cells exhibited notably decreased survival in the presence of inhibitors, both alone and with their combinations (Figure 2D,E). The addition of ATRi or CHK1i to olaparib significantly reduced the colony formation efficiency in PEO1 cells (CDI = 0.44 and 0.49), PEO4 cells (CDI = 0.20 and 0.25), and PEO1-OR cells (CDI = 0.50 and 0.63).

Moreover, the morphology of PEO1 and PEO4 cells was altered in response to all the inhibitory agents tested after a 5-day incubation period as indicated by spherical cell shape, loose adherence, or detachment from the surface, frequently with cell fragmentation (indicated by red arrows) or cell elongation conferring a spindle-like shape (indicated by blue arrows) (Figure 2F). Additionally, monolayer confluency was affected after treatments in PEO1 and PEO4 cells. In contrast, no significant evidence of PEO1-OR cell deterioration was observed in the presence of olaparib or ATRi. The combination treatment affected the population of PEO1-OR cells less notably compared with PEO1 and PEO4 cells.

Taken together, the results indicate that PEO1-OR cells display decreased sensitivity to olaparib, along with cross-resistance to ATRi and CHK1i, relative to the parental cell line. Inhibition of the ATR/CHK1 pathway synergistically promotes the cytotoxicity of olaparib more notably in sensitive PEO1 and PEO4 cells. However, we confirmed the rationale for combined treatment in all OC cells.

### 3.3. Relationship between Olaparib Resistance and Exonic Variants in Genes Involved in DNA Damage Repair, Cell Cycle Regulation, and Drug Efflux in OC Cells

Whole-exome sequencing (WES) via NGS has been employed to identify functional mutations in OC to date [45,46]. Here, we investigated variants of genes encoding proteins involved in DNA damage repair, cell cycle regulation, and drug efflux (*ABCB1*, *ATR*, *BRCA1*, *BRCA2*, *CHEK1*, *H2AX*, *PARP1*, *PARG*, *RAD51*, *TP53*, *TP53BP1*) in PEO1 olaparib-sensitive and -resistant cell lines to identify putative genetic drivers of resistance to PARPi (Tables 1 and S4). The average target coverage was  $132\times$  and  $156\times$  for PEO1 and PEO1-OR cells, respectively, providing a standard mean depth of coverage for clinical WES [47]. We achieved 96.3% and 96.7% breadth of coverage of the reference genome at a depth of  $30\times$  for PEO1 and PEO1-OR cells, respectively.

**Table 1.** Whole-exome sequencing-based detection of high-quality exonic variants detected in *ABCB1*, *ATR*, *BRCA1*, *BRCA2*, *CHEK1*, *H2AX*, *PARP1*, and *TP53* genes in PEO1 and PEO1-OR cell lines.

Gene	Mutation	Gene Region	Amino Acid Change	Type of Mutation	Functional Impact	Computed Pathogenicity	CADD Score	Allele Fraction [% of Total Reads]		Maximal Population Allele Frequency
								PEO1	PEO1-OR	
<i>TP53</i>	c.731G > A	CDS	p.G244D	M	loss	pathogenic	27	100%	100%	0%
<i>BRCA1</i>	c.4837A > G	CDS	p.S1613G	M	normal	benign (!)	<10	100%	100%	49% (South Asian)
	c.2082C > T	CDS	p.S694S	S	normal	benign	<10	100%	100%	49% (South Asian)
	c.2311T > C	CDS	p.L771L	S	normal	benign	<10	100%	100%	49% (South Asian)
	c.2612C > T	CDS	p.P871L	M	normal	benign (!)	18	100%	100%	81% (African)
	c.3113A > G	CDS	p.E1038G	M	normal	benign (!)	14	100%	100%	49% (South Asian)
	c.3548A > G	CDS	p.K1183R	M	normal	benign (!)	<10	100%	100%	49% (South Asian)
	c.4308T > C	CDS	p.S1436S	S	normal	benign	<10	100%	100%	49% (South Asian)
	c.-1074C > G	5' UTR	–	–	normal	benign	<10	100%	100%	82% (African)
	c.-134T > C	5' UTR	–	–	normal	benign	<10	100%	100%	49% (South Asian)
<i>BRCA2</i>	c.4965C > G	CDS	p.Y1655 *	STOP	loss	pathogenic	33	100%	100%	0.008% (European)
	c.4964A > T	CDS	p.Y1655F	M	normal	uncertain	<10	34%	94%	0%
	c.3807T > C	CDS	p.V1269V	S	normal	benign	<10	100%	100%	19% (African)
	c.4563A > G	CDS	p.L1521L	S	normal	benign	<10	100%	100%	100% (Jewish)
	c.6513G > C	CDS	p.V2171V	S	normal	benign	<10	100%	100%	100% (Jewish)
	c.7397T > C	CDS	p.V2466A	M	normal	benign	<10	100%	100%	100% (Jewish)
	c.* 105A > C	3' UTR	–	–	normal	benign	<10	100%	100%	23% (South Asian)

Table 1. Cont.

Gene	Mutation	Gene Region	Amino Acid Change	Type of Mutation	Functional Impact	Computed Pathogenicity	CADD Score	Allele Fraction [% of Total Reads]		Maximal Population Allele Frequency
								PEO1	PEO1-OR	
PARP1	c.2285T > C	CDS	p.V762A	M	loss	benign (!)	27	100%	100%	43% (East Asian)
	c.243C > T	CDS	p.D81D	S	normal	benign	12	100%	100%	43% (East Asian)
	c.852T > C	CDS	p.A284A	S	normal	benign	<10	100%	100%	81% (East Asian)
	c.-17G > C	5' UTR	–	–	normal	benign	12	100%	100%	43% (East Asian)
ATR	c.632T > C	CDS	p.M211T	M	gain	benign (!)	14	32%	34%	73% (African)
	c.1776T > A	CDS	p.G592G	S	normal	benign	<10	31%	31%	79% (African)
	c.1815T > C	CDS	p.D605D	S	normal	benign (!)	<10	32%	31%	44% (Jewish)
	c.5208T > C	CDS	p.Y1736Y	S	normal	benign (!)	<10	29%	30%	45% (Jewish)
	c.7875G > A	CDS	p.Q2625Q	S	normal	benign	<10	32%	30%	97% (African)
CHEK1	c.1411A > G	CDS	p.I471V	M	gain	benign	14	100%	100%	99.98% (East Asian)
	c.* 28–3033C > G	3' UTR	–	–	normal	benign	<10	53%	59% (LQ)	42% (South Asian)
ABCB1	c.210A > G	CDS	p.G70G	S	normal	benign	<10	100%	100%	100% (East Asian)
H2AX	c.-1420G > A	5' UTR	–	–	normal	benign	<10	53%	35% (LQ)	64% (East Asian)

!—conflicting pathogenic criteria were computationally applied to a single variant (at least one pathogenic and one benign, as described in Section 3); 3' UTR—3' untranslated region; 5' UTR—5' untranslated region; CDS—protein-coding sequence; CADD score ranges from 1 to 99 (higher value responds to more deleterious cases, i.e., 10 indicates top 1% pathogenic variants, 20 indicates top 0.1% pathogenic variants); M—missense mutation; LQ—low-quality score for the variant allele call in one sample; S—synonymous mutation; STOP—stop-gain mutation; \*—termination codon.

WES revealed 81 and 84 high-quality variants in PEO1 cells (exonic = 30, intronic = 51) and PEO1-OR cells (exonic = 30, intronic = 54), respectively, after filtering out low-quality variants as described in Section 2. Differences in intronic variants detected in PEO1 and PEO1-OR cells within intronic regions are presented in Table S4. We focused on the mutations detected in the exon regions crucial in maintaining the normal functions of encoded proteins. Sequencing data revealed that PEO1 and PEO1-OR cells harbored the same 30 exonic mutations in *ABCB1*, *ATR*, *BRCA1*, *BRCA2*, *CHEK1*, *H2AX*, *PARP1*, and *TP53* genes. Both cell lines displayed similar allele frequencies for most of these variants, indicating that the alterations had mostly no impact on the acquisition of resistance to olaparib. All variants involved a single nucleotide change, and 80% of these variants were located within the protein-coding sequences whereas alterations in untranslated regions (UTR) were less common. The highest numbers of alterations within protein-coding sequences were detected in *BRCA1* (four missense and three synonymous) and *BRCA2* (three synonymous, two missense, and one nonsense). Mutations resulting in a premature termination codon were found only in *BRCA2*, whereas synonymous (54%) and missense (42%) mutations accounted for most alterations detected. Among all 30 exonic variants, 27 were common in the general populations and 19 were classified as benign due to a lack of evidence for pathogenicity. Three alterations (two in *BRCA2* and one in *TP53*) located in a mutational hot spot and/or connected with previously reported data on pathogenicity (functional studies supportive of a damaging effect) were classified as pathogenic or of unknown significance (Table S1).

Regarding the impact of the variants on protein function, we identified three mutations predicted to cause loss of function (in *TP53*, *BRCA2*, and *PARP1*) and two causing gain of function (*ATR* and *CHEK1*). A pathogenic homozygous G244D (c.731G > A) mutation in *TP53* was present with 100% allele frequency in both OC cell lines, which is typical in 94–96% of HGSOC clinical cases [48,49]. Notably, *TP53*-mutated tumors are associated with abrogated G1/S cell cycle checkpoint and increased reliance on the G2/M checkpoint upon DNA damage [49]. While the identified *BRCA1* S1613G missense variant is localized in a mutational hot spot, functional assays have revealed no damaging effect on protein function [50,51]. Other *BRCA1* nonsynonymous variants (P871L, E1038G, K1183R) were classified as benign by the ClinVar variant database based on functional studies. Additionally, consistent with previous reports [52], *BRCA1* proteins with each missense variant (P871L, E1038G, K1183R, S1613G) identified by our group possessed HR activity similar to that of the respective wild-type counterparts, as determined using the HR reporter assay. We additionally identified five SNVs in the *ATR* gene in both OC cell lines; however, they were classified as of benign pathogenicity due to high frequencies in general populations. Sequencing results showed that PEO1 and PEO1-OR possess two exonic SNVs of *CHEK1*, one located in a protein-coding sequence (c.1411A > G, p.I471V) and the other in the 3' UTR (c.\* 28–3033C > G). Both cell lines were homozygous for the missense variant *CHEK1* I471V, which was computationally predicted to cause gain-of-function activity. A comparison of the frequencies of alterations detected in PEO1 and PEO1-OR cell lines revealed significantly different allele frequencies of one mutation in *BRCA2* (34% vs. 94%) and one in *H2AX* (53% vs. 35%).

#### 3.4. Upregulation of *BRCA2* Is Correlated with a Secondary Reversion Mutation Accounting for Acquired Resistance to Olaparib in OC Cells

Intrinsic and acquired resistance to PARPi are associated with secondary reversion mutations in *BRCA1/2* genes that restore the open reading frame (ORF) in OC [40,53]. We confirmed that the PEO1 olaparib-sensitive cell line is a carrier of the *BRCA2* Y1655\* (c.4965C > G) variant (Table 1), consistent with previous reports as PEO1 cells were originally established from a female OC patient carrying the same mutation [40]. This pathogenic variant was predicted to result in a termination signal at position 1655 resulting in a truncated protein product in case of successful translation of mRNA (Figure 3A). The same SNV was detected in the PEO1-OR cell line, with 100% allele frequency in both cases.

Within the same nucleotide triplet (TAC) at position 1655 in wild-type *BRCA2*, we identified a secondary single-nucleotide substitution (c.4964A > T, p.Y1655F) in both PEO1 and PEO1-OR cells. Notably, PEO1-OR cells were enriched (allele frequency of 94%) in the c.4964A > T variant compared to parental PEO1 cells (allele frequency of 34%). Interestingly, the c.4964A > T variant could be considered a reversion mutation, as the co-occurrence of both adjacent SNVs (c.4964A > T and c.4965C > G) may reestablish the ORF of *BRCA2* by altering a stop codon (TAG) to a nucleotide triplet encoding Leu (TTG).

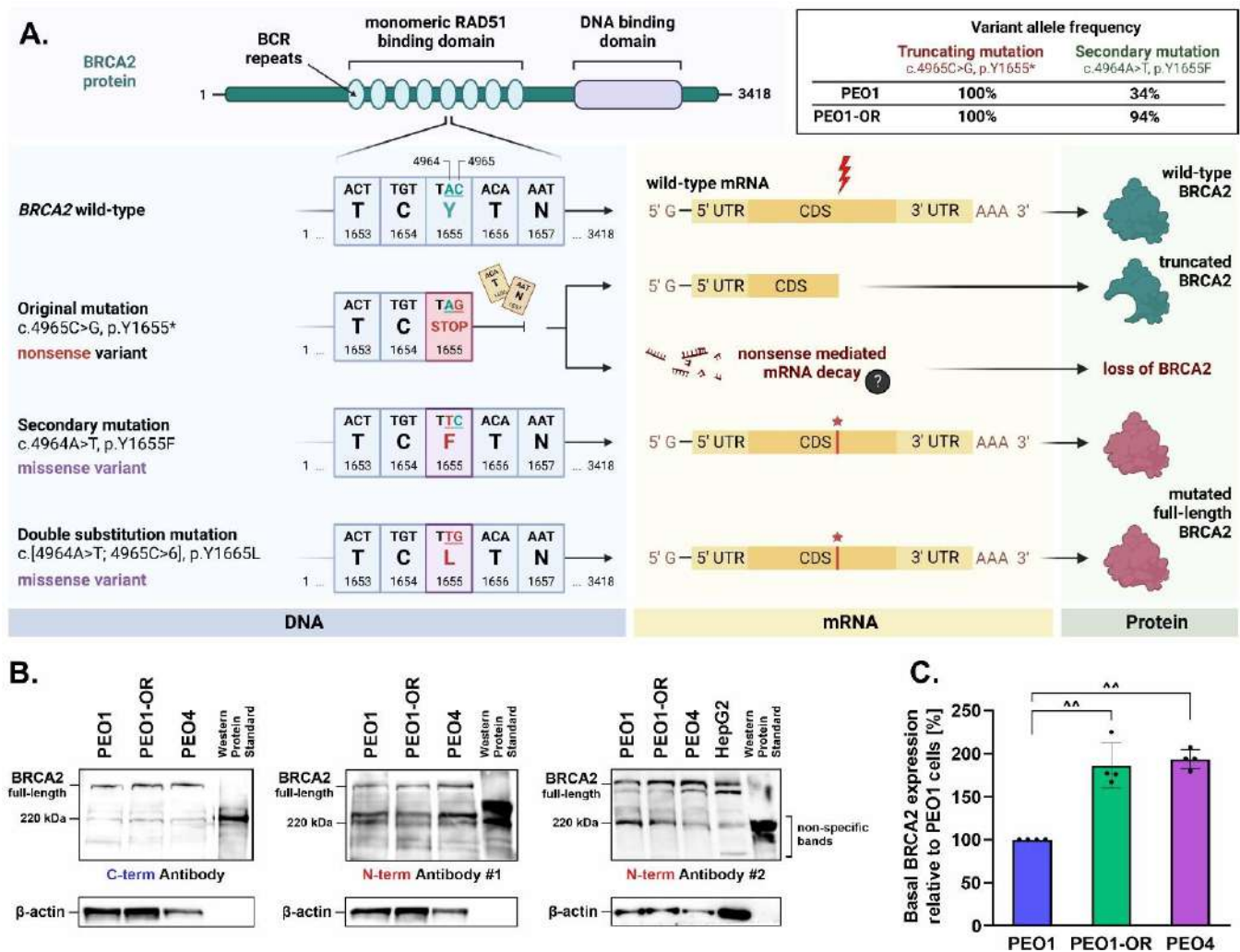


**Figure 3.** Restoration of wild-type *BRCA2* open reading frame by secondary reversion mutation promotes upregulation of *BRCA2*, potentially accounting for olaparib resistance in PEO1-OR cells. (A) Schematic representation of the biochemical consequences of key *BRCA2* variants detected using WES. PEO1-OR and PEO1 cells are homozygous for a truncating mutation (c.4965C > G, p.Y1655\*). Co-occurrence of a secondary mutation (c.[4964A > T; 4965C > G], p.Y1655L) removes the premature stop codon introduced by the truncation mutation originating from the PEO1 cell line, restoring the wild-type ORF of *BRCA2*. (B) Qualitative Western blot analysis of full-length and truncated *BRCA2* in OC cells. The HepG2 cell line was used as a negative control of truncated *BRCA2* expression to exclude non-specific bands. An anti-*BRCA2* antibody against the C-terminus and two antibodies against the N-terminus (targeting different epitopes) were used to differentiate between the two protein forms. (C) Quantitative Western blot analysis of basal expression of full-length *BRCA2* in OC using a monoclonal antibody against the N-terminus #2. The results are expressed as mean  $\pm$  SD ( $n = 4$ ). Statistical significance was assessed using ordinary one-way ANOVA followed by Tukey's test.  $^{**} p < 0.01$ : differences between cell lines. CDS—coding sequence, UTR—untranslated region.



Next, we biochemically confirmed via Western blot that PEO1 and PEO1-OR cells restored the ORF of *BRCA2* expressing full-length protein (Figure 3B). PEO4 cells with a known *BRCA2* reversion mutation (c.4965C > T, p.Y1655Y) and HepG2 cells were used as negative controls of truncated *BRCA2* expression [40]. *BRCA2* protein was detected in PEO1, PEO1-OR, and PEO4 cells using antibodies recognizing C-terminal and N-terminal regions, indicating that all the OC cell lines express full-length *BRCA2* (Figure 3B). Surprisingly, the truncated *BRCA2* variant (Y1655 \*) was not detected in PEO1 cells using two different anti-*BRCA2* (N-term) antibodies (Figure 3B), suggesting that expression of the variant possessing a single truncation mutation is abrogated in PEO1 cells, which was further confirmed using SKOV-3 and OV-90 cells as negative controls (Figure S2). Interestingly, quantitative analysis of basal intact *BRCA2* expression revealed significant upregulation of *BRCA2* levels in PEO1-OR cells compared to PEO1 cells (Figure 3C). Hence, we hypothesize that subclonal selection of the *BRCA2* reversion variant contributes to the overexpression of the protein in olaparib-resistant PEO1-OR cells.

### 3.5. Inhibition of MDR1 Drug Efflux Pump Does Not Restore Sensitivity to Olaparib, ATRi, or CHK1i in Olaparib-Resistant Cells

The MDR1 efflux pump is associated with resistance to olaparib in OC cells [54]. Hence, we examined the potential involvement of MDR1 in the cytotoxic activity of olaparib, ATRi, CHK1i, and combination treatments in HGSOc cell lines.

We observed no significant differences in the basal expression of MDR1 between PEO1 and PEO1-OR cell lines (Figure 4A). Interestingly, a 2.3-fold increase in MDR1 expression was evident in untreated PEO4 compared to PEO1 cells. Olaparib had no significant effect on MDR1 expression in OC cells after 48 h of treatment (Figure 4B). However, PEO1-OR cells with decreased sensitivity to tested inhibitors showed a significant upregulation of MDR1 after incubation with ATRi, CHK1i, or their combinations with PARPi. Next, we assessed the viability of OC cells in response to the drugs after 48 h in the presence of a non-toxic concentration (0.1  $\mu$ M) of a specific inhibitor of MDR1, tariquidar [55], using the MTT assay (Figure 4D). Simultaneous incubation with tariquidar and the above inhibitor compounds did not significantly affect the viability of OC cell lines after 48 h relative to treatment with the drugs in the absence of the MDR1 inhibitor. Blockage of MDR1 in PEO1-OR cells did not significantly restore the augmented sensitivity of parental PEO1 cells to olaparib, ATRi, and CHK1i (Figure 4D). To further clarify the role of MDR1, we employed doxorubicin (an MDR1 substrate) and P-glycoprotein inhibitors (tariquidar and verapamil) in an MDR1-expressing HepG2 cell model of drug transport (Figure S3). The addition of verapamil (50  $\mu$ M) or tariquidar (0.1  $\mu$ M) to doxorubicin led to significantly enhanced cytotoxicity in HepG2 cells in a dose-dependent manner, compared to doxorubicin alone, indicating that verapamil and tariquidar inhibit MDR1 activity. Notably, however, inhibition of MDR1 with either verapamil or tariquidar alone did not enhance the response of HepG2 cells to olaparib, ATRi, CHK1i, or their combinations (Figure S3).

### 3.6. Olaparib Synergistically Increases Cleavage of PARP1 in Olaparib-Sensitive OC Cells in Combination with ATRi or CHK1i

Next, we evaluated the mechanisms underlying the synergistic cytotoxicity of olaparib combined with ATRi or CHK1i. Basal levels of PARP1 were similar in all OC cell lines (Figure S4). The expression of PARP1 was significantly increased in all OC cells treated for 48 h with olaparib alone compared to control cells (Figure 5A); however, PEO1-OR cells exhibited the highest elevation of PARP1 expression in response to olaparib (by 2.1-fold). Compared to control cells, the addition of either ATRi or CHK1i to olaparib led to significant upregulation of PARP1, but to the same level as that observed with PARPi monotherapy. Olaparib, ATRi, and CHK1i alone induced marked elevation of the cleaved PARP1 fraction, a biomarker of caspase-dependent apoptosis [53,54], compared with the control group in PEO1 cells only (by 3.2-fold and 4.2-fold, respectively). PARPi also induced a significant synergistic increase in cleaved PARP1 compared to the control group in the presence of

ATRi or CHK1i only in olaparib-sensitive cells, in line with the results of the MTT assay (Figure 2C).

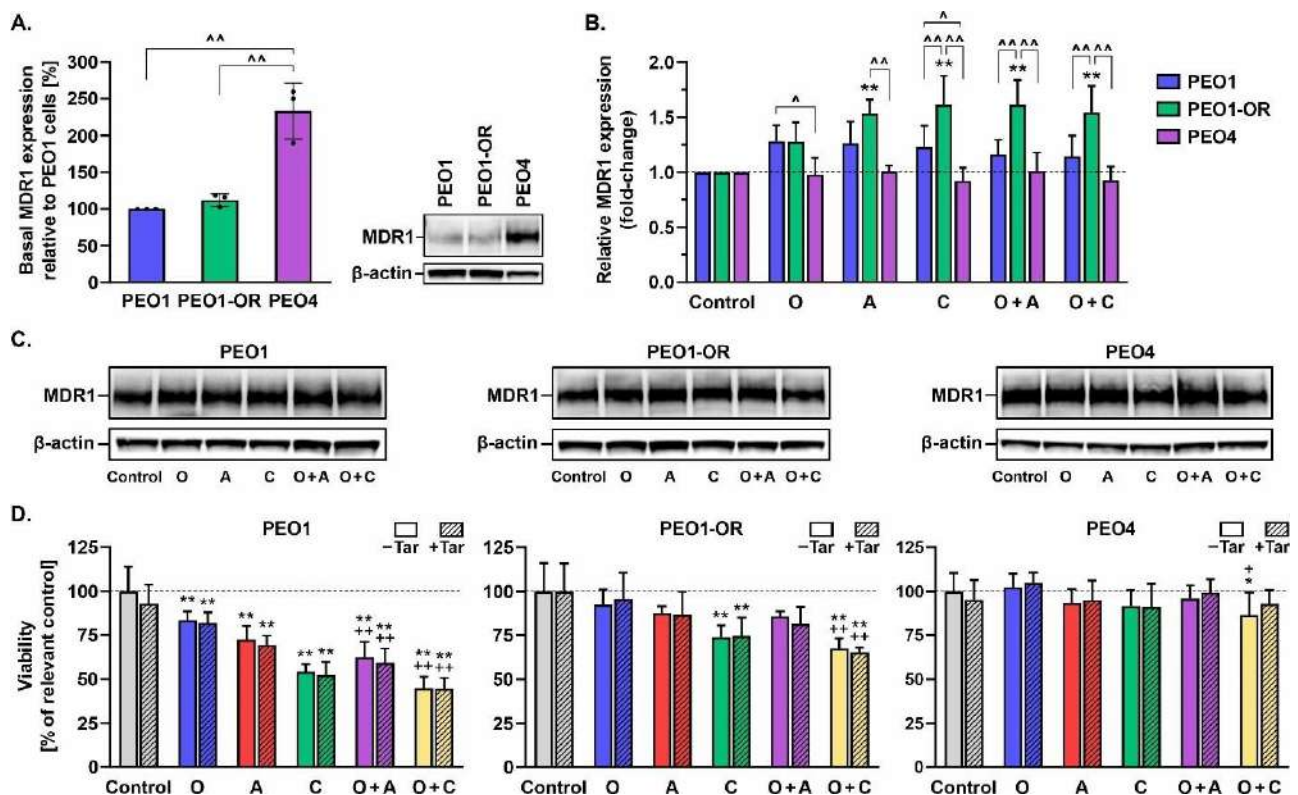


**Figure 4.** MDR1 efflux pump makes a negligible contribution to the sensitivity of HGSOc cell lines to olaparib, ATRi, and CHK1i. (A) Quantitative Western blot analysis of basal MDR1 expression in untreated OC cell lines cultured for 72 h and (B) changes in MDR1 after incubation with the inhibitor compounds for 48 h. Protein levels were quantified following normalization to  $\beta$ -actin and calculated as fold-change relative to untreated controls. Basal levels of protein were calculated relative to PEO1 cells. Results are expressed as mean  $\pm$  SD ( $n = 3$ ). Statistical significance was assessed using ordinary one-way ANOVA (basal protein expression) and two-way ANOVA (responses to tested compounds), both followed by Tukey's test. ^  $p < 0.05$ , ^^  $p < 0.01$ : differences between cell lines; \*  $p < 0.05$ , \*\*  $p < 0.01$ : treatment vs. control; +  $p < 0.05$ , ++  $p < 0.01$ : olaparib vs. combinations with ATRi or CHK1i. (C) Representative Western blot images. (D) Cell viability, defined as cellular metabolic activity, was assessed using the MTT assay in response to treatment for 2 days with olaparib (O, 5  $\mu$ M), ATRi (A, 0.5  $\mu$ M), CHK1i (C, 2.5  $\mu$ M), or their combinations for 48 h in the absence and presence of the MDR1 inhibitor tariquidar (Tar, 0.1  $\mu$ M). Data are expressed as mean  $\pm$  SD ( $n = 3$ ). Ordinary one-way ANOVA followed by Tukey's test or Brown–Forsythe version of one-way ANOVA followed by Dunnett's T3 test was used to compare the sensitivity of the cell lines to the test compounds.

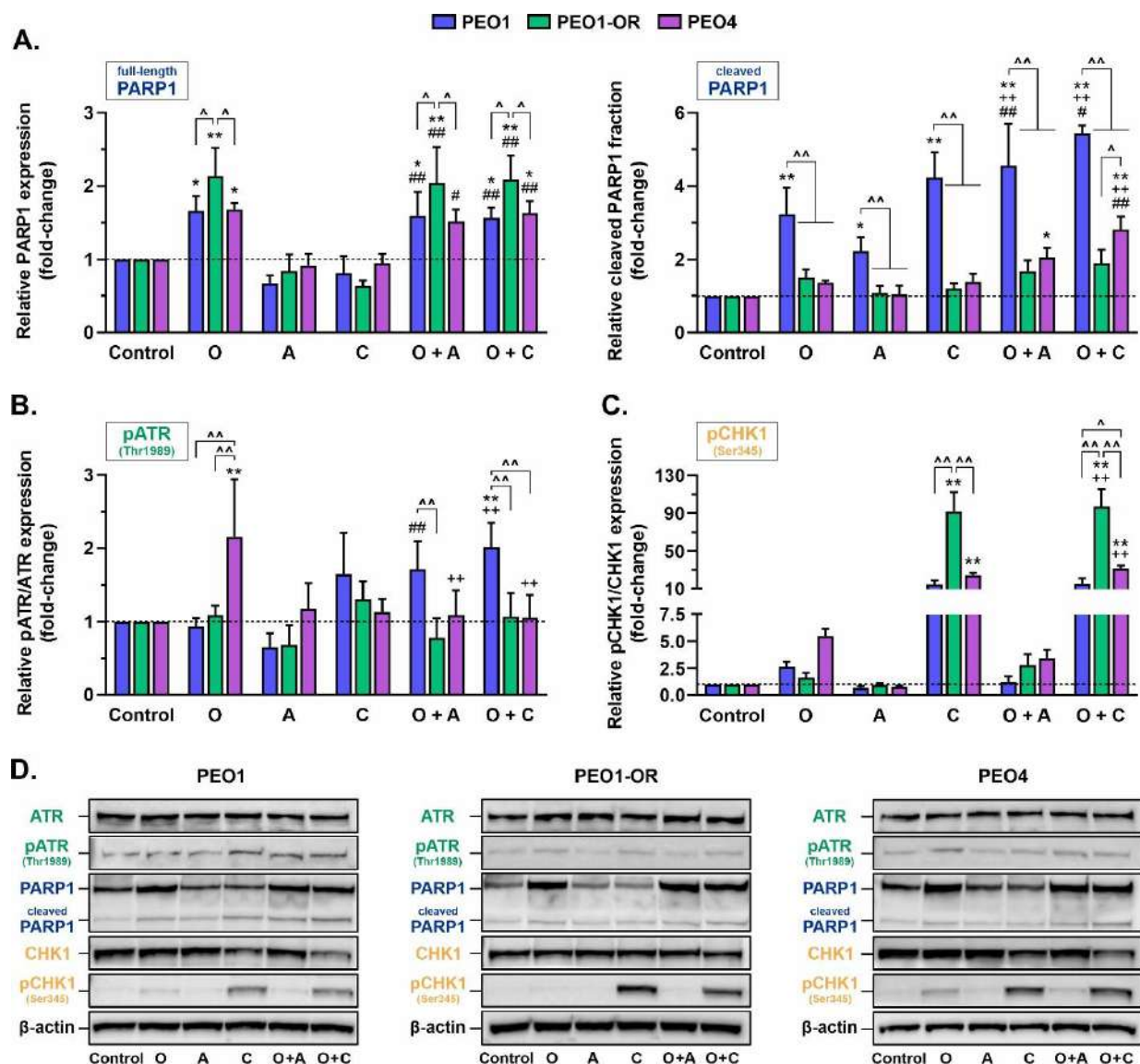


**Figure 5.** Monotherapy with olaparib, ATRi, and CHK1i or their combinations alter the expression and phosphorylation levels of targeted proteins and PARP1 cleavage in a cell-dependent manner. Quantitative Western blot analysis of (A) full-length and cleaved PARP1, (B) total and phosphorylated ATR (Thr1989), and (C) total and phosphorylated CHK1 (Ser345) in OC cell lines. Cells were incubated with olaparib (O, 5  $\mu$ M), ATRi (A, 0.5  $\mu$ M), CHK1i (C, 2.5  $\mu$ M), or their combinations for 48 h, and whole-cell lysates were prepared immediately afterward. Protein levels were quantified following normalization to  $\beta$ -actin and calculated as fold-change relative to untreated controls. The results are presented as mean  $\pm$  SD ( $n = 3$ ). Statistical significance was assessed using two-way ANOVA followed by Tukey's test. ^  $p < 0.05$ , ^^  $p < 0.01$ : differences between cell lines; \*  $p < 0.05$ , \*\*  $p < 0.01$ : treatment vs. control; ++  $p < 0.01$ : olaparib vs. combinations with ATRi or CHK1i; #  $p < 0.05$ , ##  $p < 0.01$ : ATRi or CHK1i vs. respective combinations with olaparib. (D) Representative Western blot images.

### 3.7. PEO1-OR Cells Bypass Olaparib-Induced Activation of the ATR/CHK1 Pathway

We speculated that increased G2/M checkpoint arrest in OC cell lines is primarily activated through ATR/CHK1 signaling based on the finding that olaparib-sensitive cells display increased reliance on the ATR/CHK1 axis [17,23]. To examine this hypothesis, we investigated the phosphorylation of ATR at Thr1989 and CHK1 at Ser345, events responsible for the activation of ATR/CHK1 signaling in response to DNA damage [26,27].

As shown in Figure 5, olaparib treatment had a significant impact on the ATR/CHK1 pathway. Auto-phosphorylation of ATR was significantly induced in PEO4 cells by 2.1-fold (Figure 5B), and notably increased phosphorylation of pCHK1 was observed in PEO1 and PEO4 cells by 2.7- and 5.5-fold, respectively (Figure 5C), suggesting activation of ATR/CHK1 signaling for survival. The addition of ATRi decreased PARPi-induced phosphorylation of pCHK1 in PEO1 and PEO4 cells, indicating inhibition of ATR activation. As expected [56,57], the inhibition of CHK1 caused the accumulation of CHK1 phosphorylated at Ser345 in all OC cell lines. On the contrary, olaparib alone or combined with ATRi only non-significantly increased levels of pCHK1 (by 2.8-fold) irrespective of ATR phosphorylation in PEO1-OR cells, indicating decreased reliance on ATR/CHK1 signaling for survival in olaparib-resistant cells.

### 3.8. Olaparib Combined with Blockage of ATR/CHK1 Enhances DNA Double-Strand Breaks Irrespective of RAD51-Mediated HR Activity in BRCA2<sup>MUT</sup> Ovarian Cancer Cells

PARPi agents promote the accumulation of DSBs in OC cells [17,23], resulting in phosphorylation of H2AX at serine 139, whereas RAD51 recombinase is a critical factor involved in the repair of deleterious DSBs by HR, serving as a useful marker for HR proficiency and recruitment of HR repair factors [9,58]. We hypothesized that inhibition of PARP1 and blockage of the ATR/CHK1 pathway could trigger elevated phosphorylation of H2AX, with the significant formation of  $\gamma$ H2AX only in olaparib-sensitive cells.

The basal phosphorylation level of  $\gamma$ H2AX was significantly higher in untreated PEO1 cells compared to PEO1-OR and PEO4 cells (Figure 6A). Only PEO1 cells exhibited significant changes in  $\gamma$ H2AX expression in response to all the inhibitor compounds after 48 h (Figure 6B). Upon treatment with olaparib or ATRi, similar increases in phosphorylation of H2AX were observed (by 2.0-fold), whereas CHK1i induced a 4.1-fold change in  $\gamma$ H2AX. Combined treatment with olaparib and ATRi synergistically augmented  $\gamma$ H2AX levels in olaparib-sensitive cells, indicating that olaparib-sensitive cells were the most susceptible to DNA damage. Interestingly,  $\gamma$ H2AX was increased to similar levels in the presence of CHK1i alone or combined with olaparib in all OC cells. Similar to data obtained with olaparib and ATRi, PEO1-OR cells exhibited the lowest elevation of  $\gamma$ H2AX upon co-incubation with olaparib and CHK1i (1.8-fold) relative to PEO1 (4.2-fold) and PEO4 (2.9-fold) cells. Basal RAD51 expression was comparable in untreated PEO1 and PEO1-OR cells but significantly downregulated in PEO4 cells (Figure 6B). No significant changes in RAD51 protein levels were detected in all OC cell lines exposed to the inhibitor compounds compared to untreated cells. Following olaparib treatment, PEO1-OR cells exhibited moderately increased expression of RAD51 compared to parental PEO1 cells (Figure 6B), which may be associated with resistance to PARPi.

Recruitment of RAD51 to DNA lesion sites has been proposed as a biomarker of HR proficiency in ovarian cancer cells [59]. Furthermore, we confirmed that the BRCA2 variant (c.[4964A > T; 4965C > G], p.Y1655L) harboring a missense mutation in a BRC5 repeat responsible for RAD51 binding was functional and RAD51 recruitment to DNA damage sites was not disrupted in BRCA2<sup>MUT</sup> OC cells by monitoring formation and co-localization of RAD51 and  $\gamma$ H2AX foci in OC cells (Figure 6D). RAD51 formed foci at the sites of DSBs, represented by  $\gamma$ H2AX foci, in all OC cell lines, suggesting that BRCA2<sup>MUT</sup> OC cells are HR-proficient. We observed the most apparent  $\gamma$ H2AX foci formation in PEO1 and PEO4 cells in response to olaparib combined with CHK1i (Figure 6D). In PEO4 and PEO1-OR cells, a major fraction of  $\gamma$ H2AX foci co-localized with RAD51 foci with each treatment. Lower levels of phosphorylated H2AX and reduced  $\gamma$ H2AX foci formation in PEO1-OR cells compared to PEO1 and PEO4 cells in response to studied inhibitors confirm the phenotype of decreased drug sensitivity in olaparib-resistant cells.



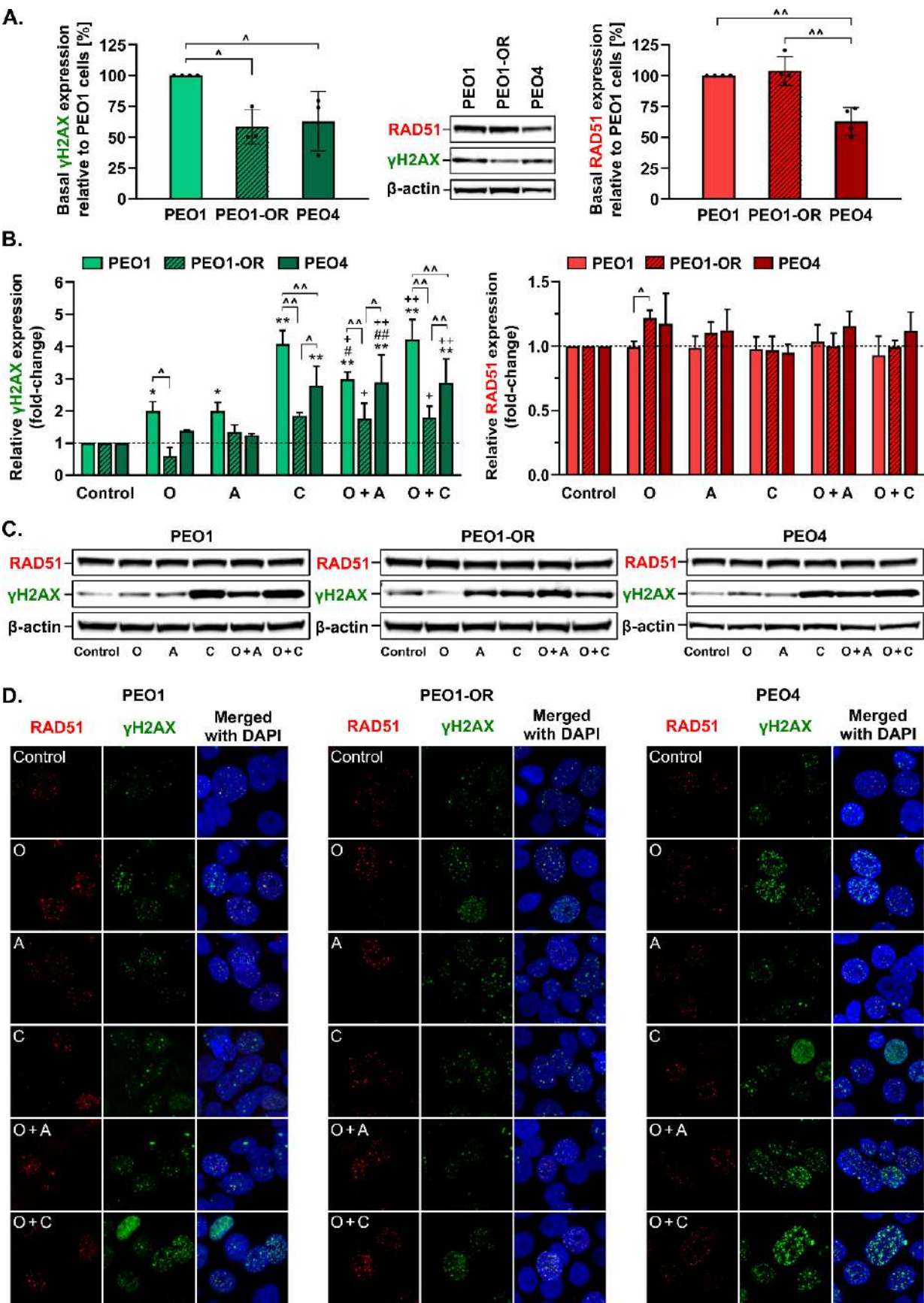


**Figure 6.** Olaparib-resistant cells exhibit decreased phosphorylation of the DSB marker H2AX in response to inhibitor treatment compared to sensitive OC cell lines. Quantitative Western blot of

(A) RAD51 and (B) phosphorylation of H2AX at Ser139 to  $\gamma$ H2AX in OC cell lines. Basal protein expression calculated from densitometric data relative to PEO1 cells. Cells were incubated for 48 h with olaparib (O, 5  $\mu$ M), ATRi (A, 0.5  $\mu$ M), CHK1i (C, 2.5  $\mu$ M), or their combinations, and whole-cell lysates prepared immediately afterward. Protein levels following treatment were quantified, with normalization to  $\beta$ -actin as a loading control, and calculated as fold-change relative to untreated controls. The results are presented as mean  $\pm$  SD ( $n = 3$ ). Statistical significance was assessed using ordinary one-way ANOVA (basal protein expression) and two-way ANOVA (responses to tested compounds), both followed by Tukey's test.  $^{\wedge} p < 0.05$ ,  $^{\sim} p < 0.01$ : differences between cell lines;  $* p < 0.05$ ,  $** p < 0.01$ : treatment vs. control;  $+ p < 0.05$ ,  $++ p < 0.01$ : olaparib vs. combinations with ATRi or CHK1i;  $\# p < 0.05$ ,  $## p < 0.01$ : ATRi or CHK1i vs. respective combinations with olaparib. (C) Representative Western blot images of RAD51 and  $\gamma$ H2AX. (D) Representative immunofluorescence images at  $63\times$  oil magnification of co-localized RAD51 foci (red) with  $\gamma$ H2AX foci (green) and nuclei stained with DAPI (blue) in OC cells exposed to the combined inhibitor compounds.

### 3.9. Olaparib-Resistant Cells Exhibit Decreased Accumulation of Chromosomal Aberrations and DNA Double-Strand Breaks Compared to Sensitive OC Cell Lines

DNA DSBs are pivotal lesions leading to the formation of structural chromosomal aberrations and HRD-associated genomic instability in OC cells [60–62]. The DNA lesion levels evaluated in studied HGSOc cell lines after 48 h of incubation (Figure 7) were correlated with the cytotoxic activity of inhibitors after 5 days, as determined with the MTT assay (Figure 2), and mostly with  $\gamma$ H2AX expression (Figure 6B).

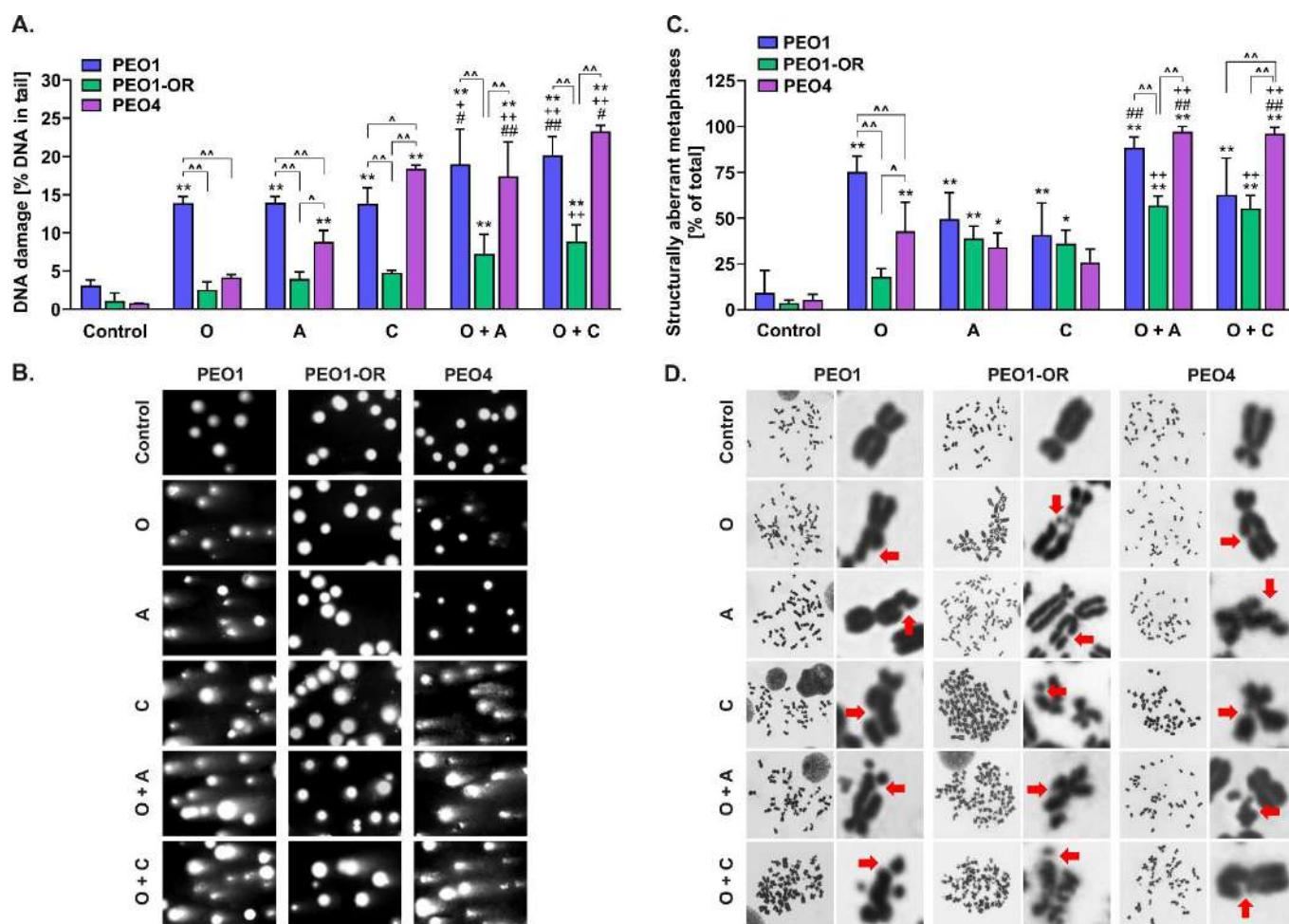


**Figure 7.** Resistance to olaparib is correlated with reduced accumulation of DSBs, generating fewer structural chromosomal aberrations in PEO1-OR cells. (A) DNA double-strand breaks examined with



the neutral comet assay in OC cells exposed to olaparib (5  $\mu$ M), ATRi (0.5  $\mu$ M), CHK1i (2.5  $\mu$ M), or their combinations for 48 h. The DNA strand-breaking agent doxorubicin (2.5  $\mu$ M) was used as a positive control in the comet assay. Results are expressed as mean  $\pm$  SD ( $n = 4$ ). (B) Representative images of DNA comets with tails. (C) Structural metaphase chromosomal aberrations induced by inhibitors in OC cells. Cells were incubated with olaparib (O, 5  $\mu$ M), ATRi (A, 0.5  $\mu$ M), CHK1i (C, 2.5  $\mu$ M), or their combinations for 48 h and arrested at the mitosis stage in the presence of colcemid (0.1  $\mu$ g/mL) for 1 h. Metaphase chromosomes were stained with Giemsa and visualized at 100 $\times$  magnification. Chromosomal structural aberrations were analyzed in 105 metaphase spreads scored for abnormalities for each group. Results are expressed as mean  $\pm$  SD ( $n = 3$ ). Statistical significance was assessed using two-way ANOVA followed by Tukey's test.  $^{\wedge} p < 0.05$ ,  $^{\wedge\wedge} p < 0.01$ : differences between cell lines;  $^* p < 0.05$ ,  $^{**} p < 0.01$ : treatment vs. control;  $^+ p < 0.05$ ,  $^{++} p < 0.01$ : olaparib vs. combinations with ATRi or CHK1i;  $^{\#} p < 0.05$ ,  $^{\#\#} p < 0.01$ : ATRi or CHK1i vs. respective combinations with olaparib. (D) Representative images of metaphase spreads with aberrant chromosomes indicated by red arrows (chromatid gaps and breaks).

The results of the neutral comet assay showed significantly increased comet tail formation after treatment with all the inhibitors in PEO1 compared to PEO1-OR cells (Figure 7A,B), indicating decreased DNA damage in olaparib-resistant cells. Treatment of PEO1-OR and PEO4 with PARPi did not induce elevation of DSBs, which were significantly higher in PEO1 cells by 5.4-fold and 3.3-fold, respectively. Olaparib, ATRi, and CHK1i exerted no significant effects on DSB levels in PEO1-OR cells, while a synergistic genotoxic effect of combined treatments was observed in PEO1 and PEO4 cells. In PEO1 cells, the addition of ATRi or CHK1i to olaparib significantly augmented PARPi-induced comet tail formation from 14.0% to 19.0% and 20.2%, respectively. Moreover, combined treatment sensitized PEO4 cells to olaparib, causing a marked increase in DSB formation to levels comparable to those of PEO1 cells (Figure 7A).

We further analyzed structural chromosomal abnormalities induced by the inhibitors after 48 h in OC cell lines (Figure 7C,D). Olaparib exerted more significant structural abnormalities in PEO1 cells than in PEO1-OR and PEO4 cells (Figure 7C), in line with marked olaparib-induced accumulation of DSBs (Figure 7A). Blockage of the ATR/CHK1 pathway did not cause a significant increase in tail DNA in PEO1-OR cells (Figure 7A), suggesting that ATRi- and CHK1-induced chromosomal instability in olaparib-resistant cells is attributable to other types of DNA lesions (Figure 7C). Combination of olaparib with ATRi or CHK1i synergistically elevated olaparib-induced chromosomal alterations in PEO4 cells only, as evident from the marked increase in the aberrant metaphase (up to 97% and 96%, respectively). Notably, the addition of ATRi or CHK1i to olaparib caused a less prominent elevation in aberrant metaphase in PEO1-OR (by 32% and 8% for O + A and O + C, respectively) and PEO4 cells (by 40% for O + A and 41% O + C, respectively) relative to PEO1 cells (Figure 7C).

Our results collectively showed significantly lower levels of DSBs and chromosomal aberrations in olaparib-resistant cells compared to PEO1 and PEO4 cells. Enhanced generation of DSBs in response to the combination of olaparib with ATRi or CHK1i in olaparib-sensitive cells was correlated with increased accumulation of aberrant metaphases, indicating genotoxic instability in OC cells.

### 3.10. PEO1-OR Cells Progress Normally through the Cell Cycle upon Inhibition of PARP1 and the ATR/CHK1 Axis

Treatment with olaparib is associated with extended arrest at either the G0/G1 [63] or G2/M phase [64] of the cell cycle in OC cell lines. Therefore, we concurrently evaluated the effects of inhibitors tested on cell cycle distribution and DSB accumulation (Figure 8).

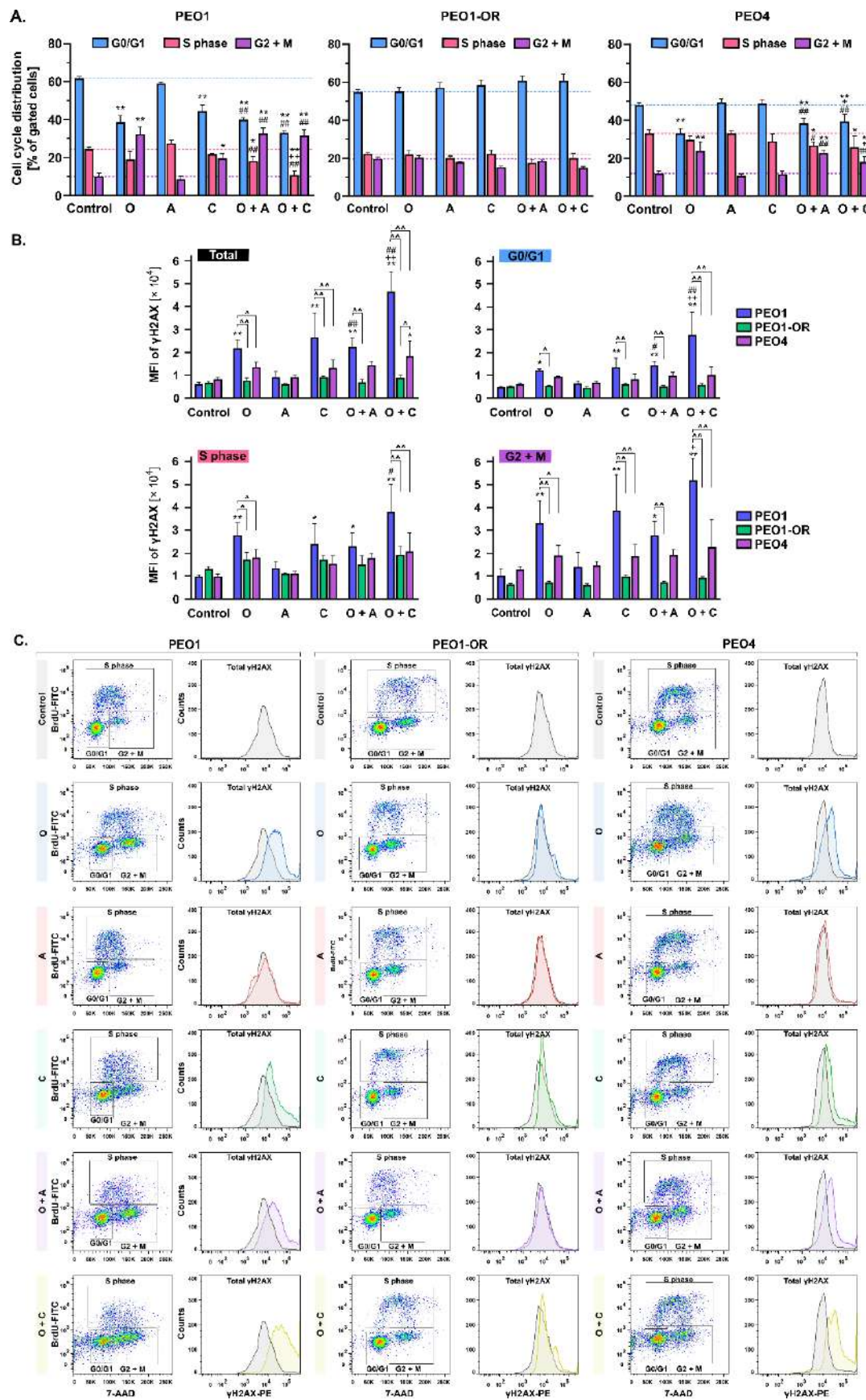


**Figure 8.** Effects of olaparib, ATRi, CHK1i, and their combinations on cell cycle distribution and accumulation of  $\gamma$ H2AX depend on the sensitivity of OC cell lines to olaparib. (A) Cell cycle analysis

with concurrent (B) quantitative assessment of  $\gamma$ H2AX levels was performed via flow cytometry. Briefly, cells were incubated for 48 h with olaparib (O, 5  $\mu$ M), ATRi (A, 0.5  $\mu$ M), CHK1i (C, 2.5  $\mu$ M), or their combinations, pulsed with BrdU during the final 3 h of the treatment, and harvested for co-staining of incorporated BrdU and intracellular  $\gamma$ H2AX. Levels of  $\gamma$ H2AX were assessed based on geometric mean fluorescence intensity (MFI). Results are expressed as mean  $\pm$  SD ( $n = 3$ ). Statistical significance was assessed using two-way ANOVA followed by Tukey's test.  $^{\wedge} p < 0.05$ ,  $^{\wedge} p < 0.01$ : differences between cell lines;  $* p < 0.05$ ,  $** p < 0.01$ : treatment vs. control;  $+ p < 0.05$ ,  $++ p < 0.01$ : olaparib vs. combinations with ATRi or CHK1i;  $\# p < 0.05$ ,  $## p < 0.01$ : ATRi or CHK1i vs. respective combinations with olaparib. (C) Dot plots of BrdU/FITC and 7-AAD stained cells and histograms with overlay signals of PE-conjugated anti- $\gamma$ H2AX antibody from untreated (gray) and treated (color) cells.

As expected, following 48 h incubation, olaparib induced a G2/M block in PEO1 cells compared to untreated cells where the G2/M phase subpopulation increased from 10% to 32%, accompanied by a 23% decrease in the G0/G1 phase subpopulation (Figure 8A). However, the addition of ATRi or CHK1i had an effect similar to that of PARPi alone on G2/M arrest in PEO1 cells. Analogous to PEO1 cells, olaparib alone and combined with ATRi or CHK1i induced notable G2/M arrest in PEO4 cells. Interestingly, olaparib-resistant cells progressed normally through all phases of the cell cycle following treatment with the inhibitors, both alone and in combination (Figure 8A).

Simultaneously, we did not observe significant changes in phosphorylation of H2AX in PEO1-OR cells treated with either single or combined inhibitors in contrast to parent PEO1 cells (Figure 8), which correlated with analysis of  $\gamma$ H2AX by Western blot (Figure 6B). Phosphorylation of H2AX increased substantially in all subpopulations of PEO1 cells in response to olaparib (by 3.6-fold), CHK1i (by 4.5-fold), and the combination of olaparib with either ATRi (by 3.7-fold) or CHK1i (by 7.8-fold) relative to untreated cells, indicating that H2AX phosphorylation occurs throughout the entire cell cycle. Interestingly, co-treatment of PEO1 cells with olaparib and CHK1i synergistically promoted the  $\gamma$ H2AX level compared to monotherapies. In all subpopulations of PEO4 cells, significant changes in  $\gamma$ H2AX levels were detected only upon co-treatment with olaparib and CHK1i compared to untreated cells, where S and G2/M phases predominantly contributed to the increase in  $\gamma$ H2AX levels (Figure 8).

Overall, the distribution of PEO1-OR cells in the cell cycle was relatively unchanged in response to the inhibitor treatments. Moreover, combined treatment with olaparib and blockers of the ATR/CHK1 axis led to G2/M phase arrest in olaparib-sensitive cells.

### 3.11. Crosstalk between BRCA1 and 53BP1 as an Indicator of Sensitivity to Olaparib and ATR/CHK1 Pathway Blockers

HR repair may be reactivated and potentially drive resistance to PARPi by reacquisition of DNA end resection via loss of 53BP1 in *BRCA1*-depleted cells [5]. Therefore, we examined the expression levels of BRCA1 (mediating RAD51 loading and HR-dependent DSB repair) and 53BP1 (promoting NHEJ-dependent repair) via Western blotting after 48 h of incubation with studied inhibitors (Figure 9).

Our data showed that basal levels of 53BP1 protein were similar across all HGSOC cell lines (Figure 9A). Moreover, basal BRCA1 expression was significantly upregulated in untreated PEO1-OR and PEO4 cells by 2.4-fold and 1.9-fold, respectively, compared to PEO1 cells (Figure 9B). In PEO1-OR cells, single treatment with olaparib and CHK1i induced a significant increase in BRCA1 expression by about 1.4-fold compared to untreated cells, with no concomitant changes in 53BP1 levels. Interestingly, a combination of both drugs induced the opposite response in PEO1-OR cells. Indeed, the addition of CHK1i to olaparib reduced BRCA1 expression to control levels and synergistically reduced expression of 53BP1 by 38% to a level similar to that in PEO4 cells. However, ATRi had no influence on 53BP1 and BRCA1 expression in PEO1-OR cells, and combined treatment with olaparib and ATRi exerted an effect similar to that of olaparib and CHK1i. In PEO4 cells, incubation with



single inhibitors and their combinations caused a significant decrease in BRCA1 expression to similar levels (by ~34–43%), along with 53BP1 (by ~41–48%), compared to untreated cells.

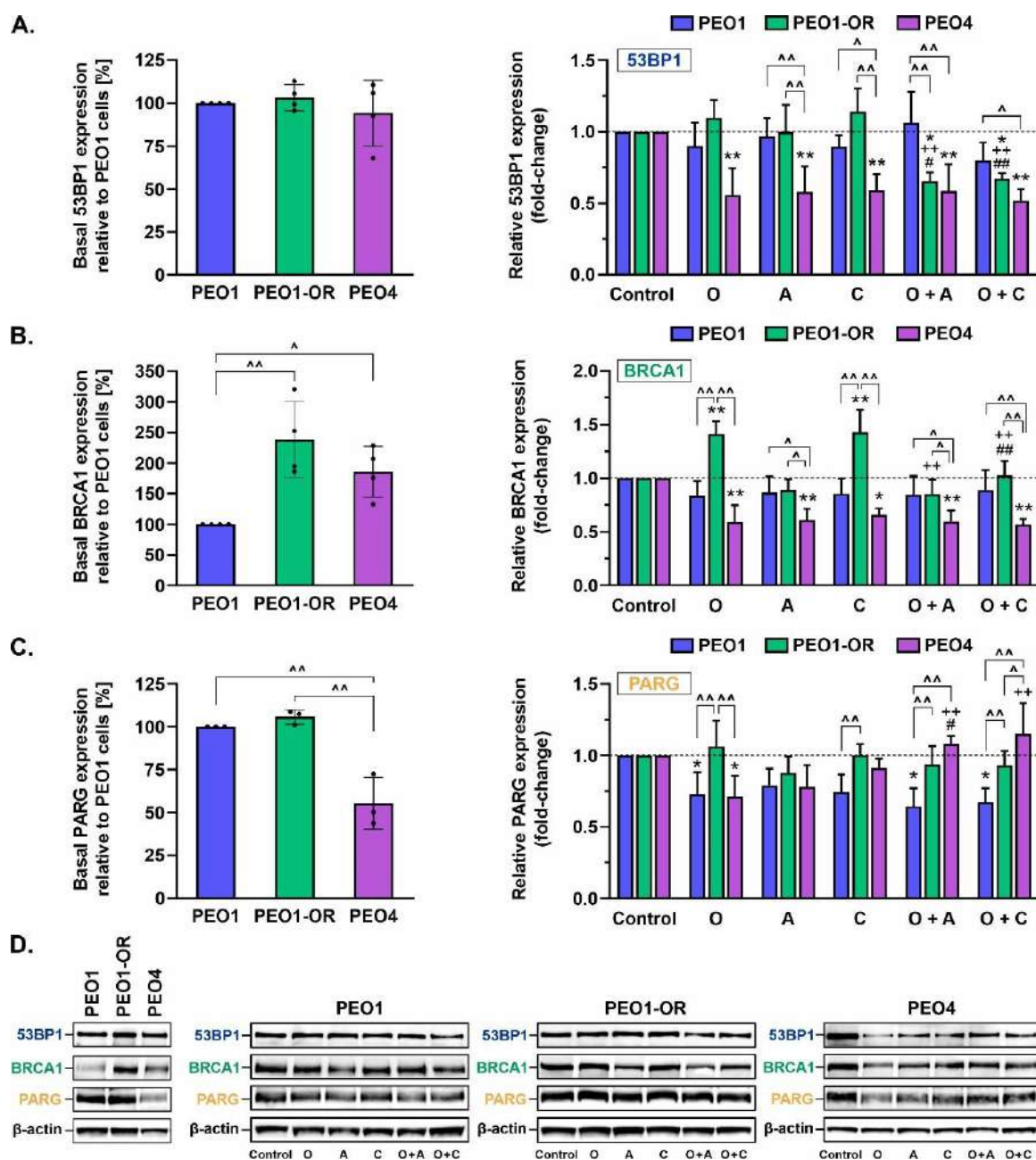


**Figure 9.** Changes in 53BP1, BRCA1, and PARG expression in OC cell lines treated with olaparib or inhibitors of the ATR/CHK1 pathway. Quantitative Western blot analysis was performed to assess basal expression of (A) 53BP1, (B) BRCA1, and (C) PARG. Protein levels upon treatment were quantified following normalization to  $\beta$ -actin as a loading control and calculated as fold-change relative to untreated controls. Cells were treated for 48 h with olaparib (O, 5  $\mu$ M), ATRi (A, 0.5  $\mu$ M), CHK1i (C, 2.5  $\mu$ M), or their combinations, and whole-cell lysates were prepared immediately afterward. Data are expressed as mean  $\pm$  SD ( $n = 3$ –4). Statistical significance was assessed using ordinary one-way ANOVA (basal protein expression) and two-way ANOVA (responses to tested compounds), both followed by Tukey's test.  $^{\wedge} p < 0.05$ ,  $^{\wedge\wedge} p < 0.01$ : differences between cell lines;  $^* p < 0.05$ ,  $^{**} p < 0.01$ : treatment vs. control;  $^{++} p < 0.01$ : olaparib vs. combinations with ATRi or CHK1i;  $^{\#} p < 0.05$ ,  $^{##} p < 0.01$ : ATRi or CHK1i vs. respective combinations with olaparib. (D) Representative Western blot images.

### 3.12. Olaparib Alone and Combined with Blockage of the ATR/CHK1 Pathway Suppresses PARG Expression in PEO1 Olaparib-Sensitive OC Cells

Next, we examined protein levels of poly(ADP-ribose) glycohydrolase (PARG) in response to inhibitor treatment (Figure 9C), as its loss is associated with PARPi resistance through suppression of olaparib-induced abrogation of PARP signaling and DNA damage [65].

Basal levels of PARG were unchanged among PEO1-OR and parental PEO1 cells. Notably, a significant reduction in basal PARG expression (by ~45%) was observed in PEO4 cells relative to the other two cell lines. The inhibitors had no significant effects on PARG levels in PEO1-OR cells; however, olaparib induced a decrease in PARG levels by 27% and 29% compared to untreated PEO1 and PEO4 cell lines, respectively. In PEO1 cells, the combination of olaparib with ATRi or CHK1i resulted in a similar decline in PARG levels to that observed upon PARPi treatment alone. PARG was restored to the basal level observed in untreated PEO4 cells upon the addition of ATRi or CHK1i. Interestingly, partial loss of PARG in PEO1 olaparib-sensitive cells accompanied upregulation of PARP1 in response to olaparib alone and in combination with ATRi and CHK1i (Figure 5A). Combined treatment with olaparib and ATRi and CHK1i also upregulated PARP1 in PEO1-OR and PEO4 cells, as shown previously (Figure 5A), but induced no significant changes in PARG levels (Figure 9C).

## 4. Discussion

Increasingly frequent clinical usage of PARPi inevitably leads to the emergence of resistance, constituting a growing problem for OC patients who relapse after treatment. Interestingly, prior exposure to PARPi is reported to decrease response to subsequent platinum-based chemotherapy in OC patients [2], which limits further therapeutic options. Over the past decade, numerous intracellular events that confer resistance to PARPi have been uncovered, including HR-dependent and HR-independent mechanisms, which are not mutually exclusive [11,16]. However, findings to date are insufficient to establish the mechanisms underlying the resensitization of OC cells to PARPi. Here we investigated how *BRCA2*<sup>MUT</sup> HGSOC cells confer resistance to olaparib and the therapeutic benefits of combined treatment with PARPi and inhibitors of the ATR/CHK1 pathway in olaparib-sensitive and -resistant cells in vitro. Furthermore, we compared cellular and molecular responses to studied treatments, with the aim of developing a promising strategy to sensitize OC to olaparib [16,17,22,23,66].

Firstly, we successfully developed a PEO1-OR olaparib-resistant cell line from PEO1 HGSOC cells harboring deleterious *BRCA2* mutations as novel OC models displaying the PARPi-resistant phenotype are indispensable for the elucidation of cellular events that contribute to a compromised response to olaparib [40]. The PEO1-OR cell model was established in vitro using moderate, stepwise increasing doses of olaparib to select stable cells with decreased sensitivity to PARPi. Considering the selection strategy and 3.3-fold decrease in olaparib cytotoxicity (according to IC<sub>50</sub> values), the newly developed cell line was classified as a clinically relevant model [35]. Data from the clonogenic assay confirmed significantly increased resistance of PEO1-OR cells to olaparib.

Following the confirmation of olaparib resistance, we showed that PEO1-OR cells acquire resistance following prolonged treatment with olaparib through multiple co-existing mechanisms (Figure 10). Data from WES analysis showed that PEO1-OR cells are enriched for a double mutation (c.[4964A > T; 4965C > G], p.Y1655L) restoring functional full-length *BRCA2* protein, suggesting that PARPi promoted subclonal selection for the variant present in a small subpopulation of parental PEO1 cells. This observation is in line with the finding of *BRCA2* reversion mutations after treatment of OC patients with PARPi [41,53,67]. However, previous works have demonstrated that PEO1 cells may acquire resistance to olaparib with or without restoration of *BRCA2* [68,69], which indicates that conferring resistant phenotype in *BRCA2*<sup>MUT</sup> HGSOC cells can occur in various ways. Moreover, Sakai et al. [40] showed that the selection of PEO1 cells with cisplatin may also induce the secondary mutation (4964A > T) restoring the *BRCA2* ORF, which is crucial for acquired resistance to chemotherapy. Unexpectedly, we did not detect expression of the truncated

BRCA2 protein in PEO1 cells, which could be attributed to nonsense-mediated mRNA decay of *BRCA2* gene transcripts with a premature stop codon, a cellular mechanism that prevents expression of truncated proteins [70]. Our findings are consistent with previous studies reporting the occurrence of a secondary *BRCA2* mutation and the presence of full-length *BRCA2* in PEO1 cells [71,72]. Interestingly, various variants of *BRCA2* have been detected in different stocks of PEO1 cells, which has been already extensively discussed [38,72]. We speculate that divergent genetic alterations of *BRCA2* may affect the expression of the full-length protein. As reported by Ciucci et al. [73], cells with *BRCA2* deficiency display decreased survival in vitro, which encourages selective pressure for reversion of the deleterious mutation. Similar restoration of functional *BRCA2* was identified in PEO1 cells following treatment with AG14361, a precursor of the PARPi talazoparib [40]. Accordingly, we propose that sub-dominant populations of OC cells harboring secondary reversion mutations undergo selection pressure against nonsense *BRCA2*<sup>MUT</sup> in response to long-term treatment with olaparib. Post-treatment analysis of tumor biopsies revealed that most patients with platinum-resistant recurrent OC harboring secondary mutations restoring *BRCA2* activity exhibited progressive disease following olaparib therapy [41]. Hence, awareness of the potential risk of developing resistance to olaparib in *BRCA2*<sup>MUT</sup> tumors should be implemented in customized regimes involving combination treatment with ATR/CHK1 inhibitors to bypass PARPi limitations. Moreover, we demonstrated significant upregulation of full-length *BRCA2* in PEO1-OR cells compared to sensitive parental cells, which could contribute to decreased sensitivity to olaparib. *BRCA2* is one of the key factors promoting HR repair and is directly associated with diminished antitumor activity of olaparib [4,7]. We also confirmed the functionality of mutant *BRCA2* in PEO1-OR cells in terms of RAD51 foci formation indicating proficiency in HR repair activity [15]. Recent studies have shown abrogated HR repair in a *BRCA2* missense variant harboring the R3052W mutation within the DNA binding domain due to disruption of translocation of *BRCA2* to the nucleus and sequestering of RAD51 in the cytoplasm [74]. Using the RAD51 functional assay, we showed that PEO1-OR cells carrying the missense *BRCA2* variant Y1655L recruit RAD51 recombinase at DNA damage sites, whereby RAD51 co-localizes with a surrogate marker of DSBs,  $\gamma$ H2AX. Similarly, PEO1 and PEO4 cells were able to induce RAD51 foci formation upon DNA damage. However, further work might be needed to comprehensively relate HRR functionality and activity with PARPi resistance in this model by HR reporter assay and/or by monitoring RAD51 foci formation in cells at the S/G2 phase where HR is most predominant.

While PARPi agents show the greatest efficacy in HRD tumors, efficacy has also been reported in a percentage of OC patients with HR proficiency [1,67]. Hence, we analyzed *BRCA1* protein based on the finding that in HR-proficient tumors, RAD51 is recruited not only by *BRCA2* but also by *BRCA1* to promote HR repair [29,75]. *BRCA1* is also an upstream regulator of *BRCA2* that directly recruits *BRCA2* at DSB sites via interactions with PALB2 [76]. Downregulation of *BRCA1* in OC cell lines has been shown to increase sensitivity to olaparib and decrease cell survival. Here, we demonstrated in PEO1-OR cells upregulation of basal levels of *BRCA1*, as well as in response to olaparib. Our findings support the hypothesis that decreased sensitivity to olaparib in OC cells is conferred through the induction of HR repair-promoting factors [77]. On the other hand, 53BP1 normally inhibits *BRCA1* to favor NHEJ repair [16]. Notably, loss of *TP53BP1* in *BRCA1*<sup>MUT</sup> OC cells was previously associated with increased HR activity as a mechanism of resistance to PARPi veliparib [5]. In our study, 53BP1 expression remained unchanged in *BRCA1*-proficient PEO1-OR cells, suggesting that accurate HR repair is favored over error-prone NHEJ through upregulation of *BRCA1*.



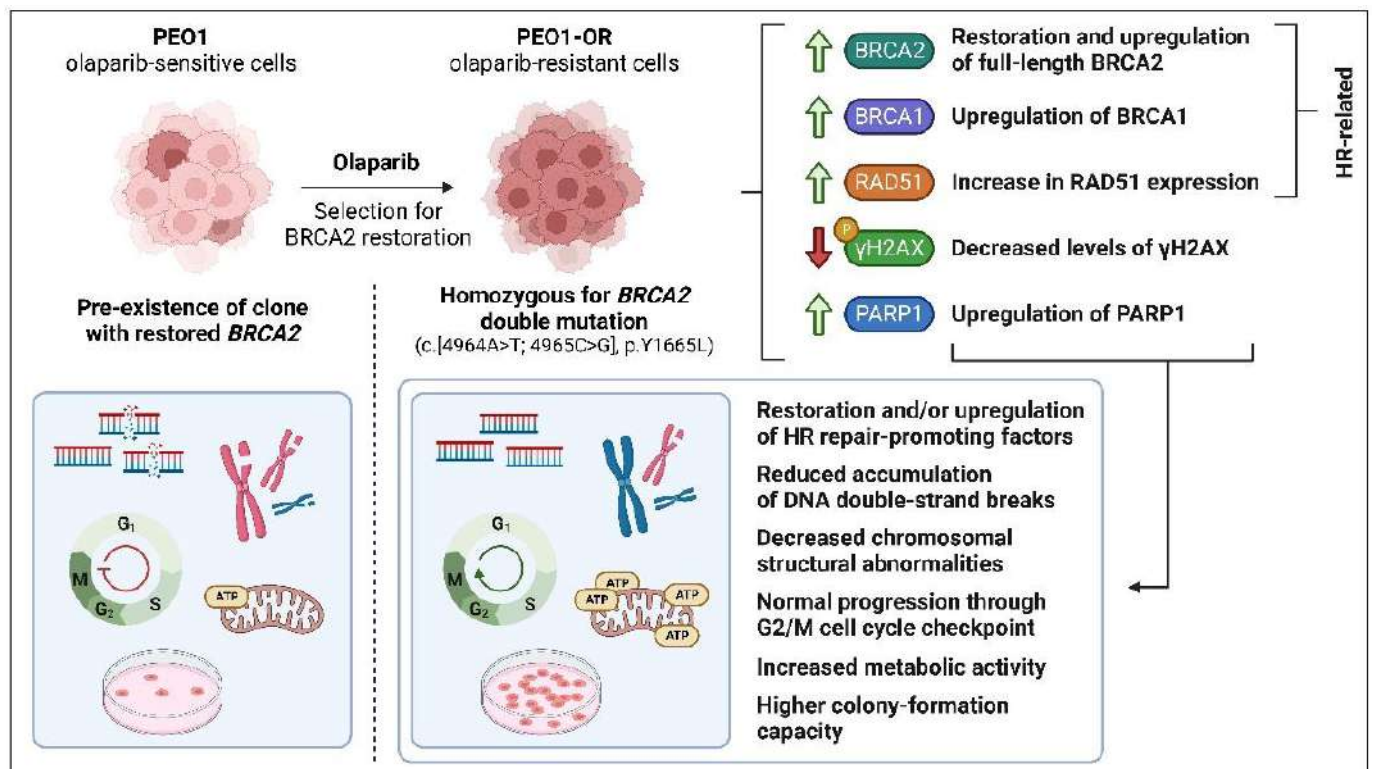


**Figure 10.** Co-existing mechanisms conferring resistance to olaparib in PEO1-OR *BRCA2*<sup>MUT</sup> HGSOC cells. PEO1-OR cells underwent selection for *BRCA2* restoration following prolonged treatment with olaparib, which led to enrichment in sub-dominant clones present in parental cells harboring the *BRCA2* double mutation (c.[4964A > T; 4965C > G], p.Y1655L) removing the premature termination codon. Upregulation of *BRCA2*, *BRCA1*, *RAD51*, and *PARP1*, along with a concurrent decrease in γH2AX levels, contributed to decreased sensitivity to olaparib.

Notably, ATR/CHK1 signaling is associated with the regulation of HR repair. CHK1 kinase phosphorylates *RAD51* and *BRCA2* to facilitate *RAD51*-*BRCA2* complex recruitment to DNA damage sites [78,79]. More recent studies have shown that *BRCA1* phosphorylation at Thr1394 by ATR also plays an important role in promoting HR repair [80]. Our findings regarding *BRCA1* and *RAD51* upregulation in PEO1-OR in response to olaparib support the rationale for combining ATR/CHK1 pathway inhibitors with olaparib to disrupt HR repair and overcome resistance to PARPi. Accordingly, we addressed ATR/CHK1 axis activity, which orchestrates HR repair in the DDR pathway and may thus constitute a biomarker of PARPi response and a promising therapeutic target. The ATR/CHK1 pathway is also implicated in controlling G2/M checkpoint transition in *TP53*<sup>MUT</sup> OC cells with abrogated S phase arrest to prevent entry into mitosis with damaged DNA [17,19,64,81]. However, the role of olaparib in the regulation of ATR/CHK1 is poorly understood in olaparib-resistant OC cells. Here, the ATR/CHK1 pathway was not activated in response to non-toxic doses of olaparib in PEO1-OR cells. Previous studies have also shown that treatment with PARPi alone has no impact on CHK1 phosphorylation in HGSOC cell lines with acquired and de novo resistance to olaparib [19]. Furthermore, contrary to PEO1-OR olaparib-resistant cells, PARPi-sensitive PEO1 HGSOC cells were arrested in the G2/M phase in response to olaparib, consistent with previous findings [19]. Cell cycle progression profiling with concurrent γH2AX monitoring highlighted that olaparib-resistant cells progressed normally through checkpoints with reduced DNA damage, indicative of genomic stability in the presence of PARPi. This observation confirms previous results showing that olaparib does not induce γH2AX accumulation in OC cells with intrinsic or acquired resistance to PARPi [19,82]. We propose that PEO1-OR cells limit their dependence on

the ATR/CHK1 checkpoint pathway following treatment with olaparib at doses exerting significant cytotoxicity in sensitive OC cell lines.

Next, we addressed HR-independent modes of olaparib resistance as the absence of functional PARP1 itself, either due to loss of expression or inactivating mutations, may abrogate the cytotoxic mechanism of action of PARPi [83]. A PARP1 missense variant (p.V762A) was identified by us in PEO1 and PEO1-OR cells, which has been previously associated with decreased PARylation activity due to localization in the catalytic domain of PARP1 [84]. Our data are in keeping with previous findings showing that PARP1 expression remains unchanged in HGSOC cells with acquired resistance to olaparib [12] and no correlation between PARP1 levels and resistance to olaparib in clinical samples [5]. Noteworthy, in this study, treatment with DNA-damaging olaparib led to upregulation of PARP1 in olaparib-resistant cells, which may be correlated with PARP1's ability to detect SSBs and DSBs mainly in late S and G2 cells [85]. Indeed, our cytogenetic and  $\gamma$ H2AX analyses showed a significantly lower accumulation of structural chromosomal abnormalities and DSBs in PEO1-OR compared to olaparib-sensitive cells. These observations are in line with previous works showing that olaparib has minimal effect on DNA damage in *BRCA2*<sup>MUT</sup> olaparib-resistant cells [68,82]. Regarding PARP signaling, loss of PARG is reported to contribute to decreased PARPi trapping and resistance. Moreover, loss or inhibition of PARG may increase cellular PARylation and decrease PARPi cytotoxicity [86], suggesting that endogenous PARG is needed for PARPi cytotoxicity. Further studies demonstrated that loss of PARG in HR-proficient HGSOC cells contributes to resistance to PARPi [12]. However, the same study also revealed that the generation of acquired resistance to olaparib from an HR-deficient OC cell line resulted in clones with unchanged or decreased levels of PARG [12]. Our results showed that basal expression of PARG in PEO1-OR remained unchanged compared to parental olaparib-sensitive cells downregulating PARG, suggesting that *BRCA2*<sup>MUT</sup> OC cells do not acquire resistance to olaparib through loss of PARG. Overall, the observation of no changes in basal levels of PARP1 and PARG in PEO1-OR cell lines supports the theory that OC cells with restored *BRCA2* protein activity confer resistance independently of the PARP signaling pathway.

Previous studies demonstrated that olaparib-resistant OC cell lines display upregulation of MDR1 and inhibition of this efflux pump, with non-specific MDR1 inhibitor veliparib [87,88] partially restoring sensitivity to PARPi [19]. However, verapamil is an L-type calcium channel blocker rather than a specific MDR1 inhibitor [89,90]. The MDR1 efflux pump was not upregulated in PEO1-OR cells in our study, indicating no contribution of increased drug efflux to olaparib resistance. In our biological model, MDR1 made no or minor contributions to acquired resistance to olaparib, based on results obtained with the specific third-generation inhibitor of MDR1 tariquidar [90], which is consistent with earlier reports that resistance to PARPi is acquired independently of the MDR1 efflux pump [91].

Furthermore, we explored the differences in response to olaparib treatment with concurrent blockage of the ATR/CHK1 pathway in HGSOC cells. The rationale for combination therapy is based on the concept that treatment with two or more agents with different molecular targets should induce a synergistic antitumor effect. Combinations of PARPi with inhibitors of the ATR/CHK1 pathway are under investigation for OC in vitro and in clinical trials for PARPi-naïve HGSOC patients and those who previously received PARPi [17,20,22,23,43,66,92]. However, further molecular studies are crucial to characterize the cellular response to this combination treatment in OC cells with distinct HR activities and resistance mechanisms. In OC cells, the majority of which are *TP53*<sup>MUT</sup>, the G1/S cell cycle checkpoint is lost, and tumor cells are dependent on the remaining checkpoints regulated by the ATR/CHK1 pathway. Hence, inhibitors of ATR or CHK1 can hinder cell cycle-dependent DNA repair and promote progression through the cell cycle with unrepaired DNA damage induced by olaparib. Moreover, our work has revealed genetic premises underlying the use of an inhibitor of ATR and CHK1 kinases in OC. One of the missense variants detected by WES in *ATR* (c.632T > C, p.M211T) in PEO1 and PEO1-OR cells is predicted to induce gain-of-function activity, supporting the idea behind the inhibi-

tion of ATR kinase. Interestingly, this uncharacterized alteration has been documented in numerous tumor and control samples from breast and/or ovarian cancer families [87]. We also showed that studied *BRCA2*<sup>MUT</sup> HGSOC cell lines carry a nonsynonymous mutation in *CHEK1* (c.1411A > G, p.I471V) and we speculate that it has no impact on the binding of MK-8776 to CHK1, as it occurs outside the binding pocket [88]. Recent studies suggest that this *CHEK1* variant is extremely common in primary and recurrent HGSOC, but undetectable in a clear-cell carcinoma subtype of EOC [93]. Accordingly, we believe that ATR and CHK1 present favorable molecular targets for combination treatment of HGSOC.

In studies aimed at assessing the effectiveness of combined treatment, we selected the minimal doses of drugs that inhibited cell growth and proliferation more significantly in olaparib-sensitive (PEO1, PEO4) than in olaparib-resistant cells (PEO1-OR) in response to a relatively long 5-day treatment period, as effective PARP inhibition in vitro requires several rounds of cell division. Interestingly, PEO4 cells seemed to be more sensitive to olaparib after 5 days of incubation than PEO1 cells based on the results of the MTT assay, which was further confirmed by the colony formation capacity of olaparib-sensitive cells. However, previous reports showed that PEO1 and PEO4 cells may exert distinct sensitivity to PARPi [40,42], suggesting it depends on the type of inhibitor used. We believe that changes induced by olaparib are more dynamic in PEO1 than PEO4 cells (reduced metabolic activity, greater accumulation of DNA damage) and are revealed as soon as after two days due to the higher proliferation rate of PEO1 than PEO4 cells and olaparib's cytotoxic mode of action. Here, we showed that olaparib combined with ATRi or CHK1i exerted early cellular changes occurring after 48 h including synergistic antitumor activity in terms of inhibiting cellular metabolic activity and colony formation capacity in olaparib-sensitive OC cell lines. Combinations of ATRi or CHK1i with PARPi were also effective in olaparib-resistant cells, most notably as a long-term effect of the strategy, confirmed based on synergistic reduction in colony formation capacity. Our results are in keeping with published data showing that olaparib combined with inhibitors of the ATR/CHK1 pathway act synergistically in BRCA1/2-proficient and BRCA1/2-deficient OC cells in vitro and in vivo [18,19,23]. Previous studies have shown that ATRi compounds can sensitize *BRCA1*-deficient OC cells with acquired resistance to olaparib. Given that PEO1-OR cells contain higher levels of BRCA1 compared to olaparib-sensitive cells, we speculate that the BRCA1 protein may partially contribute to desensitization to ATRi [91]. In agreement with data from cytotoxic assays, blockage of the ATR/CHK1 pathway enhanced the accumulation of olaparib-induced DSBs and chromosomal aberrations in olaparib-sensitive cells, whereas PEO1-OR cells were less susceptible. We propose that olaparib-induced mechanisms involved in upregulating HR repair-promoting factors contribute to the PEO1-OR response. Notably, truncated PARP1 was not detected in olaparib-resistant cells, in contrast to the significant increase in the parental cell line in response to the inhibitors and their combinations. As cleavage of PARP1 is a surrogate marker of apoptosis and truncated PARP1 directly induces this type of cell death [94], it is inferred that PEO1-OR cells are less susceptible to programmed cell death induced by drug combinations.

Levels of  $\gamma$ H2AX, a surrogate marker of DSBs, were elevated following combination treatment, relative to each monotherapy in the olaparib-sensitive OC cell lines. Upon combination treatments, phosphorylation of H2AX was less significant in PEO1-OR than in olaparib-sensitive cells, in agreement with results from the comet assay and evaluation of chromosome aberrations. Our findings were confirmed by the assessment of  $\gamma$ H2AX phosphorylation throughout the cell cycle. Modest genotoxic activity resulting from concurrent blockage of PARP1 and the ATR/CHK1 pathway had no impact on RAD51 expression in all OC cell lines. However, data from functional assays confirmed that the inhibitor compounds induced co-localization of RAD51 foci with  $\gamma$ H2AX at DNA damage sites to promote the assembly of HR pathway repair machinery in OC cell lines. Moreover, olaparib and inhibitors of ATR/CHK1 synergistically suppressed NHEJ-mediating 53BP1 levels in PEO1-OR cells. Furthermore, blockage of the ATR/CHK1 pathway had no impact on olaparib-induced G2/M arrest in sensitive OC cell lines, which is in line with previous

studies [25]. In contrast, a previous study by Brill et al. [81] showed that the addition of ATRi or CHK1i to PARPi released G2/M arrest to a limited extent in PEO1 and PEO4 cells. We speculate that following combination treatments, which induce modest DNA damage, PEO1-OR cells progress through the cell cycle with unrepaired DNA, which could contribute to partial resensitization to olaparib in the presence of inhibitors of the ATR or CHK1 pathway. Indeed, the ATR/CHK1 pathway was not activated in PEO1-OR cells in response to co-treatment with olaparib with ATRi, suggesting that cells were not arrested in the G2/M phase to repair DNA lesions. CHK1 and ATR are reported to promote HR repair via phosphorylation of repair factors, such as RAD51, BRCA1, and BRCA2 [78–80]. In PEO1-OR cells, combination treatment exerted modest but promising cytotoxic activity via upregulation of RAD51, BRCA1, and BRCA2 due to the inhibition of ATR and CHK1 kinases.

In this paper, we successfully identified mechanisms of resistance to PARPi in one *BRCA2*<sup>MUT</sup> HGSOC cell line with decreased sensitivity to olaparib, which surely does not fully reflect the complexity of this phenomenon in heterogeneous OC cells. However, some olaparib-resistant OC cell lines have already been developed from OC cells harboring *BRCA1* or *BRCA2* mutations showing a 2.1-fold to 13-fold increase in resistance [18,19]. Nevertheless, our findings provide a valuable addition to the understanding of PARPi resistance, especially in terms of the resensitization of HGSOC cells to olaparib.

## 5. Conclusions

In this study, we showed that PARPi-resistant PEO1-OR cells exhibit decreased sensitivity to olaparib due to reduced susceptibility to PARPi-induced DNA damage and G2/M arrest. Mechanistically, PEO1-OR cells are homozygous for a *BRCA2* double mutation (c.[4964A > T; 4965C > G], p.Y1655L) and show upregulation of functional intact *BRCA2*, increased expression of HR-promoting *BRCA1* with unchanged *RAD51* and *53BP1* levels, partially restored PARP signaling, and decreased phosphorylation of *H2AX*. Resistance to PARPi was acquired irrespective of *MDR1* efflux pump activity. Integration of diverse mechanisms of resistance resulted in reduced accumulation of DNA DSBs and structural chromosomal aberrations and allowed cells to progress normally through the ATR/CHK1-regulated cell cycle. At sublethal doses of inhibitors for olaparib-sensitive cells, combination treatments exerted promising synergistic antitumor effects on PEO1-OR cells. Moreover, co-treatment with ATR/CHK1 inhibitors and olaparib induced a synergistic decrease in cell viability and survival and increase in DNA damage in the cell models examined, most notably in olaparib-sensitive cells. These findings support the potential utility of combinations of inhibitors of the ATR/CHK1 pathway together with olaparib in avoiding or overcoming drug resistance of OC.

**Supplementary Materials:** The following supporting information can be downloaded at: <https://www.mdpi.com/article/10.3390/cells12071038/s1>, Figure S1: Growth curves and population doubling times for ovarian cancer (OC) cell lines; Figure S2: Qualitative Western blot analysis of full-length and truncated *BRCA2* in PEO1, PEO1-OR, and PEO4 ovarian cancer (OC) cell lines; Figure S3: Effect of *MDR1* inhibition with tariquidar or verapamil on cytotoxicity of the *MDR1* substrate doxorubicin and olaparib, ATRi, CHK1i, or their combinations after 48 h of treatment in HepG2 cell line and qualitative Western blot analysis of *MDR1* expression in untreated HepG2 cells; Figure S4: Quantitative Western blot analysis of PARP1 basal expression in untreated PEO1, PEO1-OR, and PEO4 ovarian cancer (OC) cell lines with a representative blot; Table S1: Key materials and reagents used in the study; Table S2: Primary antibodies used in the study. Table S3: Secondary antibodies used in the study; Table S4: High-quality exonic and intronic variants detected in *ABCB1*, *ATR*, *BRCA1*, *BRCA2*, *CHEK1*, *H2AX*, *PARP1*, *PARG*, *RAD51*, *TP53*, and *TP53BP1* genes in PEO1 and PEO1-OR cell lines by whole-exome sequencing.

**Author Contributions:** Conceptualization, Ł.B., A.G., A.M. and A.R.; methodology, Ł.B., A.G. and A.R.; formal analysis, Ł.B., A.G. and A.R.; investigation, Ł.B. and A.G.; resources, A.M. and A.R.; writing—original draft preparation, Ł.B.; writing—review and editing, Ł.B., A.G., A.M. and A.R.;

visualization, Ł.B., A.G. and A.R.; supervision, A.R.; funding acquisition, A.R. All authors have read and agreed to the published version of the manuscript.

**Funding:** This research was funded by the National Science Centre, Poland (Project grant number: Sonata Bis 2019/34/E/NZ7/00056).

**Institutional Review Board Statement:** Not applicable.

**Informed Consent Statement:** Not applicable.

**Data Availability Statement:** The data presented in this study are available from the corresponding author upon a reasonable request.

**Acknowledgments:** Images of metaphase chromosome spreads were acquired in the Laboratory of Microscopic Imaging and Specialized Biological Techniques (Faculty of Biology and Environmental Protection, University of Lodz). This work was supported by the National Science Centre, Poland (Project grant number: Sonata Bis 2019/34/E/NZ7/00056). Illustrations have been created with BioRender.com.

**Conflicts of Interest:** The authors declare no conflict of interest.

## Abbreviations

A	ATR inhibitor (ceralasertib)
ABC	ATP-binding cassette
ATCC	American Type Culture Collection
ATR	ataxia telangiectasia and RAD3-related protein
ATRi	ATR inhibitor(s)
BRCA1	breast cancer type 1 susceptibility protein
BRCA2	breast cancer type 2 susceptibility protein
BrdU	bromodeoxyuridine
C	CHK1 inhibitor (MK-8776)
CDI	coefficient of drug interaction
CHK1	checkpoint kinase 1
CHK1i	CHK1 inhibitor(s)
DDR	DNA damage response
DSB	double-strand break
ECACC	The European Collection of Authenticated Cell Cultures
HGSOC	high-grade serous ovarian cancer
HI-FBS	heat-inactivated fetal bovine serum
IC <sub>50</sub>	concentration of drug required to reduce cell viability to 50%
MDR	multidrug resistance
MDR1	multidrug resistance protein 1
MDRi	multidrug resistance inhibitor(s)
MFI	geometric mean fluorescence intensity
NGS	next-generation sequencing
NHEJ	non-homologous end joining
O	olaparib
OC	ovarian cancer
ORF	open reading frame
PARG	poly(ADP-ribose) glycohydrolase
PARP1	poly(ADP-ribose) polymerase 1
PARPi	PARP inhibitor(s)
PDT	population doubling time
PEO1-OR	PEO1 olaparib-resistant cell line
QCI-IT	Qiagen Clinical Insight Interpret Translational
SF	surviving fraction
Tar	tariquidar
WES	whole-exome sequencing



## References

- Ledermann, J.A.; Pujade-Lauraine, E. Olaparib as maintenance treatment for patients with platinum-sensitive relapsed ovarian cancer. *Ther. Adv. Med. Oncol.* **2019**, *11*, 1758835919849753. [\[CrossRef\]](#) [\[PubMed\]](#)
- Rose, P.G.; Yao, M.; Chambers, L.M.; Mahdi, H.; DeBernardo, R.; Michener, C.M.; AlHilli, M.; Ricci, S.; Vargas, R. PARP inhibitors decrease response to subsequent platinum-based chemotherapy in patients with BRCA mutated ovarian cancer. *Anticancer Drugs* **2021**, *32*, 1086–1092. [\[CrossRef\]](#) [\[PubMed\]](#)
- Moubarak, M.; Harter, P.; Ataseven, B.; Traut, A.; Welz, J.; Baert, T.; Heitz, F. Re-treatment with PARPi in patients with recurrent epithelial ovarian cancer: A single institutional experience. *Gynecol. Oncol. Rep.* **2022**, *40*, 100939. [\[CrossRef\]](#) [\[PubMed\]](#)
- Konstantinopoulos, P.A.; Ceccaldi, R.; Shapiro, G.I.; D'Andrea, A.D. Homologous Recombination Deficiency: Exploiting the Fundamental Vulnerability of Ovarian Cancer. *Cancer Discov.* **2015**, *5*, 1137–1154. [\[CrossRef\]](#) [\[PubMed\]](#)
- Hurley, R.M.; Wahner Hendrickson, A.E.; Visscher, D.W.; Ansell, P.; Harrell, M.I.; Wagner, J.M.; Negron, V.; Goergen, K.M.; Maurer, M.J.; Oberg, A.L.; et al. 53BP1 as a potential predictor of response in PARP inhibitor-treated homologous recombination-deficient ovarian cancer. *Gynecol. Oncol.* **2019**, *153*, 127–134. [\[CrossRef\]](#)
- Kristeleit, R.; Lisyanskaya, A.; Fedenko, A.; Dvorkin, M.; de Melo, A.C.; Shparyk, Y.; Rakhmatullina, I.; Bondarenko, I.; Colombo, N.; Svintsitskiy, V. 1Rucaparib versus chemotherapy in patients with advanced, relapsed ovarian cancer and a deleterious BRCA mutation: Efficacy and safety from ARIEL4, a randomized phase III study. *Gynecol. Oncol.* **2021**, *162*, S3–S4. [\[CrossRef\]](#)
- Creeden, J.F.; Nanavaty, N.S.; Einloth, K.R.; Gillman, C.E.; Stanbery, L.; Hamouda, D.M.; Dworkin, L.; Nemunaitis, J. Homologous recombination proficiency in ovarian and breast cancer patients. *BMC Cancer* **2021**, *21*, 1154. [\[CrossRef\]](#)
- Ngoi, N.Y.L.; Tan, D.S.P. The role of homologous recombination deficiency testing in ovarian cancer and its clinical implications: Do we need it? *ESMO Open* **2021**, *6*, 100144. [\[CrossRef\]](#)
- van Wijk, L.M.; Nilas, A.B.; Vrieling, H.; Vreeswijk, M.P.G. RAD51 as a functional biomarker for homologous recombination deficiency in cancer: A promising addition to the HRD toolbox? *Expert Rev. Mol. Diagn.* **2022**, *22*, 185–199. [\[CrossRef\]](#)
- Murai, J.; Huang, S.Y.; Das, B.B.; Renaud, A.; Zhang, Y.; Doroshow, J.H.; Ji, J.; Takeda, S.; Pommier, Y. Trapping of PARP1 and PARP2 by Clinical PARP Inhibitors. *Cancer Res.* **2012**, *72*, 5588–5599. [\[CrossRef\]](#)
- Biegala, L.; Gajek, A.; Marczak, A.; Rogalska, A. PARP inhibitor resistance in ovarian cancer: Underlying mechanisms and therapeutic approaches targeting the ATR/CHK1 pathway. *Biochim. Biophys. Acta Rev. Cancer* **2021**, *1876*, 188633. [\[CrossRef\]](#) [\[PubMed\]](#)
- Gomez, M.K.; Illuzzi, G.; Colomer, C.; Churchman, M.; Hollis, R.L.; O'Connor, M.J.; Gourley, C.; Leo, E.; Melton, D.W. Identifying and Overcoming Mechanisms of PARP Inhibitor Resistance in Homologous Recombination Repair-Deficient and Repair-Proficient High Grade Serous Ovarian Cancer Cells. *Cancers* **2020**, *12*, 1503. [\[CrossRef\]](#) [\[PubMed\]](#)
- Kim, D.S.; Camacho, C.V.; Kraus, W.L. Alternate therapeutic pathways for PARP inhibitors and potential mechanisms of resistance. *Exp. Mol. Med.* **2021**, *53*, 42–51. [\[CrossRef\]](#) [\[PubMed\]](#)
- Boussios, S.; Karihtala, P.; Moschetta, M.; Karathanasi, A.; Sadauskaite, A.; Rassy, E.; Pavlidis, N. Combined Strategies with Poly (ADP-Ribose) Polymerase (PARP) Inhibitors for the Treatment of Ovarian Cancer: A Literature Review. *Diagnostics* **2019**, *9*, 87. [\[CrossRef\]](#)
- Feng, W.; Dean, D.C.; Hornicek, F.J.; Wang, J.; Jia, Y.; Duan, Z.; Shi, H. ATR and p-ATR are emerging prognostic biomarkers and DNA damage response targets in ovarian cancer. *Ther. Adv. Med. Oncol.* **2020**, *12*, 1758835920982853. [\[CrossRef\]](#)
- Gupta, N.; Huang, T.T.; Horibata, S.; Lee, J.M. Cell cycle checkpoints and beyond: Exploiting the ATR/CHK1/WEE1 pathway for the treatment of PARP inhibitor-resistant cancer. *Pharmacol. Res.* **2022**, *178*, 106162. [\[CrossRef\]](#)
- Gralewska, P.; Gajek, A.; Marczak, A.; Mikula, M.; Ostrowski, J.; Sliwinska, A.; Rogalska, A. PARP Inhibition Increases the Reliance on ATR/CHK1 Checkpoint Signaling Leading to Synthetic Lethality—An Alternative Treatment Strategy for Epithelial Ovarian Cancer Cells Independent from HR Effectiveness. *Int. J. Mol. Sci.* **2020**, *21*, 9715. [\[CrossRef\]](#) [\[PubMed\]](#)
- Burgess, B.T.; Anderson, A.M.; McCorkle, J.R.; Wu, J.; Ueland, F.R.; Kolesar, J.M. Olaparib Combined with an ATR or Chk1 Inhibitor as a Treatment Strategy for Acquired Olaparib-Resistant BRCA1 Mutant Ovarian Cells. *Diagnostics* **2020**, *10*, 121. [\[CrossRef\]](#)
- Kim, H.; Xu, H.; George, E.; Hallberg, D.; Kumar, S.; Jagannathan, V.; Medvedev, S.; Kinose, Y.; Devins, K.; Verma, P.; et al. Combining PARP with ATR inhibition overcomes PARP inhibitor and platinum resistance in ovarian cancer models. *Nat. Commun.* **2020**, *11*, 3726. [\[CrossRef\]](#)
- Mahdi, H.; Hafez, N.; Doroshow, D.; Sohal, D.; Keedy, V.; Do, K.T.; LoRusso, P.; Jurgensmeier, J.; Avedissian, M.; Sklar, J.; et al. Ceralasertib-Mediated ATR Inhibition Combined with Olaparib in Advanced Cancers Harboring DNA Damage Response and Repair Alterations (Olaparib Combinations). *JCO Precis. Oncol.* **2021**, *5*, 1432–1442. [\[CrossRef\]](#)
- Do, K.T.; Kochupurakkal, B.; Kelland, S.; de Jonge, A.; Hedglin, J.; Powers, A.; Quinn, N.; Gannon, C.; Vuong, L.; Parmar, K.; et al. Phase 1 Combination Study of the CHK1 Inhibitor Prexasertib and the PARP Inhibitor Olaparib in High-grade Serous Ovarian Cancer and Other Solid Tumors. *Clin. Cancer Res.* **2021**, *27*, 4710–4716. [\[CrossRef\]](#)
- Wethington, S.L.; Shah, P.D.; Martin, L.P.; Tanyi, J.L.; Latif, N.A.; Morgan, M.A.; Torigian, D.A.; Pagan, C.; Rodriguez, D.; Domchek, S.M.; et al. Combination of PARP and ATR inhibitors (olaparib and ceralasertib) shows clinical activity in acquired PARP inhibitor-resistant recurrent ovarian cancer. *J. Clin. Oncol.* **2021**, *39*, 5516. [\[CrossRef\]](#)



23. Kim, H.; George, E.; Ragland, R.; Rafail, S.; Zhang, R.; Krepler, C.; Morgan, M.; Herlyn, M.; Brown, E.; Simpkins, F. Targeting the ATR/CHK1 Axis with PARP Inhibition Results in Tumor Regression in BRCA-Mutant Ovarian Cancer Models. *Clin. Cancer Res.* **2017**, *23*, 3097–3108. [[CrossRef](#)] [[PubMed](#)]
24. Li, L.Y.; Guan, Y.D.; Chen, X.S.; Yang, J.M.; Cheng, Y. DNA Repair Pathways in Cancer Therapy and Resistance. *Front. Pharmacol.* **2020**, *11*, 629266. [[CrossRef](#)]
25. Molinaro, C.; Martoriati, A.; Cailliau, K. Proteins from the DNA Damage Response: Regulation, Dysfunction, and Anticancer Strategies. *Cancers* **2021**, *13*, 3819. [[CrossRef](#)] [[PubMed](#)]
26. Marechal, A.; Zou, L. DNA damage sensing by the ATM and ATR kinases. *Cold Spring Harb. Perspect. Biol.* **2013**, *5*, a012716. [[CrossRef](#)] [[PubMed](#)]
27. Nam, E.A.; Zhao, R.; Glick, G.G.; Bansbach, C.E.; Friedman, D.B.; Cortez, D. Thr-1989 phosphorylation is a marker of active ataxia telangiectasia-mutated and Rad3-related (ATR) kinase. *J. Biol. Chem.* **2011**, *286*, 28707–28714. [[CrossRef](#)] [[PubMed](#)]
28. Sun, Y.; McCorvie, T.J.; Yates, L.A.; Zhang, X. Structural basis of homologous recombination. *Cell. Mol. Life Sci.* **2020**, *77*, 3–18. [[CrossRef](#)] [[PubMed](#)]
29. Zhao, W.; Steinfeld, J.B.; Liang, F.; Chen, X.; Maranon, D.G.; Jian Ma, C.; Kwon, Y.; Rao, T.; Wang, W.; Sheng, C.; et al. BRCA1-BARD1 promotes RAD51-mediated homologous DNA pairing. *Nature* **2017**, *550*, 360–365. [[CrossRef](#)]
30. Lopez-Acevedo, M.; Grace, L.; Teoh, D.; Whitaker, R.; Adams, D.J.; Jia, J.; Nixon, A.B.; Secord, A.A. Dasatinib (BMS-35482) potentiates the activity of gemcitabine and docetaxel in uterine leiomyosarcoma cell lines. *Gynecol. Oncol. Res. Pract.* **2014**, *1*, 2. [[CrossRef](#)]
31. Zhang, J.; Yao, Y.; He, H.; Shen, J. Clinical Interpretation of Sequence Variants. *Curr. Protoc. Hum. Genet.* **2020**, *106*, e98. [[CrossRef](#)] [[PubMed](#)]
32. Li, M.M.; Datto, M.; Duncavage, E.J.; Kulkarni, S.; Lindeman, N.I.; Roy, S.; Tsimberidou, A.M.; Vnencak-Jones, C.L.; Wolff, D.J.; Younes, A.; et al. Standards and Guidelines for the Interpretation and Reporting of Sequence Variants in Cancer: A Joint Consensus Recommendation of the Association for Molecular Pathology, American Society of Clinical Oncology, and College of American Pathologists. *J. Mol. Diagn.* **2017**, *19*, 4–23. [[CrossRef](#)] [[PubMed](#)]
33. Richards, S.; Aziz, N.; Bale, S.; Bick, D.; Das, S.; Gastier-Foster, J.; Grody, W.W.; Hegde, M.; Lyon, E.; Spector, E.; et al. Standards and guidelines for the interpretation of sequence variants: A joint consensus recommendation of the American College of Medical Genetics and Genomics and the Association for Molecular Pathology. *Genet. Med.* **2015**, *17*, 405–424. [[CrossRef](#)] [[PubMed](#)]
34. Howe, B.; Umrigar, A.; Tsien, F. Chromosome preparation from cultured cells. *J. Vis. Exp.* **2014**, *83*, e50203. [[CrossRef](#)]
35. McDermott, M.; Eustace, A.; Busschots, S.; Breen, L.; Clynes, M.; O'Donovan, N.; Stordal, B. In vitro Development of Chemotherapy and Targeted Therapy Drug-Resistant Cancer Cell Lines: A Practical Guide with Case Studies. *Front. Oncol.* **2014**, *4*, 40. [[CrossRef](#)]
36. Liu, L.; Cai, S.; Han, C.; Banerjee, A.; Wu, D.; Cui, T.; Xie, G.; Zhang, J.; Zhang, X.; McLaughlin, E.; et al. ALDH1A1 Contributes to PARP Inhibitor Resistance via Enhancing DNA Repair in BRCA2(-/-) Ovarian Cancer Cells. *Mol. Cancer Ther.* **2020**, *19*, 199–210. [[CrossRef](#)]
37. Stukova, M.; Hall, M.D.; Tsotsoros, S.D.; Madigan, J.P.; Farrell, N.P.; Gottesman, M.M. Reduced accumulation of platinum drugs is not observed in drug-resistant ovarian cancer cell lines derived from cisplatin-treated patients. *J. Inorg. Biochem.* **2015**, *149*, 45–48. [[CrossRef](#)]
38. Ng, C.K.; Cooke, S.L.; Howe, K.; Newman, S.; Xian, J.; Temple, J.; Batty, E.M.; Pole, J.C.; Langdon, S.P.; Edwards, P.A.; et al. The role of tandem duplicator phenotype in tumour evolution in high-grade serous ovarian cancer. *J. Pathol.* **2012**, *226*, 703–712. [[CrossRef](#)]
39. Langdon, S.P.; Lawrie, S.S.; Hay, F.G.; Hawkes, M.M.; McDonald, A.; Hayward, I.P.; Schol, D.J.; Hilgers, J.; Leonard, R.C.; Smyth, J.F. Characterization and properties of nine human ovarian adenocarcinoma cell lines. *Cancer Res.* **1988**, *48*, 6166–6172.
40. Sakai, W.; Swisher, E.M.; Jacquemont, C.; Chandramohan, K.V.; Couch, F.J.; Langdon, S.P.; Wurz, K.; Higgins, J.; Villegas, E.; Taniguchi, T. Functional restoration of BRCA2 protein by secondary BRCA2 mutations in BRCA2-mutated ovarian carcinoma. *Cancer Res.* **2009**, *69*, 6381–6386. [[CrossRef](#)]
41. Norquist, B.; Wurz, K.A.; Pennil, C.C.; Garcia, R.; Gross, J.; Sakai, W.; Karlan, B.Y.; Taniguchi, T.; Swisher, E.M. Secondary somatic mutations restoring BRCA1/2 predict chemotherapy resistance in hereditary ovarian carcinomas. *J. Clin. Oncol.* **2011**, *29*, 3008–3015. [[CrossRef](#)]
42. Dickson, K.A.; Xie, T.; Evenhuis, C.; Ma, Y.; Marsh, D.J. PARP Inhibitors Display Differential Efficacy in Models of BRCA Mutant High-Grade Serous Ovarian Cancer. *Int. J. Mol. Sci.* **2021**, *22*, 8506. [[CrossRef](#)]
43. Chiappa, M.; Guffanti, F.; Anselmi, M.; Lupi, M.; Panini, N.; Wiesmuller, L.; Damia, G. Combinations of ATR, Chk1 and Wee1 Inhibitors with Olaparib Are Active in Olaparib Resistant Brca1 Proficient and Deficient Murine Ovarian Cells. *Cancers* **2022**, *14*, 1807. [[CrossRef](#)] [[PubMed](#)]
44. Franken, N.A.; Rodermond, H.M.; Stap, J.; Haveman, J.; van Bree, C. Clonogenic assay of cells in vitro. *Nat. Protoc.* **2006**, *1*, 2315–2319. [[CrossRef](#)] [[PubMed](#)]
45. Subramanian, D.N.; Zethoven, M.; McInerney, S.; Morgan, J.A.; Rowley, S.M.; Lee, J.E.A.; Li, N.; Gorringer, K.L.; James, P.A.; Campbell, I.G. Exome sequencing of familial high-grade serous ovarian carcinoma reveals heterogeneity for rare candidate susceptibility genes. *Nat. Commun.* **2020**, *11*, 1640. [[CrossRef](#)] [[PubMed](#)]

46. Alenezi, W.M.; Fierheller, C.T.; Revil, T.; Serruya, C.; Mes-Masson, A.M.; Foulkes, W.D.; Provencher, D.; El Haffaf, Z.; Ragoussis, J.; Tonin, P.N. Case Review: Whole-Exome Sequencing Analyses Identify Carriers of a Known Likely Pathogenic Intronic BRCA1 Variant in Ovarian Cancer Cases Clinically Negative for Pathogenic BRCA1 and BRCA2 Variants. *Genes* **2022**, *13*, 697. [\[CrossRef\]](#)
47. Kong, S.W.; Lee, I.H.; Liu, X.; Hirschhorn, J.N.; Mandl, K.D. Measuring coverage and accuracy of whole-exome sequencing in clinical context. *Genet. Med.* **2018**, *20*, 1617–1626. [\[CrossRef\]](#)
48. Garziera, M.; Roncato, R.; Montico, M.; De Mattia, E.; Gagno, S.; Poletto, E.; Scalone, S.; Canzonieri, V.; Giorda, G.; Sorio, R.; et al. New Challenges in Tumor Mutation Heterogeneity in Advanced Ovarian Cancer by a Targeted Next-Generation Sequencing (NGS) Approach. *Cells* **2019**, *8*, 584. [\[CrossRef\]](#)
49. Guo, T.; Dong, X.; Xie, S.; Zhang, L.; Zeng, P.; Zhang, L. Cellular Mechanism of Gene Mutations and Potential Therapeutic Targets in Ovarian Cancer. *Cancer Manag. Res.* **2021**, *13*, 3081–3100. [\[CrossRef\]](#)
50. Carvalho, M.A.; Marsillac, S.M.; Karchin, R.; Manoukian, S.; Grist, S.; Swaby, R.F.; Urmenyi, T.P.; Rondinelli, E.; Silva, R.; Gayol, L.; et al. Determination of cancer risk associated with germ line BRCA1 missense variants by functional analysis. *Cancer Res.* **2007**, *67*, 1494–1501. [\[CrossRef\]](#) [\[PubMed\]](#)
51. Fernandes, V.C.; Golubeva, V.A.; Di Pietro, G.; Shields, C.; Amankwah, K.; Nepomuceno, T.C.; de Gregoriis, G.; Abreu, R.B.V.; Harro, C.; Gomes, T.T.; et al. Impact of amino acid substitutions at secondary structures in the BRCT domains of the tumor suppressor BRCA1: Implications for clinical annotation. *J. Biol. Chem.* **2019**, *294*, 5980–5992. [\[CrossRef\]](#)
52. Anantha, R.W.; Simhadri, S.; Foo, T.K.; Miao, S.; Liu, J.; Shen, Z.; Ganesan, S.; Xia, B. Functional and mutational landscapes of BRCA1 for homology-directed repair and therapy resistance. *eLife* **2017**, *6*, e21350. [\[CrossRef\]](#)
53. Lin, K.K.; Harrell, M.I.; Oza, A.M.; Oaknin, A.; Ray-Coquard, I.; Tinker, A.V.; Helman, E.; Radke, M.R.; Say, C.; Vo, L.T.; et al. BRCA Reversion Mutations in Circulating Tumor DNA Predict Primary and Acquired Resistance to the PARP Inhibitor Rucaparib in High-Grade Ovarian Carcinoma. *Cancer Discov.* **2019**, *9*, 210–219. [\[CrossRef\]](#)
54. Vaidyanathan, A.; Sawers, L.; Gannon, A.L.; Chakravarty, P.; Scott, A.L.; Bray, S.E.; Ferguson, M.J.; Smith, G. ABCB1 (MDR1) induction defines a common resistance mechanism in paclitaxel- and olaparib-resistant ovarian cancer cells. *Br. J. Cancer* **2016**, *115*, 431–441. [\[CrossRef\]](#) [\[PubMed\]](#)
55. Fox, E.; Bates, S.E. Tariquidar (XR9576): A P-glycoprotein drug efflux pump inhibitor. *Expert Rev. Anticancer Ther.* **2007**, *7*, 447–459. [\[CrossRef\]](#) [\[PubMed\]](#)
56. Leung-Pineda, V.; Ryan, C.E.; Piwnica-Worms, H. Phosphorylation of Chk1 by ATR is antagonized by a Chk1-regulated protein phosphatase 2A circuit. *Mol. Cell Biol.* **2006**, *26*, 7529–7538. [\[CrossRef\]](#) [\[PubMed\]](#)
57. Nair, J.; Huang, T.T.; Murai, J.; Haynes, B.; Steeg, P.S.; Pommier, Y.; Lee, J.M. Resistance to the CHK1 inhibitor prexasertib involves functionally distinct CHK1 activities in BRCA wild-type ovarian cancer. *Oncogene* **2020**, *39*, 5520–5535. [\[CrossRef\]](#)
58. Miller, R.E.; Leary, A.; Scott, C.L.; Serra, V.; Lord, C.J.; Bowtell, D.; Chang, D.K.; Garsed, D.W.; Jonkers, J.; Ledermann, J.A.; et al. ESMO recommendations on predictive biomarker testing for homologous recombination deficiency and PARP inhibitor benefit in ovarian cancer. *Ann. Oncol.* **2020**, *31*, 1606–1622. [\[CrossRef\]](#)
59. Tumati, M.; Hietanen, S.; Hynninen, J.; Pietila, E.; Farkkila, A.; Kaipio, K.; Roering, P.; Huhtinen, K.; Alkods, A.; Li, Y.; et al. A Functional Homologous Recombination Assay Predicts Primary Chemotherapy Response and Long-Term Survival in Ovarian Cancer Patients. *Clin. Cancer Res.* **2018**, *24*, 4482–4493. [\[CrossRef\]](#)
60. Tamura, N.; Shaikh, N.; Muliaditan, D.; Soliman, T.N.; McGuinness, J.R.; Maniati, E.; Moralli, D.; Durin, M.A.; Green, C.M.; Balkwill, F.R.; et al. Specific Mechanisms of Chromosomal Instability Indicate Therapeutic Sensitivities in High-Grade Serous Ovarian Carcinoma. *Cancer Res.* **2020**, *80*, 4946–4959. [\[CrossRef\]](#)
61. Cope, L.; Wu, R.C.; Shih, Ie, M.; Wang, T.L. High level of chromosomal aberration in ovarian cancer genome correlates with poor clinical outcome. *Gynecol. Oncol.* **2013**, *128*, 500–505. [\[CrossRef\]](#) [\[PubMed\]](#)
62. Wang, Z.C.; Birkbak, N.J.; Culhane, A.C.; Drapkin, R.; Fatima, A.; Tian, R.; Schwede, M.; Alsop, K.; Daniels, K.E.; Piao, H.; et al. Profiles of genomic instability in high-grade serous ovarian cancer predict treatment outcome. *Clin. Cancer Res.* **2012**, *18*, 5806–5815. [\[CrossRef\]](#)
63. Wang, Z.; Gao, J.; Zhou, J.; Liu, H.; Xu, C. Olaparib induced senescence under P16 or P53 dependent manner in ovarian cancer. *J. Gynecol. Oncol.* **2019**, *30*, e26. [\[CrossRef\]](#) [\[PubMed\]](#)
64. Vescarelli, E.; Gerini, G.; Megiorni, F.; Anastasiadou, E.; Pontecorvi, P.; Solito, L.; De Vitis, C.; Camero, S.; Marchetti, C.; Mancini, R.; et al. MiR-200c sensitizes Olaparib-resistant ovarian cancer cells by targeting Neuropilin 1. *J. Exp. Clin. Cancer Res.* **2020**, *39*, 3. [\[CrossRef\]](#)
65. Gogola, E.; Duarte, A.A.; de Ruiter, J.R.; Wiegant, W.W.; Schmid, J.A.; de Bruijn, R.; James, D.I.; Guerrero Ilobet, S.; Vis, D.J.; Annunziato, S.; et al. Selective Loss of PARG Restores PARylation and Counteracts PARP Inhibitor-Mediated Synthetic Lethality. *Cancer Cell* **2018**, *33*, 1078–1093.e12. [\[CrossRef\]](#)
66. Shah, P.D.; Wethington, S.L.; Pagan, C.; Latif, N.; Tanyi, J.; Martin, L.P.; Morgan, M.; Burger, R.A.; Haggerty, A.; Zarrin, H.; et al. Combination ATR and PARP Inhibitor (CAPRI): A phase 2 study of ceralasertib plus olaparib in patients with recurrent, platinum-resistant epithelial ovarian cancer. *Gynecol. Oncol.* **2021**, *163*, 246–253. [\[CrossRef\]](#)
67. Del Campo, J.M.; Matulonis, U.A.; Malander, S.; Provencher, D.; Mahner, S.; Follana, P.; Waters, J.; Berek, J.S.; Woie, K.; Oza, A.M.; et al. Niraparib Maintenance Therapy in Patients With Recurrent Ovarian Cancer After a Partial Response to the Last Platinum-Based Chemotherapy in the ENGOT-OV16/NOVA Trial. *J. Clin. Oncol.* **2019**, *37*, 2968–2973. [\[CrossRef\]](#) [\[PubMed\]](#)

68. Yamamoto, T.M.; McMellen, A.; Watson, Z.L.; Aguilera, J.; Ferguson, R.; Nurmemmedov, E.; Thakar, T.; Moldovan, G.L.; Kim, H.; Cittelly, D.M.; et al. Activation of Wnt signaling promotes olaparib resistant ovarian cancer. *Mol. Carcinog.* **2019**, *58*, 1770–1782. [\[CrossRef\]](#)
69. Lin, Z.P.; Al Zouabi, N.N.; Xu, M.L.; Bowen, N.E.; Wu, T.L.; Lavi, E.S.; Huang, P.H.; Zhu, Y.L.; Kim, B.; Ratner, E.S. In silico screening identifies a novel small molecule inhibitor that counteracts PARP inhibitor resistance in ovarian cancer. *Sci. Rep.* **2021**, *11*, 8042. [\[CrossRef\]](#)
70. Ware, M.D.; DeSilva, D.; Sinilnikova, O.M.; Stoppa-Lyonnet, D.; Tavtigian, S.V.; Mazoyer, S. Does nonsense-mediated mRNA decay explain the ovarian cancer cluster region of the BRCA2 gene? *Oncogene* **2006**, *25*, 323–328. [\[CrossRef\]](#)
71. Mesquita, K.A.; Ali, R.; Doherty, R.; Toss, M.S.; Miligy, I.; Alblihy, A.; Dorjsuren, D.; Simeonov, A.; Jadhav, A.; Wilson, D.M., 3rd; et al. FEN1 Blockade for Platinum Chemo-Sensitization and Synthetic Lethality in Epithelial Ovarian Cancers. *Cancers* **2021**, *13*, 1866. [\[CrossRef\]](#)
72. Stordal, B.; Timms, K.; Farrelly, A.; Gallagher, D.; Busschots, S.; Renaud, M.; Thery, J.; Williams, D.; Potter, J.; Tran, T.; et al. BRCA1/2 mutation analysis in 41 ovarian cell lines reveals only one functionally deleterious BRCA1 mutation. *Mol. Oncol.* **2013**, *7*, 567–579. [\[CrossRef\]](#) [\[PubMed\]](#)
73. Ciucci, A.; Buttarelli, M.; Fagotti, A.; Scambia, G.; Gallo, D. Preclinical models of epithelial ovarian cancer: Practical considerations and challenges for a meaningful application. *Cell. Mol. Life Sci.* **2022**, *79*, 364. [\[CrossRef\]](#)
74. Jimenez-Sainz, J.; Krysztofiak, A.; Garbarino, J.; Rogers, F.; Jensen, R.B. The Pathogenic R3052W BRCA2 Variant Disrupts Homology-Directed Repair by Failing to Localize to the Nucleus. *Front. Genet.* **2022**, *13*, 884210. [\[CrossRef\]](#)
75. Mukhopadhyay, A.; Elattar, A.; Cerbinskaite, A.; Wilkinson, S.J.; Drew, Y.; Kyle, S.; Los, G.; Hostomsky, Z.; Edmondson, R.J.; Curtin, N.J. Development of a functional assay for homologous recombination status in primary cultures of epithelial ovarian tumor and correlation with sensitivity to poly(ADP-ribose) polymerase inhibitors. *Clin. Cancer Res.* **2010**, *16*, 2344–2351. [\[CrossRef\]](#)
76. Zhang, F.; Ma, J.; Wu, J.; Ye, L.; Cai, H.; Xia, B.; Yu, X. PALB2 links BRCA1 and BRCA2 in the DNA-damage response. *Curr. Biol.* **2009**, *19*, 524–529. [\[CrossRef\]](#)
77. Gupta, A.; Hunt, C.R.; Chakraborty, S.; Pandita, R.K.; Yordy, J.; Ramnarain, D.B.; Horikoshi, N.; Pandita, T.K. Role of 53BP1 in the regulation of DNA double-strand break repair pathway choice. *Radiat. Res.* **2014**, *181*, 1–8. [\[CrossRef\]](#) [\[PubMed\]](#)
78. Bahassi, E.M.; Ovesen, J.L.; Riesenberg, A.L.; Bernstein, W.Z.; Hasty, P.E.; Stambrook, P.J. The checkpoint kinases Chk1 and Chk2 regulate the functional associations between hBRCA2 and Rad51 in response to DNA damage. *Oncogene* **2008**, *27*, 3977–3985. [\[CrossRef\]](#) [\[PubMed\]](#)
79. Narayanaswamy, P.B.; Tkachuk, S.; Haller, H.; Dumler, I.; Kiyani, Y. CHK1 and RAD51 activation after DNA damage is regulated via urokinase receptor/TLR4 signaling. *Cell Death Dis.* **2016**, *7*, e2383. [\[CrossRef\]](#) [\[PubMed\]](#)
80. Foo, T.K.; Vincelli, G.; Huselid, E.; Her, J.; Zheng, H.; Simhadri, S.; Wang, M.; Huo, Y.; Li, T.; Yu, X.; et al. ATR/ATM-Mediated Phosphorylation of BRCA1 T1394 Promotes Homologous Recombinational Repair and G2-M Checkpoint Maintenance. *Cancer Res.* **2021**, *81*, 4676–4684. [\[CrossRef\]](#)
81. Brill, E.; Yokoyama, T.; Nair, J.; Yu, M.; Ahn, Y.R.; Lee, J.M. Prexasertib, a cell cycle checkpoint kinases 1 and 2 inhibitor, increases in vitro toxicity of PARP inhibition by preventing Rad51 foci formation in BRCA wild type high-grade serous ovarian cancer. *Oncotarget* **2017**, *8*, 111026–111040. [\[CrossRef\]](#) [\[PubMed\]](#)
82. Pillay, N.; Tighe, A.; Nelson, L.; Littler, S.; Coulson-Gilmer, C.; Bah, N.; Golder, A.; Bakker, B.; Spierings, D.C.J.; James, D.I.; et al. DNA Replication Vulnerabilities Render Ovarian Cancer Cells Sensitive to Poly(ADP-Ribose) Glycohydrolase Inhibitors. *Cancer Cell* **2019**, *35*, 519–533.e8. [\[CrossRef\]](#) [\[PubMed\]](#)
83. Pettitt, S.J.; Krastev, D.B.; Brandsma, I.; Dréan, A.; Song, F.; Aleksandrov, R.; Harrell, M.I.; Menon, M.; Brough, R.; Campbell, J.; et al. Genome-wide and high-density CRISPR-Cas9 screens identify point mutations in PARP1 causing PARP inhibitor resistance. *Nat. Commun.* **2018**, *9*, 1849. [\[CrossRef\]](#) [\[PubMed\]](#)
84. Wang, X.G.; Wang, Z.Q.; Tong, W.M.; Shen, Y. PARP1 Val762Ala polymorphism reduces enzymatic activity. *Biochem. Biophys. Res. Commun.* **2007**, *354*, 122–126. [\[CrossRef\]](#)
85. Yang, G.; Liu, C.; Chen, S.H.; Kassab, M.A.; Hoff, J.D.; Walter, N.G.; Yu, X. Super-resolution imaging identifies PARP1 and the Ku complex acting as DNA double-strand break sensors. *Nucleic Acids Res.* **2018**, *46*, 3446–3457. [\[CrossRef\]](#)
86. Slade, D. PARP and PARG inhibitors in cancer treatment. *Genes Dev.* **2020**, *34*, 360–394. [\[CrossRef\]](#)
87. Heikkinen, K.; Mansikka, V.; Karppinen, S.M.; Rapakko, K.; Winqvist, R. Mutation analysis of the ATR gene in breast and ovarian cancer families. *Breast Cancer Res.* **2005**, *7*, R495–R501. [\[CrossRef\]](#)
88. Lv, M.; Ma, S.; Tian, Y.; Zhang, X.; Lv, W.; Zhai, H. Computational studies on the binding mechanism between triazolone inhibitors and Chk1 by molecular docking and molecular dynamics. *Mol. Biosyst.* **2015**, *11*, 275–286. [\[CrossRef\]](#)
89. Kelley, S.R.; Kamal, T.J.; Molitch, M.E. Mechanism of verapamil calcium channel blockade-induced hyperprolactinemia. *Am. J. Physiol.* **1996**, *270*, E96–E100. [\[CrossRef\]](#)
90. Kannan, P.; Telu, S.; Shukla, S.; Ambudkar, S.V.; Pike, V.W.; Halldin, C.; Gottesman, M.M.; Innis, R.B.; Hall, M.D. The “specific” P-glycoprotein inhibitor Tariquidar is also a substrate and an inhibitor for breast cancer resistance protein (BCRP/ABCG2). *ACS Chem. Neurosci.* **2011**, *2*, 82–89. [\[CrossRef\]](#)

91. Yazinski, S.A.; Comaills, V.; Buisson, R.; Genois, M.M.; Nguyen, H.D.; Ho, C.K.; Todorova Kwan, T.; Morris, R.; Lauffer, S.; Nussenzweig, A.; et al. ATR inhibition disrupts rewired homologous recombination and fork protection pathways in PARP inhibitor-resistant BRCA-deficient cancer cells. *Genes Dev.* **2017**, *31*, 318–332. [[CrossRef](#)] [[PubMed](#)]
92. McMullen, M.; Karakasis, K.; Loembe, B.; Dean, E.; Parr, G.; Oza, A.M. DUETTE: A phase II randomized, multicenter study to investigate the efficacy and tolerability of a second maintenance treatment in patients with platinum-sensitive relapsed epithelial ovarian cancer, who have previously received poly(ADP-ribose) polymerase (PARP) inhibitor maintenance treatment. *Int. J. Gynecol. Cancer* **2020**, *30*, 1824–1828. [[CrossRef](#)] [[PubMed](#)]
93. Nagasawa, S.; Ikeda, K.; Horie-Inoue, K.; Sato, S.; Takeda, S.; Hasegawa, K.; Inoue, S. Identification of novel mutations of ovarian cancer-related genes from RNA-sequencing data for Japanese epithelial ovarian cancer patients. *Endocr. J.* **2020**, *67*, 219–229. [[CrossRef](#)] [[PubMed](#)]
94. Chen, Q.; Ma, K.; Liu, X.; Chen, S.H.; Li, P.; Yu, Y.; Leung, A.K.L.; Yu, X. Truncated PARP1 mediates ADP-ribosylation of RNA polymerase III for apoptosis. *Cell Discov.* **2022**, *8*, 3. [[CrossRef](#)] [[PubMed](#)]

**Disclaimer/Publisher’s Note:** The statements, opinions and data contained in all publications are solely those of the individual author(s) and contributor(s) and not of MDPI and/or the editor(s). MDPI and/or the editor(s) disclaim responsibility for any injury to people or property resulting from any ideas, methods, instructions or products referred to in the content.

## Supplementary Information

### Olaparib-Resistant *BRCA2*<sup>MUT</sup> Ovarian Cancer Cells with Restored *BRCA2* Abrogate Olaparib-Induced DNA Damage and G2/M Arrest Controlled by the ATR/CHK1 Pathway for Survival

Łukasz Biegała, Arkadiusz Gajek, Agnieszka Marczak, Aneta Rogalska \*

#### Supplementary Figure S1 (Figure S1)

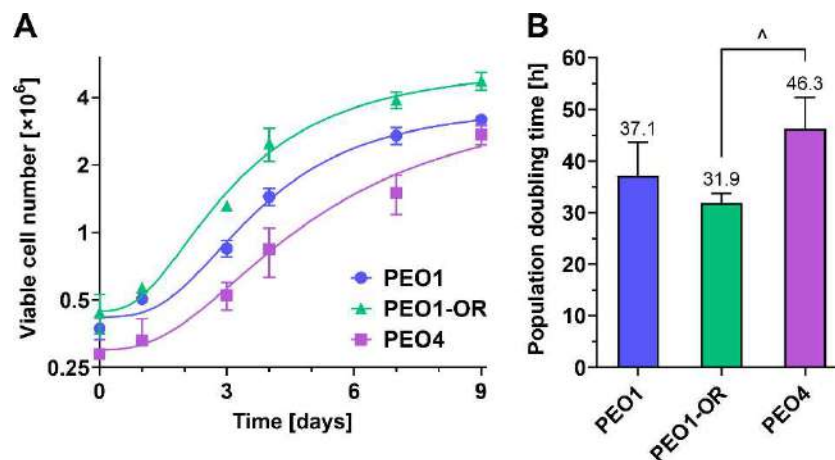


**Figure S1. Growth curves and population doubling times for ovarian cancer (OC) cell lines.** Cells seeded in 6-well plates were cultured up to 9 days and periodically subjected to endpoint counting from individual wells to determine the number of viable cells using trypan blue exclusion assay. **(A)** Growth curves of OC cell lines cultured under optimal conditions for 9 days. The results are shown as mean  $\pm$  SD ( $n = 3$ ). **(B)** Population doubling times of OC cell lines estimated in populations exhibiting exponential growth (days 2 – 5). Ordinary one-way ANOVA followed by Tukey's multiple comparison test was used to compare population doubling times between cell line:  $^{\wedge}p < 0.05$  statistically significant.



## Supplementary Figure S2 (Figure S2)

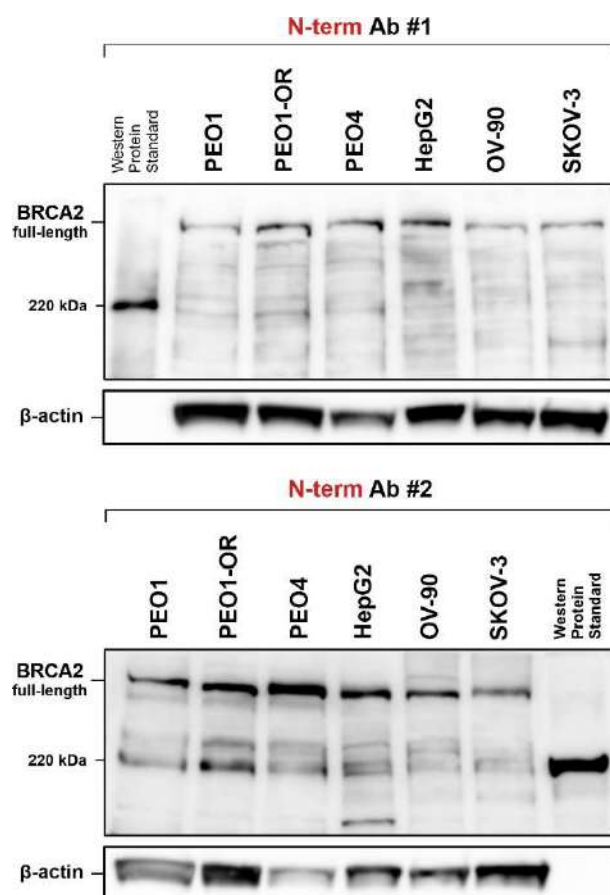


**Figure S2. Qualitative western blot analysis of full-length and truncated BRCA2 in PEO1, PEO1-OR, and PEO4 ovarian cancer (OC) cell lines.** HepG2, OV-90, and SKOV-3 cell lines were used as negative controls of truncated BRCA2 expression. Whole-cell lysates (30  $\mu$ g of protein) were loaded into each lane and separated using 8% Bis-Tris gels by SDS-PAGE. Two various antibodies targeting different epitopes within N-terminus of the protein were used for immunodetection to confirm obtained results (N-term Ab #1 and #2). Sharp band from a western protein standard (MagicMark™ XP Western Protein Standard, Thermo Fisher Scientific) corresponds to the protein molecular weight of 220 kDa. Truncated form of BRCA2 (calculated molecular weight of 186 kDa) was undetectable.



### Supplementary Figure S3 (Figure S3)

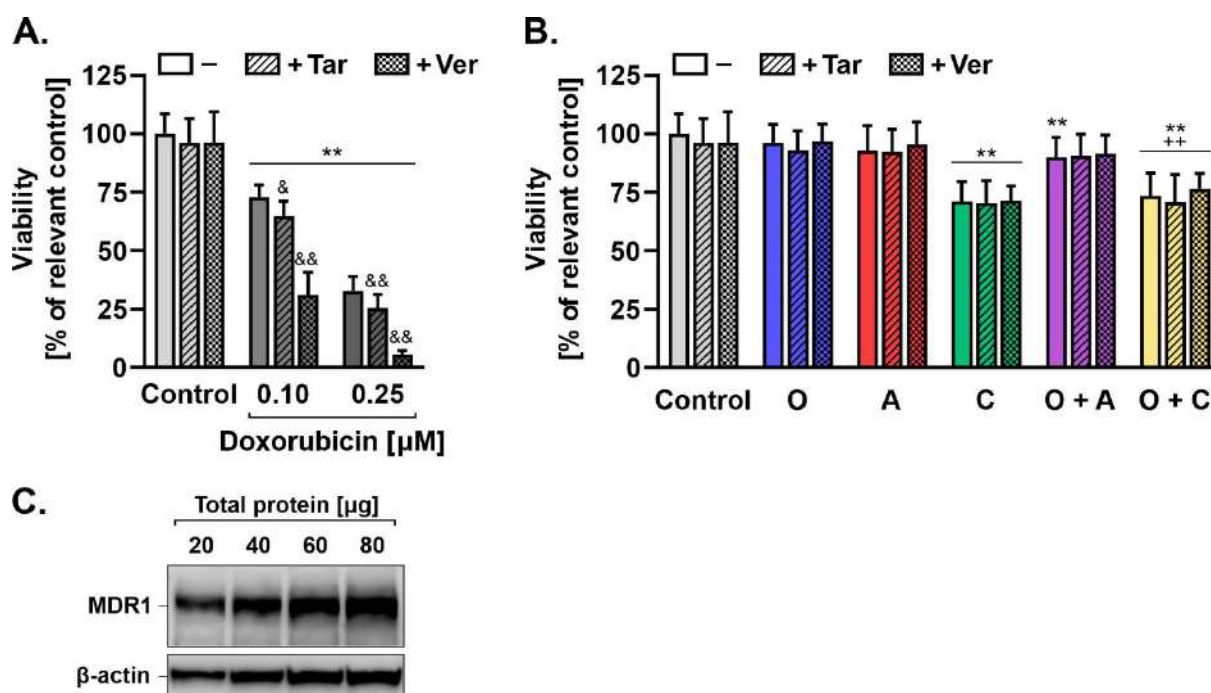


**Figure S3. Effect of MDR1 inhibition with tariquidar (Tar) or verapamil (Ver) on cytotoxicity of a MDR1 substrate doxorubicin and olaparib, ATRi, CHK1i, or their combinations after 48 h of treatment in HepG2 cell line and qualitative western blot analysis of MDR1 expression in untreated HepG2 cells.** Cell viability was assessed by MTT assay after treatment with (A) doxorubicin or (B) olaparib, ATRi, CHK1i, or their combinations, and expressed as the percentage of relevant control cells (untreated control for cells treated with tested drugs only; control with tariquidar or verapamil for cells treated with tested drugs and a relevant MDR1 inhibitor). Briefly, HepG2 cells were pre-treated with MDR inhibitors for 1 h (0.1  $\mu$ M Tar or 50  $\mu$ M Ver) following incubation with olaparib (O, 5  $\mu$ M), ATRi (A, 0.5  $\mu$ M), CHK1i (C, 2.5  $\mu$ M) or their combinations in the absence and presence of MDR1 inhibitors. Co-treatment of tariquidar (0.1  $\mu$ M, striped bars) or verapamil (50  $\mu$ M, checked bars) with doxorubicin (0.10  $\mu$ M and 0.25  $\mu$ M) was used as a positive control of enhanced cytotoxicity of a known MDR1 substrate due to MDR1 inhibition. Data was expressed as mean  $\pm$  SD (n = 3–4). Welch's ANOVA followed by Dunnett T3 multiple comparison test was used to compare viability of each group (with unequal variances) in response to the treatments: \* $p$  < 0.05, \*\* $p$  < 0.01 treatment vs. control without MDR1 inhibitor;  $\&p$  < 0.05,  $\&p$  < 0.01 treatment vs. treatment with MDR1 inhibitor (tariquidar or verapamil). (C) Qualitative western blot analysis of MDR1 expression in untreated HepG2 cells confirming protein expression in the cells.

**Supplementary Figure S4 (Figure S4)**

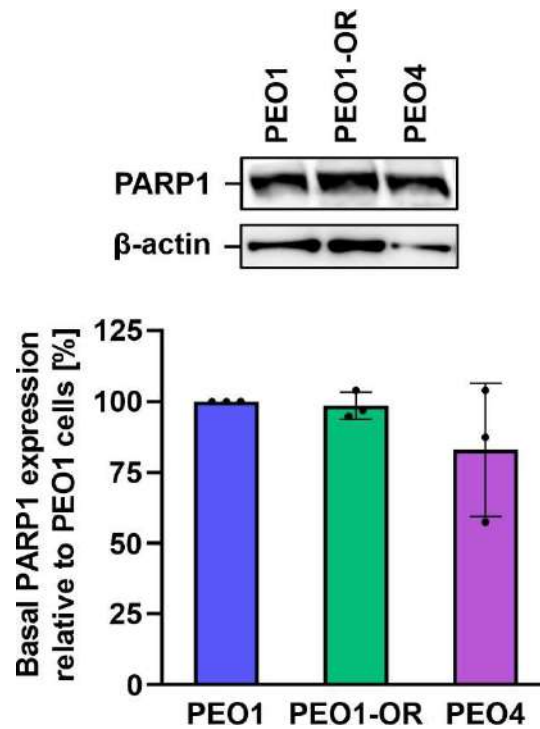


**Figure S4. Quantitative western blot analysis of PARP1 basal expression in untreated PEO1, PEO1-OR, and PEO4 ovarian cancer (OC) cell lines with a representative blot.** Whole-cell lysates (30  $\mu$ g of protein) were loaded into each lane and separated in 8% Bis-Tris gels by SDS-PAGE following protein transfer and immunodetection. The results are shown as mean  $\pm$  SD (n = 3). Individual data points are shown in bar charts presenting basal expression levels. Ordinary one-way ANOVA followed by Tukey's multiple comparison test was used to compare basal protein expression between cell lines:  $^{\wedge}p < 0.05$ ,  $^{\wedge\wedge}p < 0.01$  differences between cell lines.

## **Supplementary Table S1 (Table S1)**

### **Key materials and reagents used in the study.**

<b>Reagent</b>	<b>Catalogue Number</b>	<b>Manufacturer</b>
(±)-Verapamil HCl	V4629	Sigma-Aldrich (Merk)
BD Pharmingen™ FITC BrdU Flow Kit	557891	BD Biosciences
Colcemid	10295892001	Roche (Merck)
Crystal violet	911517ZA	VWR
DMEM, high glucose (4.5 g/L), GlutaMAX™ Supplement, HEPES	32430-027	Gibco (Thermo Fisher Scientific)
Doxorubicin HCl	SRP04600d	Sequoia Research Products Limited
FBS, heat-inactivated, qualified	10270106	Gibco (Thermo Fisher Scientific)
GenElute™ Mammalian Genomic DNA Miniprep Kits	G1N10	Sigma-Aldrich (Merk)
Giemsa Dilution Buffer (20X)	1062.3	AQUA-MED
Giemsa Stain (10X)	1020.1	AQUA-MED
Halt™ Phosphatase Inhibitor Cocktail (100X)	78420	Thermo Fisher Scientific
Halt™ Protease Inhibitor Cocktail (100X)	87786	Thermo Fisher Scientific
HiMark™ Pre-stained Protein Standard	LC5699	Invitrogen (Thermo Fisher Scientific)
MagicMark™ XP Western Protein Standard		Invitrogen (Thermo Fisher Scientific)
MOPS Running Buffer	MPM0PS	Millipore (Merck)
mPAGE® 4X LDS Sample Buffer	MPSB	Millipore (Merck)
mPAGE® Bis-Tris Precast Gels 10%	MP10W10	Millipore (Merck)
mPAGE® Bis-Tris Precast Gels 12%	MP12W10	Millipore (Merck)
mPAGE® Bis-Tris Precast Gels 8%	MP8W10	Millipore (Merck)
mPAGE® Transfer Buffer	MPTRB	Millipore (Merck)
MTT	20395.03	SERVA Electrophoresis
Pierce™ Detergent Compatible Bradford	23246	Thermo Fisher Scientific
PVDF Membrane	IPVH85R	Millipore (Merck)
RIPA Lysis and Extraction Buffer	89900	Thermo Fisher Scientific
RPMI 1640, GlutaMAX™ Supplement, HEPES	72400-021	Gibco (Thermo Fisher Scientific)
Spectra™ Multicolor Broad Range Protein Ladder	26634	Thermo Fisher Scientific
Spectra™ Multicolor High Range Protein Ladder	26625	Thermo Fisher Scientific
SuperBlock™ (TBS) Blocking Buffer	37581	Thermo Fisher Scientific
SuperSignal™ West Atto Ultimate Sensitivity Substrate	A38555	Thermo Fisher Scientific

SuperSignal™ West Pico PLUS Chemiluminescent Substrate	34577	Thermo Fisher Scientific
Tariquidar	SML1790	Sigma-Aldrich (Merk)
Trypsin-EDTA	25200072	Gibco (Thermo Fisher Scientific)
β-mercaptoethanol	M6250	Sigma-Aldrich (Merck)

### **Supplementary Table S2 (Table S2)**

**Primary antibodies used in the study.**

<b>Target</b>	<b>Host and Clonality</b>	<b>Supplier</b>	<b>Catalogue Number</b>	<b>Dilution</b>	<b>Dilution buffer</b>	<b>Blocking agent</b>	<b>Application</b>
53BP1	Mouse monoclonal	Sigma-Aldrich (Merck)	MAB3802	1:1000	5% BSA in TBST	SuperBlock™ (TBS) Blocking Buffer	WB
ATR	Mouse monoclonal	Invitrogen (Thermo Fisher Scientific)	MA1-23158	1:1000	5% BSA in TBST	5% non-fat milk in TBST	WB
BRCA1	Rabbit polyclonal	Cell Signaling Technology	9010	1:1000	5% BSA in TBST	SuperBlock™ (TBS) Blocking Buffer	WB
BRCA2 (N-term) #1	Rabbit polyclonal	Thermo Fisher Scientific	A303-434A	1:10 000	5% non-fat milk in TBST	SuperBlock™ (TBS) Blocking Buffer	WB
BRCA2 (N-term) #2	Mouse monoclonal	Invitrogen (Thermo Fisher Scientific)	MA523942	1:1000	5% non-fat milk in TBST	SuperBlock™ (TBS) Blocking Buffer	WB
BRCA2 (C-term)	Rabbit polyclonal	Thermo Fisher Scientific	A300-005A	1:1000	5% BSA in TBST	SuperBlock™ (TBS) Blocking Buffer	WB
CHK1	Rabbit monoclonal	Thermo Fisher Scientific	MA5-32180	1:1000	5% BSA in TBST	5% non-fat milk in TBST	WB
MDR1	Rabbit monoclonal	Invitrogen (Thermo Fisher Scientific)	MA5-32282	1:1000	5% BSA in TBST	SuperBlock™ (TBS) Blocking Buffer	WB
PARG	Mouse monoclonal	Invitrogen (Thermo Fisher Scientific)	MA5-27034	1:1000	5% BSA in TBST	SuperBlock™ (TBS) Blocking Buffer	WB



Target	Host and Clonality	Supplier	Catalogue Number	Dilution	Dilution buffer	Blocking agent	Application
PARP1	Rabbit monoclonal	Cell Signaling Technology	9532	1:1000	5% BSA in TBST	5% non-fat milk in TBST	WB
pATR (Thr1989)	Rabbit monoclonal	Cell Signaling Technology	30632	1:1000	5% BSA in TBST	5% non-fat milk in TBST	WB
pCHK1 (Ser345)	Rabbit monoclonal	Cell Signaling Technology	2348	1:1000	5% BSA in TBST	5% non-fat milk in TBST	WB
RAD51	Rabbit polyclonal	Sigma-Aldrich (Merck)	ABE257	1:1000 (WB) 1:500 (IF)	5% BSA in TBST	SuperBlock™ (TBS) Blocking Buffer	WB, IF
β-actin	Mouse monoclonal	Sigma-Aldrich (Merck)	A1978	1:10 000	5% BSA in TBST	5% non-fat milk in TBST or SuperBlock™ (TBS) Blocking Buffer	WB
γH2AX (Ser139)	Mouse monoclonal	Sigma-Aldrich (Merck)	05-636	1:1000 (WB) 1:500 (IF)	5% BSA in TBST	SuperBlock™ (TBS) Blocking Buffer	WB, IF
γH2AX (Ser139)	Mouse monoclonal	Invitrogen (Thermo Fisher Scientific)	12-9865-42	1:20	N/A	1X BD Perm/Wash Buffer	FC

### Supplementary Table S3 (Table S3)




Secondary antibodies used in the study.

Species Reactivity	Conjugate	Host	Manufacturer	Catalogue Number	Dilution	Dilution buffer	Application
Mouse	HRP	Goat	Invitrogen (Thermo Fisher Scientific)	A28177	1:10 000	5% non-fat milk in TBST	WB
Rabbit	HRP	Goat	Cell Signaling Technology	7074	1:10 000		WB
Mouse	Alexa Fluor™ Plus 488	Goat	Invitrogen (Thermo Fisher Scientific)	A32723	1:1000	DPBS 1X with 1% BSA and 0.3% Triton X-100	IF
Rabbit	Alexa Fluor® 555	Goat	Cell Signaling Technology	4413	1:1000		IF



















### Supplementary Table S4 (Table S4)

High-quality exonic and intronic variants detected in *ABCB1*, *ATR*, *BRCA1*, *BRCA2*, *CHEK1*, *H2AX*, *PARP1*, *PARG*, *RAD51*, *TP53*, and *TP53BP1* genes in PEO1 and PEO1-OR cell lines by whole-exome sequencing.











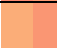
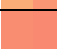




Gene	Mutation	Gene region	Variant type	Amino acid change	Type of mutation	Functional impact	Computed pathogenicity	CADD score	Allele fraction [% of total reads]		Maximal population allele frequency	
									PEO1	PEO1-OR		
TP53	c.731G>A	CDS	SNV	p.G244D	missense	loss	pathogenic	27	100% (of 83 reads)	<div></div>	100% (of 90 reads)	0%
	c.993+409delT	intron	deletion	–	–	normal	benign	<10	53% (of 19 reads)	<div></div>	absent	11% (African)
BRCA1	c.4837A>G	CDS	SNV	p.S1613G	missense	normal	benign (!)	<10	100% (of 140 reads)	<div></div>	100% (of 180 reads)	49% (South Asian)
	c.2082C>T	CDS	SNV	p.S694S	synonymous	normal	benign	<10	100% (of 183 reads)	<div></div>	100% (of 242 reads)	49% (South Asian)
	c.2311T>C	CDS	SNV	p.L771L	synonymous	normal	benign	<10	100% (of 197 reads)	<div></div>	100% (of 262 reads)	49% (South Asian)
	c.2612C>T	CDS	SNV	p.P871L	missense	normal	benign (!)	18	100% (of 135 reads)	<div></div>	100% (of 159 reads)	81% (African)
	c.3113A>G	CDS	SNV	p.E1038G	missense	normal	benign (!)	14	100% (of 189 reads)	<div></div>	100% (of 240 reads)	49% (South Asian)
	c.3548A>G	CDS	SNV	p.K1183R	missense	normal	benign (!)	<10	100% (of 190 reads)	<div></div>	100% (of 198 reads)	49% (South Asian)
	c.4308T>C	CDS	SNV	p.S1436S	synonymous	normal	benign	<10	100% (of 120 reads)	<div></div>	100% (of 160 reads)	49% (South Asian)
	c.-1074C>G	5' UTR	SNV	–	–	normal	benign	<10	100% (of 70 reads)	<div></div>	100% (of 109 reads)	82% (African)
	c.-134T>C	5' UTR	SNV	–	–	normal	benign	<10	100% (of 32 reads)	<div></div>	100% (of 32 reads)	49% (South Asian)
	c.5468-121delA	intron	deletion	–	–	normal	uncertain significance	<10	50% (of 20 reads)	<div></div>	absent	0.40% (East Asian)
	c.4987-144_4987-142dupAAA	intron	insertion	–	–	normal	likely benign	<10	absent	<div></div>	100% (of 23 reads)	4% (African)
	c.134+224delT	intron	deletion	–	–	normal	benign	<10	94% (of 16 reads)	<div></div>	95% (of 20 reads)	52% (South Asian)
	c.213-161A>G	intron	SNV	–	–	normal	benign	<10	100% (of 37 reads)	<div></div>	100% (of 40 reads)	82% (African)
	c.441+36_441+49delCTTTTCTTTTTTTT	intron	deletion	–	–	normal	benign	<10	100% (of 68 reads)	<div></div>	97% (of 131 reads)	49% (South Asian)

Gene	Mutation	Gene region	Variant type	Amino acid change	Type of mutation	Functional impact	Computed pathogenicity	CADD score	Allele fraction [% of total reads]		Maximal population allele frequency
									PEO1	PEO1-OR	
	c.441+64delT	intron	deletion	–	–	normal	benign	<10	100% (of 65 reads)	 94% (of 126 reads)	75% (African)
	c.547+146A>T	intron	SNV	–	–	normal	benign	<17	100% (of 25 reads)	100% (of 25 reads)	49% (South Asian)
	c.548-58delT	intron	deletion	–	–	normal	benign	<12	100% (of 93 reads)	100% (of 89 reads)	49% (South Asian)
	c.593+167T>C	intron	SNV	–	–	normal	benign	<10	100% (of 34 reads)	100% (of 49 reads)	49% (South Asian)
	c.4097-141A>C	intron	SNV	–	–	normal	benign	<10	100% (of 41 reads)	100% (of 67 reads)	67% (African)
	c.4357+117G>A	intron	SNV	–	–	normal	benign	<10	100% (of 19 reads)	100% (of 45 reads)	12% (South Asian)
	c.4358-2885G>A	intron	SNV	–	–	normal	benign	<10	100% (of 109 reads)	100% (of 150 reads)	49% (South Asian)
	c.4358-2590T>G	intron	SNV	–	–	normal	benign	<10	100% (of 18 reads)	100% (LQ) (of 24 reads)	49% (South Asian)
	c.4485-203_4485-199 delAACCC	intron	deletion	–	–	normal	benign	<10	100% (of 12 reads)	100% (of 7 reads)	49% (South Asian)
	c.4485-137T>A	intron	SNV	–	–	normal	benign	<10	100% (of 29 reads)	100% (of 23 reads)	69% (African)
	c.4485-63C>G	intron	SNV	–	–	normal	benign	<10	100% (of 62 reads)	100% (of 63 reads)	49% (South Asian)
	c.4987-92A>G	intron	SNV	–	–	normal	benign	<10	100% (of 47 reads)	100% (of 68 reads)	49% (South Asian)
	c.4987-68A>G	intron	SNV	–	–	normal	benign (!)	<10	100% (of 67 reads)	100% (of 104 reads)	49% (South Asian)
	c.5074+65G>A	intron	SNV	–	–	normal	benign	<10	100% (of 85 reads)	100% (of 138 reads)	46% (South Asian)
	c.5152+66G>A	intron	SNV	–	–	normal	benign	11	100% (of 74 reads)	100% (of 85 reads)	49% (South Asian)
BRCA2	c.4965C>G	CDS	SNV	p.Y1655*	stop gain	loss	pathogenic	33	100% (of 64 reads)	 100% (of 78 reads)	0.008% (European)
	c.4964A>T	CDS	SNV	p.Y1655F	missense	normal	uncertain significance	<10	34% (of 64 reads)	 94% (of 79 reads)	0%
	c.3807T>C	CDS	SNV	p.V1269V	synonymous	normal	benign	<10	100% (of 56 reads)	100% (of 81 reads)	19% (African)
	c.4563A>G	CDS	SNV	p.L1521L	synonymous	normal	benign	<10	100% (of 77 reads)	100% (of 105 reads)	100% (Jewish)

Gene	Mutation	Gene region	Variant type	Amino acid change	Type of mutation	Functional impact	Computed pathogenicity	CADD score	Allele fraction [% of total reads]		Maximal population allele frequency
									PEO1	PEO1-OR	
	c.6513G>C	CDS	SNV	p.V2171V	synonymous	normal	benign	<10	<b>100%</b> (of 88 reads)	<b>100%</b> (of 84 reads)	100% (Jewish)
	c.7397T>C	CDS	SNV	p.V2466A	missense	normal	benign	<10	<b>100%</b> (of 67 reads)	<b>100%</b> (of 83 reads)	100% (Jewish)
	c.*105A>C	3' UTR	SNV	–	–	normal	benign	<10	<b>100%</b> (of 30 reads)	<b>100%</b> (of 37 reads)	23% (South Asian)
	c.793+98G>A	intron	SNV	–	–	normal	benign	<10	<b>100%</b> (of 49 reads)	<b>100%</b> (of 48 reads)	100% (Jewish)
	c.6938-120T>C	intron	SNV	–	–	normal	benign	<10	<b>100% (LQ)</b> (of 16 reads)	<b>100%</b> (of 21 reads)	100% (Jewish)
PARP1	c.2285T>C	CDS	SNV	p.V762A	missense	loss	benign (!)	27	<b>100%</b> (of 49 reads)	<b>100%</b> (of 36 reads)	43% (East Asian)
	c.243C>T	CDS	SNV	p.D81D	synonymous	normal	benign	12	<b>100%</b> (of 106 reads)	<b>100%</b> (of 127 reads)	43% (East Asian)
	c.852T>C	CDS	SNV	p.A284A	synonymous	normal	benign	<10	<b>100%</b> (of 56 reads)	<b>100%</b> (of 52 reads)	81% (East Asian)
	c.-17G>C	5' UTR	SNV	–	–	normal	benign	12	<b>100%</b> (of 32 reads)	<b>100%</b> (of 71 reads)	43% (East Asian)
	c.286+206G>A	intron	SNV	–	–	normal	benign	<10	<b>100%</b> (of 45 reads)	<b>100%</b> (of 83 reads)	81% (East Asian)
	c.617+64C>A	intron	SNV	–	–	normal	benign	<10	<b>100%</b> (of 60 reads)	<b>100%</b> (of 114 reads)	43% (East Asian)
	c.617+12A>G	intron	SNV	–	–	normal	benign	<10	<b>100%</b> (of 83 reads)	<b>100%</b> (of 43 reads)	94% (East Asian)
	c.717+87T>C	intron	SNV	–	–	normal	benign	<10	<b>100%</b> (of 47 reads)	<b>100%</b> (of 106 reads)	47% (East Asian)
ATR	c.632T>C	CDS	SNV	p.M211T	missense	gain	benign (!)	14	<b>32%</b> (of 285 reads)	<b>34%</b> (of 359 reads)	73% (African)
	c.1776T>A	CDS	SNV	p.G592G	synonymous	normal	benign	<10	<b>31%</b> (of 1002 reads)	<b>31%</b> (of 1133 reads)	79% (African)
	c.1815T>C	CDS	SNV	p.D605D	synonymous	normal	benign (!)	<10	<b>32%</b> (of 1108 reads)	<b>31%</b> (of 1274 reads)	44% (Jewish)
	c.5208T>C	CDS	SNV	p.Y1736Y	synonymous	normal	benign (!)	<10	<b>29%</b> (of 172 reads)	<b>30%</b> (of 185 reads)	45% (Jewish)
	c.7875G>A	CDS	SNV	p.Q2625Q	synonymous	normal	benign	<10	<b>32%</b> (of 335 reads)	<b>30%</b> (of 345 reads)	97% (African)

Gene	Mutation	Gene region	Variant type	Amino acid change	Type of mutation	Functional impact	Computed pathogenicity	CADD score	Allele fraction [% of total reads]		Maximal population allele frequency
									PEO1	PEO1-OR	
	c.1885+97_1885+100 delATTT	intron	deletion	–	–	normal	benign	<10	32% (of 462 reads)	 32% (of 532 reads)	44% (Jewish)
	c.2341+185G>A	intron	SNV	–	–	normal	benign	<10	43% (of 444 reads)	 39% (of 322 reads)	48% (African)
	c.3357+128G>A	intron	SNV	–	–	normal	benign	<10	38% (of 48 reads)	 34% (of 53 reads)	24% (Jewish)
	c.4852+39delT	intron	deletion	–	–	normal	uncertain significance	<10	41% (of 87 reads)	 <b>absent</b>	0.3% (South Asian)
	c.5288+130G>A	intron	SNV	–	–	normal	benign	<10	31% (of 62 reads)	 29% (of 75 reads)	45% (Jewish)
	c.5898+25T>G	intron	SNV	–	–	normal	benign	<10	75% (of 32 reads)	 85% (of 34 reads)	79% (African)
	c.5898+82delA	intron	deletion	–	–	normal	benign	<10	100% (of 19 reads)	 100% (of 22 reads)	71% (African)
	c.5898+67_5898+79 delTATATATATATAT	intron	deletion	–	–	normal	benign	<10	100% (of 19 reads)	 59% (of 17 reads)	39% (East Asian)
	c.5898+65_5898+79 delTATATATATATATA T	intron	deletion	–	–	normal	benign	<10	<b>absent</b>	 41% (of 17 reads)	5% (Jewish)
	c.5898+54A>G	intron	SNV	–	–	normal	benign	<10	100% (of 18 reads)	 62% (LQ) (of 21 reads)	30% (African)
	c.5898+52A>G	intron	SNV	–	–	normal	likely benign	<10	<b>absent</b>	 24% (of 21 reads)	3% (Jewish)
	c.1171-58A>C	intron	SNV	–	–	normal	benign	10	64% (of 70 reads)	 67% (of 101 reads)	6% (European)
	c.2342-175A>G	intron	SNV	–	–	normal	benign	<10	33% (of 18 reads)	 28% (LQ) (of 29 reads)	44% (Jewish)
	c.2634-37_2634-36dupGT	intron	insertion	–	–	normal	benign	<10	89% (of 142 reads)	 86% (of 170 reads)	42% (European)
	c.2634-74C>T	intron	SNV	–	–	normal	benign	<10	34% (of 156 reads)	 34% (of 217 reads)	79% (African)
CHEK1	c.1411A>G	CDS	SNV	p.I471V	missense	gain	benign	14	100% (of 105 reads)	 100% (of 105 reads)	99.98% (East Asian)
	c.*28-3033C>G	3' UTR	SNV	–	–	normal	benign	<10	53% (of 17 reads)	 59% (LQ) (of 22 reads)	42% (South Asian)
	c.66-36G>T	intron	SNV	–	–	normal	benign	<10	52% (of 79 reads)	 57% (of 94 reads)	42% (East Asian)



Gene	Mutation	Gene region	Variant type	Amino acid change	Type of mutation	Functional impact	Computed pathogenicity	CADD score	Allele fraction [% of total reads]		Maximal population allele frequency	
									PEO1	PEO1-OR		
ABCB1	c.1101+111T>A	intron	SNV	–	–	normal	benign	<10	45% (of 91 reads)		51% (of 92 reads)	42% (East Asian)
	c.1233+35G>A	intron	SNV	–	–	normal	benign	<10	52% (of 126 reads)		42% (of 132 reads)	57% (Latino)
	c.210A>G	CDS	SNV	p.G70G	synonymous	normal	benign	<10	100% (of 109 reads)		100% (of 100 reads)	100% (East Asian)
	c.530+139C>T	intron	SNV	–	–	normal	benign	<10	100% (of 24 reads)		100% (of 39 reads)	64% (East Asian)
RAD51	c.645-108delA	intron	deletion	–	–	normal	uncertain significance	–	absent		37% (of 57 reads)	0%
	c.645-110_645-108delAAA	intron	deletion	–	–	normal	likely benign	<10	absent		54% (of 57 reads)	2.8% (African)
	c.225+190delT	intron	deletion	–	–	normal	benign	<10	86% (of 69 reads)		100% (of 400 reads)	64% (East Asian)
	c.226-70T>A	intron	SNV	–	–	normal	benign	<10	68% (of 79 reads)		55% (of 89 reads)	36% (European)
	c.226-33T>G	intron	SNV	–	–	normal	benign	11	26% (of 109 reads)		38% (of 118 reads)	67% (East Asian)
H2AX	c.-1420G>A	5' UTR	SNV	–	–	normal	benign	<10	53% (of 19 reads)		35% (LQ) (of 34 reads)	64% (East Asian)
TP53BP1	c.3813+58delT	intron	deletion	–	–	normal	uncertain significance	<10	28% (of 347 reads)		26% (of 415 reads)	0.48% (Latino)
	c.1165+217delT	intron	deletion	–	–	normal	likely benign	<10	absent		64% (of 11 reads)	1.6% (South Asian)
	c.272-49G>A	intron	SNV	–	–	normal	benign	<10	100% (of 165 reads)		100% (of 185 reads)	100% (Jewish)
PARG	c.1456-88_1456-87dupTA	intron	insertion	–	–	normal	benign	<10	100% (of 45 reads)		100% (of 70 reads)	59% (East Asian)
	c.1663-116A>C	intron	SNV	–	–	normal	benign	<10	100% (of 58 reads)		100% (of 84 reads)	59% (East Asian)
	c.1830+132_1830+133 delAG	intron	deletion	–	–	normal	benign	<10	20% (of 35 reads)		17% (of 23 reads)	32% (European)

Color scale visualizes allele frequency of each variants (red – absent or low, yellow – moderate, green – high); ! – conflicting pathogenic criteria has been computationally-applied to a single variant (at least one pathogenic and one benign criterion described in Results section); **3' UTR** – 3' untranslated region; **5' UTR** – 5' untranslated region; **CDS** – protein coding sequence; **CADD score** ranges from 1 to 99 (the higher the value the more deleterious case i.e., 10 indicates top 1% pathogenic variants, 20 indicates top 0.1% pathogenic variants); **LQ** – low quality score for the variant allele call in one sample. **Maximal population allele frequency** was obtained from The Genome Aggregation Database (gnomAD).

## **PUBLIKACJA #3**



# OPEN Targeted inhibition of the ATR/CHK1 pathway overcomes resistance to olaparib and dysregulates DNA damage response protein expression in *BRCA2*<sup>MUT</sup> ovarian cancer cells

Łukasz Biegała<sup>1,2</sup>, Arkadiusz Gajek<sup>1</sup>, Izabela Szymczak-Pajor<sup>3</sup>, Agnieszka Marczak<sup>1</sup>, Agnieszka Śliwińska<sup>3</sup> & Aneta Rogalska<sup>1</sup> ✉

Olaparib is a PARP inhibitor (PARPi) approved for targeted treatment of ovarian cancer (OC). However, its efficacy is impeded by the inevitable occurrence of resistance. Here, we investigated whether the cytotoxic activity of olaparib could be synergistically enhanced in olaparib-resistant OC cells with *BRCA2* reversion mutation by the addition of inhibitors of the ATR/CHK1 pathway. Moreover, we provide insights into alterations in the DNA damage response (DDR) pathway induced by combination treatments. Antitumor activity of olaparib alone or combined with an ATR inhibitor (ATRi, ceralasertib) or CHK1 inhibitor (CHK1i, MK-8776) was evaluated in OC cell lines sensitive (PEO1, PEO4) and resistant (PEO1-OR) to olaparib. Antibody microarrays were used to explore changes in expression of 27 DDR-related proteins. Olaparib in combination with ATR/CHK1 inhibitors synergistically induced a decrease in viability and clonogenic survival and an increase in apoptosis mediated by caspase-3/7 in all OC cells. Combination treatments induced cumulative alterations in expression of DDR-related proteins mediating distinct DNA repair pathways and cell cycle control. In the presence of ATRi and CHK1i, olaparib-induced upregulation of proteins determining cell fate after DNA damage (PARP1, CHK1, c-Abl, Ku70, Ku80, MDM2, and p21) was abrogated in PEO1-OR cells. Overall, the addition of ATRi or CHK1i to olaparib effectively overcomes resistance to PARPi exerting anti-proliferative effect in *BRCA2*<sup>MUT</sup> olaparib-resistant OC cells and alters expression of DDR-related proteins. These new molecular insights into cellular response to olaparib combined with ATR/CHK1 inhibitors might help improve targeted therapies for olaparib-resistant OC.

## Abbreviations

A	ATR inhibitor (cerlasertib)
ATR	Ataxia telangiectasia and RAD3-related protein
ATRi	ATR inhibitor(s)
BER	Base excision repair
BRCA1	Breast cancer type 1 susceptibility protein
BRCA2	Breast cancer type 2 susceptibility protein
C	CHK1 inhibitor (MK-8776)
CDI	Coefficient of drug interaction
CHK1	Checkpoint kinase 1

<sup>1</sup>Department of Medical Biophysics, Institute of Biophysics, Faculty of Biology and Environmental Protection, University of Lodz, 141/143 Pomorska Street, 90-236 Lodz, Poland. <sup>2</sup>Doctoral School of Exact and Natural Sciences, University of Lodz, 21/23 Jana Matejki Street, 90-237 Lodz, Poland. <sup>3</sup>Department of Nucleic Acid Biochemistry, Medical University of Lodz, 251 Pomorska Street, 92-213 Lodz, Poland. ✉email: aneta.rogalska@biol.uni.lodz.pl

CHK1i	CHK1 inhibitor(s)
CHK2	Checkpoint kinase 2
CPT	Camptothecin
DDR	DNA damage response
DR	Direct repair
DSB	Double-strand break
ECACC	European Collection of Authenticated Cell Cultures
ERCC1	Excision repair cross-complementation group 1
FBS	Fetal bovine serum
HGSOC	High-grade serous ovarian cancer
HR	Homologous recombination
MDM2	Mouse double minute 2
MGMT	O <sup>6</sup> -methylguanine-DNA methyltransferase
MMR	Mismatch repair
NBS1	Nijmegen breakage syndrome protein 1
NER	Nucleotide excision repair
NHEJ	Non-homologous end joining
O	Olaparib
OC	Ovarian cancer
OPTN	Optineurin
PARP1	Poly(ADP-ribose) polymerase 1
PARPi	PARP inhibitor(s)
PEO1-OR	PEO1 olaparib-resistant cell line
PLK1	Polo-like kinase 1
SD	Standard deviation
SSB	Single-strand break

Ovarian cancer (OC) is the most lethal gynecologic malignancy, characterized by genomic instability and aberrations in the DNA damage response (DDR)<sup>1–3</sup>. Epithelial OC accounts for about 90% of ovarian tumors and is represented by the most lethal subtype, high-grade serous OC (HGSOC)<sup>4</sup>. Currently, poly(ADP-ribose) polymerase (PARP) inhibition is part of the standard treatment regimen for HGSOC, mainly as maintenance therapy for platinum-sensitive patients with *BRCA1/2* mutations. PARP inhibitors (PARPi) have also shown efficacy in OC patients with other defects in the homologous recombination (HR) repair pathway irrespective of *BRCA1/2* status, supporting their extended clinical use<sup>5</sup>. Olaparib is an approved first-in-class small-molecule inhibitor of PARP1. Blockage of the activity of PARP1 induces accumulating DNA damage and, ultimately, death of OC cancer cells. However, with increasing use of olaparib, many OC patients ultimately develop acquired resistance to the drug and other PARPi treatments, which limits the effectiveness of this therapy<sup>6–8</sup>. Resistance of OC cells to olaparib can arise through a variety of mechanisms, including restoration of DNA repair by HR as the predominant pathway associated with secondary reversion mutations in *BRCA1/2* genes, restoration of replication fork stability, increased PARP1 expression, and other mechanisms<sup>9,10</sup>. Elucidation of alterations in DNA repair pathways beyond HR repair is of major interest in terms of understanding the development of resistance to olaparib in ovarian cancer<sup>11</sup>.

The DDR constitutes a complex network of pathways that coordinate DNA damage sensing and repair, which overlap with cell cycle control and signaling for initiation of apoptosis upon detection of severe lesions. The core DNA repair pathways include direct repair (DR), mismatch repair (MMR), nucleotide excision repair (NER), base excision repair (BER), homologous recombination (HR) repair, and non-homologous end joining (NHEJ), and involve orchestrated cooperation of numerous proteins. The choice of pathway relies on the type of DNA damage, which is repaired by specific individual or coordinated mechanisms<sup>1</sup>. In response to DNA double-strand breaks (DSB), high-fidelity HR or error-prone NHEJ repair is mainly activated. Proteins involved in DDR signaling possess distinct functions as DNA damage sensors, transducers, or effectors. Importantly, defects in one of the pathways can be compensated by the activities of others. However, when the functions of DDR-related proteins are altered, DNA damage cannot be effectively repaired, triggering cell death<sup>2</sup>.

HGSOC is hallmarked by alterations in DDR and genomic instability that are significantly associated with mutations in tumor suppressor p53 and *BRCA1/2* proteins<sup>12–14</sup>. Over recent years, knowledge of the DDR process in OC has significantly expanded to inform novel therapeutic strategies<sup>15</sup>. The well-characterized PARPi, olaparib, inhibits the activity of PARP1 involved in sensing DNA single-strand breaks (SSB) as part of a DDR, which eventually leads to repair of accumulating DSBs by HR<sup>16</sup>. Hence, PARP inhibition shows optimal efficacy in the treatment of HR repair-deficient OC cells as an example of a strategy of synthetic lethality between HR deficiency and PARPi<sup>17,18</sup>.

Targeting DDR pathways has been validated as an attractive strategy for enhancing the antitumor activity of PARPi<sup>1,15</sup>. Concurrent inhibition of the ATR/CHK1 pathway is a promising means to restore olaparib activity in some OC types, including cell lines with *BRCA1* proficiency and deficiency, as well as HGSOC patients with germline *BRCA1/2* mutations who show progression prior to PARPi therapy<sup>19–21</sup>. The ATR/CHK1 pathway is a critical component of the DDR and involved in regulating cell cycle checkpoints and DNA repair processes in OC cells<sup>2</sup>. Ataxia telangiectasia-mutated and Rad3-related (ATR) kinase functions as a sensor of the presence of SSBs arising from DSBs, stalled replication forks, and NER intermediates. Upon DNA damage and replication stress, ATR transduces the signal through effector proteins including its main target, checkpoint kinase 1 (CHK1), to exert cell cycle control at the G2/M checkpoint in OC<sup>1</sup>. Novel therapeutic opportunities for OC

have effectively exploited the ATR/CHK1 pathway. ATR or CHK1 inhibitors can enhance the cytotoxic effects of agents targeting PARP in OC cells by inhibiting HR-mediated DNA repair and promoting the accumulation of DNA damage<sup>9,22</sup>. Preclinical and clinical evidence collectively support the rationale for combining olaparib with inhibitors of the ATR/CHK1 pathway as a therapeutic option. A recent trial exploring a combination of olaparib with the ATR inhibitor (ATRi) ceralasertib in advanced cancers harboring DDR alterations showed high clinical benefit rates in a cohort of *BRCA1/2*-mutated HGSOc patients showing progression with prior PARPi-based regimens<sup>21</sup>. However, further studies are essential to clarify the potential antitumor activity of olaparib combined with inhibitors of the ATR/CHK1 pathway in OC cells harboring various DDR alterations.

Here, we aimed to provide mechanistic insights into the rationale for combining olaparib with inhibitors of the ATR/CHK1 pathway to overcome resistance to PARPi in OC cells with restored *BRCA2*. Furthermore, we explored the molecular mechanisms underlying the response of OC cells to combination treatments associated with alterations in DDR pathways. Changes in expression of proteins that sense and trigger responses to DNA damage and the pathways by which the response cascade affects effector proteins involved in DDR were comprehensively examined.

## Results

### Inhibitors of the ATR/CHK1 pathway synergistically increase the cytotoxicity of olaparib in resistant OC cells in vitro

We initially examined the hypothesis that addition of ATR/CHK1 pathway inhibitors could enhance olaparib cytotoxicity in olaparib-resistant OC cells. The cytotoxic effect of olaparib in combination with ATR/CHK1 inhibitors (ATRi/CHK1i) was evaluated in HGSOc cells treated for 2 and 5 days with 10  $\mu$ M olaparib, 5  $\mu$ M ATRi, and 1  $\mu$ M CHK1i, in addition to PEO1-OR (olaparib-resistant) cells treated with 15  $\mu$ M olaparib, 7.5  $\mu$ M ATRi, and 2.5  $\mu$ M CHK1i via the MTT assay (Fig. 1). Coefficient of drug interaction (CDI) values were calculated to determine whether the effect of combined treatment with olaparib and inhibitors was synergistic, as described in the “Materials and methods” (“MTT cell viability assay” section).

Both combination treatments exhibited nearly additive to slightly synergistic cytotoxic effects (CDI = 0.94–1.01) after 2 days of incubation in olaparib-sensitive OC cells (Fig. 1A). PEO1 cell viability was significantly reduced to ~64% in response to both combinations compared to each agent alone after 2 days. After 5 days of incubation, both ATRi and CHK1i combinations with olaparib induced a favorable synergistic reduction in PEO1 and PEO4 cell viability (CDI = 0.48–0.66) (Fig. 1A). Clearly, the addition of ATRi or CHK1i to olaparib markedly increased the cytotoxic effects of the individual agents, leading to a significant decrease in the metabolic activity of PEO1 (15.8% and 14.1%) and PEO4 (18.4% and 27.7%).

The effects of treatment of PEO1-OR cells with inhibitors at the above concentrations ranged from slightly antagonistic and nearly additive (CDI = 1.02 and 1.09) after 2 days to slightly synergistic (CDI = 0.90 and 0.93) after 5 days (Fig. S1). A satisfactory synergistic effect of olaparib with ATRi or CHK1i (CDI = 0.79 and 0.85, respectively) was achieved at higher concentrations of tested inhibitors after 5 days of incubation (Fig. 1A). Irrespective of the time of incubation, 15  $\mu$ M olaparib alone exerted only a slight cytotoxic activity in PEO1-OR cells, as evident from no significant differences in cell viability between 2 and 5 days of treatment (87.9% and 83.8%,  $p = 0.72$ ). Compared to each agent alone, combination of ATRi and CHK1i with olaparib induced a significant decrease in metabolic activity of PEO1-OR cells to about 56% and 63%, respectively. The results collectively demonstrated that after 5 days of treatment, ATR and CHK1 inhibitors synergistically enhanced the slightly cytotoxic effect of olaparib on the olaparib-resistant cell line.

### Olaparib exerts synergistic suppressive effects with inhibitors of the ATR/CHK1 pathway on clonogenic survival in olaparib-resistant OC cells

Survival of OC cell lines in response to treatments with the inhibitors alone or in combination with olaparib was investigated via the clonogenic assay (Fig. 1B–D). Colony formation of seeded OC cells treated for 5 days was examined. The results showed that untreated PEO1-OR cells exhibited two times higher plating efficiency than olaparib-sensitive cells (Fig. 1B). Importantly, both combination treatments synergistically decreased the clonogenic survival of olaparib-sensitive and -resistant OC cell lines compared to either agent alone (Fig. 1C). Interestingly, although PEO1-OR cells were significantly less sensitive to olaparib alone than PEO1 (6.5 times) and PEO4 cells (18.5 times), the addition of ATRi markedly decreased clonogenic survival, resulting in almost complete inhibition of the ability to form colonies in both olaparib-sensitive and olaparib-resistant cell lines. The colony-forming ability of all OC cell lines was also synergistically reduced in response to the combined treatment with olaparib and CHK1i. However, in the presence of olaparib, PEO1-OR cells displayed a more significant response to ATRi than CHK1i, as indicated by the higher synergistic interactions between olaparib and ATRi (CDI = 0.04) than CHK1i (CDI = 0.34) (Fig. 1C). The observed inhibitory effects of the drug combinations on clonogenic survival are in line with synergistically decreased viability of PEO1-OR cells after 5 days of incubation, as determined with the MTT assay (Fig. 1A). Our collective data indicate that addition of ATR/CHK1 kinase inhibitors to olaparib exerts a synergistic increase in cytotoxicity compared to each agent alone in PEO1-OR olaparib-resistant cells, leading to significantly decreased cell viability and clonogenic survival.

### Olaparib acts synergistically with inhibitors of the ATR/CHK1 pathway to enhance activity of caspase-3 and -7 in mediating apoptosis in olaparib-resistant cells

We examined the hypothesis that combined treatment with inhibitors of the ATR/CHK1 pathway and olaparib could enhance apoptosis in OC cells with acquired resistance to olaparib. Firstly, annexin V-FITC/PI dual staining was performed to examine the effects of combination treatments on phosphatidylserine externalization as a marker of apoptosis in OC cells after 2 days (Fig. 2A,B).

**Figure 1.** Synergistically reduced viability and clonogenic survival of PEO1-OR ovarian cancer (OC) cells resistant to olaparib in response to treatment with olaparib (O) combined with ATRi (A) or CHK1i (C) relative to each agent alone. **(A)** Cell viability was assessed using the MTT assay. OC cells were treated with the inhibitors (O, A, C) or their combinations (O + A, O + C) at the specified concentrations for 2 and 5 days. Data are presented as mean  $\pm$  SD ( $n = 4$ ). Coefficient of drug interaction (CDI) values were calculated to evaluate the effects of combination treatments. **(B)** Determination of plating efficiency of untreated OC cells following plating and incubation of 2000 control cells to form colonies in drug-free medium. Data are presented as mean  $\pm$  SD ( $n = 4$ ). **(C)** Clonogenic survival of OC cells was evaluated using a clonogenic assay. OC cells were plated and treated with the inhibitors (O, A, C) or their combinations (O + A, O + C) for 5 days, followed by incubation in drug-free medium for colony formation (7–10 days). Data are presented as mean  $\pm$  SD ( $n = 4$ ). Coefficient of drug interaction (CDI) values were calculated to evaluate the interaction effects of the combination treatments. **(D)** Representative images of colonies produced by OC cells in response to treatments. Statistical significance was assessed using ordinary one-way (plating efficiency) or two-way ANOVA (viability, colony formation efficiency) followed by the appropriate multiple comparison tests:  $^{\wedge}p < 0.05$ ,  $^{\wedge\wedge}p < 0.001$ ,  $^{\wedge\wedge\wedge}p < 0.0001$  (comparison between cell lines);  $^{**}p < 0.01$ ,  $^{***}p < 0.001$ ,  $^{****}p < 0.0001$  (treatment vs. control);  $^{*}p < 0.05$ ,  $^{****}p < 0.0001$  (olaparib vs. combination with ATRi or CHK1i);  $^{###}p < 0.0001$  (ATRi or CHK1i vs. respective combinations with olaparib).

Treatment of PEO1 cells with olaparib alone caused a significant (2.4-fold) increase in annexin V-positive cells compared with untreated cells (from 4.1% to 9.7% apoptotic cells), which was further synergistically augmented with the addition of ATRi (13.1% apoptotic cells) (Fig. 2A). In contrast, in PEO1-OR cells, olaparib or ATRi alone induced a non-significant change in the percentage of apoptotic cells (from 3.8 to 6.5% and 5.7%, respectively). Importantly, concurrent incubation with olaparib and ATRi induced a significant increase (2.2-fold) in the apoptotic cell content relative to untreated PEO1-OR cells. CHK1i alone and in combination with olaparib significantly elevated phosphatidyl externalization in PEO1-OR cells. However, the observed effect was not synergistic, with similar levels of increase in annexin V-positive cells of 8.6% and 9.6%, respectively (Fig. 2A). PEO4 cells exhibited similar minor changes in phosphatidylserine externalization as PEO1-OR cells after incubation with olaparib or ATRi alone. The most significant (almost 2.0-fold) increase in annexin V-positive cells was observed in response to a combination of olaparib and CHK1i relative to the control group (from 5.1 to 9.9%). However, this effect was similar to that of CHK1i alone (Fig. 2A).

To confirm the apoptosis-inducing effect of the combination treatment, we further investigated activation of caspase-3 and -7 in OC cells as an early event during apoptotic death and further explored whether the interaction effect between inhibitors is synergistic at the early stages at the 2-day stage (Fig. 2C,D). Olaparib alone caused significant (3.1-fold) elevation in the percentage of caspase-3 and -7-positive cells in the PEO1 cell line only (7.6% to 23.8%). Combination treatments led to a significant synergistic increase in caspase-3 and -7 activities in both PEO1 and PEO1-OR cells, although PEO1 cells were considerably more sensitive. In the olaparib-resistant cell line, olaparib and ATRi alone did not affect the activities of caspase-3 and -7. Notably, the percentage of caspase-3- and -7-positive cells increased from 13.1% in olaparib-treated cells by 1.5-fold and 2.3-fold in the presence of ATRi and CHK1i, respectively (Fig. 2C), indicating a synergistic effect. Interestingly, combination of olaparib with ATRi had a non-significant effect on phosphatidylserine externalization and caspase-3 and -7 activities in olaparib-sensitive PEO4 cells (Fig. 2A–C), which correlated with a negligible decrease in viability of this cell line in response to combination treatments after 2 days of incubation (Fig. 1A).

Caspase-3 mRNA was significantly increased in olaparib-sensitive PEO1 cells in the presence of olaparib (Fig. 2E). Moreover, the effect exerted by olaparib was synergistically augmented by ATRi and CHK1i in PEO1 cells (1.2-fold and 1.9-fold compared with olaparib alone), in line with increased activity of caspase-3 and -7, as determined with flow cytometry (Fig. 2E). In contrast, olaparib-resistant PEO1-OR cells showed no significant changes in *CASP3* levels in response to either individual inhibitors or their combinations after 2 days of incubation (Fig. 2E).

Altogether, olaparib combined with inhibitors of the ATR/CHK1 pathway exerted a slight synergistic proapoptotic effect in olaparib-resistant PEO1-OR cells after 2 days of incubation, accompanied by increased caspase-3 and -7 activities and phosphatidylserine externalization. The synergistic proapoptotic activity of the combined inhibitors in PEO1-OR cells was significantly increased with prolonged exposure up to 5 days.

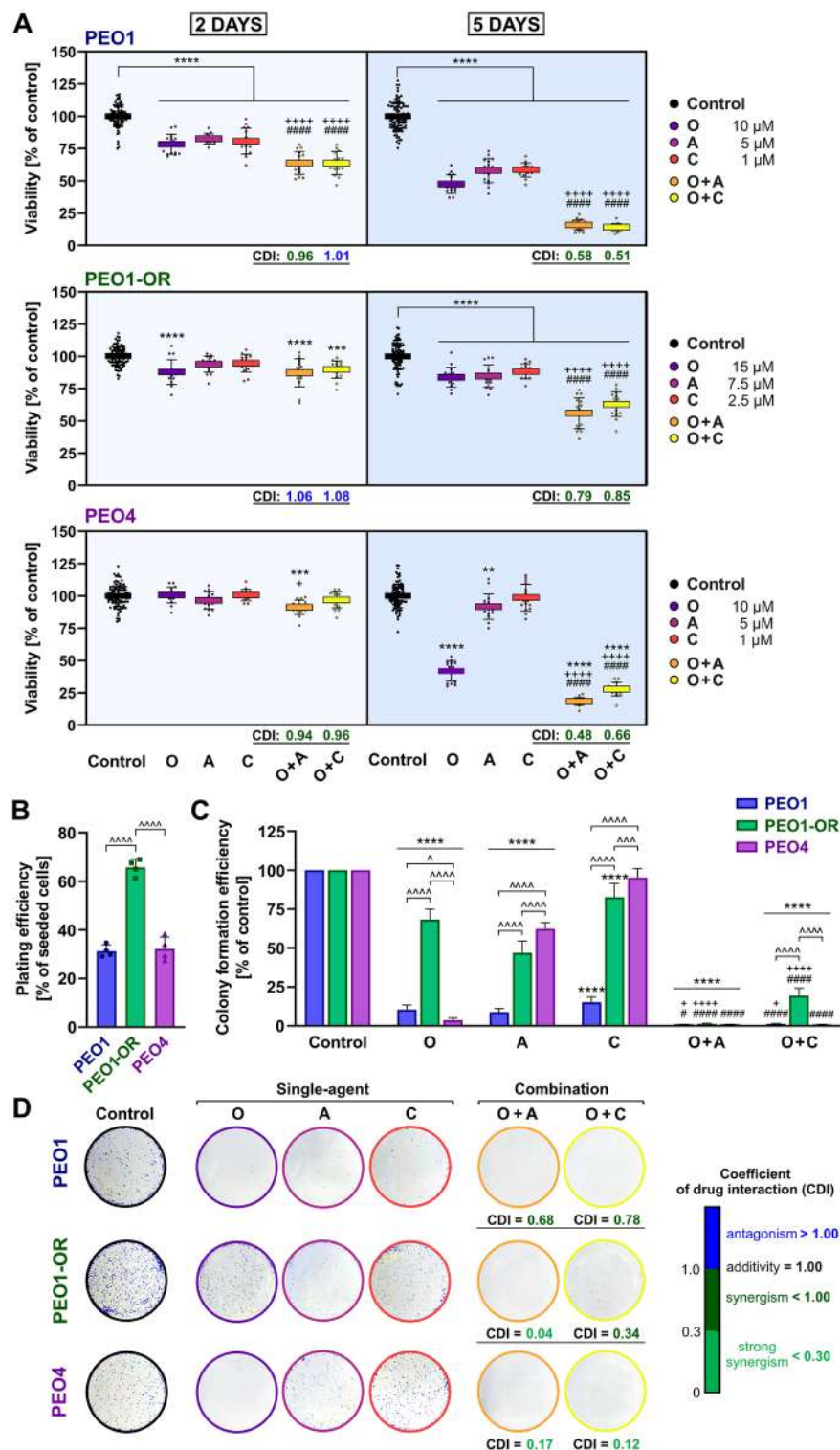
### Combination of olaparib with ATR/CHK1 inhibitors dysregulates protein expression in the DNA damage response pathway in the olaparib-resistant OC cell line

The DNA-damaging activity of olaparib plays a critical role in OC cell cytotoxicity. To establish whether restoration of olaparib cytotoxicity by inhibitors of the ATR/CHK1 pathway in resistant cells is associated with DDR-related proteins, we compared the expression profiles of 27 proteins involved in DDR in both PEO1 and PEO1-OR cells using antibody arrays (Figs. 3, 4).

Firstly, we focused on response to olaparib alone in PEO1-OR cells with markedly diminished sensitivity to this PARPi compared with PEO1 cells. A total of 7 and 9 proteins displayed significant differences in response to olaparib in PEO1 and PEO1-OR cells, respectively (Figs. 3, 4). Moreover, among all the DDR-related proteins examined, expression levels of BRCA1, BRCA2, c-Abl, CHK1, CHK2, cyclin B1, Ku80, MDM2, MGMT, and PARP1 were markedly different between the two cell lines incubated with olaparib (Figs. 3, 4).

Comparative semi-quantitative analysis of protein expression revealed that treatment with olaparib caused significant downregulation of proteins involved in promoting HR repair (BRCA1 by 2.3-fold, BRCA2 by 3.5-fold) and cell cycle control (cyclin B1 by 2.1-fold) in PEO1 cells (Fig. 4A). In contrast, treatment with olaparib had no significant effects on expression of these proteins in PEO1-OR cells (Fig. 4B). However, olaparib induced a





marked increase in expression of c-Abl (by 2.2-fold), CHK1 (by 1.8-fold), MDM2 (by 1.7-fold), Ku80 (by 1.5-fold), p21 (by 1.3-fold) and PARP1 (by 1.5-fold) in PEO1-OR cells, which was not observed in PEO1 cells (Fig. 4).

Comparison of protein levels after treatment with each agent alone and their combinations revealed significant changes in expression of seven proteins in both PEO1 (CHK2, ERCC1, MGMT, NBS1, OPTN, p21, PLK1) and PEO1-OR (c-Abl, ERCC1, MGMT, OPTN, p21, PARP1, PLK1) cell lines (Fig. 4). Expression of proteins directly targeted by the inhibitors, i.e., PARP1, ATR, and CHK1, was not significantly changed in PEO1 cells in response to treatments (Fig. 4A). These findings were confirmed at mRNA level for *PARP1* and *CHEK1* (Fig. 5). In contrast to PEO1 cells, co-treatment with ATRi and olaparib caused a 2.5-fold decrease in PARP1 expression in PEO1-OR compared to untreated cells (Fig. 4B). However, no changes in *PARP1* mRNA levels were observed in response to the combination treatment in PEO1-OR cells (Fig. 5). Moreover, combination of olaparib with

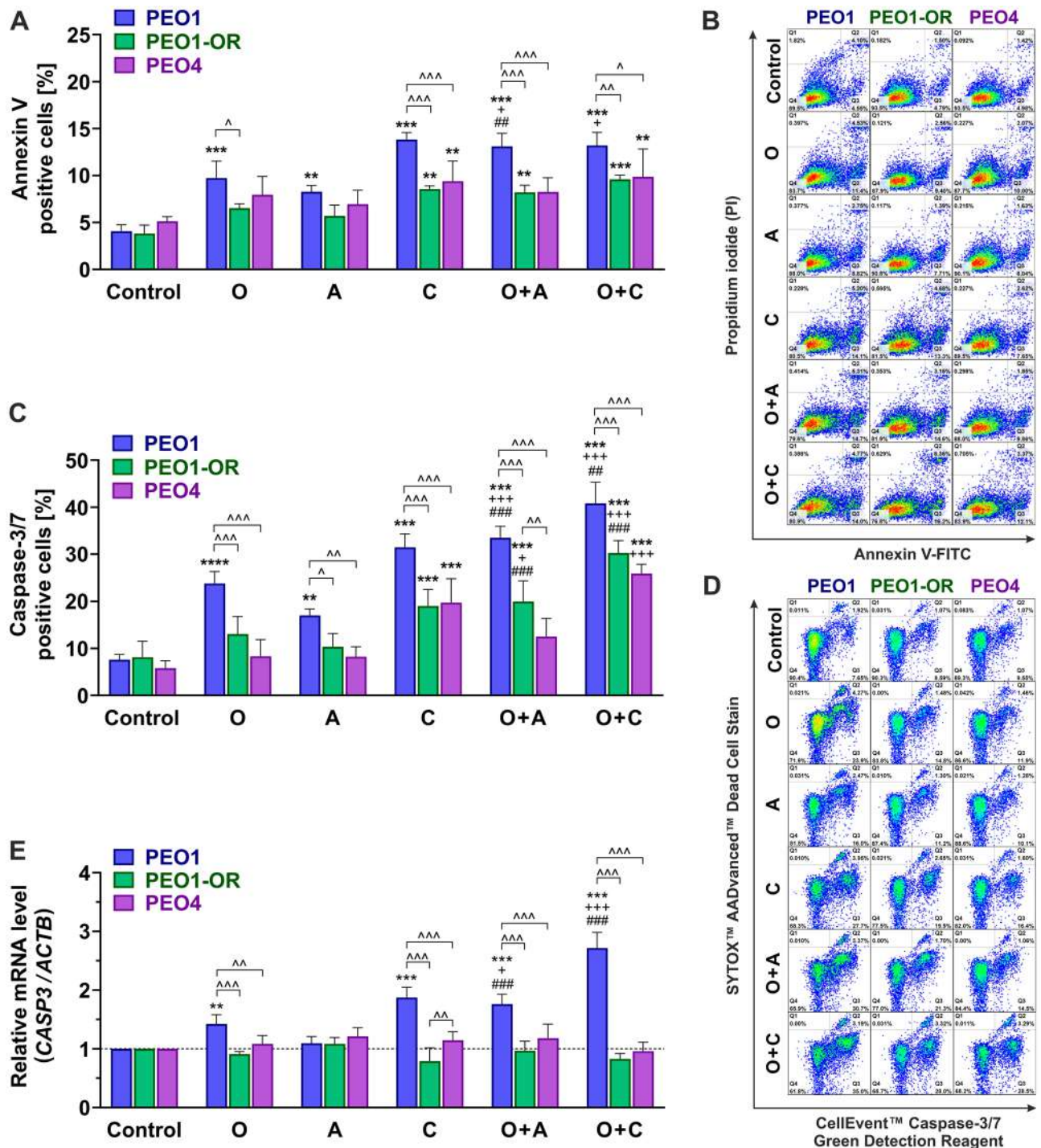


**Figure 2.** Induction of apoptosis and synergistic activation of caspase-3 and -7 in PEO1-OR ovarian cancer (OC) cells in response to olaparib (O) combined with ATRi (A) or CHK1i (C) compared to each agent alone. OC cells were treated with the inhibitors (O, A, C) or their combinations (O + A, O + C) for 2 days. (A) Apoptosis was examined via dual staining with annexin V-FITC and PI, quantified with flow cytometry, and presented as a percentage of annexin V-positive (apoptotic) relative to untreated control cells. Data are presented as mean  $\pm$  SD (n = 3). (B) Representative dot plots of annexin V-FITC- and PI-stained OC cells with the indicated percentages of non-viable cells (Q1), necrotic cells (Q2), apoptotic cells (Q3), and viable cells (Q4). (C) Activation of caspase-3 and caspase-7 in apoptotic cells examined via dual staining and flow cytometry using a CellEvent™ Caspase-3/7 Green Flow Cytometry Assay Kit, expressed as a percentage of caspase-3/7-positive relative to untreated control cells. Data are presented as mean  $\pm$  SD (n = 3). (D) Representative dot plots of a two-parameter apoptosis assay for detection of activated caspase-3/7 (CellEvent™ Caspase-3/7 Green Detection Reagent) and discrimination between live and dead cells (SYTOX™ AADvanced™ Dead Cell Stain) with the indicated percentages of necrotic cells (Q2), viable cells (Q3), and apoptotic cells with activated caspase-3/7 (Q4). (E) qRT-PCR analysis of caspase-3 mRNA. Relative mRNA expression was calculated using the  $2^{-\Delta\Delta Ct}$  method and  $\beta$ -actin (ACTB) as a reference gene. Data are presented as mean  $\pm$  SD (n = 4). Statistical significance was assessed using two-way ANOVA, followed by Tukey's multiple comparison test: \* $p < 0.05$ , \*\* $p < 0.01$ , \*\*\* $p < 0.001$  (comparison between cell lines); \* $p < 0.05$ , \*\* $p < 0.01$ , \*\*\* $p < 0.001$  (treatment vs. control); \* $p < 0.05$ , \*\* $p < 0.01$ , \*\*\* $p < 0.001$  (olaparib vs. combination with ATRi or CHK1i); \* $p < 0.05$ , \*\* $p < 0.01$ , \*\*\* $p < 0.001$  (ATRi or CHK1i vs. respective combinations with olaparib).

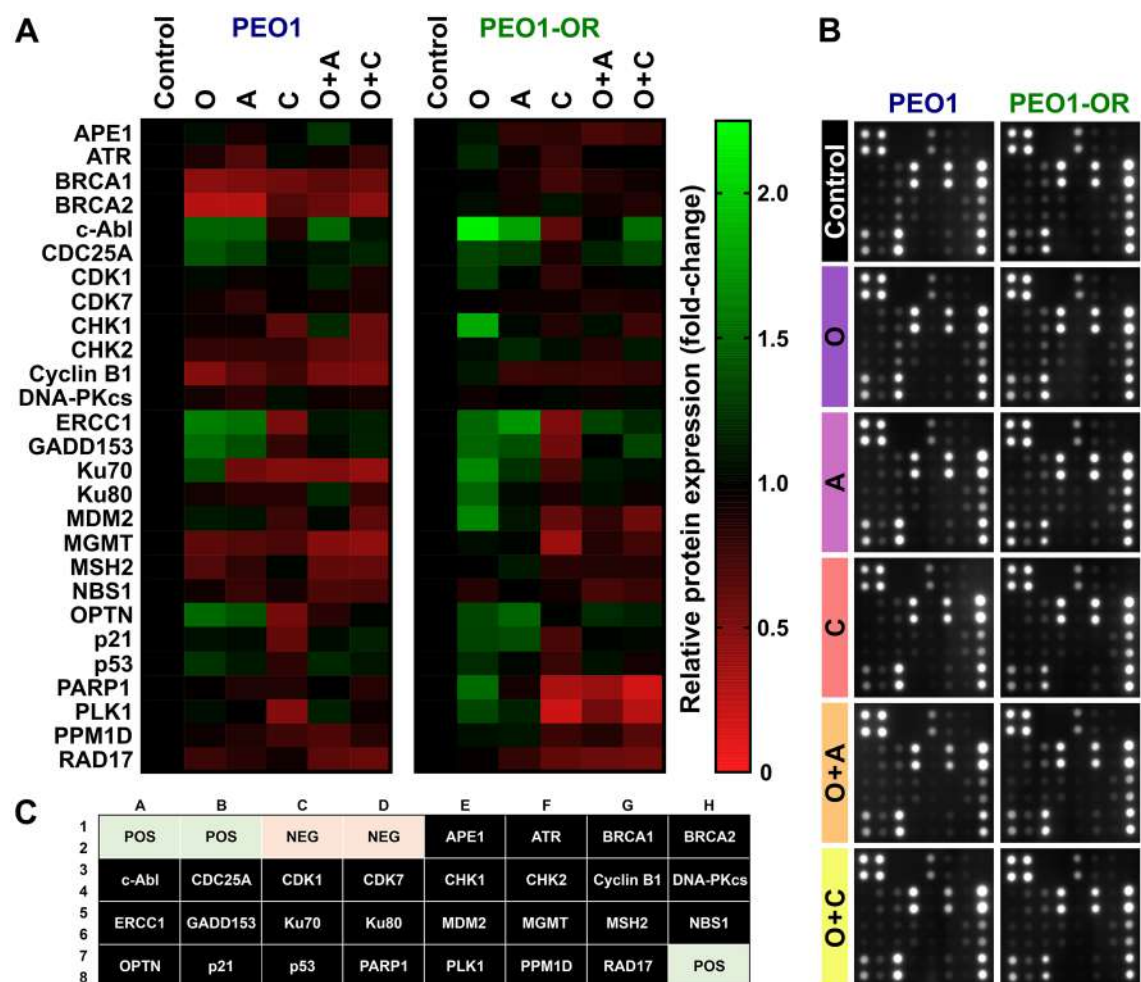


**Figure 3.** Expression profiles of DNA damage response (DDR)-related proteins in olaparib-sensitive and -resistant OC cell lines in response to olaparib (O) combined with ATRi (A) or CHK1i (C). OC cells were treated with the inhibitors (O, A, C) or their combinations (O + A, O + C) for 2 days and whole-cell lysates used for analysis of 27 DDR-related proteins via antibody arrays. **(A)** Heat map representing relative expression of DDR-associated proteins in OC cell lines treated with inhibitors (n = 4). The gradient scale represents normalized expression values. **(B)** Original representative images of antibody arrays. **(C)** Array map showing the locations of individual antigen-specific antibody spots printed in duplicate. POS positive control spots used for data normalization between arrays, NEG negative control spots used to measure the baseline signal.

either ATRi or CHK1i abolished olaparib-induced upregulation of CHK1 in PEO1-OR cells (Fig. 4B). Distinct from DDR antibody array data, a significant decrease in *CHEK1* mRNA was observed in PEO1-OR cells in response to concurrent treatment with olaparib and CHK1i (Fig. 5).

Regarding effects of the combination treatments on proteins involved in HR repair, no significant changes were observed in BRCA1 and BRCA2 representing key mediators of this pathway in PEO1-OR cells (Fig. 4B). However, inhibition of the ATR/CHK1 pathway abolished olaparib-induced upregulation of c-Abl kinase that acts as a positive regulator of HR repair. Analysis of NHEJ pathway components in PEO1-OR cells showed that protein expression of Ku70 and Ku80, but not DNA-PKcs, was significantly increased by 1.7-fold and 1.5-fold after treatment with olaparib alone. This effect was abolished with concurrent inhibition of the ATR/CHK1 pathway (Fig. 4B). In contrast, PEO1 cells showed no changes in expression of NHEJ-promoting proteins treated with either agent alone or in combination (Fig. 4A). In the case of proteins involved in other DDR pathways, the addition of either ATRi or CHK1i to olaparib restored basal levels of the NER-promoting endonuclease ERCC1 in both PEO1 and PEO1-OR cell lines (Fig. 4). Moreover, downregulation of methyltransferase MGMT, a key enzyme in the DR pathway, observed in PEO1 cells in response to olaparib combined with inhibitors of the ATR/CHK1 pathway, was abrogated in PEO1-OR cells.

Antibody array data also revealed changes in expression patterns of proteins involved in the G2/M phase transition downstream of the ATR/CHK1 pathway. We observed significant downregulation of cyclin B1 in PEO1 cells treated with both olaparib alone and combined with ATRi or CHK1i, which induced a similar decrease in cyclin B1 levels by about 2.1 times compared to untreated cells (Fig. 4A). In contrast to olaparib-sensitive cells, in PEO1-OR cells, expression of cyclin B1 remained unchanged irrespective of the treatment. However, both



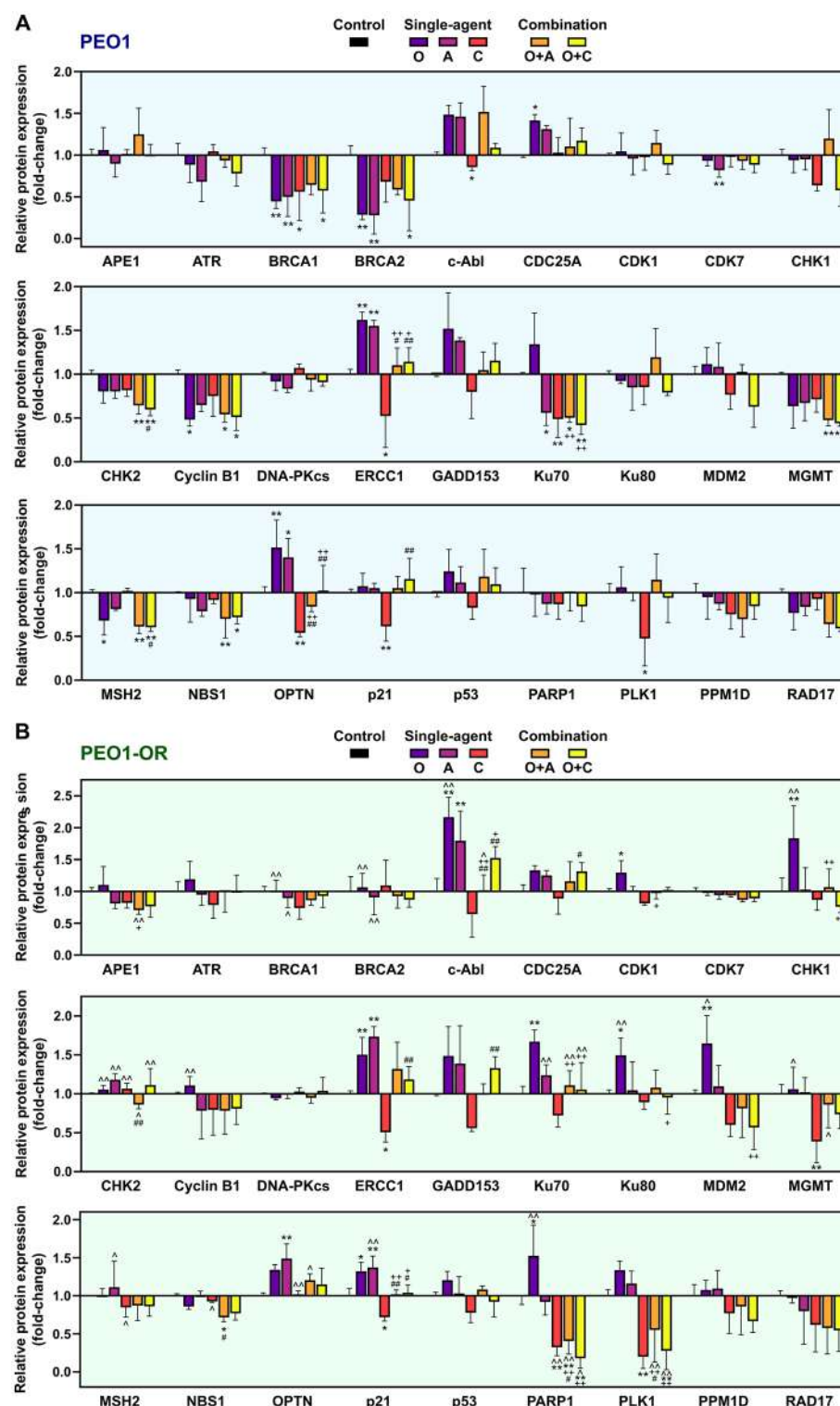


**Figure 4.** Olaparib (O) combined with ATRi (A) or CHK1i (C) dysregulates expression of DNA damage response (DDR)-related proteins in OC cells. Semi-quantitative analysis of DDR-associated proteins expression using antibody microarray in PEO1 (A) and PEO1-OR (B) cells treated with the inhibitors (O, A, C) or their combinations (O + A, O + C) for 2 days. Data are expressed as mean  $\pm$  SD (n = 4) relative to untreated control cells. Statistical significance was assessed using two-way ANOVA, followed by Tukey's multiple comparison test:  $^{\wedge}p < 0.05$ ,  $^{\wedge\wedge}p < 0.01$  (comparison between cell lines);  $^*p < 0.05$ ,  $^{**}p < 0.01$  (treatment vs. control);  $^{\#}p < 0.05$ ,  $^{\#\#}p < 0.01$  (olaparib vs. combination with ATRi or CHK1i);  $^{\#}p < 0.05$ ,  $^{##}p < 0.01$  (ATRi or CHK1i vs. respective combinations with olaparib).

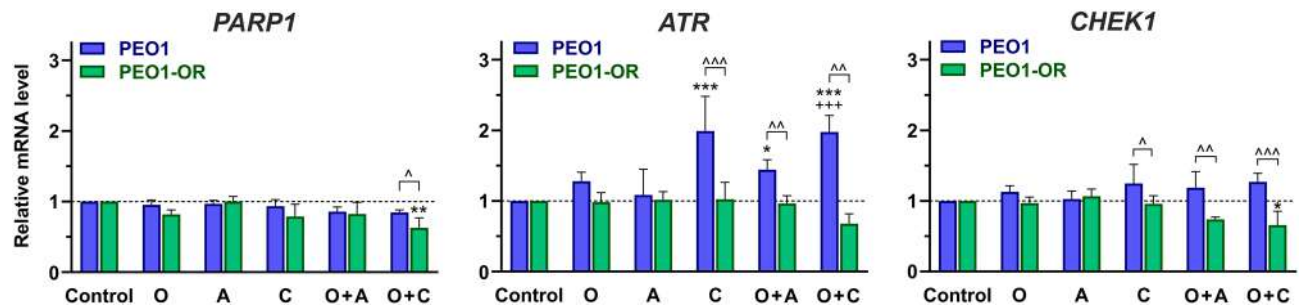


**Figure 5.** Olaparib combined with the CHK1 inhibitor decreases mRNA levels of *PARP1* and *CHEK1* in olaparib-resistant PEO1-OR cells. OC cells were treated with the inhibitors (O, A, C) or their combinations (O + A, O + C) for 2 days and mRNA levels determined via real-time qPCR. Data were normalized to  $\beta$ -actin and expressed relative to untreated cells as mean  $\pm$  SD ( $n = 4$ ). Statistical significance was assessed using two-way ANOVA, followed by Tukey's multiple comparison test:  $^{\wedge}p < 0.05$ ,  $^{\wedge\wedge}p < 0.01$ ,  $^{\wedge\wedge\wedge}p < 0.001$  (comparison between cell lines);  $^*p < 0.05$ ,  $^{**}p < 0.01$ ,  $^{***}p < 0.001$  (treatment vs. control);  $^{++}p < 0.001$  (olaparib vs. combination with ATRi or CHK1i).

combinations restored basal levels of p21 and markedly decreased PLK1 expression in PEO1-OR cells by about 1.8-fold (with ATRi) and 3.6-fold (with CHK1i) (Fig. 4B).

## Discussion

Olaparib exhibits clinical efficacy in OC patients, but PARPi resistance remains a major challenge in long-term treatment. Targeting of the ATR/CHK1 pathway with small-molecule inhibitors sensitizes OC to olaparib with distinct genetic alterations related to DDR pathways<sup>19–21,23</sup>. Importantly, ATRi<sup>21</sup> or CHK1i<sup>24</sup> kinase inhibitors combined with olaparib show favorable preliminary clinical activity in PARPi-resistant HGSOc patients. However, some of them progress after combination treatments<sup>24</sup> or do not achieve effective response<sup>25</sup>, supposedly due to unknown factors that are yet to be established. In the present study, we explored combining olaparib with ATR/CHK1 pathway inhibitors in the previously developed PEO1-OR cell line with acquired resistance to olaparib and restored *BRCA2*<sup>9</sup>. Although *BRCA2* reversion mutations occur in the minority of OC patients treated with PARPi<sup>26,27</sup>, they tend to accumulate upon progression<sup>27</sup> and represent a well-established mechanism of olaparib resistance. Importantly, our cell line serves as a valuable model of olaparib resistance, mirroring reversion mutations in *BRCA2* in PARPi-treated HGSOc patients<sup>28</sup>. Here, we addressed mechanisms associated with overcoming resistance to olaparib concerning changes in the expression of DDR-related proteins in PEO1-OR cells.

Previously we revealed differences in the responses of olaparib-sensitive and -resistant cell lines to ATR/CHK1 pathway inhibitors in the presence of PARPi at non-toxic concentrations for 2 days for PEO1-OR cells<sup>29</sup>. Here, we focused on combating resistance to olaparib via combined treatment with olaparib, ATRi, and CHK1i exerting synergistic antitumor effects. Firstly, we confirmed that inhibition of the ATR/CHK1 pathway synergistically enhanced olaparib cytotoxicity in PEO1-OR cells. Olaparib alone modestly affected the viability of PEO1-OR cells after 2 and 5 days, but combination treatment for 5 days decreased the colony-forming ability of PEO1-OR cells to similar levels as olaparib-sensitive cells, confirming durable responses. Supposedly, more than a single round of replication is required to induce significant antitumor actions in olaparib-resistant cells, affirming olaparib's need for multiple rounds of cell division to exert its cytotoxic activity<sup>30</sup>. The observations are in line with earlier reports<sup>19,23</sup> and endorse overcoming resistance to olaparib by adding ATRi or CHK1i to PARPi.

Apoptotic changes in OC cells were additionally examined. In PEO1 cells, PS externalization, caspase-3/7 activity, and *CASP3* mRNA levels synergistically increased with combination treatments compared to single-agent inhibitors within 2 days. Adding ATRi or CHK1i synergistically elevated caspase activity in PEO1-OR cells irrespective of *CASP3* transcriptional level. PS externalization tended to increase in PEO1-OR cells after 2 days in response to olaparib when combined with ATRi or CHK1i. These early membrane asymmetry changes aligned with a synergistic decrease in cell survival and growth after 5 days of treatment. Our results suggest differential control of PS exposure associated with apoptosis in olaparib-sensitive and -resistant cells. Variability in surface PS exposure within cancer types, correlating with treatment susceptibility<sup>31,32</sup>, further supports our observations. A study by Kim et al.<sup>23</sup> revealed increased PS externalization in OC olaparib-resistant cell lines after 3 days of olaparib combined with ATRi. Olaparib reportedly synergizes with arsenic trioxide in platinum-resistant OC cells to increase cleavage of caspase-3 and promote PS externalization within 2 days<sup>33</sup>. Significantly, all examined OC cells showed synergistic elevation of caspase-3/7 activity with combination treatments, indicating reduced cell growth primarily through caspase-mediated apoptosis. Our data provide evidence that relatively short incubation with combined inhibitors holds promising proapoptotic activity in PEO1-OR cells.

OC cells exhibit various changes in DDR pathways, particularly HR deficiency, which are exploited by PARPi treatments<sup>11,17,34</sup>. PARP1 inhibits DNA DSB end resection antagonizing HR and promoting NHEJ<sup>35</sup>, and regulates SSB repair through NER and BER<sup>36</sup>. Inhibition with olaparib may affect DDR pathways and drive response to PARPi beyond HR effectiveness in OC cells<sup>37</sup>. Evidence from OC indicates that concurrent downregulation of HR and either NER or MMR pathways positively correlates with sensitivity to olaparib<sup>34</sup>. Over recent years, targeting the DDR pathway has become a key strategy to overcome resistance to PARPi<sup>1,34</sup>. ATR/CHK1 inhibition shows promise in the resensitization to olaparib, especially in *BRCA1*<sup>MUT</sup> OC, but challenges exist in *BRCA2*<sup>MUT</sup>

tumors. Further investigation of the utility of ATR/CHK1 pathway inhibitors in the resensitization of OC to olaparib is necessary.

In this study, we provide evidence that a combination of olaparib with the ATR/CHK1 pathway inhibitors induces cumulative alterations in the expression of DDR-related proteins in the olaparib-resistant OC cells (Fig. 6). Olaparib-induced downregulation of BRCA1 and BRCA2 in olaparib-sensitive PEO1 cells was abrogated in PEO1-OR cells. Olaparib combined with CHK1i suppressed expression of BRCA1 and BRCA2 in PEO1 cells similarly to olaparib alone. However, despite the effective treatment of PEO1-OR cells with olaparib and ATR/CHK1 pathway inhibitors, no significant impact on BRCA1 and BRCA2 levels was observed (Fig. 6), indicating different HR-related DDR responses to combinations.

NHEJ repairs DNA DSBs throughout the cell cycle, with Ku70, Ku80, and DNA-PKcs regulating the canonical pathway<sup>2</sup>. Alternatively, DSBs are recognized by PARP1, which removes Ku70/80 complexes from damage sites exclusively during the S/G2 phase and promotes the alternative NHEJ pathway<sup>38</sup> (Fig. 6). The study by McCormick et al.<sup>39</sup> provided evidence that NHEJ is defective in 40% of ex vivo primary cultures of epithelial OC. Downregulation of Ku70, Ku80, and DNA-PKcs may promote resistance to the PARPi rucaparib, irrespective of HR repair status<sup>39</sup>. Olaparib-induced Ku70 and Ku80 overexpression in PEO1-OR cells was reversed by ATRi or CHK1i co-treatment. Simultaneously, combination treatments downregulated PARP1 in PEO1-OR. Interestingly, previous studies by our group have shown that the combination of olaparib with inhibitors of the ATR/CHK1 pathway decreases the expression of NHEJ-promoting 53BP1<sup>29</sup>.

In response to DNA damage, c-Abl tyrosine kinase mediates phosphorylation of DDR-related substrates, including proteins involved in repair mechanisms (ATR, BRCA1, PARP1, DNA-PKcs), cell cycle regulation, and apoptosis (p53, MDM2). c-Abl has been implicated in promoting DNA repair or proapoptotic signaling under unrepairable DNA damage<sup>40</sup>. For instance, phosphorylation of MDM2 by c-Abl negatively regulates the

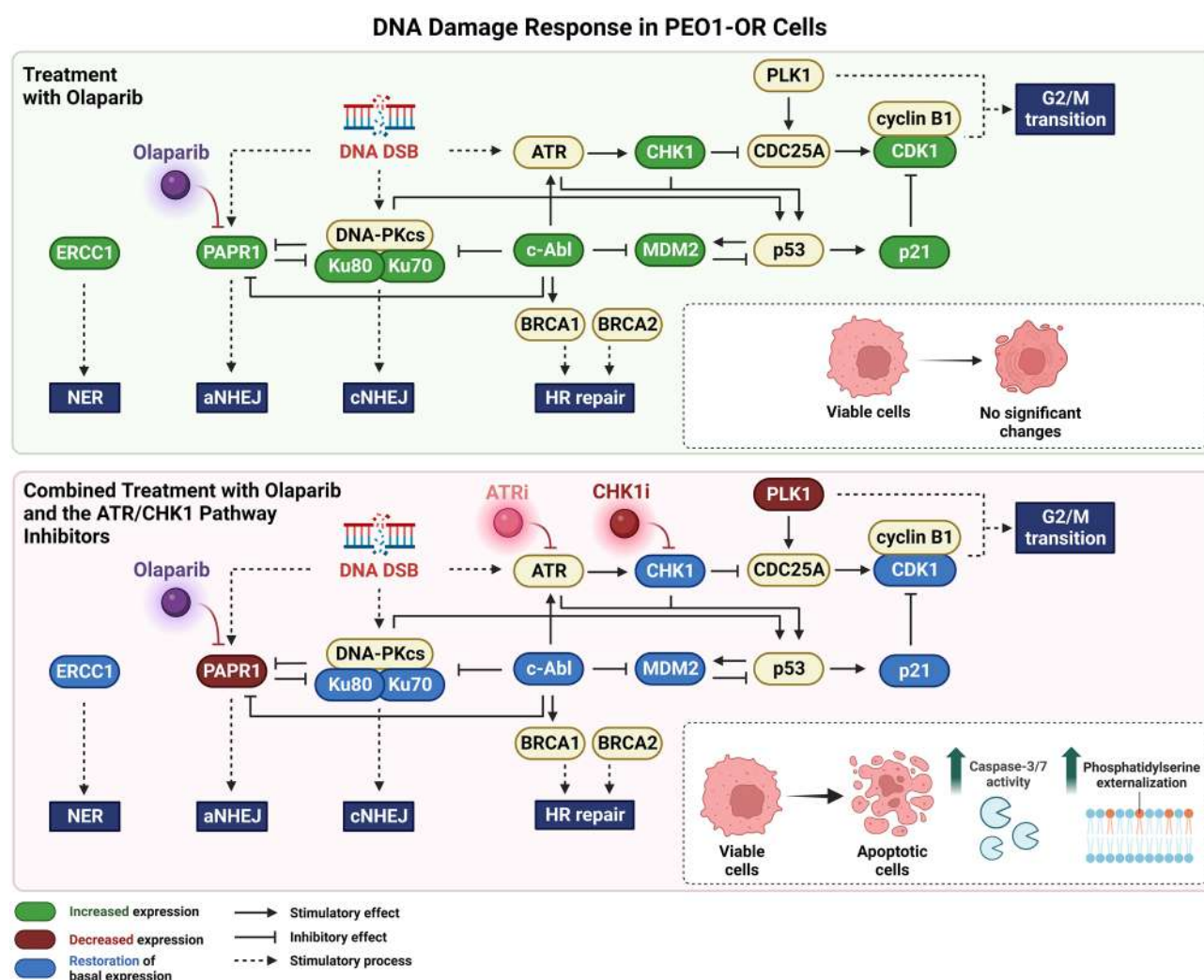


**Figure 6.** Overview of alterations in expression of proteins involved in DDR induced by inhibitors of the ATR/CHK1 pathway that potentially contribute to overcoming resistance to olaparib in PEO1-OR cells. *aNHEJ* alternative non-homologous end joining, *cNHEJ* canonical non-homologous end joining, *DSB* double-strand break, *HR* homologous recombination, *NER* nucleotide excision repair.



MDM2-dependent inhibitory effect on the tumor suppressor p53 (Fig. 6)<sup>40</sup>. Importantly, c-Abl overexpression was identified in OC specimens<sup>41,42</sup>, but studies on c-Abl's role in the DDR of olaparib-resistant OC cells are lacking. Our work revealed olaparib-induced upregulation of c-Abl and MDM2 in PEO1-OR cells, neutralized upon the addition of ATRi or CHK1i. c-Abl upregulation may contribute to decreased sensitivity to olaparib by activating alternative DNA repair pathways that compensate for loss of PARP activity. Indeed, overexpression of MDM2 is linked to increased survival, therapeutic resistance, and metastasis in OC<sup>43,44</sup>. Recent findings indicate that MDM2 inhibition enhances cisplatin's antitumor activity in platinum-resistant OC cells<sup>45</sup>. We propose that c-Abl-dependent effects on MDM2 and PARP1 may be abolished after combination treatments, and associated with overcoming resistance to olaparib. Moreover, upon DNA damage ATR-mediated phosphorylation inhibits c-Abl substrate MDM2<sup>46</sup>. In our study, olaparib-induced upregulation of c-Abl, MDM2, and CHK1 in PEO1-OR cells was abolished upon co-treatment with ATRi or CHK1i. This suggests that the reliance of olaparib-resistant OC cells on c-Abl-dependent DDR machinery plays an important role in ATR/CHK1 inhibitor-mediated suppression of resistance. Indeed, the analysis of c-Abl-mediated downstream events confirmed that combinations induced apoptosis in PEO1-OR cells.

Olaparib triggers DNA damage-induced G2/M checkpoint arrest and promotes apoptosis in sensitive OC cells<sup>23,47</sup>. We previously demonstrated that PEO1-OR cells bypass G2/M arrest induced by PARPi in olaparib-sensitive cells<sup>29</sup>. Here, we focused on changes in expression of the proteins involved in the G2/M transition (CDC25A, CDK1, CHK1, CHK2, cyclin B1, p21, PLK1). Olaparib downregulated cyclin B1 only in PEO1 cells, indicating decreased G2/M transition, consistent with previous results<sup>29</sup>. This decrease in cyclin B1 levels was abrogated in PEO1-OR cells, while simultaneous upregulation of p21 and CHK1 was observed, which could promote G2/M arrest and reflect an effective response to olaparib<sup>29</sup>. Activation of PLK1 via CHK1 upon DNA damage promotes HR-mediated DSB repair<sup>48</sup>. Moreover, in the absence of PARP1, recruitment of PLK1 to DSBs may be abolished<sup>48</sup>. In our study, combination treatment decreased the levels of PLK1 and PARP1 with concurrent normalization of CHK1 expression to basal levels in PEO1-OR cells, suggesting aberrations in HR repair.

Analysis of the DNA damage sensors provided further insights into variations in DDR among OC cells. Recent studies suggest that the DR-associated DNA damage sensor MGMT promotes chemoresistance, and its inhibition can sensitize OC to histone deacetylase inhibitors<sup>49</sup>. Large-scale screening has revealed that alterations in *MSH2*, a DNA damage recognizer, are extremely rare in OC patients<sup>50</sup>. Data from the current study showed that expression of *MSH2* and *MGMT* is suppressed in PEO1 cells in response to olaparib alone or combined with ATR/CHK1 inhibitors, suggesting deficiencies in DR and MMR pathways in olaparib-sensitive cells. However, PEO1-OR cells appear less susceptible to changes in DNA damage sensors involved in DR and MMR, indicating that alternative DDR pathways play a minor role in the resensitization of OC to olaparib.

DDR inhibitor-based combination therapies hold promise for OC treatment due to tumor susceptibility to DNA damage and reliance on response mechanisms to proliferate<sup>1,51</sup>. Recent studies link DDR signatures with response to chemotherapy in OC patients-derived tumor cells<sup>12</sup>. Dysregulation of DDR-related proteins in OC cells may be critical in selecting predictive biomarkers of treatment response and unraveling the connection between DDR and olaparib resistance. Overall, alterations in DDR-related proteins induced by the concurrent use of olaparib and ATR/CHK1 inhibitors in PEO1-OR cells show promise in postponing or preventing drug resistance in OC cells. Yet, further research is required to establish whether long-term resensitization of OC cells to olaparib combined with ATR/CHK1 pathway inhibitors is achievable.

Notably, our confirmation of overcoming olaparib resistance has been verified in one OC cell line with acquired resistance to olaparib, which limits the finding of our study to the model with *BRCA2* reversion mutation. Nonetheless, the strength of this model lies in the thorough characterization of the PEO1-OR cell line and the investigation of its response to non-toxic concentrations of PARPi in the presence of ATR/CHK1 pathway inhibitors<sup>9</sup>. Despite the potential weaknesses, we clearly showed that resistance to olaparib can be overcome with ATR/CHK1 inhibitors in OC cells.

In conclusion, ATR/CHK1 inhibitors effectively resensitize OC cells with restored *BRCA2* to olaparib in vitro, inducing apoptosis through synergistic activation of caspase-3/7. Concurrent treatment with olaparib and ATR/CHK1 pathway inhibitors induces dysregulation of proteins involved in the DDR pathway as well as the G2/M checkpoint during cell cycle control. The collective findings provide novel insights into the molecular mechanisms by which inhibitors of the ATR/CHK1 pathway act synergistically with olaparib to enhance cytotoxicity, supporting the utility of this strategy as a promising treatment for OC with restored *BRCA2*.

## Materials and methods

### Materials

PARPi (O, olaparib, AZD2281) was purchased from Selleck Chemicals (Houston, TX, USA). ATRi (A, ceralasertib, AZD6738) and CHK1i (C, MK-8776) were purchased from Wuhan ChemNorm Biotech (Wuhan, China). The stock solutions of the inhibitors were prepared in 100% dimethyl sulfoxide (DMSO) and stored at  $-80^{\circ}\text{C}$  for up to six months. RPMI 1640 culture medium, heat-inactivated fetal bovine serum (FBS), and trypsin-EDTA were obtained from Gibco (Thermo Fisher Scientific, Waltham, MA, USA). Chemicals and solvents were obtained from Sigma-Aldrich or Avantor Performance Materials Poland S.A. Other key reagents used in the studies are included in the “Materials and methods” section and Supplementary Table S1.

### Cell lines and treatment

Human HGSOC cell lines PEO1 with *BRCA2* truncating mutation (*BRCA2*<sup>MUT</sup>, c. 4965C>G, p.Y1655\*) and PEO4 with *BRCA2* reversion mutation (*BRCA2*<sup>REV</sup>, 4965C>T, p.Y1655Y) were purchased from the European Collection of Authenticated Cell Cultures (ECACC, Salisbury, UK). A human HGSOC cell line with acquired resistance to olaparib and secondary *BRCA2* mutation PEO1-OR (*BRCA2*<sup>MUT</sup>, c.[4964A>T; 4965C>G], p.Y1655L) was

developed by continuous exposure to incrementally increasing doses of olaparib as described previously<sup>29</sup>. Cells were cultured as monolayers in RPMI 1640 medium containing GlutaMAX™ supplement, HEPES, supplemented with 10% FBS and maintained in the cell culture incubator (37 °C, 5% CO<sub>2</sub>). Cells were subcultured using 0.1% trypsin solution with 0.4 mM EDTA.

Unless otherwise stated, during all experiments olaparib-sensitive cells (PEO1 and PEO4) were treated with the final concentration of 10 μM olaparib, 2.5 μM ATRi, and 1 μM CHK1i, whereas olaparib-resistant cells (PEO1-OR) were incubated with 15 μM olaparib, 7.5 μM ATRi and 2.5 μM CHK1i.

### MTT cell viability assay

Cell viability in response to tested inhibitors was evaluated with MTT assay. Cells were seeded in 96-well plates (1.0 × 10<sup>4</sup> PEO1 or PEO1-OR cells and 2.0 × 10<sup>4</sup> PEO4 cells per well for 2-day treatment, and 0.4 × 10<sup>4</sup> PEO1 or PEO1-OR cells and 0.8 × 10<sup>4</sup> PEO4 cells per well for five-day treatment) and incubated for 24 h (37 °C, 5% CO<sub>2</sub>). The next day culture medium was changed and 4 × concentrated working solutions of inhibitors or their combinations were added to wells for 2 or 5 days of incubation (37 °C, 5% CO<sub>2</sub>). Following the treatment, the medium was aspirated, 50 μL of MTT solution (0.5 mg/mL in DPBS) was added to each well, and the plates were incubated for 4 h (37 °C, 5% CO<sub>2</sub>). Afterward, 100 μL of DMSO was added to each well, plates were incubated at room temperature or 37 °C protected from light until complete solubilization of the formazan crystals, and the samples were mixed for about 30 s using a plate shaker.

The absorbance was determined spectrophotometrically on a microplate reader (Synergy HTX, BioTek, Shoreline, WA, USA) at an experimental wavelength of 580 nm, using 720 nm as a reference wavelength. To determine cell viability, the absorbance at 720 nm was subtracted from the absorbance at 580 nm ( $A_{580} - A_{720}$ ) for individual wells. Then, the mean absorbance value of background wells (DMSO with MTT) was subtracted from the absorbance readings of tested samples. Relative cell viability was calculated as the percentage of untreated control cells using corrected absorbance values. Each experiment was independently repeated four times (n = 4) with a minimum of three intraplate technical replicates and the results were presented as mean ± standard deviation (SD).

Coefficient of drug interaction (CDI) values were calculated using corrected absorbance values to determine the total cytotoxic effect of concurrent incubation with two inhibitors according to the formula:

$$CDI = \frac{AB}{A \times B} \times 100\%$$

Based on the corrected absorbance of each group, AB is the cell viability of the two-agent combination group, and each A or B is the cell viability of the single-agent group. CDI values indicated whether the effect exerted by the combination of drugs was strongly synergistic (CDI < 0.30), synergistic (0.3 ≤ CDI < 0.7), moderately synergistic (0.7 ≤ CDI < 0.85), slightly synergistic (0.85 ≤ CDI < 1.0), additive (CDI = 1.00) or antagonistic (CDI > 1.00).

### Clonogenic assay

A clonogenic assay was performed to evaluate the ability of cells to proliferate and form colonies in the presence of studied inhibitors. Cells were seeded in 6-well plates (2 × 10<sup>3</sup> cells/well) and allowed to attach for 24 h (37 °C, 5% CO<sub>2</sub>). The next day culture medium was changed and 100 × concentrated working solutions of inhibitors or their combinations were added to wells for 5 days of incubation (37 °C, 5% CO<sub>2</sub>). After the incubation period, the medium was refreshed (3 mL/well), and cells were incubated (37 °C, 5% CO<sub>2</sub>) in the absence of inhibitors for 7 days (PEO1-OR) or 10 days (PEO1, PEO4) until forming single, non-overlapping colonies. Finally, the colonies were fixed with the mixture of methanol and glacial acetic acid (7:1 (v/v)) for 10 min, stained with 1% (w/v) crystal violet in 20% (v/v) ethanol for 20 min, thoroughly rinsed with deionized water, and air-dried at room temperature. Stained colonies were photographed and counted manually. Colony formation efficiency (clonogenic survival) relative to control cells was calculated according to the formula:

$$\text{Colony formation efficiency} = \frac{\text{number of colonies in a treatment group}}{\text{number of colonies in a control group}} \times 100\%$$

Each experiment was independently repeated four times (n = 4) and the results were presented as mean ± SD. CDI values were calculated as mentioned above in “Materials and methods” (“MTT cell viability assay” section) based on clonogenic survival values for combination and single-agent groups.

### RNA isolation, cDNA synthesis, and quantitative real-time PCR

Gene expression profiling (*ATR*, *CASP3*, *CHEK1*, *PARP1*) was conducted using quantitative real-time PCR (qRT-PCR). Cells were seeded in 100 mm dishes (2 × 10<sup>6</sup> cells) and incubated for 24 h (37 °C, 5% CO<sub>2</sub>). The next day culture medium was changed and 100 × concentrated working solutions of inhibitors or their combinations were added to each dish for 2 days (37 °C, 5% CO<sub>2</sub>). After the incubation period, cells were harvested by trypsinization, centrifuged (300×g, 5 min, 4 °C) and pellets were stored at − 80 °C. Total RNA was isolated and purified using mirVana™ miRNA Isolation Kit with phenol (Invitrogen™, Thermo Fisher Scientific) according to the manufacturer's protocol and stored at − 80 °C. The quality and quantity of isolated RNA were analyzed by absorbance measurements at 230, 260, and 280 nm using a BioTek Eon™ microplate spectrophotometer.

For cDNA synthesis, 1000 ng of total RNA was reverse transcribed in 0.2 mL thin-walled tubes using High-Capacity cDNA Reverse Transcription Kit (Applied Biosystems™, Thermo Fisher Scientific) with RNase inhibitor and PTC-200 DNA Engine® Cyclor (MJ Research Inc., Canada) according to the manufacturer's instruction and cDNA was stored undiluted at − 80 °C.

qRT-PCR was performed using 10 ng of obtained cDNA, TaqMan™ Universal Master Mix II with no UNG, and predesigned TaqMan™ Gene Expression Assays listed in Table S2 (Applied Biosystems™, Thermo Fisher Scientific) in the final volume of 10 µL and run in the Rotor-Gene Q 5plex HRM (QIAGEN Inc., Germany) according to the manufacturer's protocols. Raw data was analyzed using Q-Rex Software (QIAGEN Inc., Germany).

Three widely used potential endogenous control genes (*ACTB*, *GAPDH*, and *HPRT1*) were analyzed in all OC cell lines to assess the stability of their expression across different treatment conditions and to choose a reference gene for normalization in gene expression studies. RNA for each treatment condition from two independent experiments was reversely transcribed and obtained cDNA was subjected to qRT-PCR analysis in duplicate using the abovementioned experimental conditions. Averaged threshold cycle values were compared and used to rank the genes with RefFinder web-based tool<sup>52</sup>.

Relative mRNA expression was calculated according to the comparative  $2^{-\Delta\Delta C_t}$  method using *ACTB* as a reference gene and presented as a fold-change relative to untreated control cells. Each experiment was independently repeated three to four times ( $n = 3-4$ ) with each sample run in duplicate or triplicate (SD between technical replicates  $\leq 0.3$  cycles) and the results were presented as mean  $\pm$  SD.

### Caspase 3/7 activity assay

The effect of studied inhibitors and their combinations on the activity of caspase 3 and caspase 7 (markers of apoptosis) was determined using the CellEvent™ Caspase-3/7 Green Flow Cytometry Assay Kit (Invitrogen™, Thermo Fisher Scientific) according to the manufacturer's protocols. Cells were seeded in 100 mm dishes ( $2 \times 10^6$  cells) and incubated for 24 h (37 °C, 5% CO<sub>2</sub>). The next day culture medium was changed and 100× concentrated working solutions of inhibitors or their combinations were added to each dish for 2 days (37 °C, 5% CO<sub>2</sub>). Cells were also incubated with 2.5 µM camptothecin (CPT), which was used as a positive control for the induction of caspase 3 and 7 activity. After the incubation period, cells were harvested by trypsinization, centrifuged (300×g, 5 min, room temperature), resuspended in DBPS with 5% FBS, and incubated with CellEvent™ Caspase-3/7 Green Detection Reagent for 1 h at room temperature. SYTOX™ AADvanced™ Dead Cell Stain was added during the final 5 min of staining. Labeled cells were immediately acquired by collecting at least 10,000 events with BD™ LSR II flow cytometer (Becton Dickinson, San Jose, CA, USA).

Flow cytometric data were analyzed using FlowJo v.7.6.1 analyzing software (Ashland, OR, USA). Each experiment was independently repeated three to four times ( $n = 3-4$ ) and the results were presented as mean  $\pm$  SD.

### Apoptosis assay using annexin V-FITC/PI staining

Annexin V-FITC/propidium iodide (PI) staining was performed with Dead Cell Apoptosis Kits with Alexa Fluor™ 488 annexin V/PI for flow cytometry (Invitrogen™, Thermo Fisher Scientific) according to the manufacturer's instruction to detect apoptosis in OC cells. Cells were seeded in 100 mm dishes ( $2 \times 10^6$  cells) and incubated for 24 h (37 °C, 5% CO<sub>2</sub>). The next day culture medium was changed and 100× concentrated working solutions of inhibitors or their combinations were added to each dish for 2 days (37 °C, 5% CO<sub>2</sub>). Cells were also incubated with 2.5 µM CPT, which was used as a positive control for the induction of apoptosis. After the incubation period, cells were harvested by trypsinization, centrifuged (300×g, 5 min, 4 °C), washed in ice-cold DPBS, resuspended in annexin-binding buffer containing Alexa Fluor™ 488 annexin V and PI provided with the kit, and incubated for 30 min at 4 °C. Labeled cells were immediately acquired by collecting at least 10,000 events with BD™ LSR II flow cytometer (Becton Dickinson, San Jose, CA, USA).

Flow cytometric data were analyzed using FlowJo v.7.6.1 analyzing software (Ashland, OR, USA). Each experiment was independently repeated three times ( $n = 3$ ) and the results were presented as mean  $\pm$  SD.

### DNA damage response antibody array

The expression of 27 DNA damage response-associated proteins was semi-quantitatively determined using a commercially available antibody array system RayBio™ C-Series Human DNA Damage Response Antibody Array 1 (RayBiotech Life, Inc., Peachtree Corners, USA) according to the manufacturer's instructions.

PEO1 and PEO1-OR cells were seeded in 100 mm dishes ( $2 \times 10^6$  cells) and incubated for 24 h (37 °C, 5% CO<sub>2</sub>). The next day culture medium was changed and 100× concentrated working solutions of inhibitors or their combinations were added to each dish for 2 days (37 °C, 5% CO<sub>2</sub>). After the incubation period, cells were washed twice with ice-cold DPBS and lysed directly on plates afterward using ice-cold cell lysis buffer with a protease inhibitor cocktail provided with the kit. Cell lysates were centrifuged (14,000×g, 5 min, 4 °C), supernatants were transferred to fresh microcentrifuge tubes, and clear lysates were stored at  $-80$  °C. The total protein concentration in each lysate was determined spectrophotometrically using Pierce™ BCA Protein Assay Kit (Thermo Fisher Scientific) and a Synergy HTX microplate reader (BioTek, Shoreline, WA, USA) according to the manufacturer's microplate procedure.

The antibody arrays were incubated with blocking buffer (30 min, room temperature) followed by the incubation with 1 mL of diluted samples containing 200 µg of total protein each (overnight, 4 °C). Thereafter, after repeated washings with the Wash Buffer I and II, membranes were subsequently incubated with a biotinylated antibody cocktail (overnight, 4 °C) and HRP-streptavidin (2 h, room temperature). Next, all membranes from each biological replicate were placed next to each other, and incubated with the detection buffer (2 min, room temperature), and the chemiluminescence signal was measured for 2 min with Azure 300 Imaging System (Azure Biosystems, Dublin, CA, USA) yielding non-overlapping signals.

Densitometric data were analyzed according to the manufacturer's instructions. Briefly, the integrated density of each antigen-specific antibody spot was measured using the same circle (area and shape) on every array with ImageJ software (NIH, Bethesda, MD, USA). After correcting the raw numerical densitometry data by subtracting background (negative control spots), densitometric data were further normalized to the positive control signals

from reference arrays with control cells. The changes in protein expression were calculated as a fold-change relative to untreated control cells. Each experiment was independently repeated two times ( $n = 4$ ) with two technical replicates on each membrane and the results were presented as mean  $\pm$  SD.

### Statistical analysis

Statistical analysis was performed with GraphPad Prism version 9.5.1 for Windows (GraphPad Software, San Diego, CA, USA) using the tests specified in the Results section for each experiment. Shapiro–Wilk or D’Agostino–Pearson tests were used to assess whether data come from a normal distribution. Homogeneity of variance within groups was evaluated with Brown–Forsythe or Bartlett’s tests. Ordinary one-way ANOVA followed by Tukey’s multiple comparison tests was used to assess the statistical significance of differences where three independent groups were defined by one factor (cell line). Two-way ANOVA followed by Tukey’s or Šidák multiple comparison tests was used to assess the statistical significance of differences where three independent groups were defined by two factors (drug treatment and cell line or drug treatment and time of incubation). Differences among groups were considered statistically significant at:  $^{\wedge}p < 0.05$ ,  $^{\wedge\wedge}p < 0.01$ ,  $^{\wedge\wedge\wedge}p < 0.001$ ,  $^{\wedge\wedge\wedge\wedge}p < 0.0001$  (comparison between cell lines);  $^*p < 0.05$ ,  $^{**}p < 0.01$ ,  $^{***}p < 0.001$ ,  $^{****}p < 0.0001$  (treatment vs. control);  $^{+}p < 0.05$ ,  $^{++}p < 0.01$ ,  $^{+++}p < 0.001$ ,  $^{++++}p < 0.0001$  (olaparib vs. combination with ATRi or CHK1i);  $^{\#}p < 0.05$ ,  $^{\#\#}p < 0.01$ ,  $^{\#\#\#}p < 0.001$ ,  $^{\#\#\#\#}p < 0.0001$  (ATRi or CHK1i vs. respective combinations with olaparib).

### Data availability

The datasets generated during and/or analysed during the current study are available from the corresponding author on reasonable request.

Received: 23 August 2023; Accepted: 15 December 2023

Published online: 19 December 2023

### References

- Ovejero-Sanchez, M., Gonzalez-Sarmiento, R. & Herrero, A. B. DNA damage response alterations in ovarian cancer: From molecular mechanisms to therapeutic opportunities. *Cancers* <https://doi.org/10.3390/cancers15020448> (2023).
- Gee, M. E., Faraahi, Z., McCormick, A. & Edmondson, R. J. DNA damage repair in ovarian cancer: Unlocking the heterogeneity. *J. Ovarian Res.* **11**, 50. <https://doi.org/10.1186/s13048-018-0424-x> (2018).
- Lheureux, S., Braunstein, M. & Oza, A. M. Epithelial ovarian cancer: Evolution of management in the era of precision medicine. *CA Cancer J. Clin.* **69**, 280–304. <https://doi.org/10.3322/caac.21559> (2019).
- Lisio, M. A., Fu, L., Goyeneche, A., Gao, Z. H. & Telleria, C. High-grade serous ovarian cancer: Basic sciences, clinical and therapeutic standpoints. *Int. J. Mol. Sci.* <https://doi.org/10.3390/ijms20040952> (2019).
- Wu, Y., Xu, S., Cheng, S., Yang, J. & Wang, Y. Clinical application of PARP inhibitors in ovarian cancer: From molecular mechanisms to the current status. *J. Ovarian Res.* **16**, 6. <https://doi.org/10.1186/s13048-023-01094-5> (2023).
- Miller, R. E., El-Shakankery, K. H. & Lee, J. Y. PARP inhibitors in ovarian cancer: Overcoming resistance with combination strategies. *J. Gynecol. Oncol.* **33**, e44. <https://doi.org/10.3802/jgo.2022.33.e44> (2022).
- Quigley, D. *et al.* Analysis of circulating cell-free DNA identifies multiclonal heterogeneity of BRCA2 reversion mutations associated with resistance to PARP inhibitors. *Cancer Discov.* **7**, 999–1005. <https://doi.org/10.1158/2159-8290.CD-17-0146> (2017).
- Goel, N., Foxall, M. E., Scalise, C. B., Wall, J. A. & Arend, R. C. Strategies in overcoming homologous recombination proficiency and PARP inhibitor resistance. *Mol. Cancer Ther.* **20**, 1542–1549. <https://doi.org/10.1158/1535-7163.MCT-20-0992> (2021).
- Biegala, L., Gajek, A., Marczak, A. & Rogalska, A. PARP inhibitor resistance in ovarian cancer: Underlying mechanisms and therapeutic approaches targeting the ATR/CHK1 pathway. *Biochim. Biophys. Acta Rev. Cancer* **1876**, 188633. <https://doi.org/10.1016/j.bbcan.2021.188633> (2021).
- Soberanis Pina, P. & Lheureux, S. Overcoming PARP inhibitor resistance in ovarian cancer. *Int. J. Gynecol. Cancer* **33**, 364–376. <https://doi.org/10.1136/ijgc-2022-003698> (2023).
- Tang, H. *et al.* The current status of DNA-repair-directed precision oncology strategies in epithelial ovarian cancers. *Int. J. Mol. Sci.* <https://doi.org/10.3390/ijms24087293> (2023).
- Walker, T. D. J. *et al.* The DNA damage response in advanced ovarian cancer: Functional analysis combined with machine learning identifies signatures that correlate with chemotherapy sensitivity and patient outcome. *Br. J. Cancer* **128**, 1765–1776. <https://doi.org/10.1038/s41416-023-02168-3> (2023).
- Chiang, Y. C. *et al.* A DNA damage response gene panel for different histologic types of epithelial ovarian carcinomas and their outcomes. *Biomedicine* <https://doi.org/10.3390/biomedicine9101384> (2021).
- Ghezelayagh, T. S. *et al.* Characterizing TP53 mutations in ovarian carcinomas with and without concurrent BRCA1 or BRCA2 mutations. *Gynecol. Oncol.* **160**, 786–792. <https://doi.org/10.1016/j.ygyno.2020.12.007> (2021).
- Mirza-Aghazadeh-Attari, M. *et al.* DNA damage response and repair in ovarian cancer: Potential targets for therapeutic strategies. *DNA Repair* **80**, 59–84. <https://doi.org/10.1016/j.dnarep.2019.06.005> (2019).
- Loizzi, V. *et al.* PARP inhibitors and epithelial ovarian cancer: Molecular mechanisms, clinical development and future prospective. *Oncol. Lett.* **20**, 90. <https://doi.org/10.3892/ol.2020.11951> (2020).
- Cadoo, K. *et al.* Olaparib treatment for platinum-sensitive relapsed ovarian cancer by BRCA mutation and homologous recombination deficiency status: Phase II LIGHT study primary analysis. *Gynecol. Oncol.* **166**, 425–431. <https://doi.org/10.1016/j.ygyno.2022.06.017> (2022).
- Vergote, I. *et al.* European experts consensus: BRCA/homologous recombination deficiency testing in first-line ovarian cancer. *Ann. Oncol.* **33**, 276–287. <https://doi.org/10.1016/j.annonc.2021.11.013> (2022).
- Chiappa, M. *et al.* Combinations of ATR, Chk1 and Wee1 inhibitors with olaparib are active in olaparib resistant brca1 proficient and deficient murine ovarian cells. *Cancers* <https://doi.org/10.3390/cancers14071807> (2022).
- Burgess, B. T. *et al.* Olaparib combined with an ATR or Chk1 inhibitor as a treatment strategy for acquired olaparib-resistant BRCA1 mutant ovarian cells. *Diagnostics* <https://doi.org/10.3390/diagnostics10020121> (2020).
- Mahdi, H. *et al.* Ceralasertib-mediated ATR inhibition combined with olaparib in advanced cancers harboring DNA damage response and repair alterations (olaparib combinations). *JCO Precis. Oncol.* <https://doi.org/10.1200/PO.20.00439> (2021).
- Gupta, N., Huang, T. T., Horibata, S. & Lee, J. M. Cell cycle checkpoints and beyond: Exploiting the ATR/CHK1/WEE1 pathway for the treatment of PARP inhibitor-resistant cancer. *Pharmacol. Res.* **178**, 106162. <https://doi.org/10.1016/j.phrs.2022.106162> (2022).
- Kim, H. *et al.* Combining PARP with ATR inhibition overcomes PARP inhibitor and platinum resistance in ovarian cancer models. *Nat. Commun.* **11**, 3726. <https://doi.org/10.1038/s41467-020-17127-2> (2020).



24. Do, K. T. *et al.* Phase 1 combination study of the CHK1 inhibitor prexasertib and the PARP inhibitor olaparib in high-grade serous ovarian cancer and other solid tumors. *Clin. Cancer Res.* **27**, 4710–4716. <https://doi.org/10.1158/1078-0432.CCR-21-1279> (2021).
25. Kristeleit, R. *et al.* A Phase 1/2 trial of SRA737 (a Chk1 inhibitor) administered orally in patients with advanced cancer. *Br. J. Cancer* **129**, 38–45. <https://doi.org/10.1038/s41416-023-02279-x> (2023).
26. Darabi, S. *et al.* BRCA1/2 reversion mutations in patients treated with poly ADP-ribose polymerase (PARP) inhibitors or platinum agents. *Medicina* <https://doi.org/10.3390/medicina58121818> (2022).
27. Tobalina, L., Armenia, J., Irving, E., O'Connor, M. J. & Forment, J. V. A meta-analysis of reversion mutations in BRCA genes identifies signatures of DNA end-joining repair mechanisms driving therapy resistance. *Ann. Oncol.* **32**, 103–112. <https://doi.org/10.1016/j.annonc.2020.10.470> (2021).
28. Lin, K. K. *et al.* BRCA reversion mutations in circulating tumor DNA predict primary and acquired resistance to the PARP inhibitor rucaparib in high-grade ovarian carcinoma. *Cancer Discov.* **9**, 210–219. <https://doi.org/10.1158/2159-8290.CD-18-0715> (2019).
29. Biegala, L., Gajek, A., Marczak, A. & Rogalska, A. Olaparib-resistant BRCA2 (MUT) ovarian cancer cells with restored BRCA2 abrogate olaparib-induced DNA damage and G2/M arrest controlled by the ATR/CHK1 pathway for survival. *Cells* <https://doi.org/10.3390/cells12071038> (2023).
30. Lloyd, R. L. *et al.* Combined PARP and ATR inhibition potentiates genome instability and cell death in ATM-deficient cancer cells. *Oncogene* **39**, 4869–4883. <https://doi.org/10.1038/s41388-020-1328-y> (2020).
31. Behuria, H. G., Dash, S. & Sahu, S. K. Phospholipid scramblases: Role in cancer progression and anticancer therapeutics. *Front. Genet.* **13**, 875894. <https://doi.org/10.3389/fgene.2022.875894> (2022).
32. Vallabhapurapu, S. D. *et al.* Variation in human cancer cell external phosphatidylserine is regulated by flippase activity and intracellular calcium. *Oncotarget* **6**, 34375–34388. <https://doi.org/10.18632/oncotarget.6045> (2015).
33. Tang, S. *et al.* Olaparib synergizes with arsenic trioxide by promoting apoptosis and ferroptosis in platinum-resistant ovarian cancer. *Cell Death Dis.* **13**, 826. <https://doi.org/10.1038/s41419-022-05257-y> (2022).
34. Fleury, H. *et al.* Cumulative defects in DNA repair pathways drive the PARP inhibitor response in high-grade serous epithelial ovarian cancer cell lines. *Oncotarget* **8**, 40152–40168. <https://doi.org/10.18632/oncotarget.10308> (2017).
35. Caron, M. C. *et al.* Poly(ADP-ribose) polymerase-1 antagonizes DNA resection at double-strand breaks. *Nat. Commun.* **10**, 2954. <https://doi.org/10.1038/s41467-019-10741-9> (2019).
36. Zong, C. *et al.* PARP mediated DNA damage response, genomic stability and immune responses. *Int. J. Cancer* **150**, 1745–1759. <https://doi.org/10.1002/ijc.33918> (2022).
37. Skelin, M. *et al.* The effect of PARP inhibitors in homologous recombination proficient ovarian cancer: Meta-analysis. *J. Chemother.* **35**, 150–157. <https://doi.org/10.1080/1120009X.2022.2073161> (2023).
38. Yang, G. *et al.* Super-resolution imaging identifies PARP1 and the Ku complex acting as DNA double-strand break sensors. *Nucleic Acids Res.* **46**, 3446–3457. <https://doi.org/10.1093/nar/gky088> (2018).
39. McCormick, A. *et al.* Ovarian cancers harbor defects in nonhomologous end joining resulting in resistance to rucaparib. *Clin. Cancer Res.* **23**, 2050–2060. <https://doi.org/10.1158/1078-0432.CCR-16-0564> (2017).
40. Bohio, A. A., Wang, R., Zeng, X. & Ba, X. c-Abl-mediated tyrosine phosphorylation of DNA damage response proteins and implications in important cellular functions (review). *Mol. Med. Rep.* **22**, 612–619. <https://doi.org/10.3892/mmr.2020.11156> (2020).
41. Schmandt, R. E. *et al.* Expression of c-ABL, c-KIT, and platelet-derived growth factor receptor-beta in ovarian serous carcinoma and normal ovarian surface epithelium. *Cancer* **98**, 758–764. <https://doi.org/10.1002/cncr.11561> (2003).
42. Zhou, S. *et al.* Overexpression of c-Abl predicts unfavorable outcome in epithelial ovarian cancer. *Gynecol. Oncol.* **131**, 69–76. <https://doi.org/10.1016/j.ygyno.2013.06.031> (2013).
43. Li, W., Peng, X., Lang, J. & Xu, C. Targeting mouse double minute 2: Current concepts in DNA damage repair and therapeutic approaches in cancer. *Front. Pharmacol.* **11**, 631. <https://doi.org/10.3389/fphar.2020.00631> (2020).
44. Chen, Y. *et al.* MDM2 promotes epithelial-mesenchymal transition and metastasis of ovarian cancer SKOV3 cells. *Br. J. Cancer* **117**, 1192–1201. <https://doi.org/10.1038/bjc.2017.265> (2017).
45. Xie, X., He, G. & Siddik, Z. H. Cisplatin in combination with MDM2 inhibition downregulates Rad51 recombinase in a bimodal manner to inhibit homologous recombination and augment tumor cell kill. *Mol. Pharmacol.* **97**, 237–249. <https://doi.org/10.1124/mol.119.117564> (2020).
46. Shinozaki, T., Nota, A., Taya, Y. & Okamoto, K. Functional role of Mdm2 phosphorylation by ATR in attenuation of p53 nuclear export. *Oncogene* **22**, 8870–8880. <https://doi.org/10.1038/sj.onc.1207176> (2003).
47. Vescarelli, E. *et al.* MiR-200c sensitizes Olaparib-resistant ovarian cancer cells by targeting Neuropilin 1. *J. Exp. Clin. Cancer Res.* **39**, 3. <https://doi.org/10.1186/s13046-019-1490-7> (2020).
48. Peng, B. *et al.* PARP1 and CHK1 coordinate PLK1 enzymatic activity during the DNA damage response to promote homologous recombination-mediated repair. *Nucleic Acids Res.* **49**, 7554–7570. <https://doi.org/10.1093/nar/gkab584> (2021).
49. Wu, X. *et al.* MGMT-activated DUB3 stabilizes MCL1 and drives chemoresistance in ovarian cancer. *Proc. Natl. Acad. Sci. USA* **116**, 2961–2966. <https://doi.org/10.1073/pnas.1814742116> (2019).
50. Song, H. *et al.* The contribution of deleterious germline mutations in BRCA1, BRCA2 and the mismatch repair genes to ovarian cancer in the population. *Hum. Mol. Genet.* **23**, 4703–4709. <https://doi.org/10.1093/hmg/ddu172> (2014).
51. Boubheran, S. *et al.* The evolving role of DNA damage response in overcoming therapeutic resistance in ovarian cancer. *Cancer Drug Resist.* **6**, 345–357. <https://doi.org/10.20517/cdr.2022.146> (2023).
52. Xie, F., Wang, J. & Zhang, B. RefFinder: A web-based tool for comprehensively analyzing and identifying reference genes. *Funct. Integr. Genomics* **23**, 125. <https://doi.org/10.1007/s10142-023-01055-7> (2023).

# Acknowledgements

The original illustration in Fig. 6 has been created with BioRender.com.

# Author contributions

Conceptualization, L.B., A.G., A.Ś. and A.R.; methodology, L.B., A.G., I.S.-P., A.M., A.Ś. and A.R.; formal analysis, L.B.; investigation, L.B., A.G. and I.S.-P.; resources, A.M., A.Ś. and A.R.; writing—original draft preparation, L.B.; writing—review and editing, L.B., A.G., I.S.-P., A.M., A.Ś. and A.R.; visualization, L.B., A.G. and A.R.; supervision, A.R.; funding acquisition, A.R.

# Funding

This work was supported by the National Science Centre, Poland (Project grant number: Sonata Bis 2019/34/E/NZ7/00056).

# Competing interests

The authors declare no competing interests.

### Additional information

**Supplementary Information** The online version contains supplementary material available at <https://doi.org/10.1038/s41598-023-50151-y>.

**Correspondence** and requests for materials should be addressed to A.R.

**Reprints and permissions information** is available at [www.nature.com/reprints](http://www.nature.com/reprints).

**Publisher's note** Springer Nature remains neutral with regard to jurisdictional claims in published maps and institutional affiliations.



**Open Access** This article is licensed under a Creative Commons Attribution 4.0 International License, which permits use, sharing, adaptation, distribution and reproduction in any medium or format, as long as you give appropriate credit to the original author(s) and the source, provide a link to the Creative Commons licence, and indicate if changes were made. The images or other third party material in this article are included in the article's Creative Commons licence, unless indicated otherwise in a credit line to the material. If material is not included in the article's Creative Commons licence and your intended use is not permitted by statutory regulation or exceeds the permitted use, you will need to obtain permission directly from the copyright holder. To view a copy of this licence, visit <http://creativecommons.org/licenses/by/4.0/>.

© The Author(s) 2023



# Supplementary Information

## Targeted inhibition of the ATR/CHK1 pathway overcomes resistance to olaparib and dysregulates DNA damage response protein expression in *BRCA2*<sup>MUT</sup> ovarian cancer cells

Łukasz Biegała<sup>1,2</sup>, Arkadiusz Gajek<sup>1</sup>, Izabela-Szymczak-Pajor<sup>3</sup>, Agnieszka Marczak<sup>1</sup>, Agnieszka Śliwińska<sup>3</sup>, Aneta Rogalska<sup>1,\*</sup>

### Supplementary Figure 1 (Figure S1)

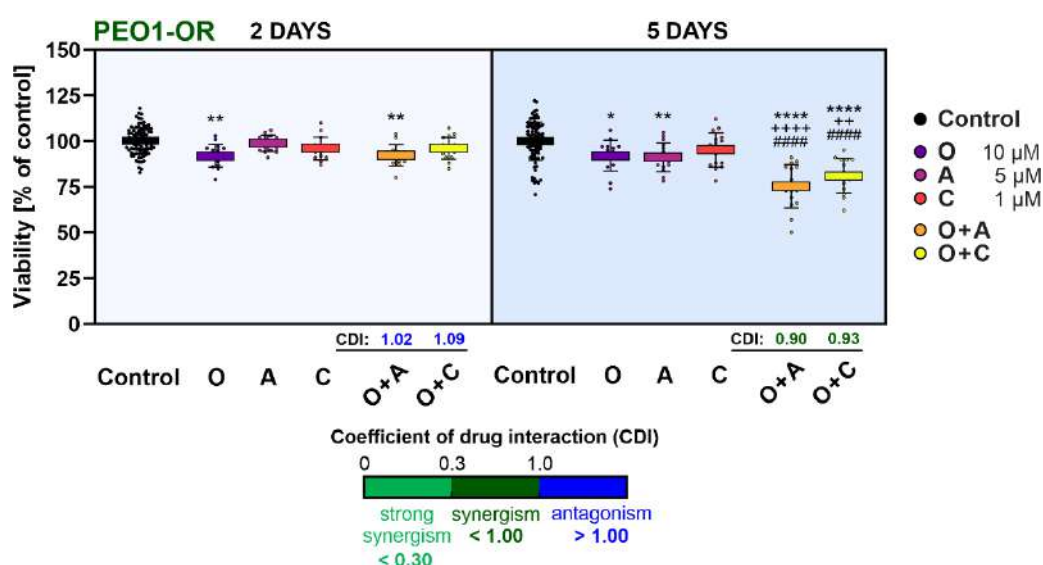


**Figure S1. Viability of PEO1-OR cells after incubation with studied inhibitors (O, A, C) or their combinations (O + A, O + C) at designated concentrations optimal for olaparib-sensitive cells (PEO1 and PEO4) for 2 days and 5 days assessed by MTT assay.** Coefficient of drug interaction (CDI) values were calculated to evaluate the interaction effect of combination treatments. Data were expressed as mean ± SD (n = 4). Statistical significance was assessed using two-way ANOVA followed by Tukey's multiple comparison test: \* $p < 0.05$ , \*\* $p < 0.01$ , \*\*\*\* $p < 0.0001$  (treatment vs. control); \*\* $p < 0.01$ , \*\*\*\* $p < 0.0001$  (olaparib vs. combination with ATRi or CHK1i); ##### $p < 0.0001$  (ATRi or CHK1i vs. respective combinations with olaparib).

## Supplementary Figure 2 (Figure S2)

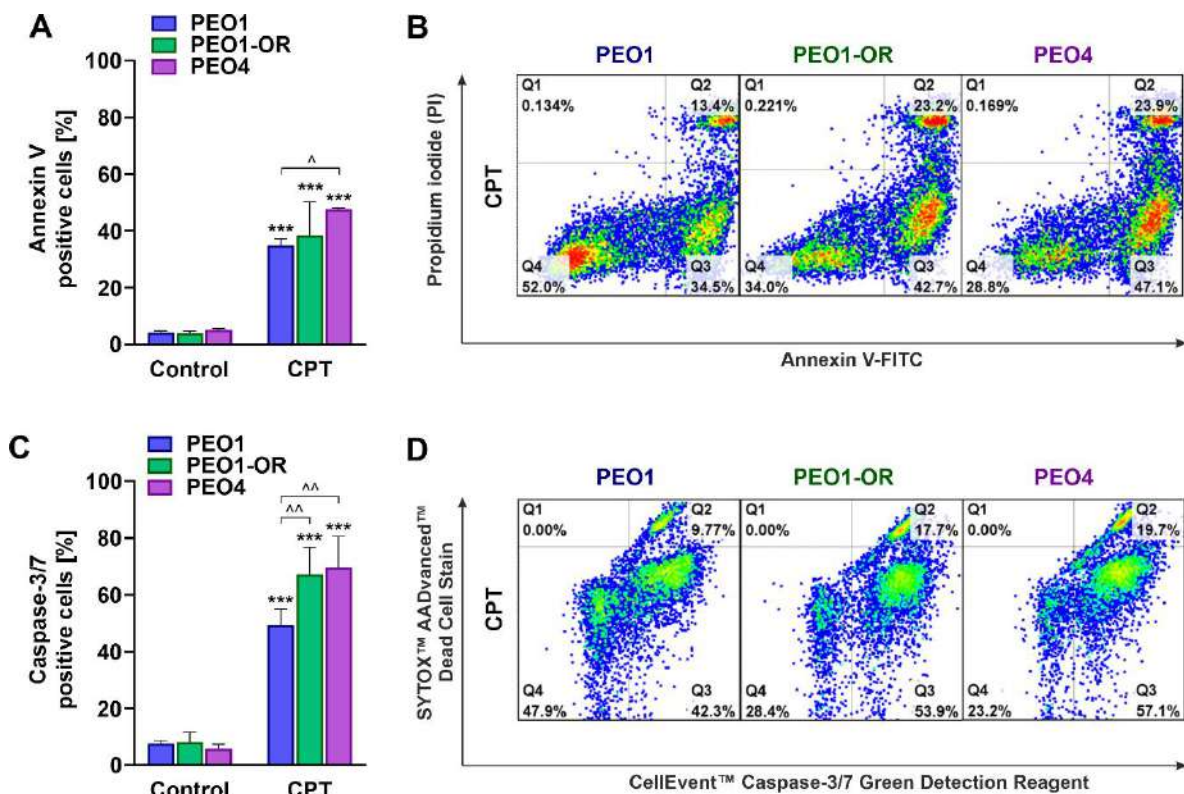


**Figure S2.**

**(A)** Apoptosis in OC cells was examined by dual staining with annexin V-FITC and PI in response to incubation with 2.5  $\mu$ M camptothecin (CPT) for 2 days as a positive control. Apoptosis rate was presented as a percentage of annexin V positive (apoptotic) cells relative to untreated control cells. Data are presented as mean  $\pm$  SD ( $n = 3$ ).

**(B)** Representative dot plots of annexin V-FITC and PI-stained OC cells with the indicated percentage of non-viable cells (Q1), necrotic cells (Q2), apoptotic cells (Q3), and viable cells (Q4).

**(C)** Activation of caspase 3 and caspase 7 in apoptotic OC cells examined by dual staining using CellEvent™ Caspase-3/7 Green Flow Cytometry Assay Kit in response to incubation with 2.5  $\mu$ M CPT for 2 days as a positive control. Caspase-3/7 activity was presented as a percentage of caspase-3/7 positive cells relative to untreated control cells. Data are presented as mean  $\pm$  SD ( $n = 3$ ).

**(D)** Representative dot plots of a two-parameter apoptosis assay for detection of activated caspase-3/7 (CellEvent™ Caspase-3/7 Green Detection Reagent) and the distinction between live and dead cell (SYTOX™ AADvanced™ Dead Cell Stain) with the indicated percentage of necrotic cells (Q2), viable cells (Q3), apoptotic cells with activated caspase-3/7 (Q4). Statistical significance was assessed using two-way ANOVA followed by Šidák multiple comparison test:  $^{\wedge}p < 0.05$ ,  $^{\wedge\wedge}p < 0.01$  (comparison between cell lines);  $^{***}p < 0.001$  (treatment vs. control).

### Supplementary Figure 3 (Figure S3)

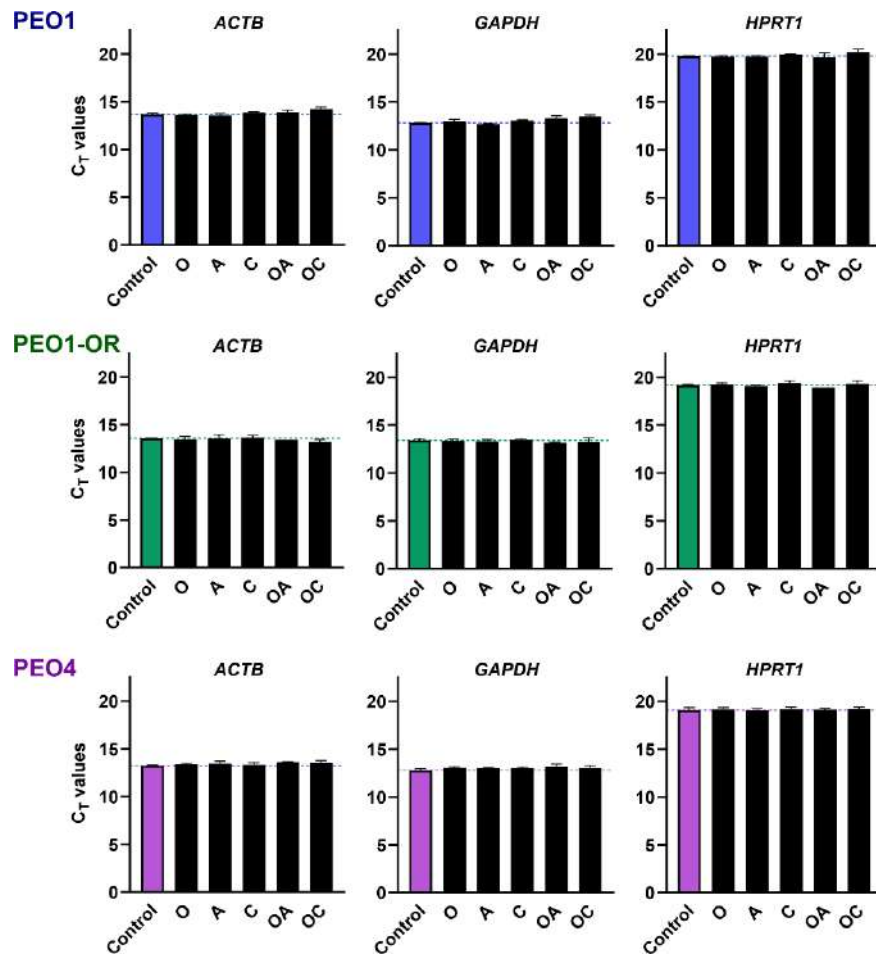


**Figure S3. Evaluation of three candidate reference genes (*ACTB*, *GAPDH*, *HPRT1*) in OC cell line for the normalization of RT-qPCR gene expression.** Graphs represent variations in threshold cycle values ( $C_T$ ) of tested genes across different treatment conditions as mean  $\pm$  SD ( $n = 2$ ). Dashed lines indicate mean  $C_T$  values for untreated control cells. The expression stability of candidate genes was evaluated based on differences in  $C_T$  values between treatments and RefFinder web-based tool.

### Supplementary Figure 4 (Figure S4)

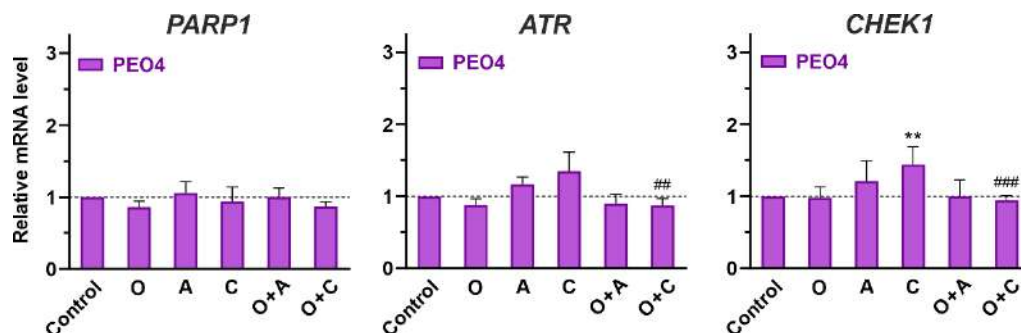


**Figure S4. Quantitative analysis of the mRNA expression of *PARP1*, *ATR*, and *CHEK1* in PEO4 cells.** OC cells were treated with studied inhibitors (O, A, C) or their combinations (O + A, O + C) for 2 days and mRNA levels were determined by real-time qPCR. Data were normalized to  $\beta$ -actin and expressed relative to untreated cells as mean  $\pm$  SD ( $n = 4$ ). Statistical significance was assessed using two-way ANOVA followed by Tukey's multiple comparison test: \*\* $p < 0.01$  (treatment vs. control); ### $p < 0.001$  (ATRi or CHK1i vs. respective combinations with olaparib).

### Supplementary Table 1 (Table S1)

List of key reagents used in the study.

Reagent	Catalog Number	Manufacturer
(S)-(+)-Camptothecin	C9911	Sigma-Aldrich
CellEvent™ Caspase-3/7 Green Flow Cytometry Assay Kit	C10427	Invitrogen™ (Thermo Fisher Scientific)
Ceralasertib	TBW02661	Wuhan ChemNorm Biotech
Crystal violet	911517ZA	VWR
FBS, heat-inactivated, qualified	10270106	Gibco (Thermo Fisher Scientific)
High-Capacity cDNA Reverse Transcription Kit	4368814	Applied Biosystems™ (Thermo Fisher Scientific)
mirVana™ miRNA Isolation Kit, with phenol	AM1560	Invitrogen™ (Thermo Fisher Scientific)
MK-8776	TBW02666	Wuhan ChemNorm Biotech
MTT	20395.03	SERVA Electrophoresis
Olaparib	S1060	Selleck Chemicals
Pierce™ BCA Protein Assay Kit	23225	Thermo Fisher Scientific
RayBio® C-Series Human DNA Damage Response Antibody Array 1	AAH-DDR-1-8	RayBiotech
RNase Inhibitor	N8080119	Applied Biosystems™ (Thermo Fisher Scientific)
RPMI 1640, GlutaMAX™ Supplement, HEPES	72400-021	Gibco (Thermo Fisher Scientific)
TaqMan™ Gene Expression Assay (FAM)	4331182	Applied Biosystems™ (Thermo Fisher Scientific)
TaqMan™ Universal Master Mix II, no UNG	4440049	Applied Biosystems™ (Thermo Fisher Scientific)
Trypsin-EDTA	25200072	Gibco (Thermo Fisher Scientific)

### Supplementary Table 2 (Table S2)

List of TaqMan™ Gene Expression Assay used for gene expression studies (RT-qPCR).

Gene	Assay ID
<i>ACTB</i>	Hs01060665_g1
<i>ATR</i>	Hs00992123_m1
<i>CASP3</i>	Hs00234387_m1
<i>CHEK1</i>	Hs00967506_m1
<i>PARP1</i>	Hs00242302_m1
<i>HPRT1</i>	Hs02800695_m1
<i>GAPDH</i>	Hs02758991_g1

## **PUBLIKACJA #4**

Article

# Uncovering miRNA–mRNA Regulatory Networks Related to Olaparib Resistance and Resensitization of *BRCA2*<sup>MUT</sup> Ovarian Cancer PEO1-OR Cells with the ATR/CHK1 Pathway Inhibitors

Łukasz Biegała <sup>1,2</sup>, Damian Kołat <sup>3,4</sup>, Arkadiusz Gajek <sup>1</sup>, Elżbieta Płuciennik <sup>3</sup>, Agnieszka Marczak <sup>1</sup>, Agnieszka Śliwińska <sup>5,\*</sup>, Michał Mikula <sup>6</sup> and Aneta Rogalska <sup>1,\*</sup>

<sup>1</sup> Department of Medical Biophysics, Institute of Biophysics, Faculty of Biology and Environmental Protection, University of Lodz, Pomorska 141/143, 90-236 Lodz, Poland; lukasz.biegala@edu.uni.lodz.pl (Ł.B.); arkadiusz.gajek@biol.uni.lodz.pl (A.G.); agnieszka.marczak@biol.uni.lodz.pl (A.M.)

<sup>2</sup> Doctoral School of Exact and Natural Sciences, University of Lodz, Jana Matejki 21/23, 90-237 Lodz, Poland

<sup>3</sup> Department of Functional Genomics, Medical University of Lodz, Żeligowskiego 7/9, 90-752 Lodz, Poland; damian.kolat@umed.lodz.pl (D.K.); elzbieta.pluciennik@umed.lodz.pl (E.P.)

<sup>4</sup> Department of Biomedicine and Experimental Surgery, Medical University of Lodz, Narutowicza 60, 90-136 Lodz, Poland

<sup>5</sup> Department of Nucleic Acid Biochemistry, Medical University of Lodz, Pomorska 251, 92-213 Lodz, Poland

<sup>6</sup> Department of Genetics, Maria Skłodowska-Curie National Research Institute of Oncology, Roentgena 5, 02-781 Warsaw, Poland; michal.mikula@nio.gov.pl

\* Correspondence: agnieszka.sliwinska@umed.lodz.pl (A.Ś.); aneta.rogalska@biol.uni.lodz.pl (A.R.)

**Citation:** Biegała, Ł.; Kołat, D.; Gajek, A.; Płuciennik, E.; Marczak, A.; Śliwińska, A.; Mikula, M.; Rogalska, A. Uncovering miRNA–mRNA Regulatory Networks Related to Olaparib Resistance and Resensitization of *BRCA2*<sup>MUT</sup> Ovarian Cancer PEO1-OR Cells with the ATR/CHK1 Pathway Inhibitors. *Cells* **2024**, *13*, 867. <https://doi.org/10.3390/cells13100867>

Academic Editor: Tohru Yamada

Received: 20 March 2024

Revised: 29 April 2024

Accepted: 16 May 2024

Published: 17 May 2024



**Copyright:** © 2024 by the authors. Licensee MDPI, Basel, Switzerland. This article is an open access article distributed under the terms and conditions of the Creative Commons Attribution (CC BY) license (<https://creativecommons.org/licenses/by/4.0/>).

**Abstract:** Resistance to olaparib is the major obstacle in targeted therapy for ovarian cancer (OC) with poly(ADP-ribose) polymerase inhibitors (PARPi), prompting studies on novel combination therapies to enhance olaparib efficacy. Despite identifying various mechanisms, understanding how OC cells acquire PARPi resistance remains incomplete. This study investigated microRNA (miRNA) expression in olaparib-sensitive (PEO1, PEO4) and previously established olaparib-resistant OC cell lines (PEO1-OR) using high-throughput RT-qPCR and bioinformatic analyses. The role of miRNAs was explored regarding acquired resistance and resensitization with the ATR/CHK1 pathway inhibitors. Differentially expressed miRNAs were used to construct miRNA–mRNA regulatory networks and perform functional enrichment analyses for target genes with miRNet 2.0. TCGA-OV dataset was analyzed to explore the prognostic value of selected miRNAs and target genes in clinical samples. We identified potential processes associated with olaparib resistance, including cell proliferation, migration, cell cycle, and growth factor signaling. Resensitized PEO1-OR cells were enriched in growth factor signaling via PDGF, EGFR, FGFR1, VEGFR2, and TGFβR, regulation of the cell cycle via the G2/M checkpoint, and caspase-mediated apoptosis. Antibody microarray analysis confirmed dysregulated growth factor expression. The addition of the ATR/CHK1 pathway inhibitors to olaparib downregulated FGF4, FGF6, NT-4, PLGF, and TGFβ1 exclusively in PEO1-OR cells. Survival and differential expression analyses for serous OC patients revealed prognostic miRNAs likely associated with olaparib resistance (miR-99b-5p, miR-424-3p, and miR-505-5p) and resensitization to olaparib (miR-324-5p and miR-424-3p). Essential miRNA–mRNA interactions were reconstructed based on prognostic miRNAs and target genes. In conclusion, our data highlight distinct miRNA profiles in olaparib-sensitive and olaparib-resistant cells, offering molecular insights into overcoming resistance with the ATR/CHK1 inhibitors in OC. Moreover, some miRNAs might serve as potential predictive signature molecules of resistance and therapeutic response.

**Keywords:** ovarian cancer; miRNA profiling; olaparib; resistance; ATR/CHK1 pathway; combination therapy; growth factors; bioinformatics; TCGA data



## 1. Introduction

Olaparib, a widely-used oral poly(ADP-ribose) polymerase inhibitor (PARPi), has demonstrated efficacy in the therapy for ovarian cancer (OC), especially high-grade serous ovarian cancer (HGSOC) with germline *BRCA1/2* mutations [1]. HGSOC is a grade 3 subtype of epithelial OC accounting for 70–80% of deaths and is often diagnosed at advanced stages [2]. Despite olaparib's efficacy in recurrent platinum-sensitive OC [3], acquired resistance to PARPi poses a significant challenge [4]. Indeed, there is a need for a precise characterization of olaparib sensitivity since some OC patients without *BRCA1/2* mutation or associated homologous recombination deficiency (HRD) may respond to PARPi. Therefore, an understanding of the molecular mechanisms underlying resistance and sensitivity to olaparib is urgently needed. Over recent years novel olaparib combinations have been evaluated to combat associated resistance and improve outcomes in OC patients. For instance, the addition of some agents, including antiangiogenic molecules or the ATR/CHK1 pathway inhibitors, has shown beneficial antitumor effects clinically in OC [5,6]. The ATR/CHK1 pathway is involved in multiple aspects of the DNA damage response, including the activation of cell cycle checkpoints, the stabilization of stalled replication forks, and the regulation of DNA repair pathways [7,8]. Given the role of the ATR and CHK1 kinases in protecting genomic integrity, targeted inhibition of the ATR/CHK1 axis constitutes a promising strategy to enhance olaparib efficacy in HGSOC. Recently, it was reported that olaparib combined with the ATR/CHK1 pathway inhibitors exerts synergistic antitumor activity in olaparib-resistant HGSOC cell lines with *BRCA1/2* mutations [7,9]. In the most recent findings from the CAPRI trial, six partial responses were observed in homologous-recombination-deficient platinum-sensitive recurrent HGSOC when olaparib was combined with the ATRi ceralasertib. This response was seen among 12 patients who were eligible for efficacy evaluation and had progressed after prior PARPi treatment [10]. However, there is still a need to unravel molecular basics explaining acquired resistance to olaparib and mechanisms associated with the resensitization of OC cells to PARPi.

MicroRNAs (miRNAs) are short non-coding RNAs that act as major post-transcriptional regulators of gene expression. Mature miRNAs can serve as oncogenes or tumor suppressors based on their modulating effect on target genes [11]. Mechanistically, a single miRNA can concurrently regulate multiple genes, and each gene can be affected by many miRNAs forming complex regulatory networks involved in diverse biological processes [12]. Aberrant miRNA expression has been linked to processes such as genomic instability, tumor progression, metastasis, and chemosensitivity in OC [11]. Numerous studies demonstrated the role of specific circulating miRNAs as diagnostic biomarkers in OC screening [13]. A model established by Yokoi et al. showed extremely high sensitivity and specificity for the detection of OC based on the expression of ten serum miRNAs [14]. Recently, a growing number of studies have demonstrated regulatory networks linking miRNAs and genes associated with resistance to cisplatin in OC [15,16]. However, the miRNA–mRNA regulations in *BRCA2*<sup>MUT</sup> olaparib-resistant HGSOC cells resensitized with the ATR/CHK1 pathway inhibitors have not been reported till now.

Our in vitro study unveils potential post-transcriptional mechanisms involved in acquiring resistance to olaparib in OC cells and their resensitization through combination treatments. In this work, differentially expressed (DE) miRNAs were linked to olaparib resistance and to response to olaparib combined with ATR/CHK1 pathway inhibitors in the PEO1-OR olaparib-resistant *BRCA2*<sup>MUT</sup> HGSOC cell line in vitro using RT-qPCR profiling. The network-based approach revealed target genes and their potential biological roles through functional enrichment analyses. Importantly, dysregulation of growth factors and their receptor expression was confirmed in olaparib-resistant PEO1-OR cells. The clinical relevance of selected miRNAs and their target genes was studied in TCGA-OV dataset by Kaplan–Meier survival analysis, stage-wise differential expression analysis, co-expression analysis, and comparison of gene expression in normal ovarian tissue and OC tumors.

## 2. Materials and Methods

### 2.1. Materials

Olaparib (O) was purchased from Selleck Chemicals (Houston, TX, USA). ATRi (A, ceralasertib) and CHK1i (C, MK-8776) were purchased from Wuhan ChemNorm Biotech (Wuhan, China). The inhibitors were dissolved in 100% dimethyl sulfoxide (DMSO) to create stock solutions, which were then stored at  $-80^{\circ}\text{C}$  for a maximum of 6 months. Cell culture reagents were purchased from Thermo Fisher Scientific (Waltham, MA, USA). Chemicals and solvents were purchased from Merck Life Science (Poznań, Poland) or Avantor Performance Materials Poland (Gliwice, Poland). The remaining reagents utilized in the study are detailed in the following sections of the Materials and Methods (Section 2), as well as in Table S1.

### 2.2. Cell Lines and Treatment

The human HGSOC cell lines, PEO1 (*BRCA2*<sup>MUT</sup>) and PEO4 (*BRCA2*<sup>REV</sup>), which are sensitive to olaparib [7,17], were purchased from the ECACC (Salisbury, UK). Both cell lines were developed from the same patient before (PEO1) and after (PEO4) development of clinical platinum resistance representing disease progression [18,19]. Acquired resistance to olaparib in the PEO1-OR (*BRCA2*<sup>MUT</sup>) human HGSOC cell line, with a double mutation in *BRCA2*, was previously established through continuous exposure of PEO1 cells to gradually escalating doses of olaparib, as detailed in a prior report [17]. Cells were grown as monolayers in RPMI 1640 medium containing GlutaMAX<sup>TM</sup> supplement, HEPES, and 10% FBS ( $37^{\circ}\text{C}$ , 5%  $\text{CO}_2$ ) and were routinely subcultured using 0.1% trypsin solution with 0.4 mM EDTA.

Before treatment, cells were seeded in 100 mm dishes ( $2 \times 10^6$  cells) and incubated for 24 h ( $37^{\circ}\text{C}$ , 5%  $\text{CO}_2$ ). The next day culture medium was changed, and cells were incubated with tested inhibitors or their combinations for 2 days ( $37^{\circ}\text{C}$ , 5%  $\text{CO}_2$ ) at concentrations previously established to exert synergistic antitumor activity [7]. PEO1 and PEO4 olaparib-sensitive cells were incubated with 10  $\mu\text{M}$  olaparib, 5  $\mu\text{M}$  ATRi, and 1  $\mu\text{M}$  CHK1i, whereas PEO1-OR olaparib-resistant cells were incubated with 15  $\mu\text{M}$  olaparib, 7.5  $\mu\text{M}$  ATRi, and 2.5  $\mu\text{M}$  CHK1i. Following the incubation, cells were harvested by trypsinization, centrifuged ( $300\times g$ , 5 min,  $4^{\circ}\text{C}$ ), washed in ice-cold PBS, and stored as pellets at  $-80^{\circ}\text{C}$  before total protein extraction and RNA isolation. Cell culture experiments were independently repeated four times ( $n = 4$ ).

### 2.3. RNA Isolation

Isolation of small-RNA-containing total RNA from four independent sets of samples ( $n = 4$ ) was performed using a *mirVana*<sup>TM</sup> miRNA Isolation Kit (Thermo Fisher Scientific, Waltham, MA, USA) according to the manufacturer's instructions. At the end of the procedure, RNA was eluted from the glass-fiber filters using 50  $\mu\text{L}$  of nuclease-free water preheated to  $95^{\circ}\text{C}$  and stored in aliquots at  $-80^{\circ}\text{C}$ . The quality and quantity of isolated RNA were analyzed by absorbance measurements at 230, 260, and 280 nm using a BioTek Eon<sup>TM</sup> microplate spectrophotometer (BioTek Instruments, Winooski, VT, USA).

### 2.4. RT-qPCR Global miRNA Expression Profiling with Predesigned TaqMan<sup>TM</sup> Array Human MicroRNA Cards in HGSOC Cell Lines

To preliminarily identify differentially expressed (DE) miRNAs, quantitative real-time PCR (qRT-PCR) global expression profiling of 754 unique human miRNAs was performed using pre-designed TaqMan<sup>TM</sup> Array Human MicroRNA A+B Cards Set v3.0 (Thermo Fisher Scientific, Waltham, MA, USA) according to the manufacturer's instructions (Part Number 4399721 Revision C from 07/2010 and Part Number 4399813 Revision D from 11/2018). The screening analysis of miRNA profiles in PEO1 and PEO1-OR cell lines was performed using equivalent amounts of total RNA pooled from four biological

replicates for each condition-specific sample to obtain one cDNA sample for each treatment condition.

Firstly, miRNAs were reverse transcribed using 1000 ng of total RNA with the TaqMan™ MicroRNA Reverse Transcription Kit and Megaplex™ RT Primers Human Pool Set v3.0 (Thermo Fisher Scientific, Waltham, MA, USA) in the final reaction volume of 7.5 µL in a PTC-200 DNA Engine® Cyclor (MJ Research Inc., St. Bruno, QC, Canada). Nuclease-free water was used instead of RNA to prepare no template control (NTC) reactions. The thermal-cycling conditions were as follows: 40 cycles of 16 °C for 2 min, 42 °C for 1 min, and 50 °C for 1 min, followed by 85 °C for 5 min and cooling at 4 °C. The ramping speed was set to 3 °C/s and the lid temperature was set to 105 °C. The obtained cDNA (133.3 ng/µL) was stored undiluted at −80 °C.

Sample-specific PCR reaction mixes were prepared to perform qRT-PCR reactions by mixing 450 µL of 2# TaqMan™ Universal Master Mix II with no UNG, 444 µL of nuclease-free water, and 6 µL of the reverse transcription product (separate for Megaplex RT pools A and B) in the final reaction volume of 900 µL. Each of the eight TaqMan® Low-density Array (TLDA) ports for both A and B cards was filled with 100 µL of a PCR reaction mix. The qPCR reactions were run in a 7900HT Fast Real-Time PCR System (Thermo Fisher Scientific, Waltham, MA, USA) using the default thermal-cycling conditions (94.5 °C for 10 min followed by 40 cycles of 97 °C for 30 s and 59.7 °C for 1 min). Raw cycle-threshold ( $C_T$ ) values were collected using automatic baseline settings and a threshold of 0.2. Informative target miRNAs were defined based on expression in untreated cells as having  $C_T$  value < 35.

Relative qPCR analysis was performed in DataAssist™ v3.01 software. The relative expression of 754 miRNAs was calculated using the comparative  $2^{-\Delta\Delta C_T}$  method [20] and global mean normalization (median  $C_T$  values of all miRNAs with  $C_T$  < 35 in each sample as the normalization factor) recommended for large-scale expression profiling [21,22]. Outliers within technical replicates were excluded from data analysis calculations by the software. Relative miRNA levels are expressed as fold changes (FCs) relative to untreated control cells. Preliminary selection of the most relevantly dysregulated miRNAs for further validation and studies assumed that miRNA was differentially expressed (up- or downregulated) with an absolute FC of at least 1.5. This FC cut-off enables the detection of subtle changes that cumulatively might have an impact on cell biology [23–25].

Next, bioinformatics selection of dysregulated miRNAs was performed to select key miRNAs for validation on the Custom TaqMan® Array MicroRNA Cards fitting 44 target miRNAs and 3 endogenous controls. Briefly, all dysregulated miRNAs were used for network-based analyses with the web tool MIENTURNET (<http://userver.bio.uniroma1.it/apps/mienturnet/>; accessed on 11 January 2023) [26]. The network was filtered with the default settings (thresholds for the minimum number of miRNA–target interactions of two and false-discovery rate of one). Dysregulated miRNAs were prioritized based on strong experimental evidence of miRNA–target interactions from miRTarBase (Release 7.0, September 2017) [27] and calculated miRNA node degree in the network.

## 2.5. RT-qPCR Validation of Dysregulated miRNA Expression with Custom TaqMan™ Array MicroRNA Cards in HGSOC Cell Lines

The expression of 44 selected miRNAs was validated using Custom TaqMan™ Array MicroRNA Cards (Thermo Fisher Scientific, Waltham, MA, USA) according to the manufacturer's instructions (Publication Part no. 4478705 Revision A from 01/2013). Customized cards were designed for 44 miRNAs of interest and 3 candidate endogenous control assays (U6 snRNA in duplicate, RNU48 snoRNA, and miR-30e-3p). The stability of endogenous control genes' expression was confirmed in all OC cell lines, and all three were used as normalizers since it is a preferred approach for miRNA normalization [24,25]. Details are included in the Supplementary Methods. The expression levels of selected miRNA were calculated in all individual samples (control, O, A, C, O + A, and O + C) and

all HGSOC cell lines (PEO1, PEO1-OR, and PEO4) using total RNA from 4 independent biological replicates ( $n = 4$ ).

Firstly, miRNAs were reverse transcribed for each sample separately (biological replicate) using 1000 ng of total RNA with the TaqMan™ MicroRNA Reverse Transcription Kit and Custom RT Primer Pool composed of individual RT primers for each target provided with the Custom TaqMan™ Array MicroRNA Cards (Thermo Fisher Scientific, Waltham, MA, USA). RT reactions were run in the final reaction volume of 15 µL according to the manufacturer's instructions in a PTC-200 DNA Engine® Cyclor (MJ Research Inc., St. Bruno, QC, Canada). NTC samples used nuclease-free water in place of RNA in the RT reaction. The thermal-cycling conditions were as follows: 16 °C for 30 min, 30 °C for 30 min, 85 °C for 5 min, followed by cooling at 4 °C. The ramping speed was set to 2.5 °C/s and the lid temperature was set to 105 °C to prevent condensation. The obtained cDNA (66.7 ng/µL) was stored undiluted at −80 °C.

Following the RT step, 3 µL of the RT reaction product (200 ng cDNA) was combined with 52 µL of nuclease-free water and 55 µL of 2× TaqMan™ Universal Master Mix II with no UNG. TLDA ports were filled with 100 µL of sample-specific PCR reaction mixes. Untreated control samples were run in duplicate, whereas treated samples and NTC samples were run in one technical replicate on one card. The qPCR reactions were run in a 7900HT Fast Real-Time PCR System (Thermo Fisher Scientific, Waltham, MA, USA) using the default thermal-cycling conditions (94.5°C for 10 min followed by 40 cycles of 97°C for 30 s and 59.7°C for 1 min). Raw  $C_T$  values were collected using automatic baseline settings and a threshold of 0.2 and exported using DataAssist™ v3.01 software. Informative target miRNAs were defined based on expression in untreated control samples as having  $C_T$  value < 32 in ≥75% of samples (at least 3 out of 4 biological replicates).  $C_T$  values ≥ 35 for miRNAs in treated samples were included in calculations if miRNA was defined as detected in untreated control cells as these values contain important biological information. Individual  $C_T$  values were averaged for control samples run in duplicate.

Relative miRNA expression was calculated as FC compared to untreated cells using the comparative  $2^{-\Delta\Delta C_T}$  method. Log-transformed relative quantity data ( $\log_2$  of FC) were used for statistical analysis. Expression of all miRNAs was visualized with a heatmap generated with GraphPad Prism. Clustering of samples with similar informative miRNA expression was performed with the ClustVis web tool using correlation distance and average linkage [28]. Significantly dysregulated miRNAs were defined as differentially expressed (up- or downregulated) with an absolute FC ≥ 1.5 ( $\log_2$  of FC ≥ 0.585) and  $p < 0.05$ .

## 2.6. Construction and Analysis of miRNA–mRNA Regulatory Networks

A regulatory network between significantly dysregulated miRNAs and their target mRNAs was constructed and analyzed using the miRNet 2.0 web-based platform [29] (accessed on 7 December 2023) and two miRNA databases with experimentally validated interactions (miRTarBase v8.0 and TarBase v8.0). The miRNA–mRNA network was integrated with protein–protein interaction (PPI) network of genes to provide deeper insight into regulatory mechanisms. The original network was simplified by reducing less important nodes and edges using a minimum network algorithm to focus on key connectivity according to the recommendations for the exploration of complex networks [29].

## 2.7. Functional Enrichment Analysis

To interpret the interactions and predict functional pathways for target genes, enrichment analyses were performed with a hypergeometric test algorithm using the Reactome database and Gene Ontology (GO) terms of the biological processes (GO:BP). Adjusted  $p$  value < 0.05 was set as the cut-off to select fifteen significantly enriched terms and pathways with the most hits. Cytoscape software (version 3.10.1) was employed to further customize, visualize, and analyze regulatory networks. The cytoHubba plug-in was used to identify hub nodes from the miRNA–mRNA network based on the maximal clique centrality (MCC) algorithm which ranks genes within the network. Out of all nodes, the top

10 genes with the highest connectivity were assigned as potential hub genes. Subnetworks of the miRNA–hub genes were constructed to visualize core interactions.

### 2.8. Growth Factor Expression Profiling with Antibody Array

The expression of 41 human growth factors (GFs) and their receptors was semi-quantitatively determined in PEO1 and PEO1-OR cells incubated with tested inhibitors or their combinations for 48 h using commercially available RayBio® C-Series Human Growth Factor Antibody Array 1 (RayBiotech Life, Inc., Peachtree Corners, GA, USA) as described previously [7]. Each array was loaded with a sample containing 150 µg of total protein and processed in accordance with the manufacturer's instructions.

The changes in protein expression were calculated as a fold change compared to untreated control cells. Each experiment was conducted independently twice, with two technical replicates on each membrane, and the results were presented as mean ± SD ( $n = 4$ ).

### 2.9. Differential Expression Analysis in Ovarian Cancer Patients

Stage-wise differential expression analysis was performed using The Cancer Genome Atlas (TCGA) repository to search and download a filtered dataset of OC patients with available clinical data as well as mRNA and miRNA expression quantification data generated using the STAR workflow [30]. The analysis was performed for serous OC samples from patients with stages II ( $n = 14$ ), III ( $n = 125$ ), and IV ( $n = 17$ ) who underwent only pharmaceutical therapy since radiation therapy is currently rarely used [31,32]. Read counts were pre-processed via calcNormFactors and subjected to differential expression analysis using the limma-voom method [33]. Genes and miRNAs with counts per million (CPM) < 10 in ≥50% of samples were filtered out as the minimal cut-off for biological relevance. Outliers were identified according to the ROUT method with 1% FDR using GraphPad Prism. The results were visualized by medians with box-and-whisker plots extending from the 25th to 75th percentiles. Statistical significance was evaluated with one-way ANOVA followed by the Tukey multiple comparison test (normally distributed data), or Kruskal–Wallis test followed by Dunn's multiple comparison test (non-normally distributed data). Pairwise co-expression analysis between miRNAs and genes was performed using Spearman's rank correlation coefficient ( $\rho$ ). Correlation with  $p < 0.05$  was considered statistically significant. Correlation matrixes were generated with GraphPad Prism.

Differential gene expression analysis between normal ovaries and tumor tissues from serous OC patients was performed using the TNMplot web tool ([www.tnmplot.com](http://www.tnmplot.com); accessed on 20 January 2024) integrating RNA-Seq data for normal and cancerous tissue from the Genotype–Tissue Expression (GTEx) and TCGA repositories, respectively [34]. Outliers were identified in each group according to the ROUT method with a 1% FDR using GraphPad Prism. The results were visualized by medians with box-and-whisker plots extending from the 25th to 75th percentiles. Statistical significance was assessed with an unpaired two-tailed Mann–Whitney test (non-normally distributed data).

### 2.10. Kaplan–Meier Survival Analysis for Ovarian Cancer Patients

Kaplan–Meier (KM) survival analysis was performed to assess prognostic values of mature miRNAs and their target genes in OC patients using a tumor online prognostic analysis platform (ToPP) (<http://biostatistics.online/topp>; accessed on 27 January 2024) with integrated data from TCGA project [35]. The analyses were restricted to HGSOc patients (grade III). For each gene, patients were split into two groups (low- and high-expression cohorts) according to the best cut-off value. A univariate module was employed to determine differences between groups regarding overall survival (OS), and progression-free interval (PFI). The difference between cohorts was characterized by the hazard ratio (HR) with 95% confidence intervals and log-rank  $p$  value.

### 2.11. Verification of Hub Genes' Expression at Protein Level in Ovarian Cancer Patients

At the protein level, normal ovarian tissues and serous OC samples were compared for selected miRNA targets by immunohistochemistry (IHC) using the Human Protein Atlas database version 23.0 (HPA, [www.proteinatlas.org](http://www.proteinatlas.org); accessed on 30 January 2024) [36]. All antibodies fulfilled the enhanced validation principles. Protein expression was compared according to antibody staining intensity and fraction of stained cells based on HPA annotations: not detected, low, medium, or high.

### 2.12. Statistical Analysis

Statistical analysis was performed with GraphPad Prism version 10.1.2 for Windows (GraphPad Software, San Diego, CA, USA). Fold change of RT-qPCR expression data, calculated using the  $2^{-\Delta\Delta Ct}$  method, was log-transformed to reduce skewness. The normality of data distribution was evaluated using either the Shapiro–Wilk or D'Agostino–Pearson test. Homogeneity of variance within groups was assessed using the Brown–Forsythe or Bartlett's test. Statistical significance of differences among multiple groups was determined using ordinary one-way ANOVA followed by Tukey's multiple comparison tests. Differences among groups were considered statistically significant at: \*  $p < 0.05$ , \*\*  $p < 0.01$ , \*\*\*  $p < 0.001$ , \*\*\*\*  $p < 0.0001$  (treatment vs. control); \*  $p < 0.05$ , \*\*  $p < 0.01$ , \*\*\*  $p < 0.001$ , \*\*\*\*  $p < 0.0001$  (olaparib vs. combination with ATRi or CHK1i); \*  $p < 0.05$ , \*\*  $p < 0.01$ , \*\*\*  $p < 0.001$ , \*\*\*\*  $p < 0.0001$  (ATRi or CHK1i vs. respective combinations with olaparib). Statistical significance for clinical data was assessed as described in the figure captions.

## 3. Results

### 3.1. Screening of Differentially Expressed miRNAs in Ovarian Cancer Cell Lines with Distinct Sensitivities to Olaparib

To establish the miRNA expression profile associated with acquired resistance to olaparib and understand the effects of combined treatments on miRNAs in HGSOC cell lines, we performed a large-scale miRNA differential expression analysis using a two-step approach (Figure 1a). A screening of 754 miRNAs was performed in PEO1 olaparib-sensitive and previously established PEO1-OR olaparib-resistant cells [17] using pre-designed TaqMan™ Array MicroRNA Cards. Based on the screening results, custom TaqMan™ Array MicroRNA Cards were designed and used for further validation of selected miRNAs in all OC cell lines.

The screening analysis revealed that 26% and 29% of all analyzed miRNAs were informative ( $C_T < 35$ ) in untreated PEO1 and PEO1-OR cells, respectively (Figure 1b). Most of the informative miRNAs were shared between both cell lines (73%), whereas PEO1 and PEO1-OR cells expressed 8% and 18% unique miRNAs, respectively (Figure 1c). Numerous miRNAs were differentially expressed in OC cell lines treated with tested inhibitors indicating significant changes in miRNA profiles (Figure 1d,e). Specifically, a combination of olaparib with ATRi or CHK1i upregulated the expression of 38 and 29 miRNAs, whereas it downregulated 85 and 82 miRNAs in PEO1-OR cells, respectively (Figure 1d,e).

To select the most likely biologically relevant miRNAs, we focused on miRNAs that fulfilled any of the following criteria: miRNAs with the highest changes in expression levels, miRNAs present in PEO1-OR but undetected in PEO1 cells or vice versa, miRNAs induced or reduced by combinations of inhibitors compared with either inhibitor alone. Based on these assumptions, 69 dysregulated miRNAs were chosen (Figure 1f) for the bioinformatics selection of miRNAs for further expression validation.

Initial bioinformatic analysis was performed to prioritize and select the most critical dysregulated miRNAs (Table S2). One miRNA (hsa-miRNA-1201) is not currently annotated as a miRNA according to the latest miRBase database (v22) and it was rejected from further analyses. A preliminary miRNA–mRNA network was created with the web tool MIENTURNET [26] only for miRNAs with strong experimental evidence of interactions (Figure S1). Among all analyzed miRNAs, 11 miRNAs had no strong experimental



evidence and were excluded from the analysis. The resulting miRNA–target interaction network topology for 57 miRNAs revealed that most miRNAs had a degree above or equal to three. However, 10 of the miRNAs were not connected with the working network and were assumed to be less biologically relevant (Figure S1).

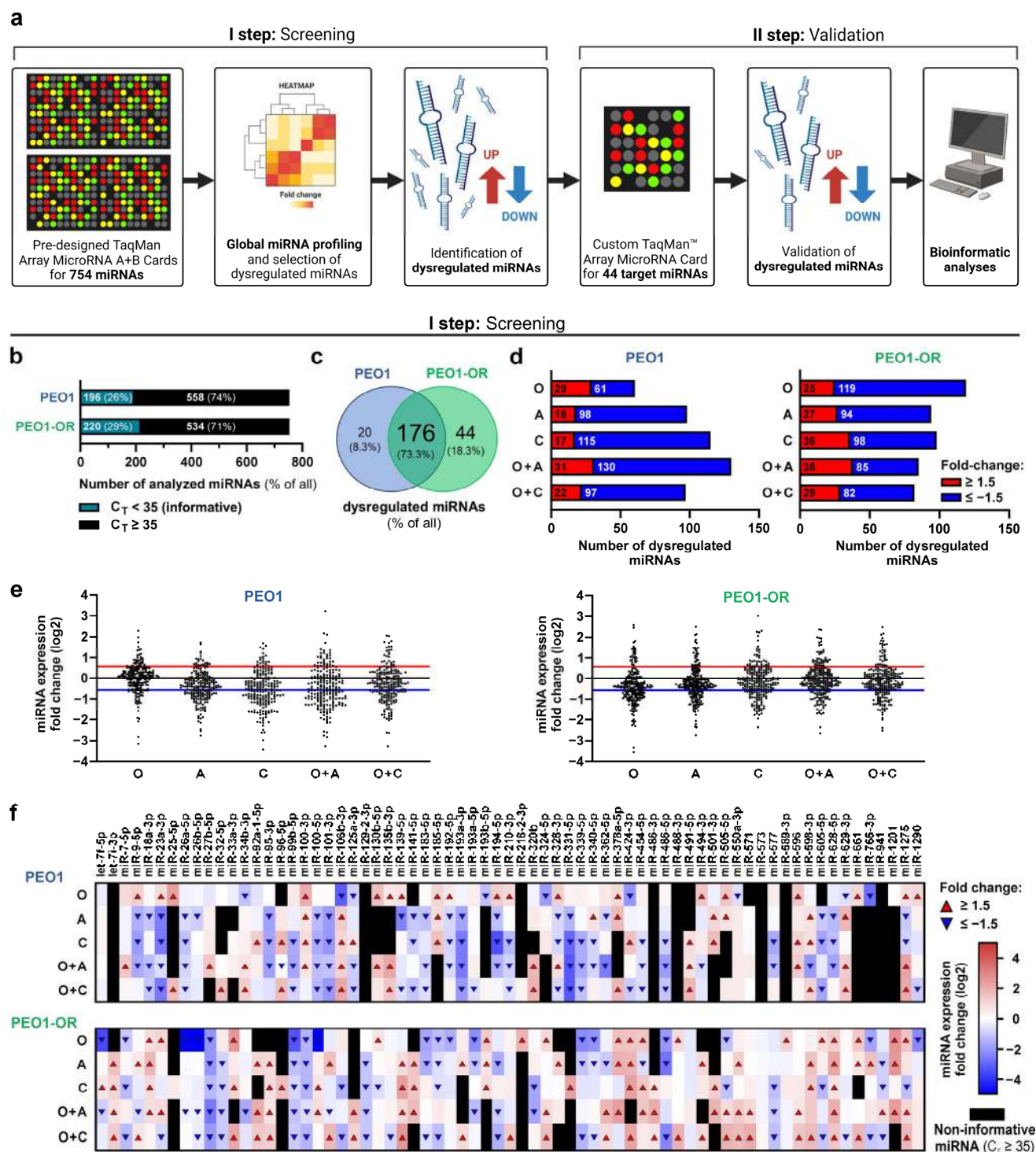


**Figure 1.** Two-step miRNA profiling strategy to screen and validate differentially expressed (DE) miRNAs in OC cell lines and miRNA screening results. (a) Workflow of the identification of DE miRNAs with pre-designed (I step) and custom (II step) TaqMan™ Array MicroRNA Cards covering 754 and 44 target miRNAs, respectively. (b) The number of informative miRNAs ( $C_T$  value  $< 35$ )

detected in untreated PEO1 and PEO1-OR cells with pre-designed TaqMan™ Array MicroRNA Cards used for relative quantification of miRNA expression. (c) Venn diagram representing informative miRNAs ( $C_T$  value < 35) overlapping or unique for PEO1 and PEO1-OR cell lines detected with pre-designed TaqMan™ MicroRNA Array Cards. (d) The number of upregulated and downregulated miRNAs in PEO1 and PEO1-OR cells in response to olaparib (O) alone or combined with ATRi (A) or CHK1i (C) based on screening analysis. (e) Scatter dot plots representing a distribution of miRNA expression (logarithmized fold changes relative to untreated cells) in response to tested inhibitors in PEO1 and PEO1-OR cells. Dots above the red line and below the blue line indicate upregulated and downregulated miRNAs (absolute  $\log_2$  of fold change  $\geq 0.585$ ), respectively. (f) Heatmap showing expression levels of 69 dysregulated miRNAs in PEO1 and PEO1-OR cells incubated with tested inhibitors. Red and blue triangles indicate upregulated and downregulated miRNA, respectively. Black rectangles indicate non-informative miRNAs in specific samples ( $C_T \geq 35$ ).

Finally, the results of bioinformatic analyses and a literature review allowed us to select 44 dysregulated miRNAs (Table S3) from screening experiments for further validation in olaparib-sensitive (PEO1, PEO4) and olaparib-resistant (PEO1-OR) cell lines.

### 3.2. Comparison of miRNA Expression Patterns in Olaparib-Sensitive and Olaparib-Resistant HGSOc Cell Lines

We first compared the miRNA expression in olaparib-resistant PEO1-OR cells relative to PEO1 olaparib-sensitive cells to differentiate miRNA profiles associated with different sensitivities to olaparib (Figure 2). Additionally, we evaluated the miRNA expression in another olaparib-sensitive cell line, PEO4 (Figure 2) [7,17]. Selection and validation of stable expression of endogenous control genes for RT-qPCR data normalization are described in the Supplementary Data and presented in Figures S2 and S3.

Most of the miRNAs among the 44 analyzed (86%) were reliably detected and quantified in untreated HGSOc cell lines (Figure S4). Significantly differentially expressed (DE) miRNAs were identified based on statistical significance ( $p < 0.05$ ) and absolute fold change  $\geq 1.5$  (i.e.,  $\log_2$  of fold change  $\geq 0.585$ ) (Figure 2a). Average fold change values for significantly dysregulated miRNA are presented in Table S4. The number of DE miRNAs in PEO1-OR cells and PEO4 cells compared to PEO1 cells amounted to 11 and 16 miRNAs, respectively. Differential miRNA expression was unbalanced, with 91% and 94% of all DE miRNAs being downregulated in PEO1-OR and PEO4 cell lines, respectively (Figure 2a,b). Comparison of miRNA profiles for all analyzed miRNAs showed substantial changes between PEO1 and PEO1-OR cells (Figure 2c). In PEO1-OR cells, miR-486-5p was the most downregulated (by 10.1-fold), whereas miR-9-5p was the most upregulated (by 1.6-fold) relative to PEO1 cells. The remaining DE miRNAs in PEO1-OR cells are as follows: miR-95-3p, miR-99b-5p, miR-100-3p, miR-100-5p, miR-125a-3p, miR-193a-3p, miR-424-3p, miR-505-5p, and miR-1290. Three of these miRNAs were uniquely downregulated in PEO1-OR cells only: miR-125a-3p, miR-193a-3p, and miR-1290 (Figure 2c).

On the whole, dysregulated expression of numerous miRNAs in the PEO1-OR cell line indicates highly likely altered post-translational regulation of gene expression associated with acquired resistance to olaparib in OC cells.

## II step: Validation

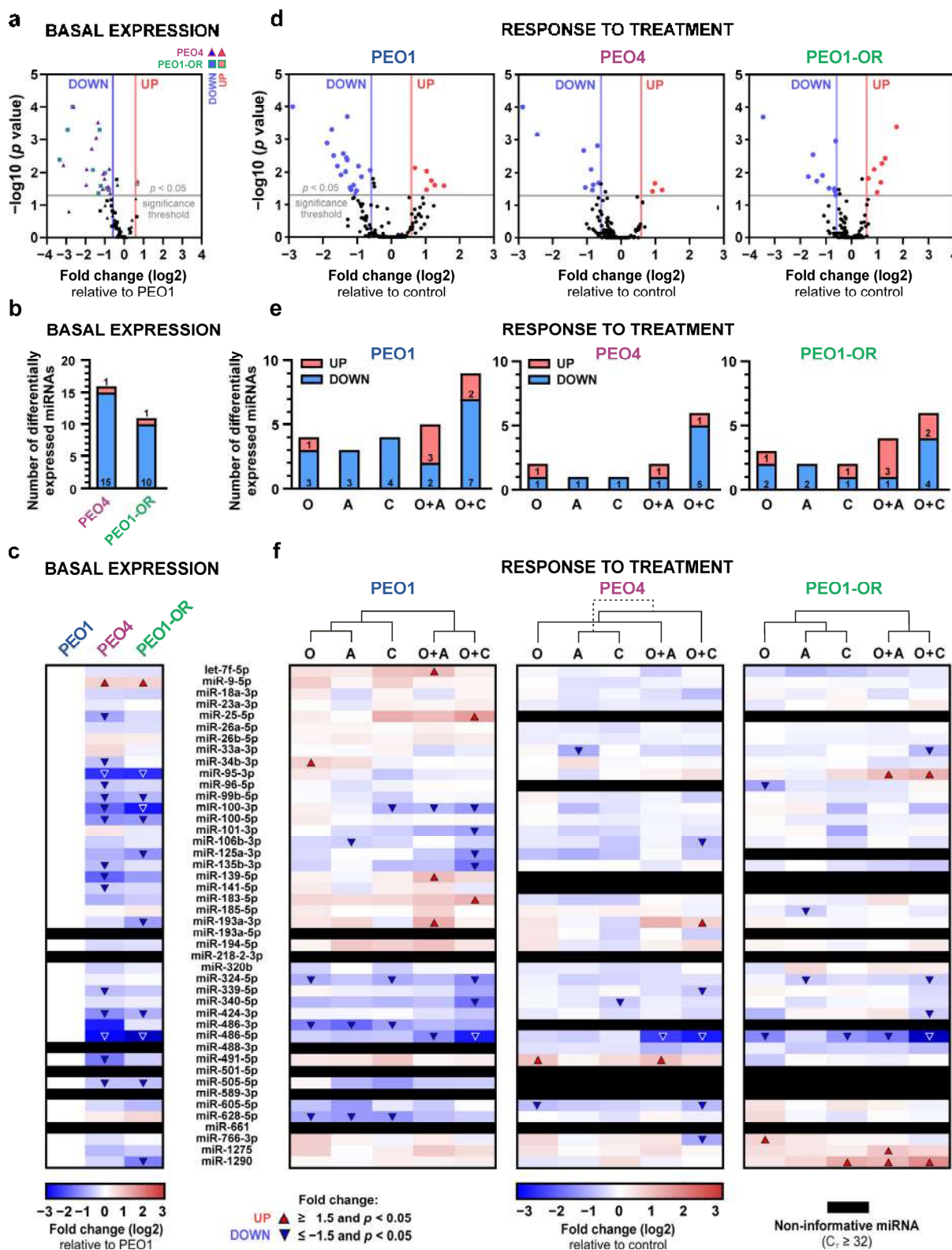


**Figure 2.** Overview of the miRNA basal expression in the absence of inhibitors and changes in miRNA levels in response to tested inhibitors in OC cell lines. (a,d) Volcano plots for miRNA expression: (a) basal expression in OC cells relative to PEO1 cells; (d) changes in expression in response to tested inhibitors or their combinations relative to untreated controls. DE miRNAs were identified

according to the following criteria: absolute fold changes of expression  $\geq 1.5$  and  $p < 0.05$  based on ordinary one-way ANOVA followed by multiple comparison tests. Significantly down- and upregulated miRNAs are highlighted with blue and red dots, respectively. Non-informative miRNAs with raw Ct values  $\geq 32$  in control cells are marked as black rectangles. (b,e) Bar charts representing the amount of significantly differentially expressed miRNAs: (b) basal expression relative to PEO1 cells; (e) changes in expression in response to tested inhibitors or their combinations relative to untreated controls. (c,f) Heatmaps for miRNA expression: (c) basal expression in OC cells relative to PEO1 cells; (f) expression changes in response to tested inhibitors or their combinations relative to untreated controls. Heatmaps were generated by a log transformation of the fold change data. Significantly ( $p < 0.05$ ) down- and upregulated miRNAs (absolute fold change  $\geq 1.5$ ) are highlighted with blue and red triangles, respectively. Hierarchical clustering via heatmap was generated to visualize the clustering based on miRNA expression profiles associated with tested inhibitors.

### 3.3. Differentially Expressed miRNAs Associated with Resensitization of PEO1-OR Cells to Olaparib with ATR/CHK1 Inhibitors

Previously we showed that ATR/CHK1 pathway inhibitors synergistically increase the cytotoxicity of olaparib in the olaparib-resistant HGSOC cell line by augmenting caspase-mediated apoptosis [7]. To identify miRNAs associated with resensitization of PEO1-OR to olaparib, we compared miRNA profiles in HGSOC cells treated for 48 h with olaparib alone or combined with ATRi or CHK1i. Most of the miRNAs were reliably detected and quantified in treated HGSOC cell lines (86% in PEO1, 75% in PEO1-OR, and 77% in PEO4 cells) (Figure 2). Expression of most miRNAs was unchanged (absolute fold change  $< 1.5$  or  $p > 0.05$ ) (Figure 2d). More DE miRNAs were identified as downregulated than upregulated in all HGSOC cells (Figure 2e). Average fold change values for significantly DE miRNAs are presented in Table S4. All results of RT-qPCR-based miRNA expression analysis in treated OC cell lines are presented in Figures S5–S7.

Cluster analysis between treatment groups revealed relatively distinct miRNA profiles between cells treated with single-agent inhibitors (O and A or C) and combined inhibitors (O + A, O + C) in PEO1 and PEO1-OR cell lines (Figure 2f). Co-clustering of olaparib combination groups indicates notable similarities at the miRNA level in PEO1-OR cells when olaparib cytotoxicity was augmented with the use of ATR/CHK1 pathway inhibitors.

In PEO1-OR cells incubated with olaparib alone, two miRNAs were downregulated (miR-96-5p, miR-486-5p), and one miRNA was upregulated (miR-766-3p) (Figure 2f). Combination treatments induced significant changes in the expression of seven miRNAs (four upregulated and three downregulated), some of which were overlapping in combination groups with either ATRi or CHK1i (Figure 2f). Four of these miRNAs (miR-33a-3p, miR-95-3p, miR-424-3p, miR-1275) were exclusively dysregulated in response to either combination in the PEO1-OR cell line, whereas they were unchanged in cells treated with single-agent inhibitors (Figure 2f). In PEO1-OR cells, four out of seven miRNAs dysregulated after olaparib combinations with ATRi or CHK1i were also changed at basal levels in the absence of inhibitors (miR-95-3p, miR-424-3p, miR-486-5p, and miR-1290) (Figure 2c,f). Interestingly, basal levels of miR-95-3p and miR-1290 were decreased in PEO1-OR cells in comparison with PEO1 cells (Figure 3a). However, the addition of ATRi or CHK1i to olaparib increased the expression of miR-95-3p and miR-1290 in PEO1-OR and appeared to partially restore miR-95-3p to the basal level in the absence of inhibitors observed in olaparib-sensitive cells (Figure 3a,b).

On the other hand, miR-424-3p and miR-486-5p were also negatively regulated in untreated PEO1-OR cells compared with PEO1 cells, but the inhibitor combinations further augmented the observed decrease in their expression levels. Interestingly, the addition of CHK1i to olaparib induced the decrease in miR-486-5p levels in both PEO1 and PEO1-OR cells (Figures 2f and 3b).

Altogether, olaparib combined with the inhibition of the ATR/CHK1 pathway seemed to re-establish the expression of miR-95-3p and miR-1290 in PEO1-OR to the level observed in parental PEO1 cells. Moreover, PEO1 and PEO1-OR cells responded in the





SD ( $n = 3-4$ ). Statistical significance was assessed with ordinary one-way ANOVA followed by multiple comparison tests: \* $p < 0.05$ , \*\* $p < 0.01$ , \*\*\* $p < 0.001$ , \*\*\*\* $p < 0.0001$  (treatment vs. control); + $p < 0.05$ , ++ $p < 0.01$ , +++ $p < 0.001$ , ++++ $p < 0.0001$  (O vs. combination with A or C); # $p < 0.05$ , ## $p < 0.001$  (A or C vs. respective combinations with O). The red and blue areas indicate FC values for upregulated and downregulated miRNAs (absolute  $\log_2$  of fold change  $\geq 0.585$ ), respectively.

### 3.4. Identification of miRNA–mRNA Regulatory Network, Enriched Pathways, and Biological Processes Related to Acquired Resistance to Olaparib in PEO1-OR Cells

To further evaluate miRNAs likely connected with resistance to olaparib in HGSOC cells, we performed bioinformatics analyses of miRNA and target genes to explore the predicted biological functions of 11 DE miRNAs. The constructed minimal regulatory network (subnetwork) for dysregulated miRNAs illustrates 205 experimentally confirmed interactions between 11 miRNAs and 38 target genes (Figure 4a). Each miRNA was predicted to regulate between 7 and 21 target genes. Among all miRNAs, the highest degree centrality (DC) in the network was confirmed for miR-9-5p (DC = 21), miR-100-5p (DC = 12), and miR-125a-3p (DC = 12), representing their high importance in the interacting subnetwork.

Functional enrichment analyses indicated the top significantly enriched Reactome pathways in untreated PEO1-OR cells, including “signaling by fibroblast growth factor receptor (FGFR)”, “signaling by epidermal growth factor receptor (EGFR)”, and other Receptor tyrosine kinase (RTK) signaling pathways associated with growth factors (Figure 4b). Pathways involved in carcinogenesis, cell proliferation, cell migration, and cell cycle were also significantly enriched (Figure 4b). Importantly, the results provided by GO analysis were similar to enriched pathways detected with Reactome, suggesting the involvement of growth factor signaling (EGFR and TGF- $\beta$  receptor) in decreased sensitivity of PEO1-OR cells to olaparib. Moreover, GO revealed significant biological processes associated with cell proliferation, cell cycle, DNA damage response, Notch signaling, and others (Figure 4b), partially in line with our previous studies [7,17]. Detailed results and target molecules involved in enriched terms for PEO1-OR cells are listed in Table S5.

Altogether, functional enrichment analysis identified pathways and processes that were likely regulated by DE miRNAs in PEO1-OR cells with acquired resistance to olaparib. Interestingly, a considerable number of their target genes were associated with the growth factor signaling pathways.





cells treated with olaparib combinations (Figure 4d). The Reactome results revealed that  $\beta$ -catenin-independent WNT signaling was the most significantly enriched pathway associated with *TNRC6A*, *CALM1*, and *CLTC* target genes. We also found a few pathways associated with growth factor signaling by TGF- $\beta$ , EGFR, FGFR1, NGF, VEGFR2, and PDGF to be significantly enriched in resensitized PEO1-OR cells (Figure 4d). Furthermore, pathways linked to apoptosis and cell cycle were found to be of significant enrichment in PEO1-OR cells. In agreement, our previous analysis indicated the role of caspase-mediated apoptosis [7] and abrogation of olaparib-induced G2/M arrest [17] in PEO1-OR cells in response to olaparib alone and combined with ATRi or CHK1i.

The GO:BP analysis showed no significantly enriched biological processes, likely due to the relatively small number of nodes in the network. Detailed results of analysis and target molecules involved in enriched terms for PEO1-OR cells are listed in Table S6. Overrepresentation analyses revealed some similarities and differences between PEO1 and PEO1-OR cells. Importantly, the most significantly enriched terms in PEO1 cells treated with either olaparib combination were also associated with various pathways and biological processes related to growth factors (Figure S8).

Overall, functional enrichment allowed us to determine pathways likely involved in the resensitization of PEO1-OR cells to olaparib in the presence of the ATR/CHK1 pathway inhibitors and focused our attention on growth factor signaling.

### 3.6. Hub Genes Associated with Olaparib Resistance and Resensitization of PEO1-OR Cells to Olaparib

To further screen out the core hub genes, we selected the top 10 genes with the highest connectivity in previously established subnetworks using the MCC algorithm in Cytoscape. Ranked hub genes and their connections with dysregulated miRNAs in PEO1 and PEO1-OR cells are illustrated in Figure 5.

From the analysis of hub genes, each was expected to be modulated by two to five DE miRNAs. Four genes seemed to be shared in untreated and combination-treated PEO1-OR cells (*SRRM2*, *DDX21*, *VIM*, *CALM1*) (Figure 5). As shown before in PEO1-OR cells, *CALM1* was associated with the top significantly enriched pathways including growth factor signaling by FGFR, EGFR, PDGF, and  $\beta$ -catenin-independent WNT signaling (Table S5). Another four genes were found to be uniquely associated with DE miRNAs in untreated PEO1-OR cells (*ESR1*, *VCP*, *CDKN1A*, and *HUWE1*) (Figure 5). *CDKN1A* was associated with most of the enriched pathways and processes in PEO1-OR cells including growth factor signaling (Table S5). Both *ESR1* and *CDKN1A* were linked with positive regulation of cell proliferation and cellular response to stress. Moreover, *VCP* and *CDKN1A* were found to be involved in response to DNA damage stimulus (Table S5). Six genes were uniquely linked with DE miRNAs in PEO1-OR cells resensitized to olaparib with ATRi or CHK1i (*YWHAQ*, *SMAD2*, *TNRC6A*, *CLTC*, *SCAF4*, and *POLR2A*) (Figure 5). These genes likely involved in resensitization to olaparib were associated with the following biological processes: beta-catenin-independent WNT signaling (*TNRC6A* and *CLTC*), G2/M DNA damage checkpoint (*YWHAQ*), loss of function of TGF $\beta$ R1 in cancer (*SMAD2*), and transcriptional regulation by small RNAs (*TNRC6A* and *POLR2A*) (Table S5). Interestingly, no genes were shared between treated PEO1 and PEO1-OR cells (Figure 5). Experimentally validated targets of DE miRNAs from minimal networks are listed in Table S7.

Considering miRNAs, the MCC algorithm captured miR-9-5p, miR-125a-3p, and miR-100-5p as the top three miRNAs with the highest importance in untreated PEO1-OR cells (Table S8). Moreover, miR-95-3p, miR-486-5p, and miR-1290 were suggested as the three most essential miRNAs in PEO1-OR cells in response to olaparib combinations. Both miR-95-3p and miR-1290 were uniquely dysregulated after O + A or O + C treatments only in PEO1-OR cells (Figure 2b) and targeted five and two hub genes, respectively. Finally, key hub genes with the highest importance were obtained as signatures in the PEO1-OR cell line.

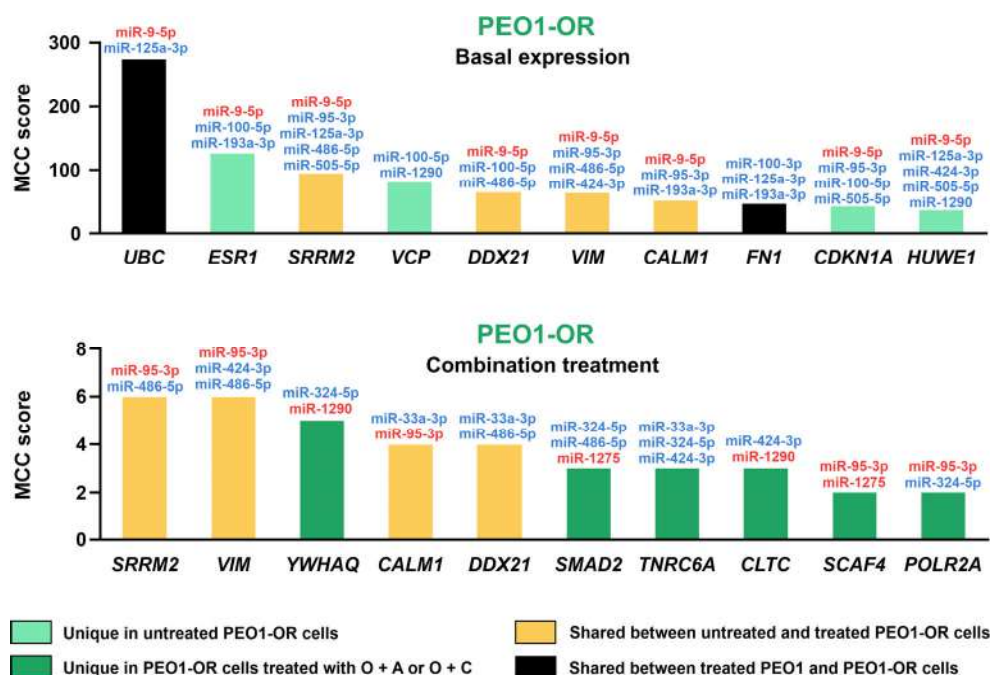


**Figure 5.** Hub genes associated with olaparib resistance and resensitization to olaparib with combination treatments in the PEO1-OR cell line. The top 10 hub genes were ranked (x-axis) based on the score (y-axis) calculated with the MCC algorithm using the cytoHubba plug-in in Cytoscape. Unique and shared genes are colored as described. Targeting miRNAs from the subnetwork are listed above bars for each hub gene from the PEO1-OR cell line and are highlighted with red (upregulated) or blue (downregulated) according to the results of relative quantity analysis.

### 3.7. Olaparib Combined with ATR/CHK1 Inhibitors Dysregulates Proteins Involved in Growth Factor Signaling in PEO1-OR Cells

Functional enrichment analyses indicated the involvement of growth factor (GF) signaling in olaparib resistance and restoration of OC cell sensitivity to olaparib with ATRi or CHK1i linked to dysregulated miRNAs. To test the biological relevance of bioinformatic analyses, we assessed the expression levels of 41 GFs and their receptors in PEO1 and PEO1-OR cells in the presence of tested inhibitors for 2 days using commercially available antibody microarrays (Figures 6 and S9).

Heatmaps displayed relative quantities of 38 detected GFs in PEO1 and PEO1-OR cells shared between both cell lines (Figure 6a). Three GFs were not detected in neither PEO1 nor PEO1-OR cells (GM-CSF, TGF $\alpha$  and TGF $\beta$ 2) (Figure S10). Single-agent inhibitors had an impact on the expression of GFs, significantly altering the levels by more than 1.5-fold ( $p < 0.05$ ) of only three and six proteins in treated PEO1-OR and PEO1 cells, respectively (Figure 6a). In PEO1-OR cells, incubation with olaparib alone caused a significant downregulation of fibroblast growth factor (FGF6) by 1.6-fold.

Comparison of protein levels after incubation with olaparib combinations with ATRi or CHK1i revealed significant changes in the expression of 7 proteins in PEO1-OR cells and 15 proteins in PEO1 cells (Figure 6a). Dysregulated GFs, shared or unique for olaparib-sensitive and -resistant cell lines, are presented on Venn diagrams (Figure 6b). In response to combination treatments, most differentially expressed GFs were downregulated in PEO1-OR cells and upregulated in PEO1 cells. FGF4, FGF7, NT-4, PLGF, and TGF $\beta$ 1 were exclusively downregulated in PEO1-OR cells in the presence of olaparib combined with either ATRi or CHK1i (Figure 6a,b).

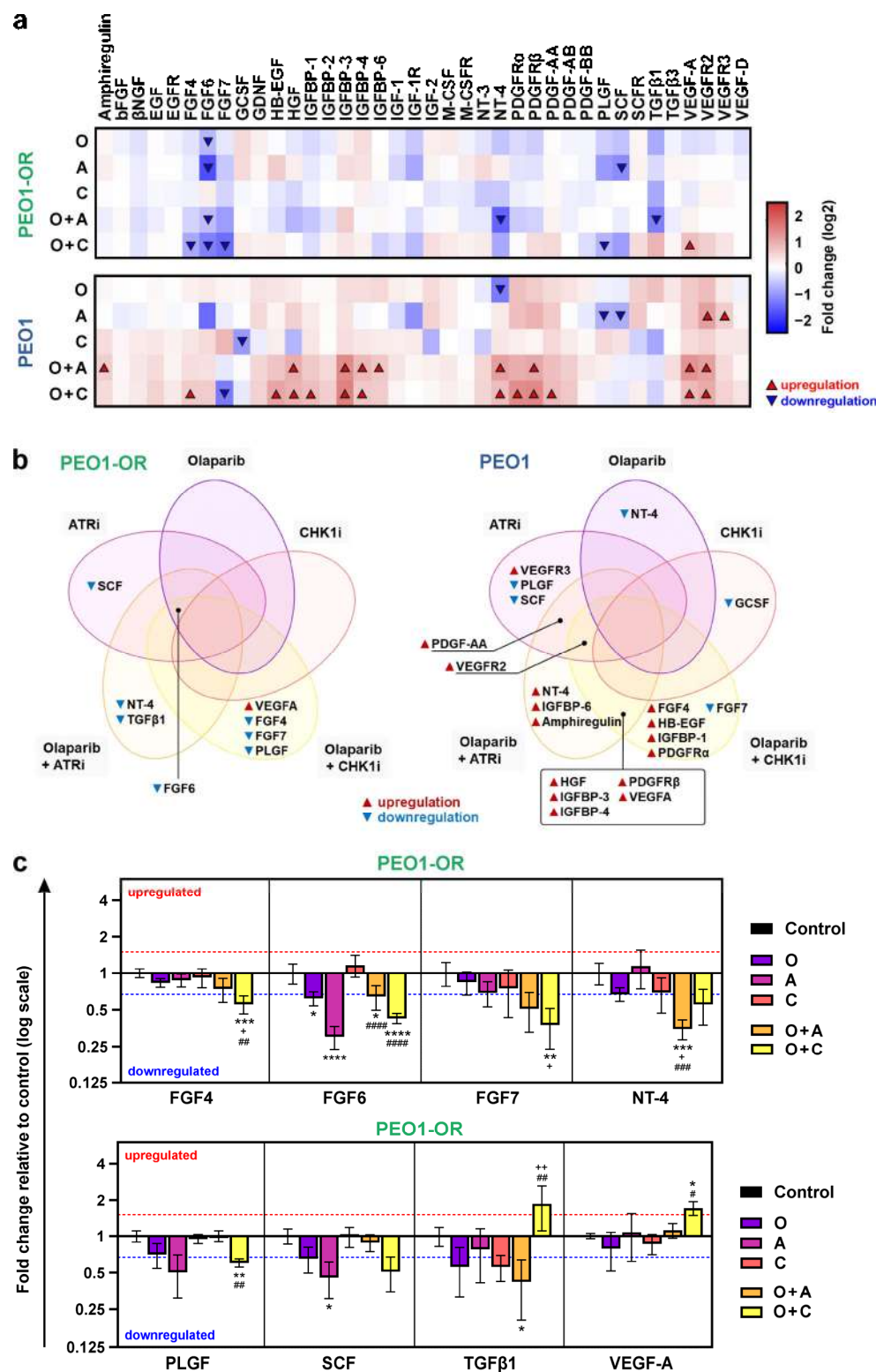


**Figure 6.** Olaparib combined with ATRi or CHK1i dysregulates the expression of growth factors (GFs) in OC cell lines. (a) Heatmaps for the expression of 41 GFs and their receptors in PEO1 and PEO1-OR cell lines. (b) Venn diagram for dysregulated GFs in PEO1 and PEO1-OR cell lines. (c) Results of semi-quantitative analysis with antibody microarrays for significantly dysregulated GFs in PEO1-OR cells (absolute fold change  $\geq 1.5$  and  $p < 0.05$ ). Cells were incubated with inhibitors (O, A, C) or their combinations (O + A, O + C) for 2 days. Data are expressed as mean fold change  $\pm$  SD

( $n = 4$ ) on a logarithmized scale relative to untreated control cells. Statistical significance was assessed using ordinary one-way ANOVA followed by multiple comparison tests: \* $p < 0.05$ , \*\* $p < 0.01$ , \*\*\* $p < 0.001$ , \*\*\*\* $p < 0.0001$  (treatment vs. control); + $p < 0.05$ , ++ $p < 0.01$  (O vs. combination with A or C); # $p < 0.05$ , ## $p < 0.01$ , ### $p < 0.001$ , #### $p < 0.0001$  (A or C vs. respective combinations with O).

The highest significant decrease in PEO1-OR cells was observed for NT-4 and FGF7, which were downregulated by 2.9-fold and 2.7-fold after olaparib treatment combined with ATRi and CHK1i, respectively (Figure 6c). VEGF-A was the only significantly upregulated GF in PEO1-OR cells (by 1.7-fold) after co-treatment with olaparib and the ATR/CHK1 pathway inhibitors, however, to a similar level as in PEO1 cells. Moreover, PEO1-OR cells abrogated combination-induced upregulation of numerous proteins associated with GFs and their receptors (amphiregulin, HB-EGF, HGF, IGFBP-1, IGFBP-3, IGFBP-4, IGFBP-6, PDGFR $\alpha$ , PDGFR $\beta$ , PDGF-AA, VEGF-A, and VEGFR2) which was observed in PEO1 cells (Figure 6a,b). Statistical analysis for significantly dysregulated GFs in PEO1 cells (Figure S9) and original representative images of antibody arrays are presented in the Supplementary Information (Figure S10).

Altogether, alterations in the expression of GFs were in line with the bioinformatic analyses indicating the association between GF signaling and miRNA dysregulation in PEO1-OR cells. Therefore, we speculated that different expression profiles could be the result of intrinsic characteristics of OC cell lines with distinct sensitivities to olaparib.

### 3.8. Differentially Expressed miRNAs and Target Genes Linked to Olaparib Resistance Predict Survival of Ovarian Cancer Patients

After overlapping miRNAs dysregulated in untreated PEO1-OR cells and in response to olaparib combinations (O + A or O + C), 14 DE miRNAs were selected for further analysis using clinical data from TCGA for stage II–IV serous OC patients (Table 1). Four miRNAs were common (miR-95-3p, miR-424-3p, miR-486-5p, and miR-1290), seven were unique in untreated PEO1-OR cells (miR-9-5p, miR-99b-5p, miR-100-3p, miR-100-5p, miR-125a-3p, miR-193a-3p, and miR-505-5p), and three were unique for treated PEO1-OR cells (miR-33a-3p, miR-324-5p, and miR-1275). Examining these miRNAs in clinical samples involved assessing their association with patient survival and expression in serous OC patient samples regarding olaparib resistance (Figure 7) and resensitization to olaparib (Figure 8).

Firstly, to highlight miRNAs that likely possess biological functions in vivo, miRNA abundance was assessed in OC samples using counts per million (CPM) values. We focused on relatively abundant miRNAs determined with a pre-defined cut-off (CPM  $\geq 10$  in  $\geq 50\%$  samples) resulting in eight miRNAs for further analysis (miR-9-5p, miR-99b-5p, miR-100-5p, miR-125a-3p, miR-324-5p, miR-424-3p, miR-486-5p, and miR-505-5p) (Table 1).

We initially focused on miRNAs associated with resistance to olaparib due to their dysregulation in untreated PEO1-OR cells relative to PEO1 cells. For clinical relevance, we used the ToPP web tool for Kaplan–Meier (KM) survival analysis on filtered HGSOV data from TCGA-OV. Notably, three of seven highly abundant miRNAs (miR-99b-5p, miR-424-3p, and miR-505-5p) showed significant prognostic value for both overall survival (OS) and progression-free intervals (PFIs) (Table 1). Low levels of miR-99b-5p, miR-424-3p, and miR-505-5p were linked to significantly worse OS times (Figure 7a). Notably, decreased expression of these miRNAs was observed in PEO1-OR cells compared to PEO1 cells (Figure 2c). KM plots for all analyzed miRNAs are presented in Figure S11. Stage-wise differential expression analysis showed no significant differences in the expression of three selected miRNAs across stages II, III, and IV of serous OC (Figure 7b). Stable expression of mature miRNAs over higher stages suggested their potential role in disease progression.

Subsequently, we created an interaction subnetwork for miR-99b-5p, miR-424-3p, and miR-505-5p and 13 target genes with two or more connections within the network (Figure 7c), reducing the previous network for untreated PEO1-OR cells (Figure 4a).



## Genes and miRNAs associated with olaparib resistance

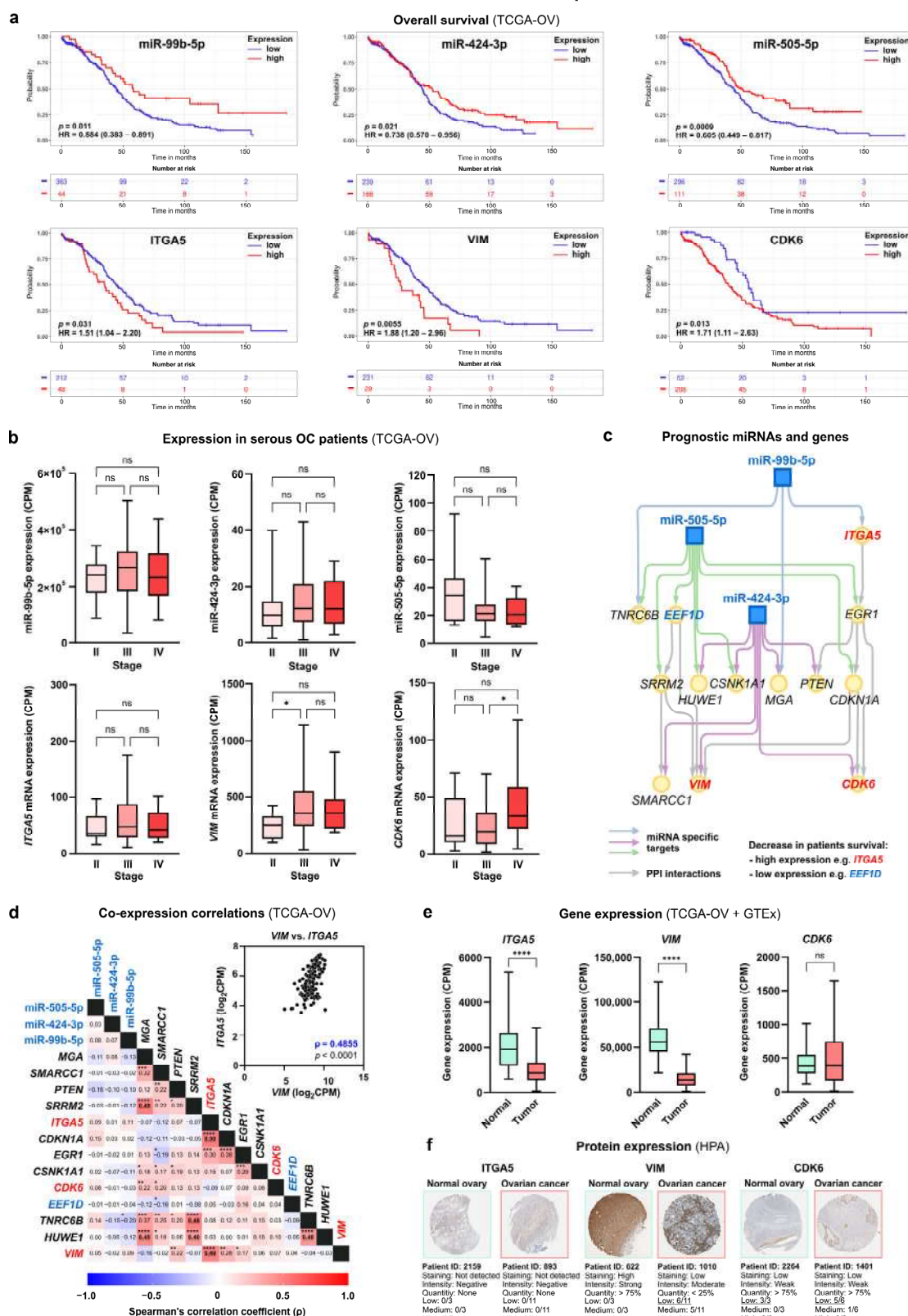


**Figure 7.** Differentially expressed miRNAs and target genes linked to olaparib resistance associated with survival in OC patients. **(a)** Interaction subnetwork between miRNAs associated with poor survival in serous OC cancer patients and target genes. The subnetwork originates from the minimal



network for PEO1-OR cells under normal conditions linked to olaparib resistance. Nodes with two or more connections (colored arrows) were analyzed to highlight critical relationships. Expression levels of miRNAs and genes in OC patients significantly associated with survival are highlighted with blue (low expression) and red (high expression). (b) Stage-wise differential expression of miRNAs and genes associated with decreased survival in serous OC patients (TCGA-OV). Box plots show normalized CPM values extending from the 25th to 75th percentiles, lines dividing boxes represent medians, and the whiskers show the highest and lowest values after outlier removal within groups (FDR = 1%). Statistical significance was calculated using the Kruskal–Wallis test followed by Dunn’s multiple comparison test: \*  $p < 0.05$ . (c) Kaplan–Meier (KM) plots display the relationship between miRNAs or genes and clinical endpoints in HGSOc patients (OS—overall survival, PFI—progression-free interval). Plots were generated with the ToPP web-based tool for HGSOc patients split into low- and high-expression groups using the best-performing threshold as a cut-off. Statistical significance between these two groups was calculated using the log-rank test: \*  $p < 0.05$ . (d) Correlation matrix of miRNA and gene expression in serous OC patients (TCGA-OV). Correlations were computed using a two-tailed Spearman’s correlation test. Spearman’s rank correlation coefficient ( $\rho$ ): 0–0.19 (no correlation), 0.20–0.39 (weak correlation), 0.40–0.59 (moderate correlation). Moderate correlations are highlighted with bold and underlined. Statistical significance: \*  $p < 0.05$ , \*\*  $p < 0.01$ , \*\*\*  $p < 0.001$ , \*\*\*\*  $p < 0.0001$ . (e) Differential expression of genes associated with decreased survival in serous OC patients (TCGA-OV) between normal ovaries (GTEx) and OC (TCGA-OV). The analysis was performed using the RNA-seq data from the TNMplot web-based tool. Box plots show CPM values extending from the 25th to 75th percentiles, lines dividing boxes represent medians, and whiskers show the highest and lowest values after outlier removal within groups (FDR = 1%). Statistical significance was calculated using a two-tailed Mann–Whitney test: \*\*\*\*  $p < 0.0001$ . (f) Verification of protein expression for selected genes in normal ovaries and serous OC using the HPA database. Images show representative immunohistochemical staining for ITGA5 (HPA002642), VIM (CAB000080), and CDK6 (CAB004363).

**Table 1.** Overview of differentially expressed miRNAs in PEO1-OR cell line selected for analysis based on their expression abundance and prognostic value in OC patient samples from TCGA database. Significant clinical endpoints are marked with bold (log-rank  $p < 0.05$ ).

miRNAs	Expression in PEO1-OR Cells		Percentage of Samples with CPM $\geq 10$ in TCGA-OV *	OS in Serous Ovarian Cancer Patients (High vs. Low Expression)		PFI in Serous Ovarian Cancer Patients (High vs. Low Expression)	
				HR	Log-Rank $p$	HR	Log-Rank $p$
	Standard Conditions	Combination Treatments					
miR-9-5p	▲		89%	0.84	0.31	1.22	0.11
miR-99b-5p	▼		100%	<b>0.58</b>	<b>0.011</b>	<b>0.539</b>	<b>0.0025</b>
miR-100-3p	▼		0%	n/a	n/a	n/a	n/a
miR-100-5p	▼		100%	1.18	0.19	<b>1.36</b>	<b>0.0088</b>
miR-125a-3p	▼		99%	<b>1.37</b>	<b>0.039</b>	1.17	0.22
miR-193a-3p	▼		1%	n/a	n/a	n/a	n/a
miR-505-5p	▼		95%	<b>0.61</b>	<b>0.0009</b>	0.793	0.065
miR-95-3p	▼	▲	4%	n/a	n/a	n/a	n/a
miR-424-3p	▼	▼	63%	<b>0.74</b>	<b>0.021</b>	<b>0.787</b>	<b>0.044</b>
miR-486-5p	▼	▼	100%	1.13	0.36	1.24	0.068
miR-1290	▼	▲	0%	n/a	n/a	n/a	n/a
miR-33a-3p		▼	0%	n/a	n/a	n/a	n/a
miR-324-5p		▼	99%	<b>0.68</b>	<b>0.0048</b>	0.821	0.094
miR-1275		▼	11%	n/a	n/a	n/a	n/a

\* miRNAs with CPM  $\geq 10$  in  $\geq 50\%$  samples from TCGA-OV were subjected to further analyses, whereas miRNAs with CPM  $< 10$  in  $\geq 50\%$  samples were rejected and designated as not applicable (n/a). CPM—counts per million, HR—hazard ratio, OS—overall survival, PFI—progression-free interval, ▲—upregulated in PEO1-OR cells, ▼—downregulated in PEO1-OR cells.

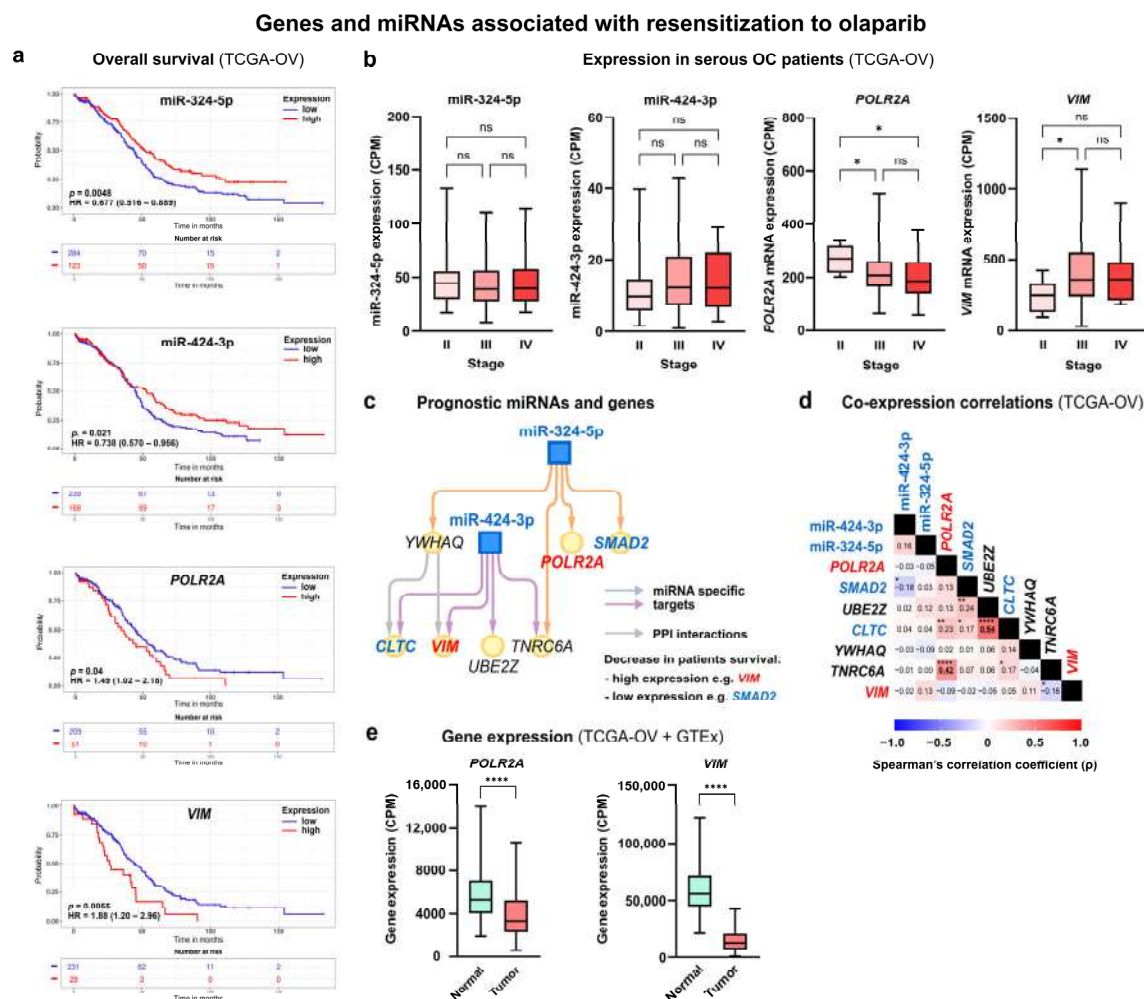


**Figure 8.** Differentially expressed miRNAs and target genes linked to resensitization to olaparib associated with survival in OC patients. **(a)** Interaction subnetwork between miRNAs associated with poor survival in serous OC cancer patients and target genes. The subnetwork originates from the minimal network for PEO1-OR cells treated with olaparib combined with ATR/CHK1 inhibitors linked to resensitization to olaparib. Expression levels of miRNAs and genes in OC patients significantly associated with survival are highlighted with blue (low expression) and red (high expression). **(b)** Stage-wise differential expression of miRNAs and genes associated with decreased survival in serous OC patients (TCGA-OV). Box plots show normalized CPM values extending from the 25th to 75th percentiles, lines dividing boxes represent medians, and the whiskers show the highest and lowest values after outlier removal within groups (FDR = 1%). Statistical significance was calculated using the Kruskal–Wallis test followed by Dunn’s multiple comparison test: \*  $p < 0.05$ . **(c)** Kaplan–Meier (KM) plots showing the relationship between miRNAs or genes and clinical endpoints in HGSOC patients (OS—overall survival, PFI—progression-free interval). Plots were generated with the ToPP web-based tool for HGSOC patients split into low- and high-expression groups using the best-performing threshold as a cut-off. Statistical significance between these two groups was calculated using the log-rank test: \*  $p < 0.05$ . **(d)** Correlation matrix of miRNA and gene expression in serous OC patients (TCGA-OV). Correlations were computed for every pair of datasets using a two-tailed Spearman’s correlation test. Spearman’s rank correlation coefficient ( $\rho$ ): 0–0.19 (no correlation), 0.20–0.39 (weak correlation), 0.40–0.59 (moderate correlation). Moderate correlations are highlighted with bold and underlined. Statistical significance: \*  $p < 0.05$ , \*\*  $p < 0.01$ , \*\*\*  $p < 0.001$ . **(e)** Differential expression of genes associated with decreased survival in serous OC patients (TCGA-OV) between normal ovaries (GTEx) and OC (TCGA-OV). The analysis was performed using the RNA-seq data from the TNMplot web-based tool integrating the data for normal and cancerous tissues. Box plots show CPM values extending from the 25th to 75th percentiles, the line dividing the box represents the median, and the whiskers show the highest and lowest values

after outlier removal within groups (FDR = 1%). Statistical significance was calculated using a two-tailed Mann–Whitney test: \*\*\*\*  $p < 0.0001$ .

Genes targeted by prognostic miRNAs from the network are listed in Table 2. Notably, target genes regulated by prognostic miRNAs were associated with 80% of the previously established pathways and biological processes enriched in PEO1-OR cells, such as signaling by GF, signaling by Wnt, and cell cycle regulation (Table S5).

**Table 2.** Overview of genes targeted by DE miRNAs associated with survival selected for analysis based on their expression abundance and prognostic value in OC patient samples from TCGA database. Significant clinical endpoints are marked with bold (log-rank  $p < 0.05$ ).

Gene	Percentage of Samples with CPM $\geq 10$ in TCGA-OV *	OS in Serous OC Patients (High vs. Low Expression Cohort)		PFI in Serous OC Patients (High vs. Low Expression Cohort)	
		HR	Log-Rank $p$	HR	Log-Rank $p$
<i>HUWE1</i>	100%	<b>1.87</b>	<b>0.013</b>	<b>0.63</b>	<b>0.043</b>
<i>TNRC6B</i>	100%	<b>1.73</b>	<b>0.0025</b>	1.31	0.11
<i>EEF1D</i>	100%	<b>0.70</b>	<b>0.026</b>	<b>0.73</b>	<b>0.039</b>
<i>CDK6</i>	74%	<b>1.71</b>	<b>0.013</b>	1.39	0.053
<i>CSNK1A1</i>	100%	1.41	0.11	<b>1.71</b>	<b>0.034</b>
<i>EGR1</i>	100%	1.36	0.055	<b>1.52</b>	<b>0.016</b>
<i>CDKN1A</i>	100%	<b>0.63</b>	<b>0.038</b>	1.49	0.076
<i>ITGA5</i>	100%	<b>1.51</b>	<b>0.031</b>	<b>1.35</b>	<b>0.045</b>
<i>SRRM2</i>	100%	<b>1.51</b>	<b>0.039</b>	1.20	0.27
<i>PTEN</i>	100%	<b>1.9</b>	<b>0.017</b>	1.34	0.12
<i>SMARCC1</i>	100%	0.84	0.43	<b>0.70</b>	<b>0.018</b>
<i>MGA</i>	99%	<b>1.44</b>	<b>0.023</b>	1.31	0.12
<i>VIM</i>	100%	<b>1.88</b>	<b>0.0055</b>	1.46	0.056
<i>TNRC6A</i>	100%	1.39	0.22	<b>0.73</b>	<b>0.043</b>
<i>YWHAQ</i>	100%	<b>0.62</b>	<b>0.0096</b>	<b>1.39</b>	<b>0.046</b>
<i>CLTC</i>	100%	<b>0.40</b>	<b>0.0039</b>	<b>0.59</b>	<b>0.021</b>
<i>UBE2Z</i>	100%	0.77	0.28	0.72	0.17
<i>SMAD2</i>	100%	<b>0.62</b>	<b>0.0077</b>	<b>0.60</b>	<b>0.0022</b>
<i>POLR2A</i>	100%	<b>1.49</b>	<b>0.04</b>	<b>1.67</b>	<b>0.0053</b>

\* All genes fulfilled a cut-off of CPM  $\geq 10$  in  $\geq 50\%$  of samples from TCGA-OV and were subjected to further analyses. CPM—counts per million, HR—hazard ratio, OS—overall survival, PFI—progression-free interval. *VIM* was considered a prognostic gene due to the highest significant HR for OS ( $p = 0.0055$ ) correlating with HR for PFI, which almost reached statistical significance ( $p = 0.056$ ).

Based on survival data, four genes (*EEF1D*, *ITGA5*, *VIM*, and *CDK6*) were associated with both OS and PFI (Figures 7a, S12 and S13). Considering that low expression of selected miRNAs was linked to worse survival, we looked for target genes with high expression showing unfavorable OS and PFI. HGSOC patients with high *ITGA5*, *VIM*, and *CDK6* showed significantly decreased survival represented by HR of 1.51 ( $p = 0.031$ ), 1.88 ( $p = 0.0055$ ), and 1.71 ( $p = 0.013$ ) (Figure 7a). Interestingly, the *CDK6* gene was associated with enriched pathways regulating the cell cycle, previously linked to olaparib resistance in PEO1-OR cells (Table S5). Stage-wise differential expression revealed upregulation of the *VIM* gene in stage III compared to stage II and upregulation of the *CDK6* gene in stage IV compared to stage III in serous OC patients (Figure 7b). These data indicate that *VIM* and *CDK6* expression may be potentially linked to tumor progression.

Next, correlation analysis revealed a positive moderate correlation between mRNA expression of *ITGA5* and *VIM* genes ( $\rho = 0.49$ ,  $p < 0.0001$ ) in serous OC patients (Figure 7d). A comparison of gene expression in normal ovaries and tumor tissue revealed decreased mRNA levels of *ITGA5* and *VIM* in OC patients (Figure 7e). Verification of gene

expression at the protein level using the HPA database showed that VIM is downregulated in most OC samples relative to normal tissue (Figure 7f) which is in line with the differential mRNA expression. Immunohistochemical images of ITGA5 showed weak staining in both normal and tumor tissue (Figure 7f), however, ITGA5 levels were annotated as “not detected” in the HPA database and rejected from interpretation.

Our analysis revealed key miRNAs associated with olaparib resistance in vitro that are also dysregulated in serous OC patients. Given that downregulated miRNAs (miR-99b-5p, miR-424-3p, and miR-505-5p) and upregulated target genes (*VIM*, *ITGA5*, *CDK6*) are also linked to worse survival of women with OC, our findings provide a theoretical foundation for exploring the link between miRNAs and resistance to olaparib in vivo.

### 3.9. Prognostic Roles of Differentially Expressed miRNAs and Target Genes Associated with Resensitization to Olaparib for Ovarian Cancer Patients

Additionally, we assessed the relevance of three miRNAs (miR-324-5p, miR-424-3p, and miR-486-5p) linked to olaparib resensitization in PEO1-OR cells based on clinical data for serous OC patients, focusing on only highly abundant miRNAs in clinical samples (Table 2). KM survival analysis indicated that low expression of miR-324-5p and miR-424-3p predicted unfavorable OS and PFI (Table 2). KM plots for OS are presented in Figure 8a. Downregulation of miR-324-5p and miR-424-3p occurred in PEO1-OR cells in response to olaparib combinations with ATRi or CHK1i (Figure 2c). Interestingly, both miRNAs exhibited unchanged expression across stages II, III, and IV in serous OC patients, indicating their potential role throughout tumor development (Figure 8b).

Using miRNAs with significant prognostic value, we created an interaction subnetwork for miR-324-5p and miR-424-3p and seven target genes (Figure 8c), reducing the previous network established for PEO1-OR cells treated with olaparib combinations (Figure 4c). Clinical prognostic significance was found for *POLR2A*, *VIM*, *CLTC*, and *SMAD2* genes (Table 2). These genes were previously established in pathways involved in the resensitization of PEO1-OR cells to olaparib (Table S6). Connecting unfavorable survival prognosis with low miRNA expression, we identified genes associated with worse survival in high-expression compared to low-expression OC cohorts. Serous OC patients with increased *VIM* and *POLR2A* had worse OS and PFI compared to low-expression groups (Figure 8a). Overexpression of the *VIM* gene was linked to the worst OS time (HR = 1.88,  $p = 0.0055$ ). Both *VIM* and *POLR2A* genes were associated with pathways enriched in resensitized PEO1-OR cells through regulation of caspase-mediated apoptosis and miRNA biogenesis (Table S6).

Considering genes associated with unfavorable survival, stage-wise differential expression analysis indicated downregulation of *POLR2A* in stages III and IV compared to stage II in OC patients and dysregulation of *VIM* (Figure 8b). Correlation analysis revealed a significant relationship between a few genes, but none were found for selected prognostic genes (Figure 8d). However, *POLR2A* showed a positive association with *TNRC6A* at the transcriptional level ( $q = 0.42$ ,  $p < 0.0001$ ). *POLR2A* and *VIM* were significantly downregulated in OC tissue in comparison with normal ovaries (Figure 8e). The HPA provided no data for *POLR2A* at the protein level which impeded validation of the expression.

Overall, miR-324-5p and miR-424-3p were significantly related to the survival of OC patients and antitumor response in resensitized PEO1-OR cells. Therefore, the abovementioned miRNAs and potentially their target genes provide promising predictive information to understand the reversal of olaparib resistance with the ATR/CHK1 pathway inhibitors in the context of serous OC.

## 4. Discussion

Olaparib exhibits significant clinical benefits in newly diagnosed and recurrent HGSOC patients, especially as maintenance therapy that prolongs overall survival in platinum-sensitive OC patients with *BRCA1/2* mutations [37]. Interestingly, responsiveness to PARPi is usually closely associated with platinum sensitivity [37,38]. However, resistance

to olaparib can develop over time in some patients, necessitating a critical understanding of associated mechanisms. Indeed, multifactorial mechanisms of resistance to PARPi and platinum analogs were demonstrated to be at least partially interrelated in OC cells [8,39]. Recent studies have demonstrated that modulators of DNA damage response, including the ATR/CHK1 pathway inhibitors, can resensitize OC cells both in vitro and in vivo [10,39,40]. Despite extensive research on resistance mechanisms, including epigenetic silencing of gene expression [41], there is still a need to better understand OC desensitization to olaparib, particularly at the post-transcriptional level. The novelty of the study is the use of the *BRCA2*<sup>MUT</sup> HGSOC cell line PEO1-OR with acquired resistance to olaparib to understand mechanisms linked to miRNA regulatory properties responsible for distinct sensitivities to olaparib alone or combined with the ATR/CHK1 pathway inhibitors. As olaparib-sensitive HGSOC models [7,17], we employed PEO1 and PEO4 cells, which were established from the same patient at the first and the second relapse following chemotherapy and represent a clinical progression of OC [18,19]. Moreover, the role of DE miRNAs and their target genes was examined in the context of serous OC patient survival to select essential signature molecules.

Considering olaparib resistance, miRNA profiling of PEO1-OR cells compared to parental PEO1 cells in the absence of inhibitors revealed 11 DE miRNAs with absolute fold change  $\geq 1.5$  and  $p < 0.05$  (miR-9-5p, miR-95-3p, miR-99b-5p, miR-100-3p, miR-100-5p, miR-125a-3p, miR-193a-3p, miR-424-3p, miR-486-5p, miR-505-5p, miR-1290). Most of them were significantly downregulated, except for upregulated miR-9-5p. The expression profile of miRNAs was also established in PEO4 cells. These cells exhibit a sensitivity to olaparib that is more similar to PEO1-OR cells after short-term incubation with olaparib (2 days), whereas after long-term incubation (5 days), their sensitivity becomes evident, similar to that of PEO1 cells [7,17]. While PEO4 cells are indeed olaparib-sensitive, it takes more time for olaparib to manifest its cytotoxic activity in these cells compared to PEO1 cells [7,17]. Therefore, we consider the drug-induced changes observed in PEO4 cells after 48 h, such as the deregulation of miRNAs, as early cellular events associated with the antitumor activity. Consequently, we hypothesize that PEO4 cells would share some DE miRNAs with both PEO1 and PEO1-OR cells. Interestingly, eight DE miRNAs were common in PEO1-OR cells and PEO4 cells, and we presumed that these miRNAs were likely associated with short-term desensitization to olaparib when both cell lines possess a phenotype of decreased sensitivity. Moreover, three DE miRNAs (miR-125a-3p, miR-193a-3p, miR-1290) were unique for PEO1-OR cells, which distinguished their characteristics of acquired long-term resistance.

Some downregulated miRNAs identified in our work were also reported in studies deciphering miRNA profiles in solid tumor samples, serum, and exosomes from serous OC cells, including miR-99b (GSE76449), miR-100-5p (GSE83693), miR-125a-3p (GSE106817), miR-193a-3p (GSE83693), miR-424-3p (GSE47841), miR-486-5p (GSE47841), and miR-505-5p (GSE76449). The study by Nam et al. demonstrated the downregulation of miR-100-5p in paired primary and recurrent HGSOC samples obtained from patients after cytoreductive surgeries compared to normal ovarian tissue [42]. Overall, we indicate that all revealed DE miRNAs contribute to the olaparib-resistant phenotype of PEO1-OR HGSOC cells in vitro.

The created minimal subnetwork with protein–protein interactions maximally connected 11 DE miRNAs in PEO1-OR cells with 38 target genes revealing essential interactions. Functional enrichment analyses indicated the potential involvement of a few interconnected biological processes and pathways in acquired resistance to olaparib. We showed that genes targeted with DE miRNAs were significantly associated with growth factor (GF) signaling, particularly signaling by fibroblast GF receptor (FGFR), epidermal GF receptor (EGFR), platelet-derived GF (PDGF), and stem cell factor (SCF)-KIT. Recently, Nicholson et al. revealed a link between FGFR signaling, DNA damage response, and resistance to cisplatin in human OC cell lines [43]. Increased activation of EGFR induced by FGFR3 overexpression was associated with decreased sensitivity to cisplatin in serous OC

cells [44]. Here, the downregulation of transforming GF beta receptor (TGF $\beta$ R) signaling was predicted as a significant change in signal transduction in PEO1-OR cells. The tumorigenic role of TGF $\beta$  has been extensively studied in OC cells regarding its association with epithelial-to-mesenchymal transition (EMT) [45]. Resistance to olaparib promoted by the TGF $\beta$  pathway has been described in various tumors [46,47], however, findings from OC are lacking. From enriched pathways linked to GF signaling, we identified a set of eleven key genes (*UBC*, *TNRC6A*, *TNRC6B*, *MTOR*, *CREB1*, *CDKN1A*, *CALM1*, *PTEN*, *XPO1*, *PPP1CB*, *SKI*). In the context of resistance, silencing of cyclin-dependent kinase inhibitor 1A (*CDKN1A*) with miRNAs was previously suggested to promote cisplatin resistance in OC cells in vivo [48]. Additionally, we identified phosphatidylinositol 3-kinase (PI3K)/AKT signaling to be significantly enriched in PEO1-OR cells. Experiments employing cisplatin-resistant OC cell lines showed that activation of the PI3K/AKT pathway desensitized cells to chemotherapy [49]. More recently, Xu et al. proposed that a combination of AKT inhibitor with olaparib slowed down tumor growth in a patient-derived xenograft (PDX) model of recurrent platinum-resistant OC with prior PARPi therapy [50].

The functional enrichment analysis also indicated GF signaling's role in decreased sensitivity of the PEO1-OR cell line to olaparib. Moreover, we found that PEO1-OR cells were enriched in biological processes related to cell cycle regulation and DNA integrity checkpoints, aligning with our previous findings of abrogated olaparib-induced G2/M arrest [17]. Here, we revealed that genes implicated in progression through the cell cycle (*MCM4*, *CDK6*, *CDKN1A*, *FEM1B*, *NDRG1*, *PTEN*, and *UBC*) may be targeted by DE miRNAs in PEO1-OR cells. Phosphatase and tensin homolog (PTEN) is a protein involved in regulating the PI3K/AKT pathway. The study by Selvendiran et al. demonstrated that upregulation of PTEN prompted G2/M arrest and apoptosis in cisplatin-resistant OC cells, however, the association with resistance to olaparib requires further investigation [51]. Altogether, we identified target genes of particular interest in the context of resistance to olaparib in our cell line model of HGSOC for potential further investigation to gain more insights into their role in vitro and in vivo.

To assess the biological relevance of our in vitro cell line data, we performed survival analysis for selected DE miRNAs and target genes in HGSOC patients using data from TCGA-OV. Based on recommendations of TCGA Research Network, clinical survival outcome for OC patients was evaluated using overall survival (OS) and progression-free intervals (PFIs) [52]. Next, we reconstructed a minimal miRNA–mRNA network associated with olaparib resistance, prioritizing prognostic miRNAs and their target genes. Kaplan–Meier analyses revealed that three miRNAs (miR-99b-5p, miR-424-3p, and miR-505-5p), downregulated in untreated PEO1-OR cells, were significantly associated with shorter OS and PFI in low-expression cohorts of HGSOC patients. A previous study demonstrated miR-99b-5p downregulation in the plasma exosomes of treatment-naïve OC patients compared to healthy individuals [53]. Additionally, we revealed that OC patients with high levels of integrin  $\alpha$ 5 (*ITGA5*), a target for miR-99b-5p, showed poorer survival compared to a low-expression cohort. *ITGA5* is a transmembrane protein reported to promote metastasis in HGSOC cells [54], which is in line with unfavorable survival. In vivo experiments revealed that loss of *ITGA5* inhibits the growth of OC xenografts [54]. A few studies examined the effect of miR-424-3p on proliferation, migration, and apoptosis in OC. A recent study suggested that miR-424-3p increases the sensitivity of OC cell lines to cisplatin by downregulating the antiapoptotic protein galectin-3 in vitro [55]. This indicates that the downregulation of miR-424-3p in PEO1-OR cells may be partially responsible for the olaparib-resistant phenotype. Moreover, we showed that high levels of genes encoding vimentin (*VIM*) and cyclin-dependent kinase 6 (*CDK6*), both targeted by miR-424-3p, were linked to shorter OS and PFI. Indeed, the upregulation of vimentin was demonstrated to induce EMT, cell growth, invasion, and chemoresistance in both OC cell lines and xenograft models of OC [56,57]. Moreover, in vitro and in vivo experiments highlighted that increased levels of *CDK6* were linked to upregulation of ATR kinase and decreased cell death in OC treated with cisplatin [58]. Altogether, we revealed important miRNA–



mRNA interactions and processes associated with decreased sensitivity to olaparib in *BRCA2*<sup>MUT</sup> OC cells in vitro.

Despite initial effectiveness, the widespread use of olaparib involves an increasing number of patients with acquired resistance and a lack of further approved therapy options [39]. Over recent years, combinations of olaparib with the ATR/CHK1 pathway inhibitors showed promising antitumor activity in OC cells [9,10,40]. The results of the CAPRI study revealed that patients with recurrent platinum-sensitive *BRCA1/2*<sup>MUT</sup> HGSOC, who had progressed upon prior PARPi, obtained promising partial responses to olaparib combined with the ATRi ceralasertib [10]. Our previous work demonstrated that inhibitors of ATR and CHK1 kinases exerted synergistic cytotoxic activity with olaparib in PEO1-OR cells [7]. Hence, the second main goal of our study was to investigate the miRNA profile of HGSOC cells resensitized to olaparib with the ATR/CHK1 pathway inhibitors.

A few previous studies analyzed the roles of specific miRNAs in the cytotoxicity of olaparib in OC cells, however, many of them utilized cell lines that do not possess features of HGSOC. The recent study suggested that overexpression of miR-200c sensitized the *BRCA1*<sup>WT</sup> SKOV-3 cells to olaparib by increasing apoptosis [59]. In another work, it was demonstrated that targeted inhibition of cyclin D1 by miR-20b increased the cytotoxicity of olaparib in SKOV-3 cells and cell-line-derived xenograft models of OC [60].

Here, we identified six dysregulated mature miRNAs that have so far not been mentioned in the context of overcoming resistance to olaparib in HGSOC cells using the ATR/CHK1 pathway inhibitors. Resensitization of PEO1-OR cells was associated with upregulation of miR-95b-3p and miR-1290 along with downregulation of miR-33a-3p, miR-324-5p, miR-424-3p, and miR-486-5p. Most of these DE miRNAs were unique for PEO1-OR cells compared to olaparib-sensitive cells. Interestingly, the addition of ATRi or CHK1i to olaparib further augmented a decrease in miR-424-3p and miR-486-5p observed in untreated PEO1-OR cells. Through analysis of miRNA–gene interactions, we found that these six miRNAs could build highly connected linkage with 17 experimentally validated target genes. Network-based approaches revealed that several pathways might be dysregulated by target genes involved in overcoming resistance to olaparib. Overrepresentation analysis found that resensitized PEO1-OR cells were mainly enriched in four groups of processes: GF signaling, apoptosis, cell cycle checkpoints, and gene silencing by RNA.

In this study, GF signaling represented a new process of particular interest associated with TGFβR1, EGFR, PDGF, and nerve growth factor (NGF). SMAD2 gene, targeted by three DE miRNAs, was found to be enriched in the pathways controlled by TGFβ receptors. Findings by Roberts et al. revealed that treatment with TGFβ induced EMT and downregulated homologous recombination repair protein, resulting in resensitization of HGSOC cells to olaparib in vitro [61]. Here, we showed that enriched signaling by FGFR1, EGFR, PDGF as well as VEGFR2 mediated cell proliferation was associated with genes encoding trinucleotide repeat-containing gene 6A protein (TNRC6A) and calmodulin 1 (CALM1), targeted by three and two DE miRNAs, respectively. Calmodulin is a calcium-dependent protein that binds and regulates the activity of EGFR [62]. EGFR and VEGFR2 are two membrane RTK proteins frequently upregulated in OC [63]. Interestingly, therapies combining platinum with VEGF/VEGFR inhibitors showed higher efficacy than monotherapies in platinum-resistant OC patients [64]. Moreover, our bioinformatic analysis confirmed that the G2/M DNA damage checkpoint may be involved in the resensitization of PEO1-OR cells, which agrees with our previous studies [17]. Here, we predicted that the YWHAQ gene, targeted by dysregulated miR-324-5p and miR-1290, may play a critical role in this process. YWHAQ, also known as 14-3-3σ, is a protein involved in the inhibition of G2/M progression [65] and contributes to the pathogenesis of epithelial OC [66]. Taken together, we predicted that a few biological processes might be implicated in the resensitization of PEO1-OR cells to olaparib using ATRi or CHK1i.

Subsequently, we validated the biological possibility of the findings concerning GF signaling through downstream expression analyses for 41 human GFs and their receptors.

PEO1-OR cells abrogated upregulation of 13 GFs observed in PEO1 cells treated with olaparib combined with the ATR/CHK1 pathway inhibitors. This suggested different responses of olaparib-sensitive and olaparib-resistant cells to combination treatments in the context of GF signaling. We uncovered altered expression of five GFs uniquely in PEO1-OR cells after combination treatments (FGF4, FGF6, NT-4, PLGF, and TGF $\beta$ 1). FGF4, neurotrophin-4 (NT-4), and TGF $\beta$ 1 were significantly downregulated and VEGF-A upregulated only in the presence of combined inhibitors. Previous research has shown that overexpression of FGF4 in fibroblast mixed cancer stem-like cells isolated from OC increases their sphere-forming capacity, however, knockdown of *FGF4* can abrogate it [67]. In epithelial OC cells, the upregulation of VEGF-A via PARP1 can promote angiogenesis [68]. Moreover, OC cells overexpressing TGF $\beta$ 1 exhibited decreased sensitivity to cisplatin [69]. Overall, dysregulation of GF expression in desensitized PEO1-OR cells confirmed our predictions from bioinformatic analyses. Accordingly, we pointed out that downregulation of FGF4, VEGF-A, TGF $\beta$ 1, and possibly NT-4 could play an important role in the resensitization of PEO1-OR cells to olaparib.

Finally, we investigated the role of DE miRNAs in combination-treated PEO1-OR cells and their target genes in the survival of HGSOC patients. Our study revealed a significant association between low levels of miR-324-5p and miR-424-3p, both downregulated in PEO1-OR cells, and poor OS and PFI times in OC patients. We investigated a set of experimentally validated targets of miR-324-5p and miR-424-3p. Importantly, low levels of two targets, vimentin and POLR2A, displayed an inverse association with OC survival compared to both miRNAs. Vimentin has been shown to promote metastatic progression by EMT in solid tumors [70]. The recent study showed that OC cells resistant to olaparib upregulate vimentin expression at the mRNA level irrespective of *BRCA1* status. Moreover, the downregulation of vimentin was associated with the inhibition of PARP1, resulting in decreased viability of OC cells in vitro [71]. Interestingly, our previous study highlighted that PEO1-OR cells incubated with olaparib and ATR/CHK1 pathway inhibitors also downregulate PARP1 [7]. POLR2A is a DNA-dependent RNA polymerase essential for cell survival. In vivo studies demonstrated that POLR2A expression level was higher in PDX models of cisplatin-resistant OC compared to sensitive cells [72].

We acknowledge that our study has several limitations. Here we experimentally confirmed dysregulation of miRNA expression in olaparib-resistant cells, however, a complex interplay among miRNAs, mRNAs, and other unexplored functional elements including long non-coding RNA requires further investigation. Furthermore, functional assays with miRNA mimics and inhibitors might support our findings concerning the role of significantly dysregulated miRNAs in acquired resistance and resensitization to olaparib. Nonetheless, this study highlights a new molecular basis associated with miRNAs for revealing mechanisms of olaparib resistance and overcoming it with the ATR/CHK1 pathway inhibitors.

## 5. Conclusions

In conclusion, we described dysregulated miRNAs and their interactions with essential target genes associated with the survival of serous OC patients. Placing these results in the context of prior studies, our findings highlight the altered miRNA profile of PARPi-resistant HGSOC cells with restored *BRCA2* in vitro. This may be especially important in the context of predicting response to olaparib in OC patients. Our data indicate that GF signaling may play an important role in acquired resistance and resensitization to olaparib. Further examination of the linkage between miRNAs and response to olaparib alone or combined with the ATR/CHK1 inhibitors in vivo may shed light on the rationale for combination therapy in HGSOC patients. Importantly, this cell-line-based miRNA profiling study could serve as a platform for further research on olaparib resistance and resensitization in ovarian cancer.

**Supplementary Materials:** The following supporting information can be downloaded at: <https://www.mdpi.com/article/10.3390/cells13100867/s1>. Supplementary Methods: Screening of endogenous control genes for qPCR studies with Custom TaqMan™ Array MicroRNA Cards; Supplementary Data: Identification of endogenous controls for use with custom TaqMan™ Array MicroRNA Cards; Figure S1: Network of miRNA–target interactions created with the MIENTURNET tool for dysregulated miRNAs identified from screening analysis with pre-designed TaqMan™ Array MicroRNA Cards and pre-selected for further validation; Figure S2: Selection of candidate endogenous control genes with the RefFinder tool based on results from pre-designed TaqMan™ Array MicroRNA Cards for further RT-qPCR studies with custom TaqMan™ Array MicroRNA Cards; Figure S3: Validation of endogenous control genes' stable expression in HGSOc cell lines for RT-qPCR data normalization from custom TaqMan™ MicroRNA Cards; Figure S4: Results of RT-qPCR-based differential miRNA basal expression analysis in untreated PEO1, PEO1-OR, and PEO4 cell lines after 2 days of cell culture (custom TaqMan™ MicroRNA Cards); Figure S5: Results of RT-qPCR-based differential miRNA expression analysis in PEO1 cell line incubated with olaparib (O), ATRi (A), CHK1i (C), or their combinations for 2 days (custom TaqMan™ MicroRNA Cards); Figure S6: Results of RT-qPCR-based differential miRNA expression analysis in PEO1-OR cell line incubated with olaparib (O), ATRi (A), CHK1i (C), or their combinations for 2 days (custom TaqMan™ MicroRNA Cards); Figure S7: Results of RT-qPCR-based differential miRNA expression analysis in PEO4 cell line incubated with olaparib (O), ATRi (A), CHK1i (C), or their combinations for 2 days (custom TaqMan™ MicroRNA Cards); Figure S8: Network-based functional enrichment analyses of significantly differentially expressed miRNAs and their target genes in PEO1 cell line incubated with olaparib combinations for 2 days; Figure S9: Results of semi-quantitative analysis with antibody microarrays for growth factors with significantly dysregulated expression in PEO1 cells (absolute fold change  $\geq 1.5$ ,  $p < 0.05$ ); Figure S10: Raw results of semi-quantitative analysis of 41 growth factors' expression in PEO1 and PEO1-OR cells incubated with tested inhibitors or their combinations for 2 days; Figure S11: Kaplan–Meier plots showing the relationship between miRNAs and clinical endpoints (OS—overall survival, PFI—progression-free interval) in serous OC patients; Figure S12: Kaplan–Meier plots showing the relationship between target genes and clinical endpoints (OS—overall survival, PFI—progression-free interval) in serous OC patients; Figure S13: Kaplan–Meier plots showing the relationship between target genes and clinical endpoints (OS—overall survival, PFI—progression-free interval) in serous OC patients (continued); Table S1: List of key reagents used in the study; Table S2: Selection of 44 out of 69 dysregulated miRNAs for validation on custom TaqMan™ MicroRNA Cards based on bioinformatics analyses and literature review; Table S3: List of analyzed miRNAs and small RNAs for miRNA validation with custom TaqMan™ MicroRNA Cards; Table S4: Average fold change values of significantly differentially expressed miRNAs in HGSOc cell lines with custom TaqMan™ MicroRNA Cards; Table S5: Top significantly enriched pathways (Reactome) and biological processes (GO:BP) associated with target genes of dysregulated miRNAs in untreated PEO1-OR cells; Table S6: Top significantly enriched pathways (Reactome) associated with target genes of dysregulated miRNAs in PEO1-OR cells in response to combinations of olaparib with the ATR/CHK1 pathway inhibitors; Table S7: Experimentally validated targets of differentially expressed miRNAs from minimal subnetworks that maximally connect seeds in the PEO1-OR cell line (established with miRNet 2.0); Table S8: Identification of hub nodes using cytoHubba plug-in based on the minimal miRNA–mRNA networks using maximal clique centrality (MCC) algorithm; Table S9: Results of stage-wise differential miRNA and gene expression analysis in serous OC patients using filtered data from TCGA-OV dataset (serous OC patients with stage II, III, or IV after pharmaceutical therapy); Table S10: Validation of endogenous control genes' stable expression in HGSOc cell lines for RT-qPCR data normalization from custom TaqMan™ MicroRNA Cards.

**Author Contributions:** Conceptualization, Ł.B., D.K., A.G., A.M., A.Ś., M.M. and A.R.; methodology, Ł.B., D.K., A.G., A.Ś. and A.R.; formal analysis, Ł.B., D.K. and E.P.; investigation, Ł.B. and A.G.; resources, A.M. and A.R.; writing—original draft preparation, Ł.B.; writing—review and editing, Ł.B., D.K., A.G., E.P., A.M., A.Ś., M.M. and A.R.; visualization, Ł.B.; supervision, A.R.; funding acquisition, A.R. All authors have read and agreed to the published version of the manuscript.

**Funding:** This work was supported by the National Science Centre, Poland (Project grant number: Sonata Bis 2019/34/E/NZ7/00056).

**Institutional Review Board Statement:** Not applicable.

**Informed Consent Statement:** Not applicable.

**Data Availability Statement:** The original TCGA data are a publicly available dataset downloaded from the National Cancer Institute Genomic Data Commons Data Portal. The data generated during the study are available from the corresponding author upon reasonable request.

**Acknowledgments:** The original illustration in Figure 1a has been created with BioRender.com. RT-qPCR experiments were carried out at the Research Laboratory CoreLab of the Medical University of Lodz.

**Conflicts of Interest:** The authors declare no conflicts of interest.

## Abbreviations

A	ATR inhibitor (ceralasertib)
ATR	ataxia telangiectasia and RAD3-related protein
ATRi	ATR inhibitor(s)
BRCA2	breast cancer type 2 susceptibility protein
C	CHK1 inhibitor (MK-8776)
CHK1	checkpoint kinase 1
CHK1i	CHK1 inhibitor(s)
C <sub>T</sub>	cycle threshold
DE	differentially expressed
DSB	double-strand break
ECACC	European Collection of Authenticated Cell Cultures
FBS	fetal bovine serum
FC	fold change
GF	growth factor
GO	Gene Ontology
HGSOC	high-grade serous ovarian cancer
HR	hazard ratio
HRD	homologous recombination deficiency
MCC	maximal clique centrality
miRNA	microRNA
O	olaparib
OC	ovarian cancer
OS	overall survival
PARP1	poly(ADP-ribose) polymerase 1
PARPi	PARP inhibitor(s)
PEO1-OR	PEO1 olaparib-resistant cell line
PFI	progression-free interval
PPI	protein–protein interaction
SD	standard deviation
TCGA	The Cancer Genome Atlas
TLDA	TaqMan® Low-density Array

## References

1. DiSilvestro, P.; Colombo, N.; Scambia, G.; Kim, B.G.; Oaknin, A.; Friedlander, M.; Lisianskaya, A.; Floquet, A.; Leary, A.; Sonke, G.S.; et al. Efficacy of Maintenance Olaparib for Patients with Newly Diagnosed Advanced Ovarian Cancer with a BRCA Mutation: Subgroup Analysis Findings from the SOLO1 Trial. *J. Clin. Oncol.* **2020**, *38*, 3528–3537. <https://doi.org/10.1200/JCO.20.00799>.
2. Lisio, M.A.; Fu, L.; Goyeneche, A.; Gao, Z.H.; Telleria, C. High-Grade Serous Ovarian Cancer: Basic Sciences, Clinical and Therapeutic Standpoints. *Int. J. Mol. Sci.* **2019**, *20*, 952. <https://doi.org/10.3390/ijms20040952>.
3. Chen, Q.; Li, X.; Zhang, Z.; Wu, T. Systematic Review of Olaparib in the Treatment of Recurrent Platinum Sensitive Ovarian Cancer. *Front. Oncol.* **2022**, *12*, 858826. <https://doi.org/10.3389/fonc.2022.858826>.
4. Wang, N.; Yang, Y.; Jin, D.; Zhang, Z.; Shen, K.; Yang, J.; Chen, H.; Zhao, X.; Yang, L.; Lu, H. PARP inhibitor resistance in breast and gynecological cancer: Resistance mechanisms and combination therapy strategies. *Front. Pharmacol.* **2022**, *13*, 967633. <https://doi.org/10.3389/fphar.2022.967633>.
5. Nicum, S.; McGregor, N.; Austin, R.; Collins, L.; Dutton, S.; McNeish, I.; Glasspool, R.; Hall, M.; Roux, R.; Michael, A.; et al. Results of a randomised Phase II trial of olaparib, chemotherapy or olaparib and cediranib in patients with platinum-resistant ovarian cancer. *Br. J. Cancer* **2024**, *130*, 941–950. <https://doi.org/10.1038/s41416-023-02567-6>.

6. Mahdi, H.; Hafez, N.; Doroshow, D.; Sohal, D.; Keedy, V.; Do, K.T.; LoRusso, P.; Jurgensmeier, J.; Avedissian, M.; Sklar, J.; et al. Ceralasertib-Mediated ATR Inhibition Combined with Olaparib in Advanced Cancers Harboring DNA Damage Response and Repair Alterations (Olaparib Combinations). *JCO Precis. Oncol.* **2021**, *5*, 1432–1442. <https://doi.org/10.1200/PO.20.00439>.
7. Biegala, L.; Gajek, A.; Szymczak-Pajor, I.; Marczak, A.; Sliwinska, A.; Rogalska, A. Targeted inhibition of the ATR/CHK1 pathway overcomes resistance to olaparib and dysregulates DNA damage response protein expression in *BRCA2*<sup>MUT</sup> ovarian cancer cells. *Sci. Rep.* **2023**, *13*, 22659. <https://doi.org/10.1038/s41598-023-50151-y>.
8. McMullen, M.; Karakasis, K.; Madariaga, A.; Oza, A.M. Overcoming Platinum and PARP-Inhibitor Resistance in Ovarian Cancer. *Cancers* **2020**, *12*, 1607. <https://doi.org/10.3390/cancers12061607>.
9. Burgess, B.T.; Anderson, A.M.; McCorkle, J.R.; Wu, J.; Ueland, F.R.; Kolesar, J.M. Olaparib Combined with an ATR or Chk1 Inhibitor as a Treatment Strategy for Acquired Olaparib-Resistant *BRCA1* Mutant Ovarian Cells. *Diagnostics* **2020**, *10*, 121. <https://doi.org/10.3390/diagnostics10020121>.
10. Wethington, S.L.; Shah, P.D.; Martin, L.; Tanyi, J.L.; Latif, N.; Morgan, M.; Torigian, D.A.; Rodriguez, D.; Smith, S.A.; Dean, E.; et al. Combination ATR (ceralasertib) and PARP (olaparib) Inhibitor (CAPRI) Trial in Acquired PARP Inhibitor-Resistant Homologous Recombination-Deficient Ovarian Cancer. *Clin. Cancer Res.* **2023**, *29*, 2800–2807. <https://doi.org/10.1158/1078-0432.CCR-22-2444>.
11. Kandettu, A.; Adiga, D.; Devi, V.; Suresh, P.S.; Chakrabarty, S.; Radhakrishnan, R.; Kabekkodu, S.P. Deregulated miRNA clusters in ovarian cancer: Imperative implications in personalized medicine. *Genes Dis.* **2022**, *9*, 1443–1465. <https://doi.org/10.1016/j.gendis.2021.12.026>.
12. Zhao, L.; Liang, X.; Wang, L.; Zhang, X. The Role of miRNA in Ovarian Cancer: An Overview. *Reprod. Sci.* **2022**, *29*, 2760–2767. <https://doi.org/10.1007/s43032-021-00717-w>.
13. Frisk, N.L.S.; Sorensen, A.E.; Pedersen, O.B.V.; Dalgaard, L.T. Circulating microRNAs for Early Diagnosis of Ovarian Cancer: A Systematic Review and Meta-Analysis. *Biomolecules* **2023**, *13*, 871. <https://doi.org/10.3390/biom13050871>.
14. Yokoi, A.; Matsuzaki, J.; Yamamoto, Y.; Yoneoka, Y.; Takahashi, K.; Shimizu, H.; Uehara, T.; Ishikawa, M.; Ikeda, S.I.; Sonoda, T.; et al. Integrated extracellular microRNA profiling for ovarian cancer screening. *Nat. Commun.* **2018**, *9*, 4319. <https://doi.org/10.1038/s41467-018-06434-4>.
15. Naghsh-Nilchi, A.; Ebrahimi Ghahnavieh, L.; Dehghanian, F. Construction of miRNA-lncRNA-mRNA co-expression network affecting EMT-mediated cisplatin resistance in ovarian cancer. *J. Cell Mol. Med.* **2022**, *26*, 4530–4547. <https://doi.org/10.1111/jcmm.17477>.
16. Wang, Y.; Bao, W.; Liu, Y.; Wang, S.; Xu, S.; Li, X.; Li, Y.; Wu, S. miR-98-5p contributes to cisplatin resistance in epithelial ovarian cancer by suppressing miR-152 biogenesis via targeting Dicer1. *Cell Death Dis.* **2018**, *9*, 447. <https://doi.org/10.1038/s41419-018-0390-7>.
17. Biegala, L.; Gajek, A.; Marczak, A.; Rogalska, A. Olaparib-Resistant *BRCA2*<sup>MUT</sup> Ovarian Cancer Cells with Restored *BRCA2* Abrogate Olaparib-Induced DNA Damage and G2/M Arrest Controlled by the ATR/CHK1 Pathway for Survival. *Cells* **2023**, *12*, 1038. <https://doi.org/10.3390/cells12071038>.
18. Langdon, S.P.; Lawrie, S.S.; Hay, F.G.; Hawkes, M.M.; McDonald, A.; Hayward, I.P.; Schol, D.J.; Hilgers, J.; Leonard, R.C.; Smyth, J.F. Characterization and properties of nine human ovarian adenocarcinoma cell lines. *Cancer Res.* **1988**, *48*, 6166–6172.
19. Cooke, S.L.; Ng, C.K.; Melnyk, N.; Garcia, M.J.; Hardcastle, T.; Temple, J.; Langdon, S.; Huntsman, D.; Brenton, J.D. Genomic analysis of genetic heterogeneity and evolution in high-grade serous ovarian carcinoma. *Oncogene* **2010**, *29*, 4905–4913. <https://doi.org/10.1038/onc.2010.245>.
20. Schmittgen, T.D.; Livak, K.J. Analyzing real-time PCR data by the comparative C<sub>T</sub> method. *Nat. Protoc.* **2008**, *3*, 1101–1108. <https://doi.org/10.1038/nprot.2008.73>.
21. Mestdagh, P.; Van Vlierberghe, P.; De Weer, A.; Muth, D.; Westermann, F.; Speleman, F.; Vandesompele, J. A novel and universal method for microRNA RT-qPCR data normalization. *Genome Biol.* **2009**, *10*, R64. <https://doi.org/10.1186/gb-2009-10-6-r64>.
22. Chekka, L.M.S.; Langaee, T.; Johnson, J.A. Comparison of Data Normalization Strategies for Array-Based MicroRNA Profiling Experiments and Identification and Validation of Circulating MicroRNAs as Endogenous Controls in Hypertension. *Front. Genet.* **2022**, *13*, 836636. <https://doi.org/10.3389/fgene.2022.836636>.
23. Pradervand, S.; Weber, J.; Thomas, J.; Bueno, M.; Wirapati, P.; Lefort, K.; Dotto, G.P.; Harshman, K. Impact of normalization on miRNA microarray expression profiling. *RNA* **2009**, *15*, 493–501. <https://doi.org/10.1261/rna.1295509>.
24. Chang, T.C.; Yu, D.; Lee, Y.S.; Wentzel, E.A.; Arking, D.E.; West, K.M.; Dang, C.V.; Thomas-Tikhonenko, A.; Mendell, J.T. Widespread microRNA repression by Myc contributes to tumorigenesis. *Nat. Genet.* **2008**, *40*, 43–50. <https://doi.org/10.1038/ng.2007.30>.
25. Guo, Y.; Zhang, Y.; Zhang, S.J.; Ma, Y.N.; He, Y. Comprehensive analysis of key genes and microRNAs in radioresistant nasopharyngeal carcinoma. *BMC Med. Genom.* **2019**, *12*, 73. <https://doi.org/10.1186/s12920-019-0507-6>.
26. Licursi, V.; Conte, F.; Fison, G.; Paci, P. MIENTURNET: An interactive web tool for microRNA-target enrichment and network-based analysis. *BMC Bioinform.* **2019**, *20*, 545. <https://doi.org/10.1186/s12859-019-3105-x>.
27. Chou, C.H.; Shrestha, S.; Yang, C.D.; Chang, N.W.; Lin, Y.L.; Liao, K.W.; Huang, W.C.; Sun, T.H.; Tu, S.J.; Lee, W.H.; et al. miRTarBase update 2018: A resource for experimentally validated microRNA-target interactions. *Nucleic Acids Res.* **2018**, *46*, D296–D302. <https://doi.org/10.1093/nar/gkx1067>.
28. Metsalu, T.; Vilo, J. ClustVis: A web tool for visualizing clustering of multivariate data using Principal Component Analysis and heatmap. *Nucleic Acids Res.* **2015**, *43*, W566–W570. <https://doi.org/10.1093/nar/gkv468>.
29. Chang, L.; Zhou, G.; Soufan, O.; Xia, J. miRNet 2.0: Network-based visual analytics for miRNA functional analysis and systems biology. *Nucleic Acids Res.* **2020**, *48*, W244–W251. <https://doi.org/10.1093/nar/gkaa467>.

30. Dobin, A.; Davis, C.A.; Schlesinger, F.; Drenkow, J.; Zaleski, C.; Jha, S.; Batut, P.; Chaisson, M.; Gingeras, T.R. STAR: Ultrafast universal RNA-seq aligner. *Bioinformatics* **2013**, *29*, 15–21. <https://doi.org/10.1093/bioinformatics/bts635>.
31. Durno, K.; Powell, M.E. The role of radiotherapy in ovarian cancer. *Int. J. Gynecol. Cancer* **2022**, *32*, 366–371. <https://doi.org/10.1136/ijgc-2021-002462>.
32. Ledermann, J.A.; Matias-Guiu, X.; Amant, F.; Concin, N.; Davidson, B.; Fotopoulou, C.; Gonzalez-Martin, A.; Gourley, C.; Leary, A.; Lorusso, D.; et al. ESGO-ESMO-ESP consensus conference recommendations on ovarian cancer: Pathology and molecular biology and early, advanced and recurrent disease. *Ann. Oncol.* **2024**, *35*, P248–P266. <https://doi.org/10.1016/j.annonc.2023.11.015>.
33. Ritchie, M.E.; Phipson, B.; Wu, D.; Hu, Y.; Law, C.W.; Shi, W.; Smyth, G.K. limma powers differential expression analyses for RNA-sequencing and microarray studies. *Nucleic Acids Res.* **2015**, *43*, e47. <https://doi.org/10.1093/nar/gkv007>.
34. Bartha, A.; Gyorffy, B. TNMplot.com: A Web Tool for the Comparison of Gene Expression in Normal, Tumor and Metastatic Tissues. *Int. J. Mol. Sci.* **2021**, *22*, 2622. <https://doi.org/10.3390/ijms22052622>.
35. Ouyang, J.; Qin, G.; Liu, Z.; Jian, X.; Shi, T.; Xie, L. ToPP: Tumor online prognostic analysis platform for prognostic feature selection and clinical patient subgroup selection. *iScience* **2022**, *25*, 104190. <https://doi.org/10.1016/j.isci.2022.104190>.
36. Uhlen, M.; Fagerberg, L.; Hallstrom, B.M.; Lindskog, C.; Oksvold, P.; Mardinoglu, A.; Sivertsson, A.; Kampf, C.; Sjostedt, E.; Asplund, A.; et al. Proteomics. Tissue-based map of the human proteome. *Science* **2015**, *347*, 1260419. <https://doi.org/10.1126/science.1260419>.
37. Poveda, A.; Floquet, A.; Ledermann, J.A.; Asher, R.; Penson, R.T.; Oza, A.M.; Korach, J.; Huzarski, T.; Pignata, S.; Friedlander, M.; et al. Olaparib tablets as maintenance therapy in patients with platinum-sensitive relapsed ovarian cancer and a *BRCA1/2* mutation (SOLO2/ENGOT-Ov21): A final analysis of a double-blind, randomised, placebo-controlled, phase 3 trial. *Lancet Oncol.* **2021**, *22*, 620–631. [https://doi.org/10.1016/S1470-2147\(21\)00073-5](https://doi.org/10.1016/S1470-2147(21)00073-5).
38. Ceccaldi, R.; O'Connor, K.W.; Mouw, K.W.; Li, A.Y.; Matulonis, U.A.; D'Andrea, A.D.; Konstantinopoulos, P.A. A unique subset of epithelial ovarian cancers with platinum sensitivity and PARP inhibitor resistance. *Cancer Res.* **2015**, *75*, 628–634. <https://doi.org/10.1158/0008-5472.CAN-14-2593>.
39. Veneziani, A.C.; Scott, C.; Wakefield, M.J.; Tinker, A.V.; Lheureux, S. Fighting resistance: Post-PARP inhibitor treatment strategies in ovarian cancer. *Ther. Adv. Med. Oncol.* **2023**, *15*, 17588359231157644. <https://doi.org/10.1177/17588359231157644>.
40. Kim, H.; Xu, H.; George, E.; Hallberg, D.; Kumar, S.; Jagannathan, V.; Medvedev, S.; Kinose, Y.; Devins, K.; Verma, P.; et al. Combining PARP with ATR inhibition overcomes PARP inhibitor and platinum resistance in ovarian cancer models. *Nat. Commun.* **2020**, *11*, 3726. <https://doi.org/10.1038/s41467-020-17127-2>.
41. Watson, Z.L.; Yamamoto, T.M.; McMellen, A.; Kim, H.; Hughes, C.J.; Wheeler, L.J.; Post, M.D.; Behbakht, K.; Bitler, B.G. Histone methyltransferases EHMT1 and EHMT2 (GLP/G9A) maintain PARP inhibitor resistance in high-grade serous ovarian carcinoma. *Clin. Epigenetics* **2019**, *11*, 165. <https://doi.org/10.1186/s13148-019-0758-2>.
42. Nam, E.J.; Kim, S.; Lee, T.S.; Kim, H.J.; Lee, J.Y.; Kim, S.W.; Kim, J.H.; Kim, Y.T. Primary and recurrent ovarian high-grade serous carcinomas display similar microRNA expression patterns relative to those of normal ovarian tissue. *Oncotarget* **2016**, *7*, 70524–70534. <https://doi.org/10.18632/oncotarget.12045>.
43. Nicholson, H.A.; Sawers, L.; Clarke, R.G.; Hiom, K.J.; Ferguson, M.J.; Smith, G. Fibroblast growth factor signalling influences homologous recombination-mediated DNA damage repair to promote drug resistance in ovarian cancer. *Br. J. Cancer* **2022**, *127*, 1340–1351. <https://doi.org/10.1038/s41416-022-01899-z>.
44. Zhao, J.; Tan, W.; Zhang, L.; Liu, J.; Shangguan, M.; Chen, J.; Zhao, B.; Peng, Y.; Cui, M.; Zhao, S. FGFR3 phosphorylates EGFR to promote cisplatin-resistance in ovarian cancer. *Biochem. Pharmacol.* **2021**, *190*, 114536. <https://doi.org/10.1016/j.bcp.2021.114536>.
45. Kumari, A.; Shonibare, Z.; Monavarian, M.; Arend, R.C.; Lee, N.Y.; Inman, G.J.; Mythreya, K. TGFbeta signaling networks in ovarian cancer progression and plasticity. *Clin. Exp. Metastasis* **2021**, *38*, 139–161. <https://doi.org/10.1007/s10585-021-10077-z>.
46. Jackson, L.M.; Dhoonmoon, A.; Hale, A.; Dennis, K.A.; Schleicher, E.M.; Nicolae, C.M.; Moldovan, G.L. Loss of MED12 activates the TGFbeta pathway to promote chemoresistance and replication fork stability in BRCA-deficient cells. *Nucleic Acids Res.* **2021**, *49*, 12855–12869. <https://doi.org/10.1093/nar/gkab1184>.
47. Le, B.V.; Podsiyalow-Bartnicka, P.; Maifrede, S.; Sullivan-Reed, K.; Nieborowska-Skorska, M.; Golovine, K.; Yao, J.C.; Nejati, R.; Cai, K.Q.; Caruso, L.B.; et al. TGFβR-SMAD3 Signaling Induces Resistance to PARP Inhibitors in the Bone Marrow Microenvironment. *Cell Rep.* **2020**, *33*, 108221. <https://doi.org/10.1016/j.celrep.2020.108221>.
48. Guo, H.; Ha, C.; Dong, H.; Yang, Z.; Ma, Y.; Ding, Y. Cancer-associated fibroblast-derived exosomal microRNA-98-5p promotes cisplatin resistance in ovarian cancer by targeting CDKN1A. *Cancer Cell Int.* **2019**, *19*, 347. <https://doi.org/10.1186/s12935-019-1051-3>.
49. Deng, J.; Bai, X.; Feng, X.; Ni, J.; Beretov, J.; Graham, P.; Li, Y. Inhibition of PI3K/Akt/mTOR signaling pathway alleviates ovarian cancer chemoresistance through reversing epithelial-mesenchymal transition and decreasing cancer stem cell marker expression. *BMC Cancer* **2019**, *19*, 618. <https://doi.org/10.1186/s12885-019-5824-9>.
50. Xu, J.; Gao, Y.; Luan, X.; Li, K.; Wang, J.; Dai, Y.; Kang, M.; Lu, C.; Zhang, M.; Lu, C.X.; et al. An effective AKT inhibitor-PARP inhibitor combination therapy for recurrent ovarian cancer. *Cancer Chemother. Pharmacol.* **2022**, *89*, 683–695. <https://doi.org/10.1007/s00280-022-04403-9>.
51. Selvendiran, K.; Tong, L.; Vishwanath, S.; Bratasz, A.; Trigg, N.J.; Kutala, V.K.; Hideg, K.; Kuppusamy, P. EF24 induces G2/M arrest and apoptosis in cisplatin-resistant human ovarian cancer cells by increasing PTEN expression. *J. Biol. Chem.* **2007**, *282*, 28609–28618. <https://doi.org/10.1074/jbc.M703796200>.



52. Liu, J.; Lichtenberg, T.; Hoadley, K.A.; Poisson, L.M.; Lazar, A.J.; Cherniack, A.D.; Kovatich, A.J.; Benz, C.C.; Levine, D.A.; Lee, A.V.; et al. An Integrated TCGA Pan-Cancer Clinical Data Resource to Drive High-Quality Survival Outcome Analytics. *Cell* **2018**, *173*, 400–416.e11. <https://doi.org/10.1016/j.cell.2018.02.052>.
53. Zhang, H.; Xu, S.; Liu, X. MicroRNA profiling of plasma exosomes from patients with ovarian cancer using high-throughput sequencing. *Oncol. Lett.* **2019**, *17*, 5601–5607. <https://doi.org/10.3892/ol.2019.10220>.
54. Gao, Q.; Yang, Z.; Xu, S.; Li, X.; Yang, X.; Jin, P.; Liu, Y.; Zhou, X.; Zhang, T.; Gong, C.; et al. Heterotypic CAF-tumor spheroids promote early peritoneal metastasis of ovarian cancer. *J. Exp. Med.* **2019**, *216*, 688–703. <https://doi.org/10.1084/jem.20180765>.
55. Bieg, D.; Sypniewski, D.; Nowak, E.; Bednarek, I. MiR-424-3p suppresses galectin-3 expression and sensitizes ovarian cancer cells to cisplatin. *Arch. Gynecol. Obstet.* **2019**, *299*, 1077–1087. <https://doi.org/10.1007/s00404-018-4999-7>.
56. Qiu, L.; Zhang, G.F.; Yu, L.; Wang, H.Y.; Jia, X.J.; Wang, T.J. Novel oncogenic and chemoresistance-inducing functions of resistin in ovarian cancer cells require miRNAs-mediated induction of epithelial-to-mesenchymal transition. *Sci. Rep.* **2018**, *8*, 12522. <https://doi.org/10.1038/s41598-018-30978-6>.
57. Zhao, L.; Zhang, P.; Su, X.J.; Zhang, B. The ubiquitin ligase TRIM56 inhibits ovarian cancer progression by targeting vimentin. *J. Cell Physiol.* **2018**, *233*, 2420–2425. <https://doi.org/10.1002/jcp.26114>.
58. Dall'Acqua, A.; Sonego, M.; Pellizzari, I.; Pellarin, I.; Canzonieri, V.; D'Andrea, S.; Benevol, S.; Sorio, R.; Giorda, G.; Califano, D.; et al. CDK6 protects epithelial ovarian cancer from platinum-induced death via FOXO3 regulation. *EMBO Mol. Med.* **2017**, *9*, 1415–1433. <https://doi.org/10.15252/emmm.201607012>.
59. Vescarelli, E.; Gerini, G.; Megiorni, F.; Anastasiadou, E.; Pontecorvi, P.; Solito, L.; De Vitis, C.; Camero, S.; Marchetti, C.; Mancini, R.; et al. MiR-200c sensitizes Olaparib-resistant ovarian cancer cells by targeting Neuropilin 1. *J. Exp. Clin. Cancer Res.* **2020**, *39*, 3. <https://doi.org/10.1186/s13046-019-1490-7>.
60. Zhong, Q.; Xiong, Y.; Ling, C.; Qian, Y.; Zhao, X.; Yang, H. Enhancing the sensitivity of ovarian cancer cells to olaparib via microRNA-20b-mediated cyclin D1 targeting. *Exp. Biol. Med.* **2021**, *246*, 1297–1306. <https://doi.org/10.1177/1535370221994077>.
61. Roberts, C.M.; Rojas-Alexandre, M.; Hanna, R.E.; Lin, Z.P.; Ratner, E.S. Transforming Growth Factor Beta and Epithelial to Mesenchymal Transition Alter Homologous Recombination Repair Gene Expression and Sensitize BRCA Wild-Type Ovarian Cancer Cells to Olaparib. *Cancers* **2023**, *15*, 3919. <https://doi.org/10.3390/cancers15153919>.
62. Li, H.; Panina, S.; Kaur, A.; Ruano, M.J.; Sanchez-Gonzalez, P.; la Cour, J.M.; Stephan, A.; Olesen, U.H.; Berchtold, M.W.; Villalobo, A. Regulation of the ligand-dependent activation of the epidermal growth factor receptor by calmodulin. *J. Biol. Chem.* **2012**, *287*, 3273–3281. <https://doi.org/10.1074/jbc.M111.317529>.
63. Ranjbar, R.; Nejatollahi, F.; Nedaei Ahmadi, A.S.; Hafezi, H.; Safaie, A. Expression of Vascular Endothelial Growth Factor (VEGF) and Epidermal Growth Factor Receptor (EGFR) in Patients With Serous Ovarian Carcinoma and Their Clinical Significance. *Iran. J. Cancer Prev.* **2015**, *8*, e3428. <https://doi.org/10.17795/ijcp-3428>.
64. Huang, D.; Ke, L.; Cui, H.; Li, S.; Sun, F. Efficacy and safety of VEGF/VEGFR inhibitors for platinum-resistant ovarian cancer: A systematic review and meta-analysis of randomized controlled trials. *BMC Womens Health* **2024**, *24*, 34. <https://doi.org/10.1186/s12905-023-02879-y>.
65. Li, Z.; Liu, J.Y.; Zhang, J.T. 14-3-3sigma, the double-edged sword of human cancers. *Am. J. Transl. Res.* **2009**, *1*, 326–340.
66. Akahira, J.; Sugihashi, Y.; Suzuki, T.; Ito, K.; Niikura, H.; Moriya, T.; Nitta, M.; Okamura, H.; Inoue, S.; Sasano, H.; et al. Decreased expression of 14-3-3 sigma is associated with advanced disease in human epithelial ovarian cancer: Its correlation with aberrant DNA methylation. *Clin. Cancer Res.* **2004**, *10*, 2687–2693. <https://doi.org/10.1158/1078-0432.ccr-03-0510>.
67. Yasuda, K.; Torigoe, T.; Mariya, T.; Asano, T.; Kuroda, T.; Matsuzaki, J.; Ikeda, K.; Yamauchi, M.; Emori, M.; Asanuma, H.; et al. Fibroblasts induce expression of FGF4 in ovarian cancer stem-like cells/cancer-initiating cells and upregulate their tumor initiation capacity. *Lab. Investig.* **2014**, *94*, 1355–1369. <https://doi.org/10.1038/labinvest.2014.122>.
68. Wei, W.; Li, Y.; Lv, S.; Zhang, C.; Tian, Y. PARP-1 may be involved in angiogenesis in epithelial ovarian cancer. *Oncol. Lett.* **2016**, *12*, 4561–4567. <https://doi.org/10.3892/ol.2016.5226>.
69. Wang, Y.; Xiang, J.; Wang, J.; Ji, Y. Downregulation of TGF-β1 suppressed proliferation and increased chemosensitivity of ovarian cancer cells by promoting BRCA1/Smad3 signaling. *Biol. Res.* **2018**, *51*, 58. <https://doi.org/10.1186/s40659-018-0205-4>.
70. Usman, S.; Waseem, N.H.; Nguyen, T.K.N.; Mohsin, S.; Jamal, A.; Teh, M.T.; Waseem, A. Vimentin Is at the Heart of Epithelial Mesenchymal Transition (EMT) Mediated Metastasis. *Cancers* **2021**, *13*, 4985. <https://doi.org/10.3390/cancers13194985>.
71. Su, S.; Lin, X.; Ding, N.; Zhang, H.; Zhang, Q.; Ding, Y.; Hou, X.; Tian, Y. Effects of PARP-1 inhibitor and ERK inhibitor on epithelial mesenchymal transitions of the ovarian cancer SKOV3 cells. *Pharmacol. Rep.* **2016**, *68*, 1225–1229. <https://doi.org/10.1016/j.pharep.2016.08.001>.
72. Li, L.Y.; Kim, H.J.; Park, S.A.; Lee, S.H.; Kim, L.K.; Lee, J.Y.; Kim, S.; Kim, Y.T.; Kim, S.W.; Nam, E.J. Genetic Profiles Associated with Chemoresistance in Patient-Derived Xenograft Models of Ovarian Cancer. *Cancer Res. Treat.* **2019**, *51*, 1117–1127. <https://doi.org/10.4143/crt.2018.405>.

**Disclaimer/Publisher's Note:** The statements, opinions and data contained in all publications are solely those of the individual author(s) and contributor(s) and not of MDPI and/or the editor(s). MDPI and/or the editor(s) disclaim responsibility for any injury to people or property resulting from any ideas, methods, instructions or products referred to in the content.

# SUPPLEMENTARY INFORMATION

## Uncovering miRNA-mRNA regulatory networks related to olaparib resistance and resensitization of *BRCA2*<sup>MUT</sup> ovarian cancer PEO1-OR cells with the ATR/CHK1 pathway inhibitors

Łukasz Biegała<sup>1,2</sup>, Damian Kołat<sup>3,4</sup>, Arkadiusz Gajek<sup>1</sup>, Elżbieta Płuciennik<sup>3</sup>, Agnieszka Marczak<sup>1</sup>, Agnieszka Śliwińska<sup>5,\*</sup>, Michał Mikula<sup>6</sup>, Aneta Rogalska<sup>1,\*</sup>

### TABLE OF CONTENTS

#### ► **Supplementary Methods:**

Screening of endogenous control genes for qPCR studies with Custom TaqMan™ Array MicroRNA Cards.

#### ► **Supplementary Data:**

Identification of endogenous controls for use with custom TaqMan™ Array MicroRNA Cards.

#### ► **Supplementary Figures:**

**Figure S1:** Network of miRNA-target interactions created with the MIENTURNET tool for dysregulated miRNAs identified from screening analysis with pre-designed TaqMan™ Array MicroRNA Cards and pre-selected for further validation.

**Figure S2:** Selection of candidate endogenous control genes with the RefFinder tool based on results from Pre-designed TaqMan™ Array MicroRNA Cards for further RT-qPCR studies with Custom TaqMan™ Array MicroRNA Cards.

**Figure S3:** Validation of endogenous control genes stable expression in HGSOC cell lines for RT-qPCR data normalization from Custom TaqMan™ MicroRNA Cards.

**Figure S4:** Results of RT-qPCR-based differential miRNA basal expression analysis in untreated PEO1, PEO1-OR, and PEO4 cell lines after 2 days of cell culture (Custom TaqMan™ MicroRNA Cards).

**Figure S5:** Results of RT-qPCR-based differential miRNA expression analysis in PEO1 cell line incubated with olaparib (O), ATRi (A), CHK1i (C), or their combinations for 2 days (Custom TaqMan™ MicroRNA Cards).

**Figure S6:** Results of RT-qPCR-based differential miRNA expression analysis in PEO1-OR cell line incubated with olaparib (O), ATRi (A), CHK1i (C), or their combinations for 2 days (Custom TaqMan™ MicroRNA Cards).

**Figure S7:** Results of RT-qPCR-based differential miRNA expression analysis in PEO4 cell line incubated with olaparib (O), ATRi (A), CHK1i (C), or their combinations for 2 days (Custom TaqMan™ MicroRNA Cards).

**Figure S8:** Network-based functional enrichment analyses of significantly differentially expressed miRNAs and their target genes in PEO1 cell line incubated with olaparib combinations for 2 days.

**Figure S9:** Results of semi-quantitative analysis with antibody microarrays for growth factors with significantly dysregulated expression in PEO1 cells (absolute fold change  $\geq 1.5$ ,  $p < 0.05$ ).

**Figure S10:** Raw results of semi-quantitative analysis of 41 growth factors expression in PEO1 and PEO1-OR cells incubated with tested inhibitors or their combinations for 2 days.

**Figure S11:** Kaplan-Meier plots showing the relationship between miRNAs and clinical endpoints (OS – overall survival, PFI – progression-free intervals) in serous OC patients.

**Figure S12:** Kaplan-Meier plots showing the relationship between target genes and clinical endpoints (OS – overall survival, PFI – progression-free intervals) in serous OC patients.

**Figure S13:** Kaplan-Meier plots showing the relationship between target genes and clinical endpoints (OS – overall survival, PFI – progression-free intervals) in serous OC patients (continued).

► **Supplementary Tables:**

**Table S1:** List of key reagents used in the study.

**Table S2:** Selection of 44 out of 69 dysregulated miRNAs for validation on Custom TaqMan™ MicroRNA Cards based on bioinformatics analyses and literature review.

**Table S3:** List of analyzed miRNAs and small RNAs for miRNA validation with Custom TaqMan™ MicroRNA Cards.

**Table S4:** Average fold change values of significantly differentially expressed miRNAs in HGSOC cell lines with (Custom TaqMan™ MicroRNA Cards).

**Table S5:** Top significantly enriched pathways (Reactome) and biological processes (GO:BP) associated with target genes of dysregulated miRNAs in untreated PEO1-OR cells.

**Table S6:** Top significantly enriched pathways (Reactome) associated with target genes of dysregulated miRNAs in PEO1-OR cells in response to combinations of olaparib with the ATR/CHK1 pathway inhibitors.

**Table S7:** Experimentally validated targets of differentially expressed miRNAs from minimal subnetworks that maximally connect seeds in the PEO1-OR cell line (established with miRNet 2.0).

**Table S8:** Identification of hub nodes using CytoHubba plug-in based on the minimal miRNA-mRNA networks using maximal clique centrality (MCC) algorithm.

**Table S9:** Results of stage-wise differential miRNA and gene expression analysis in serous OC patients using filtered data from TCGA-OV dataset (serous OC patients with stage II, III, or IV after pharmaceutical therapy).

**Table S10:** Validation of endogenous control genes stable expression in HGSOC cell lines for RT-qPCR data normalization from Custom TaqMan™ MicroRNA Cards.

## SUPPLEMENTARY METHODS

---

### Screening and validation of endogenous control genes for qPCR studies with Custom TaqMan™ Array MicroRNA Cards

The global mean normalization method, used to normalize data from RT-qPCR miRNA profiling studies with Pre-designed TaqMan™ Array MicroRNA Cards, is accurate in studies where many miRNAs are tested per sample. Custom TaqMan™ Array MicroRNA Cards contain one assay for U6 snRNA as a common candidate endogenous control gene by default. To identify additional stably expressed genes for data normalization before the design of Custom TaqMan™ Array MicroRNA Cards for 44 target miRNAs, we screened for two more reference genes based on the results from global miRNA profiling studies for 754 miRNAs. Firstly, raw  $C_T$  data from screening experiments was filtered to consider miRNAs which were reliably detected in all untreated and treated samples in PEO1 and PEO1-OR cells ( $C_T$  value < 35) and were abundantly expressed in both cell lines (average  $C_T$  value < 28). Briefly, suitable reference genes were identified based on gene stability rankings calculated with the RefFinder web-based tool. This algorithm allows the computation of the overall final ranking based on weights calculated with four different programs (geNorm, NormFinder, BestKeeper, and the comparative  $\Delta C_T$  method). Genes were prioritized according to the highest geometric mean of weights for the final rankings (stability), lowest  $C_T$  value (expression level), and lowest standard deviations of  $C_T$  (variability among groups). One gene for small RNA (RNU48 snoRNA) and one for miRNA (miRNA-30e-3p) with the highest expression stability, lowest standard deviation among groups, and highest expression level (lowest  $C_T$ ) were selected as additional candidates for reference genes in further quantitative RT-qPCR analyses.

## SUPPLEMENTARY DATA

---

### Identification of endogenous controls for use with custom TaqMan™ Array MicroRNA Cards

Small-scale miRNA gene expression studies should be preceded by a selection of the most stable small RNA controls for accurate normalization of miRNA expression data. Traditional use of a single gene for normalization might lead to relatively substantial errors. Hence, we used prior RT-qPCR data from large-scale miRNA profiling with predesigned TaqMan™ Array MicroRNA Cards to identify three reliable endogenous controls for use in normalization by multiple housekeeping genes with Custom Cards. We initially confirmed the stability of candidate endogenous control introduced on cards by default (U6 snRNA) and recommended by the manufacturer (RNU48) in both PEO1 and PEO1-OR cells. Comparison of a geometric mean of ranking values from RefFinder, average  $C_T$  values, and standard deviation of  $C_T$  for genes included in the analysis are presented in Figure S2. Out of all included miRNAs, we have evaluated 11 miRNAs meeting the inclusion criteria. miR-30e-3p was selected as the most stably and relatively abundantly expressed miRNA upon tested treatment conditions based on summed gene stability ranking evaluated with RefFinder tool, calculated average  $C_T$  values and its average standard deviation ( $C_T = 26.7 \pm 0.17$ ) in both PEO1 and PEO1-OR cells (Figure S2).

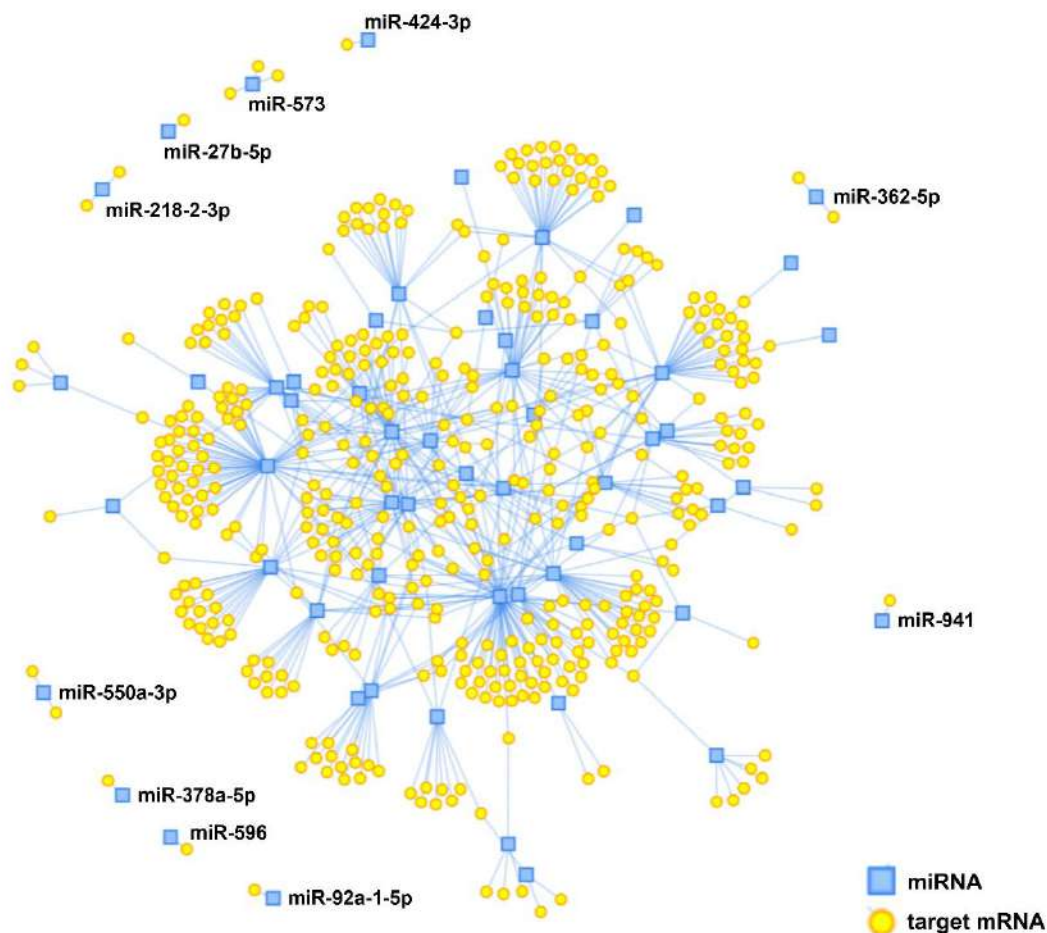
Three pre-selected endogenous control genes (U6 snRNA, RNU48 snoRNA, and miR-30e-3p) were evaluated for stable expression across treatment conditions in PEO1, PEO4, and PEO1-OR cell lines to confirm their stability in the final qPCR-based miRNA quantification experiments with Custom TaqMan™ Array MicroRNA Cards. The average  $C_T$  values and standard deviation of  $C_T$  and average  $C_T$  range across treatments in all HGSOC cell lines (Table S10) for all three endogenous control genes were used as a direct measure of the stability of these genes.

The low variation of expression values ( $C_T$  range of 0.19 – 0.67 and SD of average  $C_T$  of 0.08 – 0.22) indicated a very small dispersion among samples under studied treatment conditions (Table 2).  $C_T$  values for each group were presented on graphs in Figure S3. Comparison of  $C_T$  means among untreated and treated groups in all HGSOC cell lines showed no statistically significant difference for endogenous control gene expression (Table S10 and Figure S3). Hence, a multiple reference gene normalization strategy was applied to normalize RT-qPCR miRNA expression data for 44 target miRNAs.

## SUPPLEMENTARY FIGURES

### Supplementary Figure 1 (Figure S1)

a



b

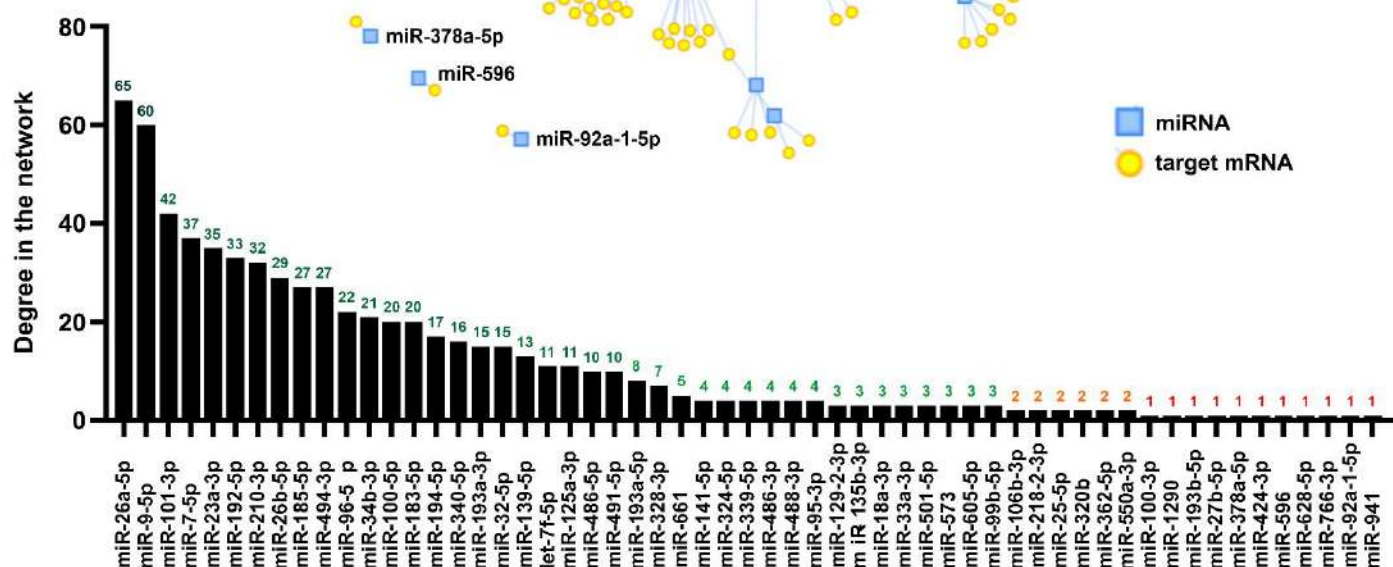


**Figure S1. Network of miRNA-target interactions created with the MIENTURNET tool for dysregulated miRNAs identified from screening analysis with pre-designed TaqMan™ Array MicroRNA Cards and pre-selected for further validation. (a)** Visualization of miRNA-target interaction network. Blue squares refer to miRNAs, while yellow circles refer to their target genes. miRNA not connected with the network were highlighted by their names. **(b)** Bar plot representing network degree for miRNAs.



## Supplementary Figure 2 (Figure S2)

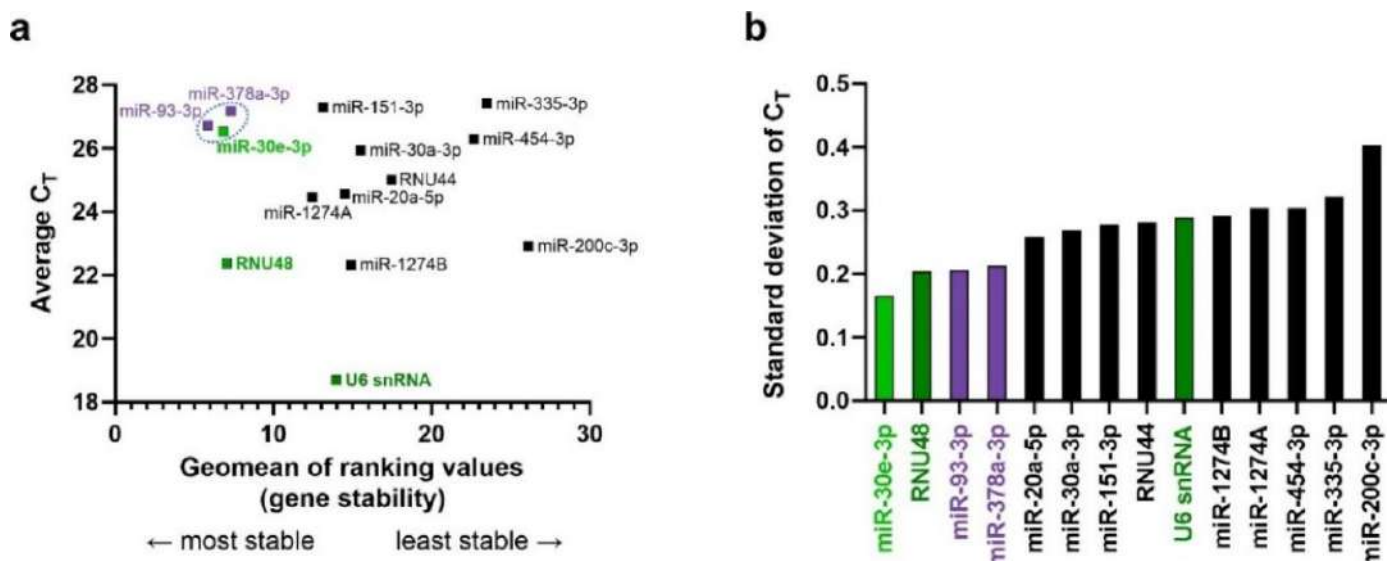


**Figure S2. Selection of candidate endogenous control genes with the RefFinder tool based on results from Pre-designed TaqMan™ Array MicroRNA Cards for further RT-qPCR studies with Custom TaqMan™ Array MicroRNA Cards.** Raw  $C_T$  values for each MicroRNA or gene were used to identify the most stable reference genes among groups in untreated and treated PEO1 and PEO1-OR cells. One small RNA from each class (snRNA, snoRNA, and miRNA) was selected as a reference gene. U6 snRNA is a fixed endogenous control introduced on TLDA Cards by the manufacturer. **(a)** Evaluation of candidate gene expression stability based on their geometric mean of ranking values calculated with RefFinder (x-axis) and average  $C_T$  values (expression level on y-axis). Undetected miRNAs in any group ( $C_T \geq 35$ ) and detected miRNAs with low expression among groups ( $C_T \geq 28$ ) were excluded from the analysis. The remaining miRNAs were used to evaluate their stability using the RefFinder web-based tool. Reference genes were prioritized according to their stability rankings derived from the four programs (geNorm, NormFinder, BestKeeper, and the comparative  $\Delta C_T$  method). Geomean of ranking values is a sum of values calculated separately for PEO1 and PEO1-OR cells. Averaged  $C_T$  is a mean value calculated separately for PEO1 and PEO1-OR cells. RNU48 exhibited the highest stability among the two analyzed snRNAs and was selected as the second reference gene. Among all analyzed miRNAs, three showed the highest gene stability and similarly modern expression levels ( $C_T$  from 26.7 – 27.2): miR-30e-3p, miR93-3p, and miR-378a-3p (marked with a blue oval). **(b)** The average standard deviation of  $C_T$  values for miRNAs among groups was used to select miRNA with the lowest expression variability. Out of three miRNAs pre-selected with RefFinder (miR-30e-3p, miR93-3p, and miR-378a-3p), miR-30e-3p expression was the most consistent among groups (SD = 0.17). Moreover, it showed the lowest average  $C_T$  and it was selected as the third reference gene.

### Supplementary Figure 3 (Figure S3)

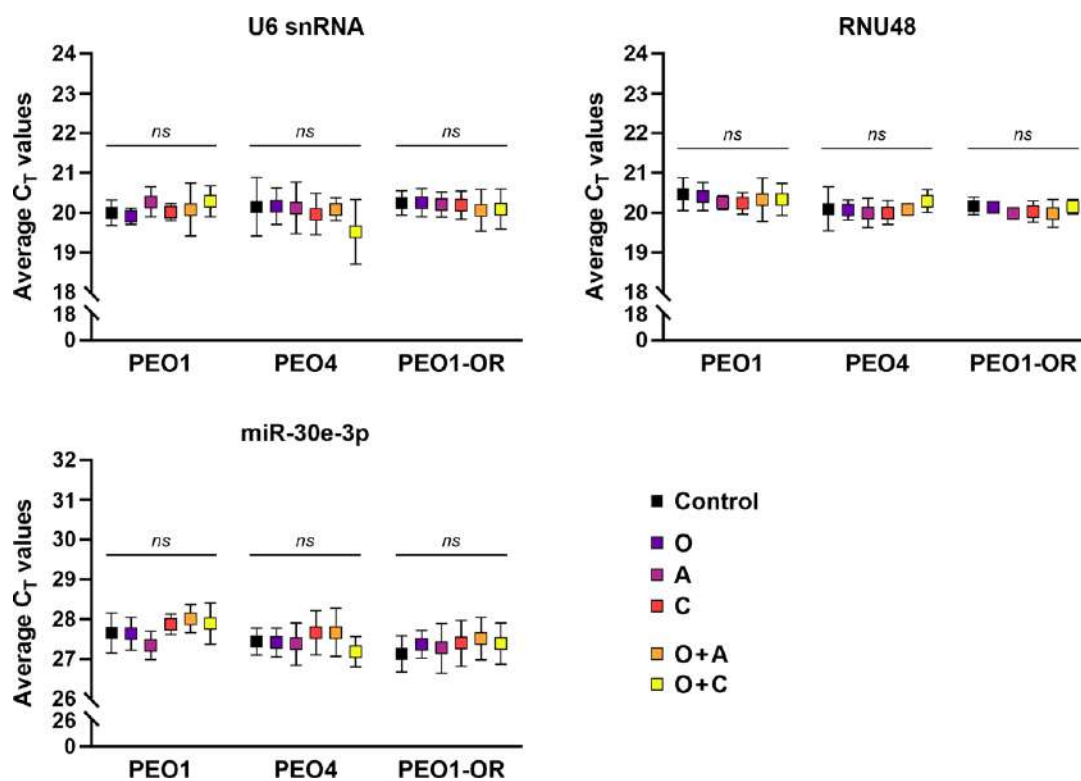


**Figure S3. Validation of endogenous control genes stable expression in HGSOC cell lines for RT-qPCR data normalization from Custom TaqMan™ MicroRNA Cards.** Symbols on graphs represent average  $C_T$  values ( $\pm$  SD) from four independent biological replicates ( $n = 4$ ). Significant differences in average  $C_T$  values between treatments for each gene and cell line were evaluated with ordinary one-way ANOVA followed by Tukey's post-hoc test. The abbreviation "ns" indicates a nonsignificant difference. O – olaparib, A – ATRi, C – CHK1i.

## Supplementary Figure 4 (Figure S4)

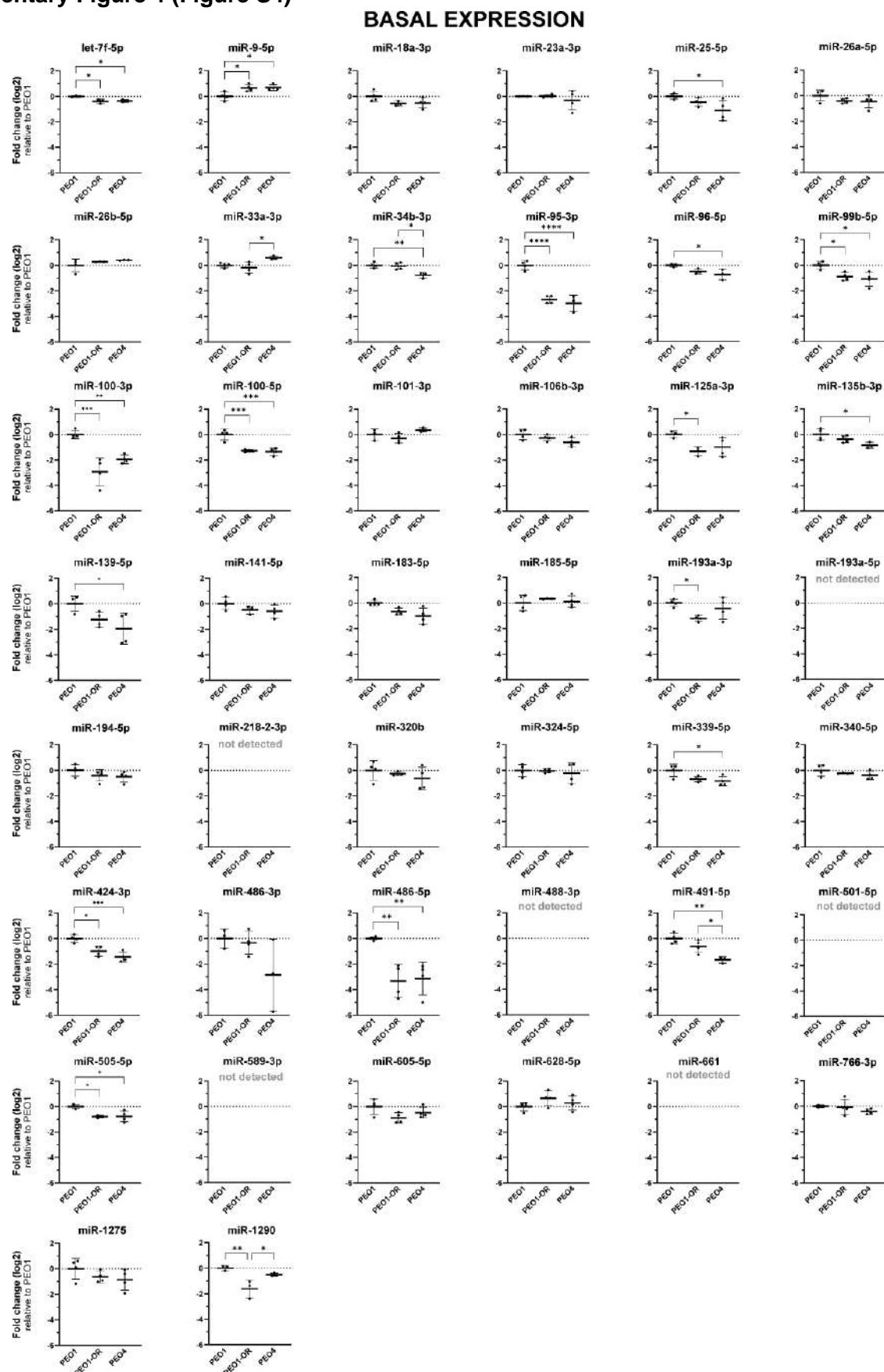


**Figure S4. Results of RT-qPCR-based differential miRNA basal expression analysis in untreated PEO1, PEO1-OR, and PEO4 cell lines after 2 days of cell culture (Custom TaqMan™ MicroRNA Cards).** Relative levels of miRNAs were expressed as means of logarithmic fold change  $\pm$  SD ( $n = 3 - 4$ ). Statistical significance was assessed compared to PEO1 cells with one-way ANOVA followed by multiple comparison tests: \* $p < 0.05$ , \*\* $p < 0.01$ , \*\*\* $p < 0.001$ , \*\*\*\* $p < 0.0001$ .

## Supplementary Figure 5 (Figure S5)

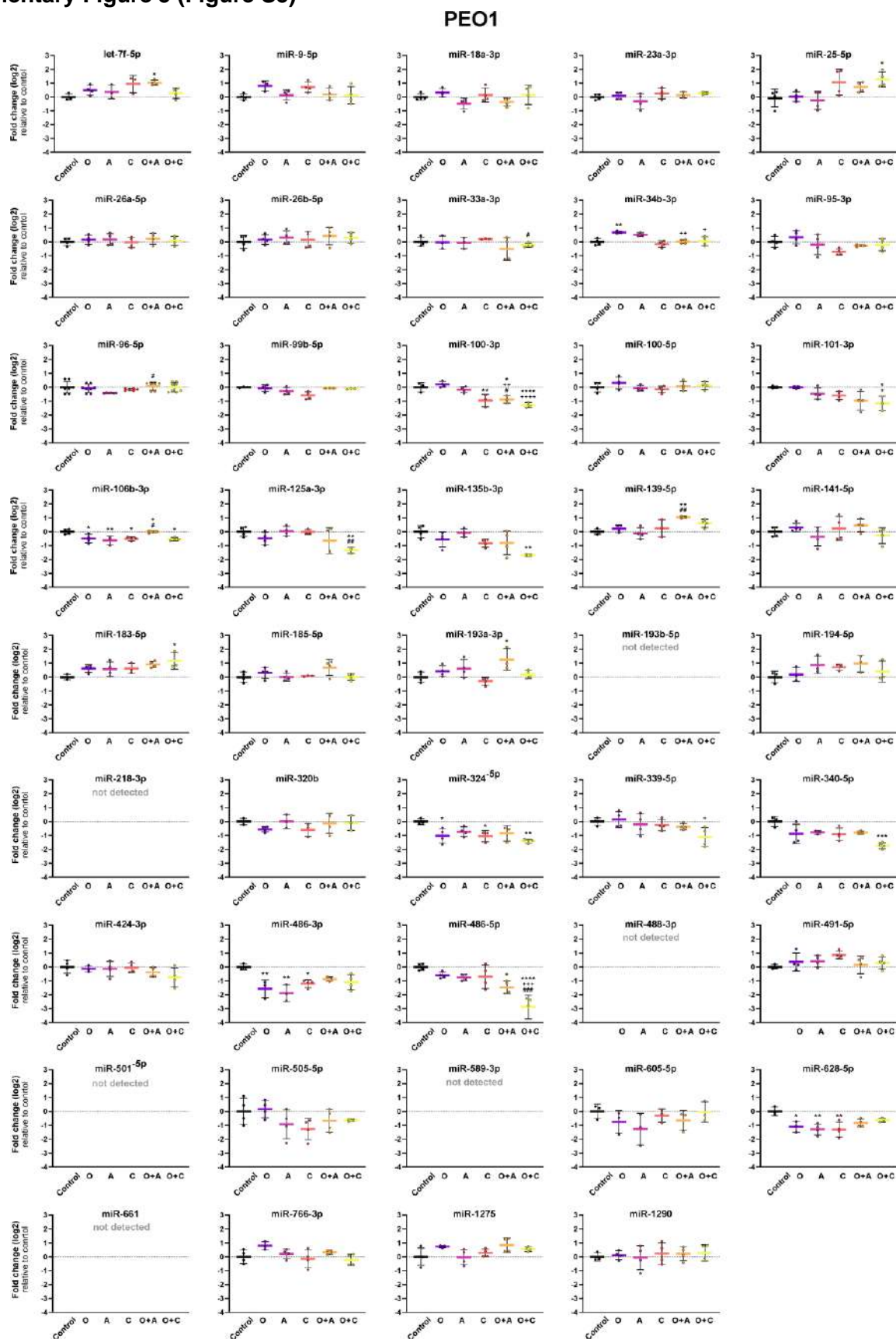


**Figure S5. Results of RT-qPCR-based differential miRNA expression analysis in PEO1 cell line incubated with olaparib (O), ATRi (A), CHK1i (C), or their combinations for 2 days (Custom TaqMan™ MicroRNA Cards).** Relative levels of miRNAs were expressed as means of logarithmic fold change  $\pm$  SD ( $n = 3 - 4$ ). Statistical significance was assessed with one-way ANOVA followed by multiple comparison tests: \* $p < 0.05$ , \*\* $p < 0.01$ , \*\*\* $p < 0.001$ , \*\*\*\* $p < 0.0001$  (treatment vs. control); + $p < 0.05$ , ++ $p < 0.01$ , +++ $p < 0.001$ , ++++ $p < 0.0001$  (O vs. combination with A or C); # $p < 0.05$ , ## $p < 0.01$ , ### $p < 0.001$ , #### $p < 0.0001$  (A or C vs. respective combinations with O).

## Supplementary Figure 6 (Figure S6)

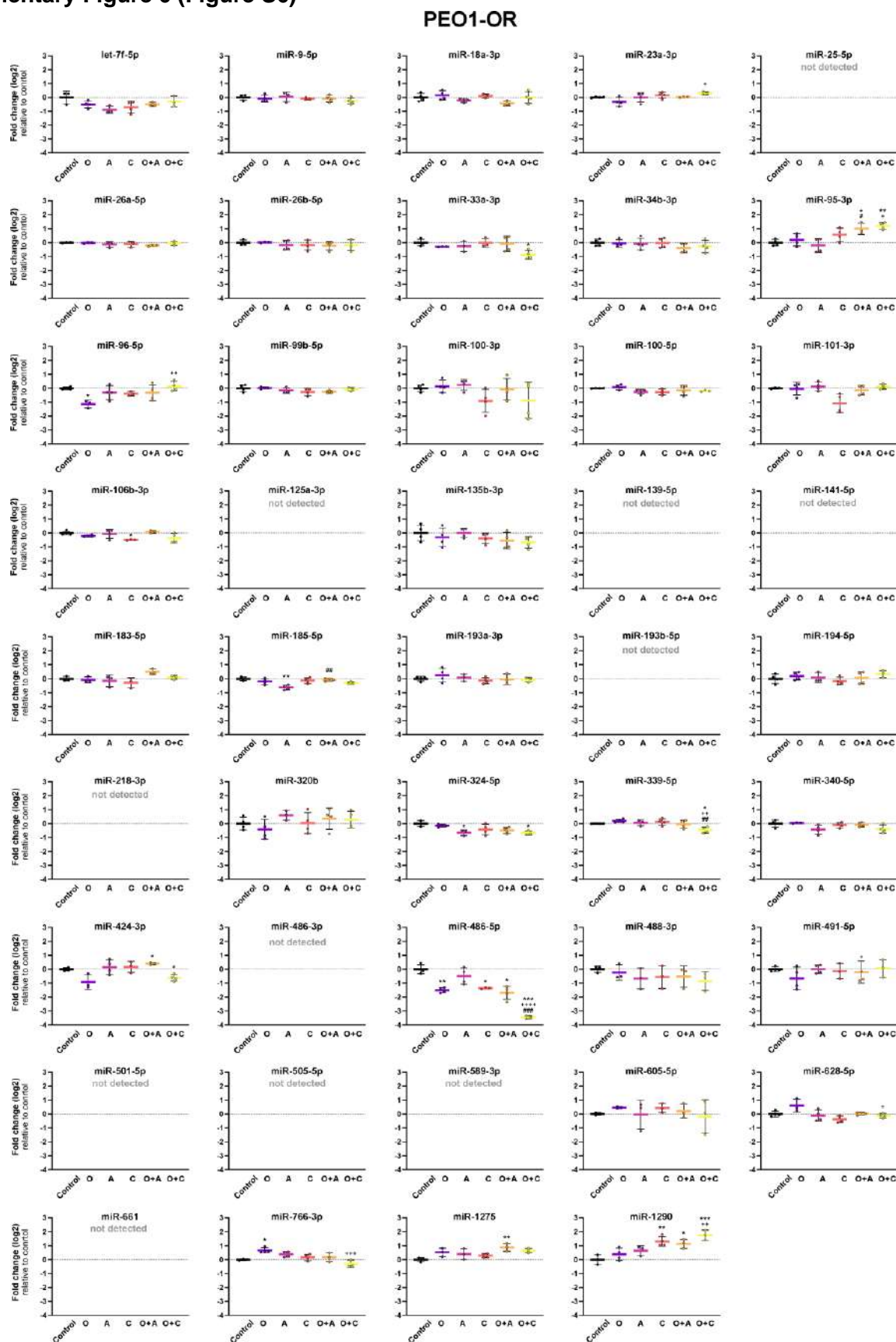


**Figure S6. Results of RT-qPCR-based differential miRNA expression analysis in PEO1-OR cell line incubated with olaparib (O), ATRi (A), CHK1i (C), or their combinations for 2 days (Custom TaqMan™ MicroRNA Cards).** Relative levels of miRNAs were expressed as means of logarithmic fold change  $\pm$  SD ( $n = 3 - 4$ ). Statistical significance was assessed with one-way ANOVA followed by multiple comparison tests:  $*p < 0.05$ ,  $**p < 0.01$ ,  $***p < 0.001$ ,  $****p < 0.0001$  (treatment vs. control);  $*p < 0.05$ ,  $**p < 0.01$ ,  $***p < 0.001$ ,  $****p < 0.0001$  (O vs. combination with A or C);  $\#p < 0.05$ ,  $\##p < 0.01$ ,  $\###p < 0.001$ ,  $\####p < 0.0001$  (A or C vs. respective combinations with O).



# Supplementary Figure 7 (Figure S7)

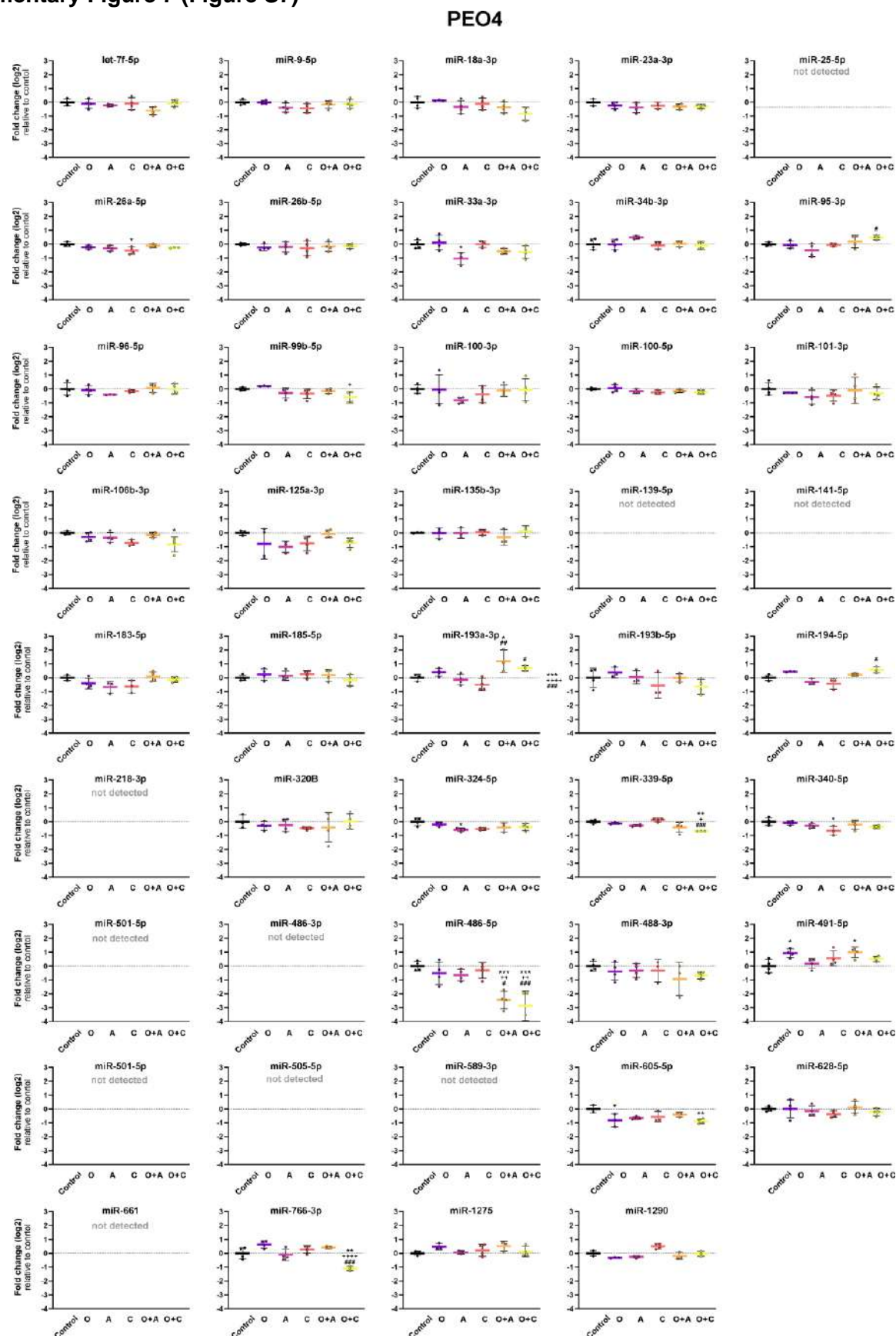


**Figure S7. Results of RT-qPCR-based differential miRNA expression analysis in PEO4 cell line incubated with olaparib (O), ATRi (A), CHK1i (C), or their combinations for 2 days (Custom TaqMan™ MicroRNA Cards).** Relative levels of miRNAs were expressed as means of logarithmic fold change  $\pm$  SD ( $n = 3 - 4$ ). Statistical significance was assessed with one-way ANOVA followed by multiple comparison tests: \* $p < 0.05$ , \*\* $p < 0.01$ , \*\*\* $p < 0.001$ , \*\*\*\* $p < 0.0001$  (treatment vs. control); + $p < 0.05$ , ++ $p < 0.01$ , +++ $p < 0.001$ , ++++ $p < 0.0001$  (O vs. combination with A or C); # $p < 0.05$ , ## $p < 0.01$ , ### $p < 0.001$ , #### $p < 0.0001$  (A or C vs. respective combinations with O).



Supplementary Figure 8 (Figure S8)

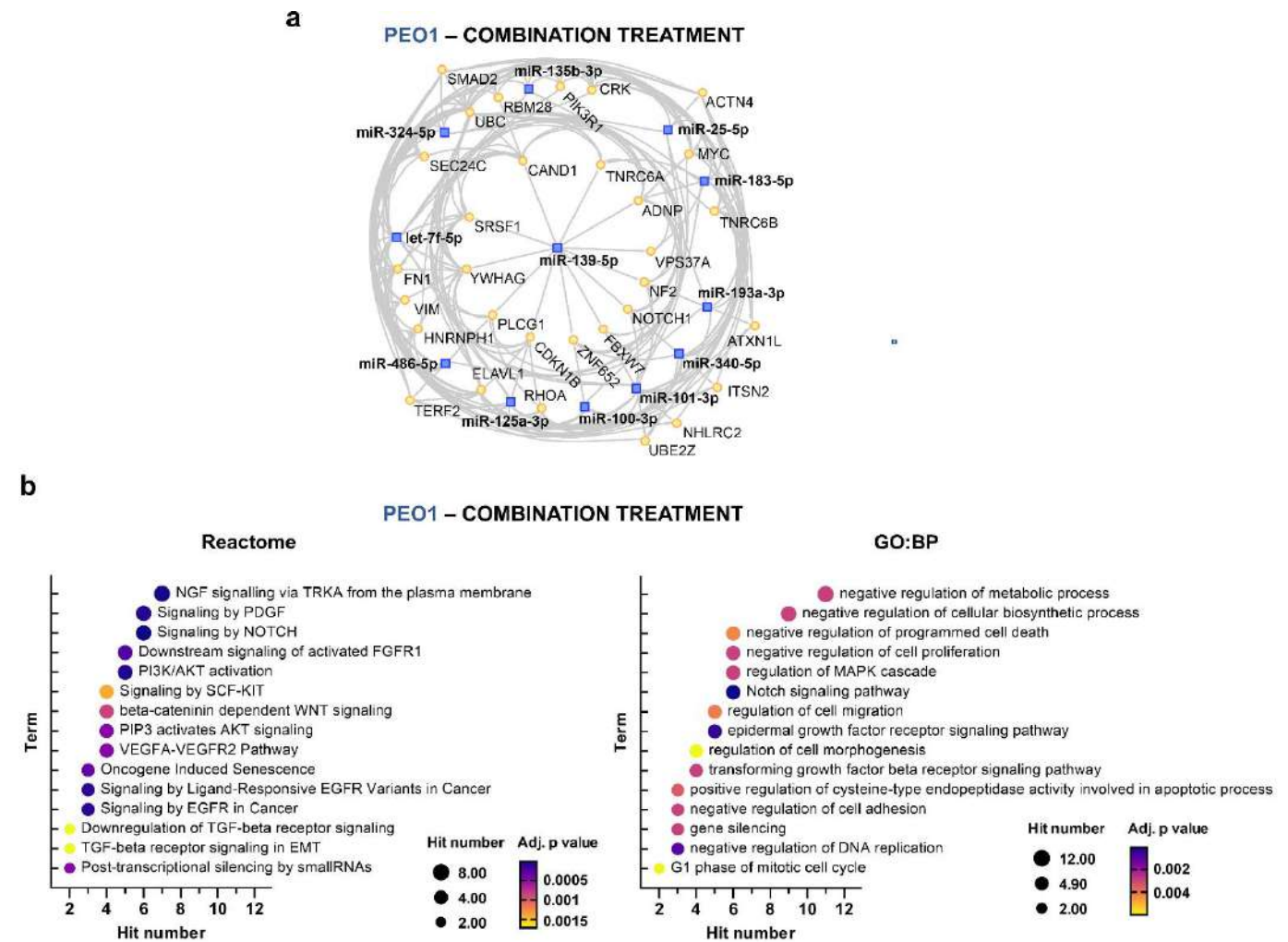


**Figure S8. Network-based functional enrichment analyses of significantly differentially expressed miRNAs and their target genes in PEO1 cell line incubated with olaparib combinations for 2 days. (a)** The minimal miRNA-mRNA interaction network. The blue square nodes represent miRNAs, and the yellow circular nodes represent target genes. **(b)** Enrichment terms visualized with bubble plots based on over-representation analysis for differentially expressed miRNA target genes in PEO1 cells. The most significantly enriched functional annotations were selected following analysis with Reactome pathways and Gene Ontology biological process (GO:BP) databases. Terms were ranked by adjusted  $p$  value and number of target genes (hit).

# Supplementary Figure 9 (Figure S9)

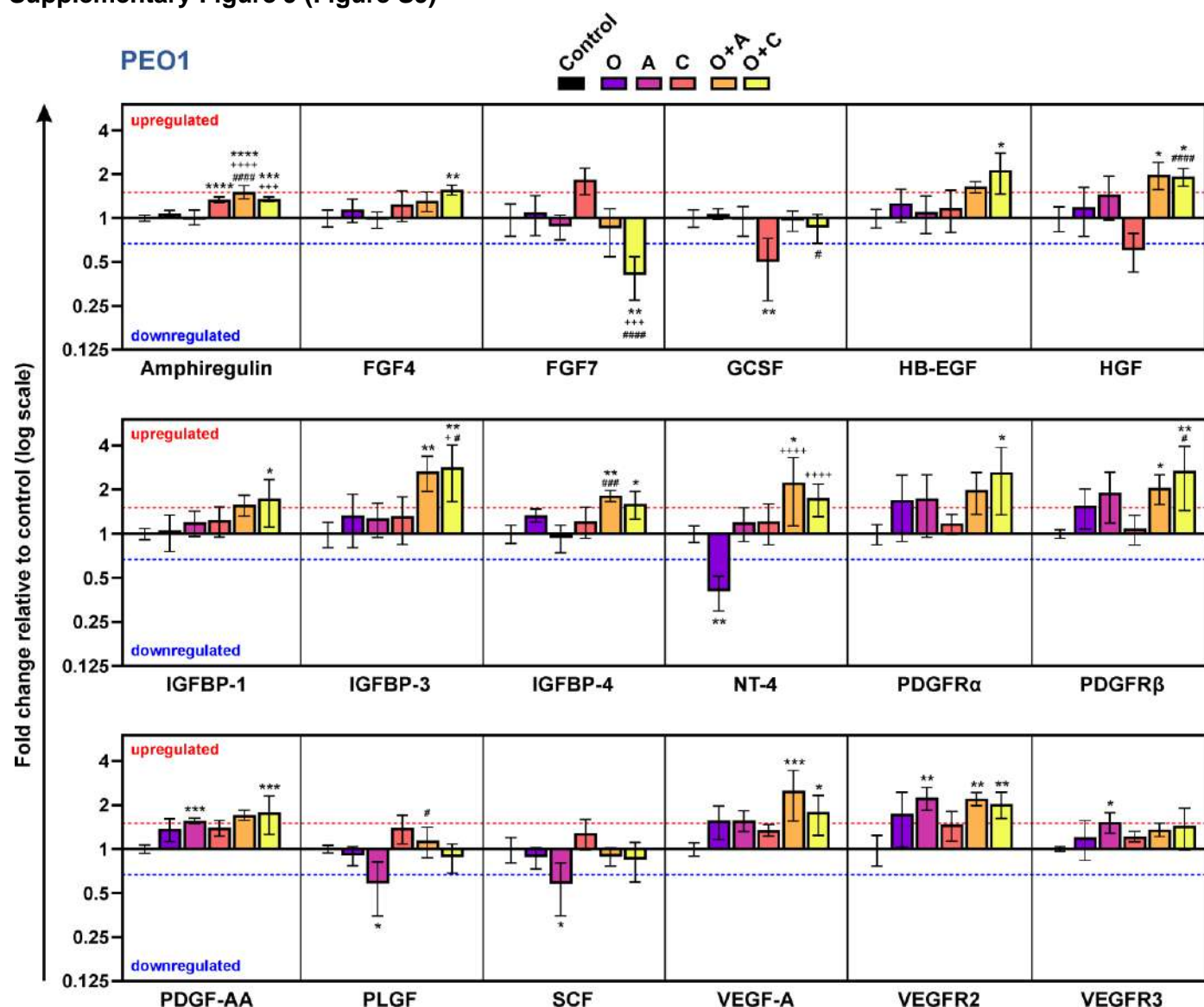


**Figure S9. Results of semi-quantitative analysis with antibody microarrays for growth factors with significantly dysregulated expression in PEO1 cells (absolute fold change  $\geq 1.5$ ,  $p < 0.05$ ).** Cells were incubated with inhibitors (O, A, C) or their combinations (O + A, O + C) for 2 days. Data was expressed as mean fold change  $\pm$  SD ( $n = 4$ ) on a logarithmized scale relative to untreated control cells. Statistical significance was assessed using one-way ANOVA followed by multiple comparison tests: \* $p < 0.05$ , \*\* $p < 0.01$ , \*\*\* $p < 0.001$ , \*\*\*\* $p < 0.0001$  (treatment vs. control); + $p < 0.05$ , ++ $p < 0.01$  (O vs. combination with A or C); # $p < 0.05$ , ## $p < 0.01$ , ### $p < 0.001$ , #### $p < 0.0001$  (A or C vs. respective combinations with O). O – olaparib, A – ATRi, C – CHK1i.

Supplementary Figure 10 (Figure S10)

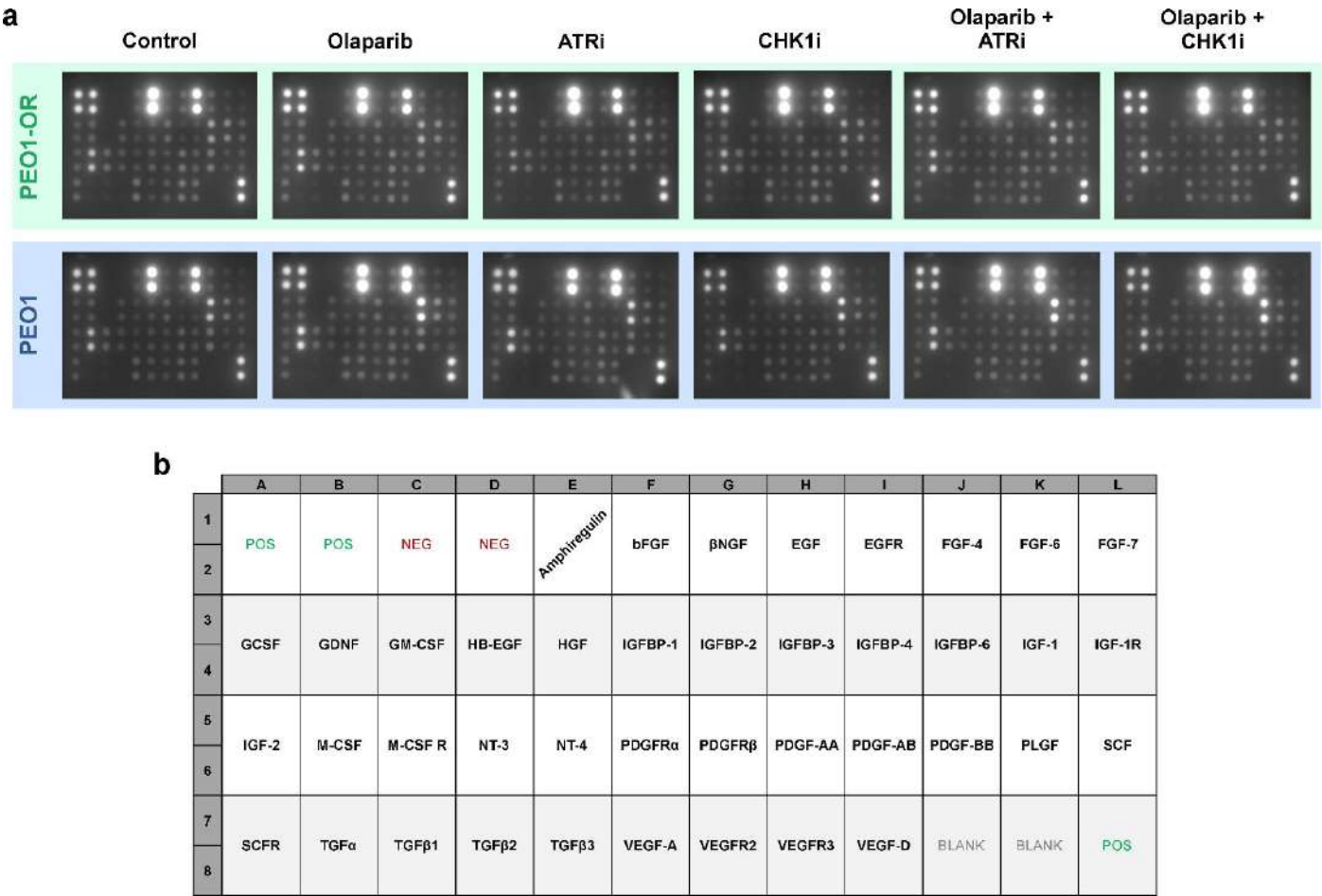


**Figure S10. Raw results of semi-quantitative analysis of 41 growth factors expression in PEO1 and PEO1-OR cells incubated with tested inhibitors or their combinations for 2 days. (a)** Representative enhanced chemiluminescence images of growth factor antibody arrays for PEO1 and PEO1-OR cell lines. **(b)** Array map with the locations of individual antigen-specific antibodies spotted in duplicate vertically. POS – positive control spots used for data normalization between arrays, NEG – negative control spots used to measure the baseline signal.

## Supplementary Figure 11 (Figure S11)

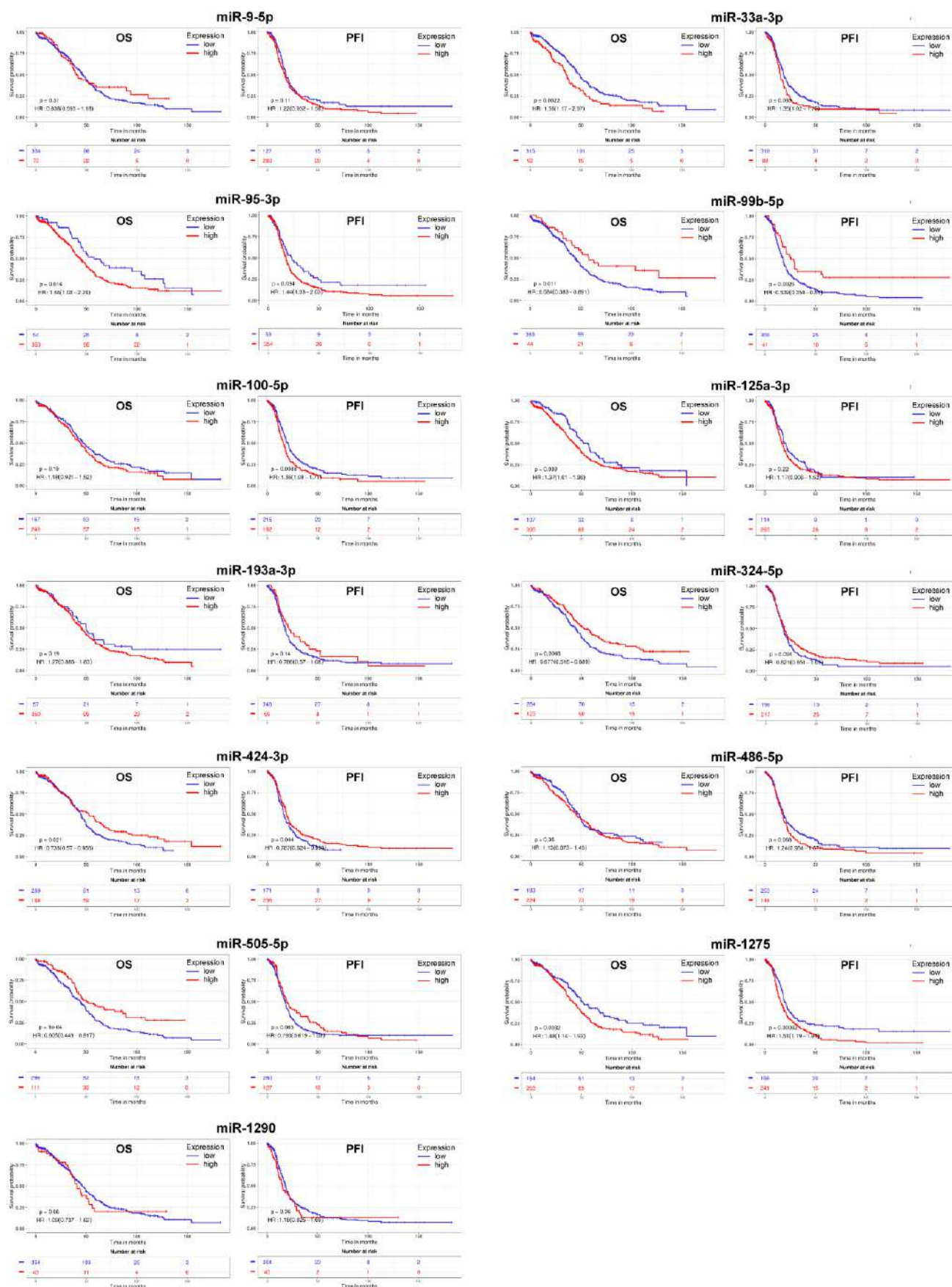


**Figure S11. Kaplan-Meier plots showing the relationship between miRNAs and clinical endpoints (OS – overall survival, PFI – progression-free intervals) in serous OC patients.** Prognostic univariate analyses were performed with the ToPP web-based tool with integrated data from TCGA-OV for HGSOc patients. Low and high expression OC cohorts were defined using the best cutoff and log-rank test. HR – hazard ratio (high vs low expression cohort).



## Supplementary Figure 12 (Figure S12)

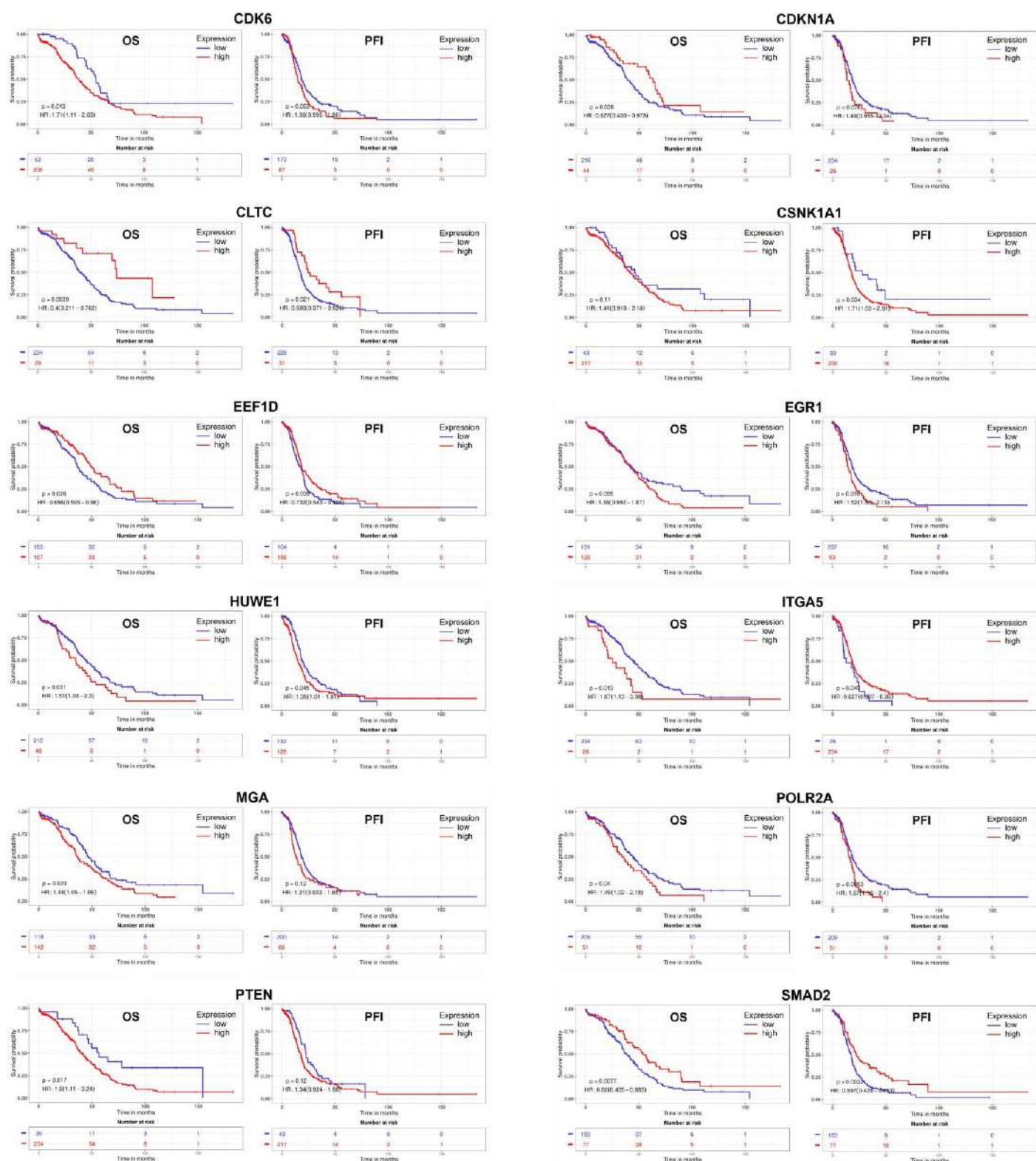


**Figure S12. Kaplan-Meier plots showing the relationship between target genes and clinical endpoints (OS – overall survival, PFI – progression-free intervals) in serous OC patients.** Prognostic univariate analyses were performed with the ToPP web-based tool with integrated data from TCGA-OV for HGSOC patients. Low and high expression OC cohorts were defined using the best cutoff and log-rank test. HR – hazard ratio (high vs low expression cohort).

## Supplementary Figure 13 (Figure S13)

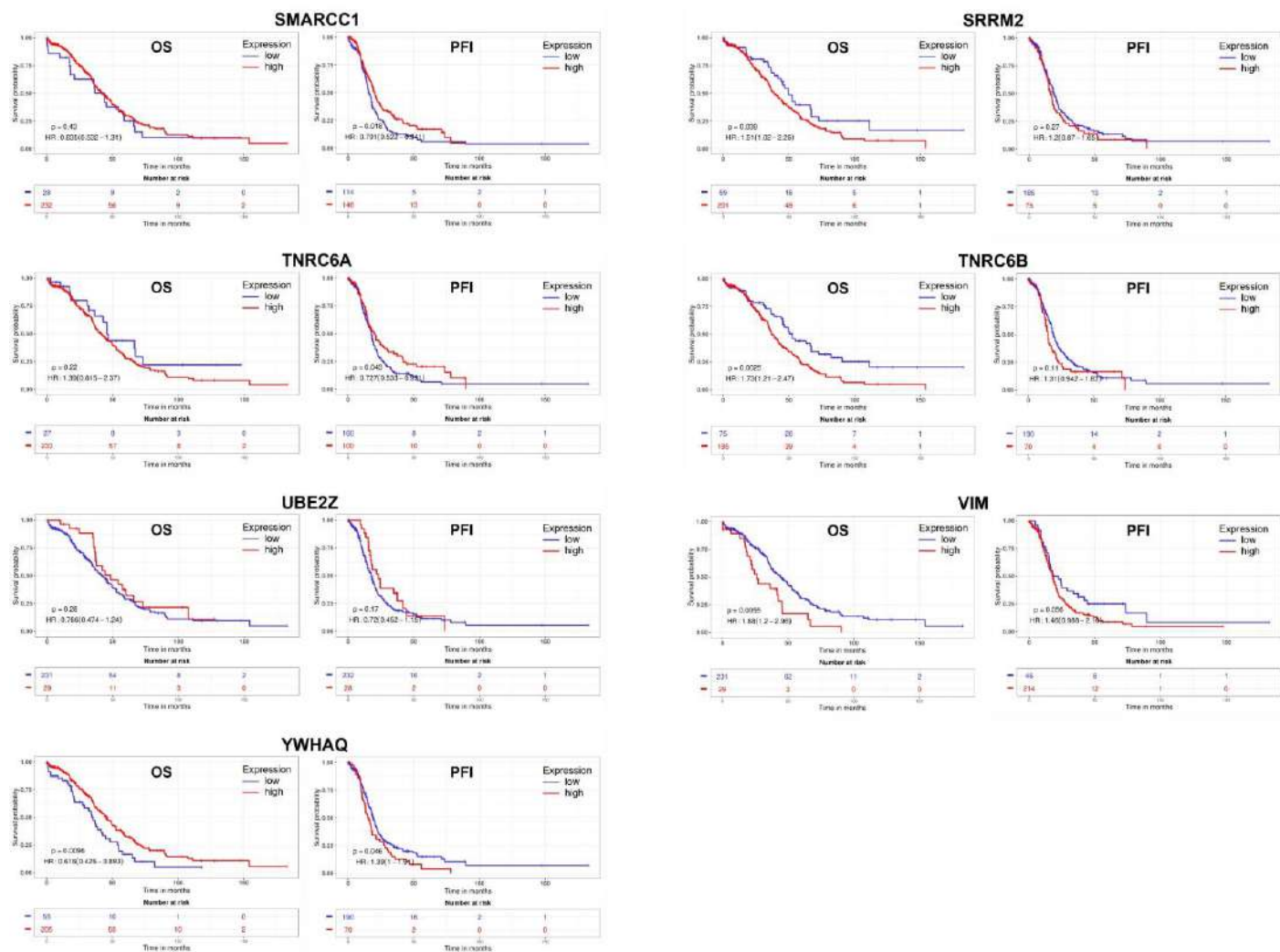


Figure S13. Kaplan-Meier plots showing the relationship between target genes and clinical endpoints (OS – overall survival, PFI – progression-free intervals) in serous OC patients (continued).



## SUPPLEMENTARY TABLES

### Supplementary Table 1 (Table S1)

List of key reagents used in the study.

Reagent	Catalog Number	Manufacturer
Megaplex™ RT Primers, Human Pool Set v3.0	4444745	Applied Biosystems™ (Thermo Fisher Scientific)
Custom TaqMan™ Array MicroRNA Card	4449139	Applied Biosystems™ (Thermo Fisher Scientific)
<i>mirVana</i> ™ miRNA Isolation Kit, with phenol	AM1560	Applied Biosystems™ (Thermo Fisher Scientific)
TaqMan™ MicroRNA Reverse Transcription Kit	4366596	Applied Biosystems™ (Thermo Fisher Scientific)
TaqMan™ Universal Master Mix II, no UNG	4440049	Applied Biosystems™ (Thermo Fisher Scientific)
Water, Nuclease-free, Molecular Biology Grade, Ultrapure, Thermo Scientific Chemicals	J71786.XCR	Applied Biosystems™ (Thermo Fisher Scientific)
TaqMan™ Array Human MicroRNA A+B Cards Set v3.0	4444913	Applied Biosystems™ (Thermo Fisher Scientific)
High-Capacity cDNA Reverse Transcription Kit	4368814	Applied Biosystems™ (Thermo Fisher Scientific)
RNase Inhibitor	N8080119	Applied Biosystems™ (Thermo Fisher Scientific)
Ceralasertib (ATRI)	TBW02661	Wuhan ChemNorm Biotech
MK-8776 (CHK1i)	TBW02666	Wuhan ChemNorm Biotech
Olaparib	S1060	Selleck Chemicals
RayBio® C-Series Human Growth Factor Antibody Array 1	AAH-GF-1-8	RayBiotech Life

## Supplementary Table 2 (Table S2)

Selection of 44 out of 69 dysregulated miRNAs for validation on Custom TaqMan™ MicroRNA Cards based on bioinformatic analyses and literature review.

#	miRNA	miRBase accession	Strong experimental evidence of miRNA-mRNA interactions *	Interaction with the network **	Node degree in the network $\geq 3$	Selected for validation
1	let-7f-5p	+	+	+	+	YES
2	let-7i-3p	+	NO	n/a	n/a	NO
3	miR-7-5p	+	+	+	+	NO
4	miR-9-5p	+	+	+	+	YES
5	miR-18a-3p	+	+	+	+	YES
6	miR-23a-3p	+	+	+	+	YES
7	miR-25-5p	+	+	+	NO	YES***
8	miR-26a-5p	+	+	+	+	YES
9	miR-26b-5p	+	+	+	+	YES
10	miR-27b-5p	+	+	NO	NO	NO
11	miR-32-5p	+	+	+	+	NO
12	miR-33a-3p	+	+	+	+	YES
13	miR-34b-3p	+	+	+	+	YES
14	miR-92a-1-5p	+	+	NO	NO	NO
15	miR-95-3p	+	+	+	+	YES
16	miR-96-5p	+	+	+	+	YES
17	miR-99b-5p	+	+	+	+	YES
18	miR-100-3p	+	+	+	NO	YES***
19	miR-100-5p	+	+	+	+	YES
20	miR-101-3p	+	+	+	+	YES
21	miR-106b-3p	+	+	+	NO	YES***
22	miR-125a-3p	+	+	+	+	YES
23	miR-129-2-3p	+	+	+	+	NO
24	miR-130b-5p	+	NO	n/a	n/a	NO
25	miR-135b-3p	+	+	+	+	NO
26	miR-139-5p	+	+	+	+	YES
27	miR-141-5p	+	+	+	+	YES
28	miR-183-5p	+	+	+	+	YES
29	miR-185-5p	+	+	+	+	YES
30	miR-192-5p	+	+	+	+	NO
31	miR-193a-3p	+	+	+	+	NO
32	miR-193a-5p	+	+	+	+	YES
33	miR-193b-5p	+	+	+	NO	NO
34	miR-194-5p	+	+	+	+	YES
35	miR-210-3p	+	+	+	+	NO
36	miR-218-2-3p	+	+	NO	NO	YES***
37	miR-320b	+	+	+	NO	YES***
38	miR-324-5p	+	+	+	+	YES
39	miR-328-3p	+	+	+	+	NO
40	miR-331-5p	+	NO	n/a	n/a	NO
41	miR-339-5p	+	+	+	+	YES
42	miR-340-5p	+	+	+	+	YES
43	miR-362-5p	+	+	NO	NO	NO
44	miR-378a-5p	+	+	NO	NO	NO
45	miR-424-3p	+	+	NO	NO	NO
46	miR-454-5p	+	NO	n/a	n/a	NO
47	miR-486-3p	+	+	+	+	YES
48	miR-486-5p	+	+	+	+	YES
49	miR-488-3p	+	+	+	+	YES
50	miR-491-5p	+	+	+	+	YES
51	miR-494-3p	+	+	+	+	NO
52	miR-501-5p	+	+	+	+	YES
53	miR-505-5p	+	NO	n/a	n/a	YES***
54	miR-550a-3p	+	+	NO	NO	NO
55	miR-571	+	NO	n/a	n/a	NO
56	miR-573	+	+	NO	NO	NO
57	miR-577	+	NO	n/a	n/a	NO
58	miR-589-3p	+	NO	n/a	n/a	YES***
59	miR-596	+	+	NO	NO	NO
60	miR-598-3p	+	NO	n/a	n/a	NO
61	miR-605-5p	+	+	+	+	YES
62	miR-628-5p	+	+	+	NO	YES
63	miR-629-3p	+	NO	n/a	n/a	NO

#	miRNA	miRBase accession	Strong experimental evidence of miRNA-mRNA interactions *	Interaction with the network **	Node degree in the network $\geq 3$	Selected for validation
64	miR-661	+	+	+	+	YES
65	miR-766-3p	+	+	+	NO	YES
66	miR-941	+	+	NO	NO	NO
67	miR-1201	NO	n/a	n/a	n/a	NO
68	miR-1275	+	NO	n/a	n/a	YES***
69	miR-1290	+	+	+	NO	YES
<b>Total number of miRNAs:</b>		<b>69</b>	<b>68</b>	<b>57</b>	<b>47</b>	<b>39</b>
					<b>39</b>	<b>44</b>

\* Experimentally validated miRNA-target interactions from the MIENTURNET web tool (using miRTarBase website release 7.0 from September 2017).

\*\* Working network created with MIENTURNET web tool.

\*\*\* miRNAs selected based on literature review (irrespective of bioinformatic analysis).

### Supplementary Table 3 (Table S3)

List of analyzed miRNAs and small RNAs for miRNA validation with Custom TaqMan™ MicroRNA Cards.

#	Assay name	Assay Type	TaqMan™ MicroRNA Assay ID
1	let-7f-5p	target	000382
2	miR-9-5p	target	000583
3	miR-18a-3p	target	002423
4	miR-23a-3p	target	000399
5	miR-25-5p	target	002442
6	miR-26a-5p	target	000405
7	miR-26b-5p	target	000407
8	miR-33a-3p	target	002136
9	miR-34b-3p	target	002102
10	miR-95-3p	target	000433
11	miR-96-5p	target	000186
12	miR-99b-5p	target	000436
13	miR-100-3p	target	002142
14	miR-100-5p	target	000437
15	miR-101-3p	target	002253
16	miR-106b-3p	target	002380
17	miR-125a-3p	target	002199
18	miR-135b-3p	target	002159
19	miR-139-5p	target	002289
20	miR-141-5p	target	002145
21	miR-183-5p	target	002269
22	miR-185-5p	target	002271
23	miR-193a-3p	target	002250
24	miR-193a-5p	target	002366
25	miR-194-5p	target	000493
26	miR-218-2-3p	target	002294
27	miR-320b	target	002844
28	miR-324-5p	target	000539
29	miR-339-5p	target	002257
30	miR-340-5p	target	002258
31	miR-424-3p	target	002309
32	miR-486-3p	target	002093
33	miR-486-5p	target	001278
34	miR-488-3p	target	002357
35	miR-491-5p	target	001630
36	miR-501-5p	target	001047
37	miR-505-5p	target	002087
38	miR-589-3p	target	001543
39	miR-605-5p	target	001568
40	miR-628-5p	target	002433
41	miR-661	target	001606
42	miR-766-3p	target	001986
43	miR-1275	target	002840
44	miR-1290	target	002863
45	miR-30e-3p	endogenous control	000422
46	RNU48	endogenous control	001006
47	U6 snRNA	endogenous control	001973
48	U6 snRNA	endogenous control	001973

## Supplementary Table 4 (Table S4)

**Average fold change values of significantly differentially expressed miRNAs in HGSOC cell lines with (Custom TaqMan™ MicroRNA Cards).** Basal expression in the absence of inhibitors was calculated in untreated PEO1-OR and PEO4 cells relative to untreated PEO1 cells. Expression in response to treatment was calculated in all HGSOC cell lines relative to respective untreated controls. Significantly down- and upregulated miRNAs (absolute fold change  $\geq 1.5$  and  $p < 0.05$ ) were highlighted with blue and red, respectively. n/d – not detected ( $C_T \geq 32$  in untreated control cells)

miRNA	BASAL LEVELS		RESPONSE TO TREATMENT														
			PEO1					PEO1-OR					PEO4				
	PEO1-OR	PEO4	O	A	C	O+A	O+C	O	A	C	O+A	O+C	O	A	C	O+A	O+C
let-7f-5p	-1.31	-1.28	1.40	1.29	1.92	2.04	1.21	-1.42	-1.86	-1.63	-1.41	-1.22	-1.08	-1.17	-1.07	-1.53	-1.05
miR-9-5p	1.59	1.62	1.75	1.10	1.63	1.14	1.09	-1.06	1.03	-1.07	-1.06	-1.20	-1.00	-1.32	-1.34	-1.13	-1.09
miR-23a-3p	1.02	-1.25	1.05	-1.23	1.19	1.11	1.21	-1.24	-1.00	1.11	1.01	1.24	-1.17	-1.31	-1.19	-1.25	-1.24
miR-25-5p	-1.37	-2.16	1.22	1.01	2.36	2.08	2.91	n/d	n/d	n/d	n/d	n/d	n/d	n/d	n/d	n/d	n/d
miR-33a-3p	-1.14	1.52	-1.03	-1.05	1.15	-1.43	-1.18	-1.24	-1.21	-1.01	-1.06	-1.84	1.07	-2.07	1.00	-1.43	-1.48
miR-34b-3p	-1.04	-1.70	1.61	1.44	-1.11	1.01	1.04	-1.04	-1.07	-1.02	-1.31	-1.21	-1.01	1.39	-1.07	1.02	-1.07
miR-95-3p	-6.37	-6.14	1.26	-1.14	-1.65	-1.21	-1.16	1.14	-1.14	1.47	1.99	2.28	-1.04	-1.36	-1.03	1.14	1.39
miR-96-5p	-1.39	-1.65	-1.06	-1.33	-1.12	1.05	1.00	-2.20	-1.24	-1.31	-1.25	1.10	n/d	n/d	n/d	n/d	n/d
miR-99b-5p	-1.86	-2.12	-1.05	-1.22	-1.51	-1.06	-1.09	1.01	-1.11	-1.20	-1.19	-1.05	1.16	-1.22	-1.27	-1.11	-1.51
miR-100-3p	-7.58	-3.85	1.15	-1.13	-1.95	-1.83	-2.44	1.10	1.18	-1.88	-1.04	-1.84	-1.02	-1.77	-1.31	-1.09	-1.04
miR-100-5p	-2.41	-2.55	1.24	-1.04	-1.11	1.06	1.08	1.05	-1.20	-1.21	-1.11	-1.14	1.03	-1.13	-1.18	-1.11	-1.18
miR-101-3p	-1.22	1.28	1.00	-1.38	-1.52	-1.97	-2.26	-1.03	1.09	-2.11	-1.11	1.08	-1.20	-1.51	-1.39	-1.08	-1.25
miR-106b-3p	-1.20	-1.54	-1.41	-1.54	-1.43	-1.01	-1.45	-1.17	-1.05	-1.42	1.05	-1.29	-1.22	-1.26	-1.64	-1.10	-1.79
miR-125a-3p	-2.52	-1.98	-1.39	1.03	-1.01	-1.56	-2.53	n/d	n/d	n/d	n/d	n/d	-1.72	-2.01	-1.68	-1.05	-1.63
miR-135b-3p	-1.29	-1.80	-1.47	-1.06	-1.76	-1.74	-3.22	-1.25	-1.00	-1.30	-1.46	-1.60	-1.02	-1.01	1.03	-1.24	1.08
miR-139-5p	-2.37	-3.88	1.16	-1.09	1.19	2.05	1.52	n/d	n/d	n/d	n/d	n/d	n/d	n/d	n/d	n/d	n/d
miR-183-5p	-1.58	-2.02	1.54	1.48	1.54	1.89	2.25	-1.05	-1.11	-1.21	1.40	1.07	-1.34	-1.60	-1.55	1.05	-1.10
miR-185-5p	1.25	1.08	1.23	1.00	1.05	1.61	-1.00	-1.14	-1.54	-1.10	-1.05	-1.22	1.17	1.11	1.19	1.13	-1.13
miR-193a-3p	-2.31	-1.35	1.34	1.53	-1.23	2.41	1.14	1.19	1.06	-1.10	-1.03	-1.04	1.31	-1.10	-1.41	2.29	1.61
miR-324-5p	-1.02	-1.15	-2.02	-1.66	-2.08	-1.79	-2.65	-1.11	-1.58	-1.34	-1.41	-1.59	-1.14	-1.50	-1.44	-1.33	-1.31
miR-339-5p	-1.59	-1.77	1.11	-1.16	-1.20	-1.29	-2.17	1.14	1.04	1.08	-1.04	-1.38	-1.09	-1.22	1.09	-1.33	-1.62
miR-340-5p	-1.17	-1.30	-1.85	-1.71	-1.89	-1.72	-3.35	1.03	-1.34	-1.08	-1.06	-1.30	-1.07	-1.23	-1.58	-1.15	-1.30
miR-424-3p	-1.99	-2.72	-1.10	-1.11	-1.04	-1.30	-1.68	-1.89	1.11	1.12	1.33	-1.54	-1.23	-1.04	-1.37	-1.16	-1.42
miR-486-3p	-1.26	-7.27	-2.98	-3.68	-2.31	-1.83	-2.13	n/d	n/d	n/d	n/d	n/d	n/d	n/d	n/d	n/d	n/d
miR-486-5p	-10.1	-8.83	-1.51	-1.70	-1.63	-2.78	-7.39	-2.84	-1.41	-2.57	-3.22	-10.9	-1.44	-1.57	-1.25	-5.47	-7.34
miR-491-5p	-1.54	-3.19	1.28	1.33	1.83	1.11	1.22	-1.57	1.01	-1.10	-1.15	1.04	1.89	1.13	1.46	1.99	1.43
miR-505-5p	-1.74	-1.71	1.12	-1.90	-2.42	-1.60	-1.57	n/d	n/d	n/d	n/d	n/d	n/d	n/d	n/d	n/d	n/d
miR-605-5p	-1.84	-1.39	-1.69	-2.41	-1.23	-1.57	-1.03	1.38	-1.03	1.34	1.15	-1.13	-1.76	-1.58	-1.48	-1.32	-1.84
miR-628-5p	1.57	1.22	-2.15	-2.44	-2.48	-1.79	-1.55	1.51	-1.08	-1.29	1.02	-1.09	1.01	-1.11	-1.29	1.08	-1.16
miR-766-3p	-1.05	-1.34	1.73	1.16	-1.10	1.25	-1.16	1.58	1.30	1.11	1.12	-1.23	1.55	-1.08	1.22	1.34	-2.13
miR-1275	-1.56	-1.83	1.65	-1.03	1.21	1.80	1.46	1.43	1.31	1.22	1.84	1.56	1.39	1.05	1.16	1.43	1.09
miR-1290	-3.06	-1.42	1.08	-1.04	1.18	1.17	1.21	1.30	1.57	2.48	2.20	3.37	-1.26	-1.20	1.42	-1.14	-1.03

## Supplementary Table 5 (Table S5)

Top significantly enriched pathways (Reactome) and biological processes (GO:BP) associated with target genes of dysregulated miRNAs in untreated PEO1-OR cells.

Cell Line: PEO1-OR Treatment: Basal expression (in the absence of inhibitors)				
#	Reactome pathway	Adj. p value	Hit number	Target genes
1	Signaling by FGFR	$1.21 \times 10^{-6}$	8	UBC, TNRC6A, TNRC6B, MTOR, CREB1, CDKN1A, CALM1, PTEN
2	Signaling by EGFR	$2.16 \times 10^{-6}$	8	UBC, TNRC6A, TNRC6B, MTOR, CREB1, CDKN1A, CALM1, PTEN
3	PIP3 activates AKT signaling	$6.77 \times 10^{-6}$	6	TNRC6A, TNRC6B, MTOR, CREB1, CDKN1A, PTEN,
4	PI3K/AKT activation	$7.29 \times 10^{-6}$	6	TNRC6A, TNRC6B, MTOR, CREB1, CDKN1A, PTEN
5	Signaling by PDGF	$1.49 \times 10^{-5}$	7	TNRC6A, TNRC6B, MTOR, CREB1, CDKN1A, CALM1, PTEN,
6	Signaling by SCF-KIT	$3.24 \times 10^{-5}$	6	TNRC6A, TNRC6B, MTOR, CREB1, CDKN1A, PTEN
7	Signaling by Wnt	$9.81 \times 10^{-5}$	7	UBC, TNRC6A, TNRC6B, CSNK1A1, CALM1, XPO1, CLTC
8	beta-catenin independent WNT signaling	$1.91 \times 10^{-4}$	5	UBC, TNRC6A, TNRC6B, CALM1, CLTC
9	Downregulation of TGF-beta receptor signaling	$3.50 \times 10^{-4}$	3	UBC, XPO1, PPP1CB
10	Signaling by TGF-beta Receptor Complex	$4.24 \times 10^{-4}$	4	UBC, XPO1, PPP1CB, SKI
11	Cyclin D associated events in G1	$5.02 \times 10^{-4}$	3	UBC, CDKN1A, CDK6
12	TGF-beta receptor signaling activates SMADs	$5.68 \times 10^{-4}$	3	UBC, XPO1, PPP1CB
13	Mitotic G1-G1/S phases	$2.61 \times 10^{-4}$	4	UBC, MCM4, CDKN1A, CDK6
14	Cell Cycle, Mitotic	$6.51 \times 10^{-3}$	6	UBC, MCM4, CDKN1A, XPO1, PPP1CB, CDK6
15	DNA Replication	$8.59 \times 10^{-3}$	3	UBC, MCM4, CDKN1A
#	GO: Biological process	Adj. p value	Hit number	Target genes
1	EGFR signaling pathway	$1.32 \times 10^{-3}$	5	UBC, MTOR, CREB1, PTEN, CLTC
2	regulation of TGF-beta receptor signaling pathway	$2.02 \times 10^{-3}$	4	UBC, XPO1, PPP1CB, SKI
3	G1/S transition of mitotic cell cycle	$2.11 \times 10^{-3}$	5	UBC, MCM4, CDKN1A, PTEN, CDK6
4	cellular response to stress	$3.75 \times 10^{-3}$	12	UBC, TERF2, TNRC6A, MTOR, CREB1, VCP, NDRG1, EGR1, CDKN1A, FEM1B, CDK6, HUWE1,
5	cell cycle checkpoint	$4.35 \times 10^{-3}$	5	UBC, NDRG1, MCM4, CDKN1A, FEM1B
6	Notch signaling pathway	$5.74 \times 10^{-3}$	4	UBC, TNRC6A, TNRC6B, CDK6
7	negative regulation of cellular metabolic process	$8.31 \times 10^{-3}$	11	UBC, TERF2, TNRC6A, MTOR, CREB1, ATXN1, EGR1, CDKN1A, XPO1, PTEN, SKI
8	DNA damage response, signal transduction by p53 class mediator	$8.48 \times 10^{-3}$	3	UBC, NDRG1, CDKN1A
9	signal transduction in response to DNA damage	$9.14 \times 10^{-3}$	3	UBC, NDRG1, CDKN1A
10	DNA damage checkpoint	$9.55 \times 10^{-3}$	3	UBC, CDKN1A, FEM1B
11	response to DNA damage stimulus	$9.55 \times 10^{-3}$	7	UBC, TERF2, VCP, NDRG1, CDKN1A, FEM1B, HUWE1
12	S phase of mitotic cell cycle	$9.55 \times 10^{-3}$	3	UBC, MCM4, CDKN1A,
13	DNA integrity checkpoint	$9.92 \times 10^{-3}$	3	UBC, CDKN1A, FEM1B
14	negative regulation of cell cycle	$1.24 \times 10^{-2}$	5	UBC, MCM4, CDKN1A, PTEN, CDK6
15	positive regulation of cell proliferation	$1.49 \times 10^{-2}$	6	ESR1, MTOR, EGR1, CDKN1A, PTEN, CDK6



## Supplementary Table 6 (Table S6)

Top significantly enriched pathways (Reactome) associated with target genes of dysregulated miRNAs in PEO1-OR cells in response to combinations of olaparib with the ATR/CHK1 pathway inhibitors.

		Cell Line:	PEO1-OR		
		Treatment:	Olaparib combination with ATRi or CHK1i (O + A and O + C)		
#	Reactome pathway	Adj. p value	Hit number	Target genes	
1	beta-catenin independent WNT signaling	0.0252	3	<i>TNRC6A, CALM1, CLTC</i>	
2	Loss of Function of TGFBR1 in Cancer	0.0406	1	<i>SMAD2</i>	
3	Post-transcriptional silencing by small RNAs	0.0406	1	<i>TNRC6A</i>	
4	Signaling by TGF-beta Receptor Complex in Cancer	0.0406	1	<i>SMAD2</i>	
5	Caspase-mediated cleavage of cytoskeletal proteins	0.0406	1	<i>VIM</i>	
6	Chk1/Chk2(Cds1) mediated inactivation of Cyclin B:Cdk1 complex	0.0406	1	<i>YWHAQ</i>	
7	G2/M DNA damage checkpoint	0.0406	1	<i>YWHAQ</i>	
8	MicroRNA (miRNA) biogenesis	0.0406	1	<i>POLR2A</i>	
9	Downregulation of TGF-beta receptor signaling	0.0406	1	<i>SMAD2</i>	
10	VEGFR2 mediated cell proliferation	0.0406	1	<i>CALM1</i>	
11	Transcriptional regulation by small RNAs	0.0406	2	<i>TNRC6A, POLR2A</i>	
12	Downstream signaling of activated FGFR1	0.0406	2	<i>TNRC6A, CALM1</i>	
13	Signaling by EGFR	0.0406	2	<i>TNRC6A, CALM1</i>	
14	Signaling by PDGF	0.0406	2	<i>TNRC6A, CALM1</i>	
15	NGF signaling via TRKA from the plasma membrane	0.0406	2	<i>TNRC6A, CALM1</i>	

## Supplementary Table 7 (Table S7)

Experimentally validated targets of differentially expressed miRNAs from minimal subnetworks that maximally connect seeds in the PEO1-OR cell line (established with miRNet 2.0).

Basal expression (in the absence of inhibitors)		Olaparib combinations with ATRi or CHK1i (O + A and O + C)	
miRNA	Target genes	miRNA	Target genes
miR-9-5p	UBC, TNRC6A, CSNK1A1, ESR1, CREB1, NDRG1, DDX21, ITGA5, EGR1, MCM4, CDKN1A, NRC1, CALM1, XPO1, SRRM2, PPP1CB, VIM, CLTC, VPS4A, HUWE1, HECTD1	miR-33a-3p	TNRC6A, DDX21, CAB39, CALM1, IRF4
miR-95-3p	MTOR, CREB1, MCM4, CDKN1A, CALM1, SRRM2, VIM, SKI, ZNF131	miR-95-3p	POLR2A, CALM1, SRRM2, VIM, SCAF4, ZNF131
miR-99b-5p	TNRC6B, MTOR, ITGA5, MCM4, XPO1, MGA, PPP1CB, VPS4A	miR-324-5p	TNRC6A, SMAD2, POLR2A, YWHAQ
miR-100-3p	FN1, PNRC1, SMARCC1, PPP1CB, HNRNPH1, SKI, HECTD1	miR-424-3p	TNRC6A, VIM, UBE2Z, CLTC
miR-100-5p	CDKN1A, EE1D, PNRC1, MGA, PPP1CB, FEM1B, CDK6	miR-486-5p	DDX21, SMAD2, SRRM2, VIM, PUM2
miR-125a-3p	UBC, TERF2, FN1, EGR1, MCM4, EE1D, SRRM2, PPP1CB, CDK6, ARPC2, HUWE1, SKI	miR-1275	SMAD2, IRF4, UBE2Z, SCAF4, RPP25
miR-193a-3p	FN1, TNRC6B, ESR1, ATXN1, ARF6, CALM1, PTEN, CLTC, CDK6, HECTD1	miR-1290	CAB39, YWHAQ, PUM2, CLTC, RPP25, ZNF131
miR-424-3p	TNRC6A, CSNK1A1, MGA, SMARCC1, VIM, PTEN, CLTC, CDK6, ARPC2, HUWE1		
miR-486-5p	TERF2, DDX21, ARF6, XPO1, SRRM2, VIM, PTEN, FEM1B, HNRNPH1		
miR-505-5p	TNRC6B, CSNK1A1, EGR1, CDKN1A, EE1D, SRRM2, HUWE1, SKI		
miR-1290	VCP, NDRG1, ATXN1, FEM1B, CLTC, VPS4A, ARPC2, HUWE1, ZNF131, HECTD1		

## Supplementary Table 8 (Table S8)

**Identification of hub nodes using CytoHubba plug-in based on the minimal miRNA-mRNA networks using maximal clique centrality (MCC) algorithm.** The top 10 hub miRNA targets with the highest connectivity were assigned as potential hub genes (underlined). O – olaparib, A – ATRi, C – CHK1i.

PEO1-OR (untreated)			PEO1-OR (O + A and O + C)			PEO1 (O + A and O + C)		
Rank	Node name	Score	Rank	Node name	Score	Rank	Node name	Score
1	<u>UBC</u>	274	1	miR-486-5p	6	1	<u>UBC</u>	229
2	miR-9-5p	138	1	<u>SRRM2</u>	6	2	<u>FN1</u>	222
3	<u>ESR1</u>	126	1	miR-1290	6	3	<u>ELAVL1</u>	204
4	<u>SRRM2</u>	94	1	<u>VIM</u>	6	4	<u>YWHAG</u>	144
5	<u>VCP</u>	80	1	miR-95-3p	6	5	<u>SRSF1</u>	129
6	<u>DDX21</u>	64	6	miR-33a-3p	5	6	<u>CAND1</u>	96
7	<u>VIM</u>	63	6	<u>YWHAQ</u>	5	7	hsa-let-7f-5p	80
8	<u>CALM1</u>	51	6	miR-1275	5	8	<u>HNRNPH1</u>	51
9	<u>FN1</u>	46	9	miR-324-5p	4	9	miR-125a-3p	50
10	<u>CDKN1A</u>	42	9	<u>CALM1</u>	4	10	<u>MYC</u>	36
11	<u>HUWE1</u>	36	9	miR-424-3p	4	11	<u>CDKN1B</u>	26
12	miR-125a-3p	32	9	<u>DDX21</u>	4	12	<u>ACTN4</u>	22
13	EEF1D	27	13	<u>SMAD2</u>	3	13	SMAD2	21
14	TERF2	24	13	<u>TNRC6A</u>	3	14	ADNP	18
15	CLTC	21	13	<u>CLTC</u>	3	14	miR-101-3p	18
16	miR-100-5p	18	16	<u>SCAF4</u>	2	14	miR-324-5p	18
17	EGR1	17	16	<u>POLR2A</u>	2	17	miR-139-5p	16
18	CREB1	16	16	RPP25	2	17	miR-183-5p	16
18	NDRG1	16	16	CAB39	2	17	CRK	16
20	CDK6	15	16	ZNF131	2	20	SEC24C	15
20	ARF6	15	16	IRF4	2	21	RHOA	13
22	SMARCC1	14	16	PUM2	2	22	miR-340-5p	10
22	miR-193a-3p	14	16	UBE2Z	2	23	PIK3R1	9
22	miR-486-5p	14			6	23	VIM	9
25	miR-1290	13			6	23	TERF2	9
26	miR-95-3p	11				23	TNRC6B	9
27	XPO1	10				23	NOTCH1	9
27	HNRNPH1	10				23	PLCG1	9
27	miR-424-3p	10				29	miR-193a-3p	8
30	miR-99b-5p	8				30	miR-135b-3p	7
30	miR-505-5p	8				30	miR-486-5p	7
32	PPP1CB	7				32	RBM28	6
32	PTEN	7				32	TNRC6A	6
32	ARPC2	7				32	miR-25-5p	6
32	SKI	7				32	miR-100-3p	6
32	miR-100-3p	7				32	NF2	6
32	ITGA5	7				37	FBXW7	5
38	MTOR	6				37	ZNF652	5
38	MCM4	6				37	ATXN1L	5
40	HECTD1	5				40	UBE2Z	4
40	TNRC6B	5				40	NHLRC2	4
40	ATXN1	5				40	ITSN2	4
43	MGA	4				43	VPS37A	3
43	FEM1B	4						
43	VPS4A	4						
43	CSNK1A1	4						
43	PNRC1	4						
48	ZNF131	3						
48	TNRC6A	3						

## Supplementary Table 9 (Table S9)

Results of stage-wise differential miRNA and gene expression analysis in serous OC patients using filtered data from TCGA-OV dataset (serous OC patients with stage II, III, or IV after pharmaceutical therapy). Gene and miRNA levels were expressed as counts per million (CPM). Statistical significance for non-normally distributed data was evaluated with the Kruskal-Wallis test comparing the medians of three groups followed by Dunn's multiple comparison test (if applicable).

miRNA	Average expression (CPM)			Median expression (CPM)			Kruskal-Wallis test <i>p</i> value
	Stage II	Stage III	Stage IV	Stage II	Stage III	Stage IV	
miR-9-5p	41.6	38.7	27.5	57.2	59.1	33.8	0.2384
miR-99b-5p	226675	262851	242556	240102	265850	231672	0.4013
miR-100-5p	1848	2982	2238	1932	2395	2141	0.2324
miR-125a-3p	39.8	43.2	49.1	36.3	37.7	41.4	0.4617
miR-324-5p	47.4	43.6	45.6	44.4	38.9	39.6	0.9585
miR-424-3p	11.9	14.6	14.2	9.8	12.2	12.1	0.5566
miR-486-5p	492.9	512.6	346.2	328.1	372.9	231.1	0.3533
miR-505-5p	35.4	23.2	23.1	34.5	21.3	20.6	0.2263

Gene	Average expression (CPM)			Median expression (CPM)			Kruskal-Wallis test <i>p</i> value
	Stage II	Stage III	Stage IV	Stage II	Stage III	Stage IV	
<i>HUWE1</i>	385.5	379.6	371.3	358.1	352.8	397.5	0.9030
<i>TNRC6B</i>	74.7	56.2	54.2	70.6	55.6	50.2	0.0647
<i>EEF1D</i>	129.7	112.8	126.6	121.3	109.7	113.7	0.6075
<i>CDK6</i>	28.0	24.2	40.9	16.0	19.6	33.6	0.0255
<i>CSNK1A1</i>	86.0	79.1	84.4	89.4	75.7	83.9	0.3994
<i>EGR1</i>	297.0	276.4	177.9	272.0	211.0	148.9	0.2884
<i>CDKN1A</i>	54.6	51.8	41.7	44.9	45.17	39.8	0.4951
<i>ITGA5</i>	47.02	61.1	49.24	35.5	47.5	41.8	0.4789
<i>SRRM2</i>	973.8	754.7	756.4	933.1	745.0	754.6	0.0975
<i>PTEN</i>	89.1	101.2	94.6	88.0	96.7	103.0	0.6343
<i>SMARCC1</i>	220.0	177.5	175.5	208.6	170.9	185.3	0.1008
<i>MGA</i>	54.5	48.1	49.3	52.0	47.0	51.1	0.3749
<i>VIM</i>	239.8	418.0	390.1	250.2	360.9	361.8	0.0271
<i>TNRC6A</i>	76.7	58.8	58.93	67.2	55.9	53.1	0.0373
<i>YWHAQ</i>	400.7	438.7	421.2	395.2	407.4	352.2	0.6053
<i>CLTC</i>	298.1	285.6	299.9	295.3	271.2	260.3	0.8709
<i>UBE2Z</i>	158.6	157.4	150.3	156.9	150.3	137.7	0.7519
<i>SMAD2</i>	158.6	157.4	150.3	156.9	150.3	137.7	0.7519
<i>POLR2A</i>	271.0	220.4	195.1	270.2	207.3	186.0	0.0074

## Supplementary Table 10 (Table S10)

**Validation of endogenous control genes stable expression in HGSOC cell lines for RT-qPCR data normalization from Custom TaqMan™ MicroRNA Cards.** Average  $C_T$  values are means for all tested treatments (control, O, A, C, O+A, and O+C) among cell lines. Significant differences in average  $C_T$  values between treatments for each gene and cell line were evaluated with ordinary one-way ANOVA. O – olaparib, A – ATRi, C – CHK1i.

Endogenous Control	Cell Line	Average $C_T$	SD of $C_T$	Significant Difference Among Treatments	$C_T$ MIN	$C_T$ MAX	$C_T$ Range
U6 snRNA	PEO1	20.10	0.14	NO ( $p = 0.6844$ )	19.91	20.29	0.38
	PEO4	20.00	0.22	NO ( $p = 0.6553$ )	19.52	20.16	0.64
	PEO1-OR	20.18	0.07	NO ( $p = 0.9734$ )	20.06	20.26	0.20
RNU48	PEO1	20.34	0.08	NO ( $p = 0.9480$ )	20.24	20.47	0.24
	PEO4	20.09	0.10	NO ( $p = 0.8417$ )	20.00	20.29	0.29
	PEO1-OR	20.08	0.08	NO ( $p = 0.6809$ )	19.98	20.17	0.19
miR-30e-3p	PEO1	27.73	0.22	NO ( $p = 0.2772$ )	27.34	28.01	0.67
	PEO4	27.46	0.17	NO ( $p = 0.6857$ )	27.18	27.67	0.50
	PEO1-OR	27.34	0.12	NO ( $p = 0.9296$ )	27.12	27.51	0.39

## **MANUSKRYPT ARTYKUŁU #5**



# Olaparib Rechallenge Combined with the ATR/CHK1 Pathway Inhibitors in Olaparib-Resistant PDX Models of Ovarian Cancer: Mechanisms Behind Synergistic Tumor Growth Inhibition

Łukasz Biegała<sup>1,2</sup>, Małgorzata Statkiewicz<sup>3</sup>, Arkadiusz Gajek<sup>1</sup>, Izabela Szymczak-Pajor<sup>4</sup>,  
Natalia Rusetska<sup>5</sup>, Agnieszka Śliwińska<sup>4</sup>, Agnieszka Marczak<sup>1</sup>, Michał Mikula<sup>3</sup>,  
Aneta Rogalska<sup>1,\*</sup>

## Abstract

The clinical utility of olaparib, a poly(ADP-ribose) polymerase (PARP) inhibitor (PARPi), has been substantial for ovarian cancer (OC) patients with homologous recombination deficiencies related to *BRCA1/2* mutations. However, resistance to olaparib inevitably develops, prompting the need for combination strategies to enhance its efficacy *in vivo*.

Thus, we established the olaparib-resistant patient-derived xenograft (PDX) models of high-grade serous OC with *BRCA1/2* mutations in NSG/J mice and characterized their molecular features associated with resistant phenotype *in vivo*. Next, olaparib-resistant PDX tumors were treated with olaparib, ATR inhibitor (ATRi, ceralasertib), and CHK1 inhibitor (CHK1i, MK-8776) or their combinations to investigate treatment responses based on tumor growth and histopathological analysis on hematoxylin and eosin-stained tissues. Evaluation of molecular downstream effects included proliferation, apoptosis, the ATR/CHK1 pathway activity, PARP signaling, DNA damage response (DDR), epithelial-to-mesenchymal transition (EMT), and MDR1 efflux pump were examined by RT-qPCR, Western Blotting, and immunohistochemistry.

Tumors resistant to olaparib exhibited defects in PARP and ATR/CHK1 signaling, accompanied by the altered expression of proteins involved in the DDR and EMT process. The studies demonstrated that olaparib and ATRi alone or combined were generally well-tolerated in mice. Olaparib combinations with the ATR/CHK1 pathway inhibitors showed promising antitumor activity indicated by a synergistic tumor growth inhibition in responding mice. The addition of ATRi to olaparib provided the best response classified as stable disease reflected by tumor growth attenuation. Mechanistically, this combination decreased tumor proliferation without increasing apoptosis or necrosis, while inducing tumor cell vacuolization indicative of cell death. Molecularly, ATRi combined with olaparib-induced or augmented downregulation of ATR, CHK1, PARP1, PARG, BRCA1,  $\gamma$ H2AX, and PARylated protein content, while reversing olaparib-induced upregulation of vimentin, BRCA2, and 53BP1.

Collectively, potential mechanisms underlying acquired resistance and resensitization to olaparib were identified. Our data provide evidence that targeted inhibition of the ATR/CHK1 pathway increases the efficacy of olaparib in olaparib-resistant HGSOC tumors *in vivo*.

## Keywords

Ovarian cancer, olaparib resistance, resensitization, ATR/CHK1 pathway, patient-derived xenograft (PDX), combination therapy.

<sup>1</sup>Department of Medical Biophysics, Institute of Biophysics, Faculty of Biology and Environmental Protection, University of Lodz, 141/143 Pomorska Street, 90-236 Lodz, Poland. <sup>2</sup>Doctoral School of Exact and Natural Sciences, University of Lodz, 21/23 Jana Matejki Street, 90-237 Lodz, Poland. <sup>3</sup>Department of Genetics, Maria Skłodowska-Curie National Research Institute of Oncology, 5 Roentgena Street, 02-781, Warsaw, Poland. <sup>4</sup>Department of Nucleic Acid Biochemistry, Medical University of Lodz, 251 Pomorska Street, 92-213 Lodz, Poland. <sup>5</sup>Department of Experimental Immunology, Maria Skłodowska-Curie National Research Institute of Oncology, 5 Roentgena Street, 02-781, Warsaw, Poland.

\*Correspondence: aneta.rogalska@biol.uni.lodz.pl.

## Introduction

High-grade serous ovarian cancer (HGSOC), the most frequent histological subtype of epithelial ovarian cancer (OC), is a heterogeneous disease usually diagnosed at advanced stages (III and IV). Despite initial responses to standard therapy, it exhibits a high relapse rate of approximately 70% within three years [1]. Around 50% of HGSOC cases harbor defects in the homologous recombination (HR) DNA repair pathway, primarily due to mutations in *BRCA1/2* genes, that render sensitivity to poly(ADP-ribose) polymerase (PARP) inhibitors (PARPi) through synthetic lethality. Olaparib, the first approved PARPi, is clinically utilized in various clinical settings based on the patient's response to first-line chemotherapy, including maintenance therapy for newly diagnosed *BRCA1/2*-mutated (*BRCA1/2*<sup>MUT</sup>) and platinum-sensitive recurrent HGSOC [2].

PARP enzymes play a pivotal role in catalyzing a post-translational mono- and poly-ADP-ribosylation (PAR) of proteins involved in various cellular processes including DNA repair. PARP1 functions as a molecular sensor in DNA damage response (DDR) pathways. It is crucial in regulating the expression and recruitment of proteins mediating various DNA repair pathways, such as HR repair, single-strand break repair, and base excision repair [3].

The antitumor activity of PARPi relies primarily on two proposed mechanisms: inhibiting PARP enzymatic activity, which impairs DNA damage repair of single-strand DNA breaks, leading to their conversion into double-strand breaks (DSB) and subsequent tumor cell death in those with defective DNA damage repair mechanism; and competitively binding of PARPi to the NAD<sup>+</sup> binding domain on PARP1, resulting in PARP1 trapping at the DNA damage site and accumulation of cytotoxic PARP1-DNA complexes [4]. However, while both mechanisms

likely contribute to anticancer activity, there is a lack of comprehensive clinical evidence to fully support either theory.

Despite the evident clinical benefits of PARPi therapy in OC, acquired resistance to olaparib may develop in patients with advanced HGSOC who experience disease progression while on treatment, thereby limiting its clinical utility [5]. Recent findings from the OReO/ENGOT trial indicate that approximately half of *BRCA1/2*<sup>MUT</sup> recurrent epithelial OC patients progress during retreatment with olaparib and derive no meaningful clinical benefit [6]. Moreover, a post-hoc analysis of data from the SOLO2 trial revealed that *BRCA1/2*<sup>MUT</sup> platinum-sensitive relapsed OC patients who progressed on maintenance olaparib lack promising treatment options following disease progression [7].

Multiple complex resistance mechanisms to olaparib have been proposed in OC cells based on *in vitro* and *in vivo* models [8]. Among them, restoration of HR repair pathway activity through secondary reversion mutations in *BRCA1/2* and other genes is the well-established mechanism of acquired resistance [9, 10]. Additionally, olaparib resistance may also arise from restoration of HR functions through the loss of TP53 binding protein 1 (53BP1) in *BRCA1*-deficient tumors, restoration of replication fork stability, reduction in PARP trapping by mutation or loss of PARP1, and enhanced drug efflux [8, 11].

To enhance the clinical potential of olaparib, investigators are exploring promising combination strategies employing immune checkpoint inhibitors, anti-angiogenic drugs, and so on [2]. Significantly, targeting DDR pathways holds promise in restoring the synthetic lethality of olaparib in HR-proficient tumors and overcoming acquired PARPi resistance [11]. Recent focus has centered on inhibiting the ATR/CHK1 pathways, given the pivotal roles of ATR kinase (ataxia telangiectasia and Rad3-related) and CHK1 (checkpoint kinase 1) in DDR and cell cycle regulation [12]. Emerging evidence suggests that inhibiting the ATR/CHK1 pathway increases olaparib efficacy in epithelial OC tumors. Indeed, both ATR inhibitors (ATRi) and CHK1 inhibitors (CHK1i) demonstrated promising antitumor activity in combination with olaparib across olaparib-sensitive and olaparib-resistant OC cell lines and patient-derived xenograft (PDX) models of HGSOC [13–16]. We previously demonstrated that targeted inhibition of the ATR/CHK1 pathway can resensitize the olaparib-resistant HGSOC cell line with *BRCA2* reversion mutation to olaparib *in vitro* through caspase-mediated apoptosis and affects the expression of DDR-related proteins [13].

Currently, the combination of olaparib with ATRi ceralasertib is under investigation in women with recurrent platinum-sensitive and platinum-resistant HGSOC in the ongoing CAPRI clinical trial (NCT03462342). Initial results from a PARPi-naïve platinum-resistant cohort showed no objective responses to combination therapy, however, 75% of patients obtained stable disease as the best response [17]. Furthermore, promising antitumor activity of the above-mentioned combination has been demonstrated in HR-deficient platinum-sensitive recurrent HGSOC with acquired resistance to olaparib [18]. However, the relatively small number of patients evaluable for efficacy testing and the absence of comparator arms necessitate further investigation of the clinical utility of olaparib in combination with ceralasertib. Additionally, given the genetic and molecular heterogeneity of HGSOC cells, the rationale for combining olaparib with ATR/CHK1 pathway inhibitors requires further *in vivo* validation. Importantly, PDX models serve as indispensable tools in preclinical drug efficacy testing since they reliably resemble cellular and molecular features of original tumors [19].

In this study, olaparib-resistant *BRCA1/2*<sup>MUT</sup> PDX models of HGSOC have been established from a patient's tumor to extensively investigate the role of the ATR/CHK1 pathways inhibitors in potentiating therapeutic response to olaparib.

## Materials and Methods

### Materials

PARPi (O, olaparib, AZD2281) was purchased from MedChemExpress (Monmouth Junction, New Jersey, USA). ATRi (A, ceralasertib, AZD6738) and CHK1i (C, MK-8776) were purchased from Wuhan ChemNorm Biotech (Wuhan, China). Master liquids of each drug were prepared in 100% dimethyl sulfoxide (DMSO) and stored at  $-80^{\circ}\text{C}$  for the future preparations of *in vivo* formulations. Working solutions for *in vivo* injections were prepared by diluting master liquids in a vehicle composed of 10% (v/v) DMSO, 40% (v/v) PEG300, and 5% (v/v) Tween 80 in double-distilled water. Other key reagents used in this study are described in the Material and Methods section and **Table S1**.

### Generation of PDX models of HGSOC

All animal procedures were conducted according to the protocol approved by the Local Ethics Committee of The Warsaw University of Life Sciences in Warsaw (protocol number: WAW2/024/2021) and the consent of the Bioethics Committee at The Maria Skłodowska-Curie National Research Institute of Oncology in Warsaw (55/2017). Immunodeficient NSG/J female mice were obtained from the Jackson Laboratory and maintained in a specific pathogen-free facility. All animals were housed according to the local regulations at  $22 \pm 2^{\circ}\text{C}$  with 12-hour light/dark cycles. Mice were euthanized as soon as they appeared to be in distress or discomfort during any procedure.

Ovarian cancer tissues were collected between June 20, 2017, and September 5, 2017, from three HGSOC patients X127 (stage IV), X160 (stage IIIB), and X179 (stage IIIC) with *BRCA1/2* mutations who underwent primary debulking surgery at The Maria Skłodowska-Curie National Research Institute of Oncology before further adjuvant therapies.

To establish PDX models of HGSOC, pieces of fresh ovarian carcinoma samples ( $10\text{--}20\text{ mm}^3$ ), obtained after surgical resection, were transplanted subcutaneously into both flanks of NSG/J mice (passage 0, P0 i.e. patient's tumor first growth *in vivo*). The mice were monitored bi-weekly for tumor development. Tumor growth was evaluated by caliper measurements of tumor length (L) and width (W). Approximate tumor volume (V) was calculated using the formula  $V = \frac{1}{2} \times (L \times W^2)$ . To expand the initial tissue for further experiments and preservation, successfully engrafted tumors reaching a volume of  $\sim 500\text{ mm}^3$  were serially excised and subcutaneously retransplanted ( $10\text{--}20\text{ mm}^3$  pieces) into new recipient mice to establish further stabilized generations (P1, P2, P3, and so on). Progressively growing PDX tumors were dissected into fragments, cryopreserved, and stored in a vapor phase of liquid nitrogen for future use.

### Establishment of olaparib-resistant PDX models

A single cryopreserved tumor fragment from each treatment naïve PDX (X127, X160, and X179) was thawed, dissected into  $\sim 20\text{ mm}^3$  pieces, and engrafted subcutaneously into both flanks of two mice to grow and generate enough tissue for further transplantations. Tumor growth was monitored daily until reaching  $\sim 500\text{ mm}^3$ . Then mice were euthanized with 5%

isoflurane followed by cervical dislocation and tumors were excised. Subsequently, ~20 mm<sup>3</sup> tumor fragments from each PDX were retransplanted subcutaneously into the left flank of each of the 12–20 new recipient mice. Mice were randomized when tumor size reached ~150 mm<sup>3</sup> into two groups: vehicle control (n = 6–10), and olaparib (n = 6–10). Animals were treated 5 days a week by intra-peritoneal injections (i.p.) with olaparib (50 mg/kg) or vehicle (10% (v/v) DMSO, 40% (v/v) PEG300, and 5% (v/v) Tween 80 in double-distilled water). Tumor growth along with mice's body weight were measured two times a week. The transplanted xenografts that showed no growth in mice were rejected. Mice were sacrificed once they showed symptoms of impaired well-being or tumor size exceeded ~1200 mm<sup>3</sup>. Then tumors were dissected, cut into multiple fragments, and cryopreserved for further molecular analyses and retransplantations. Tumor sizes at treatment completion day were compared with tumor sizes at day zero of the treatment to calculate relative tumor volumes and assess sensitivity to olaparib. Tumors that expanded their final size by at least 2-fold compared to their size at the start of treatment in the presence of olaparib for more than 4 weeks were considered resistant to olaparib.

### Treatment with tested inhibitors

Cryopreserved fragments of olaparib-resistant tumors (~20 mm<sup>3</sup>) generated from PDX-X179 were thawed and expanded through subcutaneous retransplantations into new recipient mice. Finally, obtained tumors were dissected and ~20 mm<sup>3</sup> fragments were engrafted subcutaneously into the left flank of 48 mice. Subsequently, after an increase in tumor volume to more than ~50 mm<sup>3</sup>, animals were randomized into six treatment arms with 8 individuals each: vehicle control (10% (v/v) DMSO, 40% (v/v) PEG300, and 5% (v/v) Tween 80 in double-distilled water), olaparib (50 mg/kg), ATRi (25 mg/kg), CHK1i (50 mg/kg), olaparib + ATRi (50 mg/kg + 25 mg/kg), and olaparib + CHK1i (50 mg/kg + 50 mg/kg). Mice received a vehicle by i.p. injections 5 days a week, olaparib by i.p. injections 5 days a week, ATRi administered orally 5 days a week, CHK1i by i.p. injections twice a week, or combinations of tested inhibitors i.e. olaparib with ATRi or olaparib with CHK1i (each single agent administered as described above). Tumor volume and mice body weight were measured two times a week to assess the response to inhibitors. Animals were euthanized after 23 to 37 days of treatment (median 35 days) to evaluate treatment efficacy. Then, tumors were excised, dissected into pieces, and freshly prepared for pathological assessment or snap-frozen for molecular analysis. From a subset of mice from each group, hearts were harvested and cryopreserved for evaluation of potential systemic cardiotoxicity.

### Evaluation of drug efficacy and safety assessment

Growth curves were established based on tumor volumes for individual animals and mean tumor volumes in each group and at different time points. To assess the efficacy of tested inhibitors and their combinations, we evaluated several endpoint outcomes given the lack of consensus regarding the assessment of drug efficacy in PDX models [20, 21]. These include parameters that were adjusted for variation of initial tumor volumes between mice and captured the longitudinal tumor volume measurements.

Firstly, relative tumor volumes (RTV) were calculated for inhibitor-treated (T, treatment) and vehicle-treated control (C, control) animals based on the final tumor volumes on the

treatment completion day (VT or VC) divided by the initial tumor volume at the treatment initiation day (VT<sub>0</sub> or VC<sub>0</sub>) [22, 23] according to the formulas below. Responses were classified as stable disease (SD; RTV of 0.70 to 1.20) or progressive disease (PD; RTV greater than 1.20) [24, 25].

$$RTV_T = \frac{VT}{VT_0} \quad \text{and} \quad RTV_C = \frac{VC}{VC_0}$$

Next, the relative treatment-to-control (T/C) ratio on the last day of treatment was calculated by dividing RTV<sub>T</sub> values for each tumor from treatment groups by the average RTV<sub>C</sub> value for a vehicle control group to assess the treatment effect. In general, low relative T/C ratio values indicate a strong antitumor effect. Tumors were assigned according to T/C ratios as highly responsive (T/C ratio less than 0.1), responsive (T/C ratio between 0.1 and 0.42), and non-responsive (T/C ratio greater than 0.42) [26–28].

Moreover, antitumor activity was estimated using tumor growth inhibition (TGI) parameter calculated at the end of the treatment relative to initial tumor size for each animal and compared to a vehicle control group according to the formula:

$$TGI = \left[ \left( 1 - \frac{VT}{VT_0} \right) \times \left( 1 - \frac{VC_0}{VC} \right)^{-1} \right] \times 100\%$$

VC and VC<sub>0</sub> indicate average tumor volume from a vehicle control group at the completion and the initiation of the treatment, respectively, whereas VT and VT<sub>0</sub> represent volumes of tumors treated with inhibitors at the completion and the start of the treatment, respectively [23]. Based on TGI, the inhibitory effects were compared between a combination of two inhibitors (E<sub>1+2</sub>) and single-agent inhibitors (E<sub>1</sub> and E<sub>2</sub>) using the Response Additivity approach [29] to assess synergy in each PDX tumor treated with combinations. Combination index (CI) values were calculated using average TGI values for treatment groups as effects (E<sub>1</sub>, E<sub>2</sub>, and E<sub>1+2</sub>) according to the formula below. CI values > 1, = 1, and < 1 represent antagonistic, additive, and synergistic effects, respectively.

$$CI = \frac{E_1 + E_2}{E_{1+2}}$$

### Preparation of FFPE sections

Formalin-fixed paraffin-embedded (FFPE) tissue sections were prepared from harvested tumors and hearts. Tissue fragments were fixed in 4% buffered formalin for a few hours at room temperature and subsequently dehydrated in increasing concentrations of ethanol solutions (70% for 40 min, 80% for 2 h, 90% for 1 h, and 96% overnight). Next, the tissue was incubated in the mixture of ethanol and xylene (1:1) for 1 h, followed by incubation in xylene for 2 h. Then, tissue was infiltrated by transferring to a mixture of paraffin and xylene (1:1) for 2 h at 50°C, followed by incubation in liquid paraffin for 3 h at 50°C. Afterward, tissue was embedded in a paraffin block, and 3.5-μm-thick paraffin-embedded histopathological sections were obtained by cutting paraffin blocks with a Leica RM2245 microtome (Leica Biosystems, Germany). FFPE sections were dried on glass slides at 56°C for 1 h and used for further molecular analyses.

## Hematoxylin and eosin (H&E) staining

Hematoxylin and eosin (H&E) staining was performed in tumor and heart samples. Firstly, FFPE sections were deparaffinized by incubation in xylene (2 × 10 min) and rehydrated in ethanol by the following incubations: 99% for 5 min, 96% for 5 min, 90% for 3 min, 80% for 3 min. Next, FFPE sections were incubated in distilled water for 1 min, stained with Mayer's hematoxylin solution (Dako, Agilent) for 5 min, and excess dye was removed by rinsing with distilled water and incubation in distilled water for 10 min. Then, FFPE sections were incubated with eosin solution (Dako, Agilent) for 30 sec and rinsed with distilled water. Stained tissue samples were incubated with 96% and 99% ethanol for 2 min, followed by incubation with xylene for 10 min. Finally, samples were mounted with DPX Mounting Medium (Dako, Agilent) and subjected to histological analysis.

## Histopathological analysis

Histological assessment of FFPE tissue samples stained with H&E was performed by experienced histopathologists following the ISO9001 standard using ZEISS Axiolab 5 microscopes (Zeiss, Germany). Histopathological assessment criteria were based on scientific literature and recommendations included in the International Harmonization of Nomenclature and Diagnostic Criteria developed and published by The Global Editorial and Steering Committee. Tissues were evaluated at 5×, 10×, 40×, and 100× objective magnification based on the location, nature, and severity of pathological changes. Detailed scoring rules for each type of parameter are presented in **Table S2**. Tumor tissues were assessed for vacuolization of tumor cells, pleomorphism of the nuclei, and necrosis in 3–6 individuals from each treatment arm. The mitotic index (MI) was also examined to evaluate the proliferative activity. Heart tissues were assessed in 2–4 individuals from each treatment group for degeneration of myofibers (hyaline lesions) and cardiomyocytes (vacuolar degeneration).

## Immunohistochemistry

Immunohistochemical staining (IHC) was performed on FFPE tissue sections, which were deparaffinized with xylene and rehydrated in a series of ethanol solutions of decreasing concentration. Heat-induced epitope retrieval was carried out in a Target Retrieval Solution pH 6 (Dako, Agilent) in a 100°C water bath for 30 min. After cooling the retrieval solutions for 30 min at room temperature, the slides were incubated for 5 min with a Blocker of Endogenous Peroxidase (Dako, Agilent). Subsequently, slides were incubated for 1 h at room temperature with the following primary antibodies: anti-pCHK1 (Ser345) diluted 1:1000 or anti-Ki-67 diluted 1:200. Then, slides were rinsed and incubated with an appropriate Signal Stain® Boost IHC Detection Reagent (HRP) for 30 min at room temperature. Staining was visualized by a peroxidase substrate 3,3'-diaminobenzidine tetrahydrochloride (Dako, Agilent). Nuclear contrast was achieved with hematoxylin counterstaining. The images were captured at 20× and 40× magnifications.

Ki-67 proliferation index was defined as the percentage of tumor cells with positive nuclear Ki-67 staining to evaluate the growth fraction of tumor cells. Moreover, a semi-quantitative analysis of immunohistochemical nuclear reactivity for Ki-67 and pCHK1 was performed by calculating histoscore (H-score) which combines both reaction intensity (graded as 0 – none, 1 – weak, 2 – moderate, and 3 – strong staining) and percentage

of the cells with a given intensity according to the previously reported formula: H-score = [(0 × % none) + (1 × % weak) + (2 × % moderate) + (3 × % strong)] [30]. A minimum of 3 slides per group and 3 high power fields per slide at 400× magnification were used to evaluate the staining intensity of 300 cells for each sample. Protein expression was classified according to nuclear immunoreactivity as low (0–100), medium (100–200), or high (200–300) based on the average value of the H-score.

## Analysis of BRCA1/2 variants with NGS

BRCA1/2 genes were screened for the presence of single-nucleotide variants (SNV) and indel mutations in olaparib-resistant tumors by targeted next-generation sequencing (NGS). Briefly, genomic DNA was isolated from tumor tissue samples using DNeasy Blood & Tissue Kit (Qiagen) following the manufacturer's protocol. DNA concentration and purity were measured fluorescently using a Qubit instrument (Thermo Fisher Scientific). Isolated DNA was stored at –20°C until further analysis. Next, targeted DNA libraries were prepared using the Oncomine™ Comprehensive Assay v3 (Thermo Fisher Scientific) according to the manufacturer's protocol. DNA libraries were sequenced using Ion Proton™ Sequencer (Thermo Fisher Scientific). Variant calling and annotation were performed using Ion Reporter Software according to the Oncomine™ BRCA Research Somatic-530-w3.6-DNA-Single Sample Workflow (v5.18). Variants were classified as pathogenic according to the NCBI ClinVar database.

## RNA isolation, cDNA synthesis, and RT-qPCR

Frozen tumor fragments were ground in a mortar and pestle with liquid nitrogen. Obtained tissue powder from each sample was split into two pre-chilled microcentrifuge tubes and used immediately for protein extraction and RNA isolation separately. Total RNA was isolated using mirVana™ miRNA Isolation Kit with phenol (Thermo Fisher Scientific) according to the manufacturer's protocol. The quality and quantity of isolated RNA were analyzed by absorbance measurements at 230, 260, and 280 nm using a BioTek Eon™ microplate spectrophotometer. Total RNA was aliquoted and stored at –80°C.

cDNA synthesis and RT-qPCR gene expression analysis were performed as described previously [13] using High-Capacity cDNA Reverse Transcription Kit (Thermo Fisher Scientific) and TaqMan™ Universal Master Mix II (no UNG) with predesigned TaqMan™ Gene Expression Assays (Thermo Fisher Scientific). Details concerning TaqMan® probes can be found in **Table S3**.

For qPCR gene expression analysis, a maximization set-up was employed to analyze all genes (*ACTB*, *ABCB1*, *ATR*, *CHEK1*, *CASP3*, *H2AFX*, and *PARP1*) in the same run and spread samples across runs. An identical pooled vehicle control cDNA sample was used as an inter-run calibrator and analyzed for all assays during each run to compare relative quantities of genes in all samples. Each sample was run in triplicate, extracted  $C_T$  values were averaged, and checked for technical variability (STD between technical replicates  $\leq 0.3$  cycles).  $C_T$  values obtained for the *ABCB1* gene encoding MDR1 were greater than a selected cut-off for reliable quantification ( $C_T < 35$  cycles) and rejected from the quantitative analysis. Relative mRNA expression was calculated according to the comparative  $2^{-\Delta\Delta C_T}$  method using *ACTB* as a reference gene for normalization. Normalized fold change data relative to vehicle-treated group were log-transformed before statistical analysis to reduce data skewness and the results were presented as mean  $\pm$  STD. Outliers were identified according to the ROUT method with 5% FDR using

GraphPad Prism. To identify highly relevant differentially expressed target genes, a cut-off of  $\geq 2.0$  absolute expression fold change with  $p < 0.05$  was selected.

### Protein extraction and Western Blotting

Whole-cell tissue lysates were prepared from tumor powder immediately after cryogenic grinding. Briefly, tumor powders were transferred to microcentrifuge tubes prefilled with 3.0 mm TriplePure™ Zirconium beads (Benchmark Scientific, UK) and ice-cold RIPA buffer (Thermo Fisher Scientific) supplemented with 1 mM with PMSF, Halt™ Protease Inhibitor Cocktail (Thermo Fisher Scientific) and Halt™ Phosphatase Inhibitor Cocktail (Thermo Fisher Scientific). Subsequently, samples were homogenized in BeadBug™ 6 microtube homogenizer (Benchmark Scientific, UK) for 30 sec at 4000 rpm, centrifuged (14 000×g, 1 min, 4°C) to reduce foaming, and incubated on ice for 15 min. Next, samples were centrifuged (14 000×g, 15 min, 4°C) and sonicated with a probe sonicator (2 pulses, 10 sec, 15% amplitude). Total protein concentration was quantified in clear tissue lysates with Pierce™ BCA Protein Assay Kit (Thermo Fisher Scientific) according to the manufacturer's instructions. Subsequently, protein samples were prepared in LDS Buffer, separated by SDS-PAGE, and transferred by semi-dry transfer, followed by immunodetection as described previously [13]. Primary antibodies used in the study are listed in **Table S4**.

Enhanced chemiluminescence images were captured with Azure 300 Imaging System (Azure Biosystems, Dublin, CA, USA). Densitometric quantification of the bands was performed with ImageJ software (NIH, Bethesda, MD, USA). Protein expression was normalized using  $\beta$ -actin, expressed as fold change values relative to vehicle-treated cells and presented on graphs with a logarithmic scale. Fold change data were log-transformed before statistical analysis to reduce skewness. Outliers were identified according to the ROUT method with 5% FDR using GraphPad Prism. To identify highly relevant differentially expressed proteins, a cut-off of  $\geq 2.0$  absolute expression fold change with  $p < 0.05$  was selected.

### Statistical Analysis

Statistical analysis was performed with GraphPad Prism version 10.2.1 for Windows (GraphPad Software, San Diego, CA, USA) using the appropriate tests specified in Figure captions. Shapiro–Wilk test was used to assess the normality of data distribution. Homogeneity of variance was evaluated with Brown–Forsythe and Bartlett's tests. Student t-test was used to compare means between two groups drawn from normally distributed data. Ordinary one-way ANOVA followed by Tukey's or Šidák multiple comparison tests and Brown–Forsythe ANOVA followed by Dunnett's T3 multiple comparison test were used to assess the statistical significance of differences where more than two groups were defined by one factor (treatment) with normally and non-normally distributed data, respectively. Two-way ANOVA followed by Dunnett's multiple comparison tests was used to assess the statistical significance of differences where more than two groups were defined by two factors (treatment and timepoint). Unless otherwise stated, differences between groups were considered statistically significant at: \* $p < 0.05$ , \*\* $p < 0.01$ , \*\*\* $p < 0.001$ , \*\*\*\* $p < 0.0001$  (vehicle vs. inhibitor(s)); \* $p < 0.05$ , \*\* $p < 0.01$ , \*\*\* $p < 0.001$ , \*\*\*\* $p < 0.0001$  (olaparib vs. combination with ATRi or CHK1i); \* $p < 0.05$ , \*\* $p < 0.01$ , \*\*\* $p < 0.001$ , \*\*\*\* $p < 0.0001$  (ATRi or CHK1i vs. respective combinations with olaparib).

## Results

### Characterization of the olaparib-resistant PDX model of HGSOC

Ovarian tumors with *BRCA1/2* mutations generally respond well to olaparib, but may eventually acquire decreased sensitivity to the treatment, thereby reducing its clinical utility [31, 32]. In this study, we established the olaparib-resistant PDX models of HGSOC to investigate mechanisms driving resistance to PARPi and evaluated the efficacy of combinations of olaparib with the ATR/CHK1 pathway inhibitors.

Initially, three olaparib-naïve PDX models of HGSOC (X127, X160, and X179), developed from tumor samples obtained from patients diagnosed with HGSOC, were used to induce resistance to olaparib *in vivo*. NGS-based analysis of *BRCA1/2* genes revealed pathogenic exonic variants with loss-of-function mutations in PDX-X179 (*BRCA1/2*<sup>MUT</sup>) and PDX-X127 (*BRCA1/2*<sup>MUT</sup>) tumors (**Table 1**). Treatment-naïve PDX-X179 HGSOC model exhibited a total of 9 exonic variants in both *BRCA1* and *BRCA2* genes (**Table 1**) identified by targeted NGS. Importantly, PDX-X179 carried a heterozygous *BRCA1* missense mutation (c.181T>G; p.Cys61Gly) located in a mutational hot spot and *BRCA2* truncating mutation (c.4677delT; p.Phe1559LeufsTer9), both classified as pathogenic (**Table 1**). These genetic alterations mirrored the HRD status commonly found in approximately 50% of HGSOC patients [33], which is crucial for recommending olaparib maintenance therapy in clinical practice [34].

Importantly, PDX-X179 with clinically-relevant *BRCA1/2* mutations fulfilled a genetic prerequisite for further studies. To induce resistance to olaparib *in vivo*, PDX-X179 tumors were transplanted into 16 female mice, allowed to reach a volume of  $\sim 150$  mm<sup>3</sup>, and animals with successful engraftments were randomized into vehicle control ( $n = 6$ ), and olaparib ( $n = 8$ ) groups. Mice with stable well-being and tumor growth during treatment with a vehicle ( $n = 4$ ) or 50 mg/kg olaparib ( $n = 5$ ) 5 days a week for over 4 weeks were selected for sensitivity comparison to PARPi (**Figure 1a**). Four-week treatment duration was chosen based on the typical cycle length of olaparib therapy in clinical practice, usually lasting 28 days, each followed by a treatment response assessment [17, 35, 36]. Importantly, two tumors (#11 and #14) from the PDX-X179 model successfully acquired resistance to PARPi throughout 42 days of continuous olaparib treatment (**Figure 1b**).

As presented, vehicle-treated tumors ( $n = 4$ ) exhibited stable dynamic growth (**Figure 1b-c**) and increased relative volume by about 8.0 times within 31 days of treatment initiation day. In the presence of olaparib, the treatment response was heterogeneous among mice. The comparison of tumor sizes at the completion and the initiation of treatments showed that two xenografts (#5 and #9) were sensitive displaying relative tumor volumes of 0.16 (decrease by 6.2-fold) and 0.59 (decrease by 1.7-fold), respectively (**Figure 1b-c**). One tumor (#12) was partially sensitive to PARPi with no meaningful changes in relative tumor volume. Two xenografts (#11 and #14) remained on olaparib treatment for 42 days and gradually acquired resistance to PARPi exhibiting relative tumor volumes of 2.7 and 2.0, respectively (**Figure 1b-c**). In PDX tumors #11 and #14, there was an initial period of tumor growth reaching a peak at days 21–24 before short-term tumor regression, followed by recurrence and growth stabilization indicating desensitization to PARPi. (**Figure 1b**). Notably, no significant body-weight loss was observed in any group during (**Figure 1d**), and at the end of treatment



(Figure 1e), indicating no apparent toxicity of the vehicle or olaparib in mice.

Despite successful engraftments, PDX-X127 and PDX-X160 models were excluded from further experiments due to atypical growth kinetics characterized by unexpectedly rapid growth rates and variability among animals. The growth curves for the abovementioned PDX tumors and mice body weights throughout the treatment with olaparib or vehicle were presented in Figure S1.

To preliminarily assess changes associated with varied responses to olaparib in PDX-X179 xenografts, we examined the expression of proteins involved in PARP signaling (PARP1, PARG), HR repair pathway (RAD51), and MDR1 efflux pump. Protein expression was evaluated in untreated PDX-X179 at P5 and PDX-X179 treated with the vehicle (#6, #7, #8) or olaparib (#5, #9, #11, #12, #14) (Figure 1f). Changes in protein levels of at least 2-fold

relative to primary PDX-X179 at P5 were considered biologically meaningful. Additionally, both xenografts that acquired resistance to olaparib (#11 and #14) exhibited similar expression patterns of PARP1, PARG, and RAD51, which distinguished them from primary PDX-X179 at P5, vehicle-treated xenografts (#6, #7, #8), and most olaparib-sensitive xenografts (#9 and #12). Tumors with acquired resistance to olaparib notably downregulated PARP1, PARG, and RAD51, whereas vehicle-treated tumors upregulated PARG and RAD51. In all xenografts, there were no significant changes in MDR1 expression (Figure 1f).

Overall, novel olaparib-resistant PDX models of HGSOc were developed in two tumors, allowing further investigation into the mechanism underlying the resistant phenotype and the evaluation of the effective combinations of inhibitors to restore olaparib efficacy *in vivo*.

**Table 1. Treatment-naïve PDX-X127 and PDX-179 models established from HGSOc patients tumors carry *BRCA1/2* variants with loss-of-function mutations classified as pathogenic.**

PDX	Gene	Exon	Variant Type	Function	Gene Change	Protein Change	Allele Frequency [%]	ClinVar Classification
X127	BRCA1	10	INDEL	frameshift deletion	c.1728delT	p.Glu577AsnfsTer11	34.3	Pathogenic (!)
		10	SNV	missense	c.1114A>C	p.Asn372His	90.8	Benign
		11	SNV	synonymous	c.4563A>G	p.Leu1521=	100.0	Benign
	BRCA2	11	INDEL	frameshift deletion	c.5946delT	p.Ser1982ArgfsTer22	89.1	Pathogenic (!)
		11	SNV	synonymous	c.6513G>C	p.Val2171=	99.9	Benign
		14	SNV	missense	c.7397T>C	p.Val2466Ala	100.0	Benign
X179		23	INDEL	frameshift deletion	c.9097delA	p.Thr3033LeufsTer29	15.3	Pathogenic (!)
		4	SNV	missense	c.181T>G	p.Cys61Gly	58.9	Pathogenic (♦)
		10	SNV	missense	c.1067A>G	p.Gln356Arg	51.9	Benign
		10	SNV	synonymous	c.2082C>T	p.Ser694=	43.4	Benign
		10	SNV	synonymous	c.2311T>C	p.Leu771=	43.7	Benign
	BRCA1	10	SNV	missense	c.2612C>T	p.Pro871Leu	44.2	Benign
		10	SNV	missense	c.3113A>G	p.Glu1038Gly	41.7	Benign
		10	SNV	missense	c.3548A>G	p.Lys1183Arg	43.9	Benign
		12	SNV	synonymous	c.4308T>C	p.Ser1436=	43.2	Benign
		15	SNV	missense	c.4956G>A	p.Met1652Ile	41.6	Benign
	BRCA2	10	SNV	missense	c.978C>A	p.Ser326Arg	33.8	Benign
		10	SNV	missense	c.1114A>C	p.Asn372His	99.3	Benign
		10	SNV	missense	c.1151C>T	p.Ser384Phe	54.8	Benign
		11	SNV	synonymous	c.3396A>G	p.Lys1132=	55.8	Benign
		11	SNV	synonymous	c.4563A>G	p.Leu1521=	99.9	Benign
		11	INDEL	frameshift deletion	c.4677delT	p.Phe1559LeufsTer9	48.3	Pathogenic (!)
		11	SNV	synonymous	c.6513G>C	p.Val2171=	100.0	Benign
		14	SNV	synonymous	c.7242A>G	p.Ser2414=	58.6	Benign
		14	SNV	missense	c.7397T>C	p.Val2466Ala	99.9	Benign

(♦) Mutation located in a mutational hot spot, (!) Truncating mutation, SNV – single-nucleotide variant, INDEL - insertion-deletion mutation.



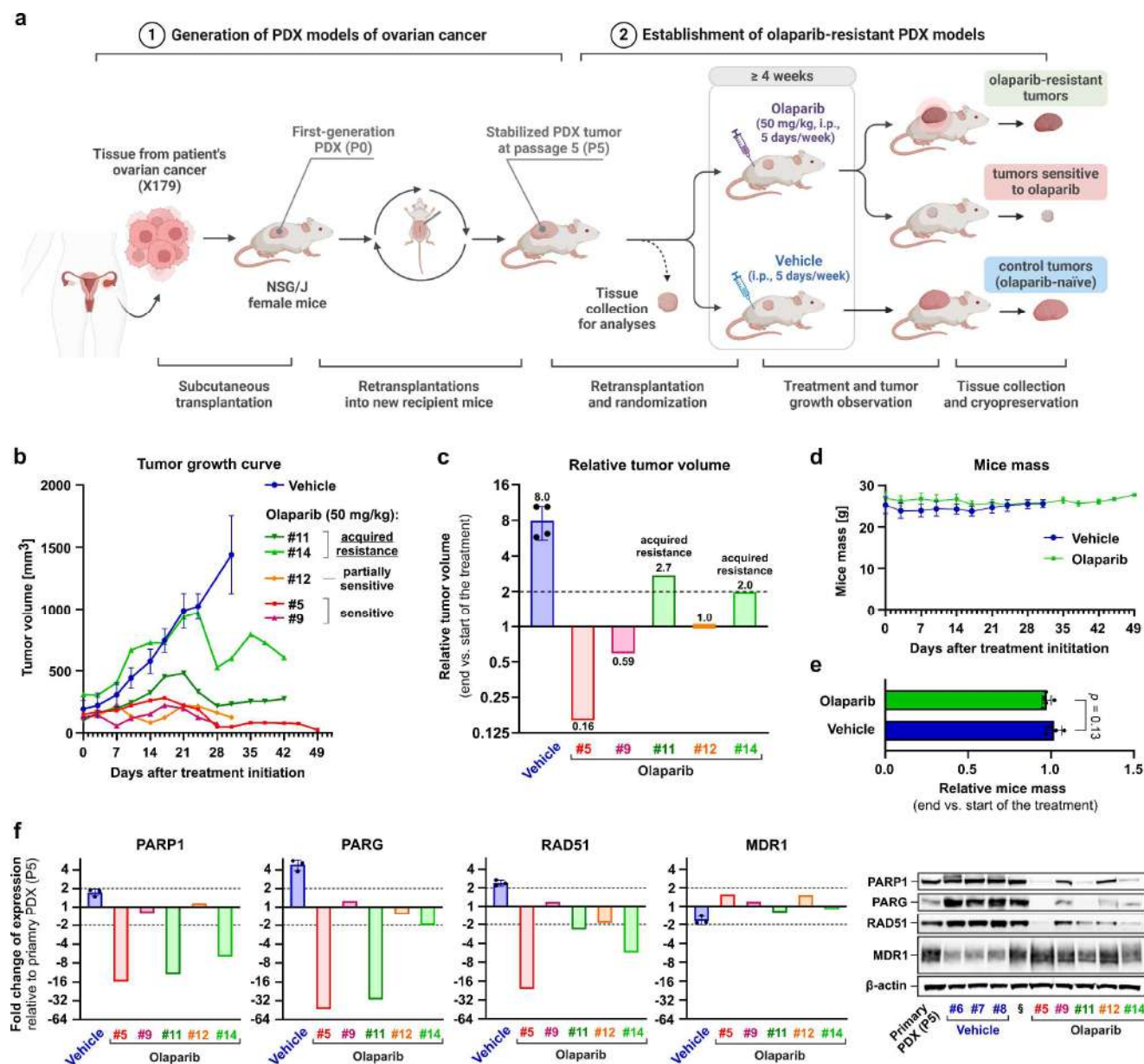


**Figure 1. Development of acquired resistance to olaparib in the PDX-X179 model of HGSOC *in vivo*.** (a) Overview of the establishment process of olaparib-resistant PDX models of HGSOC. (b) Tumor growth curves for mice treated 5 days a week with olaparib (50 mg/kg,  $n = 8$ ) or vehicle control ( $n = 6$ ). Results for mice with successful engraftment that were treated for over 4 weeks with olaparib ( $n = 5$ ) or vehicle ( $n = 4$ ) were presented. Tumor volumes for a vehicle control group are presented as mean  $\pm$  STD. (c) A bar graph with a logarithmic scale showing relative tumor volumes at harvest compared to initiation of the treatment. The results for a vehicle control group are presented as mean  $\pm$  STD ( $n = 4$ ). (d) Mice body weights during treatment with olaparib (50 mg/kg,  $n = 5$ ) or vehicle ( $n = 4$ ). Statistical significance was assessed for each timepoint between groups using multiple t-tests followed by the Holm-Sidak post-hoc test:  $^*p < 0.05$ . (e) Comparison of changes in mice masses (fold change) between groups at harvest day relative to day zero of treatment using unpaired t-test:  $^*p < 0.05$ . (f) Bar graphs with a logarithmic scale showing results of quantitative Western Blotting analysis of PARP1, PARG, RAD51, and MDR1 in PDX-X179 tumors (olaparib-resistant, -sensitive, and -naïve). Primary, early-generation PDX-X179 at passage 5 (P5) was used for transplantation to mice, which were randomized to vehicle-treated (#6, #7, #8) and olaparib-treated (#5, #9, #11, #12, #14) groups. Protein expression in treated tumors was calculated as a fold change relative to primary PDX-X179 at P5 and presented for vehicle control as mean  $\pm$  STD ( $n = 3$ ). Dashed lines indicate at least 2-fold changes in the protein levels. Representative Western Blotting images were presented. Symbol § indicates the protein sample from PDX-X179 tumor #2, which was randomized to the olaparib-treated cohort and rejected from the study due to insufficient tumor growth after transplantation.

### Conferring resistance to olaparib impairs PARP signaling in the PDX models of HGSOC

Olaparib exerts dual cytotoxic activity by catalytic inhibition of PARP1, blocking PARylation and affecting DDR, and PARP1 trapping at DNA damage sites leading to its inactivation and accumulation of cytotoxic DNA lesions [4]. Depletion of PARP1 has been linked to olaparib resistance, as PARP1 is essential for the cytotoxicity of PARPi [4]. To investigate the relationship between mechanisms of resistance to olaparib and PARP signaling, we evaluated the expression of PARP1 polymerase,

PARG glycohydrolase, and total PARylation level in PDX tumors collected after resistance induction (Figure 2a).

Relative protein levels in vehicle-treated (#6, #7, #8, and #10) and olaparib-resistant tumors (#11 and #14) were compared to untreated PDX from P5 to investigate changes associated with tumor progression (vehicle group) and induction of resistance (olaparib group). Tumors with acquired resistance to olaparib showed significantly decreased levels of PARP1 by 13.8-fold, accompanied by a significant reduction in total PARylation levels by 5.6-fold (Figure 2a), consistent with the olaparib pharmacodynamics in OC cells [37]. Additionally, PARG expression was

significantly decreased by 5.3-fold in tumors with acquired resistance to olaparib. Conversely, vehicle-treated tumors with progressive disease significant increases in PARP1 expression (by 2.1-fold) and PARG expression (by 3.2-fold), and PARylation level (by 10.6-fold) (**Figure 2a**). Importantly, there was a strong positive correlation ( $r = 0.89\text{--}0.98$ ) between the expression of PARP1 and PARG and PARylated protein content among vehicle-treated and olaparib-resistant tumors (**Figure 2b**).

Altogether, vehicle-treated PDX tumors in the absence of olaparib exerted increased PARP1 activity compared to olaparib-naïve tumors. Conversely, induction of resistance to olaparib was associated with deregulated PARP signaling in PDX models of HGSOC, leading to a decrease in PARylation of target proteins along with downregulation of PARP1 and upregulation of PARG. The findings indicate that partial loss of PARP1 may contribute to acquired resistance to olaparib through reduced PARylation and diminished PAR trapping.

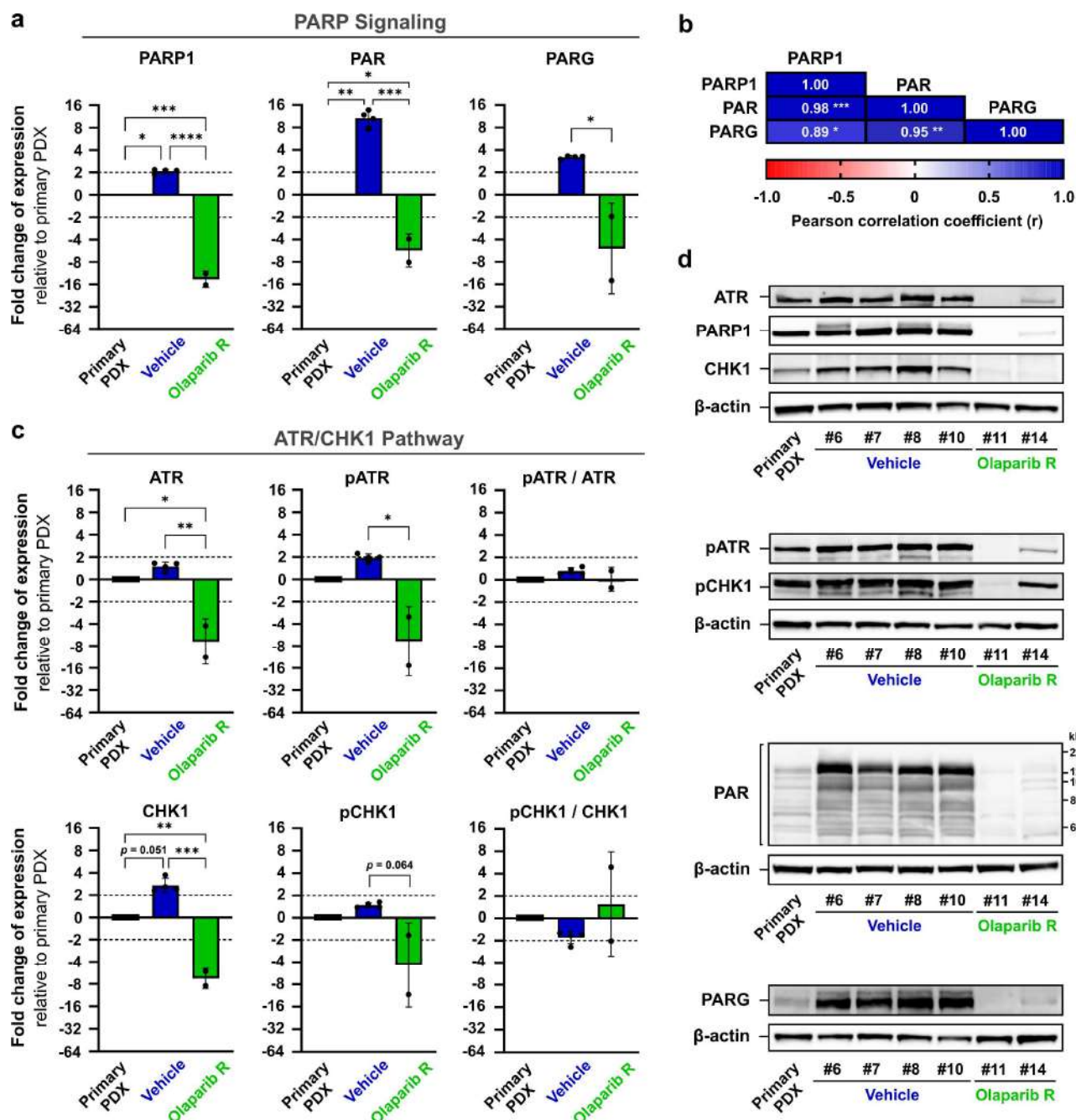


**Figure 2. Induction of resistance to olaparib in PDX models of HGSOC inhibits PARP1-mediated PARylation and downregulates the expression and phosphorylation of both ATR and CHK1 kinase with preserved relative pathway activation.** Upon the completion of the development of olaparib-resistant (R) PDX models, vehicle-treated xenografts (#6, 7, 8, and 10), and tumors with acquired resistance in the presence of 50 mg/kg olaparib (#11 and 14) were harvested, and whole tissue lysates were prepared for Western Blotting analysis. Protein expression was normalized to  $\beta$ -actin and presented on graphs with a logarithmic scale as a fold-change (mean  $\pm$  STD) relative to untreated primary PDX-X179 at P5 used for the development of tumors for both treatment arms. Dashed lines indicate expression cut-off of  $\pm 2$ -fold to indicate relevant changes (**a**) Quantitative Western Blotting analysis of PARP1 and PARG expression and PARylation level of target proteins (~50–220 kDa). (**b**) Pearson correlation analysis between PARP1 and PARG expression and PARylated protein content. (**c**) Quantitative Western Blotting analysis of total expression of ATR and CHK1, and phosphorylation of ATR (Thr1989) and (C) and CHK1 (Ser345). Phosphorylation levels of kinase were also expressed compared to the total levels of each protein (pATR/ATR and pCHK1/CHK1) to assess the relative activation of the ATR/CHK1 pathway. (**d**) Representative Western Blotting images. For quantitative Western Blotting, statistical significance between groups was assessed using ordinary one-way ANOVA followed by Tukey's post-hoc test: \* $p < 0.05$ , \*\* $p < 0.01$ , \*\*\* $p < 0.001$ , \*\*\*\* $p < 0.0001$ . For correlation analysis, statistical significance was assessed based on computed two-tailed  $p$  values: \* $p < 0.05$ , \*\* $p < 0.01$ , \*\*\* $p < 0.001$  (every pair of data set).

## Acquired resistance to olaparib affects the expression of ATR and CHK1 kinases in HGSOc tumors

Previous reports have suggested that olaparib-resistant OC cells exhibit decreased dependence on the ATR/CHK1 pathway for survival in the presence of olaparib compared to OC cell lines *in vitro* [14, 38]. Here, we investigated the role of the ATR/CHK1 pathway activity in acquiring resistance to olaparib in HGSOc cells *in vivo* (Figure 2c). In olaparib-resistant tumors, both ATR expression and ATR phosphorylation levels were significantly decreased by 11.8-fold and 17.7-fold respectively relative to vehicle-treated tumors. Similarly, CHK1 expression and its phosphorylation were notably decreased in resistant tumors. However, when considering the total expression of ATR and CHK1, relative phosphorylation levels of pATR (pATR/ATR) and pCHK1 (pCHK1/CHK1) did not significantly change in both olaparib-resistant and vehicle-treated xenografts (Figure 2c).

These observations indicate that the induction of resistance to olaparib downregulated both ATR and CHK1 expression and their phosphorylation, suggesting reduced dependence on the ATR/CHK1 axis activity of resistant tumor during progression.

## Protein biomarkers associated with DNA damage repair and epithelial-to-mesenchymal transition distinguish olaparib-naïve from olaparib-resistant HGSOc tumors

The sensitivity of OC cell lines to olaparib has previously been linked to EMT-induced deregulation of HR repair [39]. In this study, we investigated the association between acquired resistance to olaparib in PDX tumors and the expression of proteins involved in DDR pathways (BRCA1, BRCA2, 53BP1, RAD51,  $\gamma$ H2AX), EMT (E-cadherin, vimentin, MMP2) (Figure 3), caspase-mediated apoptosis (caspase-3) and multidrug resistance MDR1 efflux pump (Figure S2). Relative protein levels in vehicle-treated (#6, #7, #8, and #10) and olaparib-resistant (#11, and #14) tumors were compared to untreated PDX from P5 to investigate changes associated with tumor progression and induction of resistance.

Regarding alterations in the HR repair pathway, olaparib-resistant xenografts abrogated a significant upregulation of BRCA1 observed upon tumor progression in vehicle-treated mice and remained unchanged levels of BRCA1 relative to untreated primary PDX (Figure 3a).

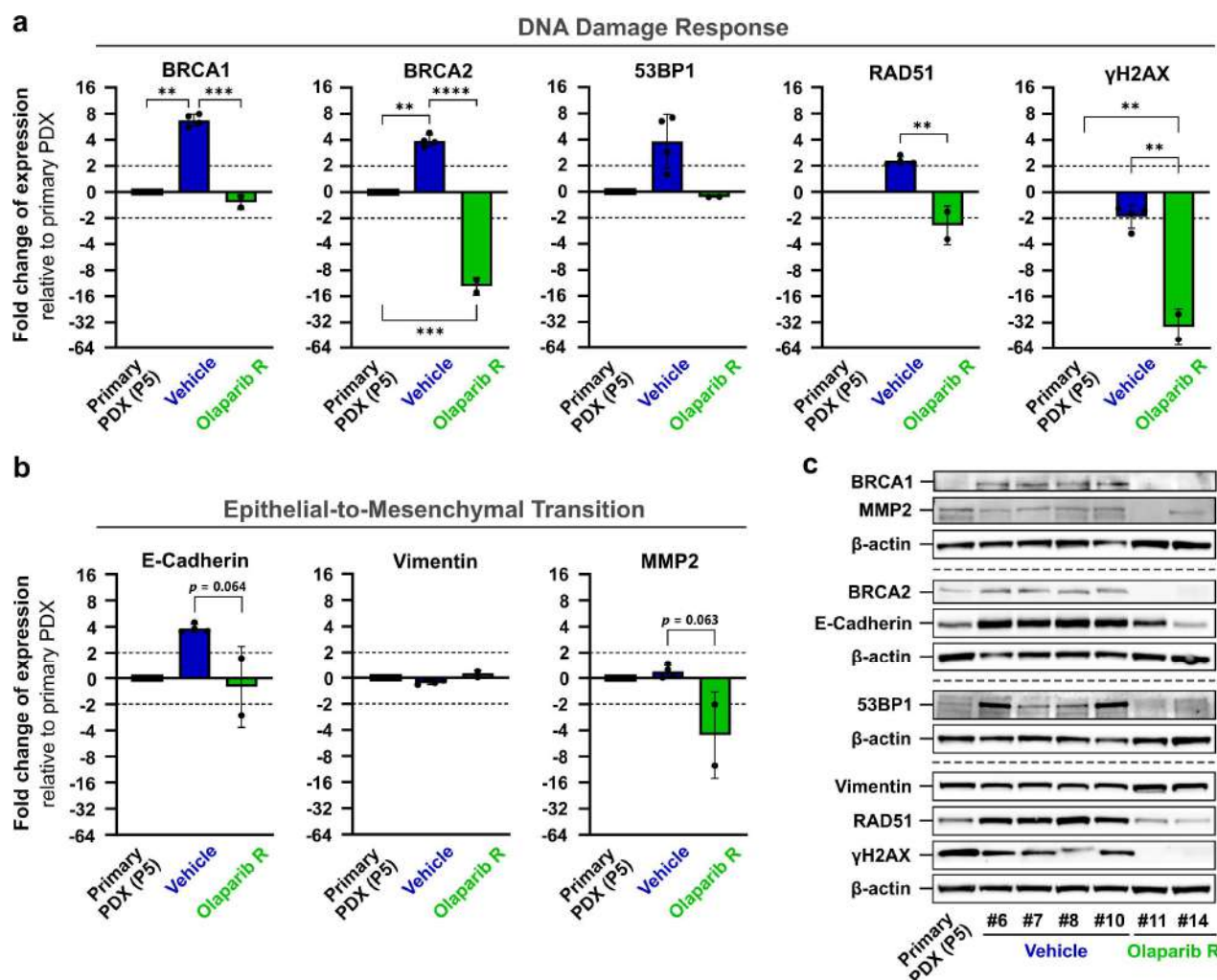


**Figure 3. Induction of resistance to olaparib in PDX models of HGSOc is associated with the downregulation of HR repair-promoting factors and the deregulation of proteins involved in EMT.** Upon the completion of the development of olaparib-resistant (R) PDX models, vehicle-treated xenografts (#6, 7, 8, and 10), and tumors with acquired resistance in the presence of 50 mg/kg olaparib (#11 and 14) were harvested, and whole tissue lysates were prepared for Western Blotting analysis. Protein expression was normalized to  $\beta$ -actin and presented on graphs with a logarithmic scale as a fold-change (mean  $\pm$  STD) relative to untreated primary PDX-X179 at P5 used for the development of tumors for both treatment arms. Dashed lines indicate expression cut-off of  $\pm 2$ -fold to indicate relevant changes (a) Quantitative Western Blotting analysis of expression of proteins associated with DNA damage response (BRCA1, BRCA2, 53BP1, RAD51, and  $\gamma$ H2AX (Ser139)). (b) Quantitative Western Blotting analysis of expression of proteins associated with epithelial-to-mesenchymal transition (E-cadherin, vimentin, and MMP2). (c) Representative Western Blotting images. Statistical significance between groups was assessed using ordinary one-way ANOVA followed by Tukey's post-hoc test: \* $p < 0.05$ , \*\* $p < 0.01$ , \*\*\* $p < 0.001$ , \*\*\*\* $p < 0.0001$ .



Moreover, BRCA2 expression was strikingly downregulated by 12.2-fold in tumors with acquired resistance, whereas vehicle-treated xenografts increased BRCA2 levels by 3.9-fold. Similarly, RAD51 and DSB biomarker  $\gamma$ H2AX levels were significantly decreased in olaparib-resistant tumors relative to vehicle-treated PDX by 5.6-fold and 18.8-fold, respectively (**Figure 3a**). BRCA1 and BRCA2 expression, along with phosphorylation of H2AX, were nearly abolished in tumors with acquired resistance to olaparib. The expression of the NHEJ-mediating 53BP1 protein was notably downregulated in resistant PDX relative to vehicle-treated tumors, however, the decrease was not significant ( $p = 0.106$ ) (**Figure 3a**).

Considering the EMT process, we evaluated the association between epithelial (E-cadherin) or mesenchymal (vimentin, MMP2) markers expression and acquiring resistance to olaparib (**Figure 3b**). Both olaparib-resistant and vehicle-treated tumors showed no changes in vimentin expression. Compared to vehicle-treated tumors, xenografts with acquired resistance notably downregulated E-cadherin and MMP2 by 4.8-fold and 5.4-fold, respectively. However, the magnitude of these changes was noteworthy, and the statistical significance was relatively weak ( $p = 0.064$  and  $p = 0.063$ , respectively) (**Figure 3b**). Assessment of the role of MDR1 and caspase-3 expression in the induction of resistance to olaparib revealed no significant changes in protein expression between cohorts (**Figure S2**).

Overall, olaparib-resistant PDX tumors exhibited decreased levels of  $\gamma$ H2AX and downregulation of HR repair-promoting factors, indicating increased repair capacity, reduced accumulation of DSB, and diminished dependence on the HR repair pathway. Furthermore, induction of resistance was linked to the deregulation of protein mediating EMT. The resistant phenotype was associated with the expression pattern of proteins involved in HR repair and EMT, potentially distinguishing olaparib-resistant from olaparib-naïve tumors.

### The addition of ATRi or CHK1i to olaparib induces antitumor activity towards olaparib-resistant PDX tumors

To investigate the antitumor effect of olaparib combined with ATR/CHK1 pathway inhibitors, we utilized olaparib-resistant PDX-X179 models and determined the efficacy of tested inhibitors *in vivo*. Mice received olaparib (O, 50 mg/kg), ATRi (A, 25 mg/kg), CHK1i (C, 50 mg/kg), or their combinations (O + A or O + C). Treatment duration lasted up to 37 days (median 35 days) according to the described schedule in the Methods section. The efficacy of inhibitors and tumor responses were evaluated based on tumor growth curves, relative tumor volumes (RTV), relative tumor-to-control (T/C) ratios, tumor growth inhibition (TGI) compared to vehicle-treated animals, and combination indices (CI) (**Figure 4**). Endpoint measurements were calculated as ratios of the post- to pre-treatment tumor volumes.

Response to olaparib was heterogeneous concerning growth curve patterns among five olaparib-treated mice (**Figure 4a**). However, the growth of olaparib-resistant tumors was not significantly affected by olaparib alone, with an average RTV increase of 4.2-fold, compared to the average 7.0-fold elevation in the vehicle-treated cohort (**Figure 4b**). This observation confirmed that tumors with acquired resistance maintained their phenotype *in vivo* after retransplantations. None of the single-agent inhibitors had a significant effect on the growth of olaparib-resistant tumors, according to RTV values and T/C ratios

(**Figure 4a-b**). In contrast, combination treatments demonstrated significant antitumor activity. As shown on tumor growth curves, the addition of ATRi or CHK1i to olaparib significantly reduced tumor volumes in the last days of treatments (**Figure 4a**). Importantly, combining olaparib with either ATRi or CHK1i significantly reduced the average RTV increase in vehicle-treated mice from 7.0-fold to about 1.4-fold and 2.6-fold in each combination cohort, respectively (**Figure 4b**). When we looked at individual tumor responses, the criterion for stable disease (RTV was between 0.70 and 1.20) was met in two of five mice treated with the combination of olaparib and ATRi (#47 and #22) with RTV values of 1.00 and 1.06, respectively. Additionally, mouse #30 from the olaparib + ATRi cohort nearly reached the cut-off value for stable disease with a 1.25-fold RTV increase.

Considering relative T/C ratio endpoint measurements, both combination groups were generally classified as responsive ( $0.10 \leq \text{relative T/C ratio} \leq 0.42$ ) (**Figure 4c**). Consistent with the antitumor effect evaluated with RTV, the addition of ATRi to olaparib exhibited a higher antitumor effect than co-treatment with CHK1i, resulting in a relative T/C ratio of 0.21. Examination of individual tumor responses revealed that all five mice receiving olaparib combined with ATRi, three of five animals receiving olaparib combined with CHK1i (#25, #35, and #10), and one individual in ATRi (#46) and olaparib (#27) cohorts were classified as positive responders (**Figure 4c**).

Evaluation of TGI values for animals treated with either combination indicated a significant inhibition of tumor enlargement (**Figure 4d**). The addition of ATRi or CHK1i to olaparib exerted synergistic inhibitory effects, resulting in TGI of 96% (CI = 0.84) and 85% (CI = 0.75), respectively, suggesting that combinations of inhibitors were more effective than single agents (**Figure 4d**). Consistent with previous efficacy measures, the best response was achieved in three PDX treated with olaparib combined with ATRi (#47, #22, and #30) resulting in a  $102 \pm 2\%$  of TGI (slight RTV increase by  $1.10 \pm 0.10$ ) and growth stabilization compared to vehicle-treated mice (**Figure 4d**). In the group receiving olaparib with CHK1i, the best antitumor response was obtained for tumor #25 characterized by 96% TGI accompanied by a moderate RTV increase of 1.40. Importantly, all tested treatments were well-tolerated in mice, with no significant effect of the change on the body weight of animals assessed at each time point relative to the vehicle control cohort (**Figure 4f**). Mice receiving single-agent inhibitors or olaparib combined with CHK1i showed no significant drug-induced weight loss after treatments compared to vehicle-treated animals (**Figure 4g**). A minor, but statistically significant reduction of body weight by 4% from the initiation until the end of the treatment was observed in mice treated with a combination of olaparib and ATRi. However, this slight reduction of mice masses is not generally considered biologically relevant [40].

Overall, tumor responses revealed synergistic inhibition of xenograft growth during treatment with combinations of olaparib with ATRi or CHK1i, yet no tumor shrinkage was achieved. Nevertheless, olaparib-resistant PDX tumors generally exhibited sustained resensitization to olaparib in the presence of ATR/CHK1 inhibitors compared to single-agent inhibitors. Although responses among xenografts in combination cohorts were heterogeneous, all mice receiving olaparib combined with ATRi were classified as responders. Significant antitumor effects leading to stable disease were observed in two of five xenografts receiving the combination of olaparib and ATRi.

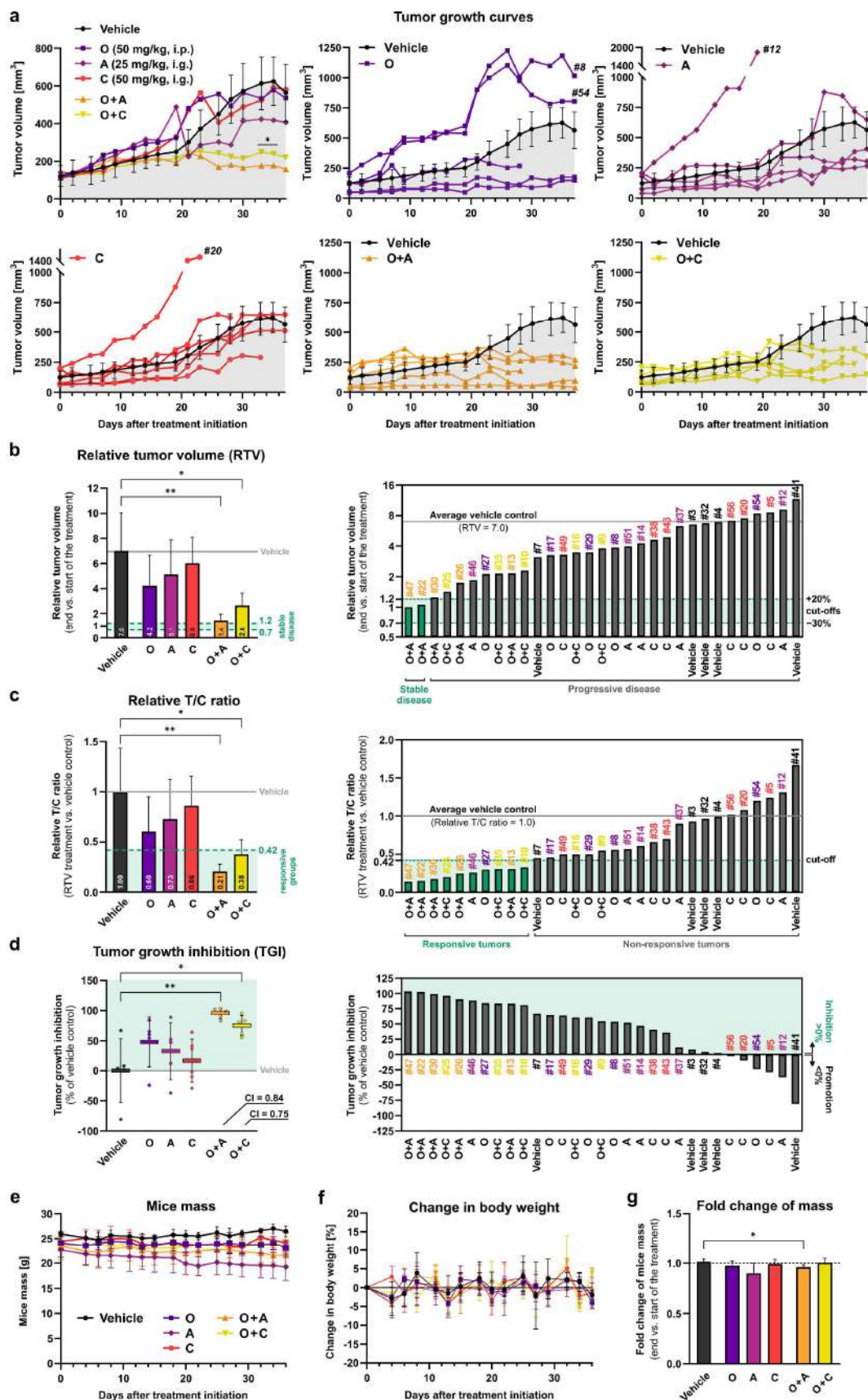


**Figure 4. Olaparib in combination with inhibitors of the ATR/CHK1 pathway exerts antitumor activity in olaparib-resistant PDX models of HGSOC.** Mice bearing olaparib-resistant tumors were treated with vehicle (n = 5), olaparib (O, 50 mg/kg, n = 5), ATRi (A, 25 mg/kg, n = 5), CHK1i (C, 50 mg/kg, n = 6) or olaparib combinations with either ATRi (O + A, n = 5) or CHK1i (O + C, n = 5). **(a)** Tumor growth inhibition curves for mice treated with vehicle (mean  $\pm$  STD) and tested inhibitors (mean). Error bars for mean tumor volumes in inhibitor-treated groups at each time point were excluded for clarity. The following curves show the growth of tumors in each mouse in the group. The area under the curve for a vehicle-treated group was tinted in grey. Statistical significance between vehicle- and inhibitor-treated groups at each timepoint was determined using ordinary two-way ANOVA followed by Dunnett's post-hoc test. **(b)** Relative tumor volume (RTV) was calculated by dividing final tumor volumes (the treatment completion day) by the initial tumor volume (the treatment initiation day). Responses were categorized as stable disease (RTV of 0.70 to 1.20) or progressive

disease (RTV greater than 1.20). Data was presented as mean  $\pm$  STD for each group and all individual PDX tumors. Statistical significance between groups was determined using ordinary one-way ANOVA followed by Šidák post-hoc test. **(c)** The relative treatment-to-control (T/C) ratio was calculated by dividing the RTV for PDX tumors treated with inhibitor(s) by the average RTV for the vehicle-treated group on the treatment completion day. Data was presented as mean  $\pm$  STD for each group and all individual PDX tumors. Statistical significance between groups was determined using ordinary one-way ANOVA followed by Šidák post-hoc test. **(d)** Tumor growth inhibition (TG) values for each group (mean  $\pm$  STD) and each PDX tumor. The synergy between each agent alone in mice treated with combinations of inhibitor groups was assessed based on combination indices (CI) values, where  $CI < 1$  indicates a synergistic effect. Statistical significance between groups was determined using ordinary one-way ANOVA followed by Šidák post-hoc test. **(e)** Overview of mice bodyweights (mean  $\pm$  STD) among groups during treatment. **(f)** Changes in mice mass (mean  $\pm$  STD) among groups throughout treatment at each timepoint relative to the previous measurement. Statistical significance between vehicle- and inhibitor-treated groups at each timepoint was determined using ordinary two-way ANOVA followed by Dunnett's post-hoc test. **(g)** Fold change (ratio) of mice mass (mean  $\pm$  STD) at completion of the treatment (end) relative to initiation of the treatment (start). Statistical significance between groups was determined using Brown-Forsythe ANOVA followed by Dunnett's T3 post-hoc test. \* $p < 0.05$ , \*\* $p < 0.01$  (vehicle vs. inhibitor(s)).

### Antitumor efficacy of olaparib and ATRi affects histology and proliferation of resensitized tumors but does not induce changes in apoptosis or MDR1 expression

To further examine the antitumor response of olaparib-resistant PDX tumors to olaparib alone or combined with ATR/CHK1 pathway inhibitors, we conducted a comprehensive histopathological analysis and evaluated the expression of proliferative marker Ki-67, apoptotic marker cleaved caspase-3, and the activation of CHK1 kinase through phosphorylation on Ser345 (**Figure 5**). One tumor with stable disease obtained in response to olaparib combined with ATRi (#47) was excluded from the histopathological and IHC analyses due to insufficient tumor tissue for the preparation of FFPE sections.

The detailed results of tumor morphology analysis, including the location, nature, and severity of pathological changes in PDX tissues stained with H&E, are presented in **Table 2**. Histological criteria for evaluating measured parameters are outlined in **Table S2**. Representative H&E-stained images of tumor tissues and identified changes are provided in **Figure 5a**. Given the efficacy of the treatments tested, our focus was on the histopathological assessment of responding tumors from combination cohorts. Generally, H&E-based evaluation of tissue from vehicle-treated tumors revealed densely distributed cell populations. In contrast, the best-responding tumors from combination groups mainly displayed bland fibrous-looking tissue with scattered tumor cells (**Figure 5a**). Additionally, evaluation of mitoses revealed no mitotic cells in the three best-responding tumors available for the analysis according to RTV values (#22, #30, #25) or minimal mitotic indices in other responders, contrasting with most vehicle-treated xenografts with minimal to slight mitotic indices (**Table 2**). Regarding necrosis, the necrotic area was undetectable in tumors #22 and #30 from the olaparib + ATRi cohort and minimal ( $< 1\%$ ) or slight (1–5%) in the remaining responders. Single-cell necrosis scoring ranged from undetected to moderate in all responsive xenografts from combination cohorts. On the contrary, most vehicle-treated tumors exhibited greater signs of necrosis likely associated with the increased growth rate. Relative to the vehicle-treated cohort, the majority of responding tumors showed increased nuclear pleomorphism with evident nucleoli and increased tumor cell vacuolization (**Table 2**) indicating histological changes accompanied by antitumor activity.

The histopathological analysis of heart tissues from a panel of twenty randomly selected mice after treatments (**Figure S3**) revealed no degeneration of myofibers (hyaline lesions) or cardiomyocytes (vacuolar degeneration) in most samples following treatment with the vehicle, olaparib, and ATRi alone or combined. Minimal hyaline degeneration in heart muscle fibers was observed in one mouse from olaparib (#54), CHK1i (#43), and olaparib + CHK1i (#10) arms. Minimal vacuolar degenerative changes in cardiomyocytes were found after administration of CHK1i (#5, #38, #43), olaparib + CHK1i (#9, #10, #16), and in one individual from the olaparib + ATRi cohort (#30) (**Figure S3**).

The evaluation of protein biomarkers by IHC staining revealed a significant decrease in the Ki-67 index from 82.4% in a vehicle arm to 56.8% for the cohort treated with the combination of olaparib and ATRi (**Figure 5b**). However, no significant differences in the immunoreactivity (H-scores) of proliferative marker Ki-67 and phosphorylation of CHK1 between groups were observed (**Figure 5b-c**). Generally, the analyses confirmed medium expression Ki-67 (average H-score range from 133 to 186) and pCHK1 (average H-score range from 159 to 208) in tumor cells across groups (**Figure 5b**). Although H-scores for Ki-67 were lower in the two best-responding tumors treated with the combination of olaparib and ATRi (H-score of 145 for #22 and 105 for #30) compared to a vehicle control group (H-score of  $162 \pm 28$ ), the differences between cohorts were not significant. Administration of olaparib with ATRi significantly decreased caspase-3 expression at the mRNA level compared to mice treated with vehicle, olaparib, or ATRi alone (**Figure S4**), although the expression of full-length and cleaved caspase-3 remained unchanged at protein level relative to vehicle-control cohort (**Figure 5d-e**), indicating no signs of increased apoptosis.

Because the sensitivity of OC cells to olaparib has been previously associated in some reports with MDR1 efflux pump *in vitro* [15, 42, 43], we investigated whether treatment efficacy could be associated with the expression of glycoprotein P *in vivo*. In line with our previous reports on the role of MDR1 in *BRCA2*<sup>MUT</sup> olaparib-resistant HGSOC cells *in vitro* [38], we showed that the response to olaparib alone or combined with the ATR/CHK1 pathway inhibitors was not associated with the expression of MDR1 in olaparib-resistant PDX tumors (**Figure S4**).

Mice that achieved stable disease after treatment with the combination of olaparib and ATRi showed minor signs of necrosis in tumor tissue. However moderate indications of increased nuclear pleomorphism with visible nucleoli were observed in some specimens, a class of nuclear atypia generally typical for HGSOC [41]. Increased vacuolization of tumor cells in response to olaparib combinations could be associated with antitumor effects resulting in vacuolization-induced cell death. Importantly, no cardiac toxicity was observed in response to olaparib alone or in combination with the ATRi indicating adequate safety and tolerability.

Altogether, given the heterogeneous responses observed in combination groups, no significant differences in the apoptosis and activation of CHK1 kinase were detected between vehicle- and inhibitor-treated PDX tumors. Moreover, there were no differences in the phosphorylation of CHK1 in a responsive cohort receiving ATRi and olaparib, suggesting that the activity of ATRi was independent of disrupting CHK1 activation. Therefore, the expression of total CHK1 and its activation was further examined. Nonetheless, administration of olaparib and ATRi notably reduced the Ki-67 index, suggesting decreased proliferation of tumor cells in the best-responding cohort.



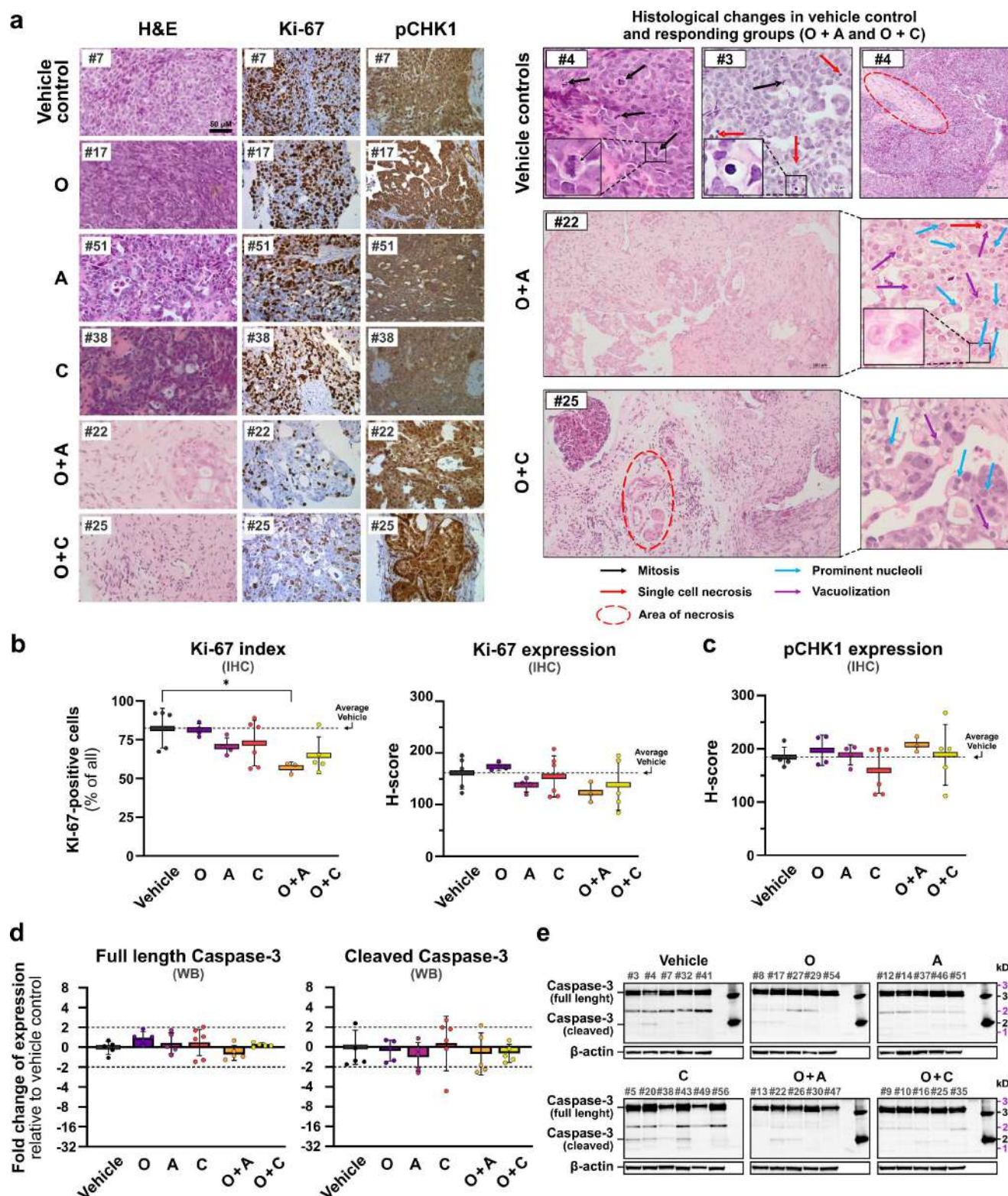


**Figure 5. Detailed characterization of the response of olaparib-resistant PDX tumors to tested inhibitors based on histopathological assessment of tumor tissue and evaluation of the Ki-67 proliferative marker and pCHK1 levels by IHC and cleavage of caspase-3 by Western Blotting.** (a) Representative images of H&E-stained tumor tissue and IHC staining of Ki-67 and pCHK1 (Ser345). (b) Evaluation of Ki-67 index, and Ki-67 expression (H-score) determined by IHC. (c) Evaluation of pCHK1 (Ser345) levels (H-score) determined by IHC. Results of IHC analyses are presented as mean  $\pm$  STD relative to a vehicle-treated group. Dashed lines indicate average values for vehicle-treated groups. (d) Evaluation of full-length caspase-3 expression and caspase-3 cleavage based on semi-quantitative Western Blotting analysis. Protein expression was normalized to  $\beta$ -actin and presented on graphs with a logarithmic scale as a fold-change (mean  $\pm$  STD) relative to a vehicle-treated group. Dashed lines indicate an expression cut-off of  $\pm 2$ -fold to indicate relevant changes. For IHC and Western Blotting analyses, statistical significance between groups was assessed using ordinary one-way ANOVA followed by Tukey's post-hoc test (normally distributed data) or Kruskal-Wallis test followed by Dunn's post-hoc test (non-normally distributed data): \* $p < 0.05$ , \*\* $p < 0.01$ , \*\*\* $p < 0.001$ , \*\*\*\* $p < 0.0001$  (vehicle vs. inhibitor(s)); \*\* $p < 0.01$ , \*\*\* $p < 0.001$ , \*\*\*\* $p < 0.0001$  (olaparib vs. combination with ATRi or CHK1i); \*\* $p < 0.01$ , \*\*\*\* $p < 0.0001$  (ATRi or CHK1i vs. respective combinations with olaparib). (e) Representative Western Blotting images with indicated migration pattern of bands corresponding to proteins from MagicMark™ XP Western Protein Standard (black) and Spectra™ Multicolor Broad Range Protein Ladder (violet).

**Table 2. Results of histopathological assessments of H&E-stained in olaparib-resistant tumors after completion of the treatment.** Mice bearing olaparib-resistant tumors were treated with vehicle (n = 5), olaparib (O, 50 mg/kg, n = 5), ATRi (A, 25 mg/kg, n = 5), CHK1i (C, 50 mg/kg, n = 6) or olaparib combinations with either ATRi (O + A, n = 5) or CHK1i (O + C, n = 5). Upon the completion, tumors were harvested and the FFPE sections were stained with H&E for the analysis of histopathological changes. In total, twenty-seven tumor samples were available for the histopathological assessment, at least three from each group. Each parameter was assessed on the scale: none/undetected (-); minimal (+); slight (++) ; moderate (+++) and high/severe (++++ according to the histological criteria presented in Table S2.

Group	Tumor # (efficacy)	Mitotic index	Area of necrosis	Single cell necrosis	Nuclear pleomorphism	Vacuolization of tumor cells
Vehicle	3	+	++	++	+	-
	4	++	+++	+++	+	-
	7	+	++++	+	+	-
	32	-	++++	++	++	-
	41	+	++	++	+	-
Olaparib	8	-	-	++	++++	++
	17	+	++++	+++	++	-
	27 (R)	-	-	+	++	+
	54	-	+++	+++	++	++++
ATRi	11	++	++++	++	++	+
	12	+++	-	+++	+	++
	46 (R)	-	-	++++	+++	+++
	51	-	-	+	+++	+
CHK1i	5	-	-	+	++	++
	20	+++	++++	+++	++	-
	38	+	-	+	++++	+
	43	-	+	+	+	-
	49	+	+	+++	+	-
	56	+	++++	++	+++	+
Olaparib + ATRi	13 (R)	+	++	+++	++++	++
	22 (R + SD)	-	-	++	++++	+++
	30 (R)	-	-	-	++	-
Olaparib + CHK1i	9	+	+	+	++++	-
	10 (R)	+	-	++	+++	+
	16	+	-	++++	+++	+
	25 (R)	-	++	+	+++	++
	35 (R)	-	+	+	++	-
	3	+	++	++	+	-

Antitumor efficacy: SD – stable disease ( $0.70 \leq \text{RTV} \leq 1.20$ ), R – responders ( $0.10 \leq \text{relative T/C ratio} \leq 0.42$ ). The remaining tumors were classified as non-responders (T/C ratio > 0.42) and/or exhibiting progressive disease ( $\text{RTV} > 1.20$ ).

### Olaparib combined with ATRi impairs the ATR/CHK1 pathway in resensitized PDX tumors

Upon DNA damage, ATR kinase is activated through autophosphorylation at Thr1989 [44], initiating the ATR/CHK1 pathway, which regulates DDR and cell cycle control [45]. The ATR/CHK1 pathway activation among the olaparib-resistant xenografts after the completion of the treatment with tested inhibitors was further assessed based on the phosphorylation of ATR (Thr1989) and CHK1 (Ser345) relative to vehicle-treated mice by Western Blotting analysis of tumor lysates from all xenografts (**Figure 6a**).

Olaparib alone affected only CHK1 phosphorylation, which was manifested by a 3.5-fold decrease in pCHK1. As expected, CHK1i administration paradoxically increased the level of pCHK1 by 4.1-fold [46, 47], although the relative increase in pCHK1 level by 4.2-fold (pCHK1/CHK1) was non-significant ( $p = 0.12$ ). Considering combination treatments, olaparib with ATRi blocked the phosphorylation of ATR and CHK1 kinase, leading to a significant decline in pATR and pCHK1 levels by 4.7-fold and 2.5-fold, respectively (**Figure 6a**). Given that total levels of ATR and CHK1 were downregulated in the presence of olaparib combined with ATRi, the activity of ATR and CHK1 relative to total levels of kinases remained unchanged. In accordance with protein expression, RT-qPCR analysis confirmed that the addition of ATRi to olaparib significantly induced a decrease in ATR and CHK1 at the mRNA level (**Figure S4**).

Overall, the combination of olaparib with ATRi decreased the expression of ATR and CHK1 kinases simultaneously with their phosphorylation levels. A significant decrease in the autophosphorylation of ATR indicated that ATR activity was notably impaired. Based on these observations, we hypothesized that the

antitumor response to olaparib combinations could be associated with alterations in downstream DDR induced by a compromised ATR/CHK1 pathway activity.

### The addition of ATRi to olaparib impedes PARylation in resensitized PDX tumors through downregulation and inhibition of PARP1

Given that olaparib inhibits PARP1, we hypothesized that restoring olaparib's inhibitory activity with ATR/CHK1 inhibitors in olaparib-resistant PDX tumors might affect PARP signaling and PARylation-dependent DNA repair. As expected, olaparib as a single agent efficiently, but only partially, inhibited PARP1 activity, leading to a 2.4-fold decrease in PARylation without affecting PARP1 or PARG expression relative to vehicle-treated tumors (**Figure 6b**). Neither ATRi nor CHK1i alone affected PARP1 expression or the content of PARylated proteins. On the contrary, ATRi or CHK1i combined with olaparib decreased PAR levels, however, only the addition of ATRi to olaparib augmented the PARPi-induced decline in PAR levels by 4.7-fold, leading to dramatic disruption of PARP signaling. Moreover, the combination of olaparib with ATRi significantly downregulated PARP1 expression by 6.5-fold, indicating that inhibition of PARylation was mediated by combination-induced downregulation and inhibition of PARP1.

RT-qPCR analysis confirmed that the addition of ATRi to olaparib significantly induced a decrease in PARP1 expression at the mRNA level (**Figure S4**). Interestingly, olaparib combined with ATRi also decreased PARG expression without restoring PAR levels compared with the vehicle-treated and single-agent-treated groups. Conversely, we did not observe significant

differences between olaparib alone or combined with CHK1i regarding the expression of PARP1 and PARG.

Therefore, in olaparib-resistant tumors resensitized to olaparib with ATRi, PARP1 downregulation was triggered, along with inhibition of its enzymatic activity, leading to a substantial blockage of PAR-mediated post-translational modification of

target proteins. This could represent another way through which ATRi restores the antitumor efficacy of olaparib. Given that the combination of ATRi with olaparib markedly decreased PARP1 expression, it is unlikely that antitumor activity was attributed to the induction of cytotoxic PARP1-DNA complexes and trapping.

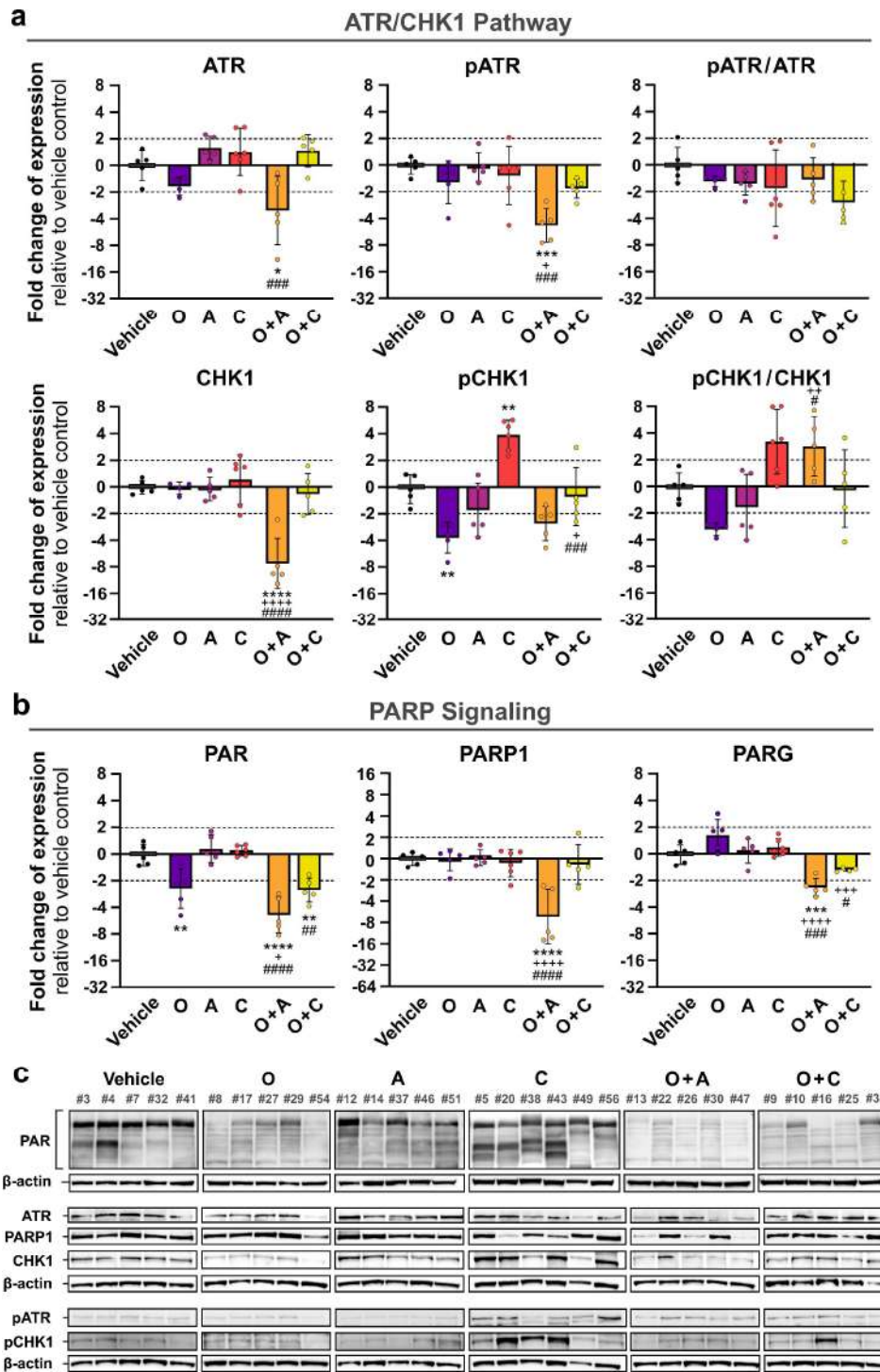


**Figure 6. The addition of ATRi to olaparib impairs ATR/CHK1 pathways and PARP signaling in olaparib-resistant PDX of HGSOC.** Mice bearing olaparib-resistant tumors were treated with vehicle ( $n = 5$ ), olaparib (O, 5- mg/kg,  $n = 5$ ), ATRi (A, 25 mg/kg,  $n = 5$ ), CHK1i (C, 5- mg/kg,  $n = 6$ ) or olaparib combinations with either ATRi (O + A,  $n = 5$ ) or CHK1i (O + C,  $n = 5$ ). Upon treatment completion, tumors were harvested and whole tissue lysates were prepared for Western Blotting analysis. Protein expression was normalized to  $\beta$ -actin and presented on graphs with a logarithmic scale as a fold-change (mean  $\pm$  STD) relative to a vehicle-treated group. Dashed lines indicate an expression cut-off of  $\pm 2$ -fold to indicate relevant changes. Statistical significance between groups was assessed using ordinary one-way ANOVA followed by Tukey's post-hoc test (normally distributed data): \* $p < 0.05$ , \*\* $p < 0.01$ , \*\*\* $p < 0.001$ , \*\*\*\* $p < 0.0001$  (vehicle vs. inhibitor(s)); \* $p < 0.05$ , \*\* $p < 0.01$ , \*\*\* $p < 0.001$ , \*\*\*\* $p < 0.0001$  (olaparib vs. combination with ATRi or CHK1i); \* $p < 0.05$ , \*\* $p < 0.01$ , \*\*\* $p < 0.001$ , \*\*\*\* $p < 0.0001$  (ATRi or CHK1i vs. respective combinations with olaparib). (a) Quantitative Western Blotting analysis of expression of total ATR and CHK1 kinases and their phosphorylation levels (pATR (Thr1989) and pCHK1 (Ser345)). (b) Quantitative Western Blotting analysis of PARP signaling proteins (PARP1, PARG) and PARylated proteins content. (c) Representative Western Blotting images.



### Olaparib treatment with targeted inhibition of ATR affects the expression of DNA damage response-mediating proteins in olaparib-resistant PDX tumors

Upon DNA damage, H2AX becomes phosphorylated by the ATR or ATM kinase to induce a response cascade that mediates DNA repair pathways, including HR repair and NHEJ [48, 49]. Olaparib, by inhibiting PARP, induces DNA damage accompanied by an increase in DSB marker  $\gamma$ H2AX in olaparib-sensitive tumors [38, 50]. To assess combinations-induced changes in DDR pathways in olaparib-resistant xenografts, we subjected tumor lysates to analysis of expression of HR-mediating BRCA1, BRCA2, and RAD51, and HNEJ-promoting 53BP1.

Inhibition of PARP1 with olaparib in olaparib-resistant PDX caused a non-significant decrease by 2.0-fold in  $\gamma$ H2AX levels relative to vehicle-treated tumors, indicating no detectable accumulation of unrepaired DSB. The addition of ATRi or CHK1 slightly augmented the downregulation of  $\gamma$ H2AX resulting in a significant decrease by 2.8 and 2.3 times, respectively (Figure 7a). Additionally, RT-qPCR confirmed a significant decrease in H2AX mRNA in both olaparib combination cohorts (Figure S4). These observations suggest that durable combination-induced antitumor activity either caused degradation of  $\gamma$ H2AX or abrogated ATR-dependent H2AX phosphorylation affecting DSB repair signaling.

Phosphorylation of H2AX facilitates the recruitment of repair factors after DNA damage [49]. Therefore, we assessed whether components involved in HR repair and NHEJ were affected. The expression of RAD51 recombinase, which is co-recruited with  $\gamma$ H2AX to DSBs to promote HR repair, was not affected by tested inhibitors, including olaparib combinations with either ATRi or CHK1i (Figure S5). This further supports the absence of DSB accumulation or defects in their detection by cellular systems. Treatment of non-responsive tumors with olaparib alone increased the expression of BRCA2 and 53BP1 while down-regulating BRCA1 (Figure 7a). On the contrary, the addition of ATRi to olaparib decreased BRCA2 and 53BP1 expression and augmented the decrease of BRCA1 in responding PDX. Administration of olaparib with CHK1 also reversed olaparib-induced upregulation of BRCA2 and 53BP1 (Figure 7a).

Altogether, the accumulation of DSB and the promotion of HR repair, as measured by the level of  $\gamma$ H2AX and RAD51, appeared unrelated to the long-term antitumor response to a combination of olaparib with ATR/CHK1 pathway inhibitors. Conversely, we confirmed decreased  $\gamma$ H2AX, suggesting potential DNA repair defects. Moreover, we showed that olaparib combined with ATRi or CHK1 modulated HR repair- and NHEJ-promoting factors. Specifically, the best-responding tumors treated with the addition of ATRi to olaparib downregulated  $\gamma$ H2AX, BRCA1, BRCA2, and 53BP1, indicating impaired DNA damage repair response in xenografts resensitized to olaparib.

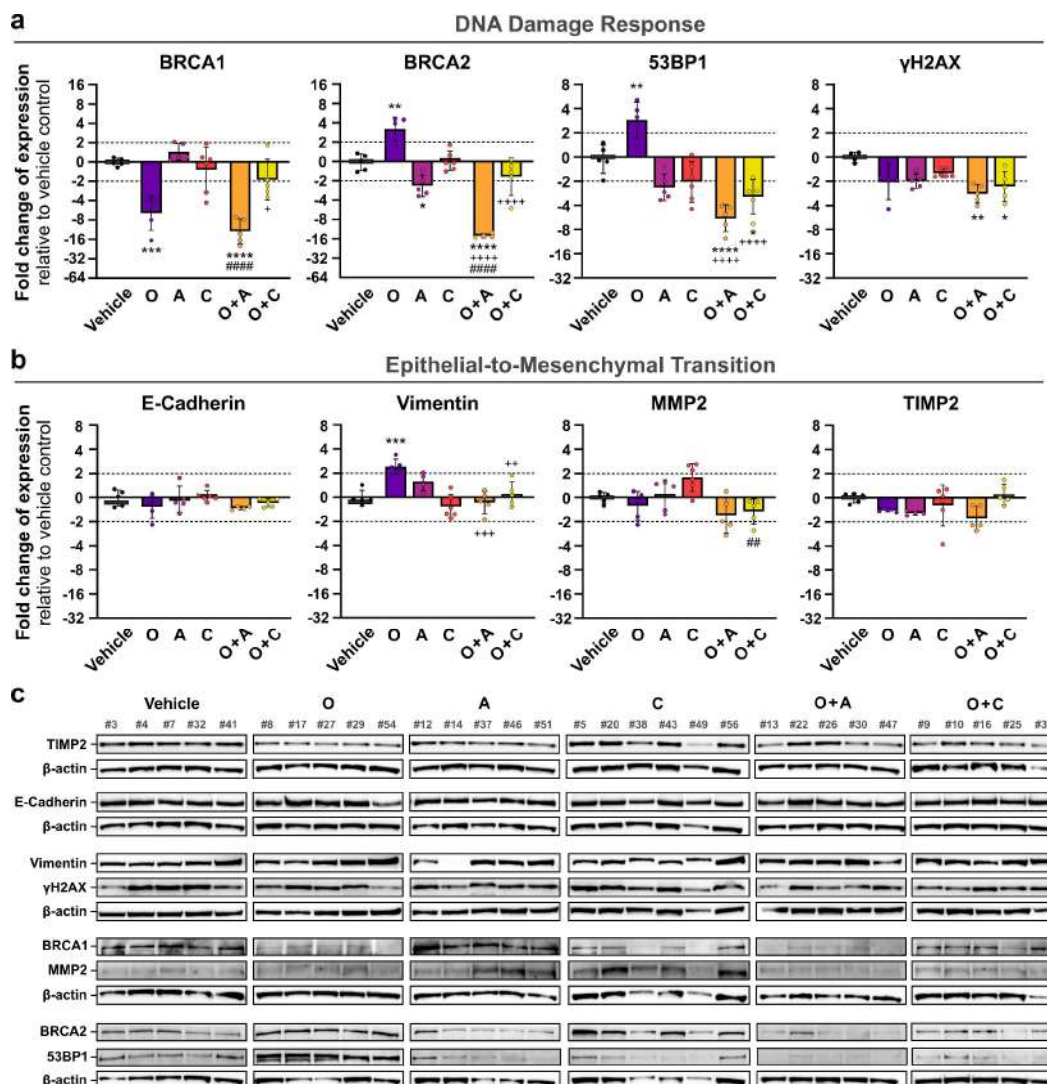


**Figure 7. The addition of ATRi to olaparib affects the expression of HR repair and NHEJ-associated DNA damage response irrespective of EMT in olaparib-resistant PDX of HGSOc.** Mice bearing olaparib-resistant tumors were treated with vehicle (n = 5), olaparib (O, 50 mg/kg, n = 5), ATRi (A, 25 mg/kg, n = 5), CHK1i (C, 50 mg/kg, n = 6) or olaparib combinations with either ATRi (O + A, n = 5) or CHK1i (O + C, n = 5). Upon treatment completion, tumors were harvested and whole tissue lysates were prepared for Western Blotting analysis. **(a)** Quantitative Western Blotting analysis of expression of proteins associated with DNA damage response (BRCA1, BRCA2, 53BP1, γH2AX (Ser139)). **(b)** Quantitative Western Blotting analysis of expression of proteins associated with epithelial-to-mesenchymal transition (E-cadherin, vimentin, MMP2, TIMP2). Protein expression was normalized to β-actin and presented on graphs with a logarithmic scale as a fold-change (mean ± STD) relative to a vehicle-treated group. Dashed lines indicate an expression cut-off of ± 2-fold to indicate relevant changes. Statistical significance between groups was assessed using ordinary one-way ANOVA followed by Tukey's post-hoc test (normally distributed data) or Kruskal-Wallis test followed by Dunn's post-hoc test (non-normally distributed data): \**p* < 0.05, \*\**p* < 0.01, \*\*\**p* < 0.001, \*\*\*\**p* < 0.0001 (vehicle vs. inhibitor(s)); \**p* < 0.01, \*\*\**p* < 0.001, \*\*\*\**p* < 0.0001 (olaparib vs. combination with ATRi or CHK1i); ##*p* < 0.01, \*\*\*\**p* < 0.0001 (ATRi or CHK1i vs. respective combinations with olaparib). **(c)** Representative Western Blotting images.

### The addition of the ATR/CHK1 pathway inhibitors to olaparib abrogates olaparib-induced upregulation of vimentin related to EMT in resensitized PDX tumors

EMT has previously been implicated in OC progression, and resistance to cisplatin therapy [51]. Recently, transforming growth factor beta-induced EMT has been associated with sensitization of *BRCA2* wild-type OC cell lines to olaparib through the downregulation of HR repair genes [39]. Based on the observed DDR deregulation, we investigate whether the addition of ATRi or CHK1i to olaparib also affects the EMT of *BRCA1/2*<sup>MUT</sup> olaparib-resistant tumors *in vivo*. We evaluated the expression of epithelial marker E-cadherin, mesenchymal markers (vimentin and MMP2), and MMP2 irreversible inhibitor TIMP2 (**Figure 7b**). The analyses revealed that the administration of olaparib alone induced a significant upregulation of mesenchymal marker vimentin in non-responding tumors, suggesting increased migration capacity. Notably, responsive tumors treated with combinations of olaparib and the ATR/CHK1 inhibitors showed no significant changes in the expression of both epithelial and mesenchymal markers relative to vehicle-treated xenografts. Importantly, in the presence of ATRi or CHK1i, olaparib-induced upregulation of vimentin was abolished (**Figure 7b**). Thus, we propose that restoration of olaparib antitumor activity through inhibition of the ATR/CHK1 pathway may prevent mesenchymal properties of olaparib-resistant PDX tumors and abolish their migration and invasion *in vivo*.

## Discussion

In the current report, we evaluated the *in vivo* antitumor efficacy and systemic tolerability of the olaparib combinations with the ATR/CHK1 pathway inhibitors in PDX models of HGSOc with acquired olaparib resistance established from the *BRCA1/2*<sup>MUT</sup> tumor. Previously, we demonstrated how the HGSOc cell line PEO1-OR with *BRCA2* reversion mutation confers resistance to olaparib, and how targeting the ATR/CHK1 pathway overcomes PARPi resistance *in vitro* [13, 38]. Prior *in vivo* studies have provided the rationale for combining olaparib with ATRi in olaparib-resistant HGSOc harboring mutations in *BRCA1* or *BRCA2*, reversion mutation in *BRCA1*, or tumors with wild-type *BRCA1/2* genes [14]. Our findings here further support the idea of combining olaparib with the ATR/CHK1 pathway inhibitors, ceralasertib or MK-8776, in the context of olaparib-resistant HGSOc PDX models established from the treatment-naïve patient's tumor carrying pathogenic mutations in both *BRCA1/2* genes, filling in a gap in the existing literature. Importantly, we demonstrated novel mechanistic evidence for conferring and overcoming resistance to olaparib in HGSOc.

As the clinical use of PARPi increases, acquired resistance to olaparib becomes common in HGSOc patients. About 50% of platinum-sensitive relapsed *BRCA1/2*<sup>MUT</sup> OC patients, previously treated with olaparib, fail to derive clinical benefits with PARPi rechallenge [6], prompting the development of new strategies to

increase olaparib efficacy. So far, several resistance mechanisms to olaparib have been identified [6]. More recently, resistance to olaparib has been associated with the generation of desensitized HGSOc daughter cells from polyploid giant cancer cells following PARPi exposure [52]. Despite these insights, further understanding of resistance events in OC is crucial, especially in the context of combination therapies targeting cancer vulnerabilities associated with a resistant phenotype.

In the first part of the study, we developed olaparib-resistant PDX models of HGSOc and provided molecular aspects associated with acquisition of resistant phenotype (part I) and linked to a subsequent response to olaparib rechallenge in resistant tumors with non-significant tumor growth inhibition (part II). Lastly, we revealed molecular insights into resensitization of olaparib-resistant tumors to olaparib using the ATR/CHK1 pathway inhibitors (part III).

Firstly, we employed the commonly used subcutaneous implantation method to establish heterotopic PDX models of HGSOc *in vivo*. Notably, subcutaneous PDX models maintain the molecular and genetic characteristics of original tumors [53]. Among the three established PDX models of HGSOc, acquired resistance to olaparib was successfully developed in *BRCA1/2*<sup>MUT</sup> PDX-X179 xenograft, which was subsequently used in further inhibitor efficacy studies. Initially, the PDX was established from an individual HGSOc patient who had not undergone any systemic antitumor therapy before debulking surgery, providing a treatment-naïve context for this *in vivo* study. Importantly, the PDX-X179 model used to successfully induce resistance carried both a missense mutation in the *BRCA1* gene and a truncating mutation in the *BRCA2* gene, reflecting clinically relevant HRD status [54, 55]. The recent screening revealed that concurrent occurrence of two or more *BRCA1/2* pathogenic mutations is present in some HGSOc patients [56]. Interestingly, *BRCA1* p.Cys61Gly substitution detected in our PDX model is a well-known Polish founder mutation associated with Hereditary Breast and Ovarian Cancer syndrome [57].

Acquired resistance to olaparib was induced in PDX-X179 xenografts through continuous intraperitoneal injections of olaparib (50 mg/kg) over 6 weeks, resulting in doubled tumor sizes. Significantly, decreased sensitivity to olaparib was further verified by olaparib rechallenge and continuation of the treatment during inhibitor efficacy studies in olaparib-resistant xenografts that were retransplanted and expanded in different mice, warranting a stable resistant phenotype. With olaparib-resistant models established, we aimed to provide detailed molecular characterization of PDX tumors with acquired resistance.

PARP1-mediated PARylation initiates signaling upon DNA damage, setting off a series of protein recruitment processes aimed at DNA repair. However, PAR chains must be removed by dePARylating enzymes, including PARG glycohydrolase, to release DDR factors so that they can act on the damaged DNA [58]. We found that acquired olaparib resistance correlated with

decreased PARylation of target proteins, alongside PARP1 and PARG downregulation. Despite PARG downregulation, PARylation rescue was unlikely due to concurrent PARP1 downregulation. This affirmed olaparib's inhibition of PARP1 activity, aligning with its mode of action but exerting minimal effects on resistant cell growth. Concurrent PARP1 downregulation suggests that olaparib favored the survival of cells with reduced PARP1 expression, further decreasing PARylation. However, PARylation was not completely inhibited in resistant tumors, indicating retained PARylation ability to some extent. As PARG acts akin to PARPi in the context of decreasing PARylation, we suggest that the downregulation of PARG allowed sufficient PAR formation in the presence of PARPi. Indeed, previous reports linked PARG loss to PARPi resistance in *BRCA2*<sup>MUT</sup> ovarian and breast cancer tumors [59]. Moreover, we propose that partial loss of PARP1, the drug target, likely enabled olaparib-resistant cells to limit PARPi-induced trapping of PARP1, leading to HGSOc desensitization. To better understand the olaparib's pharmacodynamic effect in resistant tumors, we examined PARP signaling in retransplanted xenografts with acquired resistance in response to olaparib rechallenge. Retreatment with PARPi decreased PARylation, yet PARP1 and PARG expression remained unaffected compared to vehicle-treated tumors. This finding confirmed that olaparib-induced inhibition of PARP1 enzymatic activity, and supposedly PARP1 trapping, was insufficient to exert antitumor activity in olaparib-resistant tumors *in vivo*.

To assess the impact of reduced PARylation and PARP1 expression on DNA damage repair factors in HGSOc cells that acquired resistance to olaparib, we examined the expression of the DSB biomarker  $\gamma$ H2AX and proteins involved in HR repair (RAD51, BRCA1, and BRCA2). We found that resistance to olaparib was accompanied by a decrease in  $\gamma$ H2AX expression, indicating reduced accumulation of DSB. In contrast to other studies using PDX models of HGSOc, we observed that retreatment with olaparib alone decreased H2AX phosphorylation in retransplanted olaparib-resistant tumors. The observed decrease of  $\gamma$ H2AX aligns with pharmacodynamic results from a clinical trial, where platinum-resistant OC patients receiving olaparib showed decreased  $\gamma$ H2AX in response to PARPi, in contrast to the platinum-sensitive cohort [35].

As tumors downregulated RAD51, BRCA1, and BRCA2 after conferring resistance to olaparib compared to olaparib-naïve xenografts, we speculate that conferring PARPi resistance decreased the tumor's dependence on the HR repair pathway for survival. Thus, we assessed the expression of the NHEJ-promoting factor 53BP1 in olaparib-resistant PDX tumors. Previous studies have shown that 53BP1 loss reactivates HR repair activity in *BRCA1*<sup>MUT</sup> ovarian and breast cancer cell lines, reducing sensitivity to PARPi [60, 61]. We found that *BRCA1/2*<sup>MUT</sup> olaparib-resistant tumors downregulated 53BP1 upon resistance induction, partially aligning with other *in vivo* reports indicating decreased 53BP1 expression in some *BRCA1*<sup>MUT</sup> HGSOc tumors with intrinsic resistance to olaparib [16]. Similarly, loss of 53BP1 in *BRCA1*-deficient mammary tumors was associated with reduced PARPi sensitivity through partial restoration of HR repair function [62]. However, the potential restoration of HR repair due to concurrent downregulation of 53BP1 and BRCA1 in our *BRCA1/2*<sup>MUT</sup> model of HGSOc warrants further investigation. Moreover, olaparib retreatment in retransplanted xenografts with acquired resistance upregulated BRCA2 and 53BP1, while further downregulating BRCA1. Our findings suggest that conferring resistance to olaparib was associated with

downregulation of HR- and NHEJ-promoting factors, while rechallenge with olaparib stimulated restoration of DDR-promoting BRCA2 and 53BP1 expression associated with desensitization to PARPi alone.

The ATR/CHK1 pathway regulates the response to DNA damage, orchestrating subsequent cellular processes for DNA repair, including replication fork stabilization and cell cycle checkpoint regulation. Given that the H2AX phosphorylation is mediated by ATR, we evaluated whether  $\gamma$ H2AX decrease in olaparib-resistant xenografts upon desensitization to PARPi was dependent on ATR. Notably, PDX models with acquired resistance downregulated ATR expression and ATR auto-phosphorylation, the latter suggesting a decrease in ATR activity. This reduction was further evidenced by decreased CHK1 phosphorylation. Therefore, we propose that the acquisition of olaparib-resistant phenotype was associated with decreased reliance on the ATR/CHK1 pathway for survival in the presence of olaparib. Furthermore, rechallenge with olaparib in retransplanted olaparib-resistant xenografts failed to increase phosphorylation of H2AX, ATR, and CHK1, suggesting no olaparib-induced accumulation of DSB or ATR/CHK1 activation for DNA repair and maintenance of olaparib resistant phenotype.

EMT is a crucial process associated with metastasis in OC increasing cell motility, migration, and conferring invasive phenotype [51]. Investigation of molecular hallmarks of EMT upon conferring resistance to olaparib revealed that PDX tumors with acquired resistance to olaparib downregulated E-cadherin and MMP2 after obtaining resistant phenotype, while no changes in vimentin expression were observed relative to olaparib-naïve xenografts. For this reason, an increase in migration potential was unlikely associated with the acquisition of olaparib resistance in the established PDX models. Surprisingly, olaparib retreatment upregulated vimentin expression in olaparib-resistant tumors, highlighting that repeated administration of olaparib could potentiate migratory capacities of non-responsive HGSOc cells with acquired resistance. This result sheds light on a potential unfavorable effect of retreatment with olaparib alone and further supports the rationale for employing ATR/CHK1 inhibitors in HGSOc previously treated with olaparib.

Lastly, we investigated the response of olaparib-resistant HGSOc resensitized to olaparib rechallenge using the ATR/CHK1 pathway inhibitors, focusing on associated molecular changes. Previous reports showed that olaparib antitumor activity can be potentiated in olaparib-sensitive and olaparib-resistant HGSOc cells *in vivo* with small-molecule inhibitors including VEGFR inhibitor cediranib [63], DDR, and cell cycle checkpoint inhibitors [15, 16, 64]. In this study, we have supported the concept that targeting the ATR/CHK1 pathway with the concurrent re-administration of olaparib is an effective approach to suppress tumor growth in olaparib-resistant HGSOc. Although combining olaparib with either ATRi or CHK1 synergistically inhibited tumor growth of PDX, mice receiving olaparib combined with ATRi, rather than CHK1i, obtained better response reflected by more prominent tumor suppression. Treatment response classification based on the tumor-to-control method confirmed that some mice bearing olaparib-resistant PDX tumors were responsive to olaparib in the presence of the ATR/CHK1 pathway inhibitors. In general, the addition of ATRi to olaparib resulted in a prolonged inhibition and stabilization of tumor growth, however, tumor regression was not observed. Importantly, the combination of olaparib with ATRi was well tolerated with a minor body weight



loss of mice over the course of the experiment and no notable cardiac toxicity.

Our results support previous reports showing that targeted inhibition of ATR or CHK1 kinase enhances olaparib antitumor in olaparib-resistant HGSOc tumors *in vivo* [14, 16]. The efficacy of olaparib with ATRi was previously demonstrated in genetically distinct orthotopic olaparib-resistant PDX models carrying either a truncating *BRCA2* mutation, missense mutation in *BRCA1*, or a reversion mutation in *BRCA1* [14]. These models were established from drug-resistant patients who progressed on olaparib, rucaparib, or carboplatin-based chemotherapy. In contrast, our olaparib-resistant model was established from the tumor harboring pathogenic mutations in both *BRCA1* and *BRCA2* genes, obtained from a treatment-naïve patient. Importantly, both mutations have been previously reported in breast and ovarian cancer patients [65]. Considering CHK1i, the rationale for combining olaparib with prexasertib was demonstrated in the HR-proficient PDX model established from patient's ascites-derived HGSOc cells harboring *BRCA1* missense mutation, however, in the context of intrinsic resistance to olaparib [16]. These models showed increased tumor growth inhibition in response to the combination treatment, however, in the presence of higher doses of olaparib (up to 100 mg/kg, daily) [16].

Next, extensive histopathological and molecular analyses were performed to uncover several molecules and pathways that could play a significant role in the restoration of olaparib efficacy using ATR/CHK1 pathway inhibitors. Based on our drug efficacy studies, we propose a model to elucidate the mechanism of overcoming resistance to olaparib in HGSOc cells *in vivo* with targeted inhibition of the ATR/CHK1 pathway, with a focus on the use of ATRi ceralasertib.

Histopathologically, tumors resensitized with the ATR/CHK1 pathway inhibitors seemed to have less sites of growth within a tissue mirrored by minimal mitotic indices and reduced Ki-67 levels in response to olaparib combined with ATRi, while moderate signs of necrosis were observed. Notably, olaparib combinations increased nuclear pleomorphism with evident nucleoli and augmented tumor cell vacuolization, which might be regarded as indicative of antitumor activity in resensitized HGSOc xenografts. Simultaneously, HGSOc cell death was independent of caspase 3 activity mediating apoptosis. These data indicate that an alternative cell death pathway characterized by vacuolization of multinucleated cells might be associated with synergistic tumor growth suppression of olaparib-resistant HGSOc tumors *in vivo*. Recent studies demonstrated that in OC cells *in vivo*, olaparib efficacy can be enhanced by employing different combination treatments through augmentation of apoptosis [66, 67]. Our study indicates that the induction of cell death pathways independent of the classical apoptosis is also of interest for the resensitization of olaparib-resistant HGSOc cells to PARPi in the context of targeting the ATR/CHK1 pathway.

In tumors that have acquired resistance to olaparib, re-exposure to olaparib combined with ATRi induced synergistic downregulation of PARP1 and PARG expression along with augmentation of olaparib-induced decrease in PARYlation, potentially affecting recruitment of the DNA repair proteins. Given that PARYlation plays a major role in various cellular processes other than DDR [67, 68], the downstream effects need further investigation. Nonetheless, our analysis suggests that downregulation of PARP1-mediated PARYlation might be an important effect underpinning the combination's benefit.

Recent data indicate that ATR inhibition may be more beneficial for increasing the antitumor activity of olaparib than CHK1 inhibition, given that ATR regulates some cellular functions independently of CHK1. For instance, ATR has been implicated in the CHK1-independent regulation of replication fork protection, so that only ATR inhibition impairs replication fork stability leading to resensitization to olaparib [69]. In line with our data, different outcomes resulting from combining PARPi with either ATR or CHK1 inhibition were also observed in olaparib-sensitive PDX models of HGSOc. Specifically, ATRi ceralasertib in combination with olaparib resulted in tumor regression, whereas treatment with CHK1i MK-8776 caused only tumor suppression in the same xenograft models [64]. Moreover, an effective combination of olaparib with ATRi leads to decreased activity of the ATR/CHK1 pathway, suggesting disturbed regulation of downstream processes critical for cell survival. Notably, ATRi alone did not affect the autophosphorylation of ATR or its downstream target CHK1 in non-responsive tumors. Thus, the concurrent use of olaparib and ATRi seems to be essential for pharmacological inhibition of the ATR/CHK1 pathway leading to tumor growth suppression. Although olaparib combined with CHK1i also inhibited tumor growth, no significant changes in the CHK1 activity were observed. Thus, we provide data suggesting that ATR kinase targets beyond CHK1 play a major role in obtaining significant antitumor response in HGSOc tumors with acquired resistance to olaparib.

Since phosphorylation of H2AX serves as a biomarker of DSB and a platform for DNA damage repair proteins [49], a decrease of  $\gamma$ H2AX level in HGSOc xenografts resensitized to olaparib with ATR/CHK1 pathways inhibitors indicated disturbed recruitment of DNA repair factors. Notably, decreased  $\gamma$ H2AX levels were accompanied by the downregulation of ATR, which is one of the main kinases responsible for H2AX phosphorylation. Considering the role of  $\gamma$ H2AX as a DSB biomarker, in this study levels of  $\gamma$ H2AX were assessed in response to long-term treatments lasting on average 5 weeks. Phosphorylation of H2AX in response to DNA damage is a dynamic process, thus, we cannot exclude the usefulness of  $\gamma$ H2AX as a marker of DNA-damaging antitumor activity in earlier time points. Thus,  $\gamma$ H2AX may not mirror any DNA damage in resensitized olaparib-resistant tumors once treatments exert significant tumor inhibitory activity.

Investigation of HR repair-promoting factors expression in resensitized tumors revealed more changes in tumors treated with olaparib combined with ATRi, than with CHK1i. Combining olaparib with ATRi resulted in notable downregulation of *BRCA1* and *BRCA2*, indicating impairment of key HR repair components in tumors resensitized to olaparib. These observations highlight the significance of HR repair disruption mediated by the combination of olaparib and ATRi as a therapeutic strategy for overcoming resistance to PARPi. Demonstrated changes indicate augmentation of HRD phenotype in olaparib-resensitized PDX tumors in the presence of ATRi, which is in line with increased sensitivity to olaparib in HGSOc cells with defects in HR repair [70]. Moreover, targeted inhibition of the ATR/CHK1 pathways in resensitized tumors decreased 53BP1 expression. Overall, inhibition of olaparib-resistant tumor growth in response to olaparib combined with ATRi was associated with multifactorial defects in DDR-promoting factors. Lastly, given no changes in the expression of epithelial (E-cadherin, TIMP2) and mesenchymal (vimentin, MMP2) markers in response to olaparib combinations with either ATRi or CHK1i, migratory capabilities of resensitized tumors seemed unaffected in responding PDX tumors. However,

the long-term metastatic potential of tumors resensitized to olaparib using ATR/CHK1 pathway inhibitors *in vivo* needs further investigation.

We recognize that the presented data rely on olaparib-resistant PDX models established from one HGSOC patient, necessitating caution when interpreting and generalizing these findings. Nevertheless, we have shown here that the addition of ATR/CHK1 pathway inhibitors synergistically enhances tumor growth inhibition in olaparib-resistant *BRCA1/2*<sup>MUT</sup> xenografts rechallenged with olaparib. Importantly, this study provides the molecular rationale for studied combinations in a comprehensively characterized *in vivo* model of HGSOC. Moreover, PDX models of HGSOC generally recapitulate key features of the original tumors [71], they might not fully account for tumor

heterogeneity in patients. Given that, additional studies employing HGSOC tumors with different characteristics are essential to increase the applicability of our report.

Overall, the above results provide a proof of concept that the addition of ATR/CHK1 pathway inhibitors to olaparib can exert a tumor growth inhibition effect in *BRCA1/2*<sup>MUT</sup> patients who have acquired resistance to olaparib. Importantly, our findings indicate that combining olaparib with ATRi, rather than CHK1i, demonstrated enhanced efficacy in the novel olaparib-resistant PDX models of HGSOC established from olaparib-naïve *BRCA1/2*<sup>MUT</sup> tumors. Additionally, we provide comprehensive molecular insights into the development of acquired olaparib resistance and resensitization of HGSOC cells to olaparib *in vivo* using the ATR/CHK1 pathway inhibitors.

## Abbreviations

<b>A</b>	ATR inhibitor (ceralasertib)	<b>NHEJ</b>	non-homologous end joining
<b>ATR</b>	ataxia telangiectasia and RAD3-related protein	<b>NGS</b>	next-generation sequencing
<b>ATRi</b>	ATR inhibitor(s)	<b>O</b>	olaparib
<b>C</b>	CHK1 inhibitor (MK-8776)	<b>OC</b>	ovarian cancer
<b>CHK1</b>	checkpoint kinase 1	<b>PAR</b>	poly(ADP-ribosylation)
<b>CHK1i</b>	CHK1 inhibitor(s)	<b>PARP1</b>	poly(ADP-ribose) polymerase 1
<b>CI</b>	combination index	<b>PARPi</b>	PARP inhibitors
<b>DSB</b>	double-strand break	<b>PDX</b>	patient-derived xenograft
<b>DDR</b>	DNA damage response	<b>RTV</b>	relative tumor volume
<b>EMT</b>	epithelial-to-mesenchymal transition	<b>SD</b>	stable disease
<b>FFPE</b>	formalin-fixed paraffin-embedded	<b>SNV</b>	single nucleotide variant
<b>H&amp;E</b>	hematoxylin and eosin	<b>STD</b>	standard deviation
<b>HGSOC</b>	high-grade serous ovarian cancer	<b>T/C</b>	treatment-to-control
<b>HR</b>	homologous recombination	<b>TGI</b>	tumor growth inhibition

## Author Contributions

Conceptualization, Ł.B., M.S., A.G., M.M. and A.R.; methodology, Ł.B., M.S., A.G., N.R., A.Ś., A.M. and A.R.; formal analysis, Ł.B.; investigation, Ł.B., M.S., A.G., I.S.-P. and N.R.; resources, A.Ś., A.M., M.M. and A.R.; writing—original draft preparation, Ł.B.; writing—review and editing, Ł.B., M.S., A.G., I.S.-P., N.R., A.M., A.Ś., M.M. and A.R.; visualization, Ł.B. and N.R.; supervision, A.R.; funding acquisition, A.R. All authors have read and approved the final version of the manuscript.

## Conflict of interests

The authors declare no conflicts of interest.

## Funding

This work was supported by the National Science Centre, Poland (Project grant number: Sonata Bis 2019/34/E/NZ7/00056).

## Data availability

The data generated during the study are available from the corresponding author upon reasonable request.

## Acknowledgment

The original illustrations in figures have been created with BioRender.com.

## References

- Mahmood, R.D., et al., *First-Line Management of Advanced High-Grade Serous Ovarian Cancer*. *Curr Oncol Rep*, **2020**. 22(6): p. 64.
- Maiorano, B.A., M.F.P. Maiorano, and E. Maiello, *Olaparib and advanced ovarian cancer: Summary of the past and looking into the future*. *Front Pharmacol*, **2023**. 14: p. 1162665.
- Zheng, F., et al., *Mechanism and current progress of Poly ADP-ribose polymerase (PARP) inhibitors in the treatment of ovarian cancer*. *Biomed Pharmacother*, **2020**. 123: p. 109661.
- Murai, J., et al., *Trapping of PARP1 and PARP2 by Clinical PARP Inhibitors*. *Cancer Res*, **2012**. 72(21): p. 5588-99.
- DiSilvestro, P., et al., *Overall Survival With Maintenance Olaparib at a 7-Year Follow-Up in Patients With Newly Diagnosed Advanced Ovarian Cancer and a BRCA Mutation: The SOLO1/GOG 3004 Trial*. *J Clin Oncol*, **2023**. 41(3): p. 609-617.
- Veneziani, A.C., et al., *Fighting resistance: post-PARP inhibitor treatment strategies in ovarian cancer*. *Ther Adv Med Oncol*, **2023**. 15: p. 17588359231157644.
- Frenel, J.S., et al., *Efficacy of subsequent chemotherapy for patients with BRCA1/2-mutated recurrent epithelial ovarian cancer progressing on olaparib versus placebo maintenance: post-hoc analyses of the SOLO2/ENGOT Ov-21 trial*. *Ann Oncol*, **2022**. 33(10): p. 1021-1028.
- Cordani, N., et al., *An Overview of PARP Resistance in Ovarian Cancer from a Molecular and Clinical Perspective*. *Int J Mol Sci*, **2023**. 24(15).
- Burdett, N.L., et al., *Small-scale mutations are infrequent as mechanisms of resistance in post-PARP inhibitor tumour samples in high grade serous ovarian cancer*. *Sci Rep*, **2023**. 13(1): p. 21884.
- Tobalina, L., et al., *A meta-analysis of reversion mutations in BRCA genes identifies signatures of DNA end-joining repair mechanisms driving therapy resistance*. *Ann Oncol*, **2021**. 32(1): p. 103-112.
- Miller, R.E., K.H. El-Shakankery, and J.Y. Lee, *PARP inhibitors in ovarian cancer: overcoming resistance with combination strategies*. *J Gynecol Oncol*, **2022**. 33(3): p. e44.
- Blackford, A.N. and S.P. Jackson, *ATM, ATR, and DNA-PK: The Trinity at the Heart of the DNA Damage Response*. *Mol Cell*, **2017**. 66(6): p. 801-817.
- Biegala, L., et al., *Targeted inhibition of the ATR/CHK1 pathway overcomes resistance to olaparib and dysregulates DNA damage response protein expression in BRCA2(MUT) ovarian cancer cells*. *Sci Rep*, **2023**. 13(1): p. 22659.
- Kim, H., et al., *Combining PARP with ATR inhibition overcomes PARP inhibitor and platinum resistance in ovarian cancer models*. *Nat Commun*, **2020**. 11(1): p. 3726.
- Chiappa, M., et al., *Combinations of ATR, Chk1 and Wee1 Inhibitors with Olaparib Are Active in Olaparib Resistant Brca1 Proficient and Deficient Murine Ovarian Cells*. *Cancers (Basel)*, **2022**. 14(7).

16. Parmar, K., et al., *The CHK1 Inhibitor Prexasertib Exhibits Monotherapy Activity in High-Grade Serous Ovarian Cancer Models and Sensitizes to PARP Inhibition*. Clin Cancer Res, **2019**. 25(20): p. 6127-6140.
17. Shah, P.D., et al., *Combination ATR and PARP Inhibitor (CAPRI): A phase 2 study of ceralasertib plus olaparib in patients with recurrent, platinum-resistant epithelial ovarian cancer*. Gynecol Oncol, **2021**. 163(2): p. 246-253.
18. Wethington, S.L., et al., *Combination ATR (cerlasertib) and PARP (olaparib) Inhibitor (CAPRI) Trial in Acquired PARP Inhibitor-Resistant Homologous Recombination-Deficient Ovarian Cancer*. Clin Cancer Res, **2023**. 29(15): p. 2800-2807.
19. Liu, Y., et al., *Patient-derived xenograft models in cancer therapy: technologies and applications*. Signal Transduct Target Ther, **2023**. 8(1): p. 160.
20. Zhang, F., et al., *Characterization of drug responses of mini patient-derived xenografts in mice for predicting cancer patient clinical therapeutic response*. Cancer Commun (Lond), **2018**. 38(1): p. 60.
21. Savage, P., et al., *A Targetable EGFR-Dependent Tumor-Initiating Program in Breast Cancer*. Cell Rep, **2017**. 21(5): p. 1140-1149.
22. Xu, S., et al., *Combined targeting of mTOR and AKT is an effective strategy for basal-like breast cancer in patient-derived xenograft models*. Mol Cancer Ther, **2013**. 12(8): p. 1665-75.
23. Guo, Z., et al., *Proteomic Resistance Biomarkers for PI3K Inhibitor in Triple Negative Breast Cancer Patient-Derived Xenograft Models*. Cancers (Basel), **2020**. 12(12).
24. Reissig, T.M., et al., *Lasting response by vertical inhibition with cetuximab and trametinib in KRAS-mutated colorectal cancer patient-derived xenografts*. Mol Oncol, **2023**. 17(11): p. 2396-2414.
25. Rivera, M., et al., *Patient-derived xenograft (PDX) models of colorectal carcinoma (CRC) as a platform for chemosensitivity and biomarker analysis in personalized medicine*. Neoplasia, **2021**. 23(1): p. 21-35.
26. Malcolm, J.E., et al., *Factors that influence response classifications in chemotherapy treated patient-derived xenografts (PDX)*. PeerJ, **2019**. 7: p. e6586.
27. Ng, W.H., K.C. Soo, and H. Huynh, *Vinorelbine Improves the Efficacy of Sorafenib against Hepatocellular Carcinoma: A Promising Therapeutic Approach*. Int J Mol Sci, **2024**. 25(3).
28. Arango, N.P., et al., *Selinexor (KPT-330) demonstrates anti-tumor efficacy in preclinical models of triple-negative breast cancer*. Breast Cancer Res, **2017**. 19(1): p. 93.
29. Duarte, D. and N. Vale, *Evaluation of synergism in drug combinations and reference models for future orientations in oncology*. Curr Res Pharmacol Drug Discov, **2022**. 3: p. 100110.
30. McCarty, K.S., Jr., et al., *Use of a monoclonal anti-estrogen receptor antibody in the immunohistochemical evaluation of human tumors*. Cancer Res, **1986**. 46(8 Suppl): p. 4244s-4248s.
31. Poveda, A., et al., *Olaparib tablets as maintenance therapy in patients with platinum-sensitive relapsed ovarian cancer and a BRCA1/2 mutation (SOLO2/ENGOT-Ov21): a final analysis of a double-blind, randomised, placebo-controlled, phase 3 trial*. Lancet Oncol, **2021**. 22(5): p. 620-631.
32. Wang, N., et al., *PARP inhibitor resistance in breast and gynecological cancer: Resistance mechanisms and combination therapy strategies*. Front Pharmacol, **2022**. 13: p. 967633.
33. Iijima, M., et al., *Genome-wide analysis of gynecologic cancer: The Cancer Genome Atlas in ovarian and endometrial cancer*. Oncol Lett, **2017**. 13(3): p. 1063-1070.
34. Gonzalez-Martin, A., et al., *Newly diagnosed and relapsed epithelial ovarian cancer: ESMO Clinical Practice Guideline for diagnosis, treatment and follow-up*. Ann Oncol, **2023**. 34(10): p. 833-848.
35. Del Conte, G., et al., *Phase I study of olaparib in combination with liposomal doxorubicin in patients with advanced solid tumours*. Br J Cancer, **2014**. 111(4): p. 651-9.
36. Ni, J., et al., *Olaparib in the therapy of advanced ovarian cancer: first real world experiences in safety and efficacy from China*. J Ovarian Res, **2019**. 12(1): p. 117.
37. Bankhead, P., et al., *QuPath: Open source software for digital pathology image analysis*. Sci Rep, **2017**. 7(1): p. 16878.
38. Biegala, L., et al., *Olaparib-Resistant BRCA2(MUT) Ovarian Cancer Cells with Restored BRCA2 Abrogate Olaparib-Induced DNA Damage and G2/M Arrest Controlled by the ATR/CHK1 Pathway for Survival*. Cells, **2023**. 12(7).
39. Roberts, C.M., et al., *Transforming Growth Factor Beta and Epithelial to Mesenchymal Transition Alter Homologous Recombination Repair Gene Expression and Sensitize BRCA Wild-Type Ovarian Cancer Cells to Olaparib*. Cancers (Basel), **2023**. 15(15).
40. van Berlo, D., et al., *10% Body weight (gain) change as criterion for the maximum tolerated dose: A critical analysis*. Regul Toxicol Pharmacol, **2022**. 134: p. 105235.
41. De Leo, A., et al., *What Is New on Ovarian Carcinoma: Integrated Morphologic and Molecular Analysis Following the New 2020 World Health Organization Classification of Female Genital Tumors*. Diagnostics (Basel), **2021**. 11(4).
42. Vaidyanathan, A., et al., *ABC1 (MDR1) induction defines a common resistance mechanism in paclitaxel- and olaparib-resistant ovarian cancer cells*. Br J Cancer, **2016**. 115(4): p. 431-41.
43. Klotz, D.M., et al., *Establishment and Molecular Characterization of an In Vitro Model for PARPi-Resistant Ovarian Cancer*. Cancers (Basel), **2023**. 15(15).
44. Liu, S., et al., *ATR autophosphorylation as a molecular switch for checkpoint activation*. Mol Cell, **2011**. 43(2): p. 192-202.
45. Gupta, N., et al., *Cell cycle checkpoints and beyond: Exploiting the ATR/CHK1/WEE1 pathway for the treatment of PARP inhibitor-resistant cancer*. Pharmacol Res, **2022**. 178: p. 106162.
46. Leung-Pineda, V., C.E. Ryan, and H. Piwnica-Worms, *Phosphorylation of Chk1 by ATR is antagonized by a Chk1-regulated protein phosphatase 2A circuit*. Mol Cell Biol, **2006**. 26(20): p. 7529-38.
47. Nair, J., et al., *Resistance to the CHK1 inhibitor prexasertib involves functionally distinct CHK1 activities in BRCA wild-type ovarian cancer*. Oncogene, **2020**. 39(33): p. 5520-5535.
48. Krum, S.A., et al., *BRCA1 Forms a Functional Complex with gamma-H2AX as a Late Response to Genotoxic Stress*. J Nucleic Acids, **2010**. 2010.
49. Collins, P.L., et al., *DNA double-strand breaks induce H2AX phosphorylation domains in a contact-dependent manner*. Nat Commun, **2020**. 11(1): p. 3158.
50. Hong, T., et al., *PARP inhibition promotes ferroptosis via repressing SLC7A11 and synergizes with ferroptosis inducers in BRCA-proficient ovarian cancer*. Redox Biol, **2021**. 42: p. 101928.
51. Loret, N., et al., *The Role of Epithelial-to-Mesenchymal Plasticity in Ovarian Cancer Progression and Therapy Resistance*. Cancers (Basel), **2019**. 11(6).
52. Zhang, X., et al., *Targeting polyploid giant cancer cells potentiates a therapeutic response and overcomes resistance to PARP inhibitors in ovarian cancer*. Sci Adv, **2023**. 9(29): p. eadf7195.
53. Cybula, M. and M. Bieniasz, *Patient-derived tumor models are attractive tools to repurpose drugs for ovarian cancer treatment: pre-clinical updates*. Oncotarget, **2022**. 13: p. 553-575.
54. da Cunha Colombo Bonadio, R.R., et al., *Homologous recombination deficiency in ovarian cancer: a review of its epidemiology and management*. Clinics (Sao Paulo), **2018**. 73(suppl 1): p. e450s.
55. Zhang, H., et al., *Integrated Proteogenomic Characterization of Human High-Grade Serous Ovarian Cancer*. Cell, **2016**. 166(3): p. 755-765.
56. Ratajska, M., et al., *Detection of BRCA1/2 mutations in circulating tumor DNA from patients with ovarian cancer*. Oncotarget, **2017**. 8(60): p. 101325-101332.
57. Kowalik, A., et al., *BRCA1 founder mutations and beyond in the Polish population: A single-institution BRCA1/2 next-generation sequencing study*. PLoS One, **2018**. 13(7): p. e0201086.
58. Kassab, M.A. and X. Yu, *The role of dePARylation in DNA damage repair and cancer suppression*. DNA Repair (Amst), **2019**. 76: p. 20-29.
59. Gogola, E., et al., *Selective Loss of PARG Restores PARylation and Counteracts PARP Inhibitor-Mediated Synthetic Lethality*. Cancer Cell, **2018**. 33(6): p. 1078-1093 e12.
60. Hurley, R.M., et al., *53BP1 as a potential predictor of response in PARP inhibitor-treated homologous recombination-deficient ovarian cancer*. Gynecol Oncol, **2019**. 153(1): p. 127-134.
61. Jaspers, J.E., et al., *Loss of 53BP1 causes PARP inhibitor resistance in Brca1-mutated mouse mammary tumors*. Cancer Discov, **2013**. 3(1): p. 68-81.
62. Yang, Z.M., et al., *Combining 53BP1 with BRCA1 as a biomarker to predict the sensitivity of poly(ADP-ribose) polymerase (PARP) inhibitors*. Acta Pharmacol Sin, **2017**. 38(7): p. 1038-1047.
63. Bizzaro, F., et al., *VEGF pathway inhibition potentiates PARP inhibitor efficacy in ovarian cancer independent of BRCA status*. J Hematol Oncol, **2021**. 14(1): p. 186.
64. Kim, H., et al., *Targeting the ATR/CHK1 Axis with PARP Inhibition Results in Tumor Regression in BRCA-Mutant Ovarian Cancer Models*. Clin Cancer Res, **2017**. 23(12): p. 3097-3108.
65. Li, H., et al., *Risks of breast and ovarian cancer for women harboring pathogenic missense variants in BRCA1 and BRCA2 compared with those harboring protein truncating variants*. Genet Med, **2022**. 24(1): p. 119-129.
66. Wilson, A.J., et al., *Panobinostat enhances olaparib efficacy by modifying expression of homologous recombination repair and immune transcripts in ovarian cancer*. Neoplasia, **2022**. 24(2): p. 63-75.
67. Tang, S., et al., *Olaparib synergizes with arsenic trioxide by promoting apoptosis and ferroptosis in platinum-resistant ovarian cancer*. Cell Death Dis, **2022**. 13(9): p. 826.
68. Kang, M., et al., *A Double-Edged Sword: The Two Faces of PARylation*. Int J Mol Sci, **2022**. 23(17).
69. Haynes, B., J. Murai, and J.M. Lee, *Restored replication fork stabilization, a mechanism of PARP inhibitor resistance, can be overcome by cell cycle checkpoint inhibition*. Cancer Treat Rev, **2018**. 71: p. 1-7.
70. Miller, R.E., et al., *Ovarian Cancer Therapy: Homologous Recombination Deficiency as a Predictive Biomarker of Response to PARP Inhibitors*. Onco Targets Ther, **2022**. 15: p. 1105-1117.
71. Cybula, M., et al., *Patient-Derived Xenografts of High-Grade Serous Ovarian Cancer Subtype as a Powerful Tool in Pre-Clinical Research*. Cancers (Basel), **2021**. 13(24).

## Supplementary Information

### Olaparib Rechallenge Combined with the ATR/CHK1 Pathway Inhibitors in Olaparib-Resistant PDX Models of Ovarian Cancer: Mechanisms Behind Synergistic Tumor Growth Inhibition

Łukasz Biegała<sup>1,2</sup>, Małgorzata Statkiewicz<sup>3</sup>, Arkadiusz Gajek<sup>1</sup>, Izabela-Szymczak-Pajor<sup>4</sup>,  
Natalia Rusetska<sup>5</sup>, Agnieszka Śliwińska<sup>4</sup>, Agnieszka Marczak<sup>1</sup>, Michał Mikula<sup>3</sup>,  
Aneta Rogalska<sup>1,\*</sup>

<sup>1</sup> Department of Medical Biophysics, Institute of Biophysics, Faculty of Biology and Environmental Protection, University of Lodz, 141/143 Pomorska Street, 90-236 Lodz, Poland

<sup>2</sup> Doctoral School of Exact and Natural Sciences, University of Lodz, 21/23 Jana Matejki Street, 90-237 Lodz, Poland

<sup>3</sup> Department of Genetics, Maria Skłodowska-Curie National Research Institute of Oncology, 5 Roentgena Street, 02-781, Warsaw, Poland

<sup>4</sup> Department of Nucleic Acid Biochemistry, Medical University of Lodz, 251 Pomorska Street, 92-213 Lodz, Poland

<sup>5</sup> Department of Experimental Immunology, Maria Skłodowska-Curie National Research Institute of Oncology, 5 Roentgena Street, 02-781, Warsaw, Poland

#### TABLE OF CONTENTS

##### Supplementary Figures:

**Figure S1:** The growth curves of PDX-X127 and PDX-X160 tumors and mice body weights following treatment with olaparib (50 mg/kg) or vehicle during the attempt to induce olaparib resistance *in vivo*.

**Figure S2:** The expression of MDR1 and caspase-3 after the induction of resistance to olaparib in PDX-X179 models of HGSOc.

**Figure S3:** Histopathological assessment of heart tissue from selected olaparib-resistant PDX tumors treated with tested inhibitors or their combinations.

**Figure S4:** Results of RT-qPCR gene expression analysis for *CASP3*, *PARP1*, *ATR*, *CHEK1*, and *H2AFX* in olaparib-resistant PDX-X179 tumors treated with tested inhibitors or their combinations.

**Figure S5:** Quantitative Western Blotting analysis of RAD51 and MDR1 in olaparib-resistant PDX-X179 tumors treated with tested inhibitors or their combinations.

##### Supplementary Tables:

**Table S1:** List of key reagents used in the study.

**Table S2:** Histopathological assessment criteria assessing the severity of pathological changes in H&E-stained tumor tissues based on scientific literature and recommendations included in the INHAND criteria developed and published by GESC.

**Table S3:** List of TaqMan™ Gene Expression Assay used for gene expression studies (RT-qPCR).

**Table S4:** List of primary antibodies used for Western Blotting.

## Supplementary Figure 1 (Figure S1)

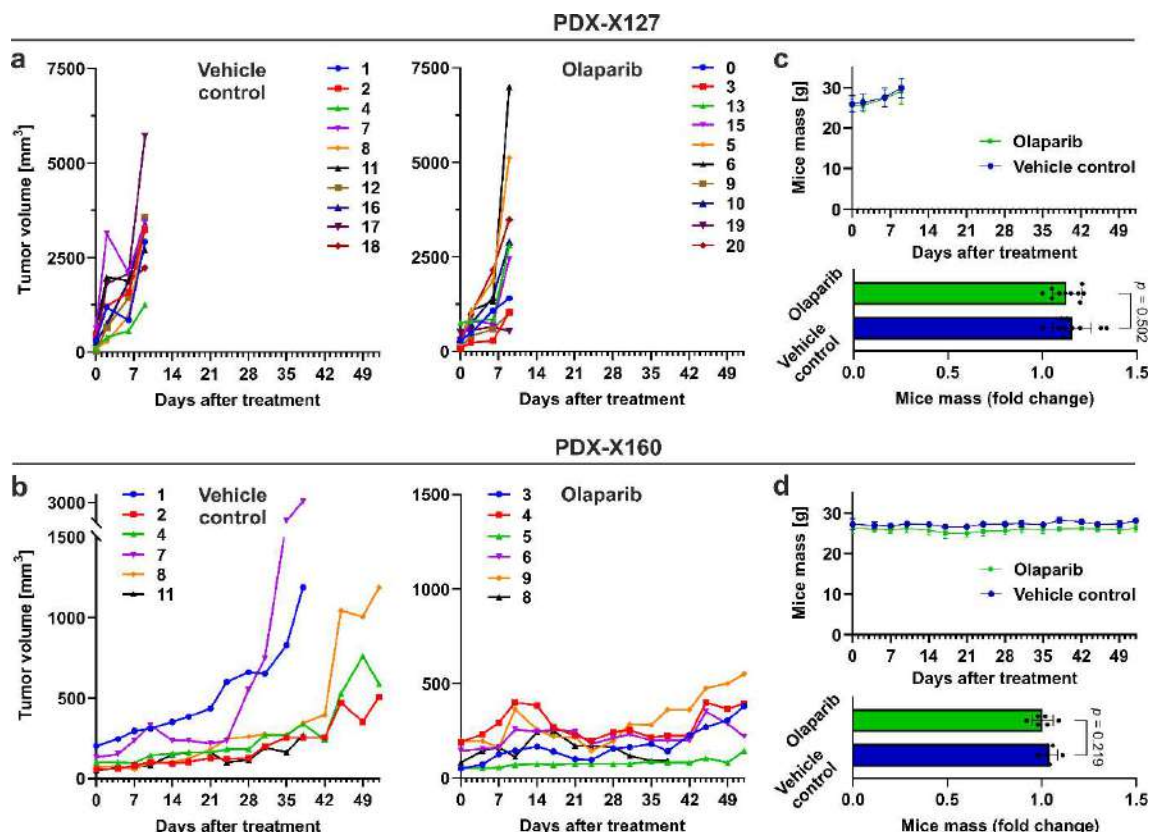


**Figure S1. The growth curves of PDX-X127 and PDX-X160 tumors and mice body weights following treatment with olaparib (50 mg/kg) or vehicle during the attempt to induce olaparib resistance *in vivo*.** Both models were not suitable for the induction of resistance to olaparib and were rejected. **(a)** Vehicle-treated xenografts from PDX-X127 increased their volume about 19.2 times during the first 9 days of treatment, reaching on average as much as  $3174 \pm 1077$  mm<sup>3</sup> ( $n = 10$ ). Tumors among vehicle control groups from PDX-X127 showed growth speed differences and exhibited unexpectedly elevated growth rates. **(b)** Vehicle-treated xenografts from PDX-X160 exhibited major intragroup differences in tumor growth. **(c, d)** Mice body weights harboring PDX-X127 and -X160 during treatment with olaparib (50 mg/kg) or vehicle and comparison of changes in mice masses (fold change) between groups at harvest day relative to day zero of treatment using unpaired t-test:  $*p < 0.05$ .

## Supplementary Figure 2 (Figure S2)

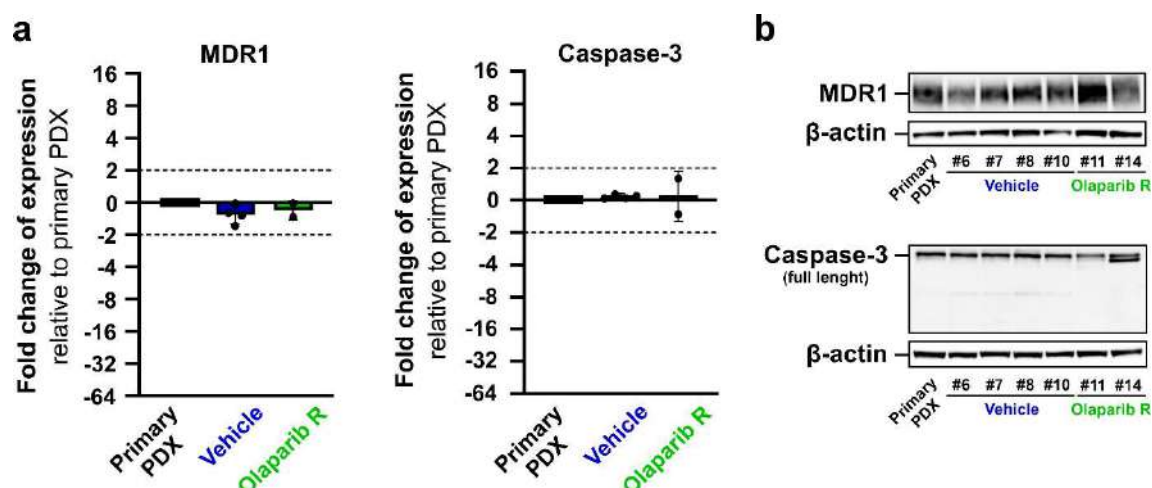


**Figure S2. The expression of MDR1 and caspase-3 after the induction of resistance to olaparib in PDX-X179 models of HGSOc.**

Upon the completion of the development of olaparib-resistant (R) PDX models, vehicle-treated xenografts (#6, 7, 8, and 10), and tumors with acquired resistance in the presence of 50 mg/kg olaparib (#11 and 14) were harvested, and whole tissue lysates were prepared for Western Blotting analysis of MDR1 (**a**) and caspase-3 (**b**). Protein expression was normalized to β-actin and presented on graphs with a logarithmic scale as a fold-change (mean ± STD) relative to untreated primary PDX-X179 at P5 used for the development of tumors for both treatment arms. Dashed lines indicate an expression cut-off of ± 2-fold to indicate relevant changes. Statistical significance between groups was assessed using ordinary one-way ANOVA followed by Tukey's post-hoc test: \* $p < 0.05$ . (**c**) Representative Western Blot images.



## Supplementary Figure 3 (Figure S3)

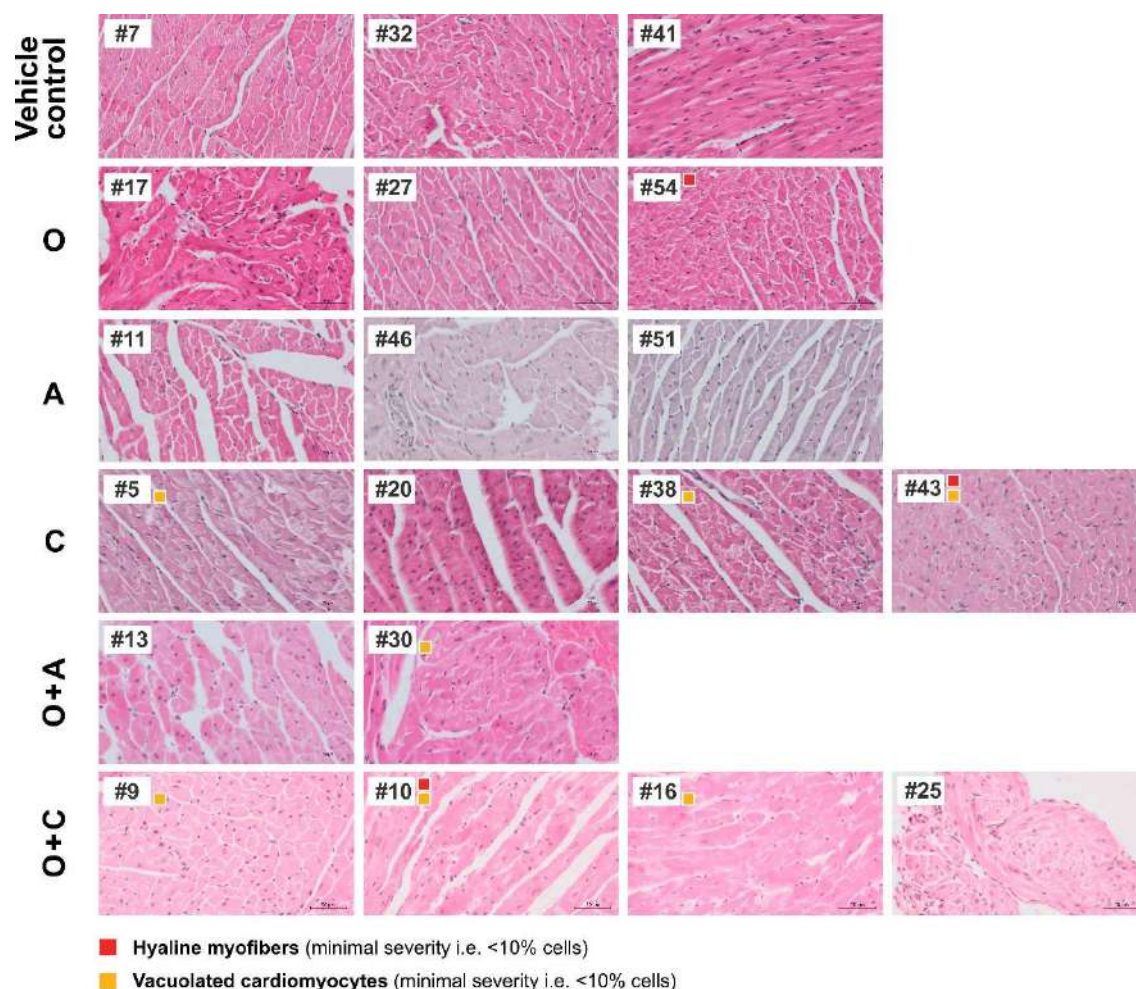


**Figure S3. Histopathological assessment of heart tissue from selected olaparib-resistant PDX tumors treated with tested inhibitors or their combinations.** Mice bearing olaparib-resistant tumors were treated with vehicle (n = 5), olaparib (O, 50 mg/kg, n = 5), ATRi (A, 25 mg/kg, n = 5), CHK1i (C, 50 mg/kg, n = 6) or olaparib combinations with either ATRi (O + A, n = 5) or CHK1i (O + C, n = 5). Upon treatment completion, hearts were harvested and FFPE tissue sections were stained with H&E for the evaluation of the presence of hyaline myofiber degeneration and cardiomyocyte vacuolization. The abundance and severity of each lesion were scored on the scale: none (0%); minimal (<10%); slight (10–39%); moderate (40–79%) and high/severe (80–100%). All detected degenerative changes in heart tissue in marked individuals were assigned as minimal.

## Supplementary Figure 4 (Figure S4)

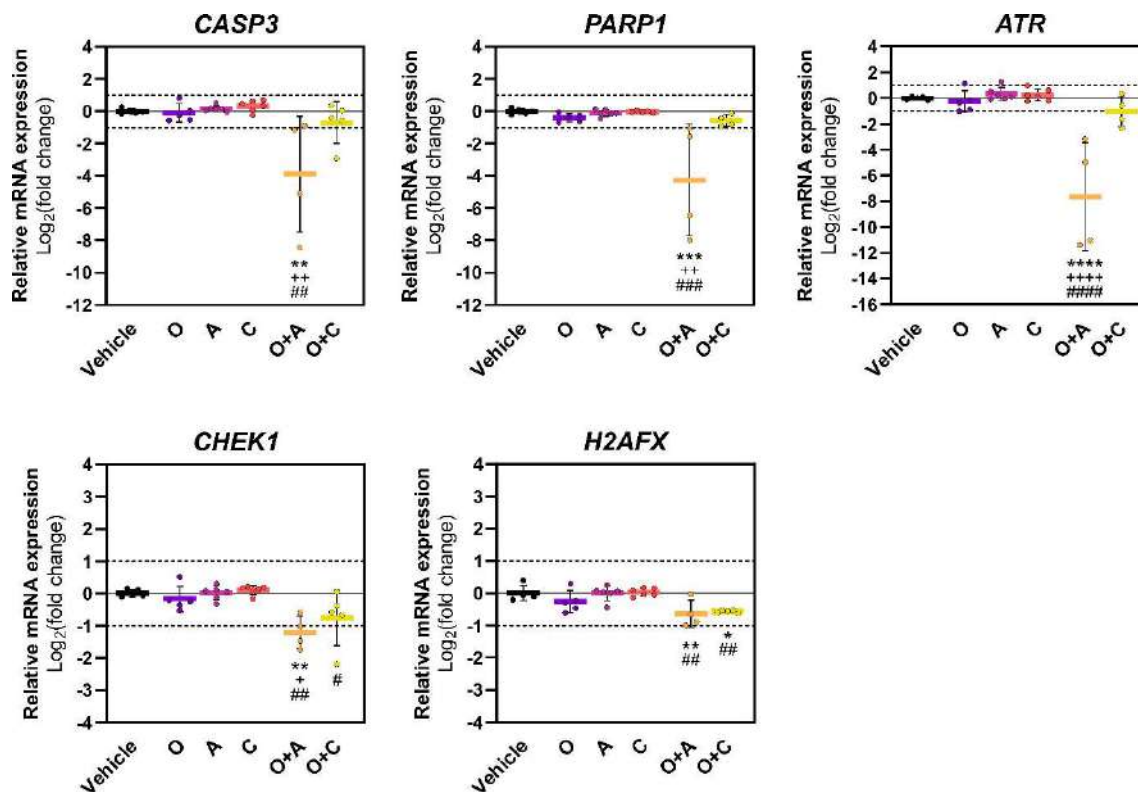


**Figure S4. Results of RT-qPCR gene expression analysis for *CASP3*, *PARP1*, *ATR*, *CHEK1*, and *H2AFX* in olaparib-resistant PDX-X179 tumors treated with tested inhibitors or their combinations.** Mice bearing olaparib-resistant tumors were treated with vehicle (n = 5), olaparib (O, 50 mg/kg, n = 5), ATRi (A, 25 mg/kg, n = 5), CHK1i (C, 50 mg/kg, n = 6) or olaparib combinations with either ATRi (O + A, n = 5) or CHK1i (O + C, n = 5). Upon treatment completion, tumors were harvested, and RNA was isolated for cDNA synthesis and determination of mRNA levels via RT-qPCR. Data were normalized to the *ACTB* gene and expressed relative to vehicle-treated tumors as mean  $\pm$  STD. Statistical significance between groups was assessed using ordinary one-way ANOVA followed by Tukey's post-hoc test: \* $p$  < 0.05, \*\* $p$  < 0.01, \*\*\* $p$  < 0.001, \*\*\*\* $p$  < 0.0001 (vehicle vs. inhibitor(s)); + $p$  < 0.05, ++ $p$  < 0.01, +++ $p$  < 0.0001 (olaparib vs. combination with ATRi or CHK1i); # $p$  < 0.05, ## $p$  < 0.01, ### $p$  < 0.001, #### $p$  < 0.0001 (ATRi or CHK1i vs. respective combinations with olaparib).

## Supplementary Figure 5 (Figure S5)

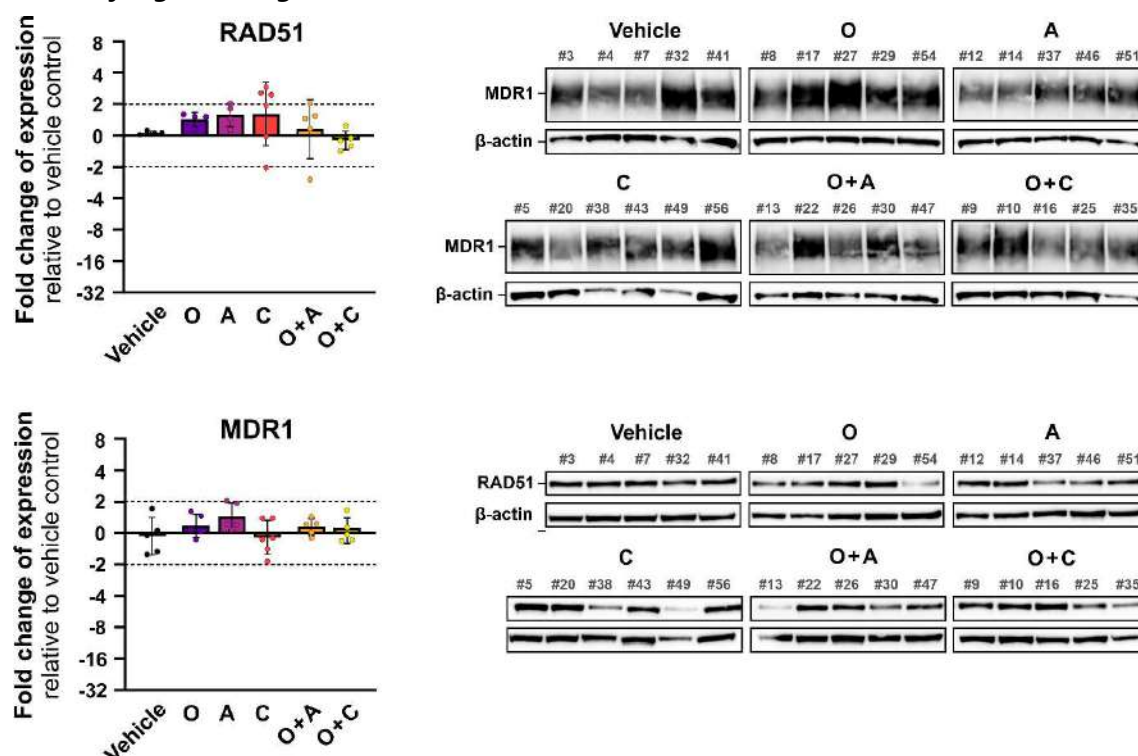


**Figure S5. Quantitative Western Blotting analysis of RAD51 and MDR1 in olaparib-resistant PDX-X179 tumors treated with tested inhibitors or their combinations.** Mice bearing olaparib-resistant tumors were treated with vehicle (n = 5), olaparib (O, 50 mg/kg, n = 5), ATRi (A, 25 mg/kg, n = 5), CHK1i (C, 50 mg/kg, n = 6) or olaparib combinations with either ATRi (O + A, n = 5) or CHK1i (O + C, n = 5). Upon treatment completion, tumors were harvested and whole tissue lysates were prepared for Western Blotting analysis. Protein expression was normalized to β-actin and presented on graphs with a logarithmic scale as a fold-change (mean ± STD) relative to a vehicle-treated group. Dashed lines indicate an expression cut-off of ± 2-fold to indicate relevant changes. Statistical significance between groups was assessed using ordinary one-way ANOVA followed by Tukey's post-hoc test (normally distributed data) or Kruskal-Wallis test followed by Dunn's post-hoc test (non-normally distributed data).

## Supplementary Table 1 (Table S1)

### List of key reagents used in the study.

Reagent	Catalog Number	Manufacturer
Anti-Ki-67 antibody	MA5-14520	Invitrogen™ (Thermo Fisher Scientific)
Anti-phospho-CHK1 (Ser345) antibody	PA5-34625	Invitrogen™ (Thermo Fisher Scientific)
Ceralasertib (ATR inhibitor)	TBW02661	Wuhan ChemNorm Biotech
DMSO, Anhydrous	D12345	Thermo Fisher Scientific
Halt™ Phosphatase Inhibitor Cocktail (100X)	78420	Thermo Fisher Scientific
Halt™ Protease Inhibitor Cocktail (100X)	87786	Thermo Fisher Scientific
High-Capacity cDNA Reverse Transcription Kit	4368814	Applied Biosystems™ (Thermo Fisher Scientific)
HiMark™ Pre-stained Protein Standard	LC5699	Invitrogen™ (Thermo Fisher Scientific)
MagicMark™ XP Western Protein Standard	LC5602	Invitrogen™ (Thermo Fisher Scientific)
mirVana™ miRNA Isolation Kit, with phenol	AM1560	Invitrogen™ (Thermo Fisher Scientific)
MK-8776 (CHK1 inhibitor)	TBW02666	Wuhan ChemNorm Biotech
MOPS Running Buffer	MPM0PS	Millipore (Merck)
mPAGE® 4X LDS Sample Buffer	MPSB	Millipore (Merck)
mPAGE® Bis-Tris Precast Gels 10%	MP10W10	Millipore (Merck)
mPAGE® Bis-Tris Precast Gels 12%	MP12W10	Millipore (Merck)
mPAGE® Bis-Tris Precast Gels 8%	MP8W10	Millipore (Merck)
mPAGE® Transfer Buffer	MPTRB	Millipore (Merck)
Olaparib	HY-10162	MedChemExpress
Pierce™ BCA Protein Assay Kits	23227	Thermo Fisher Scientific
Poly(ethylene glycol), average M.W. 300 (PEG300)	192220010	Thermo Fisher Scientific
PVDF Membrane	IPVH85R	Millipore (Merck)
RIPA Lysis and Extraction Buffer	89900	Thermo Fisher Scientific
RNase Inhibitor	N8080119	Applied Biosystems™ (Thermo Fisher Scientific)
SignalStain® Boost IHC Detection Reagent (HRP, Mouse)	8125	Cell Signaling Technology
SignalStain® Boost IHC Detection Reagent (HRP, Rabbit)	8114	Cell Signaling Technology
Spectra™ Multicolor Broad Range Protein Ladder	26634	Thermo Fisher Scientific
Spectra™ Multicolor High Range Protein Ladder	26625	Thermo Fisher Scientific
SuperBlock™ (TBS) Blocking Buffer	37581	Thermo Fisher Scientific
SuperSignal™ West Atto Ultimate Sensitivity Substrate	A38555	Thermo Fisher Scientific
SuperSignal™ West Pico PLUS Chemiluminescent Substrate	34577	Thermo Fisher Scientific
TaqMan™ Gene Expression Assay (FAM)	4331182	Applied Biosystems™ (Thermo Fisher Scientific)
TaqMan™ Universal Master Mix II, no UNG	4440049	Applied Biosystems™ (Thermo Fisher Scientific)
Target Retrieval Solution, pH 6	S2369	Dako (Agilent)
TWEEN® 80	P4780	Sigma-Aldrich (Merck)
Water, Nuclease-free, Molecular Biology Grade, Ultrapure, Thermo Scientific Chemicals	J71786.XCR	Applied Biosystems™ (Thermo Fisher Scientific)
β-mercaptoethanol	M6250	Sigma-Aldrich (Merck)

### Supplementary Table 2 (Table S2)

Histopathological assessment criteria assessing the severity of pathological changes in H&E-stained tumor tissues based on scientific literature and recommendations included in the INHAND criteria developed and published by GESC.

Scoring scale	Mitotic index (assessed in 10 fields from magnification x40)	Area of necrosis	Single-cell necrosis (assessed in 10 fields from magnification x40)	Nuclear pleomorphism	Vacuolization of tumor cells
<b>0</b> <b>none</b> <b>(-)</b>	< 1 mitosis	0 %	< 2 single cell necrosis	no pathological changes	0–5%
<b>1</b> <b>minimal</b> <b>(+)</b>	2–5 mitoses	< 1%	2–7 single cell necrosis	the cell nuclei nearly normal, the nucleoli hardly visible/evident	5–25%
<b>2</b> <b>slight</b> <b>(++)</b>	6–10 mitoses	1–5%	8–12 single cell necrosis	mild pleomorphism, visible/ evident nucleoli	26–50%
<b>3</b> <b>moderate</b> <b>(+++)</b>	11–15 mitoses	6–10%	13–17 single cell necrosis	moderate pleomorphism, prominent, distinct nucleoli	51–75%
<b>4</b> <b>severe</b> <b>(++++)</b>	> 15 mitoses	> 10%	> 17 single cell necrosis	marked pleomorphism, prominent/ numerous nucleoli	76–100%

### Supplementary Table 3 (Table S3)

List of TaqMan™ Gene Expression Assay used for gene expression studies (RT-qPCR).

Gene	Assay ID
<b>ABCB1</b>	Hs00184500_m1
<b>ACTB</b>	Hs01060665_g1
<b>ATR</b>	Hs00992123_m1
<b>CASP3</b>	Hs00234387_m1
<b>CHEK1</b>	Hs00967506_m1
<b>GAPDH</b>	Hs02758991_g1
<b>H2AXF</b>	Hs00266783_s1
<b>HPRT1</b>	Hs02800695_m1
<b>PARP1</b>	Hs00242302_m1

## Supplementary Table 4 (Table S4)

### List of primary antibodies used for Western Blotting.

Target	Supplier	Catalog Number	Dilution Factor	Antibody Dilution Buffer
<b>53BP1</b>	Sigma-Aldrich (Merck)	MAB3802	1:1250	5% BSA in TBST
<b>ATR</b>	Invitrogen™ (Thermo Fisher Scientific)	MA1-23158	1:1000	5% non-fat milk in TBST
<b>BRCA1</b>	Cell Signaling Technology	9010	1:1000	5% BSA in TBST
<b>BRCA2 (C-term)</b>	Thermo Fisher Scientific	A300-005A	1:1000	5% BSA in TBST
<b>Caspase-3</b>	Cell Signaling Technology	14220	1:1000	5% BSA in TBST
<b>CHK1</b>	Invitrogen™ (Thermo Fisher Scientific)	MA5-32180	1:1000	5% BSA in TBST
<b>E-Cadherin</b>	Cell Signaling Technology	3195	1:1000	5% BSA in TBST
<b>MDR1</b>	Invitrogen™ (Thermo Fisher Scientific)	MA5-32282	1:1000	5% BSA in TBST
<b>MMP2</b>	Cell Signaling Technology	40994	1:1000	5% BSA in TBST
<b>PAR</b>	Cell Signaling Technology	83732	1:1000	5% BSA in TBST
<b>PARG</b>	Invitrogen™ (Thermo Fisher Scientific)	MA5-27034	1:1500	5% BSA in TBST
<b>PARP1</b>	Cell Signaling Technology	9532	1:1000	5% non-fat milk in TBST
<b>pATR (Thr1989)</b>	Cell Signaling Technology	30632	1:1000	5% BSA in TBST
<b>pCHK1 (Ser345)</b>	Cell Signaling Technology	2348	1:1250	5% BSA in TBST
<b>RAD51</b>	Sigma-Aldrich (Merck)	ABE257	1:1250	5% BSA in TBST
<b>TIMP2</b>	Cell Signaling Technology	5738	1:1000	5% BSA in TBST
<b>Vimentin</b>	Cell Signaling Technology	5741	1:1000	5% BSA in TBST
<b>β-actin</b>	Sigma-Aldrich (Merck)	A1978	1:10 000	5% BSA in TBST
<b>γH2AX (Ser139)</b>	Sigma-Aldrich (Merck)	05-636	1:1000	5% BSA in TBST



**OŚWIADCZENIA  
WSPÓŁAUTORÓW PUBLIKACJI**

---

Łódź, 20.05.2024

**Mgr inż. Łukasz Biegała**

<sup>1</sup> Katedra Biofizyki Medycznej  
Uniwersytet Łódzki

<sup>2</sup> Szkoła Doktorska Nauk Ścisłych i Przyrodniczych  
Uniwersytet Łódzki

## OŚWIADCZENIE WSPÓŁAUTORA

Oświadczam, że w opublikowanej pracy:

**Biegała Ł.**, Gajek A., Marczak A., Rogalska A. *PARP inhibitor resistance in ovarian cancer: Underlying mechanisms and therapeutic approaches targeting the ATR/CHK1 pathway*. Biochim Biophys Acta Rev Cancer. 2021. 1876(2):188633. <https://doi.org/10.1016/j.bbcan.2021.188633>, mój udział wynosił **75%** i polegał na: opracowaniu koncepcji pracy przeglądowej; zebraniu danych literaturowych, przygotowaniu rycin i wstępnej wersji artykułu; redagowaniu roboczej wersji manuskryptu, wprowadzeniu poprawek merytorycznych, przygotowaniu odpowiedzi dla recenzentów, przygotowaniu i zatwierdzeniu ostatecznej wersji artykułu.

Oświadczam, że w opublikowanej pracy:

**Biegała Ł.**, Gajek A., Marczak A., Rogalska A. *Olaparib-Resistant BRCA2<sup>MUT</sup> Ovarian Cancer Cells with Restored BRCA2 Abrogate Olaparib-Induced DNA Damage and G2/M Arrest Controlled by the ATR/CHK1 Pathway for Survival*. Cells. 2023. 12(7):1038. <https://doi.org/10.3390/cells12071038>, mój udział wynosił **70%** i polegał na: opracowaniu koncepcji badań; zaplanowaniu i wdrożeniu części metodologicznej; wykonaniu części eksperymentów (prowadzenie hodowli linii komórkowych, wyprowadzenie linii komórkowej PEO1-OR odpornej na olaparib, test MTT, test wzrostu klonalnego, proliferacja komórek, izolacja DNA z linii komórkowych, przygotowanie lizatów białkowych z linii komórkowych, oznaczenie stężenia białka w lizatach komórkowych, badanie poziomu ekspresji białek metodą Western Blot, analiza wariantów genów na podstawie wyników sekwencjonowania następnej generacji, barwienie immunofluorescencyjne z wykorzystaniem mikroskopii konfokalnej, preparatyka i analiza mikroskopowa chromosomów metafazowych, analiza dystrybucji komórek w fazach cyklu komórkowego z wykorzystaniem barwienia immunofluorescencyjnego i cytometrii przepływowej); analizie, opracowaniu i interpretacji wyników; wizualizacji wyników; przygotowaniu wstępnej wersji manuskryptu; redagowaniu roboczej wersji manuskryptu, wprowadzeniu poprawek merytorycznych, przygotowaniu odpowiedzi dla recenzentów, przygotowaniu i zatwierdzeniu ostatecznej wersji artykułu.

Oświadczam, że w opublikowanej pracy:

**Biegała Ł.**, Gajek A., Szymczak-Pajor I., Marczak A., Śliwińska A., Rogalska A. *Targeted inhibition of the ATR/CHK1 pathway overcomes resistance to olaparib and dysregulates DNA damage response protein expression in BRCA2<sup>MUT</sup> ovarian cancer cells*. Sci Rep. 2023. 13(1):22659. <https://doi.org/10.1038/s41598-023-50151-y>,

*Biegała*



mój udział wynosił **65%** i polegał na: opracowaniu koncepcji badań; zaplanowaniu i wdrożeniu części metodologicznej; wykonaniu części eksperymentów (prowadzenie hodowli linii komórkowych, test MTT, test wzrostu klonalnego, proliferacja komórek, izolacja całkowitego RNA z linii komórkowych, synteza cDNA dla mRNA, przygotowanie lizatów białkowych z linii komórkowych, oznaczenie stężenia białka w lizatach komórkowych, badanie poziomu ekspresji panelu białek z wykorzystaniem macierzy przeciwciał, oznaczenie aktywności enzymatycznej kasazy-3/7 oraz oznaczenie poziomu apoptozy poprzez pomiar eksternalizacji fosfatydyloseryny za pomocą cytometrii przepływowej, walidacja ekspresji genów referencyjnych za pomocą ilościowej reakcji łańcuchowej polimerazy w czasie rzeczywistym (RT-qPCR)); analizie, opracowaniu i interpretacji wyników; wizualizacji wyników; przygotowaniu wstępnej wersji manuskryptu; redagowaniu roboczej wersji manuskryptu, wprowadzeniu poprawek merytorycznych, przygotowaniu odpowiedzi dla recenzentów, przygotowaniu i zatwierdzeniu ostatecznej wersji artykułu.

Oświadczam, że w opublikowanej pracy:

**Biegała Ł.**, Kołat D., Gajek A., Płuciennik E., Marczak A., Śliwińska A., Mikula M., Rogalska A. *Uncovering miRNA-mRNA Regulatory Networks Related to Olaparib Resistance and Resensitization of BRCA2<sup>MUT</sup> Ovarian Cancer PEO1-OR Cells with the ATR/CHK1 Pathway Inhibitors*. Cells. 2024. 13(10):864. <https://doi.org/10.3390/cells13100867>,

mój udział wynosił **70%** i polegał na: opracowaniu koncepcji badań; zaplanowaniu i wdrożeniu części metodologicznej; wykonaniu części eksperymentów (prowadzenie hodowli linii komórkowych, izolacja całkowitego RNA wraz z mikroRNA z linii komórkowych, synteza cDNA dla mikroRNA, przygotowanie lizatów białkowych z linii komórkowych, oznaczenie stężenia białka w lizatach komórkowych, badanie poziomu ekspresji panelu białek z wykorzystaniem macierzy przeciwciał, projektowanie 384-dołkowych kart mikroprzepływowych do wykonywania jednoczesnych reakcji PCR z użyciem Custom TaqMan® Array MicroRNA Cards, walidacja ekspresji genów referencyjnych oraz badanie poziomu ekspresji mikroRNA za pomocą ilościowej reakcji łańcuchowej polimerazy w czasie rzeczywistym (RT-qPCR) z wykorzystaniem Custom TaqMan® Array MicroRNA Cards); gromadzeniu, analizie i opracowaniu danych z repozytoriów; analizie wyników, w tym analizie bioinformatycznej oraz opracowaniu i interpretacji wyników; wizualizacji wyników; przygotowaniu wstępnej wersji manuskryptu; redagowaniu roboczej wersji manuskryptu, wprowadzeniu poprawek merytorycznych, przygotowaniu odpowiedzi dla recenzentów, przygotowaniu i zatwierdzeniu ostatecznej wersji artykułu.

Oświadczam, że w manuskrypcie artykułu:

**Biegała Ł.**, Statkiewicz M., Gajek A., Szymczak-Pajor I., Rusetska N., Śliwińska A., Marczak A., Mikula M., Rogalska A. pt.: „*Olaparib rechallenge combined with ATR/CHK1 pathway inhibitors in olaparib-resistant PDX models of ovarian cancer: Mechanisms behind synergistic tumor growth inhibition*”,

mój udział wynosił **60%** i polegał na: opracowaniu koncepcji badań; zaplanowaniu i wdrożeniu części metodologicznej; wykonaniu części eksperymentów (izolacja całkowitego RNA z tkanek nowotworowych, synteza cDNA dla mRNA, przygotowanie lizatów białkowych z tkanek nowotworowych, oznaczenie stężenia białka w lizatach tkankowych, badanie poziomu ekspresji

*Biegała*

białek metodą Western Blot); analizie, opracowaniu i interpretacji wyników; wizualizacji wyników; przygotowaniu wstępnej wersji manuskryptu; redagowaniu roboczej wersji manuskryptu, wprowadzeniu poprawek merytorycznych i zatwierdzeniu ostatecznej wersji manuskryptu.

*Lukasz Biegała*

---

mgr inż. Łukasz Biegała

(podpis)



Łódź, 20.05.2024

**Dr hab. Aneta Rogalska, prof. UŁ**

Katedra Biofizyki Medycznej

Uniwersytet Łódzki

## OŚWIADCZENIE WSPÓŁAUTORA

Oświadczam, że w opublikowanej pracy:

Biegała Ł., Gajek A., Marczak A., **Rogalska A.** *PARP inhibitor resistance in ovarian cancer: Underlying mechanisms and therapeutic approaches targeting the ATR/CHK1 pathway*. Biochim Biophys Acta Rev Cancer. 2021. 1876(2):188633. <https://doi.org/10.1016/j.bbcan.2021.188633>,  
mój udział wynosił **10%** i polegał na: opracowaniu koncepcji pracy przeglądowej; zebraniu danych literaturowych i przygotowaniu wstępnej wersji artykułu; redagowaniu roboczej wersji manuskryptu, przygotowaniu i zatwierdzeniu ostatecznej wersji artykułu; pozyskaniu środków finansowych na prowadzony projekt oraz sprawowaniu nadzoru nad przygotowaniem artykułu.

Oświadczam, że w opublikowanej pracy:

Biegała Ł., Gajek A., Marczak A., **Rogalska A.** *Olaparib-Resistant BRCA2<sup>MUT</sup> Ovarian Cancer Cells with Restored BRCA2 Abrogate Olaparib-Induced DNA Damage and G2/M Arrest Controlled by the ATR/CHK1 Pathway for Survival*. Cells. 2023. 12(7):1038. <https://doi.org/10.3390/cells12071038>,  
mój udział wynosił **15%** i polegał na: opracowaniu koncepcji badań; zaplanowaniu i wdrożeniu części metodologicznej; interpretacji wyników; zapewnianiu dostępu do materiałów badawczych; wizualizacji wyników; redagowaniu roboczej wersji manuskryptu, uczestniczeniu w odpowiedziach na recenzje i zatwierdzeniu ostatecznej wersji artykułu; pozyskaniu środków finansowych na prowadzony projekt oraz sprawowaniu nadzoru nad przygotowaniem artykułu.

Oświadczam, że w opublikowanej pracy:

Biegała Ł., Gajek A., Szymczak-Pajor I., Marczak A., Śliwińska A., **Rogalska A.** *Targeted inhibition of the ATR/CHK1 pathway overcomes resistance to olaparib and dysregulates DNA damage response protein expression in BRCA2<sup>MUT</sup> ovarian cancer cells*. Sci Rep. 2023. 13(1):22659. <https://doi.org/10.1038/s41598-023-50151-y>,  
mój udział wynosił **10%** i polegał na: opracowaniu koncepcji badań; zaplanowaniu części metodologicznej; wizualizacji wyników; zapewnianiu dostępu do materiałów badawczych; redagowaniu roboczej wersji manuskryptu, uczestniczeniu w odpowiedziach na recenzje i zatwierdzeniu ostatecznej wersji artykułu; pozyskaniu środków finansowych na prowadzony projekt oraz sprawowaniu nadzoru nad przygotowaniem artykułu.

Oświadczam, że w opublikowanej pracy:

Biegała Ł., Kołat D., Gajek A., Płuciennik E., Marczak A., Śliwińska A., Mikula M., **Rogalska A.** *Uncovering miRNA-mRNA Regulatory Networks Related to Olaparib Resistance and Resensitization of BRCA2<sup>MUT</sup> Ovarian Cancer PEO1-OR Cells with the ATR/CHK1 Pathway Inhibitors*. Cells. 2024. 13(10):864. <https://doi.org/10.3390/cells13100867>,

Aneta Rogalska

mój udział wynosił 5% i polegał na: opracowaniu koncepcji badań; zaplanowaniu części metodologicznej; redagowaniu roboczej wersji manuskryptu i odpowiedzi na recenzje, przygotowaniu i zatwierdzeniu ostatecznej wersji artykułu; pozyskaniu środków finansowych na prowadzony projekt oraz sprawowaniu nadzoru nad przygotowaniem artykułu.

Oświadczam, że w manuskrypcie artykułu:

Biegała Ł., Statkiewicz M., Gajek A., Szymczak-Pajor I., Rusetska N., Śliwińska A., Marczak A., Mikula M., **Rogalska A.** pt.: „*Olaparib rechallenge combined with the ATR/CHK1 pathway inhibitors in olaparib-resistant PDX models of ovarian cancer: Mechanisms behind synergistic tumor growth inhibition*”,

mój udział wynosił 4% i polegał na: opracowaniu koncepcji badań; zaplanowaniu części metodologicznej; zapewnianiu dostępu do materiałów badawczych; redagowaniu roboczej wersji i zatwierdzeniu ostatecznej wersji manuskryptu; pozyskaniu środków finansowych na prowadzony projekt oraz sprawowaniu nadzoru nad przygotowaniem artykułu.



dr hab. Aneta Rogalska, prof. UŁ

(podpis)



Łódź, 20.05.2024

**Dr Arkadiusz Gajek**

Katedra Biofizyki Medycznej

Uniwersytet Łódzki

### OŚWIADCZENIE WSPÓŁAUTORA

Oświadczam, że w opublikowanej pracy:

Biegała Ł., **Gajek A.**, Marczak A., Rogalska A. *PARP inhibitor resistance in ovarian cancer: Underlying mechanisms and therapeutic approaches targeting the ATR/CHK1 pathway*. Biochim Biophys Acta Rev Cancer. 2021. 1876(2):188633. <https://doi.org/10.1016/j.bbcan.2021.188633>, mój udział wynosił **5%** i polegał na: opracowaniu koncepcji pracy przeglądowej; zebraniu danych literaturowych, przygotowaniu części rycin i wstępnej wersji artykułu; redagowaniu roboczej wersji manuskryptu, przygotowaniu i zatwierdzeniu ostatecznej wersji artykułu.

Oświadczam, że w opublikowanej pracy:

Biegała Ł., **Gajek A.**, Marczak A., Rogalska A. *Olaparib-Resistant BRCA2<sup>MUT</sup> Ovarian Cancer Cells with Restored BRCA2 Abrogate Olaparib-Induced DNA Damage and G2/M Arrest Controlled by the ATR/CHK1 Pathway for Survival*. Cells. 2023. 12(7):1038. <https://doi.org/10.3390/cells12071038>, mój udział wynosił **10%** i polegał na: opracowaniu koncepcji badań; zaplanowaniu i wdrożeniu części metodologicznej; wykonaniu części eksperymentów (barwienie immunofluorescencyjne z wykorzystaniem mikroskopii konfokalnej, analiza mikroskopowa chromosomów metafazowych, analiza dystrybucji komórek w fazach cyklu komórkowego z wykorzystaniem barwienia immunofluorescencyjnego i cytometrii przepływowej); analizie, opracowaniu i interpretacji wyników; wizualizacji wyników; redagowaniu roboczej wersji manuskryptu, uczestniczeniu w odpowiedziach na recenzje i zatwierdzeniu ostatecznej wersji artykułu.

Oświadczam, że w opublikowanej pracy:

Biegała Ł., **Gajek A.**, Szymczak-Pajor I., Marczak A., Śliwińska A., Rogalska A. *Targeted inhibition of the ATR/CHK1 pathway overcomes resistance to olaparib and dysregulates DNA damage response protein expression in BRCA2<sup>MUT</sup> ovarian cancer cells*. Sci Rep. 2023. 13(1):22659. <https://doi.org/10.1038/s41598-023-50151-y>, mój udział wynosił **5%** i polegał na: opracowaniu koncepcji badań; zaplanowaniu i wdrożeniu części metodologicznej; wykonaniu części eksperymentów (oznaczenie aktywności enzymatycznej kasazy-3/7 oraz oznaczenie poziomu apoptozy poprzez pomiar eksternalizacji fosfatydyloseryny za pomocą cytometrii przepływowej); wizualizacji wyników; redagowaniu roboczej wersji manuskryptu, uczestniczeniu w odpowiedziach na recenzje i zatwierdzeniu ostatecznej wersji artykułu.

Arkadiusz Gajek

Oświadczam, że w opublikowanej pracy:

Biegała Ł., Kołat D., **Gajek A.**, Płuciennik E., Marczak A., Śliwińska A., Mikula M., Rogalska A. *Uncovering miRNA-mRNA Regulatory Networks Related to Olaparib Resistance and Resensitization of BRCA2<sup>MUT</sup> Ovarian Cancer PEO1-OR Cells with the ATR/CHK1 Pathway Inhibitors*. Cells. 2024. 13(10):864. <https://doi.org/10.3390/cells13100867>,

mój udział wynosił 5% i polegał na: opracowaniu koncepcji badań; zaplanowaniu i wdrożeniu części metodologicznej; wykonaniu części eksperymentów (izolacja całkowitego RNA wraz z mikroRNA z linii komórkowych); redagowaniu roboczej wersji manuskryptu i odpowiedzi na recenzje, przygotowaniu i zatwierdzeniu ostatecznej wersji artykułu.

Oświadczam, że w manuskrypcie artykułu:

Biegała Ł., Statkiewicz M., **Gajek A.**, Szymczak-Pajor I., Rusetska N., Śliwińska A., Marczak A., Mikula M., Rogalska A. pt.: „*Olaparib rechallenge combined with the ATR/CHK1 pathway inhibitors in olaparib-resistant PDX models of ovarian cancer: Mechanisms behind synergistic tumor growth inhibition*”,

mój udział wynosił 5% i polegał na: opracowaniu koncepcji badań; zaplanowaniu i wdrożeniu części metodologicznej; wykonaniu części eksperymentów (izolacja całkowitego RNA z tkanek nowotworowych, przygotowanie lizatów białkowych z tkanek nowotworowych); redagowaniu roboczej wersji i zatwierdzeniu ostatecznej wersji manuskryptu.



dr Arkadiusz Gajek

(podpis)



**Prof. dr hab. Agnieszka Marczak**  
Katedra Biofizyki Medycznej  
Uniwersytet Łódzki

## OŚWIADCZENIE WSPÓŁAUTORA

Oświadczam, że w opublikowanej pracy:

Biegała Ł., Gajek A., **Marczak A.**, Rogalska A. *PARP inhibitor resistance in ovarian cancer: Underlying mechanisms and therapeutic approaches targeting the ATR/CHK1 pathway*. Biochim Biophys Acta Rev Cancer. 2021. 1876(2):188633. <https://doi.org/10.1016/j.bbcan.2021.188633>,  
mój udział wynosił **10%** i polegał na: pracowaniu koncepcji pracy przeglądowej; przygotowaniu wstępnej wersji artykułu; redagowaniu roboczej wersji manuskryptu i zatwierdzeniu ostatecznej wersji artykułu; sprawowaniu nadzoru nad przygotowaniem artykułu.

Oświadczam, że w opublikowanej pracy:

Biegała Ł., Gajek A., **Marczak A.**, Rogalska A. *Olaparib-Resistant BRCA2<sup>MUT</sup> Ovarian Cancer Cells with Restored BRCA2 Abrogate Olaparib-Induced DNA Damage and G2/M Arrest Controlled by the ATR/CHK1 Pathway for Survival*. Cells. 2023. 12(7):1038. <https://doi.org/10.3390/cells12071038>,  
mój udział wynosił **5%** i polegał na: opracowaniu koncepcji badań; zapewnianiu dostępu do materiałów badawczych; redagowaniu roboczej wersji manuskryptu i zatwierdzeniu ostatecznej wersji artykułu.

Oświadczam, że w opublikowanej pracy:

Biegała Ł., Gajek A., Szymczak-Pajor I., **Marczak A.**, Śliwińska A., Rogalska A. *Targeted inhibition of the ATR/CHK1 pathway overcomes resistance to olaparib and dysregulates DNA damage response protein expression in BRCA2<sup>MUT</sup> ovarian cancer cells*. Sci Rep. 2023. 13(1):22659. <https://doi.org/10.1038/s41598-023-50151-y>,  
mój udział wynosił **5%** i polegał na: opracowaniu koncepcji badań; zaplanowaniu części metodologicznej; zapewnianiu dostępu do materiałów badawczych; redagowaniu roboczej wersji manuskryptu i zatwierdzeniu ostatecznej wersji artykułu.

Oświadczam, że w opublikowanej pracy:

Biegała Ł., Kołat D., Gajek A., Płuciennik E., **Marczak A.**, Śliwińska A., Mikula M., Rogalska A. *Uncovering miRNA-mRNA Regulatory Networks Related to Olaparib Resistance and Resensitization of BRCA2<sup>MUT</sup> Ovarian Cancer PEO1-OR Cells with the ATR/CHK1 Pathway Inhibitors*. Cells. 2024. 13(10):864. <https://doi.org/10.3390/cells13100867>,  
mój udział wynosił **2%** i polegał na: opracowaniu koncepcji badań; redagowaniu roboczej wersji manuskryptu i zatwierdzeniu ostatecznej wersji artykułu.

Oświadczam, że w manuskrypcie artykułu:

Biegała Ł., Statkiewicz M., Gajek A., Szymczak-Pajor I., Rusetska N., Śliwińska A., **Marczak A.**, Mikula M., Rogalska A. pt.: „*Olaparib rechallenge combined with the ATR/CHK1 pathway inhibitors in olaparib-resistant PDX models of ovarian cancer: Mechanisms behind synergistic tumor growth inhibition*”,  
mój udział wynosił **3%** i polegał na: zaplanowaniu części metodologicznej; zapewnianiu dostępu do materiałów badawczych; zatwierdzeniu ostatecznej wersji manuskryptu.

Podpis jest prawidłowy

Dokument podpisany przez  
Agnieszka Marczak  
Data: 2024.05.19 11:41:47  
CEST

Za zgodność z oryginałem

SPECJALISTA  
w Dziekanacie  
Wydziału Biologii i Ochrony Środowiska UŁ

mgr Jarosław Mrówczyński

prof. dr hab. Agnieszka Marczak

Łódź, 20.05.2024

**Dr hab. n. med. Agnieszka Śliwińska, prof. Uczelni**

Zakład Biochemii Kwasów Nukleinowych  
Uniwersytet Medyczny w Łodzi

### OŚWIADCZENIE WSPÓŁAUTORA

Oświadczam, że w opublikowanej pracy:

Biegała Ł., Gajek A., Szymczak-Pajor I., Marczak A., **Śliwińska A.**, Rogalska A. *Targeted inhibition of the ATR/CHK1 pathway overcomes resistance to olaparib and dysregulates DNA damage response protein expression in BRCA2<sup>MUT</sup> ovarian cancer cells*. Sci Rep. 2023. 13(1):22659. <https://doi.org/10.1038/s41598-023-50151-y>,

mój udział wynosił 5% i polegał na: opracowaniu koncepcji badań; zaplanowaniu części metodologicznej; zapewnianiu dostępu do materiałów badawczych; redagowaniu roboczej wersji manuskryptu i zatwierdzeniu ostatecznej wersji artykułu.

Oświadczam, że w opublikowanej pracy:

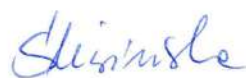
Biegała Ł., Kołat D., Gajek A., Płuciennik E., Marczak A., **Śliwińska A.**, Mikula M., Rogalska A. *Uncovering miRNA-mRNA Regulatory Networks Related to Olaparib Resistance and Resensitization of BRCA2<sup>MUT</sup> Ovarian Cancer PEO1-OR Cells with the ATR/CHK1 Pathway Inhibitors*. Cells. 2024. 13(10):864. <https://doi.org/10.3390/cells13100867>,

mój udział wynosił 4% i polegał na: opracowaniu koncepcji badań; zaplanowaniu części metodologicznej; redagowaniu roboczej wersji manuskryptu i odpowiedzi na recenzje, przygotowaniu i zatwierdzeniu ostatecznej wersji artykułu.

Oświadczam, że w manuskrypcie artykułu:

Biegała Ł., Statkiewicz M., Gajek A., Szymczak-Pajor I., Rusetska N., **Śliwińska A.**, Marczak A., Mikula M., Rogalska A. pt.: „*Olaparib rechallenge combined with the ATR/CHK1 pathway inhibitors in olaparib-resistant PDX models of ovarian cancer: Mechanisms behind synergistic tumor growth inhibition*”,

mój udział wynosił 3% i polegał na: zaplanowaniu części metodologicznej; zapewnianiu dostępu do materiałów badawczych; redagowaniu roboczej wersji i zatwierdzeniu ostatecznej wersji manuskryptu.



---

dr hab. n. med. Agnieszka Śliwińska, prof. Uczelni  
(podpis)



Łódź, 20.05.2024

**Dr n. med. Izabela Szymczak-Pajor**

Zakład Biochemii Kwasów Nukleinowych

Uniwersytet Medyczny w Łodzi

## OŚWIADCZENIE WSPÓŁAUTORA

Oświadczam, że w opublikowanej pracy:

Biegała Ł., Gajek A., **Szymczak-Pajor I.**, Marczak A., Śliwińska A., Rogalska A. *Targeted inhibition of the ATR/CHK1 pathway overcomes resistance to olaparib and dysregulates DNA damage response protein expression in BRCA2<sup>MUT</sup> ovarian cancer cells*. Sci Rep. 2023. 13(1):22659. <https://doi.org/10.1038/s41598-023-50151-y>,

mój udział wynosił 10% i polegał na: zaplanowaniu i wdrożeniu części metodologicznej; wykonaniu części eksperymentów (walidacja ekspresji genów referencyjnych oraz badanie poziomu ekspresji genów za pomocą ilościowej reakcji łańcuchowej polimerazy w czasie rzeczywistym (RT-qPCR)); redagowaniu roboczej wersji manuskryptu i zatwierdzeniu ostatecznej wersji artykułu.

Oświadczam, że w manuskrypcie artykułu:

Biegała Ł., Statkiewicz M., Gajek A., **Szymczak-Pajor I.**, Rusetska N., Śliwińska A., Marczak A., Mikula M., Rogalska A. pt.: „*Olaparib rechallenge combined with ATR/CHK1 pathway inhibitors in olaparib-resistant PDX models of ovarian cancer: Mechanisms behind synergistic tumor growth inhibition*”,

mój udział wynosił 5% i polegał na: wykonaniu części eksperymentów (walidacja ekspresji genów referencyjnych oraz badanie poziomu ekspresji genów za pomocą ilościowej reakcji łańcuchowej polimerazy w czasie rzeczywistym (RT-qPCR)); zatwierdzeniu ostatecznej wersji manuskryptu.

dr n. med. Izabela Szymczak-Pajor  
(podpis)

Warszawa, 19.05.2024

**Prof. dr hab. n. med. Michał Mikula**

Zakład Genetyki

Narodowy Instytut Onkologii im. Marii Skłodowskiej-Curie

– Państwowy Instytut Badawczy

## OŚWIADCZENIE WSPÓŁAUTORA

Oświadczam, że w opublikowanej pracy:

Biegała Ł., Kołat D., Gajek A., Płuciennik E., Marczak A., Śliwińska A., **Mikula M.**, Rogalska A.  
*Uncovering miRNA-mRNA Regulatory Networks Related to Olaparib Resistance and Resensitization of BRCA2<sup>MUT</sup> Ovarian Cancer PEO1-OR Cells with the ATR/CHK1 Pathway Inhibitors*. Cells. 2024. 13(10):864. <https://doi.org/10.3390/cells13100867>,

mój udział wynosił 2% i polegał na: opracowaniu koncepcji badań; redagowaniu roboczej wersji manuskryptu i zatwierdzeniu ostatecznej wersji artykułu.

Oświadczam, że w manuskrypcie artykułu:

Biegała Ł., Statkiewicz M., Gajek A., Szymczak-Pajor I., Rusetska N., Śliwińska A., Marczak A., **Mikula M.**, Rogalska A. pt.: „*Olaparib rechallenge combined with the ATR/CHK1 pathway inhibitors in olaparib-resistant PDX models of ovarian cancer: Mechanisms behind synergistic tumor growth inhibition*”,

mój udział wynosił 5% i polegał na: opracowaniu koncepcji badań; zapewnianiu dostępu do materiałów badawczych; redagowaniu roboczej wersji i zatwierdzeniu ostatecznej wersji manuskryptu.



Signed by /  
Podpisano przez:

Michał Marek  
Mikula

Date / Data:  
2024-05-19 10:46

---

prof. dr hab. n. med. Michał Mikula

(podpis)

Za zgodność z oryginałem

SPECJALISTA  
w Dziekanacie  
Wydziału Biologii i Ochrony Środowiska UŁ  
  
mgr Jarosław Mrówczyński



Łódź, 18.05.2024

**Mgr Damian Kołat**

<sup>1</sup> Zakład Genomiki Funkcjonalnej

Uniwersytet Medyczny w Łodzi

<sup>2</sup> Zakład Biomedycyny i Chirurgii Doświadczalnej

Uniwersytet Medyczny w Łodzi

## OŚWIADCZENIE WSPÓŁAUTORA

Oświadczam, że w opublikowanej pracy:

Biegała Ł., **Kołat D.**, Gajek A., Płuciennik E., Marczak A., Śliwińska A., Mikula M., Rogalska A.  
*Uncovering miRNA-mRNA Regulatory Networks Related to Olaparib Resistance and Resensitization of BRCA2<sup>MUT</sup> Ovarian Cancer PEO1-OR Cells with the ATR/CHK1 Pathway Inhibitors.* Cells. 2024. 13(10):864. <https://doi.org/10.3390/cells13100867>,

mój udział wynosił **10%** i polegał na: opracowaniu koncepcji badań; zaplanowaniu i wdrożeniu części metodologicznej; gromadzeniu, analizie i opracowaniu danych z repozytoriów; redagowaniu roboczej wersji manuskryptu, uczestniczeniu w odpowiedziach na recenzje i zatwierdzeniu ostatecznej wersji artykułu.



Signed by /  
Podpisano przez:

Damian Kołat  
Uniwersytet  
Medyczny w Łodzi

Date / Data:  
2024-05-18 12:11

---

mgr Damian Kołat

(podpis)

*Za zgodność z oryginałem*

**SPECJALISTA**

w Dziekanacie

Wydziału Biologii i Ochrony Środowiska UŁ

mgr Jarosław Mrówczyński

Łódź, 20.05.2024

**dr hab. n. med. Elżbieta Płuciennik, prof. Uczelni**

Zakład Genomiki Funkcjonalnej

Uniwersytet Medyczny w Łodzi

## OŚWIADCZENIE WSPÓŁAUTORA

Oświadczam, że w opublikowanej pracy:

Biegała Ł., Kołat D., Gajek A., **Płuciennik E.**, Marczak A., Śliwińska A., Mikula M., Rogalska A.  
*Uncovering miRNA-mRNA Regulatory Networks Related to Olaparib Resistance and Resensitization of BRCA2<sup>MUT</sup> Ovarian Cancer PEO1-OR Cells with the ATR/CHK1 Pathway Inhibitors*. Cells. 2024. 13(10):864. <https://doi.org/10.3390/cells13100867>,

mój udział wynosił 2% i polegał na: gromadzeniu, analizie i opracowaniu danych z repozytoriów; redagowaniu roboczej wersji manuskryptu i zatwierdzeniu ostatecznej wersji artykułu.



Signed by /  
Podpisano przez:

Elżbieta  
Płuciennik

Date / Data:  
2024-05-20 09:18

dr hab. n. med. Elżbieta Płuciennik, prof. Uczelni  
(podpis)

*Za zgodność z oryginałem*

**SPECJALISTA**  
w Dziekanacie  
Wydziału Biologii i Ochrony Środowiska UŁ  
  
mgr Jarosław Mrówczyński



Warsza...

**Dr n. med. Małgorzata Statkiewicz**

Zakład Genetyki

Narodowy Instytut Onkologii im. Marii Skłodowskiej-Curie

– Państwowy Instytut Badawczy

## OŚWIADCZENIE WSPÓŁAUTORA

Oświadczam, że w manuskrypcie artykułu:

Biegała Ł., **Statkiewicz M.**, Gajek A., Szymczak-Pajor I., Rusetska N., Śliwińska A., Marczak A., Mikula M., Rogalska A. pt.: „*Olaparib rechallenge combined with the ATR/CHK1 pathway inhibitors in olaparib-resistant PDX models of ovarian cancer: Mechanisms behind synergistic tumor growth inhibition*”,

mój udział wynosił 10% i polegał na: opracowaniu koncepcji badań; zaplanowaniu i wdrożeniu części metodologicznej; wykonaniu części eksperymentów (propagacja heteroprzeszczepów u myszy, wyprowadzenie modeli heteroprzeszczepów raka jajnika z tkanek nowotworowych pochodzących bezpośrednio od pacjentek, podawanie badanych inhibitorów myszom z heteroprzeszczepem); przygotowaniu i redagowaniu roboczej wersji oraz zatwierdzeniu ostatecznej wersji manuskryptu.

dr n. med. Małgorzata Statkiewicz  
(podpis)

Za zgodność z oryginałem

SPECJALISTA  
w Dziekanacie  
Wydziału Biologii i Ochrony Środowiska UJ.  
  
mgr Jarosław Mrówczyński



PODPIS ZAUFANY

NATALIA  
RUSETSKA16.05.2024 12:43:37 [GMT+2]  
Dokument podpisany elektronicznie  
podpisem zaufanym

Warsza..., .....

**Dr n. biol. Natalia Rusetska**

Zakład Immunoterapii Eksperymentalnej

Narodowy Instytut Onkologii im. Marii Skłodowskiej-Curie

– Państwowy Instytut Badawczy

**OŚWIADCZENIE WSPÓŁAUTORA**

Oświadczam, że w manuskrypcie artykułu:

Biegała Ł., Statkiewicz M., Gajek A., Szymczak-Pajor I., **Rusetska N.**, Śliwińska A., Marczak A., Mikula M., Rogalska A. pt.: „*Olaparib rechallenge combined with the ATR/CHK1 pathway inhibitors in olaparib-resistant PDX models of ovarian cancer: Mechanisms behind synergistic tumor growth inhibition*”,

mój udział wynosił 5% i polegał na: zaplanowaniu i wdrożeniu części metodologicznej; wykonaniu części eksperymentów (przygotowanie i badanie wycinków pobranych z guzów nowotworowych – barwienie hematoksykliną i eozyną oraz immunohistochemia, ocena mikroskopowa preparatów po barwieniu immunohistochemicznym, przygotowanie zdjęć preparatów); przygotowaniu i redagowaniu roboczej wersji oraz zatwierdzeniu ostatecznej wersji manuskryptu.

---

dr n. biol. Natalia Rusetska

(podpis)

Za zgodność z oryginałem

SPECJALISTA

w Dziekanacie

Wydziału Biologii i Ochrony Środowiska UL

  
mgr Jarosław Mrówczyński